

FIFTH EDITION

# PRINCIPLES OF YACHT DESIGN

LARS LARSSON, ROLF E ELIASSON AND MICHAL ORYCH



ADLARD COLES

FIFTH EDITION

# PRINCIPLES OF YACHT DESIGN

LARS LARSSON, ROLF E ELIASSON AND MICHAL ORYCH



LONDON • OXFORD • NEW YORK • NEW DELHI • SYDNEY



ADLARD COLES  
Bloomsbury Publishing Plc  
50 Bedford Square, London, WC1B 3DP, UK  
29 Earlsfort Terrace, Dublin 2, Ireland

BLOOMSBURY, ADLARD COLES and the Adlard Coles logo are  
trademarks of Bloomsbury Publishing Plc

First edition 1994  
Reprinted 1996, 1997  
Second edition 2000  
Third edition 2007  
Reprinted 2011, 2012  
Fourth edition 2014  
This fifth edition published in 2022

Copyright © Lars Larsson and Rolf E Eliasson 1994, 2000, 2007  
Copyright © Lars Larsson, Rolf E Eliasson and Michal Orych 2014, 2021

The Authors have asserted their right under the Copyright, Designs and  
Patents Act, 1988, to be identified as Authors of this work

This electronic edition published in 2022 by Bloomsbury Publishing Plc

All rights reserved. No part of this publication may be reproduced or  
transmitted in any form or by any means, electronic or mechanical, including  
photocopying, recording, or any information storage or retrieval system,  
without prior permission in writing from the publishers

A catalogue record for this book is available from the British Library  
Library of Congress Cataloguing-in-Publication data has been applied for

ISBN 978-1-4729-8192-9  
ePDF 978-1-4729-8194-3  
ePub 978-1-4729-8193-6

Page design and typesetting by Susan McIntyre  
Typeset in 10 on 13.75pt Adobe Caslon Pro

**Note:** while all reasonable care has been taken in the publication of this book,  
the publisher takes no responsibility for the use of the methods or products  
described in the book.

# CONTENTS

<b>PREFACE TO THE FIFTH EDITION</b>	<b>5</b>	<ul style="list-style-type: none"> <li>Added resistance in waves</li> <li>Other seakeeping aspects</li> <li>Hull statistics</li> </ul>	90 94 96
<b>LIST OF SYMBOLS</b>	<b>6</b>		
<b>INTRODUCTION</b>	<b>10</b>		
<b>1 DESIGN METHODOLOGY</b>	<b>13</b>		
<ul style="list-style-type: none"> <li>The design spiral</li> <li>Computer-aided design (CAD)</li> </ul>	13 15		
<b>2 PRELIMINARY CONSIDERATIONS</b>	<b>17</b>		
<ul style="list-style-type: none"> <li>Choice of boat-type</li> <li>Intended use</li> <li>Main dimensions</li> <li>Cost</li> <li>Checklist of considerations</li> <li>Checklist for the YD-41</li> </ul>	17 17 18 20 22 22		
<b>3 HULL GEOMETRY</b>	<b>23</b>		
<ul style="list-style-type: none"> <li>Definitions</li> <li>Line drawing</li> <li>Tools</li> <li>Work plan</li> <li>Computer-aided design of hulls</li> </ul>	23 27 29 33 35		
<b>4 HYDROSTATICS AND STABILITY</b>	<b>38</b>		
<ul style="list-style-type: none"> <li>Calculation of areas</li> <li>Wetted surface</li> <li>Displacement</li> <li>Centre of buoyancy</li> <li>Water plane area</li> <li>Transverse and longitudinal stability at small angles</li> <li>Transverse stability at large angles of heel</li> <li>Curve of static stability</li> <li>Rolling</li> <li>Influence of waves on the righting moment</li> <li>Stability statistics</li> <li>Assessment of seaworthiness</li> </ul>	38 40 40 42 46 47 50 52 54 57 59 60		
<b>5 HULL DESIGN</b>	<b>65</b>		
<ul style="list-style-type: none"> <li>Forces and moments on a sailing yacht</li> <li>Resistance components</li> <li>Viscous resistance: basic concepts</li> <li>Frictional resistance</li> <li>Viscous pressure resistance</li> <li>Roughness</li> <li>Wave resistance: basic concepts</li> <li>Wave and residuary resistance</li> <li>Heel resistance</li> </ul>	65 67 69 70 72 75 77 81 88		
		<ul style="list-style-type: none"> <li>Added resistance in waves</li> <li>Other seakeeping aspects</li> <li>Hull statistics</li> </ul>	90 94 96
<b>6 KEEL AND RUDDER DESIGN</b>	<b>102</b>		
<ul style="list-style-type: none"> <li>Flow around a wing</li> <li>Definition of the keel planform</li> <li>Classical wing theory</li> <li>Tip shape</li> <li>Lift and induced resistance of the yacht</li> <li>Advanced planform design</li> <li>Canting keels</li> <li>Evaluation of some planform concepts</li> <li>Definition of the section</li> <li>Three useful NACA sections</li> <li>Influence of shape on section characteristics</li> <li>Some practical conclusions regarding section shape</li> <li>Influence of deviations from the theoretical section shape</li> <li>Advanced section design</li> <li>Statistics on keel and rudder area</li> <li>The YD-41</li> </ul>	102 105 106 111 114 116 123 123 126 127 129 136 136 140 140 142		
<b>7 FOILING</b>	<b>144</b>		
<ul style="list-style-type: none"> <li>Foiling concepts</li> <li>Forces and moments</li> <li>Flight stability</li> <li>Planform area and shape</li> <li>Foil sections</li> <li>Example – a foiling skiff</li> <li>Computed forces</li> <li>Other aspects</li> </ul>	146 148 157 158 161 165 168 176		
<b>8 SAIL AND RIG DESIGN</b>	<b>179</b>		
<ul style="list-style-type: none"> <li>Flow around sails</li> <li>Planform</li> <li>Sail camber</li> <li>Mast interference</li> <li>Means for reducing mast disturbances</li> <li>Streamlining</li> <li>A practical model for sail and rig aerodynamics</li> <li>Sail statistics</li> </ul>	179 181 185 187 188 190 192 197		
<b>9 BALANCE</b>	<b>199</b>		
<ul style="list-style-type: none"> <li>Effect of heel</li> <li>Good balance</li> <li>Centre of effort of the underwater body</li> <li>Centre of effort of the sails</li> </ul>	199 201 201 203		



● Lead	205	<b>15 SCANTLINGS</b>	<b>304</b>
● Rudder balance	206	● Determination	304
<b>10 PROPELLER AND ENGINE</b>	<b>207</b>	● Structure of the standard	304
● Resistance in calm and rough weather	208	● Hull definitions	307
● Propeller characteristics	211	● Areas	308
● Design of an optimum propeller	213	● Dimensions of panels and stiffeners	310
● Performance of the non-optimum propeller	217	● Pressures on panels and stiffeners	310
● Check of blade area	220	● Pressure adjusting factors	313
● Propeller resistance	221	● Design loads	317
<b>11 HIGH-SPEED HYDRODYNAMICS</b>	<b>223</b>	● Design loads for the topsides	318
● Planing	223	● Design loads for the decks, superstructures and bulkheads	321
● Deadrise	226	● Summary of design loads	322
● Forces on a planing hull	228	● Mechanical properties and design stresses	323
● Spray rails, stepped bottoms and transom flaps	233	● Boatbuilding quality factor $K_{BB}$	323
● Dynamic stability	236	● Assessment method factor $K_{AM}$	324
● Alternative propulsion devices	238	● Aspect ratio factors for plating $K_{2B}$ and $K_{SH}$	325
● An example	239	● Curvature correction factor for plating $K_c$	326
<b>12 RIG CONSTRUCTION</b>	<b>243</b>	● Design stresses	326
● Definitions and scope of the standard	243	● Design shear forces and design moments $F_D$ and $M_D$	327
● Forces on the shrouds	246	● Methods for scantling determination	328
● Forces on the stays	250	● Determination of mechanical properties	328
● Comparison between wire and rod	251	● Single skin panel calculation	331
● Transverse mast stiffness	254	● Sandwich	333
● Longitudinal mast stiffness	255	● Stiffener design forces and moments	335
● Fractional mast top	256	● Stiffener curvature factor $K_{CS}$	337
● Boom	256	● Stresses in stiffeners $\tau$ and $\delta_{CRIT}$	337
● Spreaders	257	● Effective width of attached plating $B_E$	337
● Holes in the mast	258	● Stiffener construction	340
● The YD-41 rig	259	● Spade rudder stock	342
<b>13 HULL CONSTRUCTION</b>	<b>263</b>	● Keelbolts	344
● Concepts in structural mechanics	264	● Rig loads and rig attachment	346
● Global loads	265	<b>16 LAYOUT</b>	<b>351</b>
● Local hydrostatic loads	270	● Generic space requirements	351
● Local hydrodynamic loads	271	● Accommodation	352
● Transverse load distribution	273	● Deck layout	358
● Local deformations	274	● Building the YD-41	347
● Forces from the keel	275	<b>17 DESIGN EVALUATION</b>	<b>364</b>
● Forces from grounding	276	● Non-dimensional parameters	365
● Forces from the rudder	279	● The Velocity Prediction Program (VPP)	366
● Summary of loadings	281	● Towing tank testing	372
<b>14 MATERIALS</b>	<b>286</b>	● Wind tunnel testing	374
● Glass reinforcement	287	● Computational fluid dynamics (CFD)	375
● Wet laminates	291	<b>APPENDIX 1: Main particulars of the YD-41</b>	<b>385</b>
● Fatigue	291	<b>APPENDIX 2: Weight calculation</b>	<b>386</b>
● Exotic laminates	293	<b>APPENDIX 3: STIX calculation</b>	<b>393</b>
● Sandwich	295	<b>REFERENCES</b>	<b>395</b>
● Typical sandwich buckling	298	<b>INDEX</b>	<b>397</b>
● Sandwich bending	300		
● Sandwich in practice	301		
● Final remarks	303		

# PREFACE

The first edition of *Principles of Yacht Design* was published in 1994. Since then there have been three new editions, and the book has been translated into German, Japanese, Korean, Chinese, and Polish. A special edition is published in the United States. The book has thus been very well received, and in this fifth edition we have kept the structure and the main contents of the previous editions. The basic idea is to cover all aspects of yacht design, from the specification, through the hydro- and aerodynamic design, structural assessment, and layout, to the final evaluation. Emphasis is placed on concept descriptions, but formulae, separated from the text, are included in sufficient depth for a complete design of a new yacht. An important feature of the book is the example yacht, used in the book to exemplify the use of the formulae. This is now the YD-41, which replaces the original YD-40 in the fourth edition. Since that edition, the YD-41 has been built and can be seen sailing on the cover. Several pictures of the boat are also included in the book.

In this fifth edition there are minor revisions in many chapters, but the two main updates are a new chapter on foiling and a completely rewritten chapter on scantlings, following the new ISO 12215 standard. The authors owe great thanks to Nimal Sudhan Saravana Prabahar, who carried out all computations reported in the foiling chapter. Heikki Hansen, Laura Marimon Giovannetti and Adam Persson are also gratefully acknowledged for reviewing the chapter. The new ISO scantlings standard was developed under the chairmanship of Gregoire Dolto and the authors are indebted to him for his support.

*Lars Larsson  
Rolf E Eliasson  
Michal Orych  
Gothenburg*



# LIST OF SYMBOLS

In general, the symbols used in this book are those recommended by the International Towing Tank Conference (ITTC). However, in the chapters on scantling determination (hull dimensioning) and the Nordic Boat Standard (rig dimensioning) other symbols have been used. This is to simplify the later use of these standards by readers.

<b>A, A<sub>(l)</sub></b>	area, general	<b>B<sub>C</sub></b>	chine beam of hull	<b>C<sub>Lr</sub></b>	rudder lift coefficient
<b>a</b>	elongation	<b>BD</b>	boom height above deck	<b>CLR</b>	hydrodynamic centre of lateral resistance
<b>a<sub>(l)</sub></b>	distance from neutral axis to centre of area	<b>b<sub>e</sub></b>	effective width of plating	<b>C<sub>M</sub></b>	midship section coefficient
<b>A<sub>0</sub></b>	area of propeller disk	<b>BG</b>	distance between centre of buoyancy and gravity	<b>C<sub>P</sub></b>	prismatic coefficient, or pressure coefficient
<b>a<sub>1</sub></b>	distance from L <sub>WL</sub> to T1	<b>B<sub>H</sub></b>	moulded beam of hull	<b>C<sub>R</sub></b>	residuary resistance coefficient
<b>a<sub>2</sub></b>	distance from L <sub>WL</sub> to T2	<b>BM</b>	metacentric radius	<b>C<sub>S</sub></b>	aerodynamic side force coefficient
<b>ABS</b>	American Bureau of Shipping	<b>B<sub>MAX</sub></b>	maximum beam of hull	<b>c<sub>u</sub></b>	curvature height of stiffener
<b>A<sub>D</sub></b>	design area under consideration	<b>B<sub>u</sub></b>	Taylor thrust coefficient	<b>D</b>	depth of yacht, or drag, or propeller diameter
<b>A<sub>F</sub></b>	foretriangle area	<b>B<sub>WL</sub></b>	beam of waterline	<b>D1,2,3</b>	diagonal shrouds
<b>A<sub>f</sub></b>	flange area	<b>C</b>	chord length, or crown width of stiffener, or compressive strength (see also list of Indices)	<b>d<sub>kb</sub></b>	core diameter of keelbolt
<b>a<sub>k</sub></b>	distance from keel centre of gravity to canoe body	<b>C<sub>1,2</sub></b>	spreader compression force	<b>DWL</b>	designed waterline
<b>A<sub>lr</sub></b>	projected rudder area	<b>c</b>	curvature height of panel	<b>E</b>	modulus of elasticity, or base of mainsail (ISO)
<b>A<sub>M</sub></b>	mainsail area, or midship section area below designed waterline	<b>CB</b>	centreboard	<b>E<sub>C</sub></b>	compressive modulus of elasticity
<b>A<sub>min</sub></b>	keel/hull area	<b>C<sub>B</sub></b>	block coefficient	<b>E<sub>F</sub></b>	flexural modulus of elasticity
<b>AOA</b>	angle of attack	<b>C<sub>D</sub></b>	drag coefficient	<b>E<sub>T</sub></b>	tensile modulus of elasticity
<b>AP</b>	aft perpendicular	<b>C<sub>Di</sub></b>	induced drag coefficient	<b>E<sub>TC</sub></b>	average modulus of elasticity
<b>A<sub>R</sub></b>	aerodynamic driving force	<b>C<sub>D0</sub></b>	drag coefficient at zero angle of attack, or drag coefficient of mast, rig and topsides	<b>F</b>	flat factor of sails, or flexural strength, or flange width of stiffener, or design head reduction factor
<b>AR, ΔAR</b>	aspect ratio and change in aspect ratio, respectively	<b>C<sub>DP</sub></b>	viscous (parasitic) drag coefficient of sails	<b>F<sub>1,2,3</sub></b>	dimensioning transverse rig forces
<b>AR<sub>e</sub></b>	effective aspect ratio	<b>CE</b>	aerodynamic centre of effort	<b>F<sub>a</sub></b>	freeboard aft
<b>AR<sub>E</sub></b>	aspect ratio of extended keel	<b>CF</b>	centre foil	<b>F<sub>f</sub></b>	freeboard forward
<b>AR<sub>Ee</sub></b>	effective aspect ratio of extended keel	<b>C<sub>F</sub></b>	skin friction coefficient	<b>F<sub>h</sub></b>	hydrodynamic side force or horizontal boom force
<b>A<sub>S</sub></b>	sail area (main + foretriangle) or aerodynamic side force	<b>CFD</b>	computational fluid dynamics	<b>F<sub>i</sub></b>	impact force
<b>A<sub>W</sub></b>	area of water plane	<b>C<sub>H</sub></b>	heel resistance coefficient	<b>F<sub>n</sub></b>	Froude number
<b>A<sub>X</sub></b>	maximum section area below designed waterline	<b>C<sub>L</sub>, C<sub>Lmax</sub></b>	lift coefficient and maximum lift coefficient, respectively	<b>FP</b>	forward perpendicular
<b>b</b>	short edge of panel	<b>C<sub>L</sub><sup>2D</sup></b>	two-dimensional lift coefficient		
<b>B</b>	beam of hull amidships, or centre of buoyancy, hull upright	<b>C<sub>L</sub><sup>3D</sup></b>	three-dimensional lift coefficient		

$F_r$	rudder side force	$k_{BB}$	boatbuilding factor	$M_r$	rudder bending moment
$F_s$	design head reduction factor	$k_c$	curvature correction factor	$M_s$	spreader bending moment
$F_S$	freeboard at mast	$k_{DC}$	design category factor	$N$	rudder force factor
$F_v$	vertical boom force	$k_{DYN}$	dynamic load factor	<b>NBS</b>	Nordic Boat Standard
$F_\Phi$	side force at right angles to (heeled) centre plane	$k_L$	longitudinal impact factor	$n$	number of persons on board, or rate of revolutions, or number of floors in way of keel
<b>FRP</b>	fibre-reinforced plastic	$K_Q$	torque coefficient	$n_{cg}$	dynamic load factor, g:s
$g$	acceleration of gravity, or girth length, or ballast weight	$k_{SH}$	aspect ratio factor	$n_{kb}$	number of keelbolts
<b>G</b>	centre of gravity, or empty weight of yacht	$k_R$	structural component and boat type factor	<b>OF<sub>bolt</sub></b>	keel bolt offset
<b>GM</b>	metacentric height	$k_{SA}$	stiffener shear area factor	<b>ORC</b>	Offshore Racing Congress
<b>GRP</b>	glass-reinforced plastic	$k_{SHC}$	sandwich core shear coefficient	$O_x$	transverse fractional mast top length
<b>GZ</b>	righting arm	$k_{SLS}$	slamming factor for light, fast sailboats	$O_y$	longitudinal fractional mast top length
<b>H</b>	floor height or ride height	$k_{SUP}$	superstructure pressure reduction factor	<b>P</b>	height of mainsail (ISO), or propeller pitch, or load, general
$H_{1/3}$	significant wave height	$K_T$	thrust coefficient	$P_a$	dimensioning aft stay load
$h$	roughness height, rudder height, height of stiffener, local height from $L_{WL}$ or chine, mast height from deck or superstructure to the highest sail carrying forestay	$k_1$	bending stiffness coefficient	$P_{ah}$	horizontal part of aft stay load
$h_u$	distance between rudder bearings	$k_2$	aspect ratio coefficient for bending strength	$P_{av}$	vertical part of aft stay load
<b>HA</b>	heeling arm	$k_3$	aspect ratio coefficient for bending stiffness	$P_b$	bottom pressure
$h_b$	pressure head for watertight bulkhead or integral tank	$l$	long edge of panel	$P_{BMD}$	displacement powerboat bottom pressure
$I$	height of foretriangle (ISO), or moment of inertia	$L$	length, general, or length rated, or lift	$P_{BMP}$	planing powerboat bottom pressure
$I_L$	longitudinal moment of inertia of water plane area	$L_F$	floor length	$P_{BS}$	sailboat bottom pressure
<b>IACC</b>	International America's Cup Class	$L_K$	Keel root length	$P_c$	composite property
<b>IMS</b>	International Measurement System	$l_{1,2,3}$	rig panel lengths	$P_{crit}$	critical load
<b>IOR</b>	International Offshore Rule	$l_a$	distance from $L_{WL}$ to top of aft stay	$P_D$	delivered power, or design pressure
<b>ISO</b>	International Standards Organization	$l_c$	distance from leading edge to centre of effort	$P_{deck}$	compression force in deck
$I_T$	transverse moment of inertia of water plane area	$l_u$	unsupported length of stiffener	$P_{DM}$	powerboat deck pressure
$I_{yy}$	mass moment of inertia around a transverse axis through G	<b>LCB</b>	longitudinal centre of buoyancy	$P_{DS}$	sailboat deck pressure
$I_x$	transverse moment of inertia for the mast	$L_H$	length of hull	$P_{D,V}$	dimensioning shroud load
$I_y$	longitudinal moment of inertia for the mast	$L_{OA}$	length overall	$P_{fh}$	horizontal part of forestay load
<b>J</b>	base of foretriangle (ISO)	$L_{PP}$	length between perpendiculars	$P_{fi}$	dimensioning inner forestay load
$k$	gyradius in pitch, or aspect ratio factor	$L_{WL}$	length of waterline	$P_{fo}$	dimensioning outer forestay load
$k_{2b}$	aspect ratio factor	$m$	mass displacement, mass (general), or mast material factor	$P_{fv}$	vertical part of forestay load
$k_{AM}$	assessment method factor	$m_K$	mass of ballast keel	$P_{hd}$	horizontal component of stay forces
$k_{AR}$	area pressure reduction factor	$m_{LA}$	mass in loaded arrival condition	$P_{kb}$	keel bolt load tension
		$m_{LDC}$	loaded displacement mass	$P_{kt}$	total keel bolt load
		<b>M</b>	bending moment, or metacentre	$P_m$	mat property
		$M_{b_{hull}}$	hull bending moment	$P_{mast}$	mast pressure
		$M_{fi}$	floor bending moment	<b>PT</b>	dimensioning mast load
		$M_{kl}$	floor bending moment, from grounding	$P_r$	grounding load
		$M_{kt}$	transverse moment from keel	$P_{SMD}$	displacement powerboat side pressure
		$m_{MO}$	mass in minimum operating condition		



$P_{SMP}$	planing powerboat side pressure	$t, t_{max}$	thickness and maximum thickness, respectively	$Z$	height of top of hull or deck above $L_{WL}$
$P_{SS}$	sailboat side pressure	$T$	draft of yacht, or propeller thrust, or tensile strength	$Z_{CBk}$	distance from water surface to keel centre of buoyancy
$P_{SUPM}$	powerboat superstructure pressure	$T_1$	wave period, or transverse foresail force	$\alpha$	angle of attack, or scale factor
$P_{SUPS}$	sailboat superstructure pressure	$T_2$	transverse mainsail force	$\alpha_a$	aft stay angle to mast
$P_{TB}$	design pressure, integral tank	$T_{boom}$	transverse force at foot of mainsail	$\alpha_f$	forestay angle to mast
$P_{WB}$	design pressure, watertight bulkhead	$T_{bu}$	upper boom force	$\beta$	leeway angle, deadrise angle
$Q$	torque	$t_c$	core thickness, chine thickness	$\beta_{1,2,3}$	diagonal shroud angle to mast
$R$	resistance, general, or reef factor of sails	<b>TCG</b>	transverse centre of gravity	$\beta_{AW}$	apparent wind angle
$R_A$	windage	$t_f$	face thickness	$\gamma_{1,2}$	vertical shroud angle
$R_{AW}$	added resistance in waves	$T_{head}$	transverse force at top of mainsail	$\delta$	Taylor parameter, or horizontal angle of spreader
$R_F$	frictional resistance	$t_k$	keelstrake thickness	$\delta_{RM}$	additional righting moment from crew to windward
<b>RB</b>	rubber board	$T_{hl}$	lower shroud force	$\eta$	safety factor
<b>RF</b>	rubber foil	$T_{hu}$	upper shroud force	$\eta_0$	propeller efficiency
$R_H$	heel resistance	$T_K$	draft of keel below canoe body	$\Theta$	trim angle
<b>RM</b>	righting moment	$T_R$	taper ratio	$\lambda$	wavelength
$RM_1$	righting moment at 1 deg heel	<b>Tr</b>	rudder torsional moment	$\Lambda$	sweep angle
$RM_{30}$	righting moment at 30 deg heel	<b>Ts</b>	time to stop	$\nu$	kinematic viscosity
$RM_{90}$	righting moment at 90 deg heel	$t_s$	skin thickness, stemstrake thickness	$\rho$	density
$R_n$	Reynolds number	<b>V</b>	volume displacement, or yacht speed	$\sigma$	normal stress, or cavitation number
<b>RORC</b>	Royal Ocean Racing Club	<b>V1,2</b>	vertical shroud	$\sigma_{0,2}$	yield stress
$R_R$	residuary resistance	$V_{AW}$	apparent wind speed	$\sigma_c$	design stress for rudder stock
$r_t$	nose radius	$V_{AWe}$	effective apparent wind speed, yacht heeled	$\sigma_d$	design stress
$R_{vc}$	rudder centre of effort, vertical distance from top	<b>VCB</b>	vertical centre of buoyancy	$\sigma_f$	normal stress in sandwich face
<b>RYA</b>	Royal Yachting Association	<b>VPP</b>	Velocity Prediction Program	$\sigma_u$	ultimate stress
<b>s</b>	spacing of stiffeners	$V_s$	yacht speed	$\sigma_y$	yield stress
$S_{(n)}$	length of spreader	<b>W</b>	weight displacement, or fibre angle	$\tau$	Burrill parameter, or shear stress
<b>SA</b>	total triangular sail area	<b>w</b>	fibre mass	$\tau_d$	design shear stress
<b>SAF</b>	sail area, foretriangle (ISO)	<b>Wf</b>	fibre content, ratio	$\tau_u$	ultimate shear stress
<b>SAM</b>	sail area, mainsail, triangular (ISO)	$W_k$	weight of ballast	$\Phi$	heel angle
<b>SL</b>	length of spinnaker leech (ISO)	$X_0$	position of neutral axis	$\omega_\phi$	natural frequency (in roll)
<b>SM</b>	section modulus	<b>x</b>	distance of mid panel or stiffener from aft end of $L_{WL}$	$\omega_e$	frequency of wave encounter
$SM_{fi}$	floor section modulus	$x_{lc}$	distance from leading edge to centre of rudderstock	$\nabla$	volume displacement
$SM_{hull}$	hull girder section modulus	$X_m$	ratio of mat in a composite		
$SM_i$	section modulus to inside of panel	<b>X,Y,Z</b>	Cartesian coordinates. Origin at FP, X aftwards, Y to starboard, and Z upwards		
$SM_k$	section modulus increase in way of keel	<b>y</b>	deflection		
$SM_o$	section modulus to outside of panel				
<b>SMW</b>	spinnaker width (IOR)				
$S_W$	wetted surface area				
$S_{Wc}$	wetted surface area of canoe body				

## Indices

<b>c</b>	canoe body
<b>k</b>	keel
<b>r</b>	rudder
<b>u</b>	upper
<b>l</b>	lower

## ■ CONVERSION FACTORS

To convert metric measures into imperial measures, multiply by x.

To convert imperial measures into metric measures, multiply by y.

Metric	Imperial	x	y
<b>Length</b>			
Millimetres (mm)	Inches	0.039	25.40
Centimetres (cm)	Inches	0.394	2.540
Metres (m)	Inches	39.37	0.025
Metres (m)	Feet	3.281	0.305
Metres (m)	Yards	1.094	0.914
Kilometres (km)	Geographic miles	0.621	1.609
Kilometres (km)	Nautical miles	0.5397	1.8532
<b>Area</b>			
Square millimetres (mm <sup>2</sup> )	Square inches	0.0016	645.10
Square centimetres (cm <sup>2</sup> )	Square inches	0.155	6.452
Square metres (m <sup>2</sup> )	Square inches	1550	0.000645
Square metres (m <sup>2</sup> )	Square feet	10.764	0.0929
Square metres (m <sup>2</sup> )	Square yards	1.196	0.836
<b>Volume</b>			
Cubic centimetres (cm <sup>3</sup> )	Cubic inches	0.061	16.39
Cubic metres (m <sup>3</sup> )	Cubic feet	35.315	0.0283
Cubic metres (m <sup>3</sup> )	Cubic yards	1.309	0.764
Litres (L)	Cubic inches	61.024	0.0164
Litres (L)	Cubic feet	0.0353	28.317
Litres (L)	US gallons	0.264	3.785
Litres (L)	Imp. gallons	0.220	4.546
<b>Mass, weight and force</b>			
Grams (g)	Ounces	0.0353	28.350
Kilograms (kg)	Pounds	2.2046	0.4536
Tonnes, metric (T)	Pounds	2204.6	0.00045
Tonnes, metric (T)	Tons, long	0.9843	1.0160
Newton (N)	Pounds	0.2247	4.450
Kilonewton (kN)	Pounds	224.73	0.0044
<b>Density</b>			
Kilograms/m <sup>3</sup> (kg/m <sup>3</sup> )	Pounds/cubic foot	0.0624	16.026
<b>Pressure, stress, work, energy</b>			
Newton/mm <sup>2</sup> (N/mm <sup>2</sup> )	Pounds/sq inch	144.95	0.0069
Kilonewton/mm <sup>2</sup> (kN/mm <sup>2</sup> )	Pounds/sq inch	144950	0.0000069
Pascal (Pa) (= 1 N/m <sup>2</sup> )	Pounds/sq inch	0.00014	6899
Kilopascal (kPa) (= 1 kN/m <sup>2</sup> )	Pounds/sq inch	0.14495	6.899
Megapascal (MPa) (= 1 N/mm <sup>2</sup> )	Pounds/sq inch	144.95	0.0069
Gigapascal (GPa) (= 1 kN/mm <sup>2</sup> )	Pounds/sq inch	144950	0.0000069
Newton-metres (Nm)	Foot-pounds	0.7370	1.3568
Kilonewton-metres (kNm)	Foot-pounds	737.00	0.0136
Horsepower (metric)	Horsepower (imp)	0.9860	1.0142
Kilowatts (kW)	Horsepower (imp)	1.3400	0.7463
<b>Speed</b>			
Metres per second (m/s)	Feet per second	3.2808	0.3048
Metres per second (m/s)	Knots	1.9425	0.5148
Kilometres per hour (km/h)	Miles per hour	0.6214	1.6093
Kilometres per hour (km/h)	Knots	0.5397	1.8532



# INTRODUCTION

Yacht design is of interest not only to professional and amateur yacht designers; many other yachtsmen are interested in the principles behind the design of their yacht and the theory of sailing. In racing, such knowledge is important for the optimization of the equipment and the handling of the boat. Speed is also of interest in cruising; nobody is interested in a slow boat. Safety is a major issue in all kinds of sailing. Consequently, there is a need for a comprehensive book, covering all aspects of yacht design.

It is now more than 100 years since Skene wrote his now-classic *Elements of Yacht Design*, which was revised several times (see Kinney, 1973). For almost a century this book was considered the ‘bible’ in yacht design, but it is now obsolete. The most well-known books on sailing theory are the excellent ones by Marchaj: *Sailing Theory and Practice*, first published in 1964, *The Aero-Hydrodynamics of Sailing* in 1979, *Seaworthiness – the Forgotten Factor* in 1986 and *Sail Performance: Techniques to Maximize Sail Power* in 1996. Since the books deal with basic sailing theory, they are still mostly up to date, but they are not very useful for the designer, since they do not cover methodology, statistical data for existing yachts or design evaluation techniques. Furthermore, these books concentrate on the hydro- and aerodynamic aspects of the problem, while, for instance, loading, strength, and structural problems, as well as practical design considerations, are either not mentioned or treated very briefly.

By the time the first edition of the present book was published (in 1994), there was no modern textbook comparable to Skene’s as a guide for the yacht designer. Trying to replace this classic text with a modern one was a great challenge, but the new book was well-received both by professional and amateur yacht designers and translations have been made into several languages.

Since the first edition, another three high-quality books have appeared. *Sailing Yacht Design* by Claughton, Wellicome and Shenoï (1998) is published in two volumes: *Theory and Practice*, respectively. *Aero-Hydrodynamics and the Performance of Sailing Yachts* by Fossati (2009) deals with the fundamental theory of sailing yacht design and may be considered a modern version of Marchaj’s books. The same is true also for the most recent book by van Oossanen (2020): *The Science of Sailing*. This is an in-depth analysis of sailing physics in four volumes and around 1000 pages. As compared to Marchaj, and even Fossati, this book is more fundamental and goes into basic physics at a high academic level.

As the title suggests, the emphasis of this book is on yachts, rather than dinghies. However, most of the theories and concepts described apply to this class of boats as well. For specific aspects on racing dinghy design, see the excellent books by Bethwaite (1996, 2013): *High Performance Sailing* and *Higher Performance Sailing*.

For a book on yacht design to be successful, two conditions must be satisfied:

- It must cover all aspects of yacht design.
- Although it must be comprehensible for amateurs, it must be advanced enough to be of interest also to professional designers.

There follows a short presentation of this book and an explanation of the strategy adopted for satisfying these two requirements.

The book begins with a description of the methodology recommended in the design process. Specifications of the yacht and the design concept are discussed in [Chapter 2](#), and [Chapters 3](#) and [4](#) cover the geometric description of the hull and hydrostatics and stability in calm water and waves. The hydrodynamic design of the hull, keel, and rudder is explained in [Chapters 5](#) and [6](#). [Chapter 7](#) deals with foiling and [Chapter 8](#) with sail aerodynamics. In [Chapter 9](#) methods are introduced for finding the balance of the yacht. [Chapter 10](#) deals with the selection of the correct propeller and engine, and in [Chapter 11](#) planing hulls are introduced.

Structural aspects of design are treated in [Chapters 12, 13, 14](#) and [15](#). Loads acting on the rig and hull are identified and methods for computing them introduced. Dimensioning according to the ISO standard is explained and complete calculations carried out for one example. There is also a discussion on different fibre-reinforced plastic (FRP) materials, including sandwich laminates. Practical matters, such as the layout of the cockpit, deck and cabin, are discussed in [Chapter 16](#), and [Chapter 17](#) presents different means for evaluating the design. A complete weight calculation is carried out in Appendix 2.

The different aspects of the design process are therefore well covered. To satisfy the second requirement above, the material must be well presented, and we have tried to accomplish this in several ways. Yacht design is by its nature a quantitative process. A designer, professional or amateur, is not much helped by qualitative reasoning. It is not enough to know that the hull can withstand a larger load if the skin is made thicker, or that stability is increased by more lead in the keel. What he needs to know, as exactly as possible, is the *minimum* skin thickness and the least amount of lead needed in the keel for the yacht to be safe under all possible conditions. If he is not able to compute these quantities the yacht may be slower and more expensive than necessary and, worst of all, it may be unsafe. Therefore, a basic principle of this book has been to provide formulae or diagrams for all aspects of the design process. The reader should be able to evaluate quantitatively every step in the design procedure.

We are fully aware that many potential readers may be intimidated by a text loaded with formulae and would reject the book as being too technical. To avoid this, the equations have been removed from the text and inserted into the figures. A serious designer will need to work through the formulae himself for the reasons just explained, but we believe that the book could also be of interest to yachtsmen in general, since many may have a keen interest in the basic physics of sailing. They will be able to read the text without digging too deeply into the quantitative aspects. On the other hand, the equations are not very complicated from a mathematical point of view. They are numerous, and they may be lengthy, but they are all of the algebraic type. Higher mathematics, such as integral or differential calculus, have been completely avoided, and everyone with a basic mathematical background from, say, secondary school should be able to understand them.

To help the reader understand the practical application of the principles and formulae presented, the design of a new yacht, called YD-41 (Yacht Design 41-footer) is followed throughout the book. Thus, most of the formulae presented are followed by the computed value for the YD-41, and most drawings (like lines plan, interior and exterior layout, rig plan and general arrangement) are for this modern cruiser/racer. This does not mean, of course, that the book is limited to this type of yacht. The material covers other cruisers and racers, traditional and modern designs, and different rig types. Dinghies are covered as well, particularly in [Chapter 7](#) on foiling, but there is not much discussion on multihulls. Powerboats are addressed specifically in the chapters on high-speed hydrodynamics and scantlings, but much of the other material in the book applies to this type of craft as well. The YD-41 is specified in detail in Appendix 1, where all the data is given. There are two different sets of data. One is for the cruising condition, with all the necessary equipment and the tanks half full, while the other is for the light version, without cruising equipment. The latter version, or an even lighter one, is normally used in advertising material for new yachts. A weight calculation for the YD-41 is presented in Appendix 2, for different loading conditions. The boat can be seen under sail on the cover of this book.

To evaluate a new design and its qualities it is important to compare it with other yachts. Sections with statistical data are therefore included in many of the chapters. Median values for existing yachts are given and the scatter, within which approximately 95% of all yachts lie, is indicated. There is also a discussion on the effects of deviating from the median, which will enable the designer to create a yacht with special qualities. The position of the YD-41 within the statistical data is also shown and motivation for this position is given in the light of the yacht specification in [Chapter 2](#) and Appendix 1. To satisfy the more qualified readers of the book, there are sections on advanced design, where the methods and tools described are not normally available to non-professionals. Also, throughout the book, the results of the most recent research in yacht design are presented. Much of this is not discussed in yachting literature.

Finally, some general remarks on the principles and style of the book. With a few exceptions, the International System of Units (SI) is adopted. The exceptions are parts of the rig and scantling chapters where we use standards that still rely on other systems. Otherwise, it is only the yacht speed that does not always follow the SI system; it is often given in knots. This is still standard in hydrodynamics when it comes to boat speed. However, in the discussion of wings of different kinds, like keels, rudders, and hydrofoils, the aerodynamic vocabulary is used. Here speed is expressed in m/s. Resistance and drag are two words with the same meaning but from the two different disciplines. Depending on the topic both words are used in the book. A conversion table between the SI and English units may be found on [page 19](#).

Another standard adopted is the nomenclature specified by the International Towing Tank Conference (ITTC). This has been developed over a very long period and is agreed by all members of the ITTC, which include all reasonably sized towing tanks in the world, as well as most universities teaching naval architecture.

A list of references may be found at the end of the book. In the text, the references are identified by the name of the author, followed by the year of publication. It should be noted that there are more references in the list than are specifically referred to in the text.

# 1

# DESIGN METHODOLOGY

Yacht design is an iterative ‘trial and error’ procedure where the final result has to satisfy certain requirements, specified beforehand. To achieve this the designer has to start with a number of assumptions and work through the design to see if, at the end, it satisfies the requirements. This will most certainly not be the case in the first iteration, so he will have to change some assumptions and repeat the process, normally several times. The sequence of operations is often referred to as a spiral, where the designer runs through all the design steps and then returns to the starting point, whereupon a new ‘turn’ begins. After several turns the process may have produced the desired result. We will describe the design spiral in more detail below.

If all steps are taken manually the procedure can be extremely time consuming, and it is tempting to stop the iterations before the initial specifications have been fully met. A huge saving in time and accuracy is possible if modern computer-aided design (CAD) techniques are adopted, and we will discuss this possibility in the second part of the chapter.

## ■ THE DESIGN SPIRAL

In [Fig 1.1](#) the design spiral is shown. Eleven different segments may be identified, and each segment corresponds to an operation by the designer. Not all operations have to be carried out in each turn, and the tools used in each operation may vary from turn to turn. In principle, more and more segments are included, and better and better tools are used, as the process converges towards the final solution. The figure shows that each sector corresponds to a chapter (or possibly two) in this book.

From the start the designer has only the specifications of the yacht, i.e. its requested capabilities. Based on his experience, or data from other yachts, he assumes the main data of the hull. Non-dimensional parameters such as displacement/length ratio, sail area/wetted arearatio, heeling arm and metacentric height may thus be computed, and a rough check of the performance may be made based on statistics from other yachts. The procedure is summarized in [Chapters 2 and 17](#). In this first spiral turn the designer jumps from the first to the last segment directly, and the evaluation is very rough.

In the second turn, after having adjusted the main parameters, it may be time to begin the actual design of the hull, keel, rudder and sail plan. The theory for this is given in [Chapters 3, 5, 6, 7, 8 and 9](#). A rough layout of the interior and exterior design (see



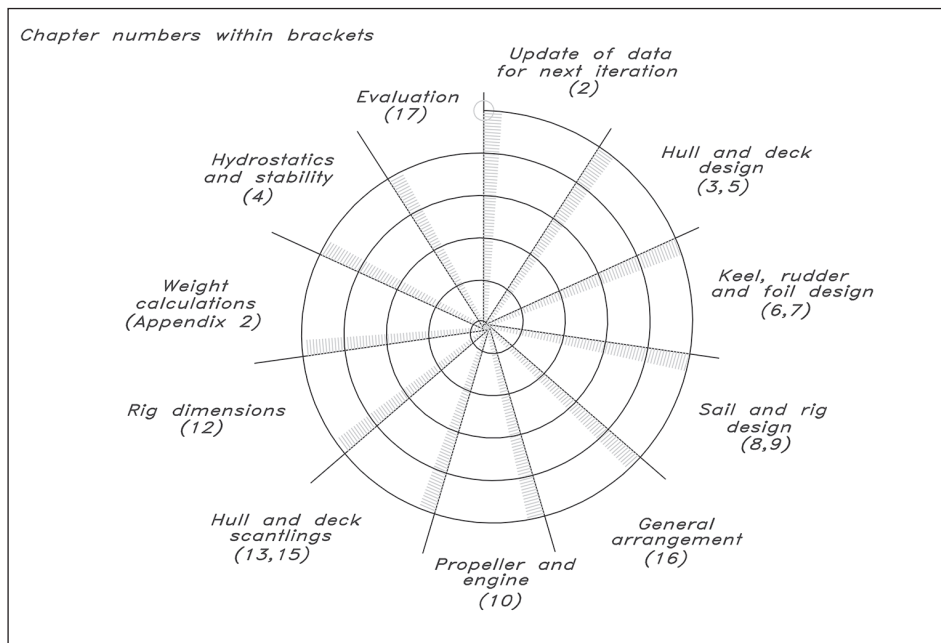


Fig 1.1 The design spiral

Chapter 16) may be made too, to give an initial weight estimate, needed for the stability calculation (see Chapter 4). It is likely that neither the weight nor the stability will be correct, so several turns may be required to satisfy these requirements reasonably. Of course, not all previous operations may have to be redone in each turn. Having found a reasonable weight and stability for the yacht, the next turn may include the detailed hull scantling calculations and the dimensioning of the rig, as well as the choice of the engine (see Chapters 10–15). Only at this stage can an exact weight calculation be carried out, as shown in Appendix 2.

As the designer approaches the final solution he may want to evaluate the design more carefully, and to do this a Velocity Prediction Program (VPP) is required. Such programs are described in Chapter 17, where other even more accurate techniques, such as towing tank testing and computational fluid dynamics (CFD), are also presented. The amateur designer may not have access to either of these tools, however, so his evaluation of the current design will have to be based on experience.

It should be pointed out that in some segments internal iterations are required. This is particularly the case in the hull design area. Here, requirements for volume and its distribution are probably specified beforehand, and it may take several iterations to satisfy them. If the process is manual, iterations between the different views to fair the lines are also required, as will be described in Chapter 3. In the hydrostatics and stability segment iterations are required to find the proper sinkage and trim when the hull heels at large angles.

## ■ COMPUTER-AIDED DESIGN (CAD)

Thanks to rapid development in recent years, computer-aided design (CAD) may be carried out efficiently on PCs or Macs. It is important to have a high resolution screen; special graphics software speeds up the process. A laser printer will produce reasonably good small-scale graphical output, but professional designers use pen plotters of various sizes to produce drawings up to full scale.

The most important module of a CAD system for yacht design is a powerful program for generating the hull lines, and such programs have been available since the early 1980s. In modern programs the hull surface is represented mathematically by one or more Non-Uniform Rational B-Splines (NURBS) patches. For a detailed description the reader is referred to the book *Computational Geometry for Ships* by Nowacki, Bloor and Oleksiewicz (1995). Any point on the surface may be found from the mathematical representation, or more precisely, if two coordinates of a point are given, the program computes the third one. Thus, if the user provides the distance from the bow, X, and the distance above the waterline, Z, the program computes the local beam, Y, at this location. Also, any cut through the surface may be obtained, for instance, any station or waterline.

There are principally two different problems in connection with the surface representation. The task can be either to generate a new hull, or to duplicate, as accurately as possible, an existing one. The latter problem is more difficult. It is certainly possible in an iterative process to approach a given shape, but it can be time consuming. Fortunately, the designer is normally interested in the first task: creating a new hull. To achieve this he has to work with a set of points, called vertices, located near the surface. By moving one vertex the hull surface is locally deformed in such a way that it is still smooth. In most programs the curvature of the surface may be plotted, thus enabling the designer to generate fair lines even on a small scale, and with the relatively low resolution of the screen. Some programs use points on the hull itself for defining its shape, but all the major programs on the international market use vertex points. There seems to be a consensus among yacht designers that this approach is very effective for creating fair lines. In [Chapter 3](#) we will show how the hull is generated by vertex points.

Most hull geometry programs have the capability to rotate the hull and show it in different perspectives on the screen. The possibility of showing a perspective plot of the hull is important and is a major improvement from the manual approach, where only three standard views are employed (see [Chapter 3](#)). For example, the shape of the sheer line may look quite different in perspective compared with the side view, since the line that meets the eye is influenced also by the beam distribution along the hull. Hulls that look good in a side view may look quite ugly in reality.

Some of the more advanced programs include the deck and superstructure as for the hull model, i.e. these parts of the yacht are represented in three dimensions and may be displayed in perspective. In other programs they are treated separately. To compute stability at large angles of heel the deck, cabin and cockpit need to be modelled, and this is frequently done in a separate module where these parts are added relatively crudely, section by section.

A keel/rudder module is often available in yacht CAD systems. The designer may choose between a number of different profiles for the cross-section and specify the planform of the keel/rudder. The code computes the volume, weight of the keel, centre of gravity and centre of effort of the hydrodynamic force. The latter is required in the balancing of the yacht, as explained in [Chapter 8](#). For this the sail plan is also required, and some systems have a simple sail module which computes sail areas and centres, given the sail corner coordinates.

The total weight and centre of gravity location (in three directions) are computed in a weight schedule monitor, which accepts the weight and position relative to a given reference point of all items on board. Appendix 2 presents the input and output from such a monitor.

Very important modules of the yacht CAD system are the hydrostatics and stability programs. These compute all the quantities discussed in [Chapter 4](#), including stability at small and large heel angles, weight per mm of sinkage, and moment per degree of trim. In the stability calculation the correct sinkage and trim are found for each heel angle – a very time consuming procedure if carried out manually.

The Velocity Prediction Program (VPP), mentioned earlier, may also be regarded as a module of the CAD system. As explained above, this program computes the speed, heel angle and leeway angle at all wind speeds and directions of interest, based on a set of dimensions for the hull, keel, rudder and sails. The very simple performance estimator, based on a few main parameters and used in the first iteration of the design spiral, may also be a module of the system.

Finally, more or less advanced programs for the structural design of the yacht may be included. Such programs can be based on the rules given by the classification societies: the American Bureau of Shipping (ABS), Lloyd's Register of Shipping (LR) and others or the ISO 12215 scantlings standard. The ISO standard will be described in [Chapter 15](#). Other methods employed in the rig and scantling calculations may be based on basic strength theory or finite element techniques.

Computer-aided design may be extended to computer-aided manufacturing, which can be used in the production of the yacht. For example, the very time consuming lofting process, where the builder produces full-scale templates, may be eliminated. Traditionally, the builder receives offset tables from the designer. Based on these offsets the templates are drawn at full scale with a reduction in dimension for the skin thickness of the hull. This is necessary, since the templates are used internally during the building process. If the hull has been CAD designed, however, the full-scale templates with the proper reduction may be plotted directly, provided a sufficiently large plotter is available. Plate expansions may also be obtained from the CAD system, simplifying the production of steel and aluminium hulls.

# 2 PRELIMINARY CONSIDERATIONS

Before actually starting the design work, we must have a clear picture of the yacht's purpose: what are the requirements, limitations and objectives of the design? In this chapter we will list the considerations that form the starting point of the design.

## ■ CHOICE OF BOAT-TYPE

Regardless of whether the client is an individual owner or a boatbuilding firm, he will have definite ideas as to the type of boat he wants. Most people have a particular yacht in mind, which, with changes in dimensions, style, arrangement, rig or hull form, satisfies their demands. These preferences are often modified by other considerations, such as local conditions, economic considerations and intended use. Personal opinion often governs the choice of type to such an extent that the more logical and scientific arguments may become of secondary concern, if not set aside entirely.

## ■ INTENDED USE

The intended use of the yacht is a matter that comes first on the list of considerations. The first distinction is that between racing and cruising. For the racer we must naturally decide to which rule the boat should be designed, and in which class it will be racing. This gives us a good starting point regarding the size of boat and crew, rig size and type, by comparing it with existing successful designs. Having established the type and size of boat, we can proceed with the design process described in the following chapters, making adjustments so as to conform to the rule we are following.

For the cruiser the primary requirement influencing the type of design to adopt regarding hull, deck, accommodation and rig is the yacht's intended use in broad terms, i.e. unlimited ocean passage-making, open or restricted offshore use, or coastal or sheltered use. Obviously, it is easier to reach high standards of safety, stability and performance with a big yacht, provided there is sufficient crew to handle the vessel.

This brings us to the question of the need for compromise. The requirements of speed, seaworthiness, dryness, weatherliness, ease of handling, comfort and other qualities often conflict, but the fewer the compromises the better the design. We must decide at an early stage what particular qualities we desire most, or require to the greatest extent. By getting

our priorities right from the start we know where compromises can be made with the least harm. Too many yachts are designed on the assumption that it is possible to achieve all of the qualities of the perfect yacht without regard for the limitations of the chosen type and its intended use. To achieve a good design it is crucial to define the intended use, weigh the requirements that these impose on the yacht and choose a type of yacht whose design elements fulfil that need. When the type of yacht is chosen we must stick to it throughout the whole design process. Of course there will be alterations along the way, but if we find that many major changes are necessary it will probably be best to start the design work from square one.

The intended use is not only about sailing area, performance, and range, but also about who is going to use the boat and under what circumstances. If we take a design intended for charter use, the requirement will usually be a large number of berths and a roomy cockpit to accommodate everyone when sailing. The time at sea will be restricted, most sleeping will be in harbour or at anchor and the handling systems must be understood by novices. By contrast, an experienced owner who wishes to make extended passages with a small crew will have the opposite requirements.

## ■ MAIN DIMENSIONS

It is generally agreed that by increasing the size of the boat a better design in terms of performance and comfort will be produced; on the other hand the boat might be more difficult to handle for a small crew. Size is also linked to the intended area of use: unlimited ocean use naturally places greater demands on a boat than sheltered water use. Not only will it need to withstand strong winds and heavy seas, but it will also need to carry more fuel, water and stores – all of which point to the bigger yacht. However, it is not self-evident that size in this respect means length; a better measure would perhaps be displacement, since this describes the volume of the boat. Take two boats of similar displacement: the longer one will usually have better performance but its carrying capabilities will be roughly the same as for the shorter one.

The requirements of engine, rig and deck equipment depend largely on size, weight and length as well as beam. To reach a certain speed with a limited power source the length–weight ratio is of vital importance, while the stability required to carry enough sail is more dependent on the beam and weight. In this context it is noticeable that the heeling moment increases with size to the power of 3, while the stability increases with size to the power of 4. So scaling a boat up linearly does not produce a design compatible with good performance and stability.

The changes in proportions with increasing size have been calculated for an allometric series of yachts from  $L_{OA} = 7\text{m}$  to  $L_{OA} = 19\text{m}$  by Barkla (1960) (see Fig 2.1). As we can clearly see, different dimensions and parameters scale differently with length. The scaling factors shown in the figure produce boats of similar behaviour regarding performance and ‘feel’ when scaled in either direction from a base model. The ‘L’ in Fig 2.1 refers to the length relation between the base model and the derivative. For example, if we increase the length of the boat by 50%, i.e. 1.5 times L, the beam, depth



**Fig 2.1** Proportions  
versus size (Barkla, 1960)

<i>PRIMARY RELATIONS – independent of basic model</i>		<i>Scale Factor</i>
<i>Assumed:</i>		$L$
<i>sail area</i>		$L^{1.85}$
<i>beam, depth, freeboard</i>		$L^{0.70}$
<i>keel &amp; rudder span, chord, thickness</i>		$L^{0.70}$
<i>Derived:</i>		
<i>areas – section</i>		$L^{1.40}$
– <i>wetted – hull</i>		$L^{1.70}$
– <i>keel &amp; rudder</i>		$L^{1.40}$
– <i>lateral – hull</i>		$L^{1.70}$
– <i>keel &amp; rudder</i>		$L^{1.40}$
<i>volumes – hull</i>		$L^{2.40}$
– <i>keel</i>		$L^{2.10}$
<i>ratios – <math>L_{WL}/\nabla^{1/3}</math> (ex-keel)</i>		$L^{0.20}$
– <i><math>SA/\nabla^{2/3}</math> (ex-keel)</i>		$L^{0.25}$
<i>Second moments of waterplane – lateral</i>		$L^{3.10}$
– <i>longitudinal</i>		$L^{3.70}$
<i>SECONDARY RELATIONS – dependent to some extent on basic model</i>		
<i>Total volume of displacement</i>		$L^{2.38}$
<i>Total wetted area</i>		$L^{1.63}$
<i>Sail area / wetted area</i>		$L^{0.22}$
<i>Sail area / <math>\nabla^{2/3}</math> (incl-keel)</i>		$L^{0.26}$
<i>Distance of VCB below <math>L_{WL}</math></i>		$L^{0.64}$
$\overline{BM}$		$L^{0.72}$
$\overline{GM}$		$L^{0.45}$
<i>Initial righting moment</i>		$L^{2.83}$
<i>Separation of centres of effort (lead)</i>		$L^{0.86}$

and freeboard will be increased by  $1.5^{0.7} = 1.33$  times the original value to keep the boat within the same performance-family.

A very good way of establishing dimensions for the hull and rig of a new design before there are any drawings or calculations is to decide on some vital dimensionless ratios that can be checked against known designs. Chapter 5 deals in more detail with this, and explains what factors are involved. Fig 2.2 shows, for the YD-41, the values of the ratios derived from first estimates of the main dimensions. Comparison is made with an existing yacht of the same size. Note that such a comparison is mostly done with several similar yachts and they do not necessarily have to be the same size. Using the relations of Fig 2.1 yachts of slightly different sizes may be scaled to the length of interest. Once we are satisfied with the numbers, we have a good starting point for the design.

<i>Design</i>	<i>LOA</i>	<i>LWL</i>	<i>B<sub>MAX</sub></i>	<i>T</i>	$\nabla$	<i>SA</i>	<i>DLR</i>	<i>LDR</i>	<i>SDR</i>	<i>SA/S<sub>w</sub></i>	<i>GPH</i>
YD-41	12.50	11.60	4.20	2.30	5.75	88.1	104	6.5	27.4	2.55	535
41' Yacht on Market	12.40	11.50	3.95	2.40	8.15	88.2	152	5.7	21.7	2.48	576

*LOA* = Length overall [m]  
*LWL* = Length in waterline [m]  
*B<sub>MAX</sub>* = Maximum beam [m]  
*T* = Maximum depth from waterline [m]  
 $\nabla$  = Light load volume displacement [m<sup>3</sup>]  
*SA* = Total triangular sail area [m<sup>2</sup>]  
*S<sub>w</sub>* = Wetted area of hull and appendages [m<sup>2</sup>]  
*DLR* = Displacement Length Ratio [ $28300 \cdot \nabla / L_{WL}^3$ ]  
*LDR* = Slenderness Ratio [ $L_{WL} / \nabla^{1/3}$ ]  
*SDR* = Sail area Displacement Ratio [ $SA / \nabla^{2/3}$ ]  
*GPH* = General Purpose Handicap, ORC

**Fig 2.2** Preliminary design parameters

## COST

No one is interested in having a boat built more expensively than necessary.

Taking only that prerequisite into account, the obvious answer seems to be to build the boat as small as possible, since building costs relate directly to size (or rather weight). However, in going for light weight we might be forced to use exotic materials and advanced building methods which in turn might increase the cost compared with using heavier materials and a more conventional building technique. At the other end of the scale are the heavy building methods needed for steel and ferrocement, for instance, which certainly provide cheap materials but produce heavy boats that need much power (sail and engine) to drive them, and robust deck equipment for handling them, all of which cost money.

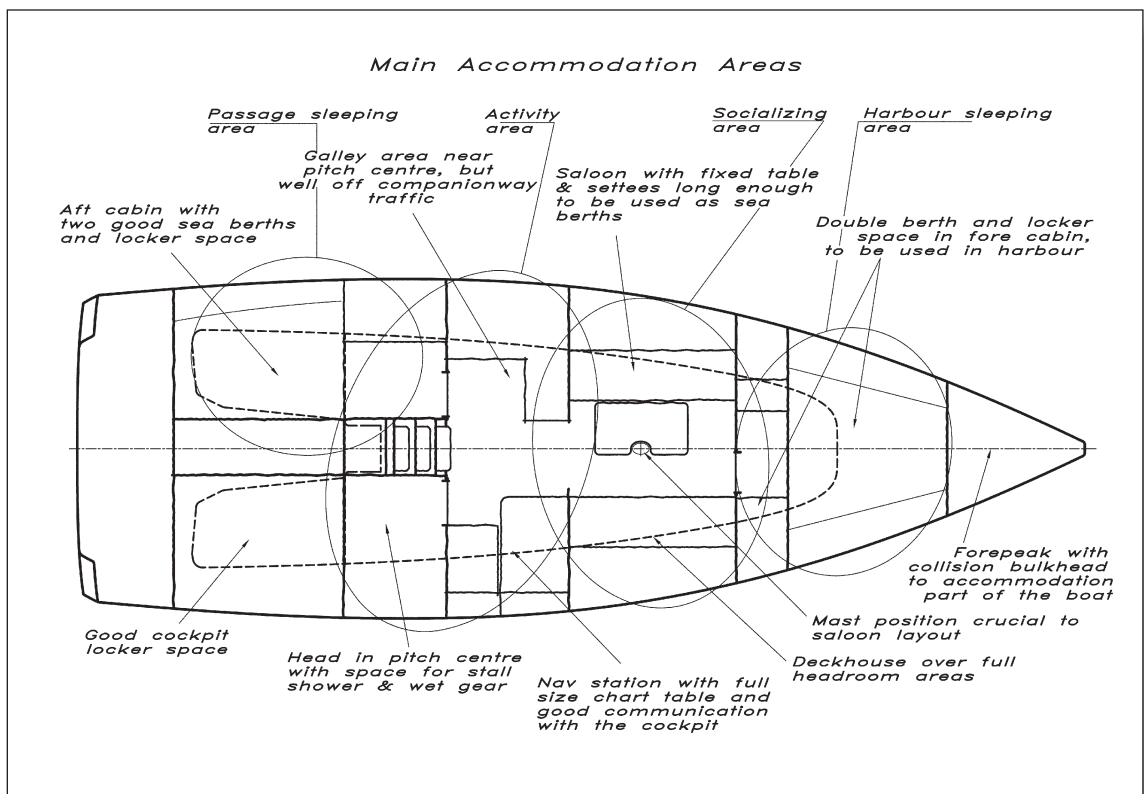
A common pitfall when designing a boat in the smaller size range to keep costs down, is to miniaturize. Everything might look well proportioned on paper, but in practice the design may not work because the human being cannot be scaled down. Moreover, trying to squeeze too much into a small volume would not produce a cost-effective design, not only because everything found in a bigger yacht would be there, but also because it would be so much harder to fit in, due to lack of space.

The hull form is basically derived from hydrodynamic and hydrostatic requirements, while the form of the deck is more open to the whim of the designer, to fashions and trends, and to what 'character' the design is intended to radiate. A deck with lots of angles and sharp turning points is much more difficult to build (FRP construction) than one with smooth areas and large radii in the corners. Here we have a choice that most definitely will affect the construction cost. Designing decks or parts of decks that require multiple moulds to make mould-release possible will also make the costs higher. We have to be quite sure that the benefits of such a design outweigh the increased cost that goes along with it.

To some extent the same reasoning can be applied to the accommodation. Obviously, a flat panel attached to another at a square angle is much cheaper to produce than a curved one attached at an oblique angle. On the other hand, rounded panels and oblique angles can be used to achieve better space utilization which, in the end, will make the boat so much better that the increased building costs can be justified. Another way of increasing usable space is to let areas and compartments overlap one another. It is not always necessary to have the full cabin height over the full length of the boat. For example, a toilet can be under a cockpit seat with the rest of the head area under the superstructure. Instead of thinking of the accommodation as a two-dimensional jigsaw puzzle, it might be fruitful to think of it as a three-dimensional puzzle to utilize the space available in the best way. A word of warning though: complicating things too much might raise the cost out of all proportion, so a better way might be to make the whole boat bigger and simpler to fulfil the requirements.

The amount of standard equipment also plays an important role in the overall cost of the boat, regardless of whether she is light or heavy. By this we mean whether to have an air-conditioner/heater, running hot and cold water, a water maker, a freezer/refrigerator, electric winches, full electronics with radar, a chart plotter and auto pilot, self-furling sails and so on. All these items can almost equal the cost of the rest of the boat.

**Fig 2.3** Preliminary layout for the YD-41



## Checklist of considerations

To summarize the above considerations the following list can be applied:

1. Define the intended use and limits.
2. Collect information about similar boats.
3. Decide on the main dimensions and ratios.
4. Decide on the preliminary layout and exterior.
5. Make a first approximation of weights and form parameters.
6. Check against 3 and correct if necessary.
7. Produce a preliminary design to work from.

## Checklist for the YD-41

Having considered these points we are now ready to lay down a preliminary design. To make that meaningful we must decide on a specific one, and in this book we will use the YD-41. The design brief for this yacht is as follows:

1. A fast ocean-going yacht, with accommodation for four, to be capable of being easily handled by a crew of two. The performance, comfort and safety shall allow for fast ocean crossings with average speeds above 10 knots in favourable conditions.
2. See [Fig 2.2](#) for comparison with a similar yacht.
3. The main dimensions and ratios are also derived from the comparison in [Fig 2.2](#).
4. [Fig 2.3 \(page 21\)](#) is a first sketch of the yacht showing the principal areas of accommodation. Basically, they are designed around the assumption that they will be functional under way with a crew of four. This means four good sea-berths, two in the aft cabin and two in the saloon, a galley, head and navigation area in the pitch centre of the boat. The saloon shall be big enough to accommodate the occasional racing crew, and other social entertaining in harbours, and the forward cabin shall be used as an in-harbour master cabin. The accommodation shall not be pressed into the ends of the boat to enhance performance and judged on a length-only basis, as this will reduce the building costs.

Having established the main dimensions, type of boat and area of use we can proceed with the more precise design work. Comparing with [Fig 2.2](#) we can see that the design brief is met quite well, with the main dimensions and their connected ratios chosen.

# 3 HULL GEOMETRY

The hull of a yacht is a complex three-dimensional shape, which cannot be defined by any simple mathematical expression. Gross features of the hull can be described by dimensional quantities such as length, beam and draft, or non-dimensional ones like prismatic coefficient or slenderness (length/displacement) ratio. For an accurate definition of the hull the traditional line drawing is still in use, although most yacht designers now take advantage of the rapid developments in CAD introduced in [Chapter 1](#).

In this chapter we start by defining a number of quantities, frequently referred to in yachting literature, describing the general features of the yacht. Thereafter, we will explain the principles of the traditional drawing and the tools required to produce it. We recommend a certain work plan for the accurate production of the drawings and, finally, we show briefly how the hull lines are generated in a modern CAD program.

## ■ DEFINITIONS

The list of definitions below includes the basic geometrical quantities used in defining a yacht hull. Many more quantities are used in general ship hydrodynamics, but they are not usually referred to in the yachting field. A complete list may be found in *Dictionary of Ship Hydrodynamics*, International Towing Tank Conference (ITTC, 2017).

### ◆ Length overall ( $L_{OA}$ )

The maximum length of the hull from the forwardmost point on the stem to the extreme after end (see [Fig 3.1](#)). According to common practice, spars or fittings, like bowsprits, pulpits, etc. are not included and neither is the rudder.

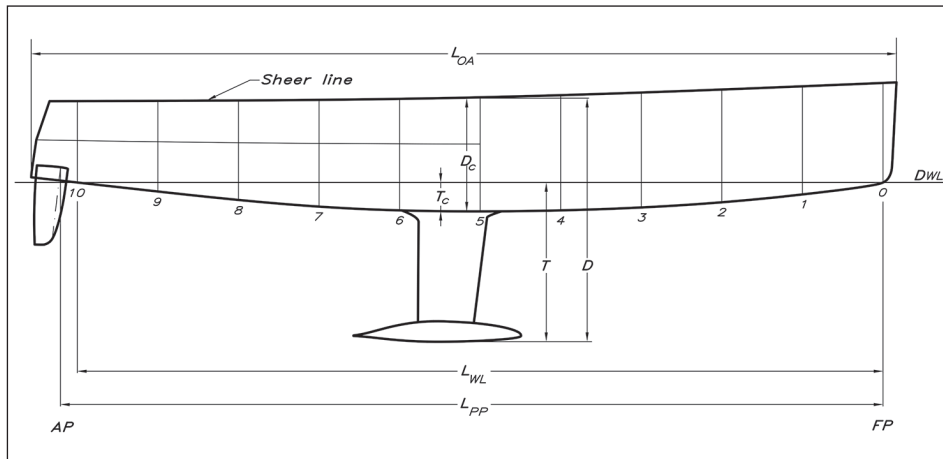
### ◆ Length of waterline ( $L_{WL}$ )

The length of the designed waterline (often referred to as the DWL).

### ◆ Length between perpendiculars ( $L_{PP}$ )

This length is not much used in yachting but is quite important for ships. The forward perpendicular (FP) is the forward end of the designed waterline, while the aft perpendicular (AP) is the centre of the rudder stock.





**Fig 3.1** Definitions of the main dimensions

### ◆ Rated length

A very important parameter in traditional rating rules. Usually  $L$  is obtained by considering the fullness of the bow and stern sections.

### ◆ Beam ( $B$ or $B_{MAX}$ )

The maximum beam of the hull excluding fittings, like rubbing strakes.

### ◆ Beam of waterline ( $B_{WL}$ )

The maximum beam at the designed waterline.

### ◆ Draft ( $T$ )

The maximum draft of the yacht when floating on the designed waterline.  $T_c$  is the draft of the hull without the keel (the 'canoe' body).

### ◆ Depth ( $D$ )

The vertical distance from the deepest point of the keel to the sheer line (see below).  $D_c$  is without the keel.

### ◆ Displacement

This could either be mass displacement ( $m$ ), i.e. the mass of the yacht, or volume displacement ( $V$  or  $\nabla$ ), the volume of the immersed part of the yacht.  $m_c$ ,  $V_c$  and  $\nabla_c$  are the corresponding notations without the keel.

### ◆ Midship section

For ships, this section is located midway between the fore and aft perpendiculars. For yachts it is more common to put it midway between the fore and aft ends of the waterline. The area of the midship section (submerged part) is denoted  $A_M$ , with an index 'c' indicating that the keel is not included.  $C_{Mc}$  is the midship sectional area coefficient defined for the canoe body as  $C_{Mc} = A_{Mc} / (B_{WL} \cdot T_c)$ .

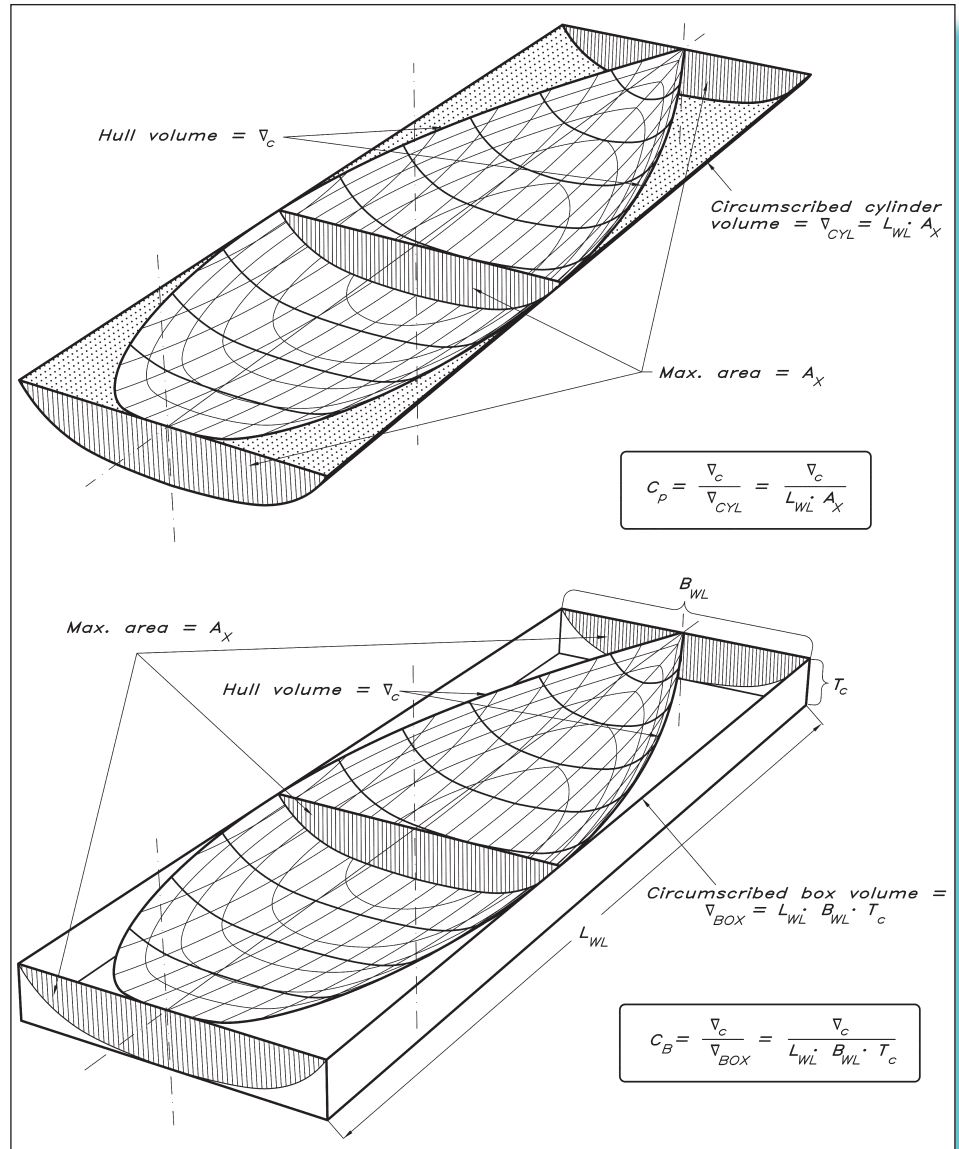
### ◆ Maximum area section

For yachts the maximum area section is usually located behind the midship section. Its area is denoted  $A_X$  ( $A_{Xc}$ ).

### ◆ Prismatic coefficient ( $C_p$ )

This is the ratio of the volume displacement and the maximum section area multiplied by the waterline length, i.e.  $C_p = \nabla / (A_X \cdot L_{WL})$ . This value is very much influenced by the keel and in most yacht applications only the canoe body is considered:  $C_{Pc} = \nabla_c / (A_{Xc} \cdot L_{WL})$ . See Fig 3.2. The prismatic coefficient is representative of the fullness of the yacht. The fuller the ends, the larger the  $C_{Pc}$ . Its optimum value depends on the speed, as explained in Chapter 5. Note that the index c is often dropped, even if the coefficient refers to the canoe body.

**Fig 3.2** The prismatic coefficient



**Fig 3.3** The block coefficient

#### ◆ Block coefficient ( $C_B$ )

Although quite important in general ship hydrodynamics this coefficient is not so commonly used in yacht design. The volume displacement is now divided by the volume of a circumscribed block (only the canoe body value is of any relevance)  $C_{Bc} = \nabla_c / (L_{WL} \cdot B_{WL} \cdot T_c)$ . See Fig 3.3.

#### ◆ Centre of buoyancy (B)

The centre of gravity of the displaced volume of water. Its longitudinal and vertical positions are denoted by LCB and VCB, respectively.

#### ◆ Centre of gravity (G)

The centre of gravity of the yacht must be on the same vertical line as the centre of buoyancy. In drawings, G is often marked with a special symbol created by a circle and a cross. This is used also for marking geometric centres of gravity. See, for instance, Fig 9.2.

#### ◆ Sheer line

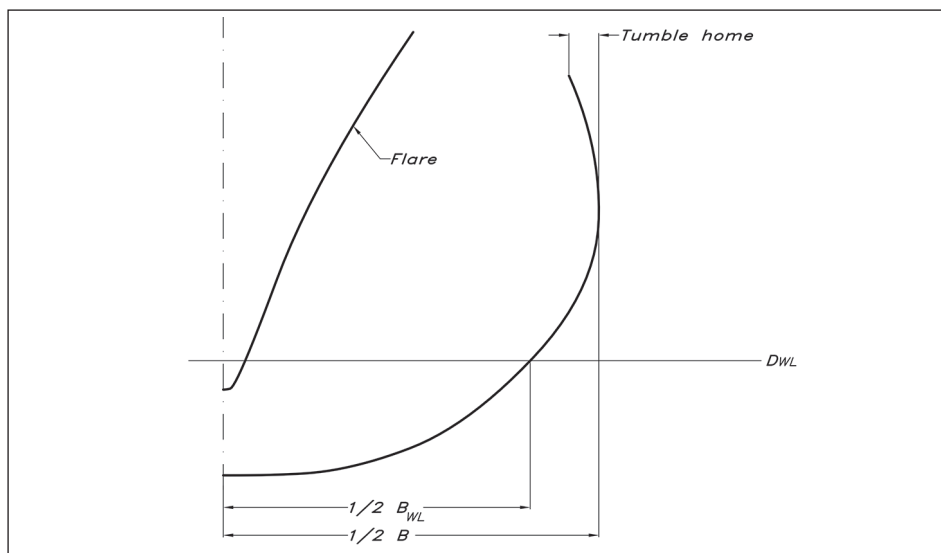
The intersection between the deck and the topside. Traditionally, the projection of this line on the symmetry plane is concave, the 'sheer' is positive. Zero and negative sheer may be found on some extreme racing yachts and powerboats.

#### ◆ Freeboard

The vertical distance between the sheer line and the waterline.

#### ◆ Tumble home

When the maximum beam is below the sheer line the upper part of the topsides will bend inwards (see Fig 3.4). To some extent this reduces the weight at deck level, but it also reduces the righting moment of the crew on the windward rail. Further, the hull becomes more vulnerable to outer skin damage in harbours.



**Fig 3.4** Definition of tumble home and flare

#### ◆ Flare

The opposite of tumble home. On the forebody in particular, the sections may bend outwards to reduce excessive pitching of the yacht and to keep it drier when beating to windward.

#### ◆ Scale factor ( $\alpha$ )

This is not a geometrical parameter of the hull, but it is very important when designing a yacht. The scale factor is simply the ratio of a length (for instance the  $L_{WL}$ ) at full scale to the corresponding length at model scale. Note that the ratio of corresponding areas (like the wetted area) is  $\alpha^2$  and of corresponding volumes (like displacement)  $\alpha^3$ .

## ■ LINE DRAWING

A complete line drawing of the YD-41 is presented in Fig 3.5 (overleaf). The hull is shown in three views: the profile plan (top left), the body plan (top right) and half breadth plan (bottom). Note that the bow is to the right.

In principle, the hull can be defined by its intersection with two different families of planes, and these are usually taken as horizontal ones (waterlines) and vertical ones at right angles to the longitudinal axis of the hull (sections). While the number of waterlines is chosen rather arbitrarily, there are standard rules for the positioning of the sections. In yacht architecture the designed waterline is usually divided into ten equal parts and the corresponding sections are numbered from the forward perpendicular (section 0) backwards. At the ends, other equidistant sections, like # 11 and # -1 may be added, and to define rapid changes in the geometry, half or quarter sections may be introduced as well. In Fig 3.5 half sections are used throughout.

The profile is very important for the appearance of the yacht, showing the shapes of the bow and stern and the sheer line. When drawing the waterlines, displayed in the half breadth plan, it is most helpful if the lines end in a geometrically well-defined way. Therefore a 'ghost' stem and a 'ghost' transom may be added. The ghost stem is the imagined sharp leading edge of the hull, which in practice often has a rounded stem, and the ghost transom is introduced because the real transom is often curved and inclined. If an imagined vertical transom is put near the real one at some convenient station, it will facilitate the fairing of the lines. The drawing of Fig 3.5 has been produced on a CAD system and no ghost stem is shown. However, a ghost transom is included.

In the body plan, the cross-sections of the hull are displayed. Since the hull is usually symmetrical port and starboard, only one half needs to be shown, and this makes it possible to present the forebody to the right and the afterbody to the left. In this way mixing of the lines is avoided and the picture is clearer. Note that in the figure the half stations are drawn with a different line type.

The above cuts through the hull are sufficient for defining the shape, but another two families of cuts are usually added, to aid in the visual perception of the body. Buttocks are introduced in the profile plan, showing vertical, longitudinal cuts through the hull at positions indicated in the half breadth plan. The diagonals in the lower part of the half breadth plan are also quite important. They are obtained by cutting the hull longitudinally

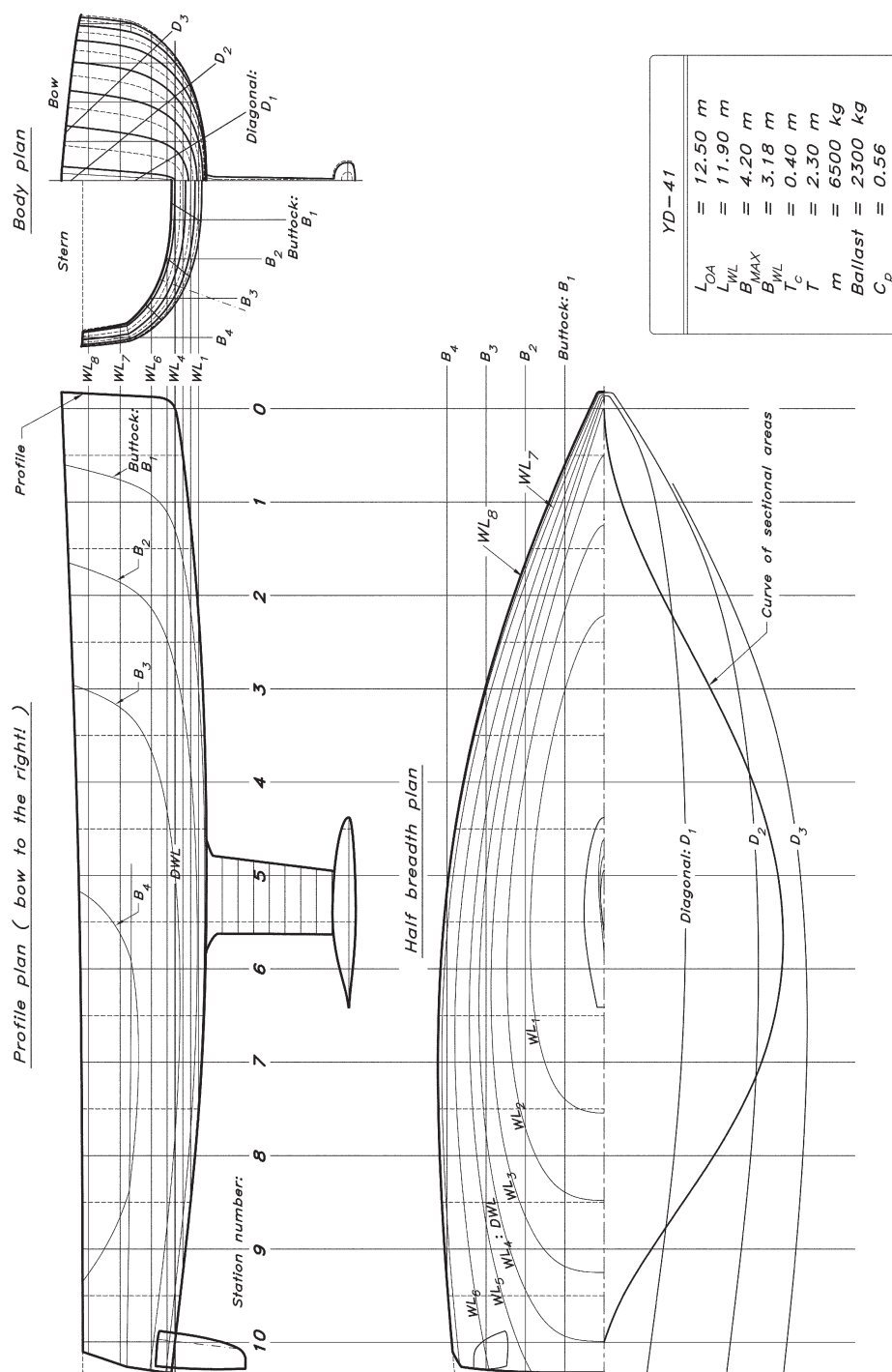


Fig 3.5 The line drawing

in different inclined planes, as indicated in the body plan. The planes should be, as much as possible, at right angles to the surface of the hull, thus representing its longitudinal smoothness. In practice, the flow tends to follow the diagonals, at least approximately, so that they are representative of the hull shape as ‘seen’ by the water. Special attention should be paid to the after end of the diagonals, where knuckles, not noticed in the other cuts, may be found, particularly on yachts designed under the International Offshore Rule (IOR) in the 1970s and 1980s. Almost certainly, such unevenness increases the resistance and reduces the speed of the yacht.

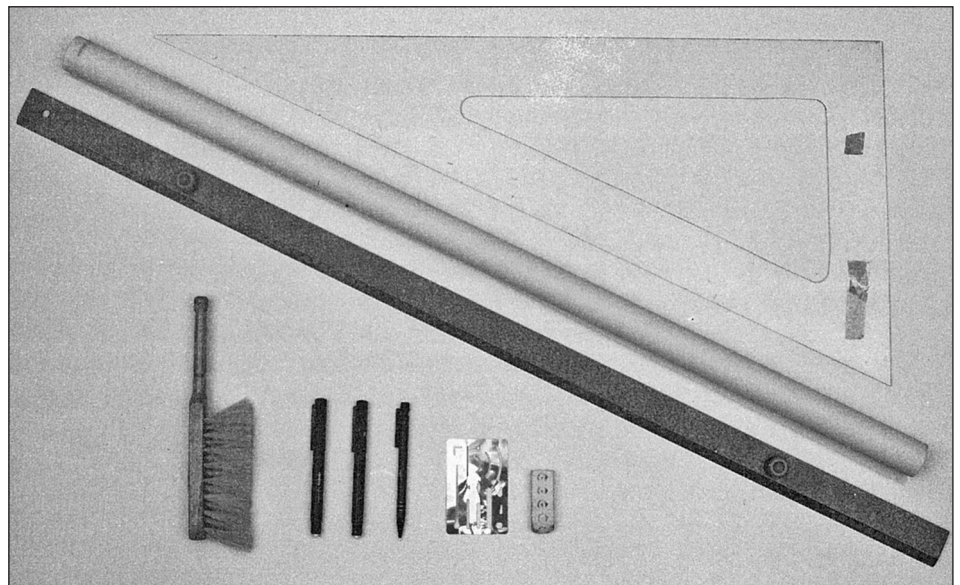
The other line in the lower part of the half breadth plan is the curve of sectional areas, representing the longitudinal distribution of the submerged volume of the yacht. The value at each section is proportional to the submerged area of that section, while the total area under the curve represents the displacement (volume). A more detailed description of the construction of the curve of sectional areas will be given in [Chapter 4](#).

If the drawing is produced manually, a table of offsets is usually provided by the designer. This is to enable the builder to lay out the lines at full size and produce his templates. Offsets are always provided for the waterlines, but the same information may be given for diagonals and/or buttocks, too. Note that all measurements are to the outside of the shell. For drawings produced by a CAD system the geometry information can be transferred directly to a numerically controlled cutting machine. Usually the international Initial Graphics Exchange Specification (IGES) standard is then used as the file format.

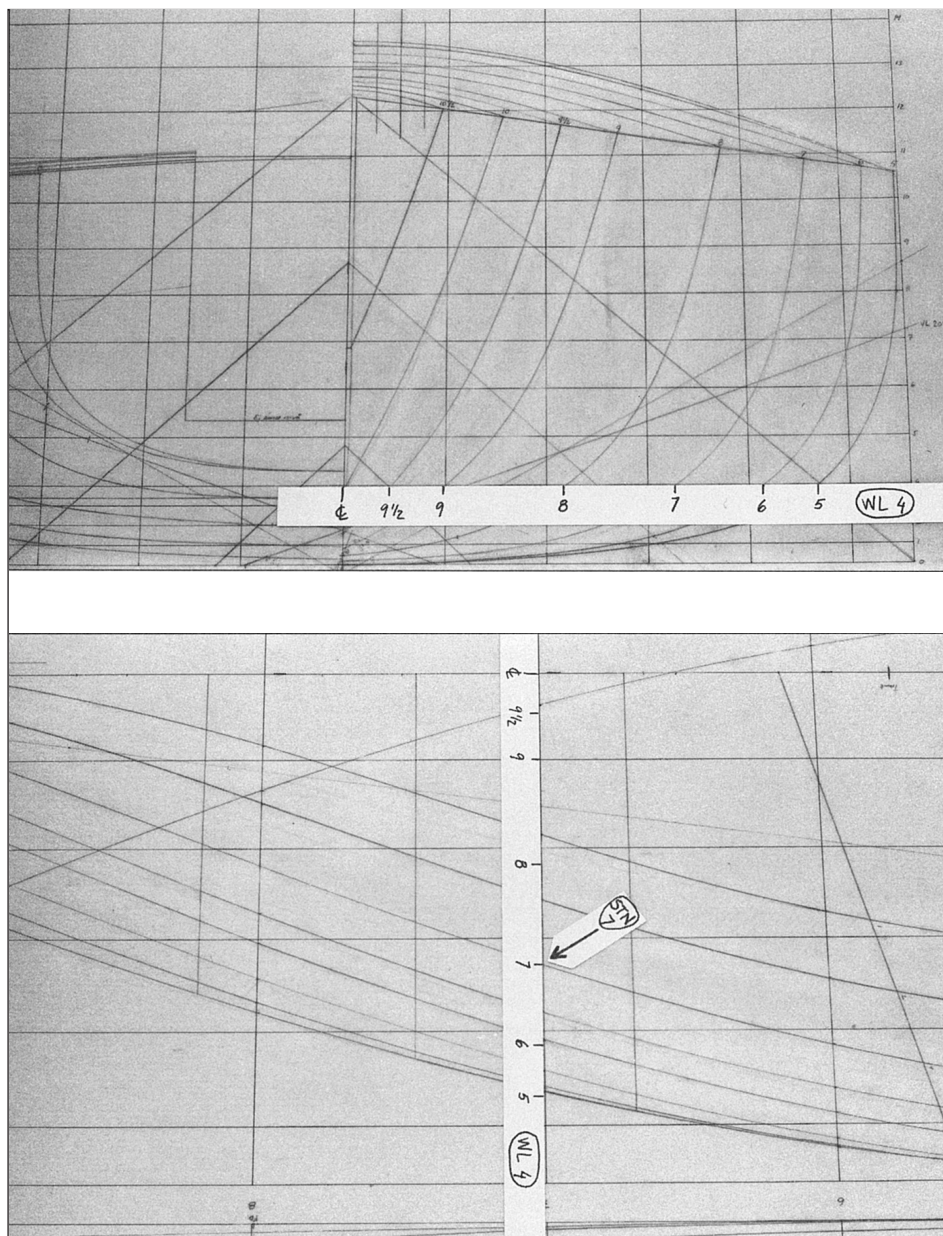
## ■ TOOLS

A manual drawing should be made on a special plastic film, available in different thicknesses. The film is robust and will not be damaged by erasing. Furthermore, it is unaffected by the humidity of the air, which may shrink ordinary paper.

**Fig 3.6** Tools (set square, plastic film, straight edge, brush, pens, pencil, erasing shield and eraser)





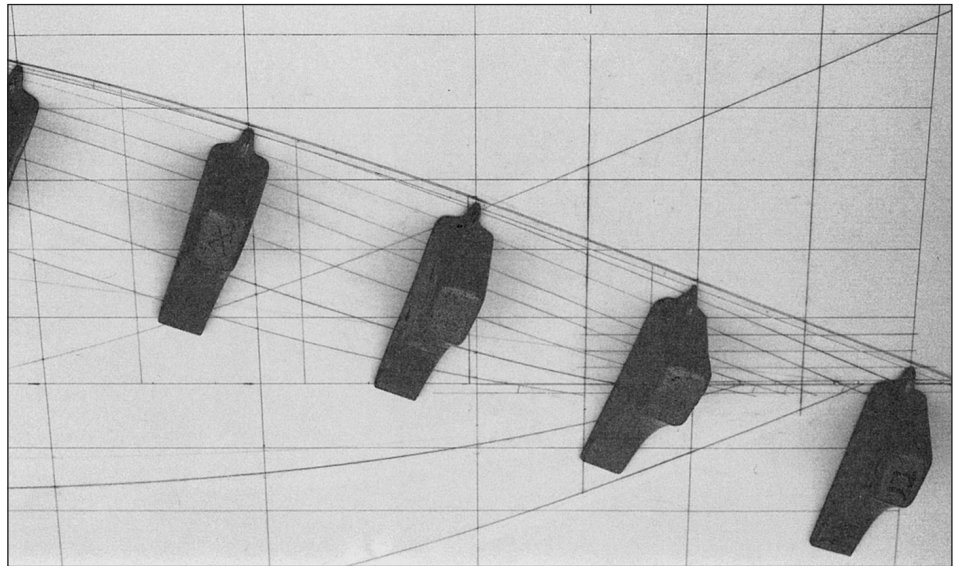


**Fig 3.7** Transfer of measures from body plan (TOP) to half breadth plan (BOTTOM) using a paper ribbon

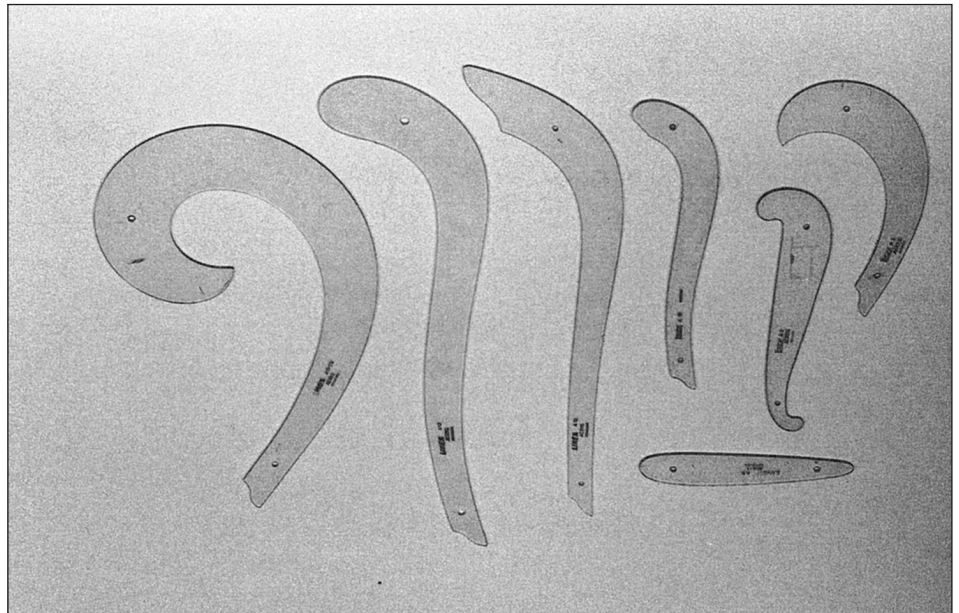
Since the film is transparent the grid for the line drawing is drawn on the back so that it will remain, even after erasing the hull lines on the front many times. Great care must be exercised when drawing the grid, making sure that the alignment and spacing are correct and that all angles are exactly 90°. In Fig 3.5 the grid is shown as thin horizontal and vertical lines, representing waterlines, buttocks and stations.

Black ink should be used when drawing the grid and preferably when finishing the hull lines too. However, when working on the lines a pencil and an eraser are needed. There are, in fact, special pencils and erasers for this type of work on plastic film. An erasing shield and a brush are also most useful (see Fig 3.6).

**Fig 3.8** Ducks and a spline used for drawing a waterline



**Fig 3.9** Templates used for drawing lines with large curvature



For creating the grid a long straight-edge is required, together with a large 90° set square. It is very convenient to have a bunch of paper ribbons, which can be used for transferring different measures from one plan to the other. For example, when drawing a waterline the offsets of this line may be marked on the ribbon directly from the body plan and moved to the half breadth plan (Fig 3.7).

To draw the hull lines it is necessary to have a set of splines and weights or ducks. Long, smooth arcs can be created when bending the splines and supporting them by the ducks at certain intervals. Fig 3.8 shows how these tools are used when drawing a waterline. The splines should be made of plastic, somewhat longer than the hull on the



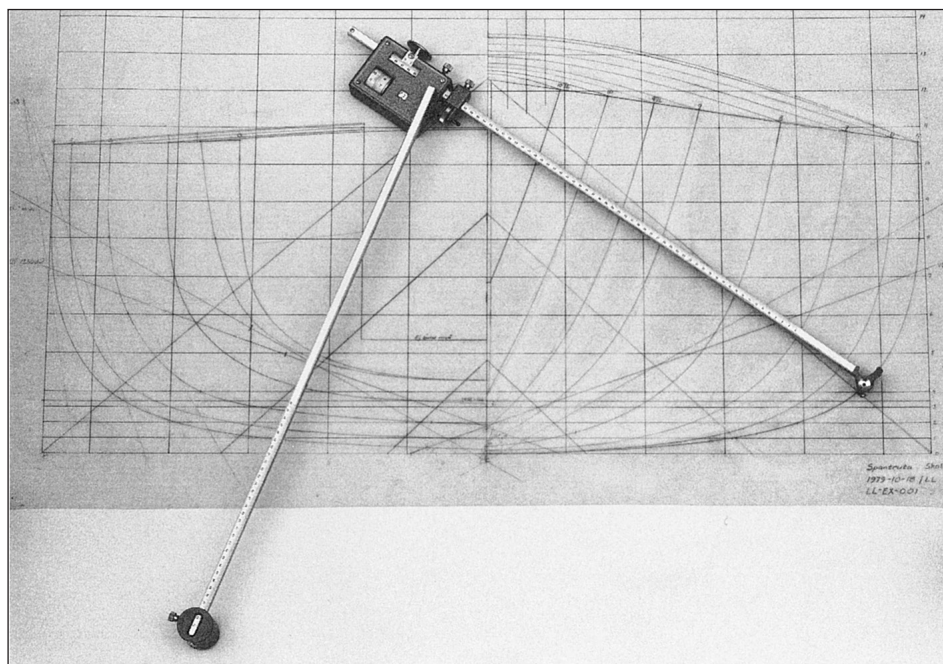


Fig 3.10 Planimeter

drawing, and with a cross-section of about  $2.5 \text{ mm}^2$ . Many different types of ducks can be found, some of them homemade. Preferably, they should be made of lead, and the weight should be between 1.5 and 2.5 kg. To be able to support the spline, they should have a pointed nose, as shown in Fig 3.8.

The splines are needed when drawing the lines in the profile and half breadth plans. However, the lines of the body plan are usually too curved for the splines, so it is necessary to make use of a set of templates especially developed for this purpose. The most well-known ones are the so-called Copenhagen ship curves, the most common of which are shown in Fig 3.9.

A very convenient instrument, well known in naval architecture, is the planimeter, used for measuring areas (see Fig 3.10). The pointer of the planimeter is moved around the area to be measured, and the change in the reading of the scale when returning to the point of departure gives the area enclosed by the path followed. Considering the difficulty in following exactly any given line the accuracy is surprisingly high, more than adequate for the present purposes. The need for measuring areas will be explained in the next chapter.



## Work plan

Designing the hull is a complex process, and many requirements have to be considered. One difficulty is that important parameters, such as the displacement, cannot be determined until the lines have been fixed. This calls for an iterative method. Such a method is also required in the fairing of the lines. The challenge is to make the lines in one projection correspond to smooth lines in the other two projections. For an inexperienced draftsman this problem is a serious one, and many trials may be needed to produce a smooth hull.

While the preferred sequence of operations may differ slightly between yacht designers, the main steps should be taken in a certain order. In the following, we propose a work plan, which has been found effective in many cases. It should be pointed out that the plan does not consider any restrictions from measurement rules.

### Step 1: Fix the main dimensions

These should be based on the general considerations discussed in [Chapter 2](#), using information on other yachts of a similar size, designed for similar purposes. This way of working is classical in naval architecture, where the development proceeds relatively slowly by evolution of previous designs. It is therefore very important, after deciding on the size of the yacht, to find as much information as possible on other similar designs. Drawings of new yachts may be found in many of the leading yachting magazines from all over the world.

The dimensions to fix at this stage are: length overall, length of the waterline, maximum beam, draft, displacement, sail area, ballast ratio, prismatic coefficient and longitudinal centre of buoyancy.

One of the aims of this book is to help in the choice of these parameters and to enable the reader to evaluate older designs when trying to find the optimum for his own special demands.

### Step 2: Draw the profile

As pointed out above, this step takes much consideration, since the aesthetics of the yacht are, to a large extent, determined by the profile.

### Step 3: Draw the midship section

The midship section can be drawn at this stage. Alternatively, if the centre of buoyancy is far aft, the maximum section may be drawn. The shape of the first section drawn is important, since it determines the character of the other sections.

### Step 4: Check the displacement

To find the hull displacement, calculate (or measure) the submerged area of the section just drawn and multiply by the waterline length and the prismatic coefficient chosen for the hull. From the ballast ratio, the keel mass can be computed and the volume can be found, dividing by the density of the material (about 7200 kg/m<sup>3</sup> for iron and 11300 kg/m<sup>3</sup> for lead). Assume that the rudder displacement is 10% that of the keel and add all three volumes together. If the displacement thus obtained is different from the prescribed one, return to step 3 and change accordingly.

The procedure described is for a fin-keel yacht. For a hull with an integrated keel, as on more traditional yachts, the prismatic coefficient usually includes both the keel and the rudder.

#### **Step 5: Draw the designed waterline**

One point at or near the midship station is now known, together with the two end points from the profile, so now a first attempt can be made to draw the designed waterline.

#### **Step 6: Draw stations 3, 7 and the transom**

The waterline breadth is now known, as well as the hull draft, and the sections should have a family resemblance to the midship section. Often it is helpful to draw a ghost transom behind the hull.

#### **Step 7: Draw new waterlines**

Two or three waterlines can now be drawn above and below the DWL. If the appearance is not satisfactory, go back to step 6 and change.

#### **Steps 8 and 9: Add new sections and waterlines**

Once this is done, sections 1–9 should be completed as well as 7–10 waterlines. Constant adjustments have to be made in order to create smooth lines in the body plan, as well as in the half breadth plan.

#### **Step 10: Recheck the displacement and the longitudinal centre of buoyancy**

The curve of sectional areas can now be constructed. Its area gives the displacement (excluding that of keel and rudder) and its centre of gravity corresponds to the longitudinal position of the centre of buoyancy. If not correct, adjustments have to be made from steps 5 or 6.

#### **Step 11: Draw diagonals**

Inspect the smoothness, particularly near the stern. Adjust if necessary.

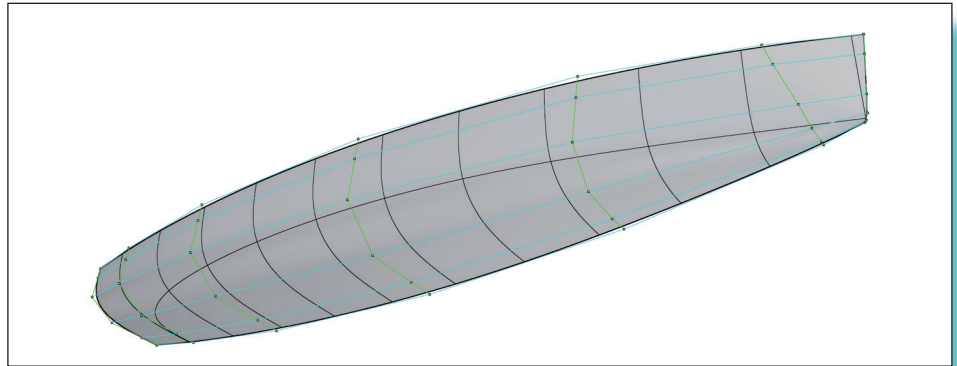
#### **Step 12: Draw buttocks**

This is the final check on the smoothness. Usually only very minor corrections have to be made at this stage.

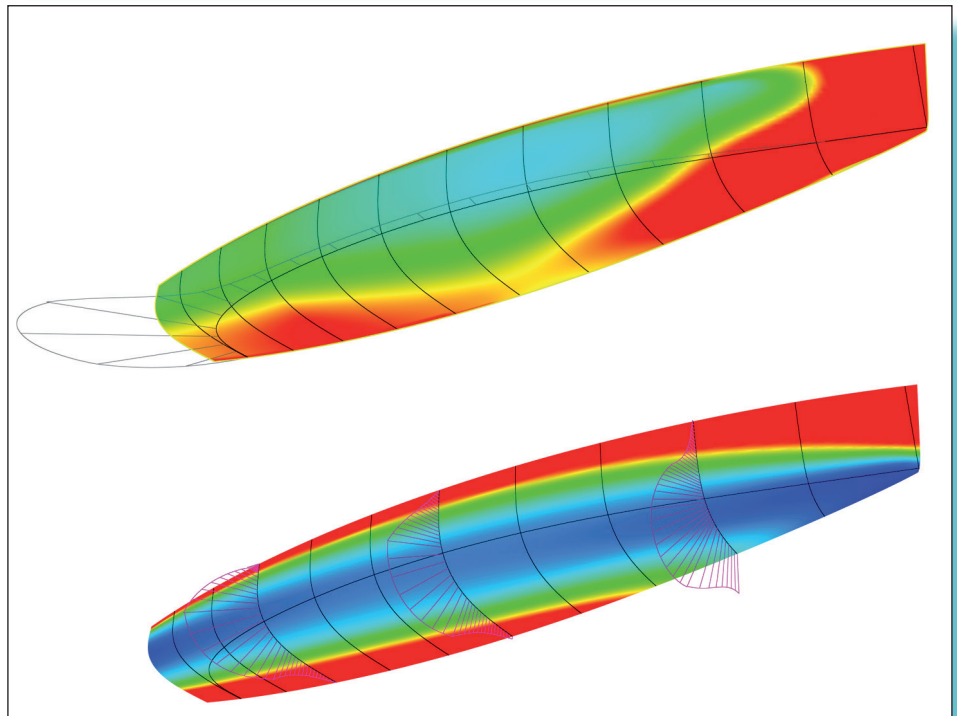
## ■ COMPUTER-AIDED DESIGN OF HULLS

As mentioned in [Chapter 1](#), most modern CAD programs use Non Uniform Rational B-Splines (NURBS) for generating the hull surface. A NURBS surface is defined by a set of vertex points normally just outside of the surface. An example is shown in [Fig 3.11](#). It can be seen that the vertices form a mesh outside of the hull. The task of the designer is to locate the vertices in such a way that the desired hull shape is created. By moving one vertex, the hull surface will change in the vicinity of that vertex, maintaining a smooth surface. In principle there are three ways to generate the hull: to start from scratch with a rectangular patch, to start from an already existing shape or to start from a generic hull created by the program based on a set of parameters specified by the user. The latter option might not be available in all programs, but it is a very useful feature.

**Fig 3.11** Hull with vertices for defining the surface



**Fig 3.12** Hull with curvature displayed in a colour scale and as a function along a line. (TOP) minimum surface curvature and curvature along waterline; (BOTTOM) maximum surface curvature and curvature along three sections





To avoid bumps on the surface the curvature may be displayed either as a colour map on the surface, or as a function plotted along a specific line. In the first case either of the two principal curvatures of the surface may be shown. At each point on the surface there are always two perpendicular directions along which the normal curvature is maximum and minimum, respectively. These are the principal curvatures at that point. If a function is plotted along a line it is the **normal** curvature of the surface along the line that is shown. Examples are given in Fig 3.12. In the upper figure the colours represent the minimum principal curvature which is essentially along the hull, while the line plot represents the normal curvature of the hull along the waterline. In the lower figure the maximum principal curvature (essentially transverse) is shown by the colours, while the line plots represent the normal curvature along three sections. Using the information on the curvatures the designer can generate a very smooth hull.

A great advantage of most CAD programs is that the hull may be shown in perspective. As pointed out in Chapter 1 it is important to study the sheer line in particular from different angles, since the impression of the hull contour in reality is also influenced by the beam distribution, which is not visible if only the profile view is studied. Fig 3.13 shows the YD-41 in perspective, and a good impression can be obtained of the shape.

By using a CAD program a fair hull can be produced rapidly and different requirements may be satisfied without too much work, such as a given prismatic coefficient or longitudinal centre of buoyancy. Meeting such requirements accurately in a manual process is extremely time consuming, so it is understandable that CAD techniques are always used nowadays by professional designers. Since the cost of modern CAD systems has dropped considerably in recent years (there are even freeware programs on the internet) they are now available to amateur designers. However, the manual approach described above is still in use and is therefore described in this book.

Having finished the CAD design a rendered picture of the yacht may be produced. There are a number of programs available for this. Here, lighting and shadows are introduced and the light is reflected by the surface of any object, creating a very realistic picture. Fig 3.14 shows rendered pictures of the YD-41 in two perspectives: one from the bow and one from the stern. Even a water surface may be added, as seen in Fig 3.15. The rendered pictures look very similar to photos of the yacht.

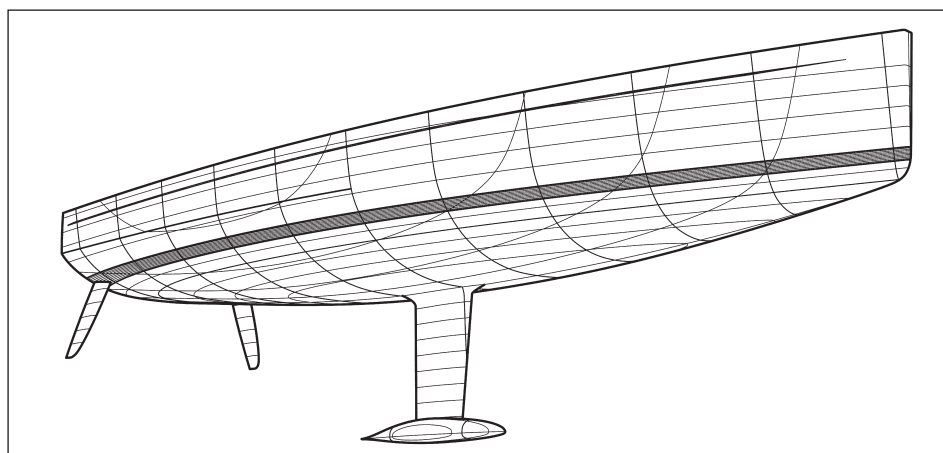


Fig 3.13 Perspective view of the YD-41

.....  
**Fig 3.14** Rendered pictures  
of the YD-41



.....  
**Fig 3.15** Rendered picture  
of the YD-41, including  
water surface.  
A picture of the real  
boat can be seen on  
the book cover



# 4 HYDROSTATICS AND STABILITY

Looking back at hull development in the history of yachting, it is obvious that opinion about the optimum shape of a yacht has changed many times. This is due in part to the changing rules, but more recently the shift in design trends reflects the increasing knowledge about the physical laws governing the behaviour of sailing yachts. The aim of this book is to present the state of the art in yacht design. While current knowledge does not provide explanations for all phenomena, there is one area where the basic laws have been known for a long time, and where the methods have been used by designers for centuries. This is the area of hydrostatics and stability.

Hydrostatics and stability represent perhaps the most important aspects of a design, since the properties of a yacht in these respects reflect its ability to carry the required weight and to withstand the heeling moment from the sails. It should be stressed that exact knowledge of stability is restricted to the static case, with no waves on the water surface. We have, however, chosen to include also dynamic stability in this chapter, although the laws are quite different.

We begin this chapter by introducing some simple ways of computing areas. This knowledge is required in subsequent paragraphs dealing with calculations of the wetted surface, displacement and its centre of gravity, the prismatic coefficient, the water plane area and the related mass per mm of immersion as well as the moment per degree of heel and trim. The discussion of dynamic stability includes stability in waves, methods for reducing roll, requirements for offshore yachts and some statistical information on the righting moment of existing yachts.

Note that all CAD programs for hydrodynamic applications have modules for the calculation of all hydrostatic data. For users of such programs the first part of this Chapter may be of less interest, but at least it can be used for understanding the background of the hydrostatic computations.

## ■ CALCULATION OF AREAS

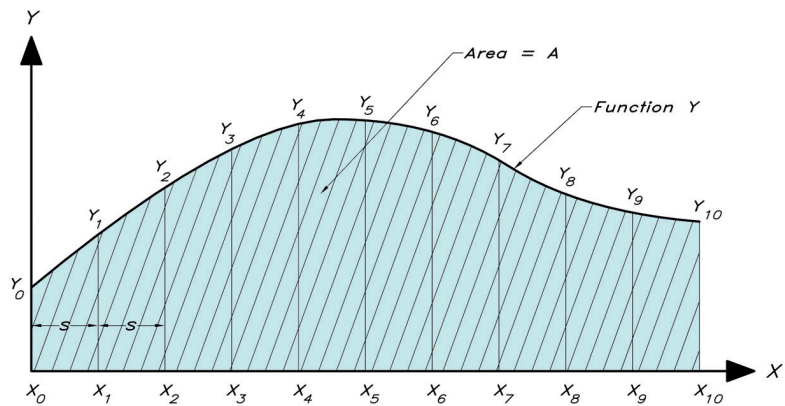
For the amateur designer, one way to obtain the area of a closed curve might be to draw it on a square grid and just count the number of squares. In most cases this method is accurate enough, but it is tedious and would hardly be used by professionals.

Another convenient way is to make use of the planimeter, as explained in the previous chapter. This method is fast and accurate, but few amateur designers have access to this handy instrument.

The best choice for many designers is to compute the area using a simple numerical method, based on the ordinates (y-values) of the curve at certain intervals.

Fig 4.1 introduces the most common numerical method for computing areas. It is called Simpson's rule, and is quite popular in naval architecture. Since the sequence of operations is always the same when applying Simpson's rule, a special scheme, shown in Fig 4.1, may be employed. The distance between the end points of the interval, in this case  $X_0$  and  $X_{10}$ , is divided into an even number of equidistant steps, in this case 10. The step size is denoted  $s$ . Values of the function  $Y$  are computed for all  $X$ -values and may be inserted into the table in the column 'ordinate value'. By multiplying each value by its Simpson multiplier, 1 for the end values and 4 and 2 alternating for the others, and adding all the products, the 'sum of products' is obtained. The area  $A$  under the curve  $Y$  is then simply obtained by multiplying this sum by the step size and dividing by 3.

Fig 4.1 Simpson's rule



Simpson's rule :

$$A = \frac{s}{3} ( Y_0 + 4Y_1 + 2Y_2 + 4Y_3 + 2Y_4 + 4Y_5 + 2Y_6 + 4Y_7 + 2Y_8 + 4Y_9 + Y_{10} )$$

*S.M. = Simpson's multipliers*

Ordinate No.	Ordinate value	S.M.	Product
0	$Y_0$	1	$Y_0$
1	$Y_1$	4	$4Y_1$
2	$Y_2$	2	$2Y_2$
3	$Y_3$	4	$4Y_3$
4	$Y_4$	2	$2Y_4$
5	$Y_5$	4	$4Y_5$
6	$Y_6$	2	$2Y_6$
7	$Y_7$	4	$4Y_7$
8	$Y_8$	2	$2Y_8$
9	$Y_9$	4	$4Y_9$
10	$Y_{10}$	1	$Y_{10}$
			Sum of products

$$A = \frac{s}{3} ( \text{Sum of products} )$$

Of course, the number of steps may be other than 10, but the number has to be even in Simpson's rule. In many applications within yacht design the number of steps is indeed 10, due to the standard division of the waterline from station 0 to station 10, but sometimes a higher accuracy is needed near the ends, where half stations may be introduced. The principle of Simpson's rule may still be used, by considering end intervals as pairs of halves, but the number of full intervals must always be even, so normally two or four intervals have to be divided. Fig 4.3 (page 42) shows the change caused by dividing an interval into two halves. In the following discussion, we will always refer to Simpson's rule for area calculations. However, the other methods mentioned above may be used as alternatives.

## ■ WETTED SURFACE

Due to the three-dimensional nature of the hull an exact calculation of the wetted surface is complicated, but a good approximation may be obtained as explained in Fig 4.2. If the girth length  $g$  along the surface from the keel to the waterline is measured at each station, and plotted against the longitudinal position on the hull from bow to stern, the area  $A$  under the curve is a reasonably good representation of the wetted surface of one half of the hull. The computation of this area is also shown in Fig 4.2. The values for the YD-41 are given in brackets.

The problem with the computed area is that the longitudinal slope of the hull, as seen in the waterlines or the diagonals, is not considered. The effect of this is small, but a more accurate result is obtained by adding 2–4%, i.e. by multiplying by a 'bilge factor'  $c$ , which is in the range 1.02–1.04. The bilge factor can be estimated by comparing the length of a typical diagonal with the straight line distance between the end points of the waterline.

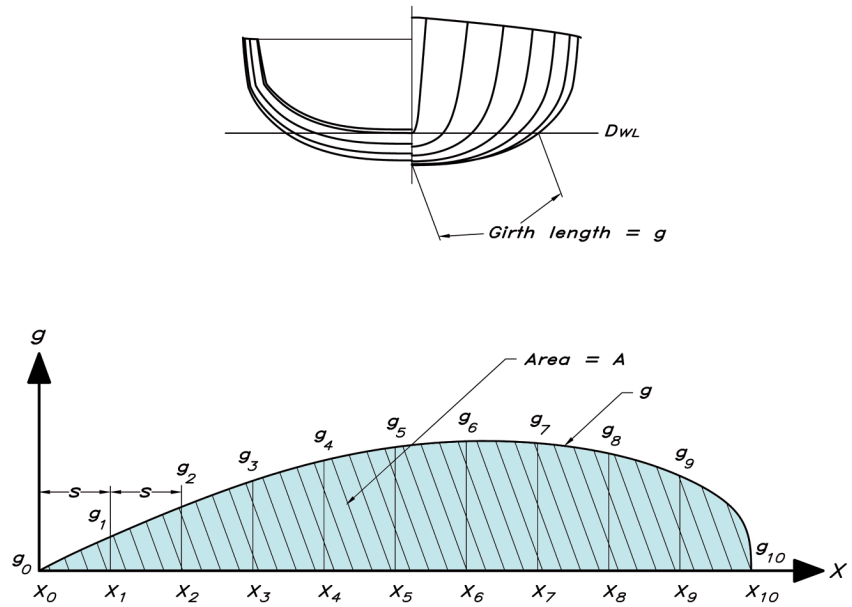
To simplify the presentation as much as possible, we have chosen to use full-scale entries for all formulae. Measures obtained from the drawings therefore have to be converted to full scale before being used in the calculations. In this way the somewhat confusing exercise with scale factors of various powers can be avoided in the different formulae. Note also that many calculations, like the present one, are made for only one half of the hull. Where this is the case the final value is therefore obtained only after multiplying by 2.

A very fast, but somewhat more approximate method to find the wetted surface is to make use of an empirical formula based on the length, beam, draft, displacement and prismatic coefficient of the canoe body (as shown in Fig 4.2). For smooth hulls this formula is surprisingly accurate, but if a drawing of the hull is available the method above is recommended.

## ■ DISPLACEMENT

According to Archimedes' principle, the mass of a floating body is equal to the mass of the displaced volume of water. Thus the volume displacement of the yacht,  $\nabla$ , multiplied by the density of water,  $\rho$  (i.e. the weight displacement  $m$ ), has to be equal to the total mass of the yacht.

**Fig 4.2** Calculation of the wetted surface



Ordinate No.	Ordinate value	S.M.	Product
0	$g_0$ [ 0.000 ]	1	$g_0$ [ 0.000 ]
1	$g_1$ [ 0.436 ]	4	$4g_1$ [ 1.742 ]
2	$g_2$ [ 0.820 ]	2	$2g_2$ [ 1.639 ]
3	$g_3$ [ 1.155 ]	4	$4g_3$ [ 4.620 ]
4	$g_4$ [ 1.417 ]	2	$2g_4$ [ 2.834 ]
5	$g_5$ [ 1.587 ]	4	$4g_5$ [ 6.349 ]
6	$g_6$ [ 1.662 ]	2	$2g_6$ [ 3.325 ]
7	$g_7$ [ 1.638 ]	4	$4g_7$ [ 6.552 ]
8	$g_8$ [ 1.506 ]	2	$2g_8$ [ 3.012 ]
9	$g_9$ [ 1.218 ]	4	$4g_9$ [ 4.870 ]
10	$g_{10}$ [ 0.000 ]	1	$g_{10}$ [ 0.000 ]
			Sum of products [ 34.95 ]

$$A = \frac{S}{3} \cdot (\text{Sum of products})$$

$$S_w = 2 \cdot c \cdot A$$

$$\left\{ \begin{array}{l} 2 = \text{both sides} \\ c = \text{bilge factor} = 1.02 - 1.04 \end{array} \right.$$

$$[S_w = 28.20 \text{ m}^2]$$

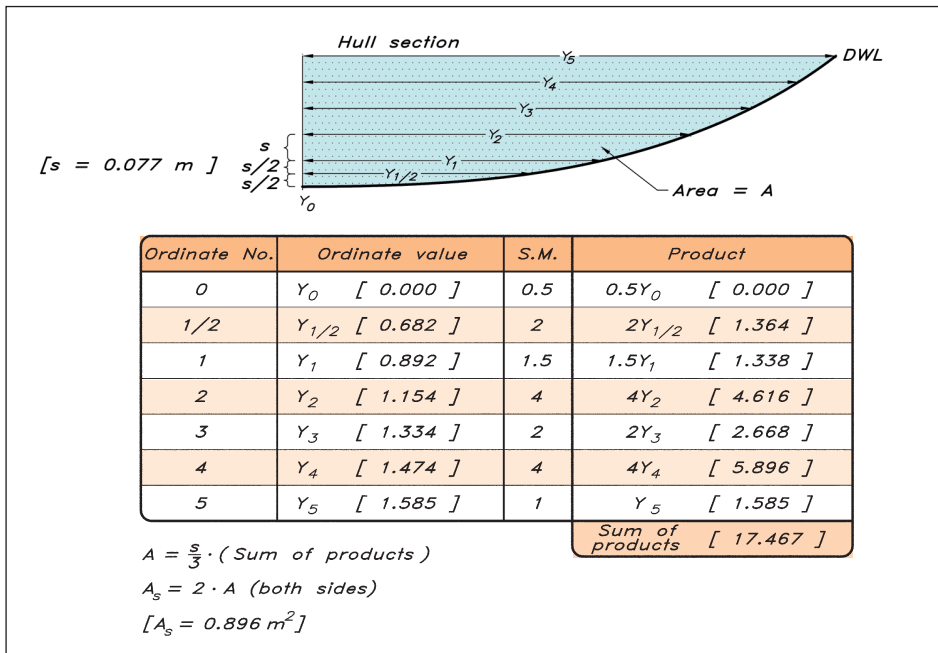
Alternatively (entirely empirical) :

$$S_w = [1.97 + 0.171 \frac{B_{WL}}{T_c}] \sqrt{\nabla_c \times L_{WL}} \cdot \sqrt[3]{\frac{0.65}{C_M}} [27.34 \text{ m}^2]$$

$$C_M = \frac{\nabla_c}{L_{WL} \cdot B_{WL} \cdot T_c \cdot C_p} [0.716]$$



**Fig 4.3** Calculation of the sectional area



In this chapter we will deal with the calculation of the volume displacement, while the mass of the yacht will be discussed in Appendix 2. It should be noted, that  $\rho$  is equal to  $1000 \text{ kg/m}^3$  for fresh water, but varies for salt water, depending on the salinity. As an average value for salt water  $1025 \text{ kg/m}^3$  may be used.

To obtain the volume, the curve of sectional areas has to be determined first. This is obtained by plotting the area of each section (the submerged part) at a suitable scale in the half breadth plan, as explained in Chapter 3. A difficulty encountered when applying Simpson's rule to compute the area  $A_s$  of a section is that the ordinates are not known at suitable intervals, so each section has to be properly divided (see Fig 4.3).

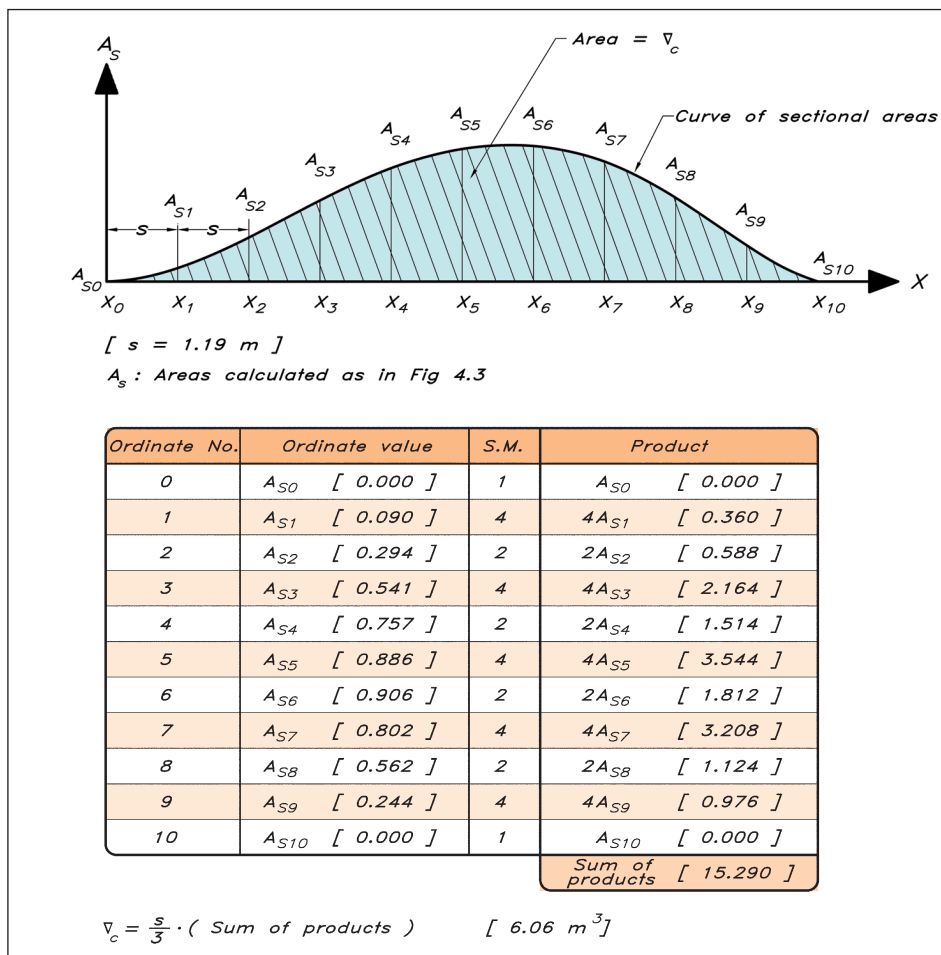
The ordinates in Fig 4.3 are the half breadths arranged in such a way that the depth at that section is divided into five parts. Half spacing is used in the lowest interval, since the ordinates vary rapidly in that region. This split interval is treated separately and the Simpson multipliers are halved, i.e. 0.5, 2, 0.5. However, the rightmost ordinate is shared with the next full interval, where the first multiplier is 1 (the first in the series 1, 4, 2, 4, 1). The total value thus becomes 1.5.

Having obtained all the areas of the sections and plotted them to obtain the curve of sectional areas (as in the line drawing of Fig 3.5), the displacement is obtained as the area under the curve. Fig 4.4 shows how this is computed using Simpson's rule. Note again that full-scale values are used throughout and that the values for the YD-41 are given in brackets.

## CENTRE OF BUOYANCY

The moment created by a force with respect to a perpendicular axis is the product of the force and the distance to the axis (the lever). This concept can be used for finding the

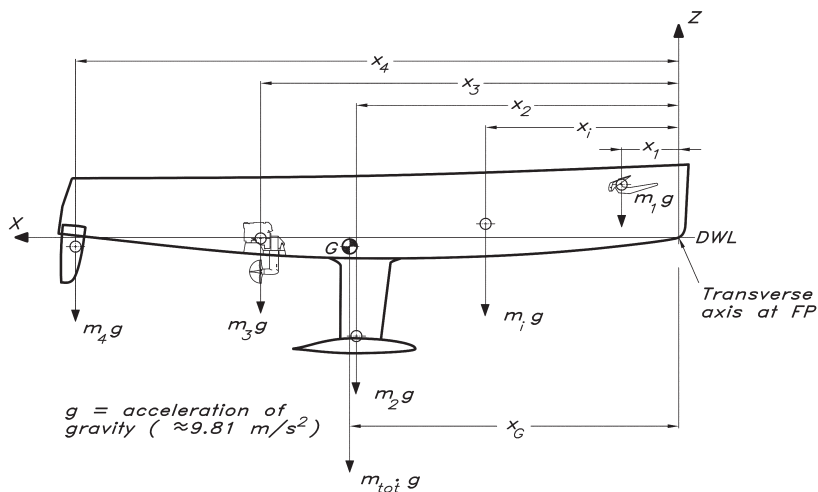
**Fig 4.4** Calculation of the volume displacement



centre of gravity of a body. By definition, the centre of gravity is the point where the mass of the body may be assumed concentrated. The gravitational force may be assumed acting at this point.

One way to calculate the distance to the centre of gravity from an arbitrary axis is to add the moments of the different parts of the body with respect to this axis. This gives a resulting moment, which must be equal to that of the concentrated mass at the centre of gravity. This method is explained in Fig 4.5, where the axis chosen is located athwartships at the forward perpendicular (FP).

A corresponding computation can be performed for the centre of gravity of the displaced volume of water, i.e. the centre of buoyancy. Let us first compute the longitudinal position, LCB, using the same axis as before. Each section of the hull may now be considered as contributing to the moment by an amount proportional to its area multiplied by its distance from the FP. Thus a 'curve of sectional moments' can be constructed in a similar way to the curve of sectional areas. The area under the new curve represents the total moment, from which the position of the centre of buoyancy can be obtained as explained in Fig 4.6 (page 45).



*x*-Values forward of FP and *z*-values below DWL are negative.

*Centre of gravity measured from FP along x-axis.*

$$m_{\text{tot}} g \cdot x_G = m_1 g x_1 + m_2 g x_2 + m_3 g x_3 + \dots + m_i g x_i + \dots$$

$$m_{\text{tot}} x_G = m_1 x_1 + m_2 x_2 + m_3 x_3 + \dots + m_i x_i + \dots$$

$$m_{\text{tot}} = m_1 + m_2 + m_3 + \dots + m_i + \dots$$

$$x_G = \frac{m_1 x_1 + m_2 x_2 + m_3 x_3 + \dots + m_i x_i + \dots}{m_1 + m_2 + m_3 + \dots + m_i + \dots}$$

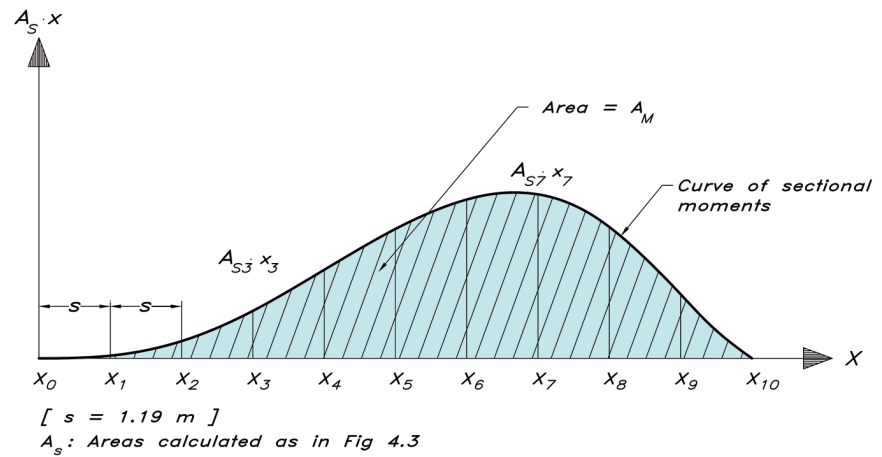
*Centre of gravity measured from DWL along z-axis:*

$$z_G = \frac{m_1 z_1 + m_2 z_2 + m_3 z_3 + \dots + m_i z_i + \dots}{m_1 + m_2 + m_3 + \dots + m_i + \dots}$$

**Fig 4.5** Method of finding the centre of gravity

There is a simple alternative method, which is used frequently for determining the longitudinal centre of buoyancy (LCB). If carefully employed, this method is probably as accurate as the numerical one. The sectional area curve is simply cut out in a piece of cardboard and the cut-out part is balanced on the edge of a knife at right angles to the longitudinal axis. When the cardboard is balanced, its centre of gravity is on the edge of the knife. This is also the position of the LCB. If the piece is hung on a needle and allowed to rotate, the vertical line through the needle crosses the centre of gravity. By hanging the piece at two positions and using a plumb bob to mark the vertical lines, the centre of gravity is found at their intersection.

**Fig 4.6** Calculation of the longitudinal centre of buoyancy of the canoe body



Ordinate No.	Ordinate value	S.M.	Product
0	$A_{S0} \cdot x_0 [ 0.000 ]$	1	$A_{S0} \cdot x_0 [ 0.000 ]$
1	$A_{S1} \cdot x_1 [ 0.107 ]$	4	$4A_{S1} \cdot x_1 [ 0.428 ]$
2	$A_{S2} \cdot x_2 [ 0.699 ]$	2	$2A_{S2} \cdot x_2 [ 1.399 ]$
3	$A_{S3} \cdot x_3 [ 1.931 ]$	4	$4A_{S3} \cdot x_3 [ 7.722 ]$
4	$A_{S4} \cdot x_4 [ 3.602 ]$	2	$2A_{S4} \cdot x_4 [ 7.203 ]$
5	$A_{S5} \cdot x_5 [ 5.269 ]$	4	$4A_{S5} \cdot x_5 [ 21.077 ]$
6	$A_{S6} \cdot x_6 [ 6.466 ]$	2	$2A_{S6} \cdot x_6 [ 12.932 ]$
7	$A_{S7} \cdot x_7 [ 6.678 ]$	4	$4A_{S7} \cdot x_7 [ 26.711 ]$
8	$A_{S8} \cdot x_8 [ 5.348 ]$	2	$2A_{S8} \cdot x_8 [ 10.696 ]$
9	$A_{S9} \cdot x_9 [ 2.612 ]$	4	$4A_{S9} \cdot x_9 [ 10.705 ]$
10	$A_{S10} \cdot x_{10} [ 0.000 ]$	1	$A_{S10} \cdot x_{10} [ 0.000 ]$
			Sum of products [ 98.617 ]

$$A_M = \frac{s}{3} \cdot (\text{Sum of products}) \quad [ 39.10 \text{ m}^4 ]$$

$$x_{LCB} = \frac{A_M}{\nabla_c} \quad [ 6.468 \text{ m } ]$$

For the determination of the vertical position of the centre of buoyancy (VCB), the vertical distribution of sectional moments must be considered. If the areas of several waterlines are known, the vertical distribution of the volume can be plotted in the form of a curve. This curve can then be treated in the same way as the sectional area curve and the location of the VCB can be found. However, the areas of the waterlines might not be known, since they are not normally required for other purposes. Another possibility is to cut out all sections of the hull from a piece of paper and glue them together just as in the body plan. The vertical position of the centre of gravity for this paper body is the desired VCB.

## ■ WATER PLANE AREA

The water plane area, i.e. the area inside the designed waterline (DWL), is important in several respects: first, its size determines ‘the weight per mm immersion’, i.e. the additional weight required to sink the hull a certain distance; secondly, its centre of gravity is located on the axis around which the hull is trimmed, when moving a weight longitudinally on board; thirdly, the so-called moment of inertia (sometimes called the second moment of area) around a longitudinal axis determines the stability at small angles of heel; and fourthly, the moment of inertia around a transverse axis through the centre of gravity (of the area) yields the longitudinal stability, i.e. the moment required to trim the hull a certain angle.

The calculation of the area is straightforward, using Simpson’s rule exactly as shown in Fig 4.1. If the area is denoted  $A_W$  (full-scale value), the additional displacement when sinking the hull 1 mm is  $0.001 \cdot A_W \text{ m}^3$ . The mass of this volume, corresponding to the applied mass on the hull, is  $\rho \cdot 0.001 \cdot A_W$ , where  $\rho$  is the water density. The mass per mm immersion is thus calculated from this simple formula.

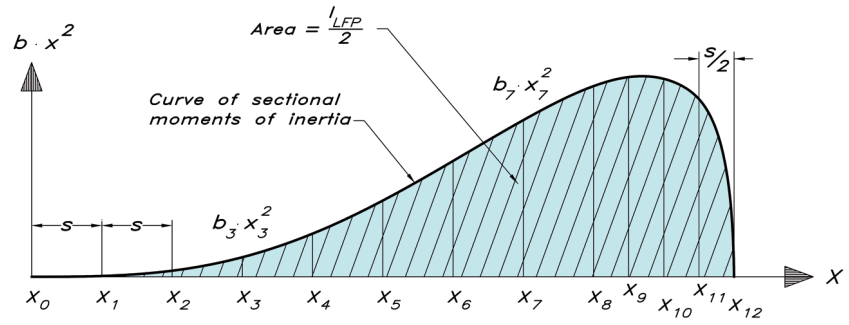
As explained earlier the centre of buoyancy is determined from the geometrical centre of gravity of the sectional area curve. Either a numerical method, like Simpson’s, or the simple ‘cardboard’ method can be used for the calculation. To obtain the geometrical centre of gravity of the water plane area, usually called the ‘centre of flotation’, the same techniques can be employed.

No simple method is available for finding the moment of inertia, but the numerical calculation is similar to that of the centre of gravity. Let us first calculate the longitudinal moment of inertia  $I_{LFP}$  about a transverse axis at the FP. A ‘curve of sectional moments of inertia’ can now be constructed, where each ordinate is the product of the waterline half-width and the *square* of the distance from the FP. The area of this curve can be used for finding the full-scale moment of inertia (both sides) in the usual way (see Fig 4.7). Note that, due to the very rapidly varying waterline beam close to the stern for the YD-41, the last two intervals have been split. This is required to get an acceptable accuracy for this shape of the waterline.

In the formula for longitudinal stability, to be presented in the next section, the moment of inertia  $I_L$  is taken about an axis, not through the FP, but through the centre of flotation. The calculated value  $I_{LFP}$  may, however, be converted to  $I_L$  quite simply, as shown in Fig 4.7.

In principle, the transverse moment of inertia  $I_T$  around the longitudinal axis, needed for the transverse stability, could be computed in a similar way, but then the water plane area would have to be divided into a set of longitudinal strips, which could be treated like the transverse ones above. This division is impractical, however, since it is not used in any other calculation. An alternative method is therefore shown in Fig 4.8 (page 48). Note that, for reasons of symmetry the longitudinal axis has to pass through the centre of flotation, so no correction need be applied.

**Fig 4.7** Calculation of the longitudinal moment of inertia



[  $s = 1.19 \text{ m}$  ]  
 $b = \text{half beam}$

Ordinate No.	Ordinate value	S.M.	Product
0	$b_0 \cdot x_0^2$ [ 0.00 ]	1	$b_0 \cdot x_0^2$ [ 0.0 ]
1	$b_1 \cdot x_1^2$ [ 0.55 ]	4	$4 b_1 \cdot x_1^2$ [ 2.2 ]
2	$b_2 \cdot x_2^2$ [ 4.23 ]	2	$2 b_2 \cdot x_2^2$ [ 8.5 ]
3	$b_3 \cdot x_3^2$ [ 13.63 ]	4	$4 b_3 \cdot x_3^2$ [ 54.5 ]
4	$b_4 \cdot x_4^2$ [ 30.08 ]	2	$2 b_4 \cdot x_4^2$ [ 60.2 ]
5	$b_5 \cdot x_5^2$ [ 53.12 ]	4	$4 b_5 \cdot x_5^2$ [ 212.5 ]
6	$b_6 \cdot x_6^2$ [ 80.73 ]	2	$2 b_6 \cdot x_6^2$ [ 161.5 ]
7	$b_7 \cdot x_7^2$ [ 109.2 ]	4	$4 b_7 \cdot x_7^2$ [ 436.8 ]
8	$b_8 \cdot x_8^2$ [ 132.9 ]	1.5	$1.5 b_8 \cdot x_8^2$ [ 199.4 ]
9	$b_9 \cdot x_9^2$ [ 139.0 ]	2	$2 b_9 \cdot x_9^2$ [ 278.4 ]
10	$b_{10} \cdot x_{10}^2$ [ 138.0 ]	1	$b_{10} \cdot x_{10}^2$ [ 138.0 ]
11	$b_{11} \cdot x_{11}^2$ [ 124.0 ]	2	$2 b_{11} \cdot x_{11}^2$ [ 248.0 ]
12	$b_{12} \cdot x_{12}^2$ [ 0.00 ]	0.5	$0.5 b_{12} \cdot x_{12}^2$ [ 0.0 ]
			Sum of products [ 1800 ]

$$I_{LFP} = 2 \cdot \frac{s}{3} \cdot (\text{Sum of products}) \quad [ 1427 \text{ m}^4 ]$$

Moment of inertia around centre of flotation

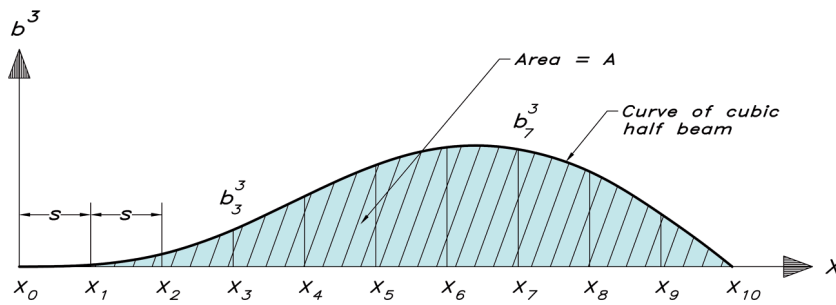
$$I_L = I_{LFP} - A_W \cdot x_F^2 \quad [ 205 \text{ m}^4 ]$$

$A_W = \text{waterline area} \quad [ 26.34 \text{ m}^2 ]$

$x_F = \text{distance from FP to centre of flotation} \quad [ 6.812 \text{ m} ]$

## TRANSVERSE AND LONGITUDINAL STABILITY AT SMALL ANGLES

The transverse stability of a yacht may be explained with reference to Fig 4.9 (page 49). When the yacht is heeled, the centre of buoyancy moves to leeward from B to B'. The buoyancy force, upwards, then creates a couple with the equally large gravity force acting downwards at G. The lever arm is usually called  $\overline{GZ}$  and the righting moment is  $m \cdot g \cdot \overline{GZ}$ , since the gravity force is the mass,  $m$ , multiplied by the acceleration of gravity,  $g$  ( $9.81 \text{ m/s}^2$ ).



$$[ s = 1.19 \text{ m } ]$$

$b = \text{half beam}$

Ordinate No.	Ordinate value	S.M.	Product
0	$b_0^3 [ 0.000 ]$	1	$b_0^3 [ 0.000 ]$
1	$b_1^3 [ 0.058 ]$	4	$4 b_1^3 [ 0.235 ]$
2	$b_2^3 [ 0.418 ]$	2	$2 b_2^3 [ 0.837 ]$
3	$b_3^3 [ 1.228 ]$	4	$4 b_3^3 [ 4.914 ]$
4	$b_4^3 [ 2.347 ]$	2	$2 b_4^3 [ 4.695 ]$
5	$b_5^3 [ 3.388 ]$	4	$4 b_5^3 [ 13.55 ]$
6	$b_6^3 [ 3.982 ]$	2	$2 b_6^3 [ 7.964 ]$
7	$b_7^3 [ 3.906 ]$	4	$4 b_7^3 [ 15.63 ]$
8	$b_8^3 [ 3.163 ]$	2	$2 b_8^3 [ 6.327 ]$
9	$b_9^3 [ 1.745 ]$	4	$4 b_9^3 [ 6.981 ]$
10	$b_{10}^3 [ 0.000 ]$	1	$b_{10}^3 [ 0.000 ]$
Sum of products			$[ 61.135 ]$

$$A = \frac{s}{3} \cdot ( \text{Sum of products} )$$

$$I_T = \frac{2}{3} \cdot A \quad [ 16.1 \text{ m}^4 ]$$

**Fig 4.8** Calculation of the transverse moment of inertia

There is another important point marked in the figure: the transverse metacentre, M. This is the intersection between the vertical line through B' and the symmetry plane of the yacht. For small angles of heel this point may be assumed fixed, which simplifies the calculations considerably. The distance between the centre of gravity G and M,  $\overline{GM}$ , is called the metacentric height and  $\overline{BM}$  is the metacentric radius. A fundamental stability formula (which will not be proven here) says that the metacentric radius is equal to the ratio of the transverse moment of inertia  $I_T$  and the volume displacement  $\nabla$ . Using this formula and some simple geometric relations the righting moment may be obtained as explained in Fig 4.9.



Fig 4.9 Transverse stability

Transverse stability relations:

$$\overline{BM} = \frac{I_T}{\nabla} \quad (\text{Fundamental stability formula}) \quad [2.55 \text{ m}]$$

$$\overline{GM} = \overline{BM} - \overline{BG} \quad (G \text{ above } B) \quad [2.52 \text{ m}]$$

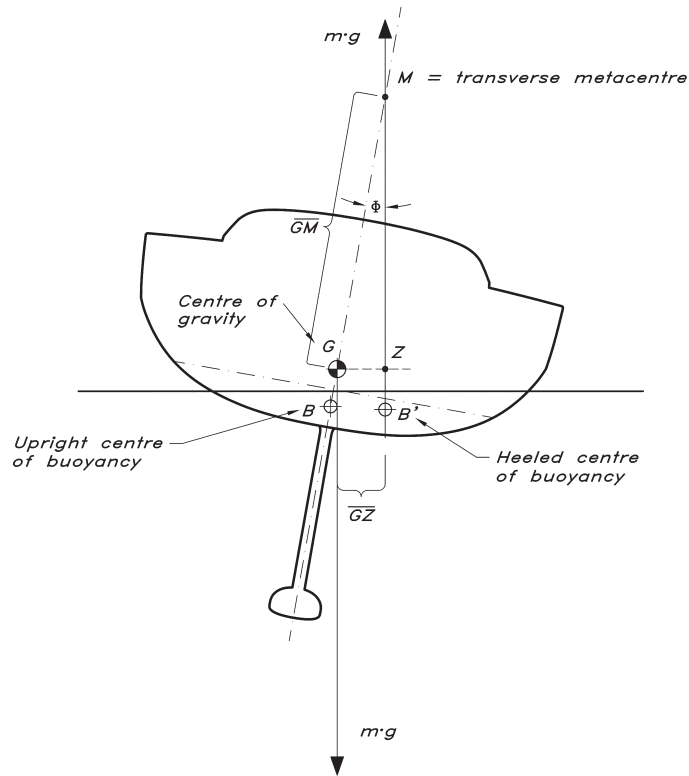
$$\overline{GZ} = \overline{GM} \cdot \sin \phi \quad (\phi = \text{heel angle})$$

$$[\overline{BG} = 0.03 \text{ m}]$$

$$[\nabla = 6.3 \text{ m}^3]$$

Transverse righting moment: [Nm]

$$RM = m \cdot g \cdot \overline{GZ}$$



Since the stability of the yacht is proportional to  $\overline{GM}$  there are two principal ways of increasing it. Either  $G$  may be lowered or  $M$  may be raised. A low  $G$  is found on narrow, heavy yachts with a large ballast ratio, like the 12 m and other R yachts. They have weight stability. Modern racing yachts, on the other hand, are wide and shallow, which raises  $M$ . They have form stability.

The method of calculating the longitudinal stability corresponds exactly to that of the transverse stability. Thus, the restoring moment when the hull gets a trim angle may be computed from the formulae of Fig 4.10, which correspond to those of the previous figure. There is also a formula for computing the trim angle obtained when moving a weight longitudinally on board the yacht.

Longitudinal stability relation:

$$\overline{BM}_L = \frac{I_L}{\nabla} \quad (\text{Fundamental stability formula}) \quad [ 33.06 \text{ m} ]$$

$$\overline{GM}_L = \overline{BM}_L - \overline{BG} \quad (G \text{ above } B) \quad [ 33.03 \text{ m} ]$$

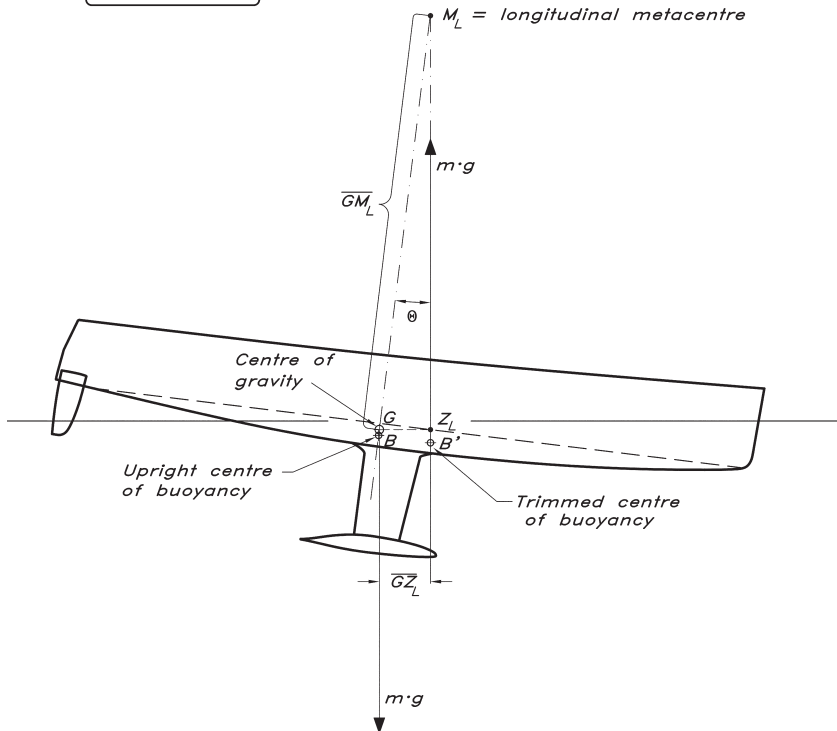
$$\overline{GZ}_L = \overline{GM}_L \cdot \sin \theta \quad (\theta = \text{trim angle})$$

$$[ \overline{BG} = 0.03 \text{ m} ]$$

$$[ \nabla = 6.3 \text{ m}^3 ]$$

Longitudinal righting moment:

$$RM_L = m \cdot g \cdot \overline{GZ}_L$$



Trim angle in degrees when moving a weight (W) a distance (x) longitudinally:

$$\theta = \frac{180}{\pi} \cdot \frac{W \cdot x}{m \cdot \overline{GM}_L}$$

Fig 4.10 Longitudinal stability

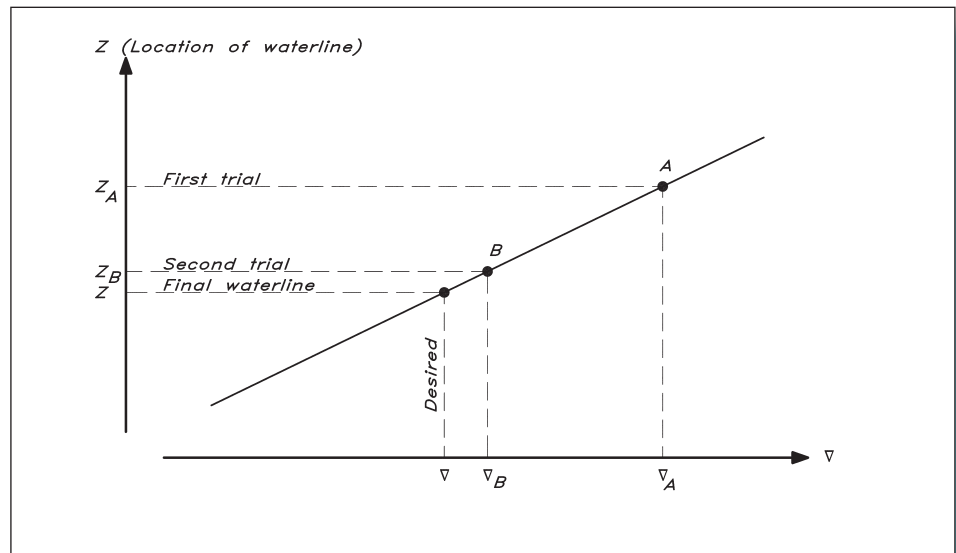
## TRANSVERSE STABILITY AT LARGE ANGLES OF HEEL

The calculation of the righting moment at large heel angles is considerably more complicated than that for small angles. One difficulty arises from the fact that the positioning of the heeled hull with respect to the water surface is not known. If the hull is just rotated about the centreline (at the level of the DWL), the displacement will generally become too large and a trimming moment will develop. The only way to overcome this difficulty is by trial

and error, i.e. by trying several attitudes, varying the sinkage and trim systematically, in order to find a position where the displacement and LCB correspond to the original ones.

After finding the right attitude a considerable amount of calculation is needed to find the righting moment, since no simple formulae, like those for small heel angles, are available. In practice, these calculations have seldom been carried out manually even for ships, because before the computer era naval architects made use of a special instrument, called an integrator, a development of the planimeter. Such an instrument is, however, rarely available to the yacht designer, so we will propose a slightly more approximate method, which is often accurate enough. The method is illustrated in Fig 4.11. Special care must be taken, however, with very beamy yachts with large fore and aft asymmetry. Such hulls will develop a considerable trim when heeling, and this effect is not considered here.

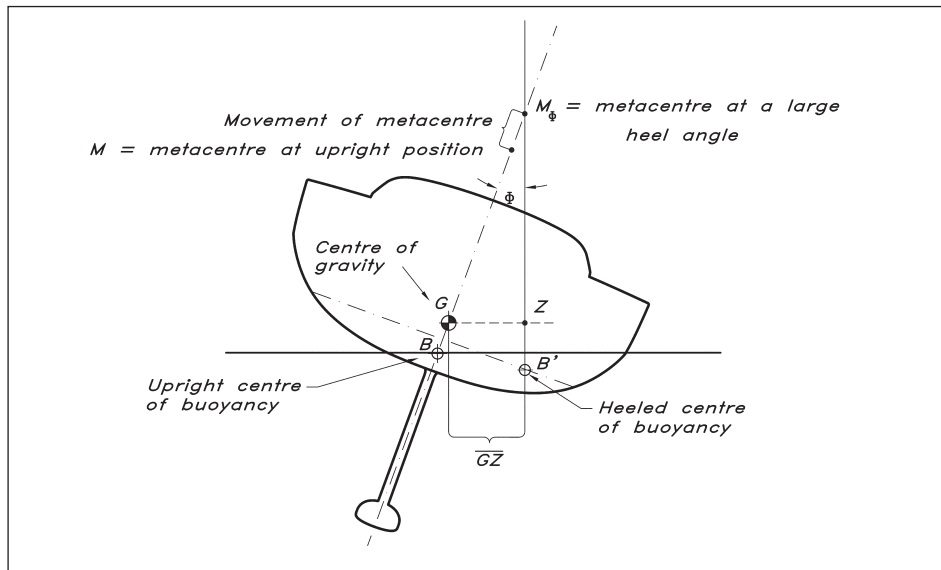
**Fig 4.11** Procedure to find the heeled waterline



To find the attitude of the hull, rotate it first around the centreline at DWL to the desired angle. Then calculate the displacement  $\nabla_A$  up to this waterline located at  $Z_A$ . This cannot be done, however, without knowing the shape of the sections on both sides of the symmetry plane, so the body plan has first to be completed to include both sides of the hull.

The displacement  $\nabla_A$  is bound to be too large, so a new waterline at  $Z_B$  has to be found. A first estimate of this line can be made by dividing the excess displacement by the area of the original DWL. This gives the approximate distance to the new waterline at  $Z_B$ , for which the displacement  $\nabla_B$  is also computed. Not even this is likely to be very accurate, but the final position  $Z$  of the waterline can be found by interpolation or extrapolation to the right, as explained in the figure. In this way the displacement will be quite accurate, although all effects of trim are neglected.

Having found the waterline, the 'cardboard method' is used to find the transverse position of the centre of buoyancy,  $B'$  in Fig 4.12 (overleaf). All heeled sections below the waterline



**Fig 4.12** Stability at large angles of heel

are cut out in cardboard and glued together in their correct positions. The centre of gravity of the cardboard body (corresponding to the centre of buoyancy of the real hull) can then be found from the intersection of two lines, obtained using a plumb bob, as explained above.

Knowing  $B'$ , the location of the point where the vertical through  $B'$  hits the centre plane  $M_\phi$  can be found (see Fig 4.12).  $\overline{BM}$  may then be measured from the figure and the remaining formulae for small angles applied.

## CURVE OF STATIC STABILITY

The curve of static stability represents the righting moment at varying angles of heel. Since the moment differs from the lever arm only with respect to the constant  $m \cdot g$ , the vertical scale could equally well represent  $\overline{GZ}$ . In Fig 4.13 the  $\overline{GZ}$ -curve for the YD-41 is presented.

For small angles  $\overline{GM}$  is constant and  $\sin \phi \approx \phi$  (in radians), so  $\overline{GZ}$  is proportional to the heel angle, i.e.  $\overline{GZ} = \overline{GM} \cdot \sin \phi \approx \overline{GM} \cdot \phi$ . The slope of the  $\overline{GZ}$  curve at the origin may thus be obtained by noting that the tangent should pass through the point  $\overline{GZ} = \overline{GM}$  for  $\phi = 1$  radian, i.e. at  $57.3^\circ$ .

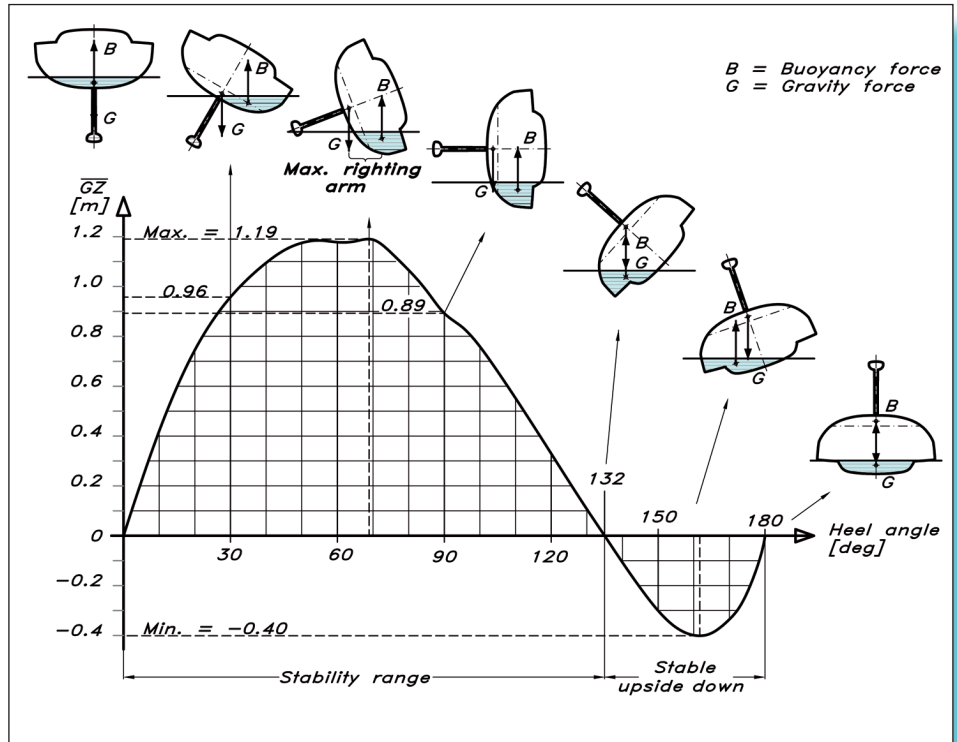
Another important aspect of the  $\overline{GZ}$  curve is the maximum, which represents the largest possible righting moment of the hull. Obviously the yacht will capsize if the heeling moment exceeds this level.

Of great interest is the so-called stability range, which is the range of angles for which a positive righting moment is developed. For larger angles the hull is stable upside-down.

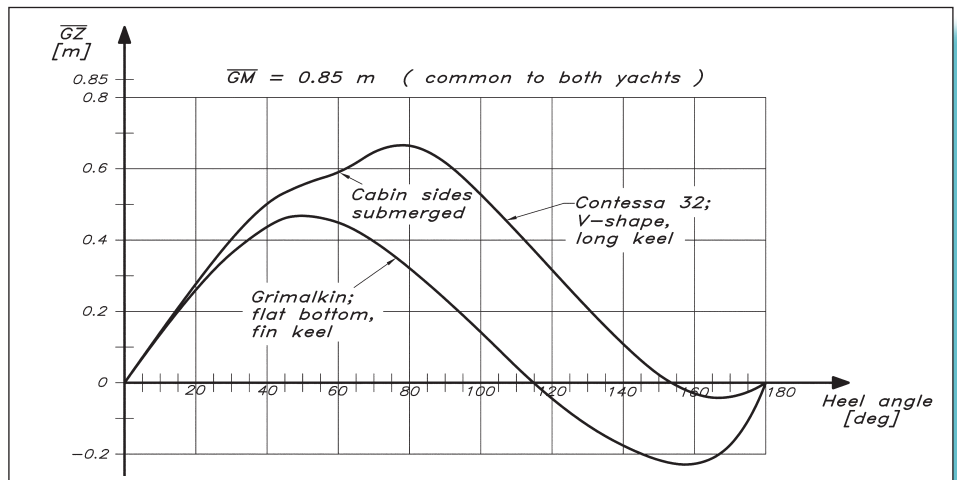
It is also of interest to note that the area under the RM curve up to a certain angle represents the work needed, by waves for instance, to heel the hull to this angle.

Large differences are found in the stability curves for modern fin-keel yachts and traditional V-shaped long keel ones. After the Fastnet Race disaster in 1979, a study was

**Fig 4.13** The curve of static stability – YD-41



**Fig 4.14**  $\overline{GZ}$ -Curves for *Grimalkin* and the *Contessa 32*



carried out at Southampton University in which two yachts of similar size were compared. Both raced in Class V. One was a cruiser-racer, the *Contessa 32*, while the other one was an extreme racer, *Grimalkin*, 30-foot  $L_{OA}$ .

Interestingly enough both yachts have the same  $\overline{GM} = 0.85 \text{ m}$  (as appears from Fig 4.14, which shows the  $\overline{GZ}$ -curves). This does not mean, however, that RM is exactly the same for small angles, since the mass differs: 4600 kg for the *Contessa 32* and 3800 kg for *Grimalkin*. At  $1^\circ$  of heel RM is 670 Nm (Newton-metres) and 550 Nm, respectively. It should be noted that the sail area is almost exactly the same for both yachts.

A larger difference is found in the maximum  $\overline{GZ}$ , which is about 40% higher for the Contessa 32. Converted into righting moment the difference is even larger. For the Contessa 32  $RM_{\max}$  occurs at about  $80^\circ$  and is equal to 30200 Nm, while for *Grimalkin*  $RM_{\max}$  is only 17900 Nm at about  $50^\circ$ .

A more significant difference is also found in the stability range. The Contessa 32 is stable up to about  $155^\circ$ , while zero righting moment occurs already at about  $115^\circ$  for *Grimalkin*. There is thus a very small range of angles,  $25^\circ$ , where the Contessa 32 is stable upside down, and the area between the RM curve and the horizontal axis is very small in this range. For *Grimalkin* the corresponding range is about  $65^\circ$  and the area is significant. This means that it is considerably more difficult to put the latter yacht into the upright position once it has capsized. The amount of work required by wind and waves is large, so this yacht may be expected to stay upside down for some time, perhaps a few minutes, while the Contessa 32 would return to the upright position almost immediately after a knockdown.

From this discussion it is clear that the traditional yacht is safer under rough conditions than the more modern one. In the following paragraphs we will elaborate further on the effects of waves on stability, before we present some statistics and criteria for the seaworthiness of ocean-racing yachts.

## ■ ROLLING

A sailing yacht in a seaway moves in all six degrees of freedom, i.e. surge, sway, heave, roll, pitch and yaw. The first three are linear motions in the longitudinal, transverse and vertical directions, while the remaining three are rotations around a longitudinal, transverse and vertical axis, respectively. From a safety point of view, rolling is the most important motion, and it will be dealt with in this and the following section. More important for the added resistance in waves are the pitching and heaving motions, and these will be discussed in [Chapter 5](#), in connection with hull design.

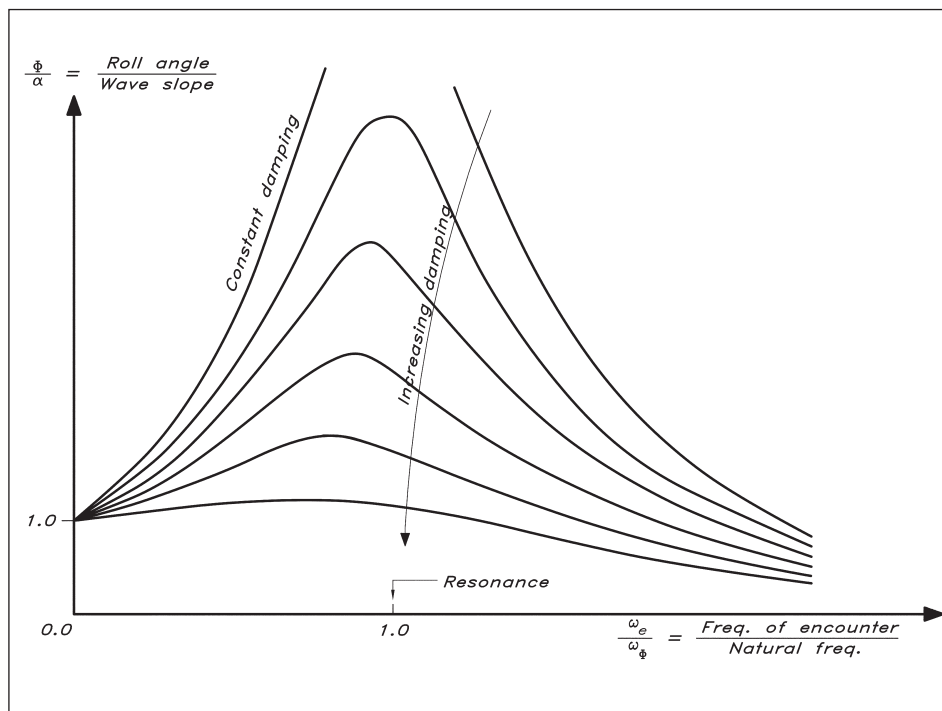
If a hull is given a heel angle in still water and is then suddenly released, the righting moment will immediately tend to put the hull upright. The hull starts rolling back to its upright position, but due to its inertia it will not stop when the heel angle is zero. Rather, it will continue to roll over to the other side, where an opposing righting moment develops. The hull then rolls back and forth, until the motion is damped out. In fact, for a sailing yacht, the damping is very large, so the motion dies rapidly.

This example contains many of the important features in connection with rolling excited by a seaway. Of great importance is the frequency with which the hull rolls in the still water test; the so-called natural frequency. The higher the stability, and the lower the inertia, the larger the natural frequency. It can easily be imagined that if the frequency of the waves hitting the hull in rough water is the same as the natural frequency (resonance), very large motions may result, at least if the damping is small.

This phenomenon is clearly borne out in [Fig 4.15](#). The horizontal scale is the frequency of encounter of the waves divided by the natural frequency of the hull, and the vertical scale is the roll angle divided by the wave slope. Several curves are shown in



**Fig 4.15** Roll amplitude for varying frequencies and damping



the diagram, each one with a constant damping. Note that the lowest curves represent the largest damping.

If the frequency of encounter is low or the natural frequency high, small values are obtained on the horizontal axis. This is where all curves converge into a value of one on the vertical axis. The roll angle is then the same as the wave slope. This may happen for long ocean waves after a gale, where most hulls will follow the wave contour. A liferaft, with a very small inertia, i.e. high natural frequency, will follow the wave contour for much shorter waves of higher frequency also, since the value on the horizontal scale is still very low. At the other end of the spectrum all curves tend to zero. This is where the waves hit the hull at such a high frequency that it does not have the time to react, an unlikely situation for waves of any significant height.

A dangerous condition is when the frequency of encounter is close to the natural frequency, i.e. close to resonance. As appears from Fig 4.15 the roll angle may then be several times larger than the wave slope and the yacht may capsize. We will now discuss the various means of avoiding this situation.

If the yacht approaches resonance, i.e. the frequency of encounter gets close to the natural frequency, one of these frequencies must be changed. The most straightforward way of doing this is to change the course. Since the frequency of encounter depends both on the wave speed (and length) and the speed component of the yacht in the direction of wave propagation, changing the course will change this frequency. If the yacht beats to windward many more waves are met per minute than if it runs downwind with the waves. This technique of avoiding excessive roll is also used on large ships under severe conditions. Speed reduction is also possible, of course.

From a theoretical point of view the natural frequency may be changed by increasing or reducing either the stability or the inertia (or more precisely, the mass moment of inertia around a longitudinal axis). To avoid the resonance situation the natural frequency can be either increased or reduced. However, in conditions where this problem occurs it is better to move to the left in Fig 4.15, either by increasing stability or reducing inertia. If weights located at a high position are moved down to the bottom of the hull (which is probably closer to the centre of gravity) both these effects are accomplished.

The technique of avoiding resonance is closely related to the operation of the yacht, while the other way to reduce roll – namely, to increase damping – is the designer's task. Damping may be caused by three things:

- Friction between the water and the yacht
- Generation of waves on the water surface
- Generation of vortices from the keel, rudder, sharp bilges and sails. This factor is by far the most important for sailing yachts.

Vortex generation depends partly on the shape of the sections (see Fig 4.16), but mainly on the size of the lateral area. Excessive rolling combined with low speed creates large angles of attack of the flow approaching the keel and rudder, which then get overloaded and stall. These phenomena will be dealt with at some length in Chapter 6. For the forces on the stalled surfaces the area is much more important than other geometrical properties, so a long keel yacht will have more damping than a fin-keel one. This is an important conclusion, which speaks in favour of traditional designs and against more modern ones with a small lateral area.

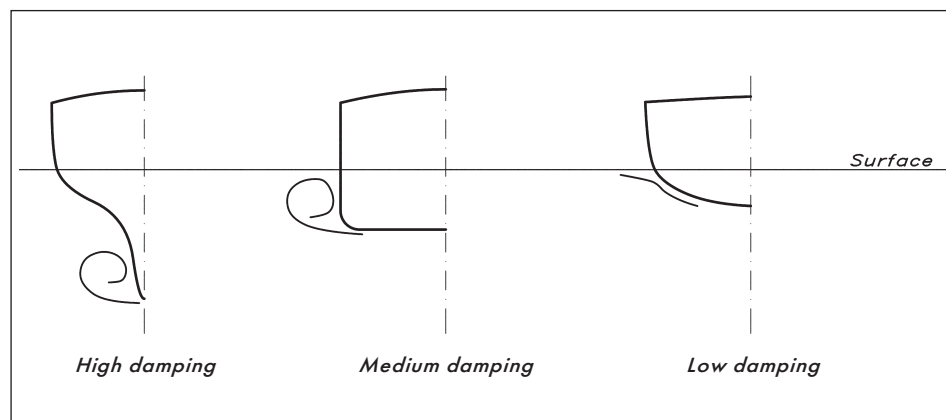
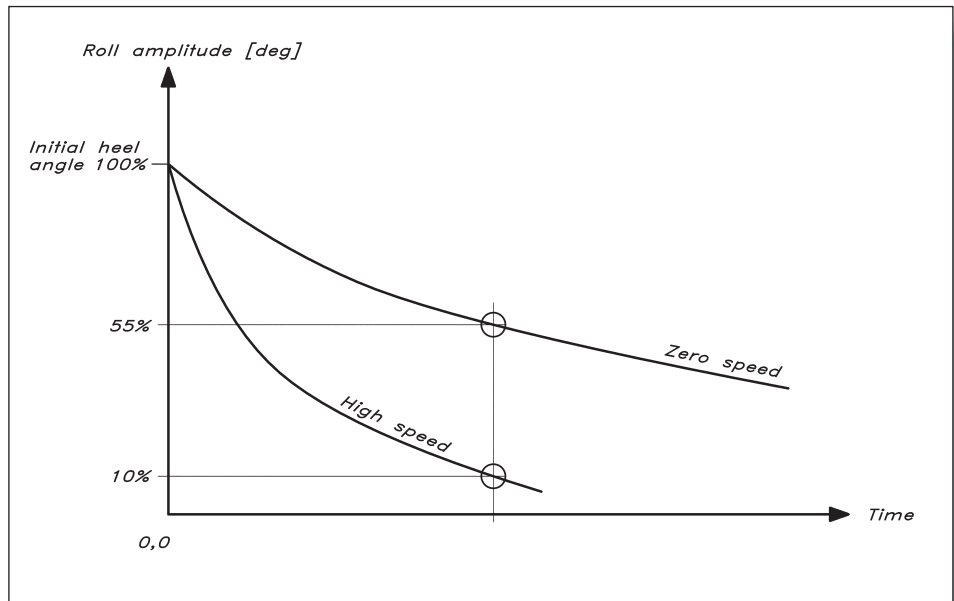


Fig 4.16 Influence of section shape on damping

It should also be pointed out that forward speed increases damping considerably, particularly for fin-keel yachts. If the speed is high enough, the keel starts working properly and the forces get much larger. Fig 4.17 shows how the roll amplitude decays with time for *Grimalkin* in still water. At zero speed the decay is much smaller than at high speed, where the rolling is rapidly damped. It is therefore important, especially for fin-keel yachts, to keep the speed up under critical conditions.

**Fig 4.17** Influence of speed on roll damping – fin-keel yacht



## ■ INFLUENCE OF WAVES ON THE RIGHTING MOMENT

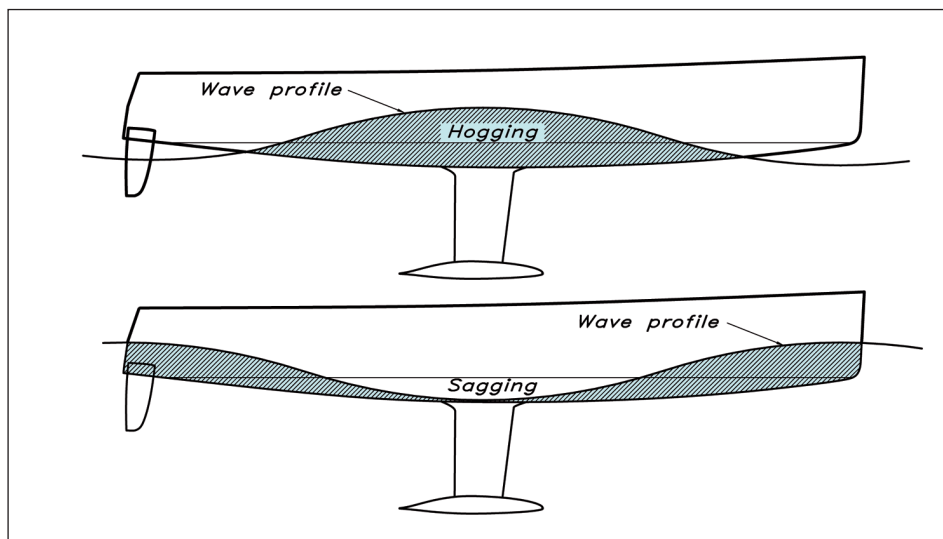
The righting moment is influenced by waves in two ways:

- The wave profile along the hull changes the waterline shape.
- The centrifugal forces on the water particles change the pressure in the wave.

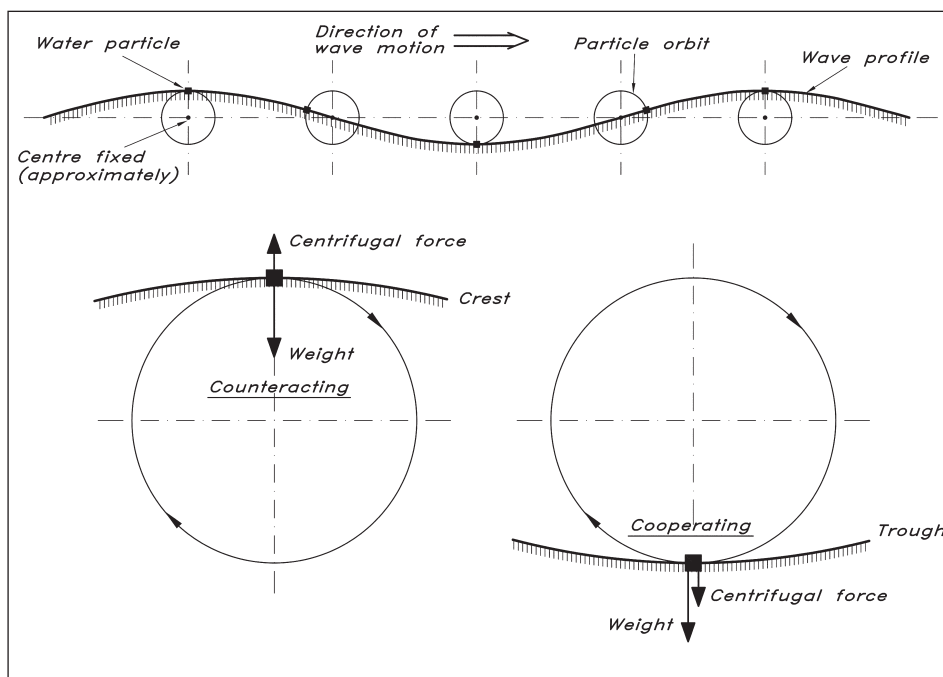
As regards the wave profile, two typical cases may be distinguished. These are shown in Fig 4.18 (overleaf). Hogging is when the wave crest is at midship, and sagging when the trough is at this position. For a sailing yacht, with some flare at all sections, hogging means that the submerged part of the hull gets thinner at the ends and beamier at midship. Since the water plane moment of inertia and the metacentric radius depend on beam cubed (Figs 4.8 and 4.9), this results in an increase in stability. In sagging the opposite occurs, with an increase in beam at the ends and a reduction at midship, i.e. a more even distribution of beam, which causes a reduction in stability. (It is worth mentioning that the effect is often the opposite for a ship with vertical sides at midship.)

For the wave profile effect to be significant the wavelength has to be of the same order as the hull length. This is not the case at sea, at least not under difficult conditions, where the waves are much longer. On the other hand, the waves generated by the hull itself often have the same length as the hull (as we will see in Chapter 5). The hull is then in a sagging condition and this may reduce stability considerably, particularly for hulls with a shallow draft, where the maximum beam may be much reduced in the wave trough. A formula for this effect will be given in the final section in this chapter.

To understand the effect of centrifugal forces some knowledge of particle motion in waves is required. This is explained in Fig 4.19. When the wave passes a certain point on



**Fig 4.18** Hogging and sagging

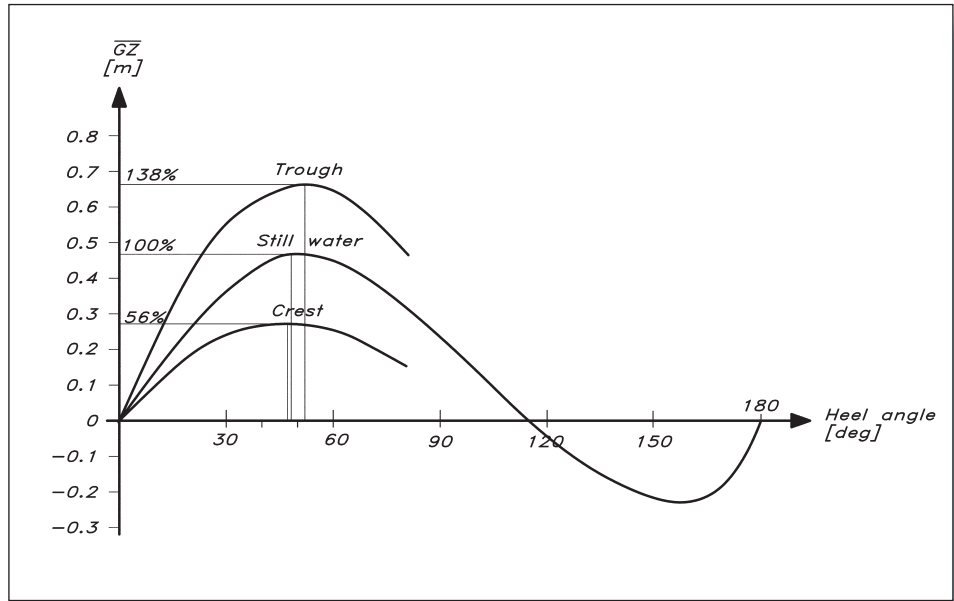


**Fig 4.19** Particle motion in a wave

the surface the water particles exhibit an orbital motion. Thus, when the particle is in a wave crest it moves with the wave, while the opposite is true in a wave trough. It is easy to compute the orbital speed, since the diameter of the circle is equal to the wave height, and the time to complete one full turn is equal to the wave period. For ocean waves this speed may be several metres per second.

The centrifugal effect on the water particles is explained in the lower part of Fig 4.19. In a crest the centrifugal force is directed upwards, i.e. opposite to the gravitational force; in a trough the two forces are in the same direction. An extreme case is when the two

**Fig 4.20** Influence of wave on the stability curve – *Grimalkin*



forces are equally large, which may happen for short and steep waves. Gravitation is then cancelled in the wave crest and the water will no longer be continuous, but will break down into droplets. A hull in this position will lose all its stability. A relevant question is whether it will still stay afloat, and the answer is yes (provided it does not capsize). It will, in fact, float at the original waterline. This is because the hull loses as much weight as the water due to the circular motion.

Complete loss of stability is, fortunately, very rare, but significant reductions may occur, as shown in Fig 4.20. *Grimalkin's* stability curve is shown for a wave height of 12 m and a wave period of 9 seconds. These extreme conditions were actually measured in the Fastnet disaster in 1979. It is seen that on a wave crest the stability is almost halved, and this is at a position when the yacht is most exposed to the wind.

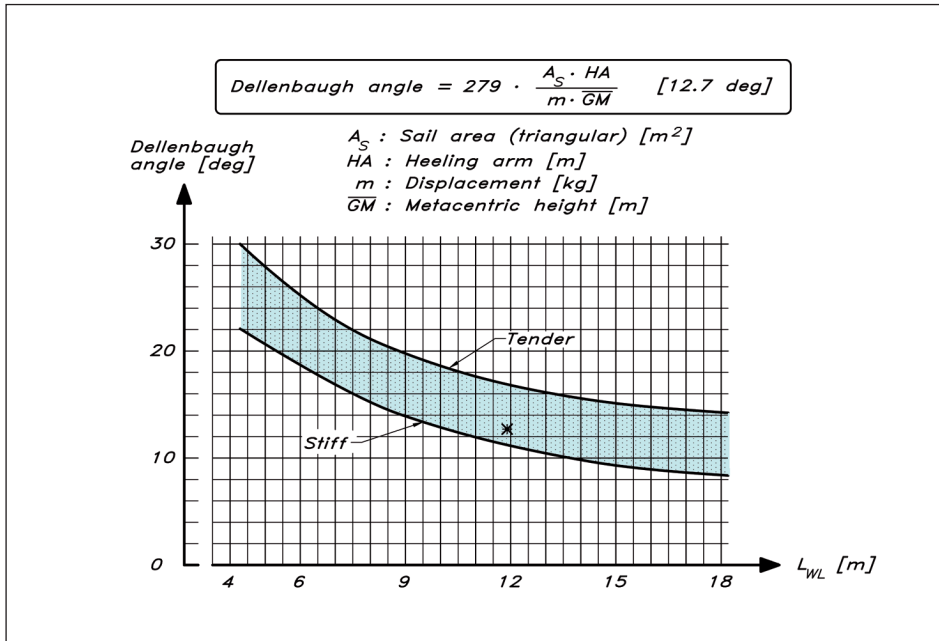
## ■ STABILITY STATISTICS

In general, modern yachts have larger  $\overline{GM}$ s than traditional ones due to their larger beam/draft ratio. The scatter is very large, however. In a survey of American IMS yachts around 1990 the lowest value was 0.67 m and the highest 2.1 m. More limited statistics for European yachts designed around 2010 show surprisingly similar results: 0.85–2.1 m for waterline lengths between 8 and 15 m. For these yachts  $\overline{GM}$  is in the range 10–15% of  $L_{WL}$ .

As for the stability range, several yachts in the IMS fleet had a positive righting moment up to 180° while there were other yachts which developed negative stability at 100° of heel. The average was 122°. The more recent survey showed stability ranges between 100 and 135°, with an average of 118°.

A rapid way of judging the stability of the yacht is to compute the so-called Dellenbaugh angle. This angle is computed from a simple formula (given in Fig 4.21),

Fig 4.21 Dellenbaugh angle



containing the sail area, heeling arm,  $\overline{GM}$  and displacement. The heeling arm is defined as the vertical distance between the centre of effort of the sails and the centre of lateral resistance of the underwater body. (Both will be discussed later, particularly in [Chapter 8](#).) Most modern yachts fall within the band of [Fig 4.21](#), which gives the Dellenbaugh angle versus the waterline length. The difference between stiff and tender yachts is about 6° for all lengths. For a 12 m  $L_{WL}$  yacht the angle is therefore between 11° and 17°, and the value for the YD-41 is 12.7°, which confirms the finding above that the yacht is quite stiff. Note that the Dellenbaugh angle says nothing about the stability at large angles of heel.

## ASSESSMENT OF SEAWORTHINESS

It is extremely difficult to find rigorous criteria for the safety of offshore yachts. We have touched upon several factors of importance in the previous sections, but when it comes to the dynamic effects in a seaway little quantitative information has been given. Nevertheless, the problem is of great importance and a new standard for boats and yachts (sail and power) of between 2.5 m and 24 m length is ratified by the International Standards Organization (ISO). In the following section we will introduce the standard ISO 12217-2 which deals with sailing yachts from 6 m to 24 m in length.

The general idea is to define a 'stability index', STIX, obtainable from the main dimensions of the yacht and its righting moment curve. Different qualities of the design, of importance from a seakeeping and safety point of view, are identified and expressed in the form of factors, which are multiplied to obtain the STIX. The factors are explained below. In [Fig 4.22](#) (page 62) the exact formulae are given.



#### ◆ Base length factor ( $L_{BS}$ )

The size of the yacht is the single most important parameter when assessing safety at sea, since it defines a scale with which to measure the waves. The larger the yacht, the smaller the relative size of the waves. In this approach the size is simply taken as a weighted average of the overall length and the waterline length. Whether or not this is a valid assumption can be discussed. To consider the waterline length twice as important as the overall length, as is done in the formula, is reasonable when it comes to the sailing performance of a yacht. But in this context, with the yacht often heeled over to  $90^\circ$  or more, the overall length should be more important than the waterline length. As the formula stands now it penalizes yachts with overhangs (old ones) and encourages yachts with square ends (modern ones).

#### ◆ Displacement length factor (FDL)

A light displacement relative to the size of the yacht may be considered a disadvantage from a control point of view and is therefore penalized, as appears in [Fig 4.22](#). The formula is designed to yield a value of 1.0 for a 'normal' yacht, and the minimum and maximum values used in the STIX computation are 0.75 and 1.25, even though the actual value may be outside this range. Similar principles apply also to the other factors below.

Penalizing light yachts may seem unfair considering experiences from races under very rough conditions, such as the Fastnet race in 1979 and the Sydney-Hobart race in 1998, where the light yachts indeed survived well. However, these yachts were handled by full racing crews. Yachts covered by the ISO standard are supposed to travel the same waters with a minimum crew, perhaps rather inexperienced. Then a very responsive and sensitive yacht is not a good asset. In the FDL-factor we have a Length factor  $F_L$ , which increases with  $L_{BS}$ . Its function is to allow larger yachts to have a lighter relative displacement than the smaller ones, without being penalized. The reason can be found in [Fig 2.1](#): stability characteristics do not scale in proportion to length.

#### ◆ Beam displacement factor (FBD)

Based on research carried out both in England (Wolfson Unit, Southampton) and the USA (Society of Naval Architects and Marine Engineers) after the Fastnet disaster, it has been concluded that large beam in combination with light displacement accentuates the risk of wave-induced capsize. The hull also gets more stable upside down, which is undesirable. This feature was demonstrated by two Open-60 yachts a few years ago. They were floating upside down with the keel intact a very long time after capsizing, before they were found.

On the other hand, a very small beam to displacement ratio may have a negative effect on the form stability, so large deviations in both directions from the norm are penalized. Particularly bad examples of narrowbeam yachts were the old English plank-on-the-edge cutters, with almost no form of stability. They were developed from a bad rating rule and depended on heavy ballast at a low position. The heel angle was excessive even in normal sailing conditions and the risk of downflooding was large.

The FBD formulae are different for narrow, 'normal' and wide hulls. The governing factor is  $FB$ , which is based on the ratio of beam to the third root of displacement. The 'normal'  $FB$ -ratio lies between 1.45 and 2.2.

Determination of monohull stability index (STIX) : [42]

$$STIX = (7 + 2.25 \cdot L_{BS}) \cdot (FDL \cdot FBD \cdot FKR \cdot FIR \cdot FDS \cdot FWM \cdot FDF)^{0.5}$$

$L_H$  = hull length (m) excluding bolted on extensions (bowsprit, stem roller, etc.)  
 $B_H$  = hull width (m) excluding bolted on extensions (cap rails, rub rails, etc.)  
 $B_{WL}$  = beam waterline (m) in the appropriate loading condition  
 $m$  = mass of the boat (kg) where more than one loading is considered  
 $m_{MO}$  = mass of the boat (kg) in the minium operating condition  
 $m_{LA}$  = mass of the boat (kg) in the loaded arrival condition  
 $h_{CE}$  = height of centre of sail area above the waterline when the boat is upright  
 $h_{LP}$  = height of centre of lateral area below the waterline when the boat is upright  
 $GZ_{90}$  = righting arm at 90° heel  $GZ_D$  = righting arm at  $\Phi_D^\circ$  heel  
 $\Phi_V$  = angle of vanishing stability  
 $\Phi_D$  = first occurring downflooding angle (For details see ISO 12217-2 standard)

Base Length Factor : [12.26]

$$L_{BS} = (L_H + 2L_{WL})/3$$

Displacement Length Factor : [0.905]

$$FDL = \left[ 0.6 + \frac{15 \cdot m \cdot F_L}{L_{BS}^3 \cdot (333 - 8 \cdot L_{BS})} \right]^{0.5} \quad 0.75 < FDL < 1.25$$

$$F_L = (L_{BS}/11)^{0.2}$$

Beam Displacement Factor : [0.831]

$$F_B = \frac{3.3 \cdot B_H}{(0.03 \cdot m)^{1/3}} \quad 0.75 < FBD < 1.25$$

$$FBD = \left[ \frac{13.31 \cdot B_{WL}}{B_H \cdot F_B^3} \right]^{0.5} \quad \text{if } F_B > 2.2$$

$$FBD = \left[ \frac{B_{WL} \cdot F_B^2}{1.682 \cdot B_H} \right]^{0.5} \quad \text{if } F_B < 1.45$$

$$FBD = 1.118 \cdot (B_{WL}/B_H)^{0.5} \quad \text{if } 1.45 \leq F_B \leq 2.2$$

Knockdown Recovery Factor : [1.216]

$$F_R = GZ_{90} \cdot m / (2 \cdot A_s \cdot h_{CE}) \quad 0.5 < FKR < 1.5$$

$$FKR = 0.875 + 0.0883 \cdot F_R \quad \text{if } F_R \geq 1.5$$

$$FKR = 0.5 + 0.333 \cdot F_R \quad \text{if } F_R < 1.5$$

$$FKR = 0.5 \quad \text{if } \Phi_V < 90^\circ$$

Inversion Recovery Factor : [1.090]

$$FIR = \Phi_V / (125 - m/1600) \quad \text{if } m < 40000 \quad 0.4 < FIR < 1.5$$

$$FIR = \Phi_V / 100 \quad \text{if } m \geq 40000$$

Dynamic Stability Factor : [1.183]

$$FDS = (A_{GZ} / (15.81 \cdot \sqrt{L_H}))^{0.3} \quad 0.5 < FDS < 1.5$$

$A_{GZ}$  = the positive area under the GZ-curve (m.deg.) as follows:  
 from upright to  $\Phi_V$ , for the appropriate loading condition

Wind Moment Factor : [1.00]

$$FWM = 1.0 \quad \text{if } \Phi_D > 90^\circ \quad 0.5 < FWM < 1.0$$

$$FWM = V_{AW} / 17 \quad \text{if } \Phi_D < 90^\circ$$

$V_{AW}$  = the steady apparent windspeed to heel the vessel to  $\Phi_D$  when carrying full sail =  $(13 \cdot m \cdot GZ_D / (A_s \cdot (h_{CE} + h_{LP}) \cdot \cos \Phi_D^{1.3}))^{0.5}$

Downflooding Factor : [1.25]

$$FDF = \Phi_D / 90 \quad 0.5 < FDF < 1.25$$

Design Categories :	A	B	C	D
STIX Lower Limits :	32	23	14	5

**Fig 4.22** STIX stability index (Blyth, Moon, Oossanen, Dolto and Eliasson)

#### ◆ Knockdown recovery factor (FKR)

This factor refers to the ability of the yacht to spill water out of the sails after a knockdown. The governing factor here is FR, which represents the ratio of the righting moment and heeling moment with sails just dipped into the water. If FR is larger than or equal to 1.5, the recovery factor is calculated using the uppermost formula in Fig 4.22, and if it is below 1.5, the second formula should be used. For yachts with an angle of vanishing stability less than 90°, FKR is set to 0.5, the minimum value.

#### ◆ Inversion recovery factor (FIR)

FIR represents the yacht's ability to recover unaided after an inversion. The important quantity here is the angle of vanishing stability. The formulae are simple, especially the last one regarding vessels with a weight of more than 40 tons. For a vessel this size, FIR is equal to the vanishing angle divided by 100. For smaller yachts the demands are larger. An 8-ton yacht requires a vanishing angle of 120° to get a FIR factor of 1.

#### ◆ Dynamic stability factor (FDS)

As shown in Fig 4.13, the area under the righting moment curve up to a certain heel angle represents the work needed by external forces (from wind and waves) to heel the yacht to this angle. This is utilized in the dynamic stability factor (FDS), which is proportional to the area under the righting arm ( $\overline{GZ}$ -) curve over the whole stability range, i.e. up to the angle of vanishing stability. The reason for not using the righting moment curve is the fact that size is already accounted for in LBS, so using this curve would give too much credit to the larger yacht. The  $\overline{GZ}$ -curve for smaller angles of heel shall be determined by inclining tests. Computed values are accepted but then with a standard reduction of the computed value to account for the generally too optimistic prediction.

#### ◆ Wind moment factor (FWM)

For hulls with a downflooding angle smaller than 90° this factor represents the risk of downflooding due to a gust heeling the unreefed yacht. FWM cannot be larger than 1. This value is accomplished if the downflooding angle is 90° or more, which is the case for most ballasted yachts, with 'normal' deck openings. If the downflooding angle is smaller than 90° the yacht must withstand an apparent wind speed of 17 m/s when carrying full sail without downflooding to achieve an FWM value of 1.

#### ◆ Downflooding factor (FDF)

This factor represents the risk of downflooding in a knockdown and it is proportional to the downflooding angle.

The downflooding angle is defined as the heel angle at which the first downflooding opening becomes immersed. The opening may be either a main companionway hatch, to a cockpit that is not quick-draining or into the hull itself. For a yacht with a quick-draining cockpit, the most crucial point is normally the top corner of the companionway hatch, not the lower corner where it meets the cockpit sole. So, if there are no abnormally large ventilation openings in the hull, the upper corner of the companionway hatch is what defines the downflooding angle. For a heavy yacht (with the hatch on the centreline) the

angle is normally in the region of  $115^\circ$ , whereas the angle for light displacement yachts is often around  $125^\circ$ . This is due to the up-floating when the yacht heels over. For offset hatches the angle obviously has to be calculated for the worst direction of heel.

Stability index is obtained from the formula at the top of Fig 4.22. Note that calculations have to be carried out both for the minimum operating condition ( $m_{MO}$ ) and the loaded arrival condition ( $m_{LA}$ ). The smallest of the computed STIX values is to be used. Based on the STIX number, the yachts are classified in four different categories, A–D. The limits for the different categories are given in Fig 4.22. A yacht in category A is considered very seaworthy and should be fit for ocean passages, while a yacht in category D should be used only in sheltered waters. To qualify for an A or B rating the yacht must have a quick-draining cockpit and a downflooding angle of at least  $90^\circ$ . For a discussion and comparison of STIX calculations of a light and a heavy yacht the reader is referred Eliasson (2003). Here we will comment on the STIX calculation for the YD–41.

As appears from Fig 4.22, the YD–41 has a STIX rating of 42 and is thus very well qualified for category A. Only the displacement length factor FDL and the beam displacement factor FBD are below 1.0 (0.905 and 0.831, respectively). The strongest points are related to the righting moment ( $FKR = 1.216$ ,  $FIR = 1.09$  and  $FDS = 1.183$ ) and the downflooding angle ( $FDF = 1.0$ ). In Appendix 3 the complete STIX calculation for the YD–41 is presented. Calculations have been carried out for the minimum operating condition and the loaded arrival condition, but only the minimum operating condition results are shown, since the loaded arrival case gives a higher STIX rating. The basis for the minimum operating condition is the light ship, corresponding to the light displacement of Appendix 1. To get the minimum operating condition two crew, a liferaft and some standard equipment have been added. Hull dimensions corresponding to this displacement have been interpolated between the two columns of Appendix 1.

The stability index was developed by van Oossanen, Dolto, Eliasson and Moon in an ISO working group under the chairmanship of A G Blyth. It is presented here by permission of the ISO. Note that it is also part of the European Directive 94/25/EC regarding strength and safety of pleasure craft with a length between 2.5 and 24 m.

# 5 HULL DESIGN

In this chapter we describe the theories behind the hydrodynamic design of the hull. We start by introducing the various forces acting on a sailing yacht and explain how the forces are created by the flow around the hull. Formulae will be given for the force components, and the trade-offs in the hull design process will be dealt with at some length. Finally, there is a section on hull statistics, which may be used as a guide for selecting the main dimensions of a new design.

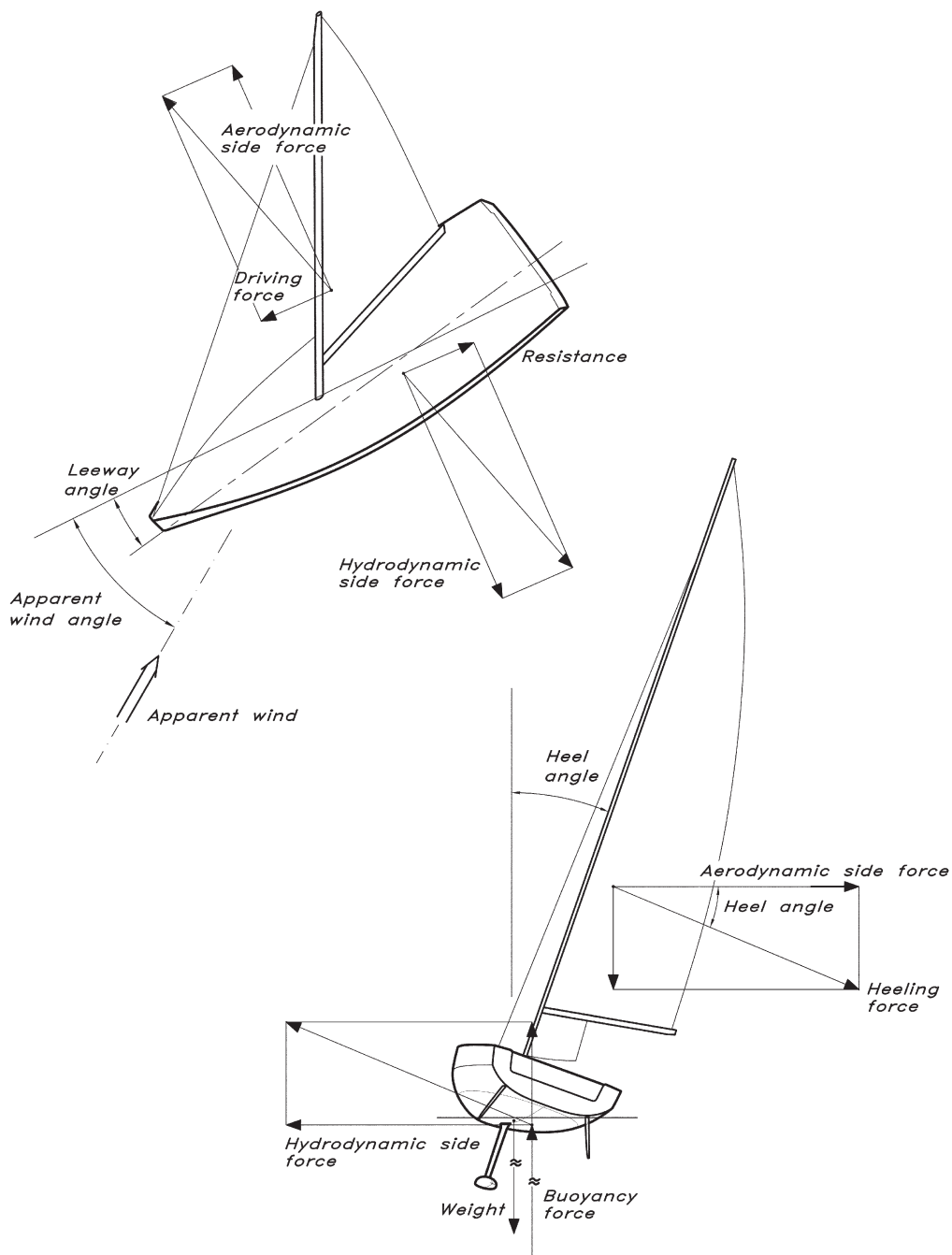
## ■ FORCES AND MOMENTS ON A SAILING YACHT

Fig 5.1 (overleaf) shows the different forces acting on a sailing yacht. In the plan view the horizontal components of the forces are displayed. When the hull is driven through the water a resistance is developed. Under equilibrium conditions, when the yacht is sailing at constant speed in a given direction, the resistance has to be balanced by a driving force from the sails. Unfortunately, this cannot be created without at the same time obtaining a side force, which in turn has to be balanced by a hydrodynamic side force. The latter is developed by the underwater body when sliding slightly sideways, i.e. when the yacht has a leeway angle. Since the turning moment under equilibrium conditions must be zero, the resulting hydro- and aerodynamic forces (in the horizontal plane) must act along the same line.

The view at the bottom of Fig 5.1 is along the direction of motion. It is seen that the resulting hydro- and aerodynamic forces are at right angles to the mast. This is not necessarily exactly true, but it is an approximation that is always made in sailing yacht theory. The heeling moment from the aerodynamic force is balanced by the righting moment from the buoyancy force and the weight.

In Fig 5.1 the apparent wind direction is marked by a fat arrow. This is not the true wind direction, since the wind felt onboard the yacht is influenced by its speed through the air. Fig 5.2 (page 67) illustrates the relations between the true and apparent wind speeds and directions, the so-called velocity triangle. Note that the wind created by the yacht speed (which must be used when adding the wind vectors) is opposite to the arrow shown as yacht speed in the figure.

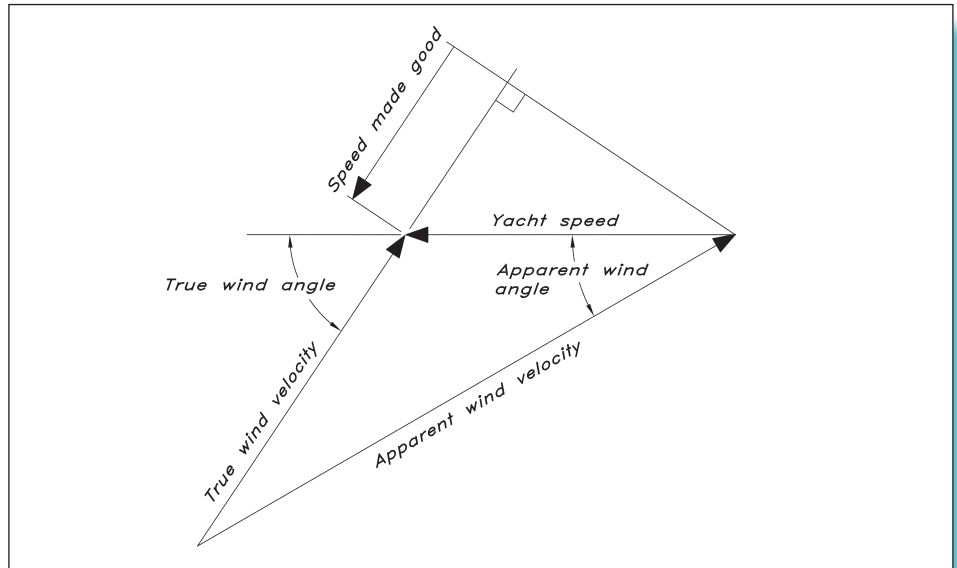
This chapter will deal mainly with the resistance force and its components, and how it can be minimized by proper design. The side force will be considered in the next chapter in connection with the discussion of keels and rudders, since these have primary responsibility for the side force production.



**Fig 5.1** Forces on a sailing yacht



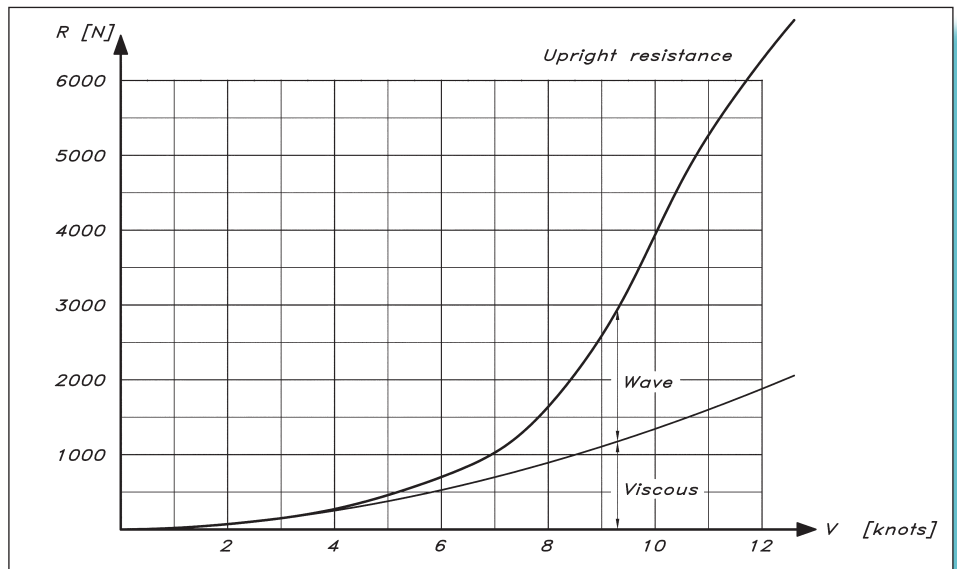
Fig 5.2 Velocity triangle



## RESISTANCE COMPONENTS

Fig 5.3 shows the resistance curve for the YD-41 if it were to be towed upright in smooth water. At low speeds the dominating component is the viscous resistance due to frictional forces between the hull and the water. The friction gives rise to eddies of different sizes, which contain energy left behind the hull in the wake. This component increases relatively slowly with speed, as opposed to the second component, the wave resistance, which occurs because the hull generates waves, transferring energy away. The sum of the viscous and wave resistance components is often referred to as the upright resistance.

Fig 5.3 Upright resistance  
– YD-41



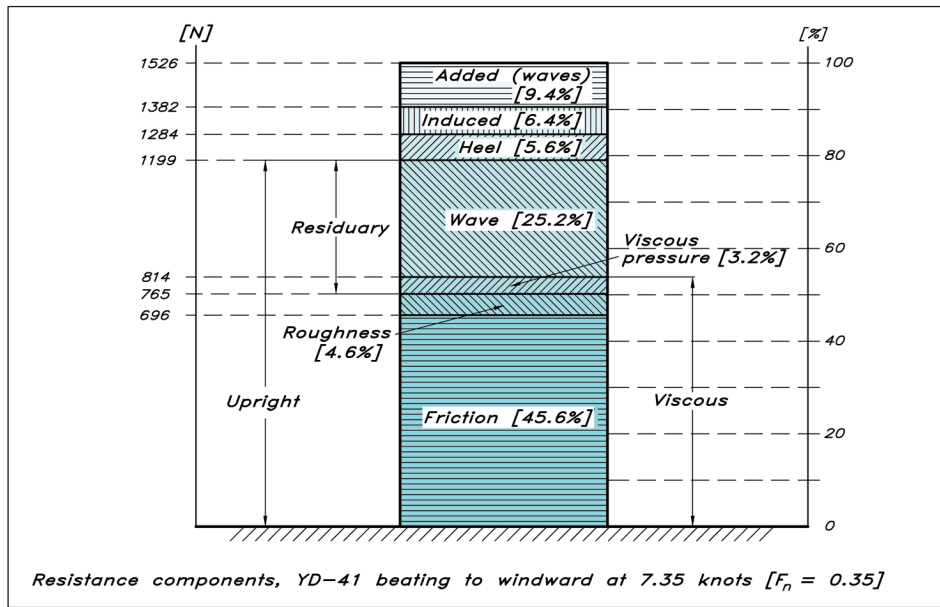


Fig 5.4 Breakdown of total resistance – YD-41

In a real sailing situation, the picture is more complicated, particularly upwind in a seaway. Fig 5.4 shows a breakdown of the total resistance of the YD-41 beating to windward offshore at 7.35 knots in a fresh breeze. The values of the resistance components are shown to the left as computed by the formulae to be given in this chapter. All components are also given as a percentage of the total force. We will refer extensively to this figure in the following discussion.

The viscous resistance has been subdivided into components, to be discussed later. As well as the viscous and wave components we have three new forces: heel, induced and added resistance. The heel resistance is the sum of the changes in the viscous and wave resistance due to heel. This component is introduced in sailing theory for convenience. Since methods for obtaining the two resistance components for upright hulls are well-established in ship hydrodynamics it is an advantage to consider the effects of heel separately.

The induced resistance is caused by the leeway. When the yacht is moving slightly sideways, water flows from the higher pressure on the leeward side, below the tip of the keel and rudder, and also below the bottom of the hull, to the lower pressure on the windward side. Longitudinal vortices are then created. Most sailors have probably seen the vortex from the keel tip at large heel angles. When the vortex gets close to the surface, air is sucked down into its centre, which makes it visible. The vortices contain rotational energy left behind the hull.

In a seaway all the calm water resistance components are increased, due to the unsteady motions of the yacht. However, it is an advantage to lump all the changes together into one component, called the added resistance in waves. This component is represented at the top of the bar in Fig 5.4.

To sum up, we have five major resistance components: viscous resistance, wave resistance, heel resistance, induced resistance and added resistance in waves. We will now discuss them in turn and show how they are affected by the shape of the hull.

## ■ VISCOUS RESISTANCE: BASIC CONCEPTS

Viscous resistance derives its name from the fact that it is the viscosity of the water that gives rise, directly or indirectly, to this resistance component. The water viscosity (kinematic), denoted  $\nu$ , depends on the water temperature. At 20°C it is  $1.0 \cdot 10^{-6} \text{ m}^2/\text{s}$ . We will use this value in the following discussion. Viscosities for other temperatures may be found in standard tables. For estimates of the viscous resistance the present value is good enough.

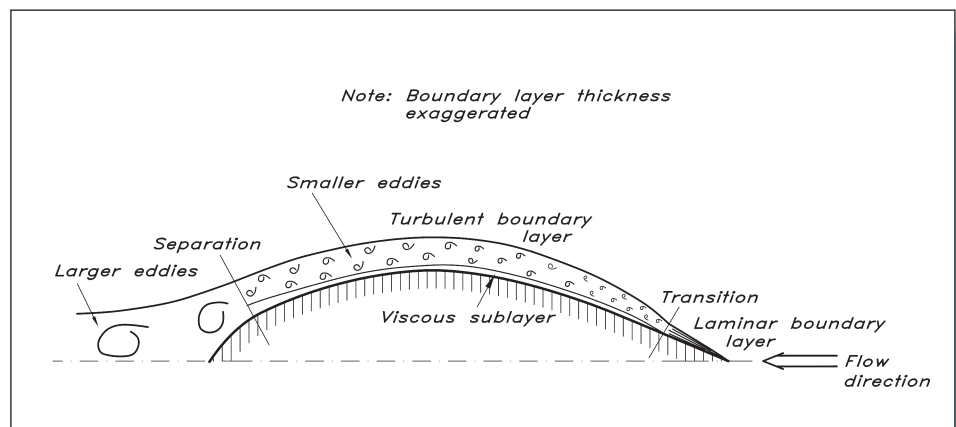
To understand the nature of viscous resistance certain concepts of fluid mechanics must be known. The most important ones from this perspective are explained in Fig 5.5.

Whoever has looked down the side of a ship moving in reasonably calm water must have seen that the water close to the hull is entrained and moves with the hull. It looks as if the water particles closest to the hull are stuck to the surface. This is in fact the case. The molecular forces between the hull and the water are strong enough to stop the relative motion in the innermost water layer. Viewed from the hull the water velocity increases gradually from zero at the surface to approximately the ship speed a certain distance away. The part of the flow within this distance, normally less than 1 m for a large ship, is called the boundary layer. On a smaller scale, the same phenomenon occurs with a sailing yacht. At the bow the boundary layer is very thin, but grows backwards, attaining a thickness of the order of 0.1 m near the stern. The boundary layer of Fig 5.5 is thus grossly exaggerated for clarity.

Near the bow the flow within the boundary layer is smooth. The velocity in one layer is slightly larger than in the layer just inside. This is the laminar part of the boundary layer. After a certain distance from the bow disturbances start to occur, and shortly thereafter the flow structure breaks down into a seemingly chaotic state: turbulence. The boundary layer is now characterized by eddies of different sizes and frequencies. The fluctuating velocities caused by the eddies are, however, considerably smaller than the mean velocity at all points in the boundary layer, so the flow is always moving backwards.

A special area can be distinguished in the inner part of the turbulent boundary layer. This area is extremely thin. If the total boundary layer thickness over the main part of the yacht is of the order of a few centimetres, the inner region, called the viscous sublayer, is of the order of 0.1 mm. Nevertheless, it plays quite an important role, particularly

**Fig 5.5** Different regions in the flow around the hull



in connection with surface roughness, as we will see. In the viscous sublayer the flow is mainly laminar, but it is sometimes disturbed by turbulent bursts, located at isolated spots, moving downstream with the flow.

The area where the flow changes from laminar to turbulent is called the transition region and is normally very short. In [Fig 5.5](#) it is marked as a point.

Close to the stern another flow phenomenon, called separation, may occur. If the stern is very full, the flow cannot follow the surface and bend inwards as rapidly as the hull. In fact, the flow closest to the surface stops and forces the flow further out to proceed in a direction more straight backwards. Large eddies develop, as indicated in the figure. It should be stressed that these eddies are much stronger than the ones in the turbulent boundary layer. The mean flow may now move forwards. While it is impossible in practice to avoid transition to turbulence in the boundary layer on a sailing yacht, separation should definitely be avoided, since it increases the resistance considerably. During one period of the IOR era, very uneven stern lines were used to 'cheat the rule', i.e. to reduce the rating, but the price paid was a slower yacht, and after some corrections had been introduced into the rule this type of stern disappeared.

The viscous resistance may be subdivided into three components: the direct friction on the smooth surface, the pressure imbalance between the fore and afterbodies due to the boundary layer, and the increase in friction due to surface roughness. We will now deal with these components individually.

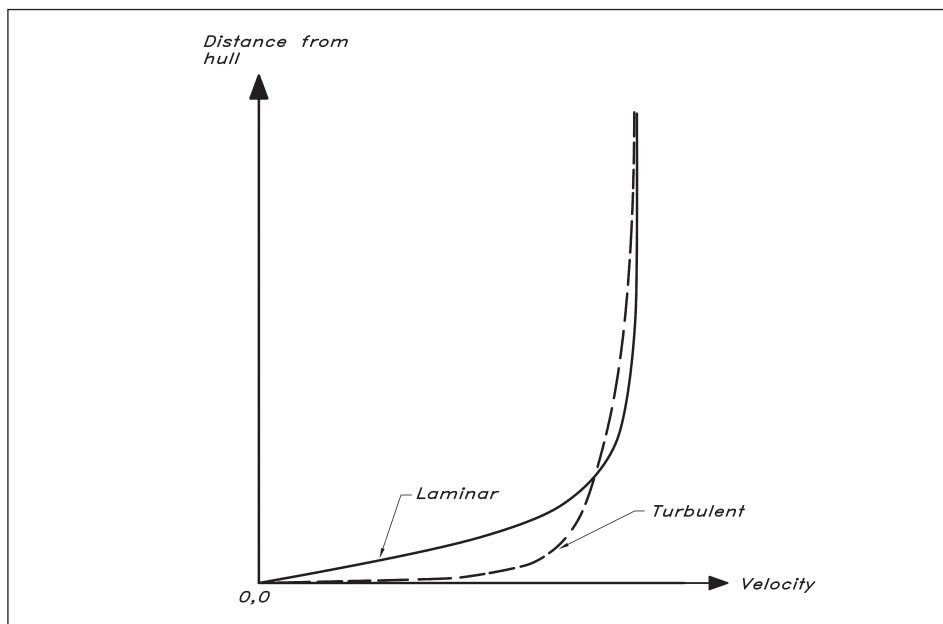
## ■ FRICTIONAL RESISTANCE

Having introduced some important concepts related to viscous resistance we are now ready to discuss the first and most important component, which is caused by direct friction between the water and the hull surface. Although the water does not slip along the surface, a resistance force is developed, because the layer of water closest to the hull is influenced by the next layer, which is moving backwards. This in turn is affected by another adjacent layer, and so on. The frictional force is in fact proportional to the rate at which the speed of water increases with the distance from the surface.

Some conclusions as to the frictional resistance may now be drawn. First, since the friction acts on the hull surface, minimizing the wetted surface area must be advantageous. When the fin keel was introduced in the 1960s, it produced a considerable reduction in the wetted surface, resulting in an increase of speed in these new designs. Secondly, since the velocity distribution in the laminar part of the boundary layer is different from that in the turbulent part, the friction is different. In the laminar case, the thin water layers affect each other only by molecular forces, which are relatively weak, while in the turbulent case adjacent layers are more strongly connected due to the 'stirring' effect of the eddies. Typical velocity distributions in the two types of boundary layers are shown in [Fig 5.6](#).

Since the velocity increases much more rapidly with the distance from the surface in the turbulent case, the friction is much larger. The laminar flow should thus be maintained as far back as possible. This effect is very important in the design of keels, rudders and

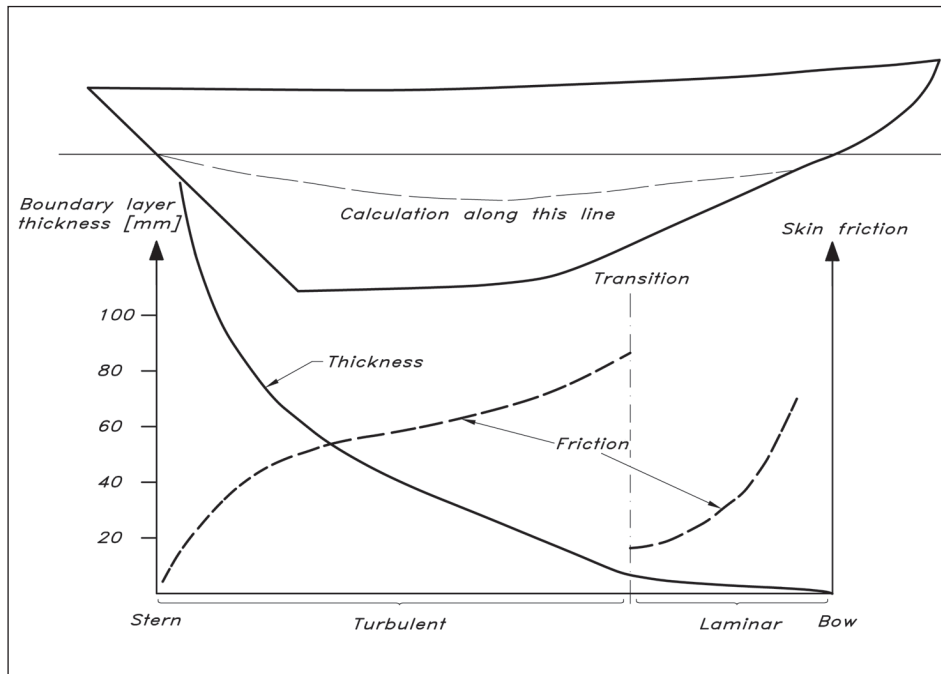
**Fig 5.6** Velocity distribution in the laminar and turbulent boundary layer



other appendices, like bulbs, where the shape can be chosen freely. However, many other effects have to be considered for the hull, so not much can be done in this respect. The technique employed in appendage design will be described in the next chapter. Here it suffices to say that straight lines on the forebody are likely to increase the laminar length, but in any case, the area covered by a laminar boundary layer will be only a small fraction of the total wetted surface of the hull.

As an example, the boundary layer and friction (often called skin friction) distributions on a 7.6 m traditional yacht, for which flow calculations have been made, are given in Fig 5.7 (overleaf). The quantities are given along one streamline from bow to stern. It may be seen that the boundary layer thickness increases slowly in the laminar part, but after transition the increase is much faster, particularly near the stern. The scale to the left in Fig 5.7 gives the thickness in mm. The friction drops rapidly in the laminar part to a very small value, but increases abruptly at transition. After transition it drops again to almost zero at the stern. This hull has a relatively long laminar part due to the straight hull lines on the forebody.

The data for Fig 5.7 was obtained by a computer program (SHIPFLOW), for the flow around ships and other bodies. This program, which will be described in Chapter 17, is used in advanced yacht design, mostly in connection with the America's Cup, but it is too complex and expensive for the amateur yacht designer. There are, however, simple formulae valid for flat plates, which can be used for estimates of the boundary layer thickness and skin friction. Like all quantities related to the viscous resistance they depend on a dimensionless number, called the Reynolds number,  $R_n$ . This is the product of the plate velocity  $V$  and length  $L$ , divided by the kinematic viscosity of the water  $\nu$ .  $R_n = V \cdot L / \nu$ . Fig 5.8 shows how the friction varies with the Reynolds number, and gives the relevant formulae for estimating the friction of the different parts of the underwater body.



**Fig 5.7** Boundary layer and skin friction distribution on a 7.6 m traditional yacht

Note that, when the friction of the hull is computed, only 70% of the waterline length is used for defining the Reynolds number. This is because water particles do not generally follow the entire length of the bottom. For instance, those hitting the hull near maximum beam will follow the hull only a short distance before leaving it for the wake behind the hull. Values within brackets in Fig 5.8 are for the YD-41.

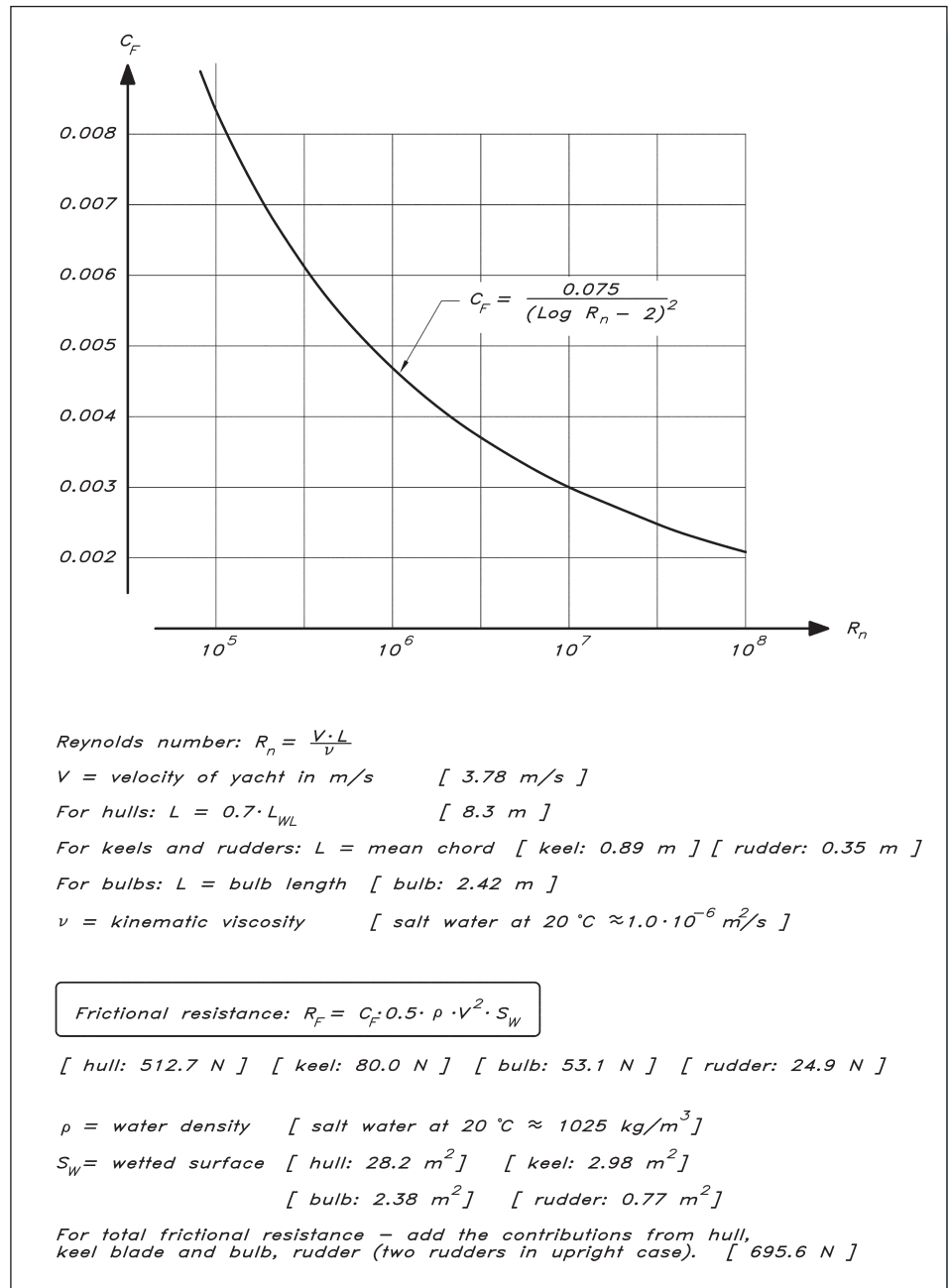
The diagram in the figure gives the total skin friction *coefficient*,  $C_F$ , which may be converted into the frictional resistance *force*  $R_F$ , using the formula inside the box. This way of representing forces by a coefficient  $C$  with an index is very common in fluid mechanics, and the force may always be obtained by multiplying by the so-called dynamic pressure  $0.5 \cdot \rho \cdot V^2$  and a representative area, here normally the wetted surface  $S_W$ .

The values computed for the YD-41 are at 3.78 m/s, or 7.35 knots, the same speed as in Fig 5.4. By adding the contributions from the hull, keel, rudder and bulb, the total friction is obtained as 696 N, also given in the bar of Fig 5.4.

## ■ VISCOUS PRESSURE RESISTANCE

Fig 5.9 (page 74) shows a typical pressure distribution on the hull at a given depth, i.e. along a certain waterline. It is seen that the bow and stern pressures are higher than in the undisturbed water at this depth, while the pressure in the middle part of the hull is lower. Had there been no boundary layer, the pressure forces over the bow would have balanced those over the stern exactly and there would have been no resulting force (neglecting for a moment the effect of the waves, which also have an influence on the pressure). The boundary layer does, however, modify the pressure distribution, and, since the layer is

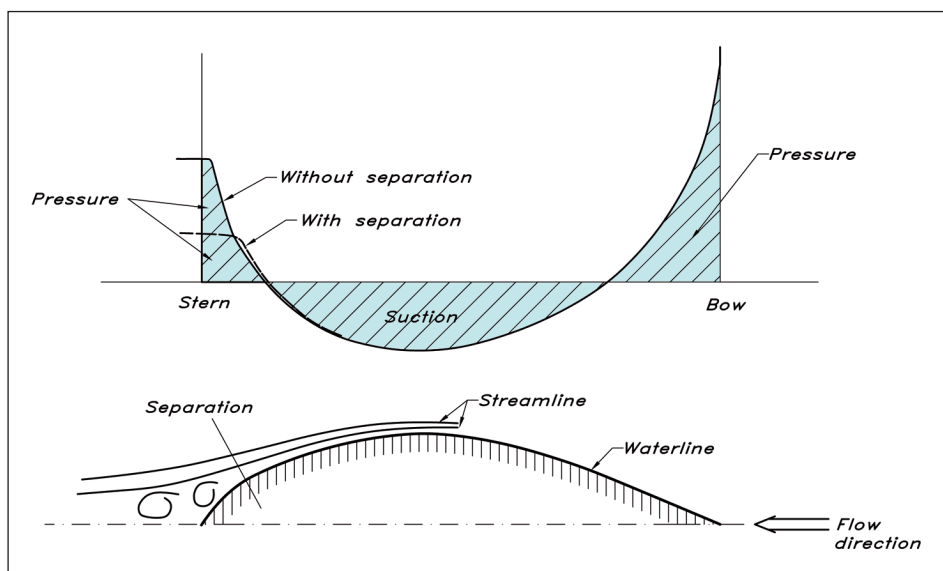
**Fig 5.8** Calculation of frictional resistance



considerably thicker around the stern than at the bow, the stern pressure is affected most. A slightly lower pressure is found at the stern, giving rise to the resistance component, which is indirectly caused by friction, through the boundary layer. For a sailing yacht it is in the range 5–10% of the direct frictional force.

The pressure resistance just described is unavoidable, but it can be minimized by proper design of the stern. Thus, the blunter the stern the larger the pressure drop. As long as separation is avoided the effects are small, but if the flow separates a large reduction in





**Fig 5.9** Pressure distribution with and without separation

pressure will occur, and the pressure resistance may be considerably larger than the 5–10% mentioned. When judging the bluntness of the stern, the shape of the diagonals should be studied, since these are closer to the flow direction than the waterlines. Maximum slopes of the diagonals have been suggested in the literature, but the values vary considerably between the different authors, ranging from about 22° to about 30°. Most likely the upper limit is too high, and to be safe it is better not to exceed the lower value.

It should be pointed out that the viscous pressure resistance is influenced by the prismatic coefficient and the location of the longitudinal centre of buoyancy. The larger the  $C_p$  the fuller the ends of the hull, and the more aft the position of the LCB the fuller the stern. In order to minimize the viscous resistance the hull should have a shape like a cod, but very slender. The  $C_p$  should be less than 0.5 and the LCB should be positioned in front of the midship section. This would be a good design were it not for the wave resistance. As will be seen later, bluff forebodies tend to increase the waves, while in fact bluff afterbodies tend to decrease them. A thick stern boundary layer (on a bluff afterbody) makes the hull appear longer than it really is, and this effect is even more pronounced if separation occurs. Some designers have therefore produced very bluff sterns with some separation, just to decrease the wave resistance. This is not likely to pay off, however, unless there are important gains, from a measuring point of view in a rating rule.

Obviously, the stern design, as well as  $C_p$  and LCB, must be optimized considering the speed for which the yacht is designed (i.e. for which wind conditions it is optimized). The higher the speed the more important the wave resistance and the bluffer the stern. Optimum values of  $C_p$  and LCB will be given later, in the discussion of wave resistance.

While the frictional resistance is set mainly by the wetted surface, the viscous pressure resistance depends on the shape of the hull. This is also the case for the wave resistance, and both appear due to pressure imbalances, so it is very common to lump both together into one component: the residuary resistance. We will not give any formulae here for the viscous pressure resistance itself, but will follow general practice and give the formula only

for the residuary resistance. This will be presented later. In Fig 5.4 we have assumed that the viscous pressure resistance is 7% of the friction, based on CFD computations.

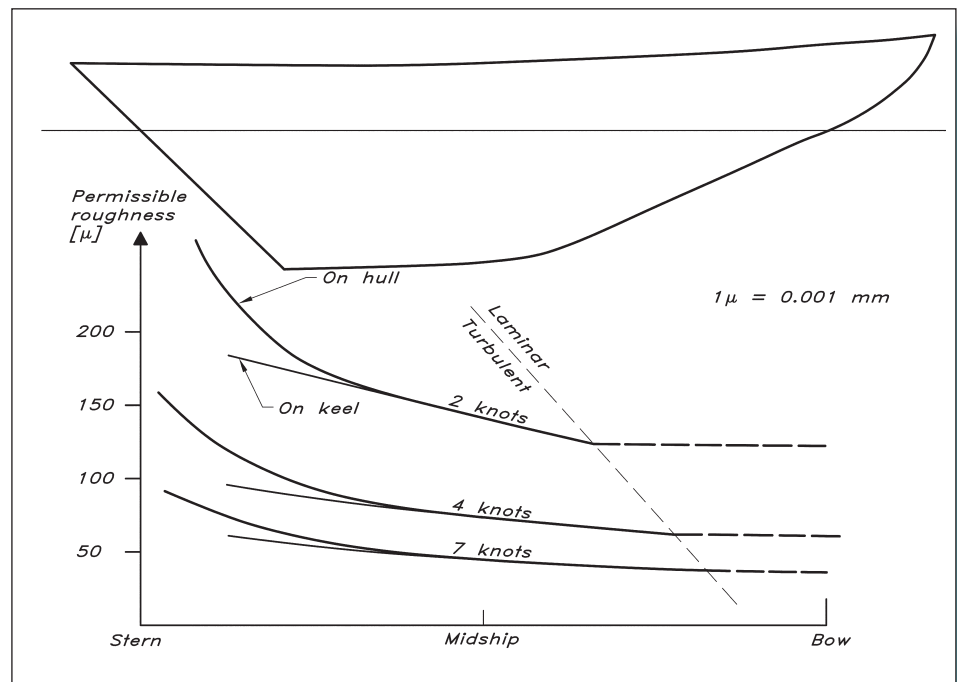
Note that the discussion above also holds for the appendages. Due to the boundary layer displacement effect, the pressure near the trailing edge becomes lower than that without a boundary layer and a pressure drag is generated. Its magnitude depends on the shape of the section, as for the hull. This will be further discussed in Chapter 6. The viscous pressure resistance in Fig 5.4 includes contributions both from the hull and the appendages.

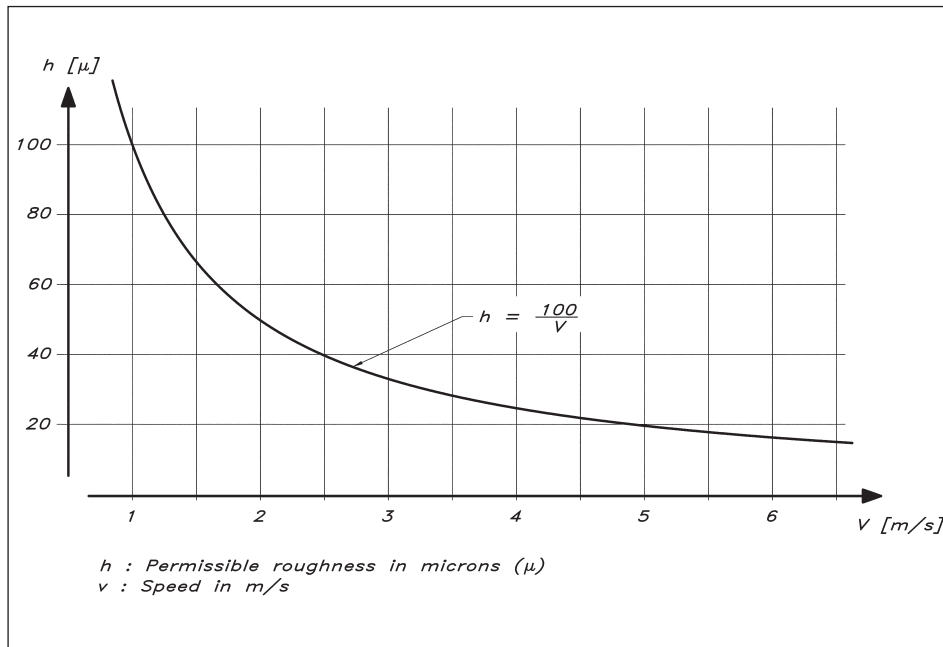
## ROUGHNESS

The third component of viscous resistance, due to surface roughness, might not be too important from a design point of view, but it is certainly of interest for the practising yachtsman and should, therefore, be discussed.

According to a large number of experiments with flows over rough surfaces, the effect of roughness disappears if the roughness elements are embedded in the viscous sublayer, introduced above. There is thus a limit, below which the surface may be considered smooth from a resistance point of view: ‘hydraulically smooth’ in fluid mechanics terminology. We have already noted that the thickness of the viscous sublayer is very small, normally of the order of 0.1 mm. Let us look at this in more detail, using the boundary layer calculation for the 7.6 m traditional yacht as an example. In Fig 5.10 the thickness of the viscous sublayer, i.e. the permissible roughness height, is given for three different speeds. One branch of the curves represents the hull, while the other is for the

**Fig 5.10** Permissible roughness – traditional yacht





**Fig 5.11** Estimation of permissible roughness at different speeds

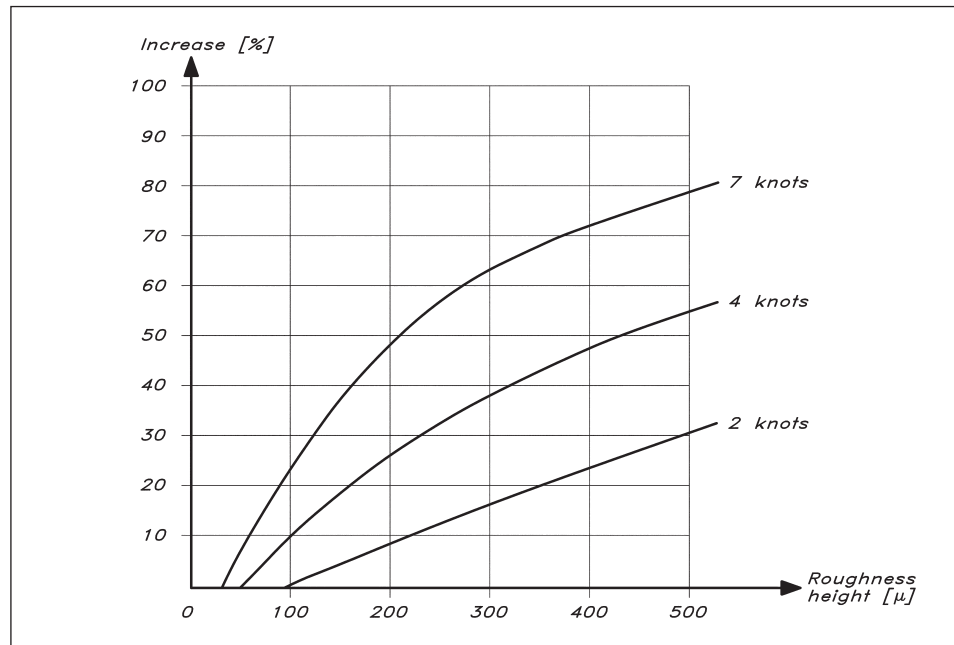
keel. At the forward end of the hull the boundary layer is laminar and, although the theories for this part are less well developed, it is safe to assume, as has been done in the figure, that the permissible roughness in this region is the same as in the most forward part of the turbulent boundary layer.

Several observations may be made concerning Fig 5.10. First, there is a strong dependence on speed. Second, there is an increase in the permissible roughness aftwards. Third, the increase is not as large on the keel as on the hull near the stern. We may also note that the most strict requirement is 0.03 mm, or 30  $\mu$ m for the highest speed on the forward half of the hull. To get a feeling for this small value we may note that a sandpaper of number 400 has a grain size of 25  $\mu$ m. This does not mean that the surface should be sanded with this paper. A considerably rougher one would yield the required smoothness, since the grooves left after the paper are much smaller than the grains.

There is a very simple relation which can be used for estimating the permissible roughness on the forward part of the hull. This relation is given in numerical and graphical form in Fig 5.11. Note that the roughness is given in microns and that it is inversely proportional to the speed.

An appropriate question now is how much the viscous resistance is increased if the requirement for a hydraulically smooth surface is not met. To answer this, we may return again to the calculations for the traditional yacht. In Fig 5.12 the increase in viscous resistance for varying roughness heights and speeds is given. It is seen that the increase is considerable, particularly at higher speeds. Fig 5.12 was computed based on measurements for flat plates, where the surface was densely covered with sand grains. This is not the case for a sailing yacht, so the values given must be considered as an upper limit. In any case, it is obvious that roughness heights above the limit for a hydraulically smooth surface cannot be tolerated for racing yachts. It should be pointed out that barnacle growth results

**Fig 5.12** Increase in viscous resistance due to roughness – traditional yacht



in much larger increases in resistance than indicated here. Two or even threefold increases in the viscous resistance have been noted for densely packed barnacles, several millimetres in height. See for instance, Leer-Andersen and Larsson (2003).

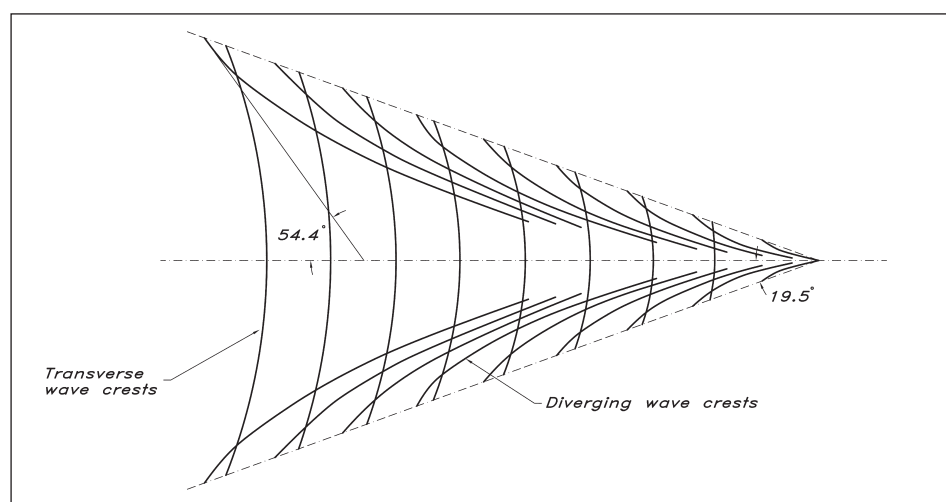
The YD-41 has a maximum speed of about 13 knots, i.e. about 6.5 m/s. According to Fig 5.11 the permissible roughness is then about 15μ. Normally, a brush-painted surface has grooves 50–100μ in height, so there is a significant resistance increase as compared to the hydraulically smooth surface. In Fig 5.4 the roughness component is 10% of the friction and the speed is 7.35 knots. This is reasonable, judging from Fig 5.12, where the 7-knot curve yields 8–23% increase for heights between 50 and 100μ. As pointed out above this is probably somewhat high for normal roughness types. The fact that the curves of the figure are for a different hull is not too important, since the speed is the most significant factor.

Roughness on appendages will be dealt with in Chapter 6. Since many foil sections are designed for laminar flow, which may be destabilized by roughness, the smoothness requirements are considerably stricter than on the hull, at least up to the point of maximum thickness of the foil.

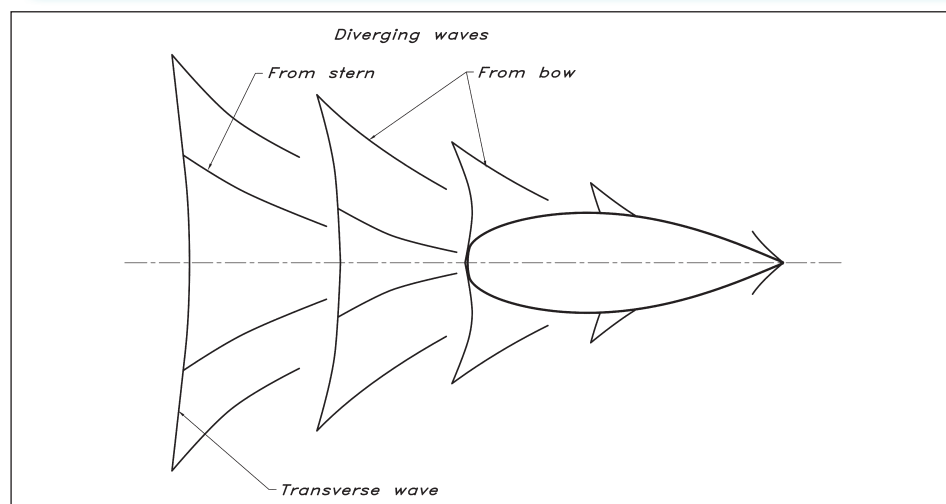
## ■ WAVE RESISTANCE: BASIC CONCEPTS

We will now turn to the second major resistance component of Fig 5.4: wave resistance. Like viscous resistance it could be split into subcomponents, but they are of interest only under certain conditions, for instance when the bow wave breaks or is transformed into spray. We will neglect these phenomena here. As in the case of viscous resistance we will start by introducing some basic concepts.

If one throws a stone into a pond, circular, concentric waves originate from the point where the stone hits the surface. If one were to throw several stones in a row along a straight line the circular waves would interfere with one another and create a wave system very similar to that far behind a yacht. This is a system with well-defined properties, called the Kelvin wave system, and is due to a travelling point disturbance on the water surface. The same system is found far behind large ships, and in fact behind all objects moving along the surface. The reason why the same system is created is that if the waves have travelled a sufficiently large distance, and occupy a large area compared to the dimensions of the object, the latter may always be considered as a point. For instance, if a ship moving in calm water is viewed from an aircraft, the ship itself is very small as compared with the area covered by the wave system, and the latter has the typical Kelvin structure. Fig 5.13 is an illustration of this phenomenon. It may be seen that two types of waves exist: diverging waves moving sideways and transverse waves at right angles to the direction of motion, moving with the ship.

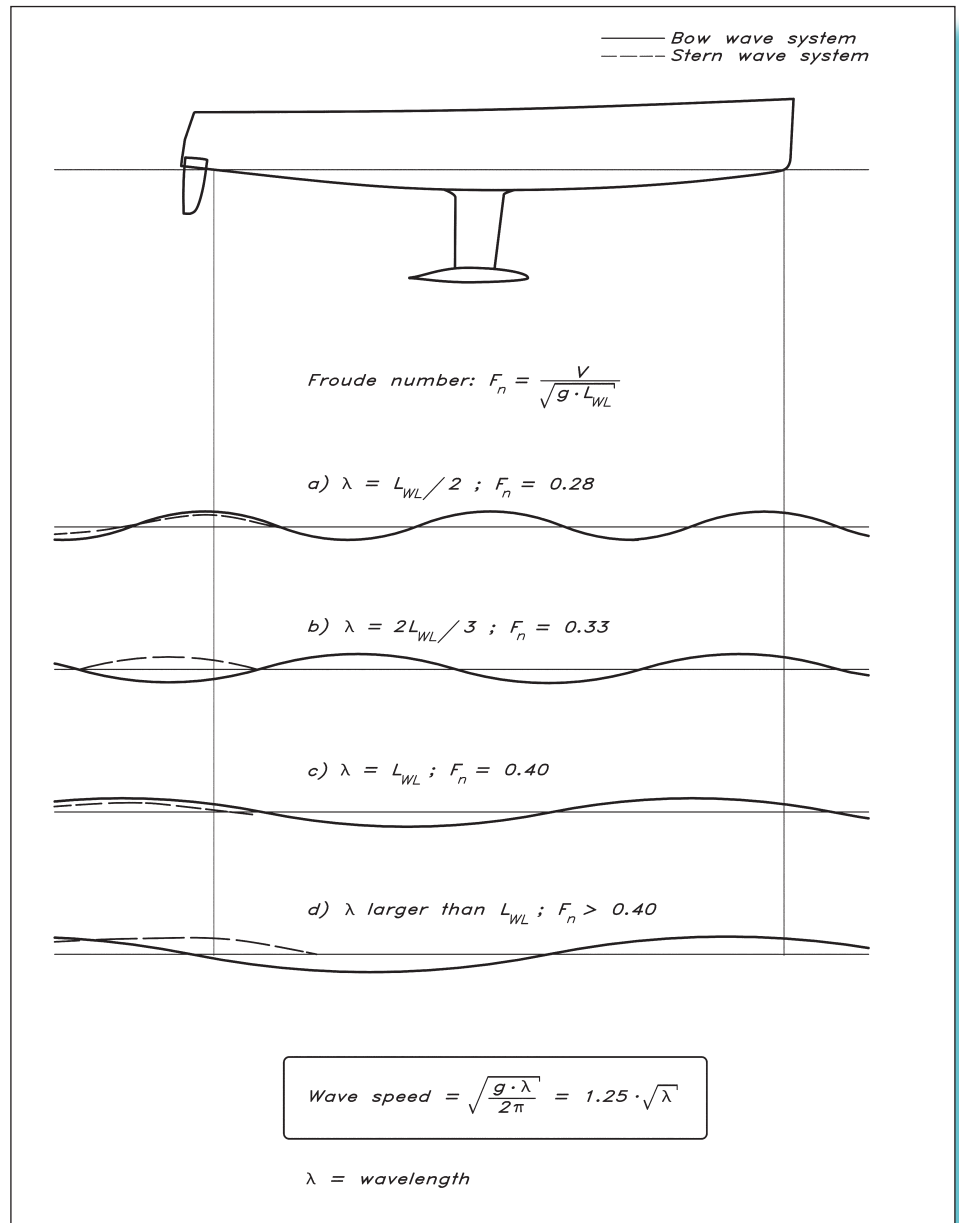


**Fig 5.13** The Kelvin wave system



**Fig 5.14** Local bow and stern wave systems

**Fig 5.15** Interference between the bow and stern waves



Locally, the situation is quite different, and the waves are highly dependent on the shape of the hull. Within distances of a few hull lengths, waves from all points on the hull surface will in theory contribute to the wave system. Some points are, however, more important than others, since the disturbance is larger. For a sailing yacht the high-pressure regions at the bow and stern are dominant, and it is usually assumed that only two wave systems exist (see Fig 5.14).

There is a very simple relation between wavelength and travelling speed for surface waves. As can be seen in Fig 5.15 the speed is equal to 1.25 times the square root of the length. For example, a 7 m long wave will have a speed of 3.3 m/s.

Since the wave system travels with the yacht, at the same speed in the longitudinal direction, the length of the generated waves will depend on the yacht speed. If, for instance, the speed is 1.25 times the square root of the waterline length, the length of the wave is the same as the waterline length. A yacht with an  $L_{WL}$  of 7 m will thus have one wave crest at the bow and the next one at the stern if the speed is 3.3 m/s.

The speed dependence of the waves gives rise to an important phenomenon: interference. An illustration of this is given in Fig 5.15. If the wave crests from the bow system coincide with those from the stern, large waves will be created. On the other hand, if the bow wave crests coincide with troughs in the stern waves, the result is an attenuated wave. The first case is illustrated in (a) and (c), where the wavelength is half and equal to the waterline length, respectively. In (b) the wavelength is  $\frac{2}{3}$  of  $L_{WL}$ , and the waves are attenuated. In the last figure (d) the wavelength is larger than the  $L_{WL}$ . The second wave crest then occurs aft of the stern, which, when the speed increases, will move into a trough, giving the hull a large trim angle.

In each of the cases (a–d) a quantity  $F_n$  is given. This is the so-called Froude number, which plays a similar role for the wave resistance as the Reynolds number does for viscous resistance. The Froude number is a dimensionless speed, where the velocity in metres per second is divided by the square root of the waterline length times the acceleration of gravity (see Fig 5.15). It is the Froude number that determines how many waves there are along the hull. For instance, at  $F_n = 0.40$  there is one wave, at 0.28 there are two, etc. The properties of the wave resistance curve are highly dependent on the Froude number, as we will see below. The Froude number is therefore a very important quantity and we use it extensively in the following discussion, rather than velocity in knots or metres per second. Using the simple definition, the Froude number can always be converted easily into these dimensional quantities.

Since the wave resistance occurs because energy is transported away in the waves, the amplification and attenuation due to interference between the wave systems must have some effect on the wave resistance curve. Thus, at speeds where there is an amplification of the waves the resistance must be relatively large, while the opposite must be true at speeds where there is an attenuation. The wave resistance curve thus exhibits what is normally referred to as humps and hollows (see Fig 5.16). It may be assumed that wave resistance increases with speed to the sixth power, but in addition there are the fluctuations due to interference.

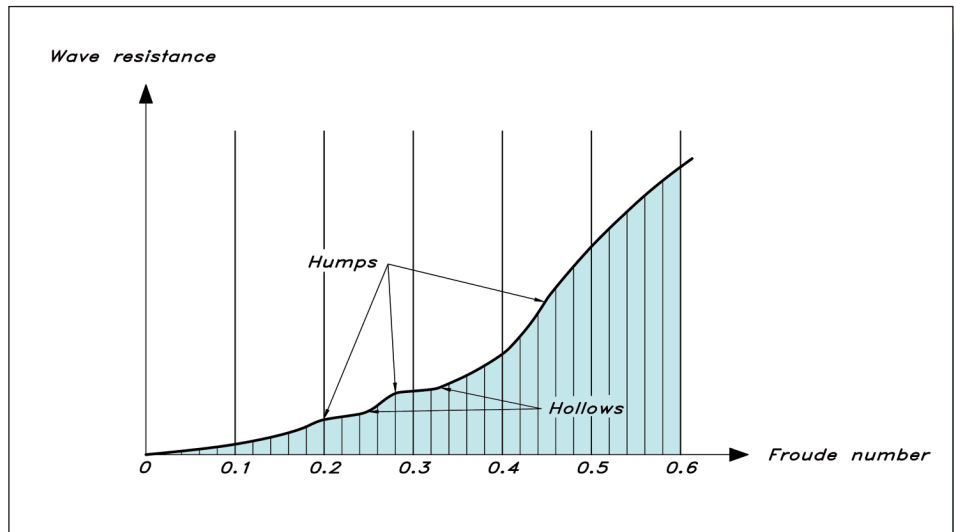
Humps and hollows may be more or less pronounced, depending on the hull shape. For many sailing yachts they are very small in the lower speed range, but the last hump is still important. The slope of the curve gets very large just below this speed and to get over the hump is difficult. If this can be achieved, however, the increase in resistance becomes more gradual, and the hull enters the semi-planing speed range.

Catamarans and extremely light canoes and dinghies may accomplish this even beating to windward, while the lightest displacement hulls enter the semi-planing range in the downwind legs. Most displacement hulls cannot, however, pass the barrier at the last hump.

According to the discussion above, the largest hump in the resistance curve should occur when the wavelength is equal to the waterline length, at  $F_n = 0.40$ , but in practice it



**Fig 5.16** Humps and hollows on the wave resistance curve



occurs at a higher Froude number, i.e. at a higher speed. This is because the overhangs at the bow and stern cause the distance between the bow and stern waves to be larger than the nominal waterline length. The last hump thus occurs normally at a Froude number of about 0.5. Heavy displacement hulls cannot reach this value, except under special conditions, as when sailing in heavy following seas. The YD-41 is, however, very light and can reach a Froude number of 0.6, corresponding to 6.5 m/s or 13 knots.

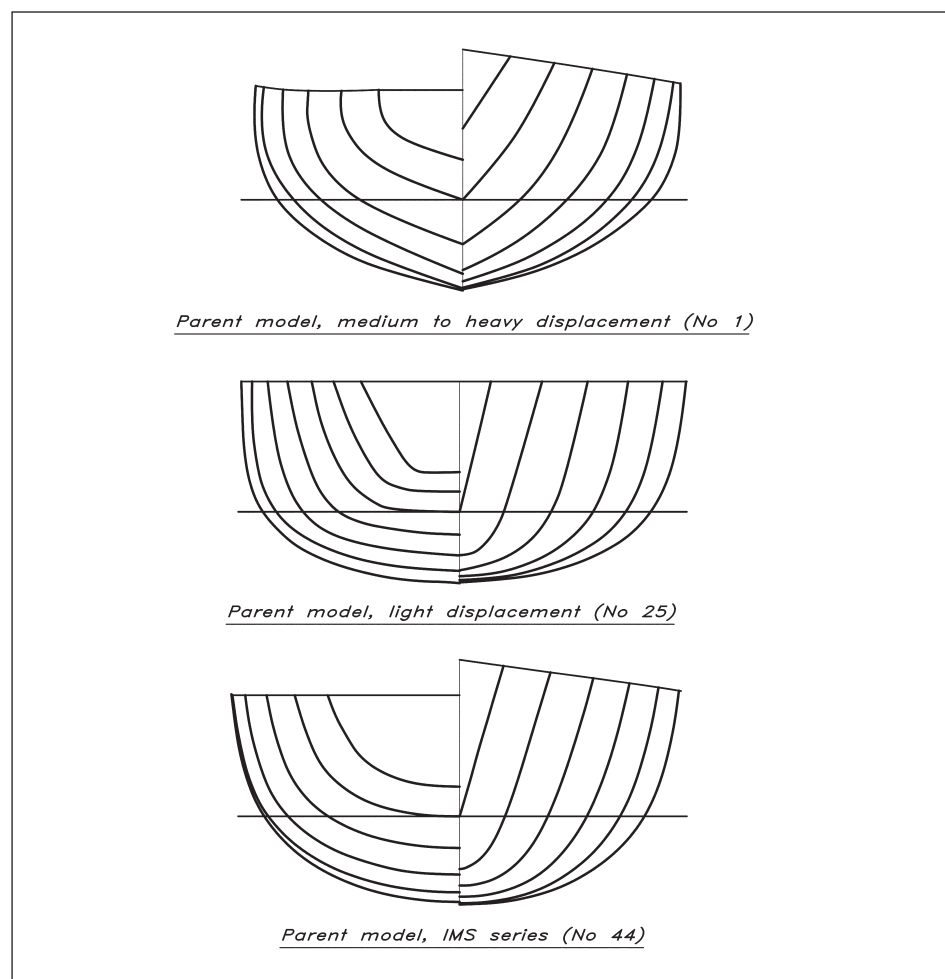
It should be mentioned that in most literature on sailing theory an older quantity, the so-called 'speed length ratio', is used instead of the Froude number. This is defined as the speed in knots, divided by the square root of the waterline length in feet. In fact it differs only by a constant from the Froude number, but its disadvantages are that it is not dimensionless and that it is not based on metric quantities. Conversion between the two numbers can be made easily using the formula: Froude number =  $0.30 \cdot [\text{speed length ratio}]$ .

## ■ WAVE AND RESIDUARY RESISTANCE

Very extensive series of tests with models of sailing yachts have been carried out at Delft University of Technology over a period of 40 years. The first series was initiated by Professor J Gerritsma in 1973 and it has been followed by several new series. Over the years, many scientists have been engaged in testing but the main supervisor succeeding Professor Gerritsma has been Dr J A Keuning. The Delft series has had a large impact on sailing yacht performance prediction methods and is used as the main source of empirical relations, for instance in the Offshore Racing Congress (ORC) Velocity Prediction Program (VPP) for sailing yacht handicap calculations. A survey of the Delft series data up to the late 1990s is given in Keuning and Sonnenberg (1998). The most recent update of the formula for residuary resistance is presented in Keuning and Katgert (2008).

The first series comprised 22 models with a systematic variation of five different hull parameters:  $L_{WL}/B_{WL}$ ,  $B_{WL}/T_c$ ,  $C_p$ , LCB and  $L_{WL}/(\nabla)^{1/3}$ . All hulls were derived from a Frans Maas designed parent model, a medium displacement, contemporary ocean racer. Its body plan is shown in Fig 5.17 (top). During the 1980s it became apparent, however, that an extension of the series to lighter displacements was required, and a new parent model was designed by van de Stadt Design in 1983, see Fig 5.17 (middle). This model was number 25 in the second series of hulls comprising models 23–28. The third series was an extension of the second one with models 29–40, based on the same parent hull, but with special emphasis on very light displacement and higher  $L_{WL}/B_{WL}$ . Finally, a new parent model was designed by Sparkman and Stephens in 1995, Fig 5.17 (bottom). It was developed as an average IMS design especially for research purposes and was given number 44. The fourth series comprised models 41–50. After that a small series of three yachts with different midship sections were added (models 60–62) together with another three hull series (models 71–73) with larger L/B, relevant for maxi yachts.

In Table 5.1 the full range of variations in the eight different parameters now used for resistance predictions is given. The loading factor, defined as  $\nabla_c^{2/3}/A_W$  – i.e. the ratio of



**Fig 5.17** Body plans of the Delft parent models

the  $\frac{2}{3}$  power of the displacement and the waterline area – is of interest at higher speeds, where hydrodynamic lift forces come into play (see [Chapter 11](#)). The formulae presented below approximate the experimental data quite well within the limits of the variations. It is strongly recommended not to use the formulae outside the limits, since extrapolation may lead to considerable errors.

Table 5.1 Range of hull form parameters in the Delft series	
$LCB_{fpp}/L_{WL}$	0.500–0.582
$C_p$	0.519–0.599
$\nabla_c^{2/3}/A_W$	0.079–0.265
$B_{WL}/L_{WL}$	0.170–0.366
$LCB_{fpp}/LCF_{fpp}$	0.920–1.002
$\nabla_c^{1/3}/L_{WL}$	0.12–0.23
$C_M$	0.646–0.790
$B_{WL}/T_c$	2.46–19.38
(LCB <sub>fpp</sub> and LCF <sub>fpp</sub> measured from FP)	

From the Delft series several important empirical relations were derived. The formula for the wetted surface was presented in [Fig 4.2](#). Now, however, we are concerned with resistance. Rather than presenting the wave resistance separately the scientists chose to give the sum of the wave and viscous pressure resistance, i.e. the residuary resistance. Since the hulls were smooth the only component missing in the total upright resistance is the friction (see [Fig 5.4](#)). As mentioned above, there is a good reason for lumping together the wave and viscous pressure resistance, since they are both dependent on the three-dimensional shape of the hull. When optimizing the hull for a certain speed, the combined effect on the wave and viscous pressure components must be considered.

The residuary resistance of the canoe body  $R_{Rc}$ , based on a statistical analysis of all hulls, may be computed from the formula of [Fig 5.18](#), which gives the resistance for one specific Froude number. The resistance is divided by the gravity force, i.e. the mass of the yacht multiplied by the acceleration of gravity. Varying the coefficients a0–a7, given in the table, Froude numbers ranging from 0.15 to 0.75 may be computed. The position of the longitudinal centre of buoyancy, LCB, and the longitudinal centre of flotation, LCF, should be given in metres measured from the forward perpendicular (section 0 in [Fig 3.5](#)).

It has long been known that the keel may contribute to the wave generation, and to test the influence on the residuary resistance of the keel several series of tests were carried out in Delft. As a result, the formula of [Fig 5.19](#) was derived. Like for the canoe body residuary resistance, the formula includes both wave resistance and viscous pressure resistance. Most likely, the accuracy of this relation is lower than that of the hull, due to the limited number of tests, but on the other hand the quantity computed is relatively small and has thus only a small effect on the total resistance. The formula contains the

draft/beam ratio of the hull, the volumes of the hull and the keel, and the vertical position of the keel centre of buoyancy. As in Fig 5.18, the formula holds for one Froude number with a given set of coefficients. In the table coefficients are given for Froude numbers in the range 0.20–0.60. At lower speeds the contribution is negligible. No information is available for the speed range up to 0.75. The formula was derived for keels without bulbs, but, lacking data for bulbous keels, it may be applied also to such keels. This has been done for the YD-41.

The interested reader may program the formulae and use the coefficients of the tables to compute the residuary resistance of yachts of varying shapes. An accurate and effective optimization of a design may then be carried out, by investigating different alternatives. This approach is more quantitative than the traditional one, where the designer has to rely on experience and rules of thumb.

In the following we shall draw some general conclusions on the influence of the hull shape on the residuary resistance.

### ◆ Displacement

In the formula of Fig 5.18 the residuary resistance is expressed as a fraction of the hull weight. This fraction is in the range 0–10% for hull speeds of practical interest. As an example, the resistance curves for the first parent models of Fig 5.17 are shown in

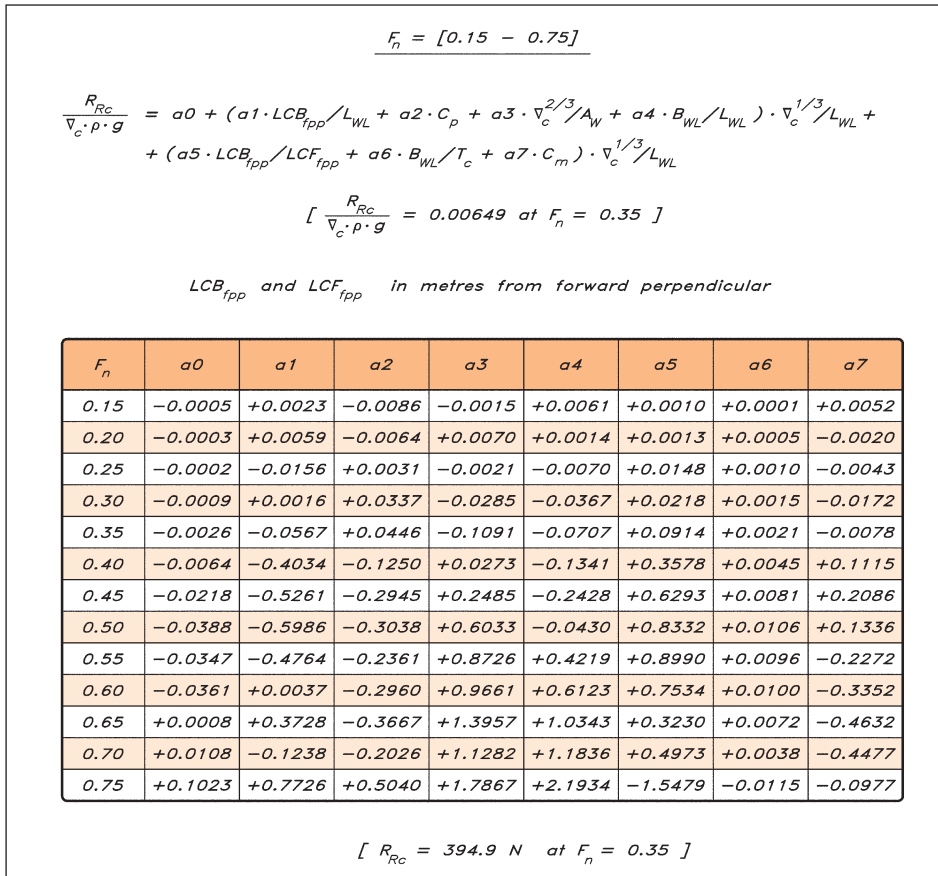


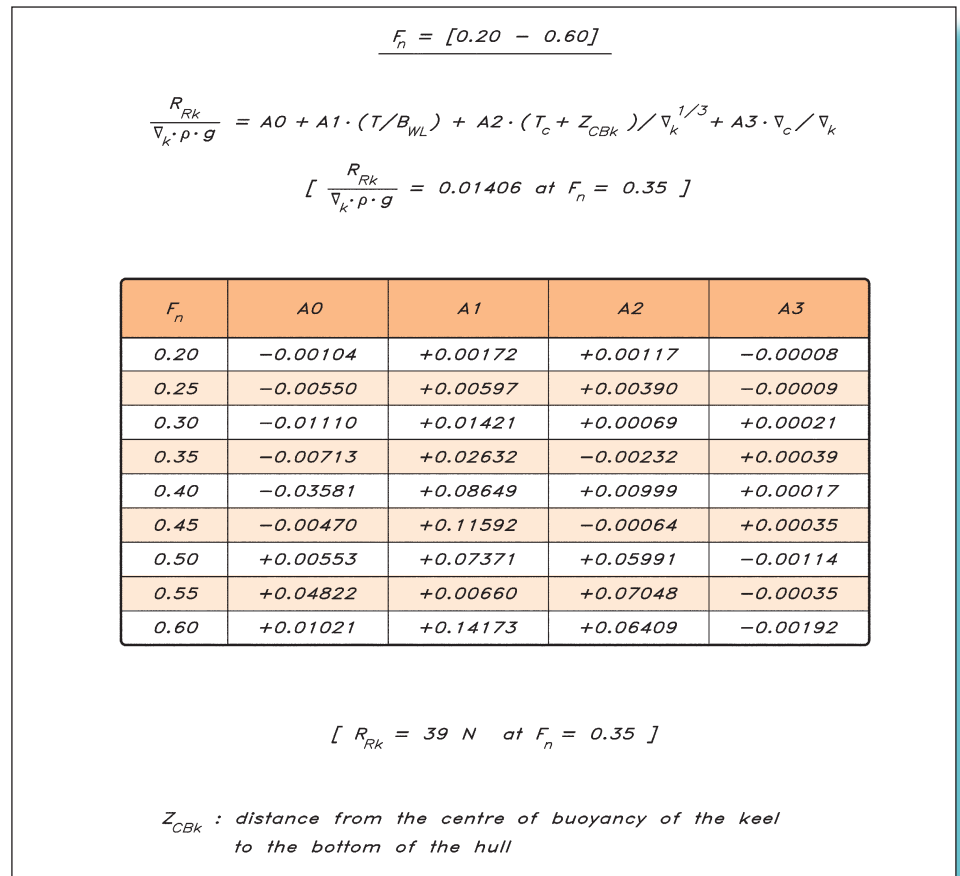
Fig 5.18 Residuary resistance of the hull

Fig 5.20 (page 87). These hulls are typical representatives of the medium/high displacement series (models 1–22) and the light displacement series (23–39), respectively. The resistance as a fraction of hull weight (top figure) is very similar up to a Froude number of around 0.4, but thereafter the curve for model 1 bends upwards, while that of model 25 exhibits an inflection after which the slope is reduced.

A quite different picture is seen in the bottom part of Fig 5.20, which shows the residuary resistance in Newtons for the two hulls at full scale, assuming an  $L_{WL}$  of 10 m. The displacement of hull no. 1 is 9.18 tons, while that of no. 25 is only 4.62 tons, so there is approximately a factor of two between the heavy and the light hull displacements. This is reflected in an approximately equally large difference in resistance for the low-speed range. Due to the very sharp increase in resistance for the heavy hull above  $F_n = 0.45$  this yacht will not reach higher Froude numbers than that, while the light hull can reach 0.60 or higher, since the slope of the curve is small.

From Fig 5.20 we learn that the displacement is a very important parameter for the residuary resistance. In the displacement speed range, up to about  $F_n = 0.45$ , the resistance is roughly proportional to the displacement. At a certain Froude number, the residuary resistance is more or less the same, expressed as a fraction of the displacement, regardless of the shape of the yacht, i.e. whether it is small or large, light or heavy, narrow or beamy, etc. For example, at  $F_n = 0.3$  the residuary resistance is normally 0.3–0.4% of the hull

**Fig 5.19** Residuary resistance of the keel



weight, at  $F_n = 0.35$  0.7–0.8%, at 0.40 2.0–2.5% and at 0.45 4.5–5.5%. Note that the resistance is given versus Froude number. If yachts of different sizes are compared the larger yacht will have a larger speed at the Froude number in question.

While the displacement, or hull weight, rather, is the major factor determining the residuary resistance, the form parameters of Fig 5.18 may change the resistance within the limits given above for a given displacement. Variations of 10–20% in the residuary resistance may thus occur due to changes in these form parameters, and at least three of them ( $\nabla_c^{1/3}/L_{WL}$ ,  $C_p$  and LCB) need to be considered if the hull is to be optimized. In the following discussion we will consider  $B_{WL}/L_{WL}$  and  $B_{WL}/T_c$  also.

### ◆ Length/displacement ratio

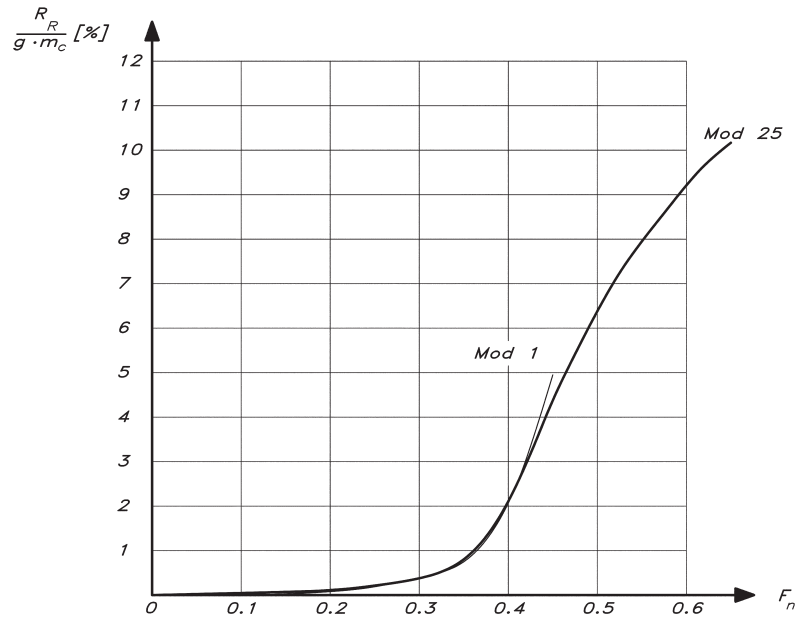
The inverse of  $\nabla_c^{1/3}/L_{WL}$  (i.e.  $L_{WL}/\nabla_c^{1/3}$ ) is called length/displacement ratio and has a somewhat unfavourable effect on the resistance per unit weight in the low-speed range. It is barely visible in Fig 5.20(a) due to the limited resolution, but the lighter hull with a larger length/displacement ratio has a slightly larger resistance per kg of displacement in this speed range. However, the major effect is in the high-speed range, which can only be reached if the length/displacement ratio is large enough. Exactly how large the ratio has to be is impossible to say, since the other parameters, as well as section shape, stability, etc. also play a role. However, values around 5.7 are often quoted in the literature. Hulls with lower values are likely to run into the ‘barrier’ at around  $F_n = 0.45$ , while those with a larger ratio may pass the hump and reach higher speeds. The larger the ratio the higher the speed possible. The YD–41 has a ratio of 6.5, which is an unusually high value for a production yacht, and it may reach Froude numbers around 0.6, as mentioned above. Racing dinghies like the 5-0-5 reach values up to 7.5, but it is difficult to beat the International Canoe with a value of 8.8. Further information on length/displacement ratios is given in the section on hull statistics.

### ◆ Prismatic coefficient

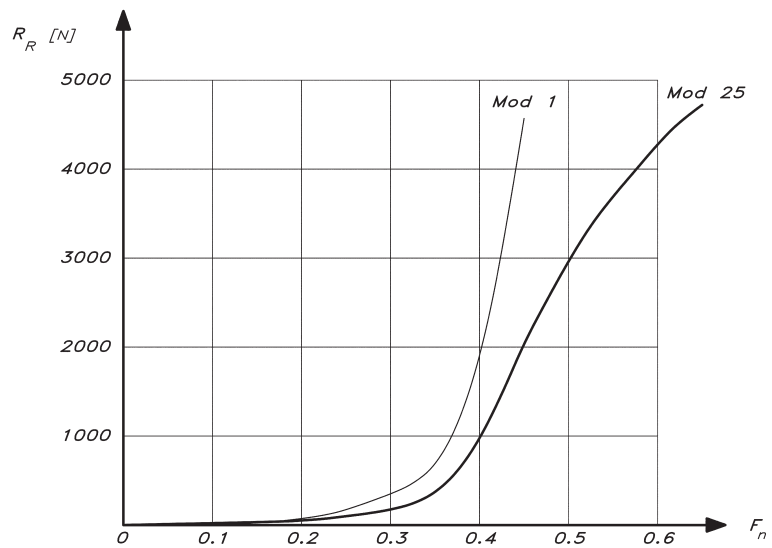
The designer has to decide at what speed his yacht shall have its optimum performance. Upwind in light wind the prismatic coefficient should be 0.5 or even lower, while downwind in more wind the coefficient should be 0.65–0.70 for lighter hulls that can reach a Froude number of 0.6. Normally, hulls are designed for maximum performance beating upwind in a breeze. The Froude number is then around 0.35, and a suitable prismatic coefficient around 0.55. The value of the YD–41 is 0.56.

It is hard to optimize the prismatic coefficient for the high-speed range. To attain high downwind speeds the aft part of the bottom has to be flat and relatively horizontal. The buttocks should be straight or concave in order not to create a low pressure, which will suck down the stern. The waterlines should be as straight as possible in order not to create a suction which will amplify the wave trough present at the afterbody at this speed. The only way to satisfy these criteria is to have a submerged transom, as on powerboats, but this is hardly possible for a sailing yacht, which has to operate in a wide speed range. The low-speed characteristics of this solution are not acceptable.

**Fig 5.20** Residuary resistance of two Delft parent models



a) Residuary resistance as a fraction of displacement.



b) Residuary resistance in Newton for a 10m  $L_{WL}$  yacht.

#### ◆ Centre of buoyancy

For low speeds, LCB should be around 3% of  $L_{WL}$  behind midship. At full upwind speeds at Froude numbers around 0.35 the position should move aftwards to 3.5–4.5%. Again, it is very difficult to optimise for a high speed at a Froude number of 0.6, since this calls for a large submerged transom and an LCB located 6–8% behind midship. Note that the transom submergence for a sailing yacht has to be considerably larger than for a power



boat due to the bow-down trimming moment from the sails. For the YD-41 the LCB is 4.2% aft of midship.

#### ◆ Length/beam and beam/draft ratio

The effect of these parameters on the residuary resistance is very small. Often, the effect on the wetted surface, and hence the frictional resistance, is as large or larger than the effect on the residuary resistance when the beam is changed. There are also other aspects on beam variations, above all the hull stability, which increases with the beam to the third power. The effect on the added resistance in waves is also quite important, and a large beam, or large fullness in the bow region in particular, increases this resistance component considerably. Finally, there is an important effect on the resistance due to heel, as will be seen below.

## ■ HEEL RESISTANCE

When the hull heels due to the side force from the sails, two resistance components develop, as explained in the first section of this chapter. The induced resistance is normally the most important one, but it will not be discussed here, since it is mainly caused by the keel and rudder, which generate the major part of the hydrodynamic side force. Induced resistance and side force will be discussed in [Chapter 6](#).

The heel resistance represents the change in total resistance due to heel alone, i.e. at zero side force. Since the submerged shape of the hull changes with heel, all resistance components change as well, to some extent. However, most changes are negligible and the only ones considered here are those related to:

- Hull friction
- Hull wave generation
- Keel wave generation.

The change in hull friction is almost exclusively due to a change in wetted surface. Using the formula of [Fig 5.21](#) for the heeled surface area the heeled friction may be obtained

*Wetted surface of hull in heeled position:*

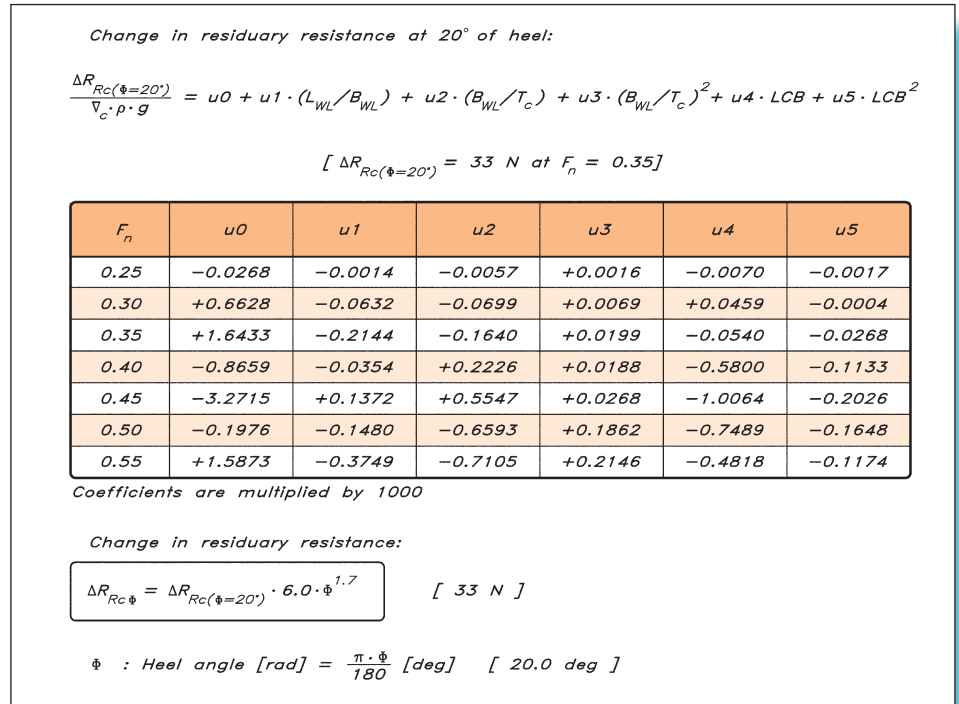
$$S_{Wc\Phi} = S_{Wc} \cdot [1 + 0.01 \cdot (s0 + s1 \cdot (B_{WL}/T_c) + s2 \cdot (B_{WL}/T_c)^2 + s3 \cdot C_{Mc})]$$

$$[S_{Wc\Phi} = 25.2 \text{ m}^2 \text{ at } \Phi = 20.0^\circ]$$

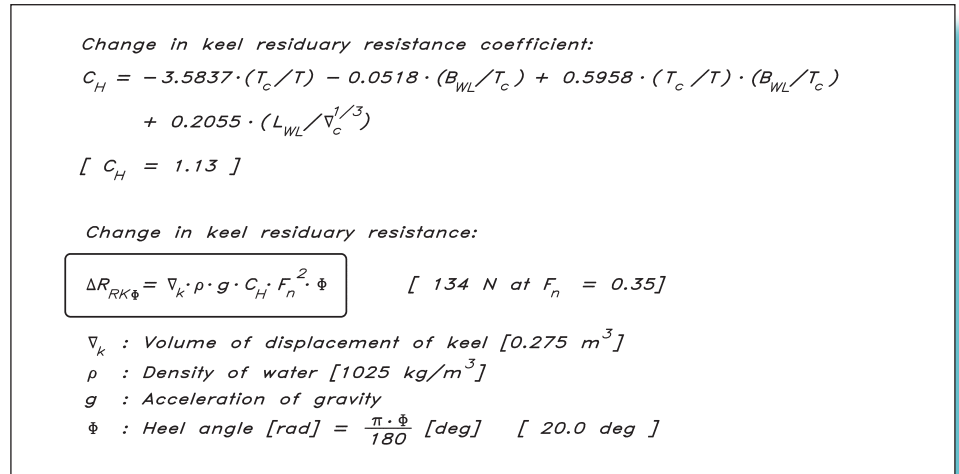
$\Phi$	$s0$	$s1$	$s2$	$s3$
5	-4.1120	+0.0540	-0.0270	+6.3290
10	-4.5220	-0.1320	-0.0770	+8.7380
15	-3.2910	-0.3890	-0.1180	+8.9490
20	+1.8500	-1.2000	-0.1090	+5.3640
25	+6.5100	-2.3050	-0.0660	+3.4430
30	+12.334	-3.9110	+0.0240	+1.7670
35	+14.648	-5.1820	+0.1020	+3.4970

**Fig 5.21** Wetted surface for non-zero heel angle

**Fig 5.22** Change in hull residuary resistance



**Fig 5.23** Change in keel residuary resistance



(cf Fig 5.8). Note that the minus signs in the table of coefficients mean that the new friction may well be smaller than the upright one. Since the keel will be submerged for reasonable heel angles its friction is assumed unchanged. If the yacht has two rudders, like the YD-41, one may be lifted out of the water. This is assumed in Fig 5.4.

Changes in the hull wave making (and possible changes in viscous pressure resistance) are taken into account using the formula of Fig 5.22. Here the change in residuary resistance with heel is given in a similar way as in the previous figures. The formula has been derived from heeled tests with most of the models in the Delft series. Fig 5.23 gives the change in keel residuary resistance.

When computing the heel resistance of the YD-41 in Fig 5.4 the heel angle has been taken as  $20^\circ$ . Deducting the reduction of frictional resistance of the hull (513 N upright and 459 N heeled) and one rudder (25 N) from the increase in residuary resistance of the hull (33 N) and keel (134 N) yields a total increase due to heel of 88 N, as seen in Fig 5.4. Note that the heel angle shall be given in radians.

## ■ ADDED RESISTANCE IN WAVES

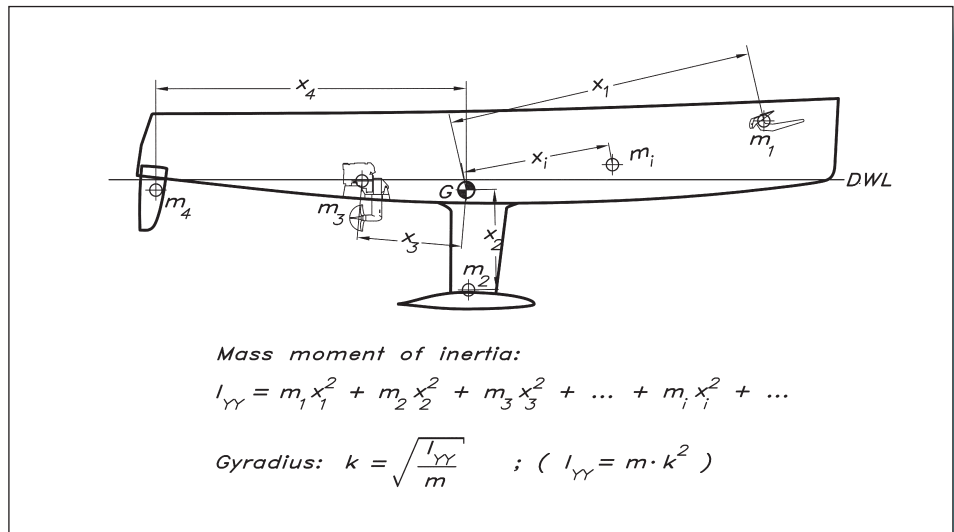
Chapter 4 introduced some basic safety factors when sailing in waves and presented and discussed the solution of the equation for the rolling motion. It was pointed out that similar equations hold for the other types of motion, provided the coupling between them can be neglected. Here we shall deal with a special aspect of seakeeping, namely the added resistance caused by the waves. As pointed out in Chapter 4, the theory of seakeeping is quite complex and cannot be treated comprehensively in this book. We will explain only some fundamental concepts related to the added resistance and give some guidelines on how to reduce it.

When a yacht moves in a seaway, the waves impose motions of all kinds on the hull. The most important ones, from a resistance point of view, are the heave and pitch motions, which are usually strongly coupled. When the hull heaves and pitches, it generates its own wave system, which carries energy away in much the same way as the still water wave pattern, thereby creating a resistance force.

Of some importance for a sailing yacht is the rolling motion too, which, as we have seen, creates vortices at the tip of the keel and rudder, i.e. a kind of induced resistance, similar to the one created by the tip vortices when the yacht is sailing in smooth water (see Chapter 6). In the following we will concentrate on heave and pitch. As in the case of rolling the yacht has natural frequencies in heave and pitch. When the frequency of encounter of the waves is equal to the natural frequency of one of these motions resonance occurs, and the corresponding motion amplitude gets very large. The added resistance is particularly serious if resonance occurs in pitch, since the resistance may then increase considerably. Ocean waves are normally considerably longer than the yacht, and the frequency of encounter is much smaller than the natural frequency, so resonance is unlikely to occur offshore. In sheltered waters, however, it may happen. To move as far away as possible from resonance, the natural frequency should be increased when the frequency of encounter is smaller and vice versa, so practically it is always beneficial to have as high a natural frequency as possible. This means that the hull will better follow the contour of the waves.

The most important quantity in connection with the natural frequency in pitch is the mass moment of inertia of the yacht around a transverse axis through the centre of gravity. This quantity may be computed, considering all weights on board, as described in Fig 5.24. Note that all parts of the yacht, including the mast, keel and hull skin, have to be considered. To make the calculation, all large components have to be divided into smaller pieces, each one with a certain mass and distance from the centre of gravity. The calculation of the mass moment of inertia could be made in connection with the weight

**Fig 5.24** Calculation of the mass moment of inertia –  $I_{YY}$



calculation, presented in Appendix 2, but this is seldom done, simply because there are no guidelines for its maximum value. We will, however, elaborate on this quantity and look at an example, to show the importance of minimizing it.

Since every object contributes to the moment of inertia not only by its mass, but also by the distance to the centre of gravity squared, objects positioned far away will have a large influence. Such objects include, for instance, lights, wind gauges or antennas at the top of the mast, or tanks, anchors and other mooring gear stowed at the ends of the yacht.

For convenience, another quantity, namely the gyradius, which is related to the moment of inertia, is defined in Fig 5.24. This is the length which, squared and multiplied by the hull mass, gives the moment of inertia. For ships the gyradius is usually assumed to be one quarter of the hull length, and this seems to be a reasonable assumption for a sailing yacht too. The mass moment of inertia may thus be approximated as one quarter of the overall hull length squared, then multiplied by the hull mass. Detailed calculations of the gyradius for the YD-41 show that it is 21.5% of the length overall.

To obtain a more exact value of the gyradius, and to study its effect, careful calculations were carried out for a three-quarter tonner, *Sunshine*, built in the early 1980s. In Table 5.2 the contribution to the mass moment of inertia of all parts of the yacht is given. Table 5.2(a) gives the values relevant for a cruising version, while the corresponding values for an extreme racing version are given in 5.2(b). The masses are also given, and it should be noted that, for rating reasons, the total mass is the same. Note also the very large contribution from the rig in both tables. It is twice as important as the hull and four to five times as important as the keel for the moment of inertia. The cruising version had a gyradius of 2.22 m, while it was only 1.85 m for the racer.

The effect of varying the gyradius was investigated by computing the motions and added resistance using a ship motions computer program, and introducing the resistance into a Velocity Prediction Program (VPP) for sailing yachts. (An introduction to VPPs will be given in Chapter 17.) The result of the calculations is presented in Figs 5.25(a) and 5.25(b). In the first figure the variation in speed made good to windward (the

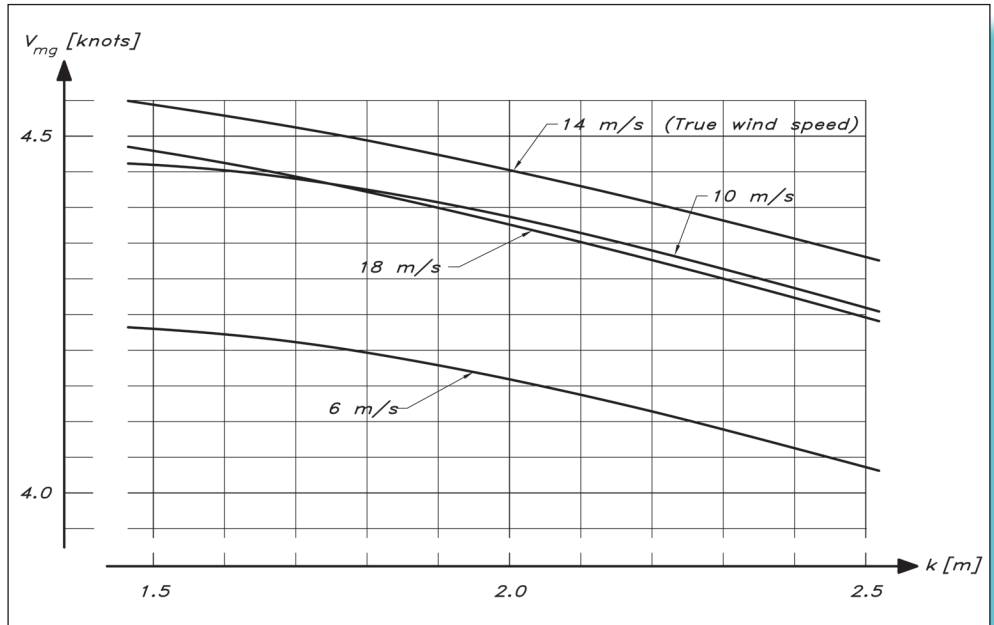
Table 5.2(a) Mass moment of inertia for <i>Sunshine</i> , cruising version				
Object	Mass (kg)	% of total mass	Moment of inertia (moi)	% of total moi
Rig	104	3.2	6798	42.0
Hull	597	18.3	3631	22.4
Deck	300	9.2	1867	11.5
Keel	1200	36.8	1296	8.0
Rudder	30	0.9	471	2.9
Motor	230	7.1	345	2.1
Others	800	24.5	1774	11.0
<b>Total</b>	<b>3261</b>	<b>100.0</b>	<b>16182</b>	<b>100.0</b>

Table 5.2(b) Mass moment of inertia for <i>Sunshine</i> , racing version				
Object	Mass (kg)	% of total mass	Moment of inertia (moi)	% of total moi
Rig	73	2.2	4759	43.1
Hull	299	9.2	1816	16.4
Deck	150	4.6	933	8.4
Keel	1200	36.8	1296	11.7
Rudder	30	0.9	471	4.3
Motor	230	7.1	0	0.0
Others	1279	39.2	1774	16.1
<b>Total</b>	<b>3261</b>	<b>100.0</b>	<b>11049</b>	<b>100.0</b>

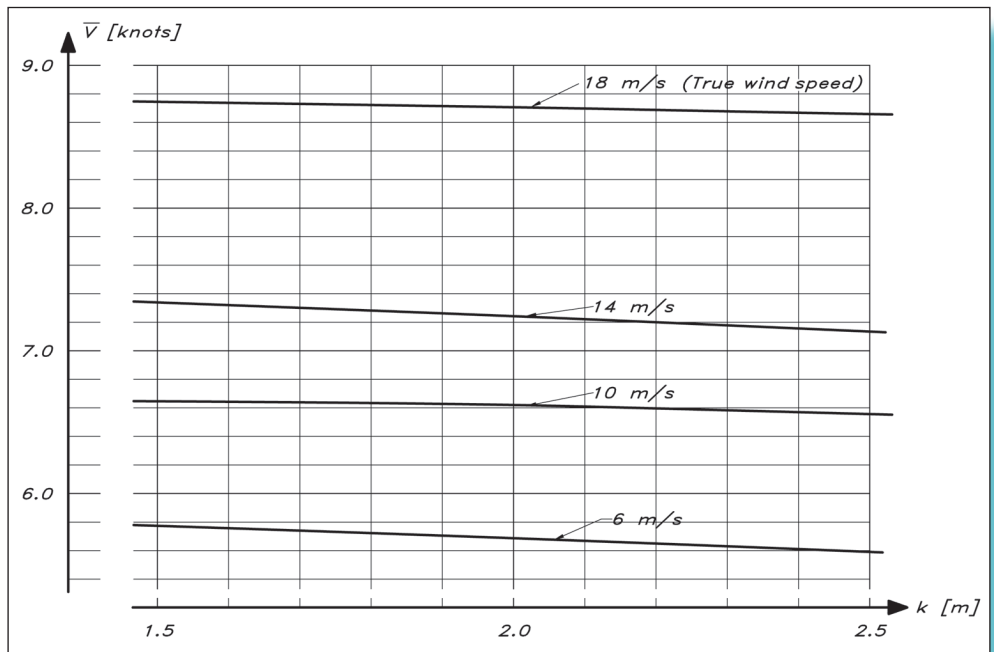
velocity component opposite the wind direction) is given for four wind speeds from 6 to 18 m/s, with a gyradius varying from 1.5 to 2.5 m. A significant drop in speed is noted between the two extremes. On the other hand, as we have seen, the range in gyradius is probably too wide. Introducing the two values computed for *Sunshine*, 2.22 m and 1.85 m respectively, it is seen that the speed of the cruiser is roughly 0.1 knots lower than that of the racer. This is a reduction in speed by 2.2%, and would render the cruiser chanceless in a race. The corresponding results, computed as an average across all wind directions, are given in Fig 5.25(b). It should be pointed out that no effect of the sails on the motions was considered in these calculations. Since only pitch and heave are taken into account, this approximation is reasonable. In rolling, the sails certainly have a large damping effect.

Based on seakeeping calculations for 16 of the Delft models, a simple statistical formula for the added resistance in waves was proposed by D M W Schaaf (see Keuning and Sonnenberg (1998). The formula is presented in Fig 5.26. Here the mean added resistance is non-dimensionalized using the waterline length and the significant wave height. The

**Fig 5.25(a)** Influence of gyradius on speed made good – *Sunshine*



**Fig 5.25(b)** Influence of gyradius on average speed – *Sunshine*



latter is defined as the mean height of the largest one third of the waves and that is what is normally estimated as the wave height by experienced sailors. The independent variable on the right hand side of the equation is the product of the displacement/length ratio and the pitch gyradius. There are two coefficients in the equation, (a) and (b), which are determined by the Froude number, the heading angle and the mean wave period, as seen in the table of Fig 5.27. Note that straight upwind corresponds to 180°.

*Added resistance in waves:*

$$\frac{\bar{R}_{AW} \cdot 10^2}{\rho \cdot g \cdot L_{WL} \cdot H_{1/3}^2} = a \cdot [10^2 \cdot (\nabla_c^{1/3} / L_{WL}) \cdot (k_{yy} / L_{WL})]^b$$

$$[ \bar{R}_{AW} = 144 \text{ N} ]$$

$\nabla_c$  : Volume displacement of hull [6.05 m<sup>3</sup>]

$\rho$  : Density of water [1025 kg/m<sup>3</sup>]

$g$  : Acceleration of gravity

$T_1$  : Wave period [2.8 s]

$H_{1/3}$  : Significant wave height [0.4 m]

$k_{yy}$  : Longitudinal radius of gyration [2.685 m]

**Fig 5.26** Added resistance in waves

A disadvantage of the formula is that the only hull parameters considered are the displacement/length ratio and the gyradius. General experience in hydrodynamics suggests that there should be an influence from other parameters like length/beam ratio, beam/draft ratio and prismatic coefficient. Therefore, a more elaborate equation, including these parameters, was also proposed. However, the number of coefficients required for this relation is so large that it will not be given here. Comparative calculations show that the results from the two equations are very similar, except in very short waves where the more elaborate one is better.

The added resistance calculations for the YD-41 are made for coastal waters with a significant wave height of 0.4 m and a mean wave period of 2.8 s. This yields an added resistance of 144 N, beating upwind at 135°. As seen in Fig 5.4, this corresponds to 9.4% of the total resistance.

## ■ OTHER SEAKEEPING ASPECTS

The two most important requirements on a sailing yacht in a seaway are that it is stable enough to avoid capsizing even under severe conditions, and that the hull can withstand the loads exerted by the waves. These aspects are dealt with in Chapters 4 and 13, respectively. For a racing yacht the added resistance comes next in order of importance, and it was therefore dealt with at some length in the previous section. However, for a cruising yacht, other aspects of the design may be equally important.

In fact, what might be termed ‘seakindliness’ may be more valuable for a crew, which has to spend months on board the yacht during long ocean crossings. A yacht that is seakind is easy to live on even under relatively difficult conditions. By its very nature this property is more difficult to quantify, but it is clear that the motions of a seakind yacht must be soft enough to enable the crew to work without problems and to relax after work.



$$T'_1 = T_1 \cdot \sqrt{g/L_{WL}}$$

		$F_n = 0.15$		$F_n = 0.25$		$F_n = 0.35$		$F_n = 0.45$		$F_n = 0.60$	
$T'_1$	$\mu$	$a$	$b$	$a$	$b$	$a$	$b$	$a$	$b$	$a$	$b$
2.0	100	0.0064	1.8012	0.0094	1.6076	0.0131	1.4260	0.0170	1.2701	0.0000	0.0000
2.0	115	0.0702	1.2351	0.1253	1.0662	0.2020	0.7105	0.2958	0.4759	0.0000	0.0000
2.0	125	0.1778	0.9700	0.2924	0.7191	0.4691	0.4367	0.6982	0.1580	0.0000	0.0000
2.0	135	0.3367	0.7520	0.4790	0.5351	0.7962	0.2292	0.0000	0.0000	0.0000	0.0000
2.0	145	0.5349	0.5876	0.7386	0.3868	1.1418	0.0633	0.0000	0.0000	0.0000	0.0000
2.5	100	0.0022	2.1441	0.0031	1.9747	0.0043	1.7986	0.0055	1.6561	0.0071	1.4768
2.5	115	0.0217	1.6837	0.0383	1.4654	0.0609	1.2603	0.0876	1.0757	0.1283	0.8442
2.5	125	0.0537	1.4670	0.0884	1.2926	0.1408	1.0782	0.2054	0.8712	0.3089	0.5981
2.5	135	0.0999	1.3090	0.1515	1.1733	0.2403	0.9466	0.3544	0.7159	0.5456	0.4009
2.5	145	0.1360	1.2874	0.2196	1.0797	0.3444	0.8444	0.5117	0.5931	0.8044	0.2401
3.0	100	0.0010	2.3044	0.0014	2.1272	0.0019	1.9711	0.0025	1.7965	0.0031	1.6447
3.0	115	0.0092	1.8811	0.0161	1.6875	0.0255	1.5033	0.0365	1.3381	0.0523	1.1408
3.0	125	0.0226	1.6904	0.0369	1.5517	0.0585	1.3686	0.0847	1.1929	0.1234	0.9741
3.0	135	0.0418	1.5562	0.0630	1.4652	0.0993	1.2809	0.1450	1.0916	0.2145	0.8488
3.0	145	0.0642	1.4592	0.0908	1.4015	0.1423	1.2141	0.2087	1.0130	0.3126	0.7488
3.5	100	0.0005	2.3809	0.0007	2.2141	0.0010	2.0250	0.0013	1.8954	0.0016	1.7004
3.5	115	0.0046	1.9846	0.0082	1.7948	0.0129	1.6215	0.0184	1.4634	0.0261	1.2793
3.5	125	0.0115	1.7995	0.0186	1.6757	0.0294	1.5105	0.0422	1.3514	0.0609	1.1546
3.5	135	0.0210	1.6782	0.0317	1.6078	0.0497	1.4467	0.0724	1.2761	0.1050	1.0676
3.5	145	0.0324	1.5891	0.0456	1.5598	0.0712	1.3989	0.1040	1.2222	0.1522	0.9995
4.0	100	0.0003	2.4046	0.0004	2.2345	0.0006	2.0808	0.0007	1.9466	0.0010	1.7326
4.0	115	0.0026	2.0357	0.0046	1.8532	0.0073	1.6824	0.0103	1.5325	0.0148	1.3493
4.0	125	0.0065	1.8550	0.0105	1.7445	0.0166	1.5870	0.0238	1.4336	0.0341	1.2495
4.0	135	0.0119	1.7434	0.0180	1.6810	0.0281	1.5238	0.0408	1.3743	0.0588	1.1803
4.0	145	0.0183	1.6596	0.0258	1.6418	0.0401	1.4981	0.0586	1.3336	0.0850	1.1309
4.5	100	0.0002	2.4482	0.0003	2.2604	0.0004	2.0584	0.0005	1.9708	0.0006	1.7525
4.5	115	0.0017	2.0487	0.0028	1.8848	0.0044	1.7216	0.0064	1.5621	0.0090	1.3874
4.5	125	0.0040	1.8939	0.0064	1.7856	0.0101	1.6294	0.0147	1.4736	0.0209	1.2971
4.5	135	0.0073	1.7805	0.0109	1.7283	0.0171	1.5848	0.0249	1.4305	0.0359	1.2425
4.5	145	0.0112	1.6989	0.0157	1.6910	0.0246	1.5529	0.0359	1.3961	0.0518	1.2037
5.0	100	0.0001	2.0466	0.0002	2.3517	0.0002	2.1274	0.0003	1.9235	0.0003	1.8738
5.0	115	0.0011	2.0596	0.0019	1.8990	0.0029	1.7384	0.0042	1.5856	0.0059	1.4108
5.0	125	0.0026	1.9051	0.0042	1.8020	0.0066	1.6550	0.0094	1.5094	0.0135	1.3302
5.0	135	0.0047	1.8004	0.0071	1.7548	0.0112	1.6107	0.0161	1.4648	0.0232	1.2797
5.0	145	0.0072	1.7275	0.0102	1.7217	0.0159	1.5872	0.0232	1.4363	0.0336	1.2460
5.5	100	6.0e-5	2.6609	0.0001	2.3753	0.0002	2.0611	0.0002	2.0358	0.0002	1.8756
5.5	115	0.0007	2.0844	0.0012	1.9306	0.0019	1.7600	0.0028	1.5994	0.0039	1.4301
5.5	125	0.0018	1.9197	0.0028	1.8161	0.0044	1.6773	0.0064	1.5267	0.0091	1.3506
5.5	135	0.0032	1.8225	0.0048	1.7664	0.0075	1.6315	0.0109	1.4841	0.0157	1.3046
5.5	145	0.0050	1.7307	0.0069	1.7372	0.0107	1.6102	0.0158	1.4579	0.0229	1.2703
6.0	100	5.0e-5	2.5121	6.0e-5	2.4574	9.0e-5	2.2831	0.0001	2.0042	0.0002	1.6893
6.0	115	0.0005	2.0700	0.0009	1.9220	0.0014	1.7578	0.0020	1.6112	0.0028	1.4332
6.0	125	0.0012	1.9246	0.0020	1.8259	0.0031	1.6867	0.0046	1.5244	0.0064	1.3600
6.0	135	0.0022	1.8258	0.0034	1.7814	0.0053	1.6457	0.0077	1.4950	0.0111	1.3136
6.0	145	0.0034	1.7506	0.0049	1.7446	0.0076	1.6232	0.0111	1.4746	0.0161	1.2867

Fig 5.27 Coefficients for added resistance in waves

As explained in [Chapter 4](#), the motions of the yacht depend on its inertia, its stability and its damping. Since pitch, roll and heave are the most important motions, the most important inertial quantities are the mass moments of inertia around a transverse and a longitudinal axis (or the corresponding gyradii), as well as the hull mass. The stability depends on the shape of the waterline area and its moment of inertia around two axes. Finally, the damping depends on the size of the keel. Most modern designers strive for small gyradii, a light hull, large stability and a small keel. All these features tend to increase the accelerations onboard the yacht, thus making it less seakind. For a cruising yacht this is unlikely to be the optimum solution. A very severe problem of this kind was experienced when the first large ships for carrying ore were taken into service. When the ore was loaded on the bottom of the hull, its stability became so large that excessive accelerations were created. In fact, some fatal accidents occurred when people were thrown towards the bulkheads in heavy seas. Modern ore carriers have the ore in a cradle lifted from the bottom of the hull, and much softer motions are obtained. Another ship type for which soft motions are important is the fishing boat, where the fishermen have to carry out their work on deck, often in heavy seas. To cope with this problem some boats have an increased transverse gyradius from weights of iron or concrete put as far sideways as possible inside the hull.

Other quantities which affect the hull's seakeeping capabilities are the overhangs fore and aft, the freeboard height and the bow flare. A large forward overhang is likely to increase pitching, since large pitching moments are created when a wave hits this part of the hull far from the centre of gravity. Aft overhangs may, of course, have a similar effect in following seas, but the frequency of encounter is then much lower so the problem is small. On the contrary, in fact, the stern overhang may be beneficial, since it may damp the pitching motions in head seas. A high freeboard forward, and a flared one in particular, prevents green water on deck, and spray hitting the cockpit is effectively avoided too. The hull thus gets much dryer.

A final point to mention is the balance between the forward and aft halves of the hull. Many modern yachts have very full stern sections, while the forward sections are very sharp. This is good for the surfing abilities of the hull, but it may not be good for the course stability when rolling. When the hull heels over, the centre of buoyancy moves much more sideways in the stern than in the bow. The force required to move the volume of water sideways comes from the hull, which by the law of action and reaction is affected by the same force from the water, but in the opposite direction. The stern is thus affected much more than the bow, and the hull changes its course in the heeling direction. This happens, of course, both to starboard and port, and the vessel becomes difficult to keep on course. The remedy for this is to design less square transoms. With more rounded transoms the waterplane area does not move so far sideways when heeling. This also reduces the bow-down trimming moment often found on wide-stern yachts.

## ■ HULL STATISTICS

To aid the designer in his choice of main proportions for the yacht, a compilation of hull statistics for the most important quantities is presented in this section. Most of the statistics are based on ORC certificates and include boats, 8–15 m  $L_{OA}$ , built from

2000 to 2012. There are about 400 different types included. Note that the data has been extrapolated down to 6 m in the figures.

Statistics will be given for the main hull dimensionless ratios: length overall/max beam, length of waterline/draft, length of waterline/canoe body draft, length of waterline/(volume displacement)<sup>1/3</sup> and length overall/length of waterline. Two ratios important for the above-water appearance of the hull will be presented too: freeboard forward/length of waterline and freeboard forward/freeboard aft. Finally, statistics for the ballast ratio will be discussed.

It should be pointed out that the data used in the statistical evaluation is for the light condition, i.e. without crew, stores, water or fuel. This condition corresponds best to the official data for a yacht and is used for rating purposes and in class rules. A fully equipped cruising yacht with the crew on board may be up to 20% heavier. In the computations for the YD-41 in this book we have assumed a half-loaded condition with the crew, which reflects reality more closely. To compare with other yachts in this section, we will, however, use the light condition. The differences are shown in Appendix 1.

#### ◆ Length overall/max beam ( $L_{OA}/B_{MAX}$ )

As seen in [Chapter 2](#) most dimensionless hull ratios exhibit a dependence on the size of the yacht. This is true also for  $L_{OA}/B_{MAX}$ . The larger the yacht the larger the ratio, i.e. large yachts are less beamy, relatively speaking. The reason for this is that if a given hull is simply scaled to a larger size its stability will increase faster than its heeling moment from the sails. The hull will thus become unnecessarily stable and a somewhat narrower yacht would suffice. It may be shown that, everything else being scaled properly, beam should be scaled as  $(\text{length})^{2/3}$ . This means that  $L_{OA}/B_{MAX}$  will be scaled as  $(\text{length})^{1/3}$ , i.e. the ratio will increase slightly with length. For example, if the length is doubled the ratio will increase by 25%. The assumption that everything else is scaled properly, like ballast ratio, position of ballast, mast height, etc., may seem an oversimplification, but the simple scaling rule above seems to fit the hull statistics over all hull lengths from 6 to 15 m  $L_{WL}$  very well. It may be seen from the figure that a 7 m ( $L_{WL}$ ) yacht typically has a length/beam ratio of 2.8, while a hull twice as long has a ratio of 3.5, i.e. an increase of 25%.

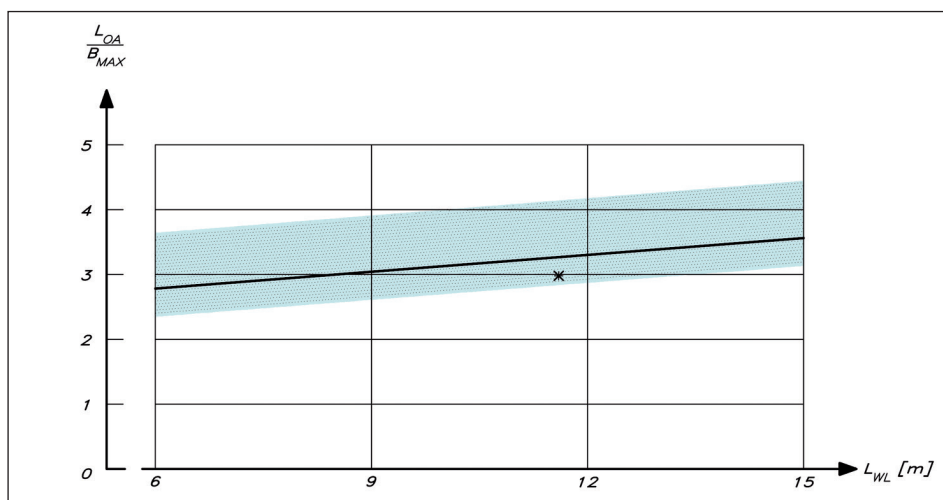
The line of [Fig 5.28](#) (overleaf) represents the median, i.e. there are approximately as many yachts above as below the line. In this case the median differs from the average, since there is a considerably larger spread upwards than downwards, as can be seen from the shaded area, representing the scatter of the data. The limits are adjusted in such a way that about 95% of all yachts fall within the shaded area. A design close to a limit is thus quite extreme.

The YD-41 has an overall length of 12.50 m and a beam of 4.20 m. Its  $L_{OA}/B_{MAX}$  is thus 3.0. For an  $L_{WL}$  in the light condition of 11.62 m this is below the line as can be seen in [Fig 5.28](#) where the YD-41 is marked with a symbol. The hull is thus a bit beamier than average.

#### ◆ Length of waterline/draft ( $L_{WL}/T$ )

$L_{WL}/T$  is plotted versus  $L_{WL}$  in [Fig 5.29](#). Obviously, this ratio increases with length as well. A larger yacht has a larger ratio, i.e. a smaller relative draft.

The choice of draft for a cruising yacht is a trade-off between performance and practical advantages, like the possibilities of entering more shallow water areas, ease of



**Fig 5.28** Length/beam ratio

handling ashore, etc., while for a racing yacht draft is penalized to cancel the performance advantage. The YD-41 has an  $L_{WL}$  of 11.62 m and a draft of 2.28 m in the light condition. This yields an  $L_{WL}/T$  of 5.1, which is close to the line in Fig 5.29.

#### ◆ Length of waterline/canoe body draft ( $L_{WL}/T_c$ )

Since modern yachts have fin keels it is possible to define the canoe body draft,  $T_c$ . As seen in Fig 5.30  $L_{WL}/T_c$  increases slightly with length, but the dependence is not very strong. Compared with the corresponding statistics in the previous editions of this book the values are larger, with median values between 21 and 23. In the old statistics, based on yachts designed in the 1970s and 1980s, the median value was 18. Modern hulls are thus shallower. It should be noted that these statistics are from a smaller database of around 30 modern hull forms. The hull draft does not appear from the ORC certificate, so a special study had to be made of this quantity.

The YD-41 is an example of a very light modern hull form, as can be seen in Fig 5.30. Its value of  $L_{WL}/T_c$  is very high, even outside of the shaded region.

#### ◆ Length/displacement ratio ( $L_{WL}/\nabla^{1/3}$ )

As explained above the length/displacement ratio is a very important quantity for the resistance of the yacht at high speeds. To enable the yacht to exceed a Froude number of about 0.45, ratios above about 5.7 are required. In Fig 5.31 the length/displacement ratio is plotted versus waterline length.

Since beam and draft do not increase linearly with length, displacement increases slightly slower than length cubed. In fact, with the same assumptions as above, the displacement increases as  $(\text{length})^{7/3}$ , which means that the length/displacement ratio increases as  $(\text{length})^{2/9}$ . Increasing the length by a factor of two increases the ratio by 17%. The increase is not as fast in the statistical data, as may be seen in Fig 5.31 (overleaf).

As was the case for the length/beam ratio the spread is asymmetric. There are, however, certain kinds of hulls outside the limits. Thus, some extreme ultra light yachts have considerably higher ratios, and since the statistics are based mainly on yachts which

Fig 5.29 Length/draft ratio

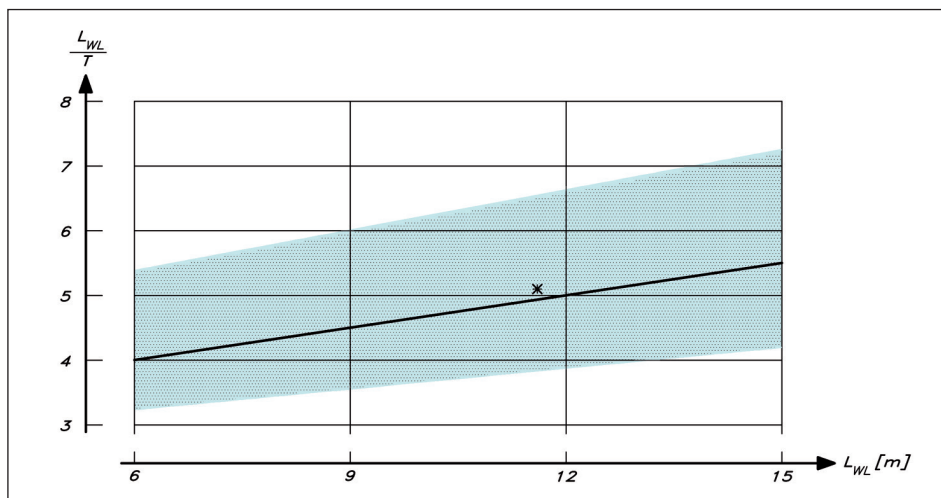
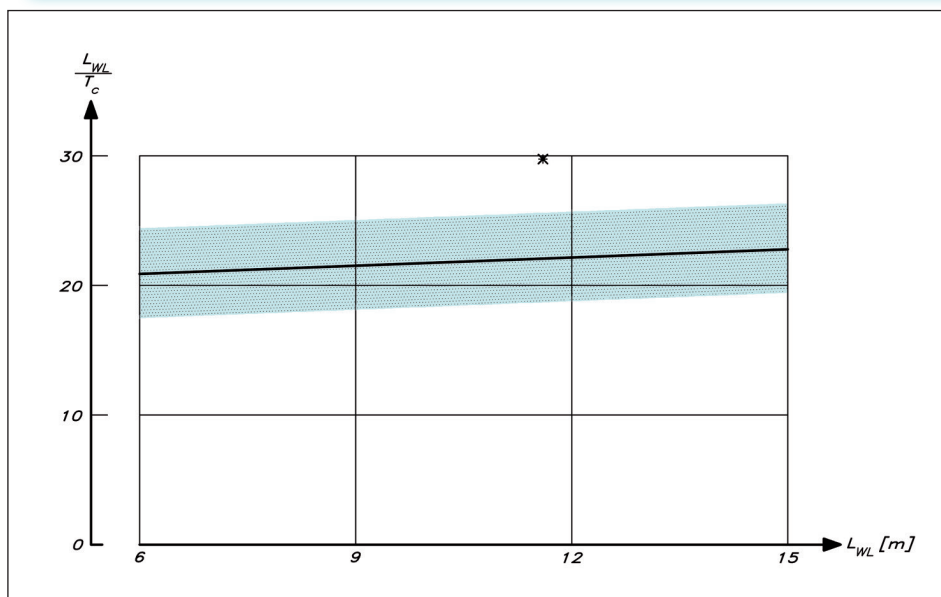


Fig 5.30 Length/hull draft ratio



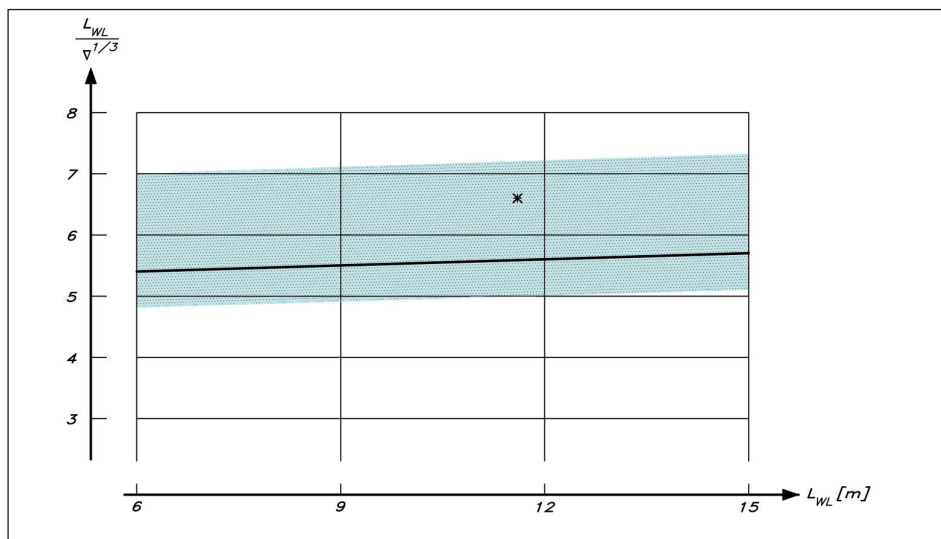
may participate in some kind of racing (since they have ORC certificates), some heavy cruising yachts may have been missed.

The length/displacement ratio is, of course, quite different between a racer and a cruiser, since the equipment required for comfortable living on board is rather heavy. For a high-performance cruiser, like the YD-41, the value is 6.5, which is well above the mean line in Fig 5.31.

#### ◆ Length overall/length of waterline ( $L_{OA}/L_{WL}$ )

The overhangs of modern hulls have decreased steadily over the past 50 years. To a certain extent this is a matter of fashion, but there are also other reasons, such as the influence of the racing rules, particularly the IOR rule, which had a considerable influence on the shape of the hull a few decades ago. For a given length overall, smaller overhangs will give





**Fig 5.31** Length/  
displacement ratio

a larger waterline length, which is beneficial. The YD-41 has  $L_{OA}/L_{WL} = 1.08$ , which may be considered typical of contemporary yachts.

#### ◆ Freeboard height

It is a well-known fact that the relative freeboard height decreases with hull length. Obviously, this is due to the requirements of the accommodation. Even on very small yachts headroom for moderately tall people is required. The trend is shown in Fig 5.32, which shows the freeboard forward versus the waterline length. This graph is based on the same limited database as Fig 5.30.

A typical value of freeboard forward/freeboard aft is 1.3. As compared to older yachts this is lower, so modern yachts have a more horizontal sheer line. Both the forward and aft freeboards are higher, however, and the camber of the sheer line, the ‘spring’, is smaller. The YD-41 has a freeboard forward/waterline length of 0.123, while the mean value is 0.130 for this size of hull, and the ratio of the two freeboards is 1.23.

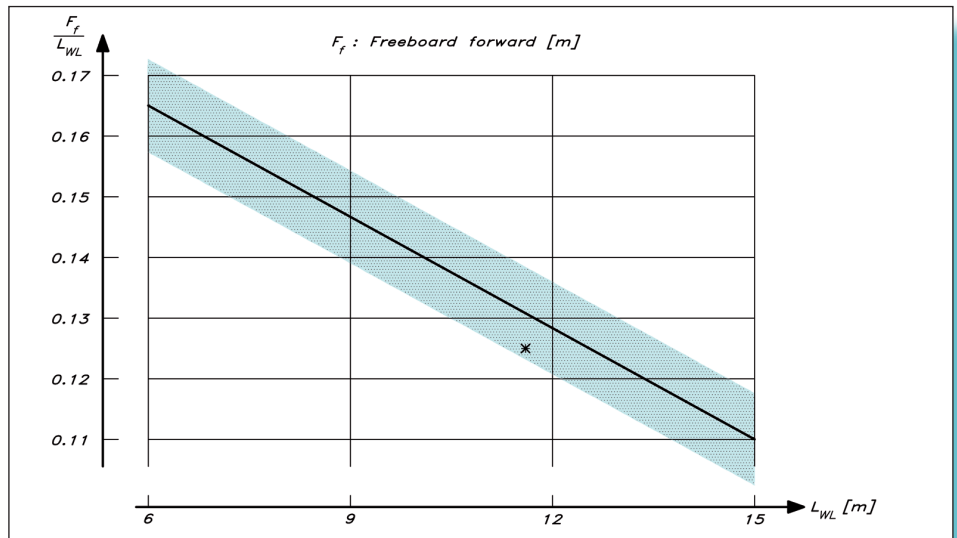
#### ◆ Ballast ratio

The ballast ratio, i.e. the ratio of keel weight to total weight, varies considerably on modern yachts. As seen in Fig 5.33 most yachts lie within the range 0.25–0.50. These numbers have been lowered in recent years due to the more common bulb keels, which can be lighter with the same stability. There does not seem to be any particular variation with length. Our YD-41 has a ballast ratio of 0.39, which is close to the median value. The keel mass is 2300 kg and the light displacement 5900 kg.

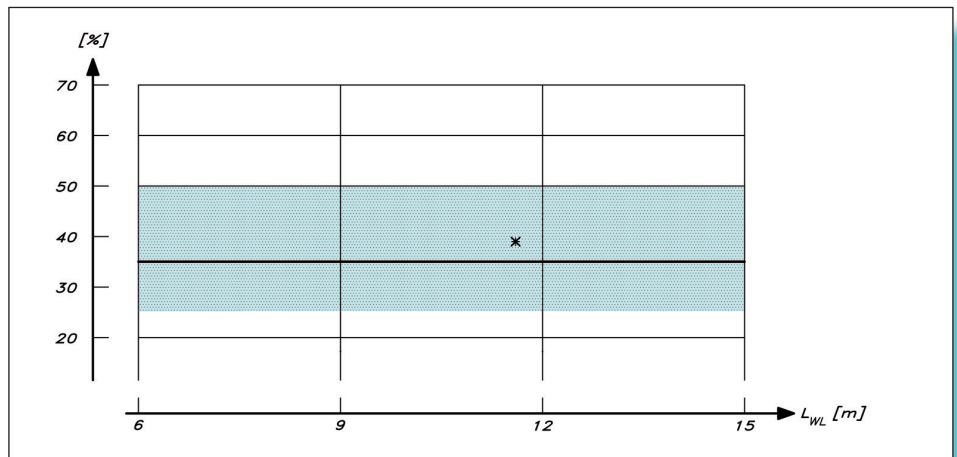
It should be mentioned, finally, that the official displacements used in the statistics may be slightly low, due to optimistic weight calculations even for the light condition. In reality, the length/displacement ratio and the ballast ratio are probably somewhat lower than the official ones. The values given for the YD-41 are realistic, however.

A photo of the YD-41 hull with keel and appendages is shown in Fig 5.34.

**Fig 5.32** Freeboard forward/length ratio



**Fig 5.33** Ballast ratio



**Fig 5.34** Launching of the YD-41 (Photo: Michal Orych)





# 6 KEEL AND RUDDER DESIGN

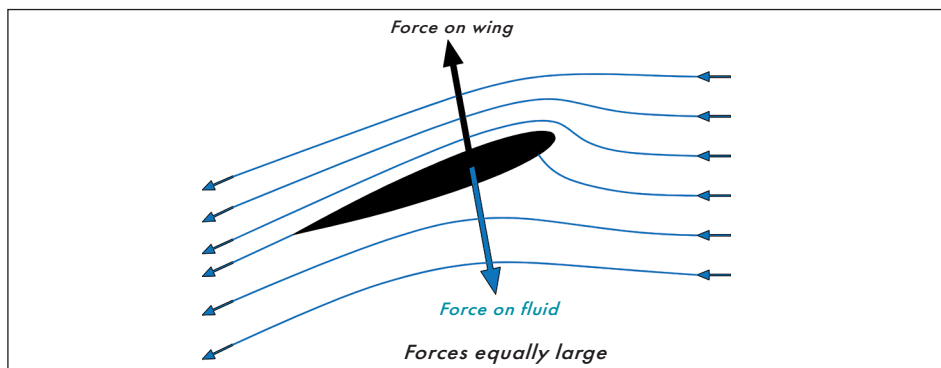
In the design of keels and rudders, well-established principles from aircraft aerodynamics can be employed. Although most aircraft today fly at speeds at which the compressibility of the air is important (more than 100 m/s), much information can be gleaned also for the incompressible water flow, partly due to the early aerodynamic research carried out more than 70 years ago. In this chapter we will first give a short introduction to the basic principles of the flow around a wing (keel or rudder) at an angle of attack, and the corresponding force generation. The remaining part of the chapter deals with the two main aspects of wing design: the planform and the wing section. As in the previous chapter we also provide statistics, enabling the designer to select a suitable size for the keel and rudder. Note that wing theory will also be the basis for [Chapter 7](#) on foiling and [Chapter 8](#) on sails.

## ■ FLOW AROUND A WING

In [Fig 6.1](#), the flow around a wing is sketched. The inflow from the right is split into two parts by the wing. One part moves above the wing and the other below. There is a dividing streamline between the two parts. If we assume, for a moment, that the wing is infinitely long with a constant cross-section and that the flow is at right angles to the span, the dividing streamline ends in a stagnation point on the wing surface. At the stagnation point itself there is no flow in either direction along the surface, and since the fluid does not penetrate the wing there is no velocity at right angles to the surface either. A similar point with zero velocity is found at the trailing edge (tail). This is the so-called two-dimensional (2D) case, where the properties at all cross-sections, regardless of spanwise position, are the same. In practice, this can be accomplished by mounting the wing between two walls at right angles to the span in a wind tunnel. The properties of the cross-section (often called just section, or profile) can then be investigated.

Since the flow follows the contour of the wing it has to leave the trailing edge in a direction different from that in front of the wing. In [Fig 6.1](#) the arrows on the streamlines show that the flow has turned from horizontal to a direction obliquely downwards. The flow is thus deflected by the wing, and this can only happen if the wing exerts a downward force on the flow, indicated by the large blue arrow. Now, there is a fundamental law in physics (Newton's third law) that says: 'If an object A exerts a force on object B, then object B must exert a force of equal magnitude and opposite direction back on object A'. This opposite force is thus directed mainly upwards. It is black in the figure and is

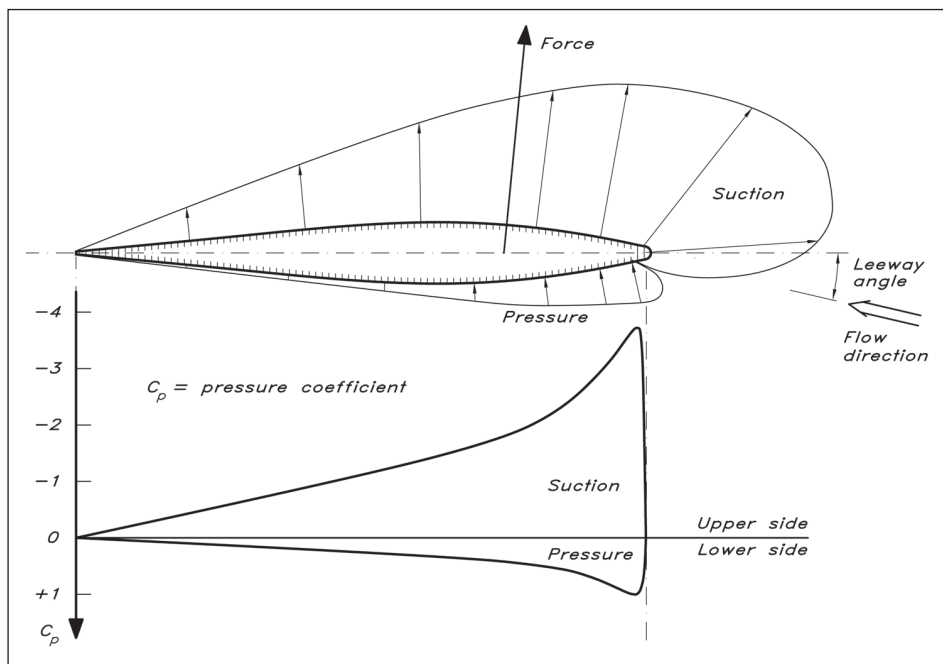
**Fig 6.1** Flow around a wing section



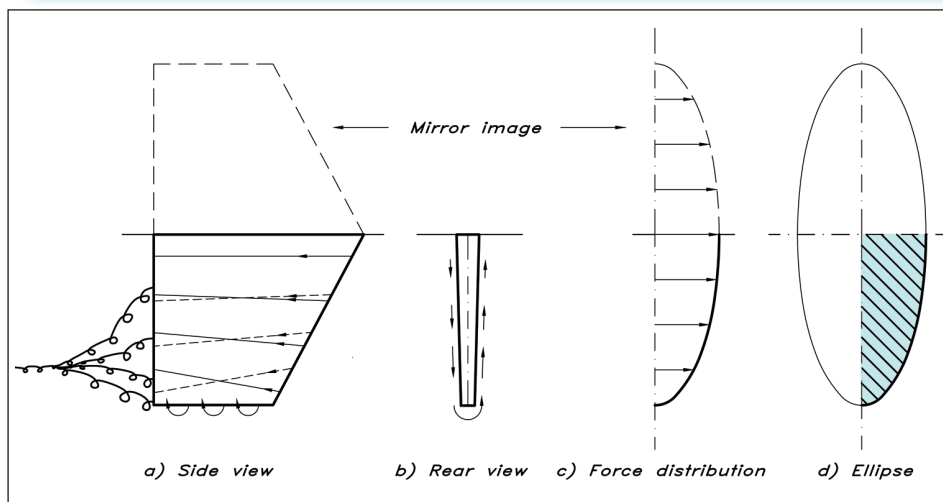
just an inevitable consequence of the fact that the flow cannot pass through the wing. The flow direction has to change. Had there been no friction, the two forces would have been exactly vertical, but the friction tilts the force on the wing slightly backwards, i.e. there is a small frictional drag component on the wing. The force on the fluid is tilted correspondingly forwards, indicating that the wing not only pushes the flow downwards, it also reduces the velocity slightly.

Most wing sections of interest in sailing yacht design are symmetric, as in Fig 6.1, since they have to work equally well on both tacks. At zero angle of attack the pressure distribution along the section looks in principle like the one along a waterline (see Fig 5.9), i.e. there is high pressure at the nose and tail, and lower pressure in between. However, at non-zero angle of attack (as in Fig 6.1), the flow becomes highly asymmetric. In particular, there is a large difference between the flow that has to move from the stagnation point past the nose on to the upper side and the one moving backwards from the stagnation point. While the former passes a region of very large curvature, the latter moves more or less straight back. There is also a difference in speed between the two sides; the upper speed being higher than the undisturbed one, and the lower speed slower. Quite different pressures are then created as shown in Fig 6.2, and it is particularly noteworthy that there is a large suction peak at the nose. Further back on the top side the suction is gradually reduced. On the lower side the pressure is positive, but its absolute value is lower than on the other side. If all the pressure forces on the section are added, a resulting force (shown as an arrow) is obtained. The angle between the undisturbed flow and the resulting force depends on the efficiency of the wing. For a two-dimensional case without friction the angle would be  $90^\circ$ . In a real situation it is always smaller than  $90^\circ$  (pointing more backwards). The designer's task is to make the angle as close to  $90^\circ$  as possible, and in the following we will explain how this can be accomplished.

Since the pressure and suction forces are much larger in the front part of the wing, the centre of effort of the resulting force is located in the forward part. In fact, it may be shown theoretically that the centre of effort is at one quarter of the distance from nose to tail for a symmetric section in a two-dimensional frictionless fluid. The lower part of Fig 6.2 shows a diagram, where the pressure is plotted in the more normal way, i.e. with the pressure on the vertical scale and the position along the section on the horizontal scale. Note, however, that negative pressures are plotted upwards. In this way the upper side of the wing corresponds to the upper part of the diagram, and conversely for the



**Fig 6.2** Pressure distribution around a wing section



**Fig 6.3** Force and vortex distribution on a wing

lower side. The distance between the upper and lower curves at any chordwise position is representative of the vertical force being generated at that position, and the total vertical force is proportional to the area between the two curves.

Real wings are not, of course, infinitely long, nor are they mounted between the walls of a tunnel. They therefore have free ends in the flow, and that creates some new phenomena. This is the three-dimensional (3D) case.

In Fig 6.3 a keel is shown from the side (a) and from behind (b). Since the pressure is higher on the leeward side of the keel than on the windward side, the flow will tend to move around the tip from the leeward to the windward side. This creates a downward motion on the leeward side, gradually increasing from zero at the root to a maximum at

the tip. A corresponding motion upwards is created to windward. Streamlines on the two sides of the keel therefore have different directions, and when they meet at the trailing edge vortices are created. This is particularly so at the tip, where a strong vortex is left behind the keel. Sometimes, when the yacht heels strongly this vortex can be seen, since air is sucked into the low-pressure core of the vortex when it gets close to the surface. As appears from the figure, all the vortices created at the trailing edge tend to roll up into a single one left behind the yacht. Since this vortex contains rotational energy it gives rise to a resistance component, the induced resistance, discussed in the previous chapter.

At the tip the side force generated must go to zero, since no pressure jump between the two sides can exist in the flow at the tip. Near the root, on the other hand, the flow is uninfluenced by the tip and a large force may be generated, since the bottom acts as a wall, preventing the overflow. The variation between root and tip depends on the shape of the keel, and it may be shown that the best distribution of the force is an elliptical one. With this distribution the minimum amount of vortex energy is left behind, which means that the induced resistance is minimized.

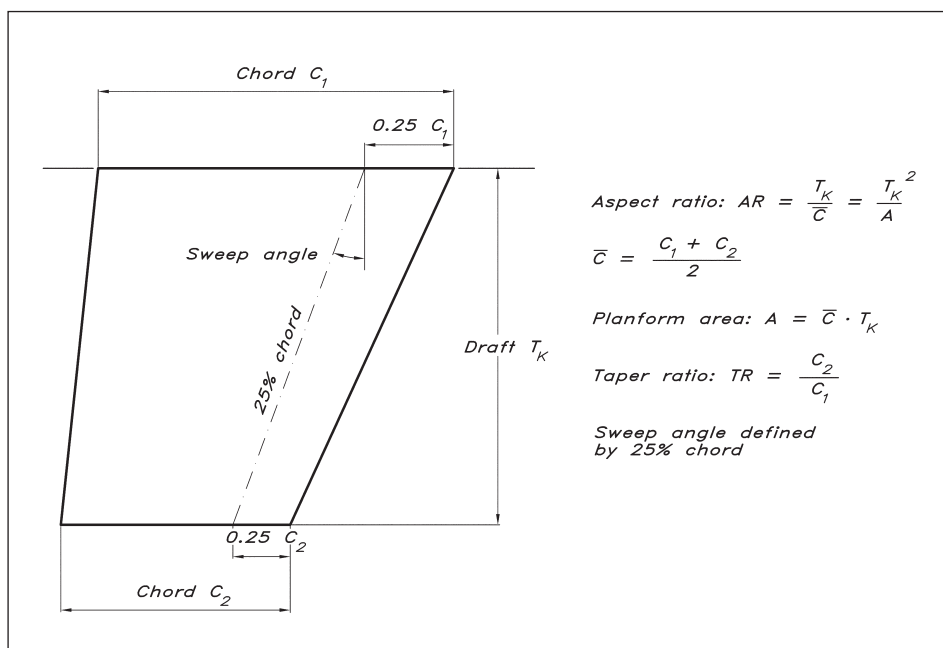
In Fig 6.3 (c) an elliptical distribution is shown. This may be imagined as one quarter of a full ellipse, as shown in (d). The simplest way to obtain an elliptical distribution of the side force is to make the keel planform elliptic. This has some disadvantages, however, and we will return shortly to the optimization of the planform.

An interesting phenomenon is indicated in Fig 6.3 (a) and (c). If the bottom of the hull may be considered as a flat plate of infinite extension, the flow around the keel would be the same as if the plate had been replaced by the mirror image of the keel in the plate. A flat wall parallel to the flow thus acts as a symmetry plane. Now, the bottom is neither flat nor infinite in reality, and the much more complex real flow will be discussed below.

## ■ DEFINITION OF THE KEEL PLANFORM

The definition of the planform of a trapezoidal keel is given in Fig 6.4 (overleaf). First, it should be mentioned that the horizontal distance from nose to tail at all depths is called the chord. Two chords are specified in the figure, namely the root and tip chords,  $C_1$  and  $C_2$ . These can be used to define a mean chord  $C = (C_1 + C_2)/2$ . The most important parameter for the efficiency of the keel is the aspect ratio, AR, defined as  $AR = T_k/C$ , i.e. the keel depth divided by the mean chord. This is the geometric aspect ratio. As explained above, the effective aspect ratio  $AR_e$  is twice as large if the keel is attached to a large flat surface. The second parameter to be defined is the taper ratio, TR, which is simply the ratio of the tip chord to the root chord, i.e.  $TR = C_2/C_1$ .

Most keels are not exactly vertical, but sweep backwards to some extent. It is not obvious, however, how to define this sweep angle,  $\Lambda$ . The leading or trailing edges might be used for defining the angle, or perhaps the mid-line between the two, but the most appropriate choice turns out to be the line 25% of the chord length from the leading edge. As pointed out above, under certain ideal conditions, the centre of effort at every section lies along this line. Even though this is not exactly true in a real case, it is still a good



**Fig 6.4** Definition of the planform

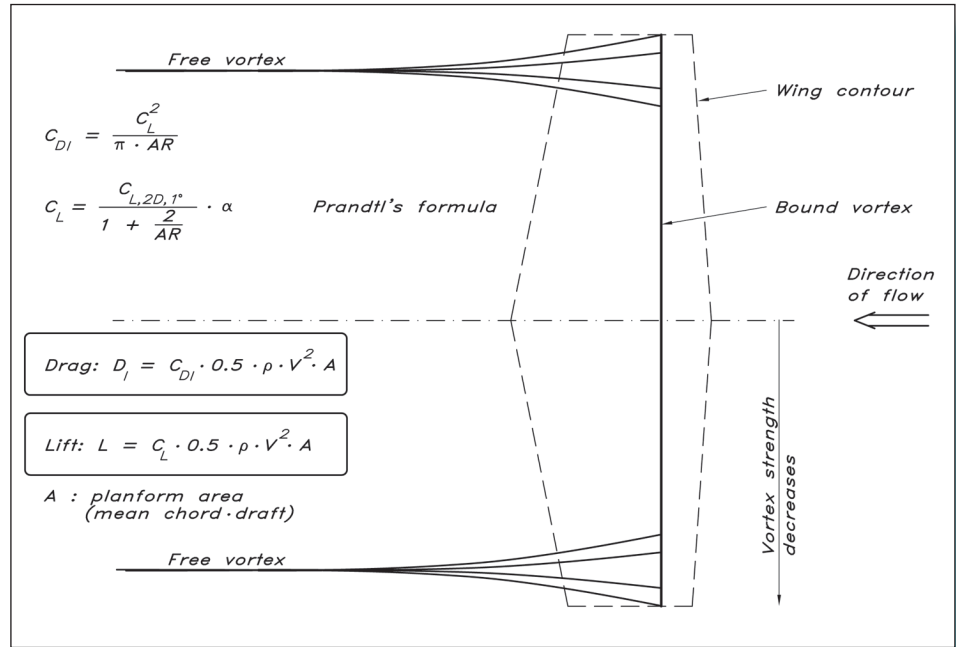
approximation for fin keels and rudders of normal aspect ratios. We will return to the location of the centre of effort in [Chapter 9](#), in connection with the balance of the yacht.

## ■ CLASSICAL WING THEORY

One of the most well-known and useful theories in aerodynamics is the so-called lifting line theory for computing the lift and induced resistance (drag) of wings. Without going deeply into the mathematics, the basics of the theory may be explained with reference to [Fig 6.5](#), which shows a wing with two free ends, symmetric about the centreline. It could also be interpreted as a keel with its image reflected in the hull bottom. The wing is dashed in the figure, since in the theory it is replaced by a set of vortices. There is thus one vortex along the span of the wing (from tip to tip). This is called the bound vortex, since it is fixed to the wing. However, as we have seen, vortices are shed backwards from the wing, particularly close to the tip. These are the free vortices, which align themselves with the local flow direction. There is a theorem stating that a vortex cannot have a free end in the flow. Thus, when a vortex filament bends backwards and leaves the bound part, the vortex strength of the latter is reduced by the strength of the filament. At the tip, all the vorticity has been shed backwards, and the bound vorticity is zero. Behind the wing, all the free vortex filaments roll up into one concentrated free vortex on each side. These two are in turn connected through the starting vortex (not shown in the figure), created when the wing started its motion.

The local force created by the vortex system is proportional to the component of the vortex at right angles to the local flow direction. Since the free vortices are parallel to the flow, they do not create any force, but the bound vortices on the wing generate a force that

Fig 6.5 Lifting line theory



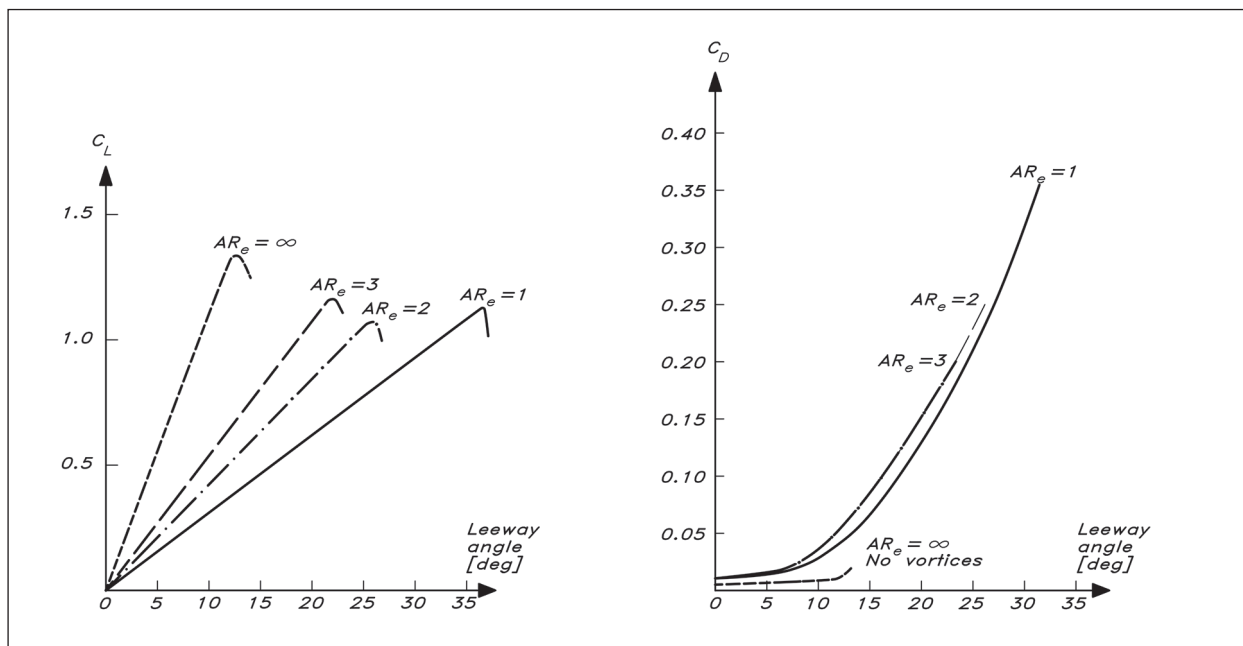
is proportional to the vortex strength. The theory also shows that the best distribution of vorticity, and hence force, on the wing is the elliptical one. In this case, the induced drag and lift coefficients,  $C_{DI}$  and  $C_L$  of the wing, and the corresponding forces, can be obtained easily, as shown in Fig 6.5.  $C_{L,2D,1^\circ}$  is the lift coefficient per degree in the two-dimensional case. For a symmetrical section in a frictionless fluid this coefficient may be obtained theoretically as  $\pi^2/90 = 0.11$ . In a real flow it is slightly smaller due to viscosity, and 0.10 is a good approximation for all symmetrical sections.

If the force distribution on the wing is not elliptic, the drag is increased while the lift is decreased. This may be accounted for in the equations by using the effective aspect ratio. As seen above this concept is introduced to account for the mirror image (by multiplication by 2), but it may also be used for the departure from the elliptical, by multiplication by a number slightly smaller than one. A departure from the elliptic distribution thus always reduces the effective aspect ratio. This effect is relatively small, as will be seen below, but it is large enough to matter, at least in the design of racing yachts.

We may summarize the most important results as follows:

- The lift and induced drag coefficients can be estimated in most cases from the formulae of Fig 6.5.
- The aspect ratio is the most important parameter for the lift and drag of a wing.
- The elliptical force distribution is the best one.

The effect of the aspect ratio appears again in Fig 6.6 (overleaf), which is based on wind-tunnel experiments with wings of different aspect ratios. Lift and drag coefficients are given for varying angles of attack. In the left-hand diagram very different curves are obtained depending on  $AR_c$ . For instance, at  $5^\circ$ , which is a typical leeway angle and hence angle



**Fig 6.6** Influence of aspect ratio on lift and drag

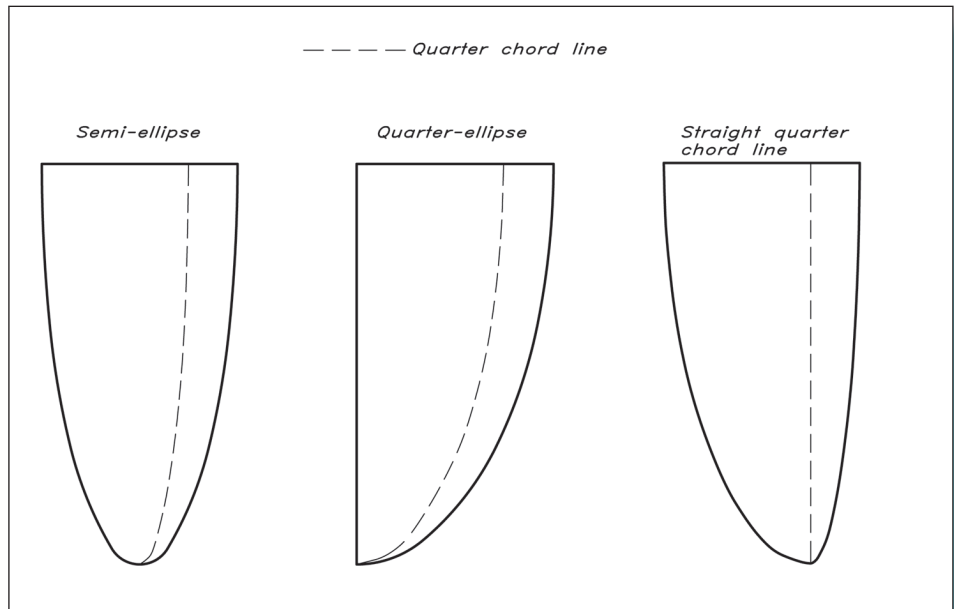
of attack for a keel, the square wing with  $AR_e = 1$  produces less than one third of the lift coefficient of the two-dimensional wing, which has  $AR_e = \infty$ . An effective  $AR_e = 3$  is relatively common for keels. It may be seen that this produces about twice as much lift as the square wing.

In the range of practical  $AR_e$  the drag is relatively unchanged, but it should be kept in mind that this is for a given angle of attack, while in reality a more interesting question is how much drag is produced for a given side force. As pointed out in [Chapter 5](#) the task of the keel is to balance the given side force from the sails at the expense of the smallest possible drag. With this in mind the lift diagram could be interpreted in a different way. For a given side force the leeway for the two-dimensional keel would be less than one third, and for the  $AR_e = 3$  keel less than half that of the  $AR_e = 1$  keel. Quite different drags would then be obtained as the right-hand drag diagram suggests. Note that  $C_D$  in [Fig 6.6](#) represents the total drag, i.e. also the viscous components, as presented in [Fig 5.4](#). This is why  $C_D$  is not zero at zero leeway angle.

The differences between traditional long keels and fin keels are now obvious. While the long keels have an effective aspect ratio considerably smaller than one, the modern fin keel  $AR_e$  values are usually larger than three. Large performance differences are therefore to be expected. However, there are also disadvantages to the fin keel. One of these was discussed in [Chapter 3](#) in connection with roll damping, and it was shown that a long keel is considerably more effective in this respect. Another disadvantage occurs at low speeds. As appears from the lift equation of [Fig 6.5](#), the lift is proportional to the lift coefficient, the speed squared and the keel area. Since fin keels have a smaller area, they operate at higher lift coefficients (which are easily obtained since they are more effective). However, the maximum  $C_L$  is about the same for all aspect ratios and it is reached much faster for a fin-keel yacht when the speed drops, if the side force is still required. This may happen



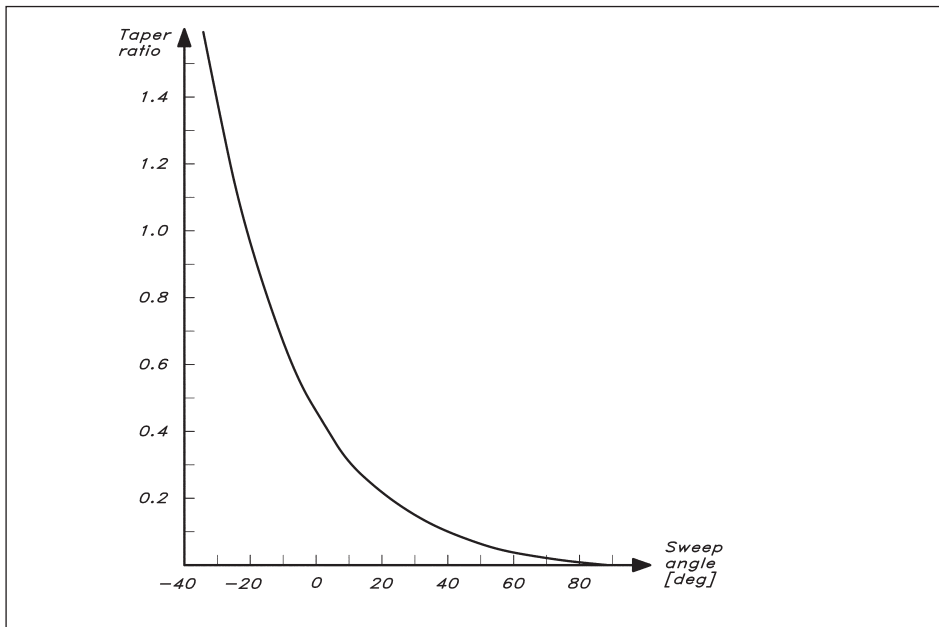
**Fig 6.7** Different elliptic keels



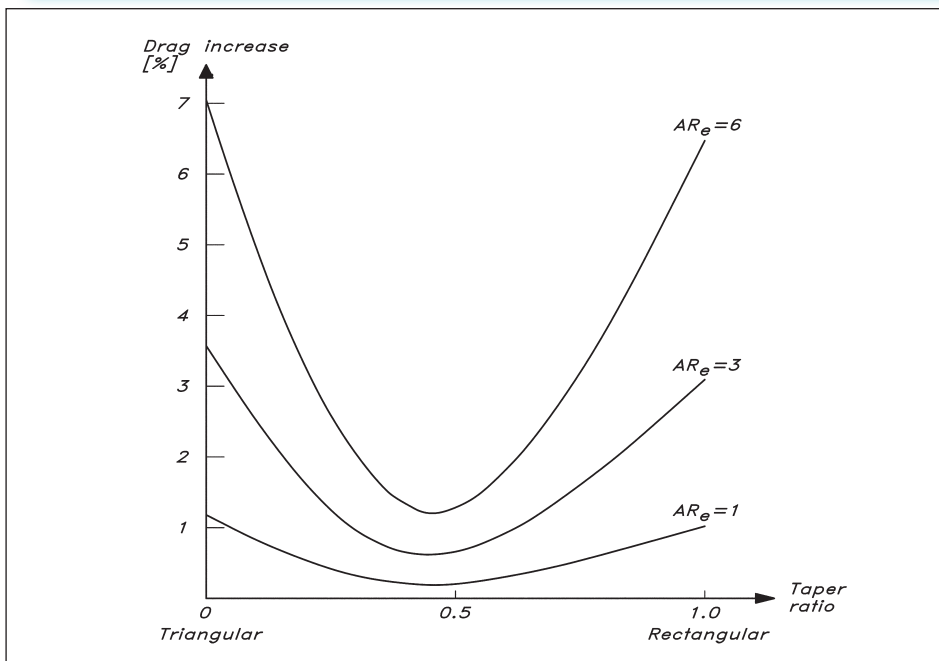
when berthing, or at the start of a race when there may be a considerable side force from the sails, but the speed is low. The keel then stalls, and the yacht starts moving sideways. The difference between long keels and fin keels is quite significant, and many owners of fin-keel yachts have experienced problems when manoeuvring in harbours.

To obtain the advantageous elliptical distribution of the side force the keel may be designed with an elliptical planform. This means that the chord length must vary elliptically from tip to root. Two geometries that would satisfy these requirements are the semi-ellipse and the quarter-ellipse (see Fig 6.7), but in both cases the important quarter chord line would be bent, so the force distribution would not be exactly elliptical. In the third alternative the design has started from a straight quarter chord line and the chord lengths have been distributed elliptically in the vertical direction, always keeping the 25% point on each chord on the line.

The elliptical planform has certain disadvantages, not least from a practical point of view, so trapezoidal keels are much more common. It is, in fact, possible to obtain a force distribution which is very nearly elliptic for this kind of keel also, provided the taper ratio is chosen to fit the sweep angle according to Fig 6.8. As can be seen in the figure, a small taper ratio requires a large sweep back and vice versa. At zero angle the taper ratio should be around 0.45, and for large ratios the keel should actually point forwards, since the angle is negative. Most keels have a sweep angle of 20–30°, which should call for a taper ratio of about 0.1. This is not practical, however, since the centre of gravity would then be too high up, and the stability poor. There is another disadvantage of small taper ratios. If the keel is unswept, and either elliptic or has a taper ratio of 0.45, the area distribution in the vertical direction corresponds to the force distribution. If smaller chords near the tip are compensated by sweepback to get large enough forces in the area, this part will be more highly loaded than the rest of the keel. The local lift coefficient will be higher, and this part will stall earlier. In practice, taper ratios lower than 0.2 are not recommended. As a



**Fig 6.8** Optimum relation between sweep angle and taper ratio



**Fig 6.9** Increase in induced drag due to non-optimum taper ratio

matter of fact, most designers use much larger ratios, 0.4–0.6, for stability reasons. Note that, if a given thickness ratio is used, the cross-sectional area of the keel increases as chord squared, which means that the amount of ballast carried near the tip is highly dependent on the tip chord.

Fig 6.8 is obtained from the lifting line theory, as is Fig 6.9, which shows the penalty if the force distribution is not elliptical. Only the zero sweep angle case is presented. The vertical axis shows the percentage increase in drag for the trapezoidal keel as compared

to the elliptic one. It may be seen that the penalty is smallest at a taper ratio of about 0.45, as expected. In this case very small drag increases are noted, for practical aspect ratios of less than 1%. If the taper is far from the optimum the increase may be up to 3–4%. It is interesting to note that the importance of a correct force distribution is quite dependent on the aspect ratio. For long keels with  $AR_c$  smaller than 1.0 the penalty is practically insignificant.

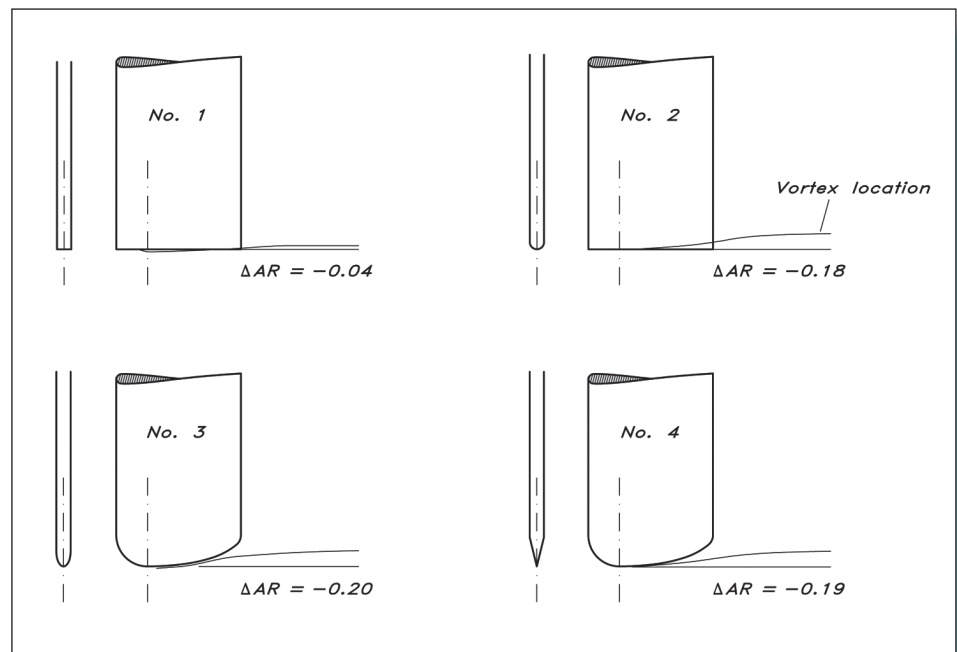
## TIP SHAPE

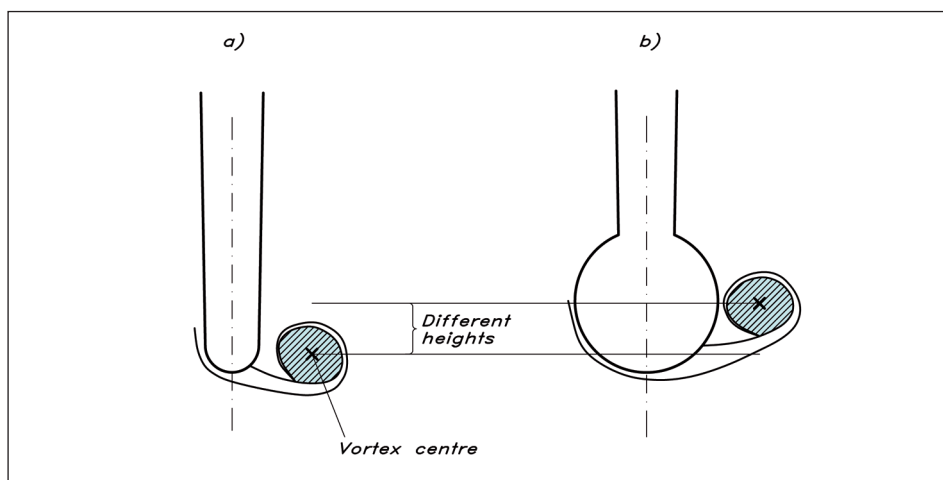
The lifting line theory is a useful tool in explaining the most important features of planform design. The most important conclusion to be drawn is that the primary parameter is the aspect ratio, whose influence on the forces can be computed with good accuracy using the formulae above. Sweep angle and taper may contribute a few per cent to the efficiency of the keel, but there are other factors not included in the theory which could also have some influence. We discuss one of them here, namely, the shape of the tip.

In the theory the wing is replaced by a vortex system, which is appropriate for the major features of the flow. However, in reality, the detailed shape of the wing tip will have some influence on the velocity distribution. One effect is that the trailing, free vortices, which are aligned with the local flow, may be positioned slightly differently, depending on the tip shape. This is important, since the effective span of the wing in Fig 6.5 is determined from the distance between the two trailing vortices far behind the wing. For a sailing yacht this means that it is the depth of the trailing vortex that defines the effective aspect ratio, rather than the actual keel depth.

Fig 6.10 shows the measured results of a series of tips. Both the planform and front

**Fig 6.10** Influence of tip shape on aspect ratio





**Fig 6.11** Location of tip vortex

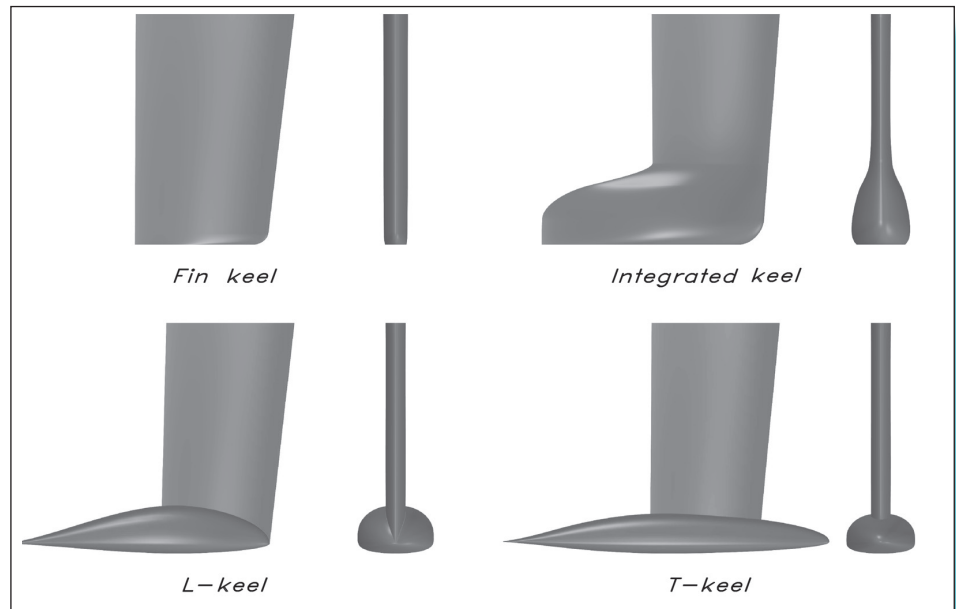
views are shown; the change in aspect ratio relative to the theory is given for each configuration. The location of the tip vortex is also given. It may be seen that the best design is the simplest one with a square cut off in both views. The worst is a tip that is rounded in both directions. In the former the geometric aspect ratio is reduced by 0.04, while in the latter the reduction is 0.20.

The reason why the square tip is better, considering first the planform view, is that the flow along the tip is guided backwards by the flat ending. It will not tend to move upwards as much as it would if the tip had been rounded. So the vortex stays further down. In fact, it would be possible to improve the tip shape even further by rounding the forward part in such a way that the flow approaches the tip smoothly, but the important thing is to keep the aft part straight.

The square shape in the front view is better than the rounded one, since the downward flow on the leeward side separates at the edge and the vortex is moved below the tip. A rounded shape permits the flow to move around to the windward side before it separates. The vortex may then be found on the windward side, not at maximum depth. [Fig 6.11](#) shows that this effect could be even larger for a bulbous keel. A disadvantage of the square ending is that separation will also occur at the corners under conditions when lift is not required. In downwind sailing an extra drag component will then appear. This disadvantage may be partly eliminated if the tip is made V-shaped and if the corners where the V meets the vertical part are rounded off.

A water-tunnel investigation of four different tip shapes (round, square, V and bulb) revealed that the best shape overall was the V, while the round shape was the best downwind. The effect of the bulb is a bit uncertain in this respect. As we have seen in [Fig 6.11](#) the large radius may help the flow pass the tip and move up on the other side, but this does not happen for all bulbs. A way to avoid this is to put a small riblet at maximum draft, thereby promoting separation of the vortex. Disadvantages of the bulb are that the wetted area increases greatly and that some interference drag is created in the corners between the bulb and the keel. These negative aspects may, however, be well compensated by the large increase in stability, and today most sailing yachts are designed with a bulbous keel.

Fig 6.12 Keels



#### ◆ Bulbous keels

To investigate the performance of different bulbous keels, several student projects were carried out at Chalmers University of Technology during 2010–2018 and were reported in Ljungqvist *et al* (2018). The four keels of Fig 6.12 were investigated. A plain fin keel was compared with the three most common bulb-type keels, referred to as ‘integrated keel’, ‘L-keel’ and ‘T-keel’. All bulb keels were designed for the same righting moment, but that of the fin keel was considerably smaller. Wind tunnel tests were carried out, as well as numerical computations. To convert the forces and moments to sailing speed, a Velocity Prediction Program (VPP) was used (see Chapter 17). Predictions were made for the 40-foot YD–40 yacht, used as an example in the first three editions of this book. Note that the wave making effect of the keels was not taken into account, but it should be very similar for all bulb keels.

Table 6.1 shows the predicted times per nautical mile for the four keels at two wind speeds. The time is given both for upwind sailing and for a combination of 50% upwind and 50% downwind. To account for the different stability between the fin keel and the others (which also differed slightly), the sail area was adjusted to give the same heel angle, 13.6° (the Dellenbaugh angle), considering the effect of the changed rig weight.

Table 6.1 Seconds per nautical mile. All keels in cast iron					
Wind speed	Course	Fin keel	Integrated keel	L-keel	T-keel
8 knots	Upwind	831	805	801	800
	Upw/Downw	918	895	893	890
20 knots	Upwind	627	615	611	611
	Upw/Downw	557	546	546	545

It can be seen that there is a considerable difference between the fin keel and the others, caused by the very different stabilities. The differences between the bulb keels are rather small, particularly at the higher wind speed, but the T-keel is slightly better than the others in all conditions except for upwind at 20 knots, where the L-keel is equally fast.

## LIFT AND INDUCED RESISTANCE OF THE YACHT

So far, the discussion of lift and induced drag has been based on lifting line theory, with the necessary modification due to the local tip flow. This is a very useful approach for optimizing the individual appendages, which are considered as wings. Through the introduction of the effective aspect ratio the mirroring effect and the departure from the elliptic loading may be taken into account. However, if the side force and induced resistance of *the whole yacht* is to be computed there are more effects to consider.

Lift coefficient:

$$C_L = 5.7 \cdot AR_e / (1.8 + \cos(\Lambda) \cdot (AR_e^2 / \cos^4(\Lambda) + 4)^{0.5}) \cdot \alpha$$

$$AR_e = 2 \cdot AR$$

$$\alpha_k = \beta \quad \text{and} \quad \alpha_r = \beta - \varepsilon + \delta_r$$

$$\varepsilon = a0 \cdot (C_{L,k} / AR_{e,k})^{0.5}$$

Lift force:

$$L_k = C_{L,k} \cdot 0.5 \cdot \rho \cdot V^2 \cdot A_k \quad L_r = C_{L,r} \cdot 0.5 \cdot \rho \cdot (0.9 \cdot V)^2 \cdot A_r$$

Hydrodynamic side force:

$$F_{h,k} = L_k \cdot c_{hull} \cdot c_{heel} \quad F_{h,r} = L_r \cdot c_{hull} \cdot c_{heel}$$

$$c_{hull} = 1.8 \cdot (T_c / T_k) + 1$$

$$c_{heel} = 1 - 0.382 \cdot \phi$$

$$F_h = F_{h,k} + F_{h,r}$$

$\rho$  : Density of water [ kg/m<sup>3</sup> ]  
 $V$  : Boat speed [ m/s ]  
 $A$  : Planform area of keel or rudder [ m<sup>2</sup> ]  
 $\Lambda$  : Sweep angle [deg]  
 $\beta$  : Leeway angle [rad]  
 $\phi$  : Heel angle [rad]  
 $\varepsilon$  : Downwash angle [rad]  
 $\delta_r$  : Rudder angle [rad]

$\phi$	$a0$
0	0.136
15	0.137

**Fig 6.13** Hydrodynamic side force of the yacht

First, there are now three bodies contributing to the forces: the keel, the rudder and the hull. Most likely, the combined side force distribution will be far from elliptic. Second, there is the effect of the water surface, which is influenced by all three bodies, particularly when the yacht heels. No simple relations exist for this flow. However, based on systematic keel variations, Keuning and Verwerft (2009) proposed a method for predicting the side fore of the yacht presented in Fig 6.13. This method takes into account the effects of the hull, the keel and the rudder, as well as the water surface. Note that the accuracy of this approach is too low for optimizing appendages. It merely serves as a means to estimate the total side force, considering all effects.

First, the upright lift coefficient is computed for the keel and the rudder using a formula derived by Whicker and Fehlner (1958) from wind tunnel tests with 3D wings. This formula should be somewhat more accurate than Prandtl's in Fig 6.5, since it includes the sweep angle. The aspect ratio is computed using the mirror image in the hull bottom, hence the factor 2 for  $AR_e$ .

The angle of attack for the keel is the leeway angle, while for the rudder the change in flow direction due to the keel is considered, as well as the rudder angle. To obtain the lift force, the lift coefficients are multiplied by the dynamic pressure ( $0.5 \times \text{density} \times \text{velocity squared}$ ) and the respective planform area. However, the water velocity at the rudder is assumed to be only 90% of the yacht speed. To obtain the hydrodynamic side force (horizontal) for the heeled yacht the lifts are multiplied by two factors, one for the effect of the hull and the other for the heel. Implicitly, the effect of the free surface is included in these factors.

There is no method presented for the corresponding induced resistance in the paper by Keuning and Verwerft, but a reasonable approach is proposed in Fig 6.14. In general, the induced resistance can be obtained from Prandtl's formula of Fig 6.5 knowing the lift coefficient and the aspect ratio. Here we know the hydrodynamic side force,  $F_h$ , for the keel and the rudder. As seen in Fig 5.1 this is horizontal. But we need the force in the heeled

**Fig 6.14** Induced resistance of the yacht

Induced resistance coefficient:

$$C_{Dl,k} = \frac{C_{L\Phi,k}^2}{\pi \cdot AR_{Ee,k}} \qquad C_{Dl,r} = \frac{C_{L\Phi,r}^2}{\pi \cdot AR_{Ee,r}}$$

$$C_{L\Phi,k} = F_{\Phi,k} / 0.5 \cdot \rho \cdot V^2 \cdot A_{E,k} \qquad C_{L\Phi,r} = F_{\Phi,r} / 0.5 \cdot \rho \cdot (0.9 \cdot V)^2 \cdot A_{E,r}$$

$$F_{\Phi,k} = F_{h,k} / \cos(\Phi) \qquad F_{\Phi,r} = F_{h,r} / \cos(\Phi)$$
  

Induced resistance:

$$R_{i,k} = C_{Dl,k} \cdot 0.5 \cdot \rho \cdot V^2 \cdot A_{E,k} \quad \text{and} \quad R_{i,r} = C_{Dl,r} \cdot 0.5 \cdot \rho \cdot (0.9 \cdot V)^2 \cdot A_{E,r}$$
  

$\rho$  : Density of water [ kg/m<sup>3</sup> ]  
 $V$  : Boat speed [ m/s ]  
 $A_E$  : Lateral area of extended blade [ m<sup>2</sup> ]  
 $AR_{Ee}$  : Effective aspect ratio, for extended blade [ m ]  
 $\Phi$  : Heel angle [deg]



plane,  $F_\phi$ , at right angles to the centreplane. This is obtained by division by the cosine of the heel angle and corresponds to the lift force. To obtain the lift coefficient we have to know the lateral area, and that is now taken as the area of the keel or rudder extended upwards to the waterplane in the upright condition. This is an approximate way of including the effect of the hull, and will be further explained in [Chapter 9](#) (see [Fig 9.2, page 202](#)). The extended aspect ratio  $AR_E$  is also computed for the extended keel or rudder. Considering the mirror effect of the free surface the geometrical  $AR_E$  is multiplied by 2 to get the effective extended aspect ratio  $AR_{Ec}$ . Then the induced resistance coefficient can be computed, and the force obtained in the normal way by use of the extended keel and rudder areas.

## ■ ADVANCED PLANFORM DESIGN

In this section we will describe some more advanced concepts used recently in keel planform design for racing yachts. In most cases a relatively detailed knowledge of the flow around the hull and keel is required, and this calls for tank testing or computational fluid dynamics (CFD) methods, not normally available to the amateur designer. It may, however, still be of interest to understand the principles behind the different concepts. A similar presentation will be made in connection with section design.

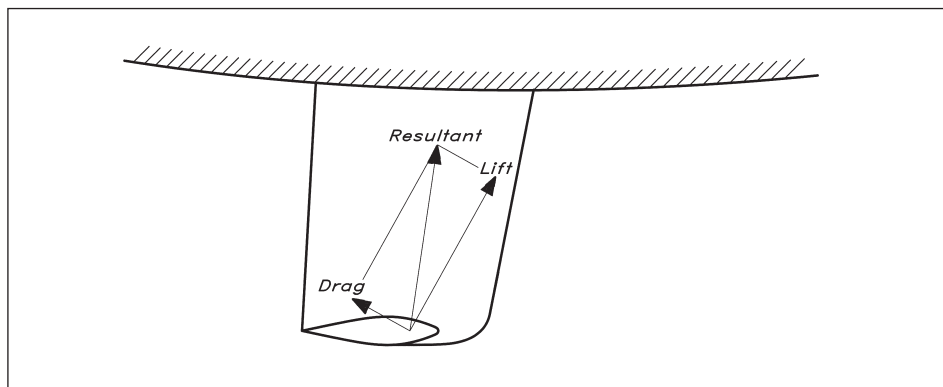
### ◆ Winged keels

An important development in keel planform design is the keel wing, used in the America's Cup from 1983 until the catamarans took over in 2010. The technique has also made its way into cruising. The basic idea is to increase the effective aspect ratio of the keel, without making it deeper, and thereby to reduce the induced resistance. Alternatively, the keel could be made shallower for a given resistance, an attractive option for cruising yachts.

The idea of manipulating the tip flow with some kind of device is quite old. Even in the 1940s experiments were made with end plates on keels at the Davidson Laboratory in New York. By putting a plate perpendicular to the keel plane at the tip, the overflow from the pressure to the suction side was reduced, and the effective aspect ratio increased. However, this was only at the expense of a large increase in viscous resistance due to the plates, so the total effect was unfavourable. It was not until the late 1960s that more effective devices with a streamlined wing shape were wind tunnel tested by the aerodynamicist S O Ridder, and used on racing yachts. The real breakthrough came after the victory of the Australian 12-metre *Australia II* in the 1983 America's Cup races.

If the tip device is to reduce the overflow it obviously has to have an angle of attack relative to the local flow direction. A device following the local streamlines would not alter the direction of the flow. With this in mind it is easy to understand why the simple plates did not work. A flat plate at an angle of attack produces a large drag, because the flow separates at the leading edge. It is therefore necessary to use well-designed foils with a minimum of viscous resistance to obtain a net positive result. Since the foils will not be aligned with the flow a lift force will develop. On the leeward side of the keel the flow is directed downwards and the wing generates a downward force. The opposite is true on the windward side, where the force points upwards. If the foil is effective enough both

**Fig 6.15** Keel wing force on windward side



forces may have a component forwards. The wing then pulls the yacht along. Fig 6.15 demonstrates that this occurs only if the drag is small enough relative to the lift. If this condition is not satisfied the wings will generate a drag force. It should now be apparent why the proper design of the wings is of the utmost importance.

Another way of looking at the effect of the wings is to consider the trailing vorticity left behind the keel. Without the wings a strong vortex is formed near the tip due to the overflow. The wing takes advantage of the vortical energy and reduces it, so that less is left in the wake, thereby reducing resistance. It should be pointed out that new vortices (of less strength) are now left behind the tips of the wings, where some overflow occurs.

Points to consider in the design of keel wings are:

- Root chord
- Pitch angle
- Span
- Longitudinal position
- Taper
- Junction fairing
- Twist
- Section characteristics
- Dihedral angle.

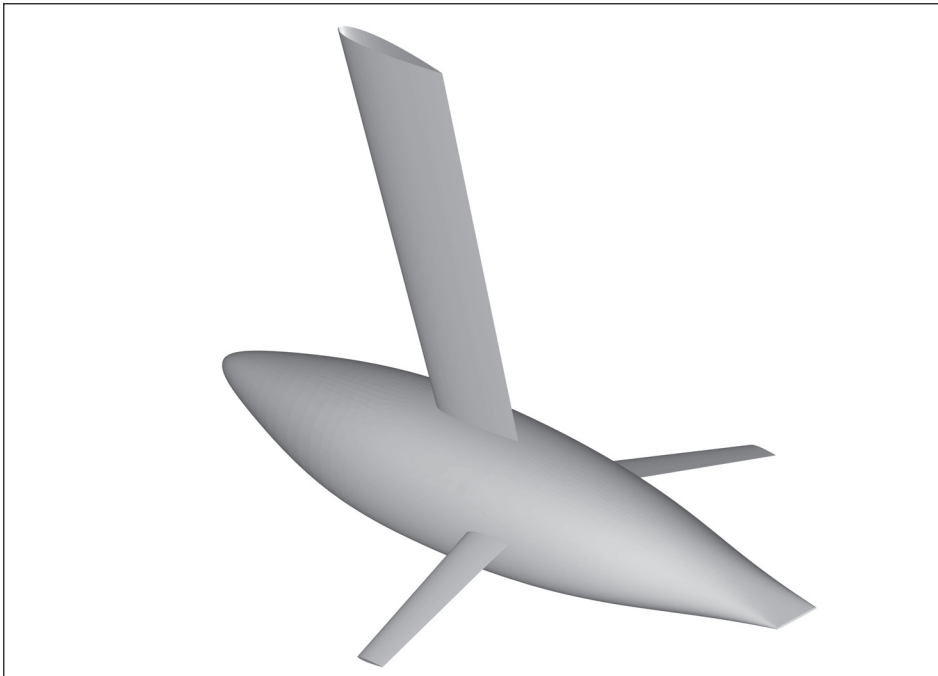
As to the root chord, there is a trade-off between frictional and induced resistance. In a frictionless fluid the root of the wing should be as large as the tip of the keel in order to avoid discontinuities in the load carried over from the keel to the wing. Such discontinuities mean shed vorticity and hence induced resistance. On the other hand, to minimize wetted surface and friction the chord should be as short as possible.

A similar situation exists for the span. In principle, the vortices shed at the wing tips are smaller for large spans, but the wetted surface is larger. Another important aspect of span size is the variation in local flow direction along the span. The larger the span, the stronger the variation. In the inner part of the wing the flow is mostly governed by the displacement of the hull, while further out the flow direction is determined by the waves. Obviously, heel angle and speed will alter these conditions. It is thus more complicated

to design large span wings. The taper and twist of the sections determine the loading and shedding of vorticity spanwise, and have to be optimized together.

The dihedral angle has caused some debate in yachting literature. This is the angle between the wing viewed from behind and the horizontal (hull upright). In our explanation above, the wings get their loading from the keel, due to the overflow from the pressure to the suction side. This is likely to be the major effect, but when the yacht heels and yaws the leeway itself causes an angle of attack on the wings, in such a way that the leeward wing becomes more heavily loaded, and the windward wing carries a reduced load. For instance, if the hull heels  $45^\circ$  and the dihedral angle is  $45^\circ$  the leeward wing will be vertical and exposed to the full leeway angle. The other wing will be horizontal and more lightly loaded. In this situation the largest vortex will be shed at the tip of the leeward wing which is at a draft that is probably larger than the nominal one. This is certainly an advantage. On the other hand, it is advantageous to equalize the vortices from the two wing tips, as will be explained below, and also, in fact, to spread them apart as much as possible. These latter effects speak in favour of small dihedral angles.

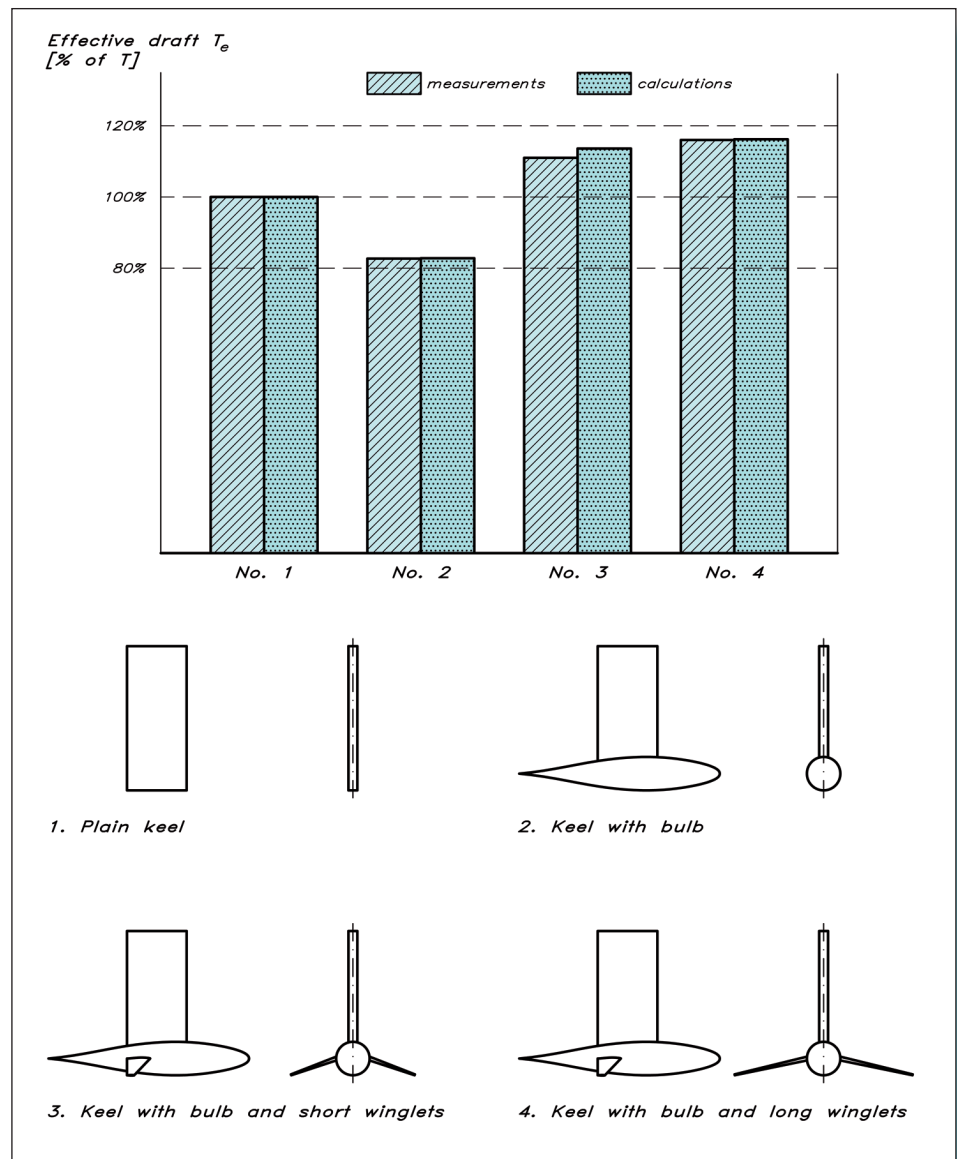
The pitch angle is defined as the angle of the wing root relative to the horizontal, viewed from the side. This has to be adjusted, as well as the angle of all sections, to the local flow direction. A common practice is to carry out the adjustment for the upright condition (where the wings are not needed) in such a way that the drag of the wings is minimized. In the early days of the winged keels this was accomplished by measuring the force on the wing and adjusting its angle in the towing tank to obtain minimum wing drag. The disadvantage of this approach is that the effect of the variation in the spanwise direction is not accounted for. It is now possible to compute the flow direction locally, and to unload each section of the wing by proper twisting.

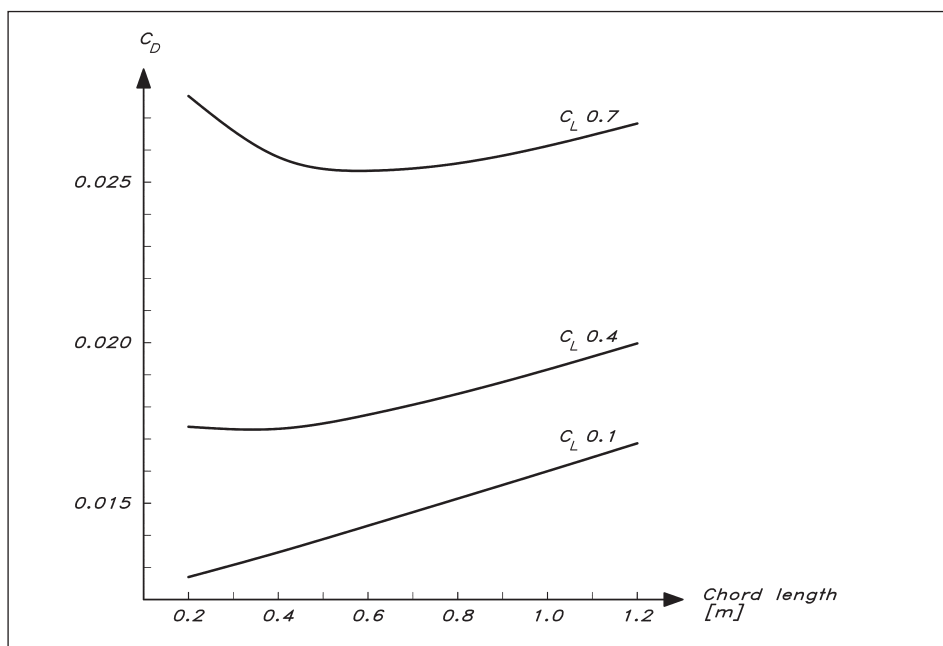


**Fig 6.16** Typical keel/bulb/wing configuration of the IACC class

A possible reason for the success of the *Australia II* may have been the large stability gain through the righting moment from the very fat wings, fitted to the keel. In view of the above, it is fairly obvious that the wings were far from optimum hydrodynamically. In modern designs the stability effect of the keel is separated from the hydrodynamic effects by adding a heavy bulb to the keel and fitting optimized wings to the bulb. A typical example is seen in Fig 6.16. This is a picture of a standard test case for numerical keel flow predictions investigated by Werner *et al* (2006). The addition of a bulb to a keel destroys the keel sections in the region covered by the bulb. Therefore, the hydrodynamic efficiency of the keel is reduced (but this is outweighed by the stability increase as we have seen above). This is borne out very clearly in the diagram of Fig 6.17, where measurements and computations of the effective draft of four different configurations are shown. The

**Fig 6.17** Comparison of measured and calculated effective draft  $T_e$  (Orych, 2005)





**Fig 6.18** Total resistance coefficient of a keel/bulb/wing configuration versus lift coefficient (Orych, 2005)

data was measured in a wind tunnel by Boeing (Tinoco *et al*, 1993) and the calculations were presented by Orych (2005). It is seen that the effective draft when adding a bulb is reduced by about 18%. On the other hand, adding wings to the bulb increases the effective draft by 14–16% relative to the bare keel. The longer wings are slightly better than the short ones.

Since the effective draft indicates how well a particular configuration performs in terms of induced resistance there is no penalty for wetted surface and friction. If friction is taken into account the keel/bulb configuration will still be worse hydrodynamically relative to the bare keel, and the advantages of the wings will be smaller. The optimum size of the wings will then depend on the required lift. Orych carried out computations with systematic variations of the wings for varying lift coefficients. The geometry corresponded to a typical former America's Cup Class (IACC) keel and one example is shown in Fig 6.18.

Here the total drag of the keel/bulb/wing configuration is shown versus root chord length. It is seen that the optimum chord for this case is about 0.6 m for a lift coefficient of 0.7 and about 0.4 m for a lift of 0.4. For a lift coefficient of 0.1 the diagram indicates that there should be no wings at all. (The curve has to be somewhat extrapolated.)

At the junction between the keel and the wing a vortex is normally created. This vortex gives rise to a resistance component. The same phenomenon also occurs in the junction between the keel and the hull. To alleviate the problem a special fairing, called a fillet, may be used. The classic design of the fillet is to start at the leading edge and increase the radius along the intersection backwards to the trailing edge, where the fairing radius should be of the order of the (largest) boundary layer thickness. In the keel/hull junction the hull boundary layer is normally a few centimetres, for a 41-footer like the YD-41 around 5 cm. In the keel/wing junction the keel boundary layer is thinner, and a radius of about 1 cm seems appropriate. It is very important that the fillet is tapered off smoothly behind the

trailing edge. Other ideas for fillet design have been suggested recently, but they do not seem to work at an angle of attack and are therefore of little use in yacht design.

Considering all the trade-offs and the detailed knowledge of the flow required, it is very unlikely that those other than experienced fluid dynamicists can design effective wings. If wings are just added without the above considerations, the chances that they will have a negative effect, rather than a positive one, are quite high.

#### ◆ Forward rudders (canard wings)

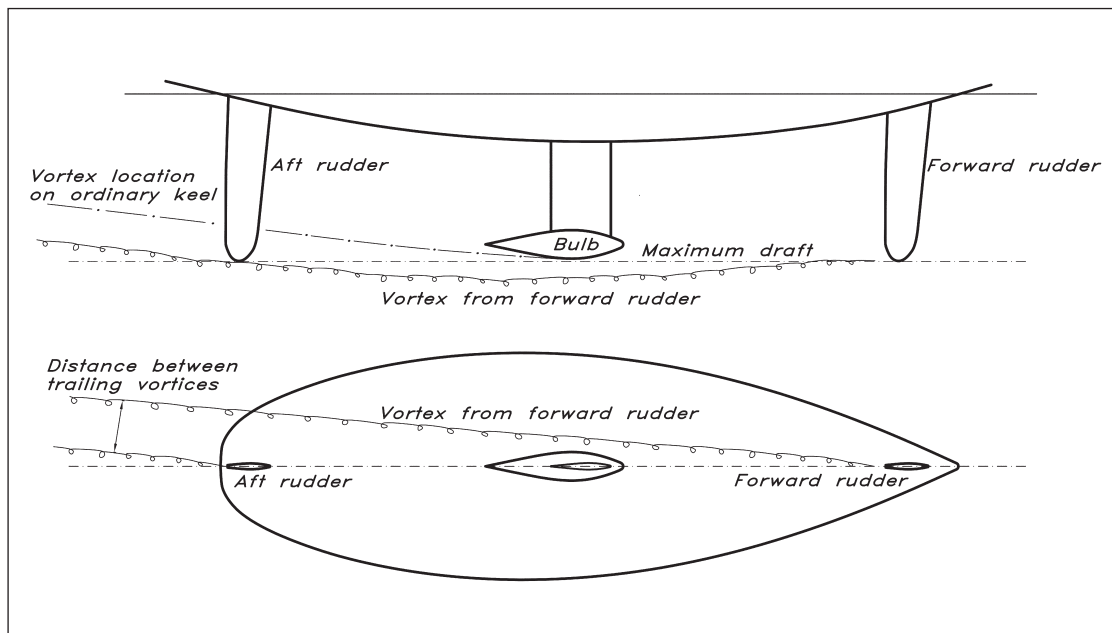
In the America's Cup races of 1987 the American yacht *USA* featured a radical underwater design, where the two normal tasks of the keel (to lower the centre of gravity and to produce a side force) were split on different devices. The ballast was put into a large bulb, kept in position below the hull by a streamlined strut, and the side force was produced by a forward and an aft rudder.

The effect of splitting the side force between two surfaces may be investigated using biplane theory. The principle is straightforward: by reducing the lift on each one of the surfaces, keeping the span unchanged, the sum of the induced resistances becomes smaller than for one surface alone. This is so because, as we have seen in the lifting line theory, the induced resistance is proportional to the lift squared. If there were no interference between the two surfaces, splitting the lift into two halves would result in a resistance of each surface of only one quarter of the original one, i.e. the total resistance would be halved. Unfortunately, the interference effects cannot be ignored, unless the trailing vortex systems are several span lengths apart. There is thus no point in putting the aft wing in the wake of the forward one. The vortex systems would then coincide and co-operate to generate the same resistance as if there had been only one wing. If the wings, or lifting surfaces, are put side by side, there is a gain. For instance, on sailing catamarans the two centreboards are several span lengths apart and may be considered independent.

At first glance, the forward and aft rudder configuration may seem a useless idea, since the rudders are located behind one another. However, because the hull has a leeway angle and the rudders are far apart the distance between the trailing vortex systems may be significant, if not large (see the bottom part of Fig 6.19, overleaf). A leeway angle of  $4^\circ$  with the rudders 15 metres apart would result in a trailing vortex separation of approximately 1 metre, which is about 40% of the draft. This should be enough for a noticeable drag reduction.

Fig 6.19 illustrates another interesting effect of the positioning of the rudders at the ends of the relatively deep hull. The trailing vortex systems are influenced by the flow around the hull, as can be seen in the top figure. The ultimate location in the wake will be further down than for an ordinary keel positioned approximately at the maximum draft of the canoe body. Since it is the location of the vortex far behind that determines the effective draft, the rudder arrangement is better, given the maximum geometric draft of the configuration.

A third possible advantage of the forward and aft rudder configuration is the effect on the wave system. While an ordinary keel has an unfavourable effect on the waves, the opposite may be true for the rudders. When the hull sails upwind at full speed, the Froude number is around 0.35 and the wavelength is slightly smaller than the waterline length. There is thus a wave trough at midship. If the hull heels significantly the suction side of



**Fig 6.19** Forward and aft rudder configuration

the keel will be close to the water surface, thus deepening the trough. The rudders, on the other hand, will apply their suction in regions where there are wave crests, which should reduce their height.

There are several practical aspects of the forward and aft rudder configuration. In principle manoeuvrability will be increased, but that requires a good control system for co-operation between the rudders. Another aspect is the risk of ventilation when the rudders are lifted due to the heeling of the yacht. Beamy yachts may lift the rudders too much to be effective. In any case, the forward and aft rudder configuration is interesting and will probably appear more frequently on fast racing yachts in the future.

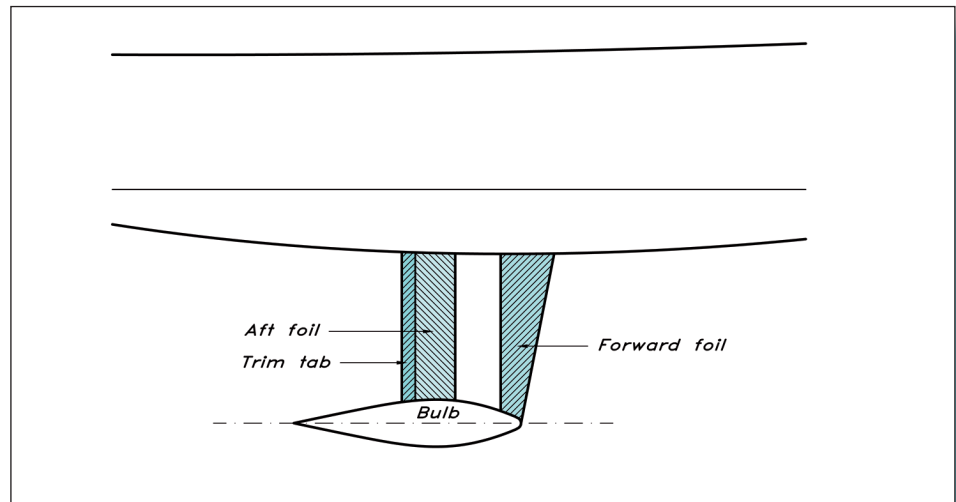
#### ◆ Tandem keels

As for the forward and aft rudders, the side force on a tandem keel is split on two foils, but much closer together. Normally they are also linked through a horizontal fin or a bulb (see Fig 6.20, where there is also a trim tab on the aft foil). There is now a strong interaction between the two foils in much the same way as between the jib and the mainsail, which will be described in the next chapter. The reader is referred to the theoretical explanation given there.

The two major positive effects of the tandem configuration are the increased maximum lift coefficient obtainable before stall, and the possibility of obtaining laminar flow over a larger area. The latter may seem surprising, but according to experiments the turbulence in the wake of the forward foil is swept sideways fast enough not to disturb the aft foil, so laminar flow may be exploited even there. The increased maximum lift coefficient means that a smaller lateral area is required, so both effects mean less friction. A further step in this direction might be taken by dropping the rudder altogether and steering the yacht with the trim tab.



**Fig 6.20** Tandem keel with trim tab



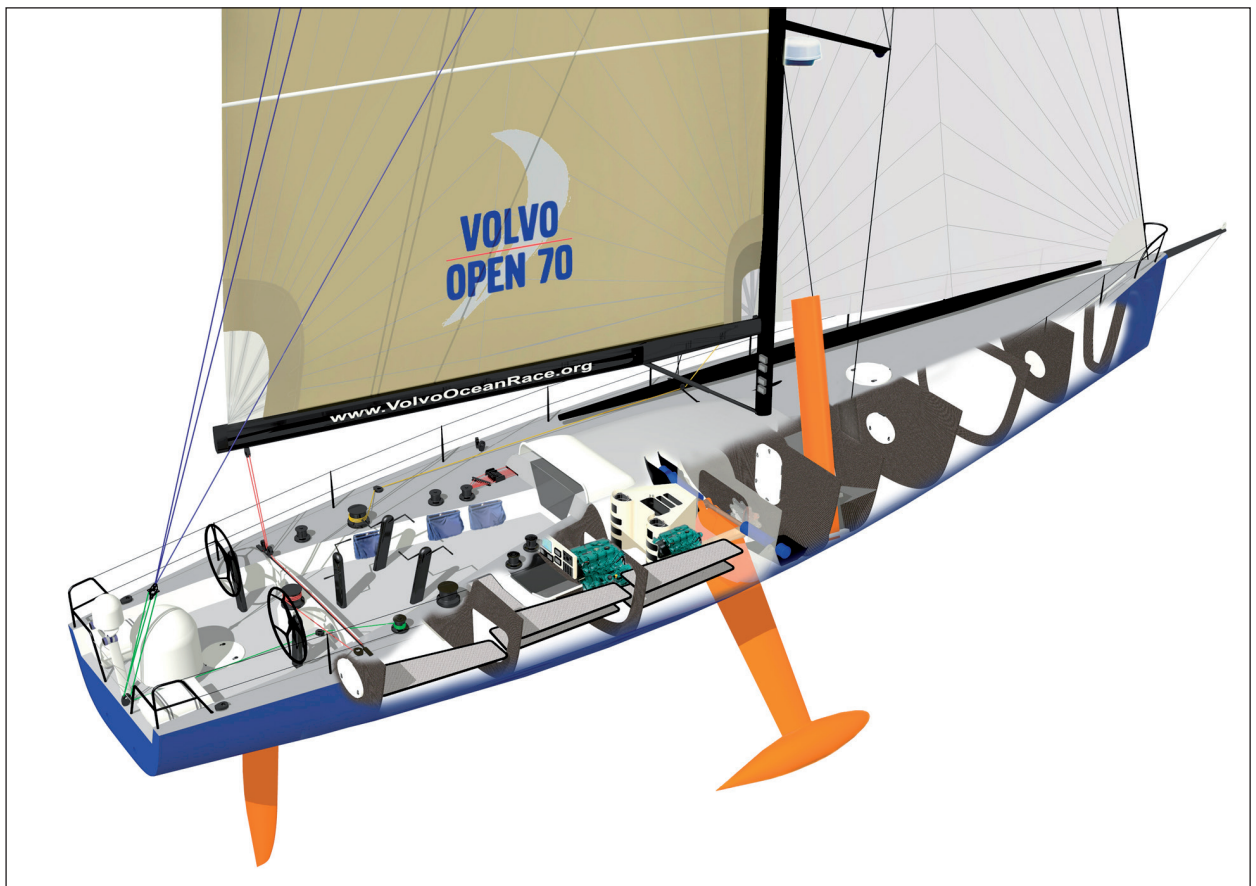
## ■ CANTING KEELS

Extreme racing yachts, such as the Volvo Open 70, exhibit canting keels for improved stability. A typical example is shown in Fig 6.21. Here the keel can swing sideways  $45^\circ$  in each direction. Going upwind a hydraulic system will swing the keel and bulb to windward, which considerably increases stability. On the other hand, the ability of the keel to produce a side force is more or less lost. Therefore, the side force generation is taken over by daggerboards, which are centreboards placed in the bilge region, i.e. far from the centreline. Since only the leeward one is lowered it may be tilted to become more vertical when the yacht heels. It may also benefit from asymmetric sections, which produce the required side force at a smaller leeway. The task of the keel blade is to support the bulb weight, so it can be designed without considering its lift-generating capability. Canting keel yachts often also have twin rudders, tilted in the same way as the daggerboards to increase efficiency.

## ■ EVALUATION OF SOME PLANFORM CONCEPTS

An evaluation of seven different keel concepts was made at the Delft University of Technology in the early 1980s. All keels were tested on the same hull, a 3.2 m model of a 63 ft fast cruising yacht. To isolate the hydrodynamic effects from the stability, which varied somewhat between the keels, all evaluations were made with the same righting moment of the yacht.

The seven keels are shown in Fig 6.22. Since the emphasis was placed on minimizing the draft of the yacht without compromising performance too much, most of the keels had a very small span: only 1.39 m. This was true for numbers 2, 3, 4, 5 and 6, while 1 and 7 had a more normal span of 2.29 m. No. 1 was a standard trapezoidal keel, with which to compare all the others, and no. 7 was elliptic. Among the shallow draft keels, no. 3 was

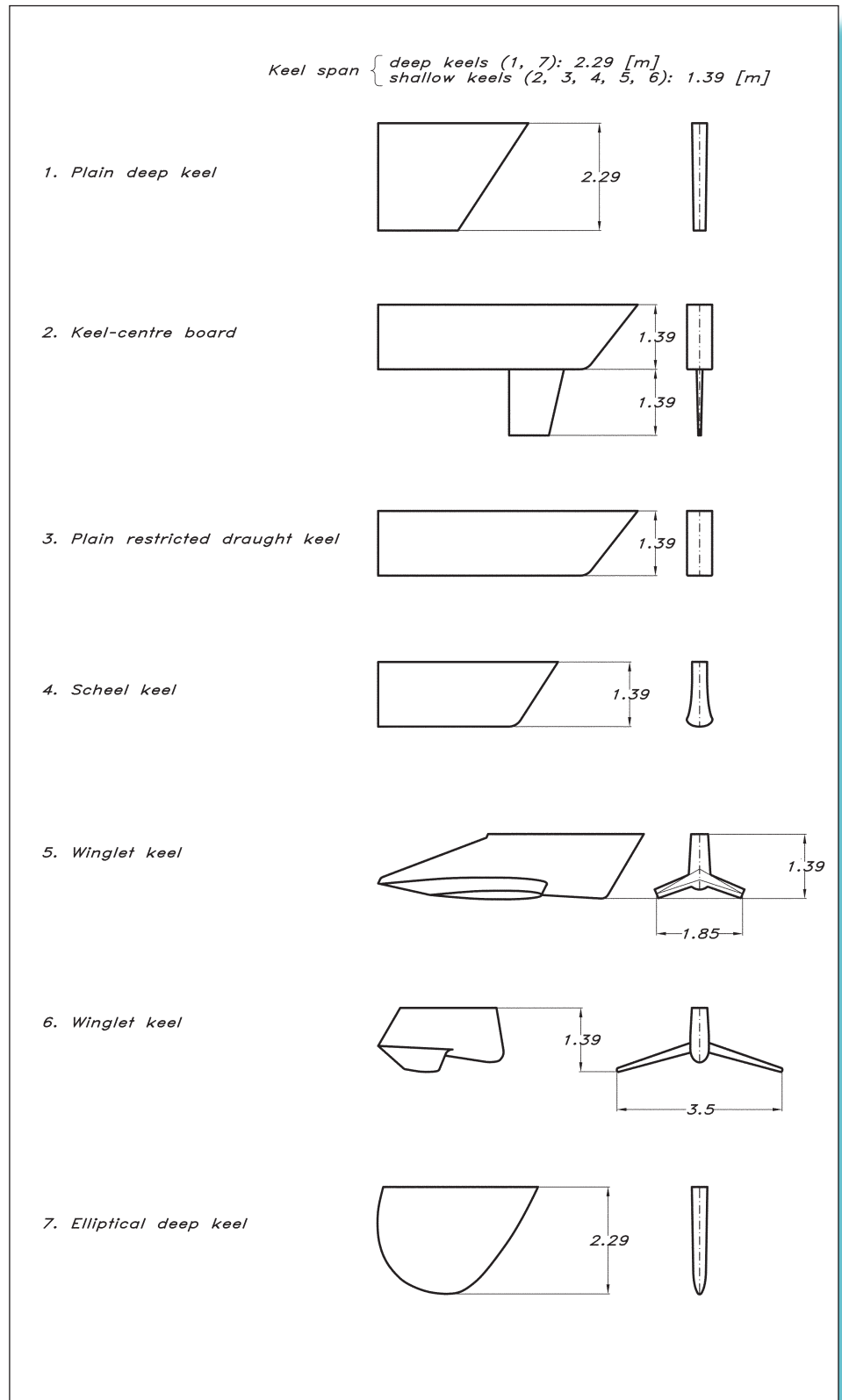


just a trapezoidal reference case, while the others exploited some kind of device at the tip. No. 2 had a centreboard, which increased the draft by 1.41 m, no. 4 was a so-called Scheel keel and nos. 5 and 6 had wings of different spans. A Scheel keel has very thick sections near the tip, as can be seen from the figure. This is to try to reduce the overflow by means of the ‘corners’ seen in the front view near the bottom of the keel.

Tests were made and evaluated using a VPP. Sailing speeds at all wind speeds and directions of interest were thus obtained, and [Table 6.2 \(page 125\)](#) presents the final outcome, namely the elapsed time on an Olympic course at two wind speeds. It may be seen that the elliptic and the basic trapezoidal keels are the best, and virtually identical. The fact that they are the best is not, of course, surprising, since they have the largest draft. More interesting perhaps is the fact that keel no. 6, which is much shallower, is almost equally good in the strong wind. It is thus possible to reduce the draft by introducing wings without much loss in performance. In fact, if the draft difference had been smaller the winged keel might have been equal, or even better. The winglet keel with the small span, the Scheel keel and the shallow trapezoidal keel were 2%, 3.5% and 5%, respectively, slower than the best on the Olympic course. A somewhat disappointing result is the performance of the centreboard keel, which had the largest draft including the board, but was 2% slower than the best. It should be noted, however, that the board was left down under all conditions, while in reality it would have been raised downwind.

**Fig 6.21** Illustration of a Volvo Open 70 with a canting keel (swung to windward) and bilge boards (windward one shown hoisted). Courtesy of Volvo Ocean Race

**Fig 6.22** Keels tested by Professor Gerritsma and others



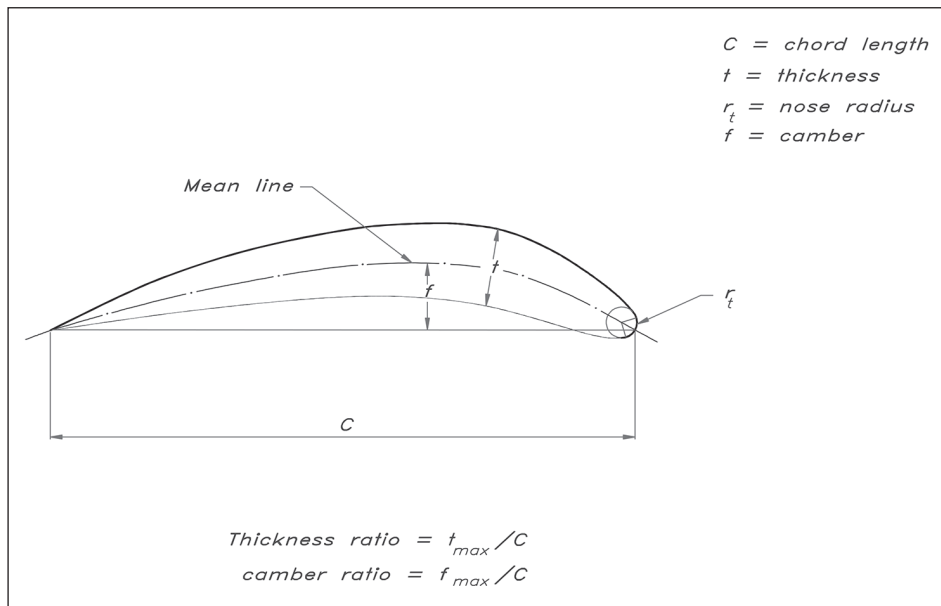
**Table 6.2** Elapsed time (hours, with decimals) on an Olympic course for the Delft Keels

Wind speed (knots)	Keel no.						
	1	2	3	4	5	6	7
15	3.96	4.06	4.13	4.10	4.04	4.01	3.96
25	3.52	3.60	3.72	3.64	3.60	3.53	3.52

## ■ DEFINITION OF THE SECTION

The sectional shape of the keel does not have such a significant effect on its characteristics as the planform, but on the other hand the most important planform parameter, the aspect ratio, is fixed in most class rules and heavily penalized in rating rules. A study of the influence of the sectional characteristics may therefore be worthwhile.

In Fig 6.23 the geometrical parameters defining a foil section are presented. The section of the figure is asymmetric, i.e. the mean line, defined as the line midway between the upper and lower surface contours, is bent. As pointed out above, asymmetric sections are rarely used for sailing yachts, since they have to perform equally well on both tacks. We will limit most of the following discussion to symmetric sections, where the mean line is straight. The thickness  $t$  is measured at right angles to the mean line, and the maximum thickness is denoted  $t_{\max}$ . The thickness ratio of the section is  $t_{\max}/C$ , where  $C$  is the chord length. An important parameter for the section characteristics is the nose radius,  $r_t$ , which is defined as the radius of curvature at the leading edge. This definition is not very practical, but as a rule of thumb the nose radius defines a circle, which follows the nose contour upwards and downwards about  $45^\circ$ .

**Fig 6.23** Definition of section shape

## ■ THREE USEFUL NACA SECTIONS

Unfortunately, many sailing yachts use foil sections that are not well designed. As a general rule the designer should not attempt to develop his own section, unless he is an experienced fluid dynamicist. There are several books listing useful sections available, and these can be used in most cases. The most well-known publication in this area is the classic *Theory of Wing Sections*, Abbott & von Doenhoff (1949). This book contains not only theories of wings and wing sections, but also an extensive presentation of the geometry and characteristics of a large number of sections.

In Table 6.3 the geometries of three useful sections are presented. The first belongs to the so-called four-digit series, where the last two digits represent the thickness ratio

Table 6.3 Three useful NACA sections			
x	y 0010	y 63-010	y 65-010
0	0	0	0
0.5	1.018	0.829	0.772
0.75	1.237	1.004	0.932
1.25	1.578	1.275	1.169
2.5	2.178	1.756	1.574
5.0	2.962	2.440	2.177
7.5	3.500	2.950	2.647
10	3.902	3.362	3.040
15	4.455	3.994	3.666
20	4.782	4.445	4.143
25	4.952	4.753	4.503
30	5.002	4.938	4.760
35	4.958	5.000	4.924
40	4.837	4.938	4.996
45	4.651	4.766	4.963
50	4.412	4.496	4.812
55	4.127	4.140	4.530
60	3.803	3.715	4.146
65	3.444	3.234	3.682
70	3.053	2.712	3.156
75	2.634	2.166	2.584
80	2.187	1.618	1.987
85	1.710	1.088	1.385
90	1.207	0.604	0.810
95	0.672	0.214	0.306
100	0.105	0	0

and the first two give information about the mean line. For a symmetric section only the last two digits are of interest. The other two sections belong to the six-series, which may be considered more modern, even though it was designed in the 1940s. The six-series contains five different groups, denoted 63, 64, 65, 66 and 67, where the second digit gives the position of minimum pressure along the chord. The 63-series thus has its minimum at 30% of the chord from the leading edge, the 64-series at 40%, etc. This information is quite important, as we will see. After the dash in the number the first digit concerns the mean line, while the last two give the thickness ratio in per cent. All three sections of Table 6.3 have a thickness ratio of 10%. The four-digit series can be scaled to any other thickness by multiplying all  $y$ -values by the thickness desired divided by the given 10%. This is not precisely true for the six-series, but it is a good approximation if the thickness ratios are not too far from 10%.

The sections are specified in the table by a set of  $x$ - $y$  values, where  $x$  is along the chord, measured from the nose and  $y$  is at right angles to  $x$ . Note that both coordinates are given in per cent of the chord length and that only one half of the (symmetric) section is defined. To be able to describe the most important part of the section, namely the nose region, the nose radius is required. This varies quadratically with the thickness ratio, as appears from Fig 6.24, which gives the radius, not only for the two series, but also for an ellipse. It is seen that the six-series is relatively close to the ellipse, while the nose radius for the four-digit series is much larger.

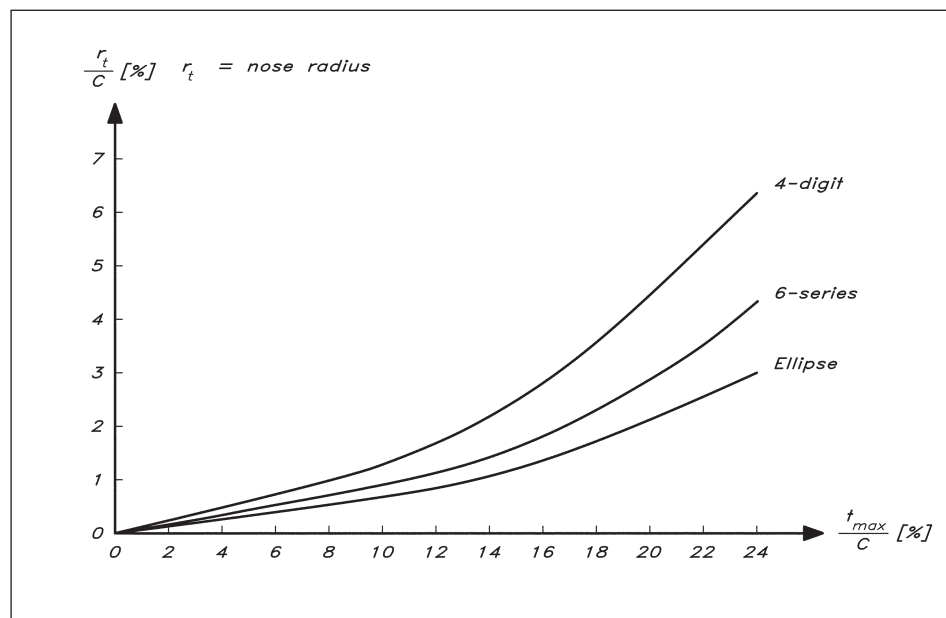


Fig 6.24 Nose radius

## ■ INFLUENCE OF SHAPE ON SECTION CHARACTERISTICS

In order to understand the influence of the shape of the section on its performance, reference should be made to Fig 5.5, which shows the boundary layer around a hull. In principle, the same picture may represent the flow around an airfoil section. There is a laminar boundary layer developing backwards from the leading edge. After a certain distance the flow becomes unstable, and shortly thereafter the boundary layer undergoes transition to the turbulent state. Under certain conditions the flow may separate, and recirculation may occur. When compared to the case of Fig 5.5, which is symmetric, one difference is that for an airfoil at an angle of attack the flow picture is not the same on the two sides. We recall from the discussion in Chapter 5 that the boundary layer development is determined from the pressure distribution, which in turn depends on the shape. A favourable pressure distribution with diminishing pressure stabilizes the flow, which is then sucked backwards. An increasing pressure works in the opposite direction and destabilizes the flow in such a way that transition moves upstream and separation occurs more easily.

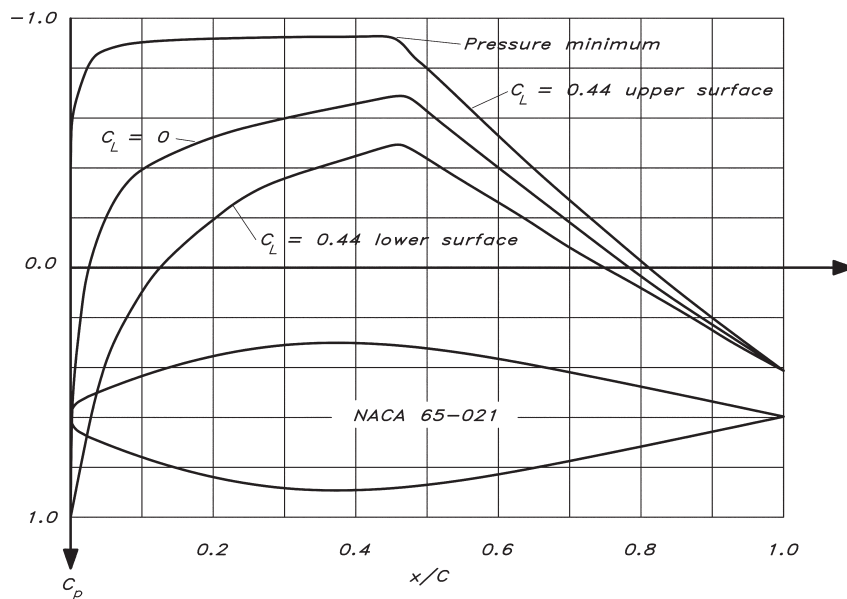
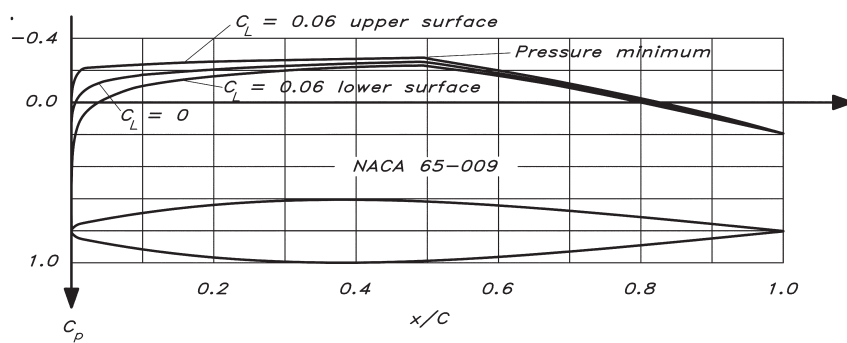
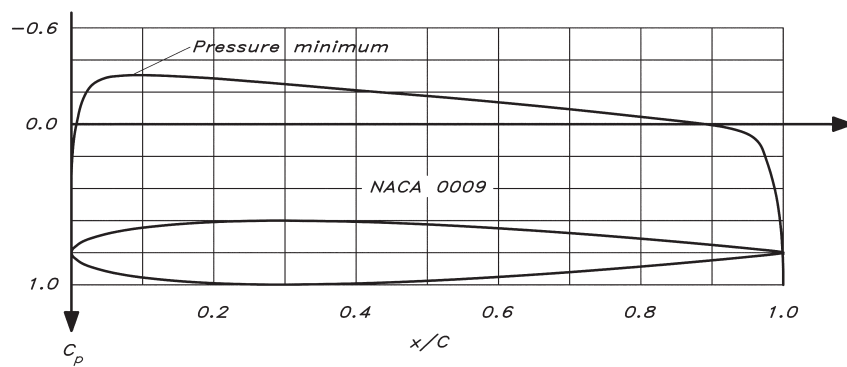
With these considerations in mind it is of interest to examine the pressure distribution on the three typical sections shown in Fig 6.25. The first is a conventional four digit NACA section with a thickness ratio of 9%, while the other two belong to the 65-series, with 9% and 21% thickness ratios, respectively. As before, negative pressure is upwards on the vertical scale. It may be seen that the four-digit section has its pressure minimum very far forward, close to 10% of the chord from the leading edge. This means that a favourable pressure distribution exists on only 10% of the chord, and that transition is likely to occur far forward. On the two other sections the maximum thickness, and hence the pressure minimum, occurs further back, and a much larger laminar zone can be anticipated, resulting in a considerable drag reduction.

For the 65-series two extra pressure distributions are given. These show the pressure on the upper and lower sides of the section at the maximum angle (i.e. maximum lift coefficient) for which it works properly. It can be seen that a favourable pressure distribution is maintained even on the suction side up to a lift coefficient of 0.06 for the thin section and 0.44 for the thick one. At higher lifts, i.e. larger angles of attack, the suction peak moves very far forward on the suction side, transition occurs close to the leading edge and the drag increases. A typical lift coefficient sailing upwind is 0.2, while it is almost zero downwind. The differences between the three sections may now be summarized as follows:

- The four-digit series has its pressure minimum further forward and has consequently a smaller region of laminar flow as compared to the 65-series.
- The thin section works well only in a small range of angles of attack, while the thick section accepts larger angles.

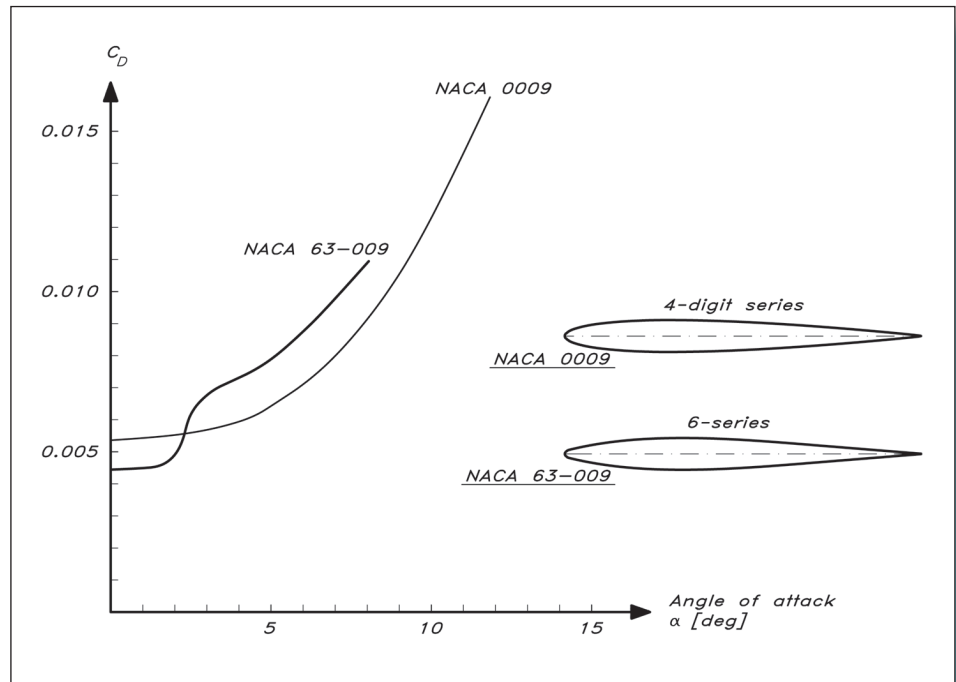
We will now turn to a more quantitative discussion of the differences in lift and drag. First the difference between the series will be presented. In Fig 6.26 two sections of the same thickness (9%) are shown, together with the corresponding drag curves. The four-digit and 63-series are compared, since the 65-series, shown in Fig 6.25, is rarely





**Fig 6.25** Influence of shape on pressure distribution

**Fig 6.26** Comparison between two sections

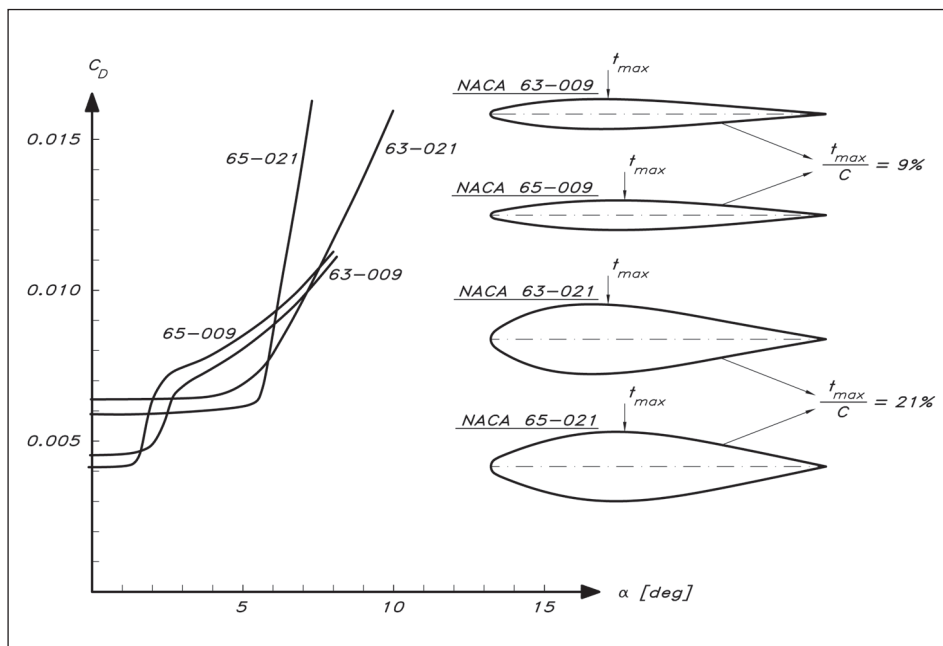


used for such small thicknesses. It appears that the 63-section has about 20% smaller drag up to about  $2^\circ$  of angle of attack, while for larger angles the four-digit section is superior. It should be pointed out that the angle is for a two-dimensional wing, i.e. with  $AR = \infty$ . For more practical  $AR$ s the angle is about twice as large, given the lift coefficient (cf Fig 6.6).

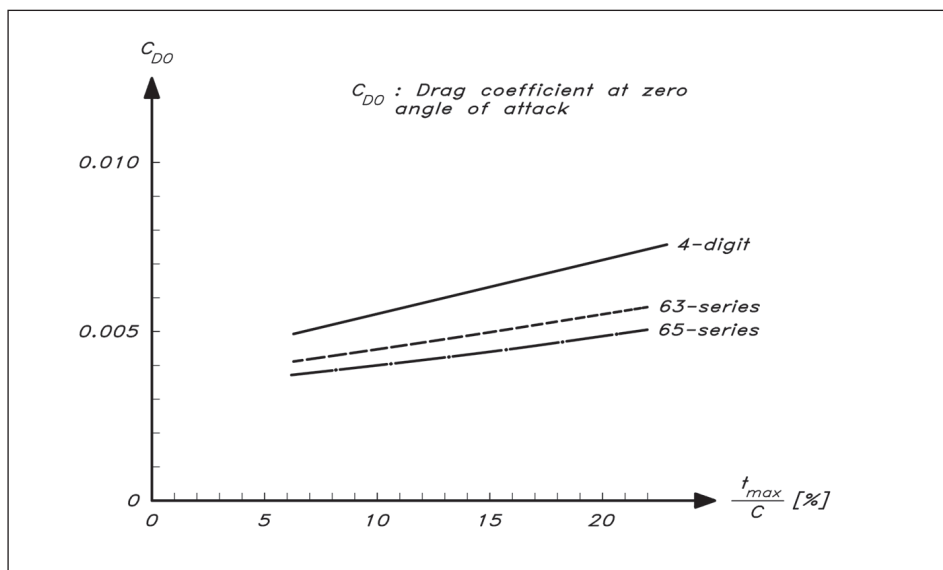
The influence of the thickness and its distribution for the same type of sections, all belonging to the 6-series, is exemplified in Fig 6.27. Two 9% and two 21% sections are shown. The sections of the same thickness differ, since they are from the 63- and 65-series, respectively. The location of the maximum thickness (and the pressure minimum) is different. It can be seen that the thin sections have the smallest drag at small angles of attack, while the so-called 'drag bucket' is much wider for the thick ones. Furthermore, the 65-sections give smaller drag than the 63-sections, but the drag bucket is slightly narrower.

To simplify the comparison at zero angle of attack, Fig 6.28 has been prepared. The drag coefficient for varying thickness ratios is given for the four-digit, as well as the 63- and 65-series. There is obviously quite a large difference, particularly between the four-digit series and the others.

The difference between the lift coefficients is much smaller, as can be seen from Fig 6.29. For the range of angles of interest ( $2-3^\circ$ , corresponding to  $4-6^\circ$  at  $AR = 3$ ), the difference is hardly noticeable and the approximate value, 0.10, of the two-dimensional lift coefficient per degree ( $C_{L, 2D, 1^\circ}$ ), given above, seems to fit the data quite well. There is, however, quite a difference at high angles of attack. The thin sections tend to stall abruptly, with a large loss in lift as a consequence. The thick sections, on the other hand, exhibit a much more gradual stall, with an almost constant lift. An explanation of the



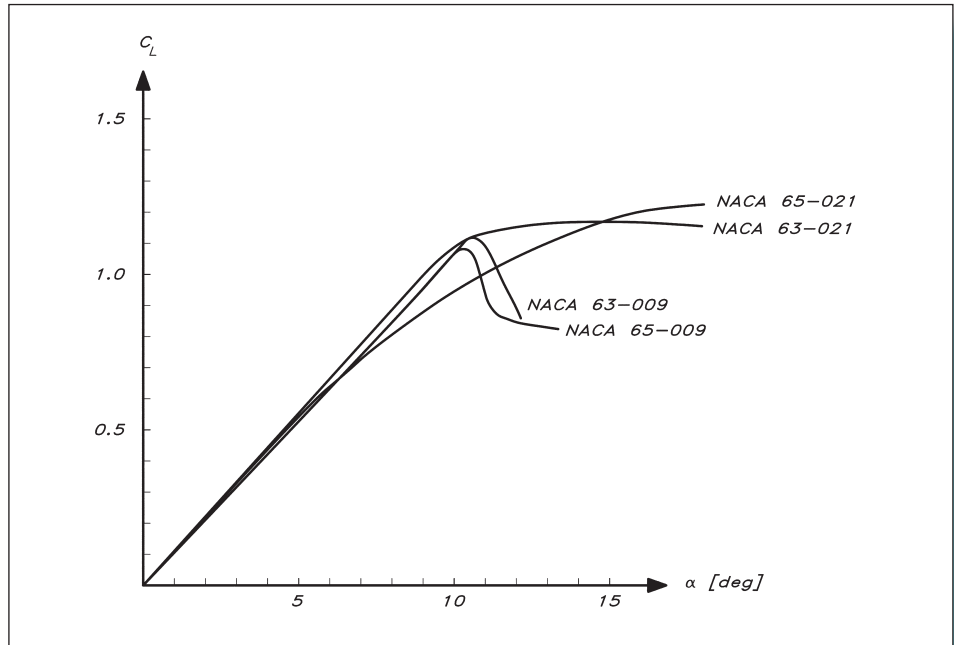
**Fig 6.27** Influence of section shape on drag



**Fig 6.28** Influence of thickness on drag at zero angle of attack

differences may be given with reference to Fig 6.30. When a thick section (Case (a)) stalls, separation occurs on the suction side near the trailing edge. The larger the angle the larger the separated zone, but the changes are smooth. In the opposite case, i.e. a very thin section (Case (b)), the flow cannot follow the sharp bend around the nose even for small angles of attack, so a separation bubble develops at the nose. When the angle is increased the bubble grows smoothly until it reaches the trailing edge and the maximum lift is developed. No jump in lift occurs, but the drag is large for all angles. On a section of medium thickness, 9–12% (Case (c)), both types of separation start to develop at relatively

**Fig 6.29** Influence of section shape on lift

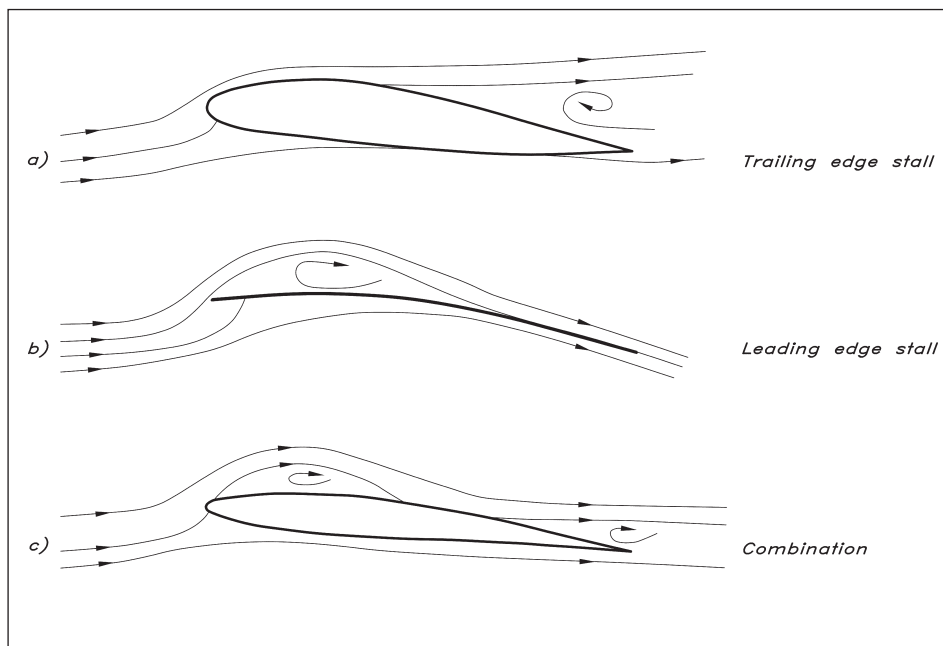


high angles of attack. The catastrophic drop in lift occurs when the separation bubbles meet and the entire suction side suddenly becomes separated.

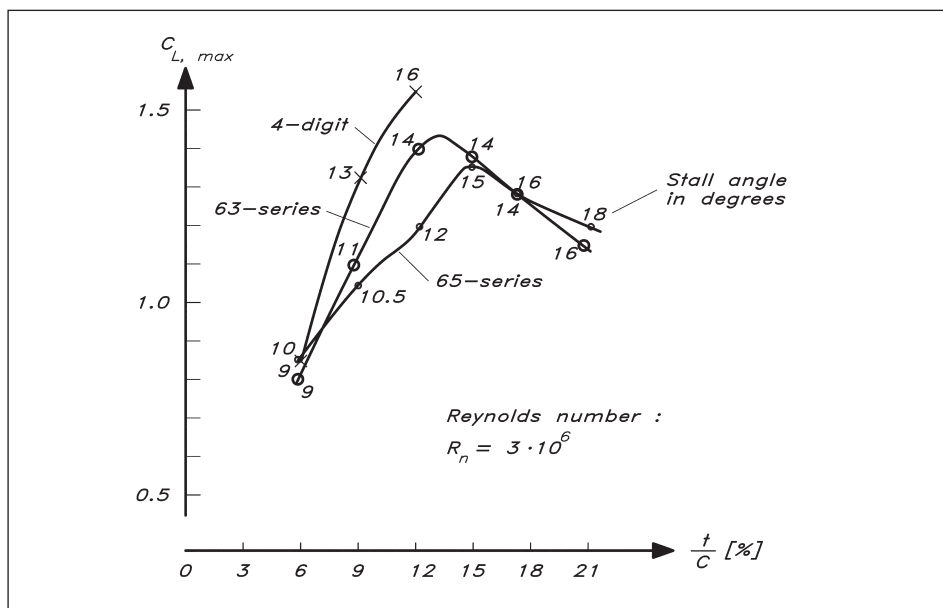
The maximum lift coefficient for the four-digit and the 63- and 65-series sections is given as a function of thickness ratio in Fig 6.31 (overleaf). It can be seen that the highest lift may be achieved by sections with a thickness ratio in the range 12–15%, and that the four-digit series is the best one in this respect. The angle at which the maximum occurs for each section is also indicated. Note again that this angle is approximately twice as large for keels of normal aspect ratio.

A possibility not discussed earlier is to divide the section into one fixed and one movable part. The mean line is then no longer straight, but exhibits a sharp corner at the hinge. This design may have several advantages, provided it is well done. An example of such a configuration is the trim tab behind a fixed keel. Fig 6.32 shows the principal effect of a deflection of the tab on the pressure distribution, as well as on the lift and drag. The stagnation point moves from its asymmetric position at the nose closer to the original symmetry line of the section, and therefore the large suction peak created by the sharp bend around the nose is reduced or even eliminated. The pressure distributions on both sides become closer to the one at zero angle of attack, and the favourable pressure decrease can be maintained at higher angles of attack. This effect is substantiated by the shift of the drag bucket to the right in the lower part of the figure. Another important effect is that the lift curve is moved to the left, giving a lift force even at zero angle of attack. By proper adjustment of the trim tab enough side force to balance the sails may be generated without leeway, which is an advantage, since the hull will then move straight through the water and thus produce minimum resistance.

When the tab is deflected there is normally a knuckle in the section at the hinge, which causes pressure spikes on both sides. This inevitably causes a drag increase, which



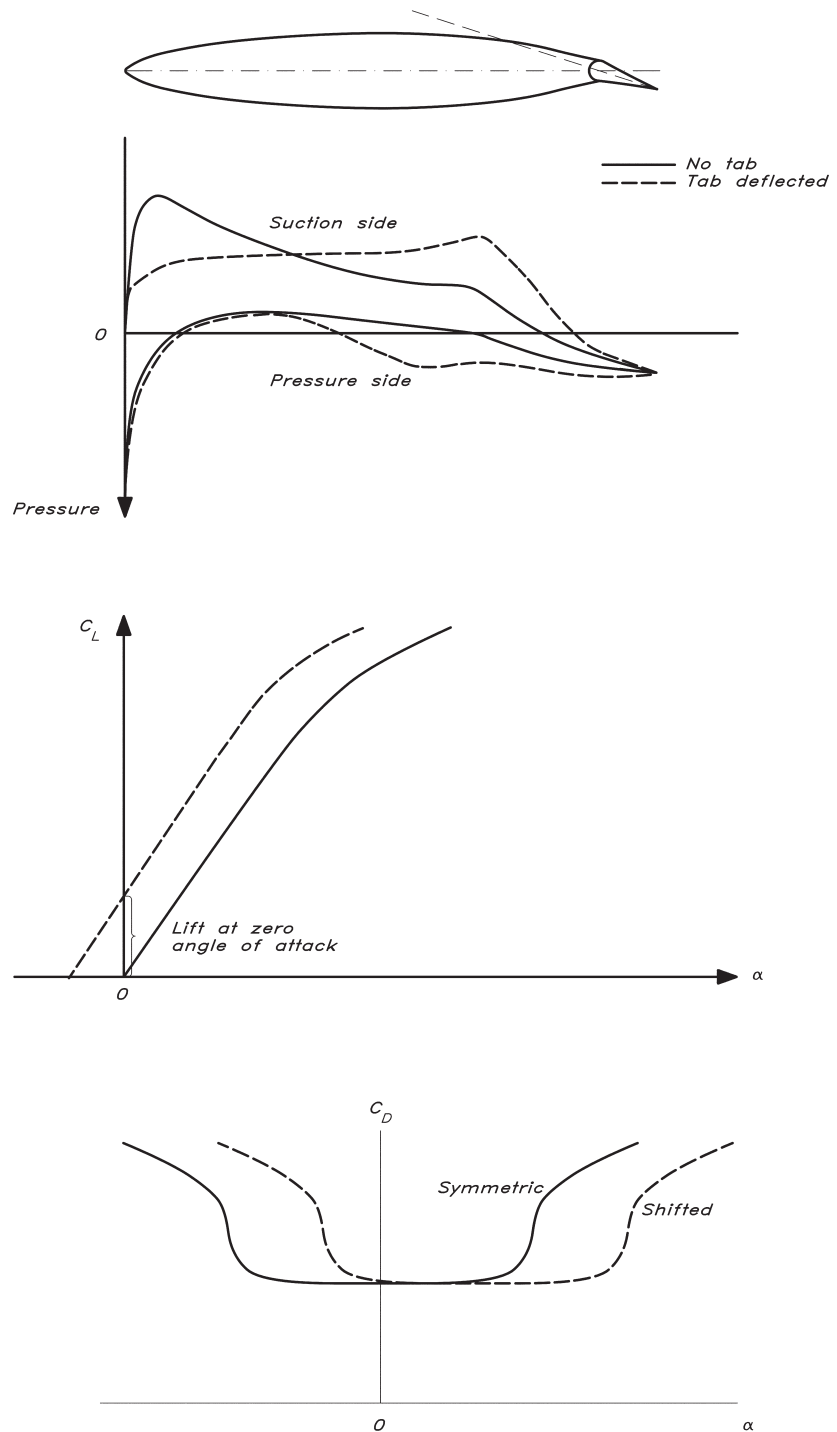
**Fig 6.30** Different types of stall



**Fig 6.31** Maximum lift for different profiles

to some extent reduces the positive effect of the tab. A way to alleviate this problem was pointed out by the yacht designer G Heyman. Since the suction side is the most sensitive one, it is advantageous to design this to be smooth with the tab deflected. The suction sides of the tab and the main part of the section are thus integrated to yield a smooth curve from nose to tail, at the tab angle of interest. Of course, this means that when the tab is set to zero angle the section will not be smooth, but this may not be so serious, since the section is then normally unloaded.

**Fig 6.32** Effect of trim tab



## ■ SOME PRACTICAL CONCLUSIONS REGARDING SECTION SHAPE

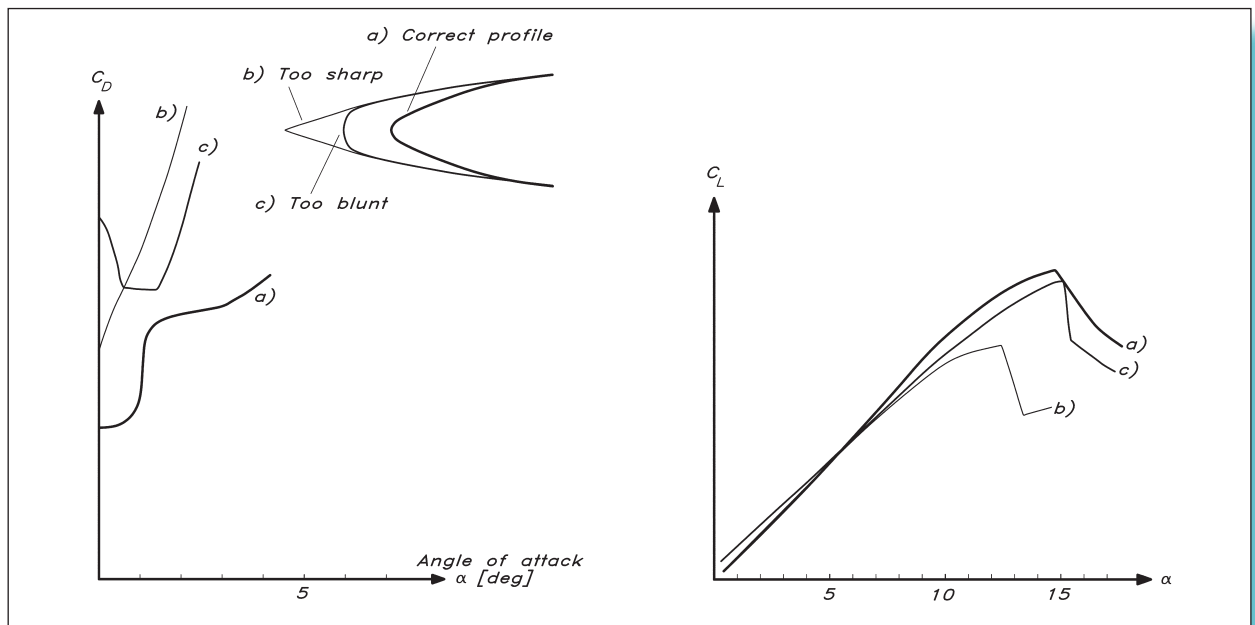
First it should be mentioned that all lift and drag coefficients presented above are for a Reynolds number of 3 million. This is the lowest Reynolds number presented in *Theory of Wing Sections*, and it is relevant for keels and rudders for most sailing yachts. It is, however, too large for the centreboard and rudder of most dinghies, at least at non-planing speeds. We will return to this problem in [Chapter 7](#).

In the discussion below, we will have to consider the keel and the rudder separately, since their function and operating conditions are different. Thus, the keel normally operates at small angles of attack and the speed of the yacht depends on the drag produced at these small angles. The rudder, on the other hand, may help the keel to produce the necessary side force, but its main task is to provide enough moment to manoeuvre the yacht under all conditions. Therefore, the rudder has to be designed with emphasis on the maximum side force required.

Since the lift and angle of attack for the keel are small, sections of the six-series are preferable. The 63- or 65-series may be used, but the thickness ratio should not be too small to keep the drag bucket wide enough for upwind sailing. Figures of 12% for the 63- and 15% for the 65-series may be considered as suitable lower limits. A thick section is, of course, favourable from a ballast point of view, but there are reasons for keeping the thickness limited. Thus, the drag at zero angle of attack increases with thickness (as seen in [Fig 6.28](#)), and experience has shown that a thick keel at the root produces unnecessary waves when the yacht heels. A good compromise is to use a relatively thick section, 15–18% for example, at the tip and gradually decrease the thickness ratio to 12%, say, at the root, at the same time gradually changing from the 65- to the 63-series.

The rudder has to be designed for the maximum side force required, and this force is proportional to the product of the maximum lift coefficient and the planform area. A large  $C_{Lmax}$  means that the area can be small, and the total wetted surface reduced. On the other hand, a larger wetted surface can be tolerated if it has an extensive area of laminar flow. Furthermore, the rudder operates most of the time at higher angles than the keel, particularly if the yacht is sailing in a seaway, and corrections to the course have to be made continuously. With all this in mind it is obvious that the more extreme laminar sections, such as the 65-series, should be avoided, since they have a lower  $C_{Lmax}$  and higher resistance at larger angles than the two other types of section discussed above. For light and fast hulls such as catamarans, dinghies and lightweight displacement hulls, relatively small rudder angles are required, which would speak in favour of the 63-series, while for heavier yachts with larger rudder angles the four-digit series might be preferable. A suitable thickness for most yachts is 12–15%, since the maximum  $C_{Lmax}$  is obtained in this range. Very fast hulls with surface-piercing rudders should use thinner sections, however, since the spray generated at the nose is proportional to the thickness squared.



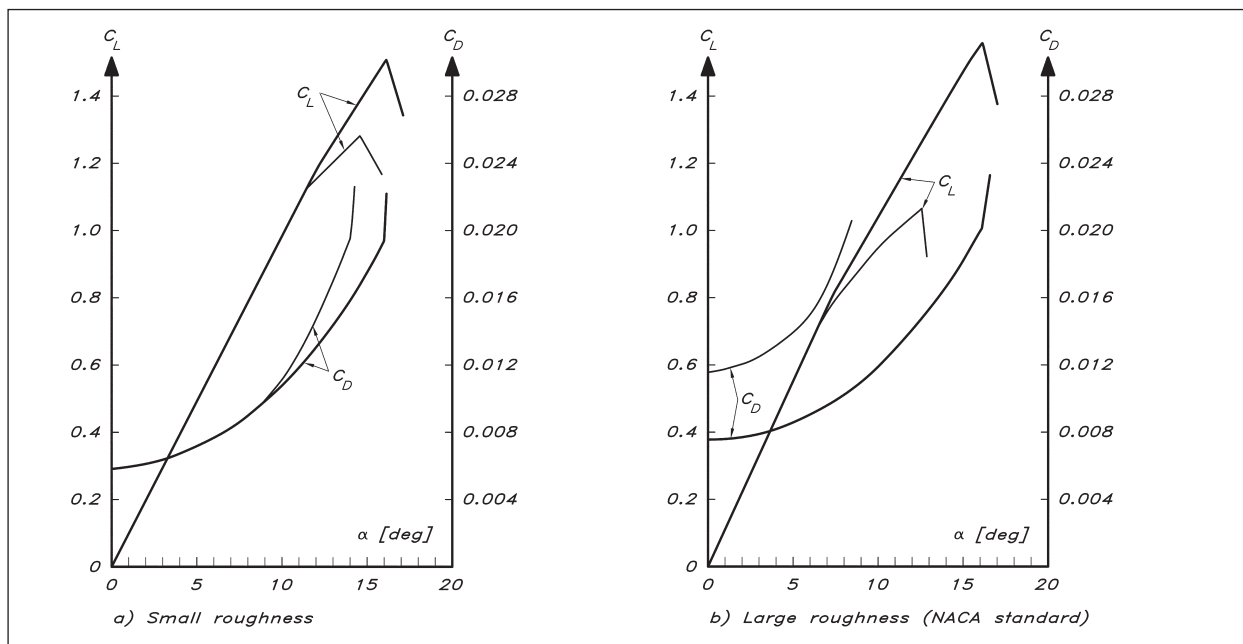


**Fig 6.33** Influence of nose shape on drag and lift

## ■ INFLUENCE OF DEVIATIONS FROM THE THEORETICAL SECTION SHAPE

The most sensitive part of the section is the nose, where the flow has to pass a region of very high curvature on its way from the stagnation point on to the suction side when the section has an angle of attack. Therefore, the nose radius as presented in Fig 6.24 should be used as closely as possible. In *Sailing Theory and Practice* (Marchaj, 1982), two investigations are reported, where the influence of imperfections at the nose was tested. First, the bluntness was altered, as indicated on the left in Fig 6.33. The figure shows that the drag increased considerably, regardless of whether the nose was made blunter or sharper, as compared with the ideal shape. A more careful variation was made in the second investigation, where the nose radius was varied for a 12% section. Special emphasis was placed on the high lift properties, and a lower  $C_{L,max}$  was obtained both for larger and smaller radii, compared to the correct one (see Fig 6.33, right).

In Chapter 5 the influence of surface roughness on the viscous resistance of the hull was discussed in some detail. The importance of a smooth surface is even greater for the keel and rudder, particularly if laminar sections are used. Small imperfections may cause premature transition, making the favourable characteristics deteriorate more than for a less advanced section from the four-digit series. However, even a section of this kind may be affected negatively. Fig 6.34 (overleaf) shows the influence of a very small roughness element, of the order of 10  $\mu\text{m}$ , on a NACA 0012 section. It may be seen that the drag is not greatly affected for small angles, but stall occurs much earlier. To the right in the same figure the influence of NACA's standard roughness on the same section is shown. This roughness is relatively large: 0.04% of the chord length, corresponding to a height of 0.4 mm on a one-metre chord, and the effect is dramatic, with a large drag increase at

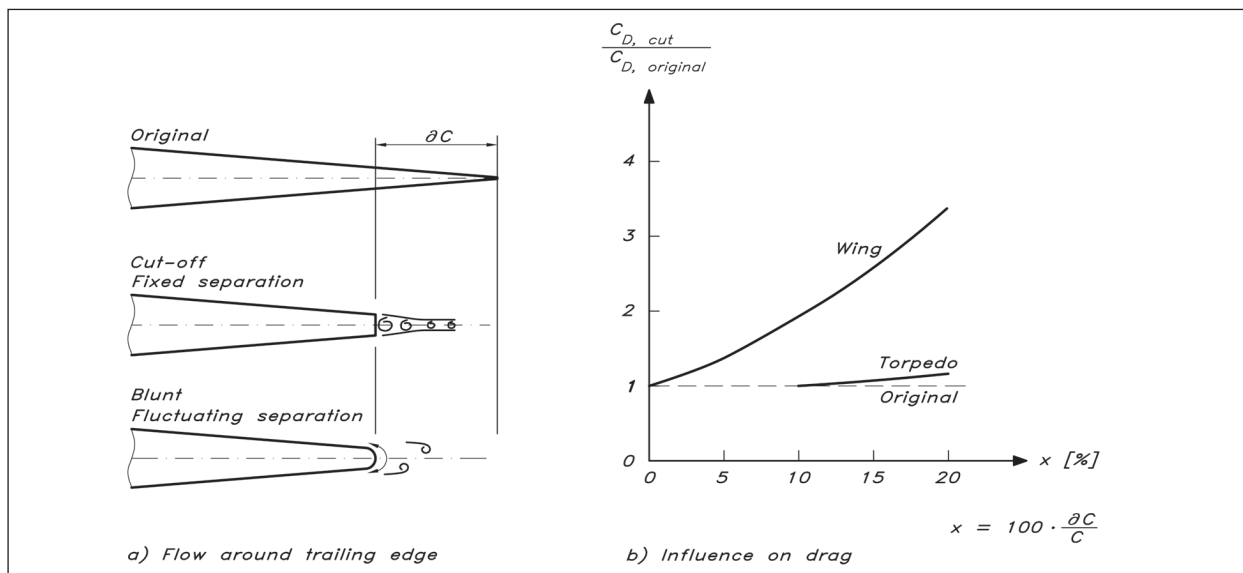


small angles and a very early stall. As pointed out in Chapter 5, the influence of roughness increases with speed, so for planing boats, great care should be taken to keep the foils (centreboard and rudder) free from surface imperfections. This is particularly important on the forward one third of the chord.

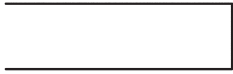
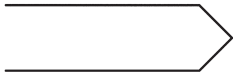






For practical reasons the trailing edge of a keel or rudder section cannot be razor-sharp. It is therefore interesting to investigate the effect of various endings of the section. Reference should be made first to Fig 6.35, which shows the effect of cutting off part of the tail. For a wing the drag starts increasing immediately, even for very small

Fig 6.34 Influence of roughness on drag and lift

Fig 6.35 Influence of trailing edge shape



**Fig 6.36** Influence of trailing edge geometry on vibration level

<i>Case</i>	<i>Geometry</i>	<i>Relative vibration amplitude</i>
1		1
2		1.9
3		3.8
4		0.43
5		0
6		0.38
7		0.03
8		0

cut-offs. This is in contrast to the effect on an axisymmetric body, like a torpedo or a keel bulb, where relatively large cut-offs are permitted without a drag penalty. Therefore, the cut-off on a wing should be kept to a minimum. The way the cutting is done is also of importance.

Fig 6.36 shows some alternatives. An interesting phenomenon is the vibration that occurs for certain shapes. The figure shows the amplitude of the vibrations at resonance for each case relative to those of a square cut-off. It can be seen that if the edge is symmetric and wedge-shaped (cases 2–5), the total wedge angle has to be 30° or smaller. For 90° and 60° much larger vibrations occur than for the square ending. This is also the case if the ending is rounded in some way, which it normally is, if the trailing edge of the keel or rudder is left without attention. An asymmetric cut-off is somewhat more forgiving, and a 45° cut-off is acceptable, provided the corner on the cut-off side is smoothed. The vibrations are not only of academic interest. On the contrary, they may cause severe vibrations and noise in the entire hull at speeds where resonance occurs. Using the information in Fig 6.36 these problems can be solved.

## ■ ADVANCED SECTION DESIGN

The NACA sections presented above are quite efficient and useful for most sailing yachts. However, with modern tools it is possible to create sections more tailor-made for their purpose. Such a tool is the freeware XFOIL, developed by Mark Drela<sup>1</sup> at Massachusetts Institute of Technology. Other useful tools are found on the site Airfoil tools.<sup>2</sup> This site contains the geometries of very many sections of different kinds, as well as the lift and drag coefficients of many of them.

When designing an optimum section the designer starts from the pressure distribution on the suction side at the design lift coefficient (angle of attack). The distribution may be divided into three zones (see Fig 6.37). To keep the boundary layer laminar the pressure must decrease, and this is what happens in zone A, where the thickness of the section increases. At some position this increase obviously has to stop, since the thickness has to go to zero at the trailing edge. This also means that the pressure has to start increasing at some position along the chord. The required slope of the pressure distribution in zone A depends on the Reynolds number and the ambient turbulence level. A higher Reynolds number and a higher turbulence level give a more unstable flow, and hence a larger slope of the pressure distribution is required to maintain the laminar boundary layer. The possible slope is set by the magnitude of the suction at the peak value and the length of zone A. Since the latter should be long the peak must be high, i.e. the maximum thickness should be as large as possible, without causing problems in the other two zones, where the pressure has to rise again.

The pressure recovery zone is split into two parts, B and C, since different strategies should be used in the early and later parts of the recovery. The problem is to avoid separation. In principle, the thicker the boundary layer and the faster the pressure increase, the larger the risk of separation. At the suction peak, where transition is assumed to occur, the boundary layer is relatively thin, and can withstand a rapid pressure increase. Approaching the tail, however, the boundary layer thickens rapidly and a much more gentle increase in pressure is required. Thus, in zone B, the pressure increase should be fast, which calls for a rapid thinning of the section. In zone C, on the other hand, the pressure should increase slowly, so the tail must taper off in a smooth manner. This gives optimized sections the typical concave appearance at the tail.

Obviously, the design of sections in the manner described takes considerable experience, and access to accurate computer programs for the computation of the pressure distribution and of the boundary layer development, including both transition and separation. Neither of these conditions is likely to be satisfied for the amateur designer, who will have to rely on standard sections, for instance from the NACA series described above.

## ■ STATISTICS ON KEEL AND RUDDER AREA

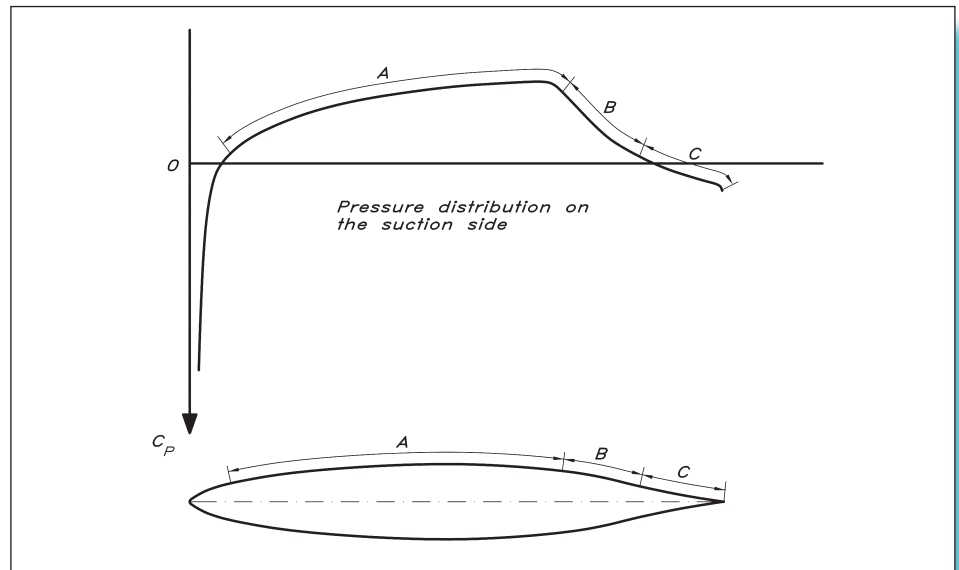
Since the task of the keel is to produce the major part of the hydrodynamic side force to balance the aerodynamic side force from the sails, it is reasonable to look at the keel area

---

<sup>1</sup><https://web.mit.edu/drela/Public/web/xfoil/>

<sup>2</sup><http://airfoiltools.com/>

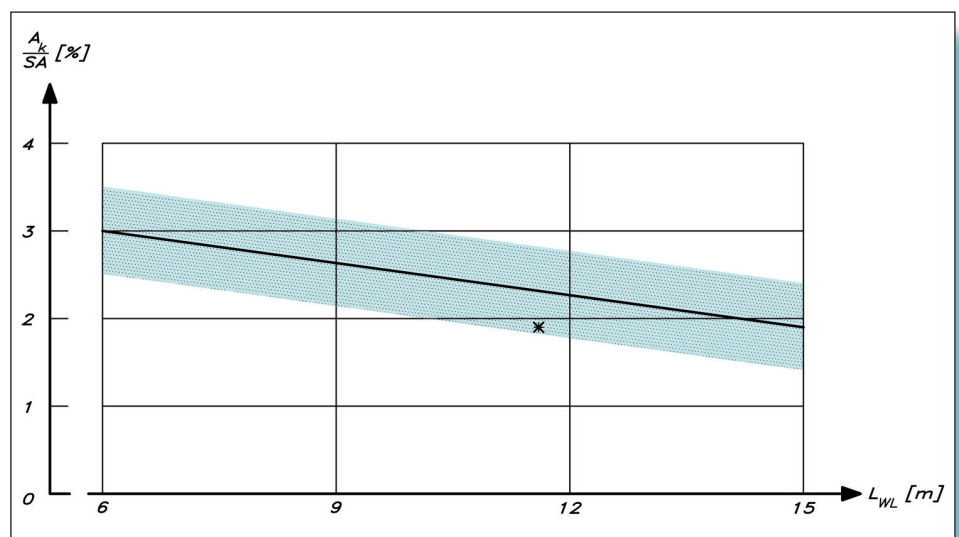
**Fig 6.37** Distribution of the three zones of interest in advanced section design

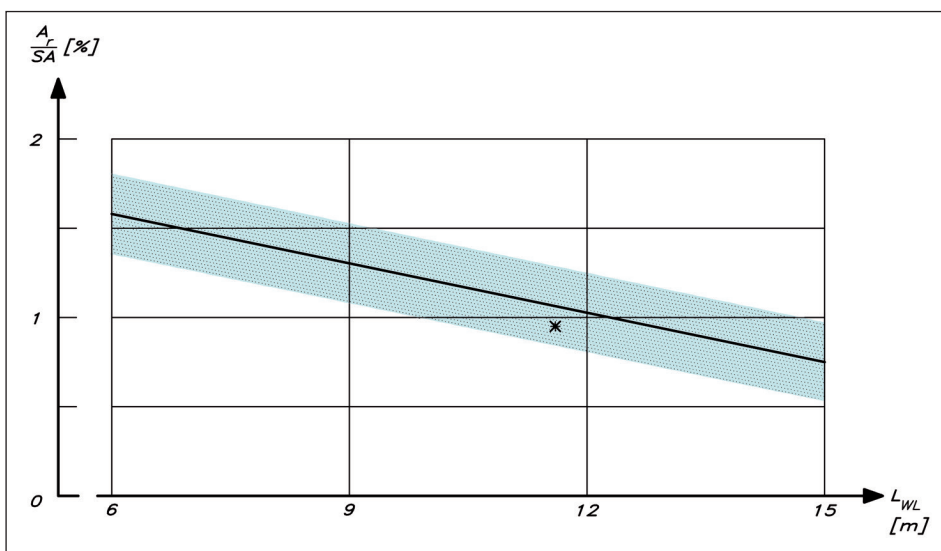


as a fraction of the sail area. We will simplify the calculation of the latter by referring to the sum of the main and foretriangles, denoted SA.

Fig 6.38 shows the keel area,  $A_k$ , as a percentage of the sail area for varying waterline lengths. The database is the same as in Figs 5.30 and 5.32. A median line is shown, as well as the region within which 95% of the entries fall. The median line starts at 3.0% for the smallest yachts and ends at 1.9% for the largest ones. The reason for the drop is that the sail force, to be balanced essentially by the keel, is proportional to the sail area for a given (apparent) wind speed, while the keel lift for a given leeway is proportional not only to the keel area, but also to the square of the yacht speed, which is higher for a larger yacht. Therefore the percentage can be reduced for this yacht. (The yacht speed also has an influence on the apparent wind speed, which reduces the effect somewhat.)

**Fig 6.38** Keel projected area/sail area





**Fig 6.39** Rudder projected area/sail area

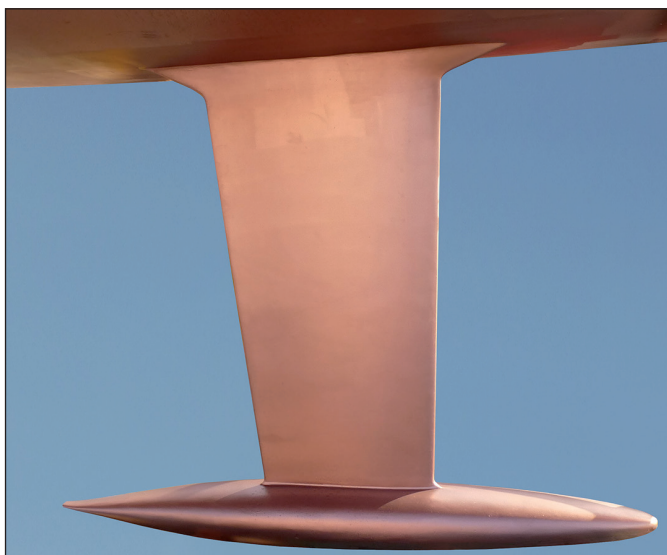
Note that the keel area is obtained by extending the blade through the bulb down to maximum draft.

The keel areas of Fig 6.38 are considerably smaller than those of older designs. In the previous editions of this book the keel area was recommended to be 3.5% of the sail area (no dependence on length was proposed). The main reason for the reduction is the bulb, which was rare on older yachts, but which is now very common. The bulb carries a substantial lift. In the bulb keel investigation reported in connection with Table 6.1 the lift was essentially the same for the bulb keels and the fin keel in spite of the fact that the lateral area of the latter was 20% smaller. Another possible reason for smaller keels on modern yachts is that their speed has increased.

In Fig 6.39 the rudder area,  $A_r$ , is presented as a percentage of the sail area. Also in this case there is a drop in percentage with length, from 1.6% to 0.8%. This is for the same reasons as for the keel, even though the rudder has a different mission. Its area is determined to give the required side force for manoeuvring even at low speeds. There is a reduction in rudder area as well, compared with older designs. In the previous editions of this book the rudder area was recommended to be 1.4% of the sail area. Here the median line in the middle of the length range gives 1.2%, so the reduction is much smaller than for the keel.

## THE YD-41

The lateral keel blade area (extended to the bottom of the bulb) of the YD-41 is 1.69 m<sup>2</sup>, while the sum of the main and foretriangles is 88.1 m<sup>2</sup>. This keel is thus 1.9% of the triangle area, a relatively small value, calling for an experienced crew to keep the speed up. The sweep angle of the keel is 5.5°, which gives a taper ratio of 0.4 according to Fig 6.8. However, the figure is for plain fin keels, and the addition of a bulb changes the required taper. Since the bulb restricts the overflow from the pressure to the suction



sides at the tip, a larger taper ratio is likely to be better. However, to the knowledge of the authors, no investigations of the optimum are available. We have selected a root chord of 1.00 m and a tip chord of 0.78 m. Keeping the upper chord relatively small (with a given thickness ratio) reduces the wave effects of the keel, but strength requirements need to be considered. Note that the keel blade of the YD-41 is manufactured with welded steel plates to put as much of the keel weight as possible in the bulb. A 10.5% NACA 63 section is selected for the whole span of the blade. The thin section creates little wave resistance and for such a thin profile the more laminar sections of the six-series should be avoided. A picture of the keel and bulb is seen in Fig 6.40.

**Fig 6.40** YD-41 keel and bulb (Photo: Michal Orych)

The YD-41 also has twin rudders to secure manoeuvrability when heeled. The stern is rather wide, so a single rudder in the centre plane would run the risk of being lifted partly out of the water at large heel angles. Since the leeward twin rudder is positioned at the deepest point of the hull when heeled  $20^\circ$ , and tilted to become vertical at this heel angle, the rudders can be made smaller than a regular single rudder. Also, they are designed such that the windward rudder is lifted entirely out of the water at  $20^\circ$  of heel, so upwind there is a reduction in wetted surface compared to a single rudder.

It is advantageous if the rudder shaft is at right angles to the bottom, where it exits, since the gap between the hull and the rudder may then be sealed for all rudder angles. This is the case for the YD-41, and since the 25% line approximately coincides with the shaft axis, this line is approximately at right angles too. In the upper part of the rudder the flow follows the bottom, so the sweep angle is zero. Further down the flow direction is more horizontal, so there is a small sweep. We have neglected this and chosen a taper ratio of 0.46, which is optimum for zero sweep according to Fig 6.8. The root chord is thus 0.48 m and the tip chord 0.22 m. A rudder span of 1.15 m gives a high geometric aspect ratio of 3.3 and an area of  $0.40 \text{ m}^2$ . The latter is 0.45% of the sail area and is thus very small compared to a single rudder. In Fig 6.39 the total lateral area, which is 0.9% of the sail area, is shown for the YD-41. It is slightly below the median line. To make the rudders as robust as possible against stalling a NACA 0012 section has been selected.

It should be noted that twin rudders are less efficient than a single rudder when manoeuvring under engine at low speed. This is because a single rudder is positioned behind the propeller and directs the slip stream. Therefore, even at zero speed the boat can be turned, a great advantage when manoeuvring in harbours. For the twin rudders, located outside the propeller slip stream, the boat must have a significant forward speed to be manoeuvrable.



# 7 FOILING

During the past decade, the interest in foiling has boomed for all sailing craft. Successful designs have been presented for dinghies, multihulls and monohulls in a wide range of sizes, from the 2.4 m long Optimist for children to the most advanced racing machines seen so far, the 22.9 m long AC75 monohulls, used in the 2021 America's Cup.

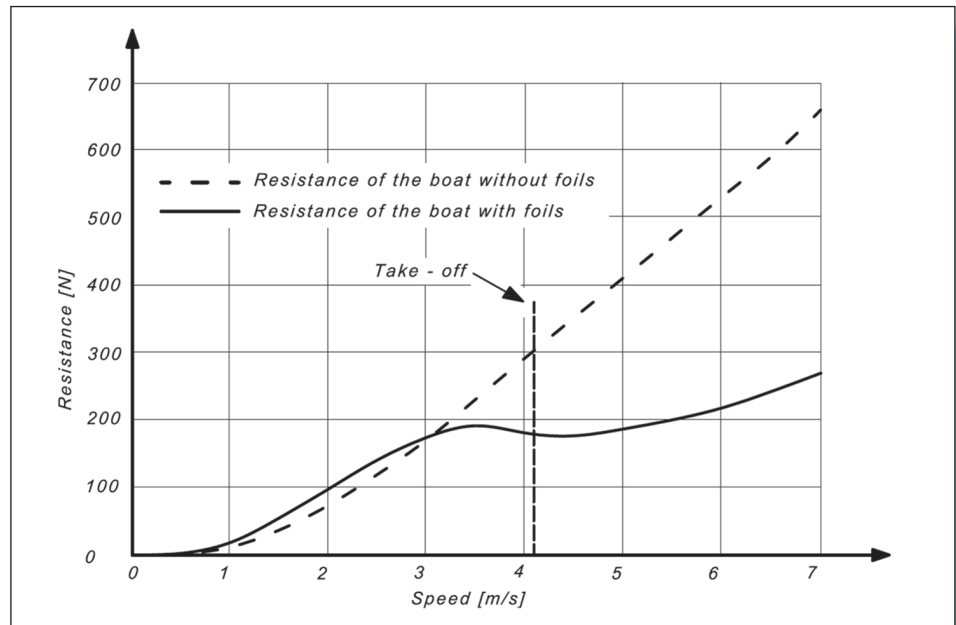
Surprisingly, interest has boomed only recently, even though foiling is not a new concept; the first patent on foiling was filed in 1869 by the Frenchman Emmanuel Denis Fargot. For a rowing boat! The first known sailboat with foils was produced by Americans R. Gilruth and Bill Carl in 1938, but it was not until the 1970s that foiling became more common. Many successful designs were presented during the following 40 years, mainly for multihulls. The most well-known one is Alain Thébault's trimaran *Hydroptère* in 2009, the first sailboat to reach an average of 50 knots over one nautical mile. By far the most well-known foiling sailboat class during the past 20 years, however, is the Moth. Much of the development has taken place in this class and many of the world's most skilled helmsmen for foiling yachts, for instance in the America's Cup, have been trained there.

The basic idea behind foiling is very tempting: to lift the boat out of the water by submerged hydrofoils, thereby reducing the hydrodynamic hull resistance to zero. Following common practice in yachting, these hydrofoils will simply be called 'foils' in the following. As we have seen in [Chapter 5](#), the hull resistance increases very rapidly for higher Froude numbers due to the abrupt increase in wave resistance, at least for displacement hulls. This severely restricts the high-speed potential for such hulls. For planing hulls, the increase is not as fast, but there is still a restriction due to wave resistance.

The complete removal of hydrodynamic hull resistance for foiling craft does come at a price: the resistance of the foils. At speeds below take-off, the total wetted surface is increased, and thus the friction. Therefore, resistance increases faster at low speeds than without the foils (see [Fig 7.1](#)). However, the lift from the foils develops gradually with speed, thus raising the hull more and more out of the water. This reduces resistance even before take-off, and for light craft it may well be smaller than without foils. Just after take-off, where the hull resistance has disappeared completely, the appendage friction is rather small, but it becomes the dominant resistance component at high speeds. Around take-off, the dominant resistance component is induced resistance, but it gradually decreases with speed. A more detailed description of these resistance components, and several others of less importance, will be presented below.

The resistance reduction due to the partly lifted hull before take-off can be utilized for heavier yachts, which are not entirely lifted out of the water. Here another effect of the

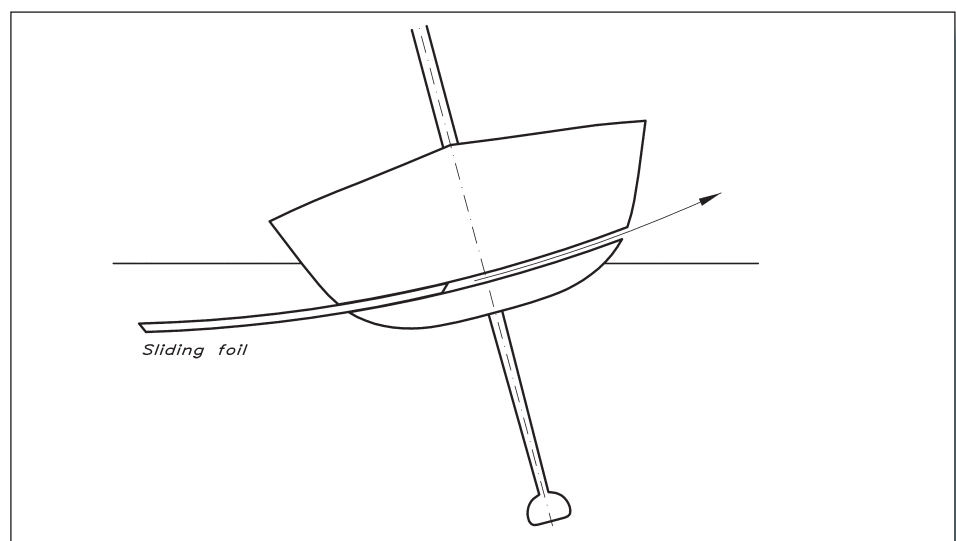
**Fig 7.1** Resistance with and without foils (for Linnea)



foils is also exploited. If the foils can be used asymmetrically on the hull, for instance by retracting a foil on the windward side, while the leeward one is in operation, the stability of the yacht may be improved. This is the idea behind the Dynamic Stability System (DSS), patented by Hugh Welbourn as late as 2007 (see Fig 7.2). Here, an essentially horizontal wing is pushed out to leeward and retracted to windward. As in the figure, it may be a single wing sliding sideways through the hull. The main idea is not to lift the hull but to increase stability.

There is also a third effect, exploited in some concepts: the generation of side forces. That may alleviate the burden of the keel and rudder, and in some cases, the keel is removed altogether.

**Fig 7.2** Dynamic Stability System



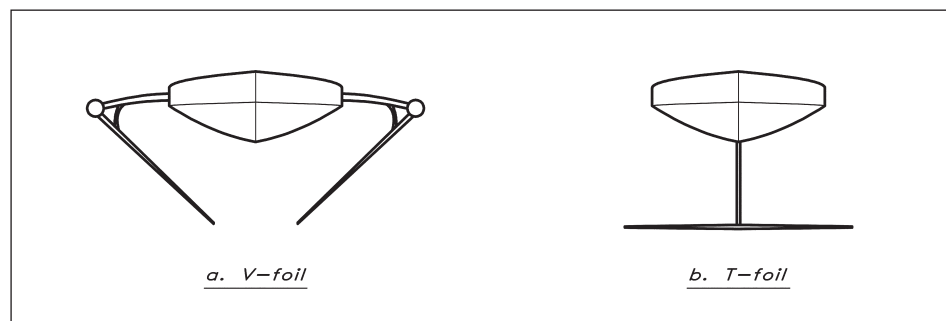
This chapter is divided into two main parts. In the first part we introduce important aspects on foiling. An overview is given of different foiling concepts, followed by an analysis of the forces and moments acting on a foiling boat. Requirements for static and dynamic flight stability are discussed and general advice on the design of all appendages given. In the second part, this qualitative discussion is followed by a quantitative description of the design of a foiling dinghy. Explanations are given for the choice of appendages, and the computation of all forces and moments are presented in detail. At the end of the chapter, some more complex aspects, not covered in detail, are introduced.

## ■ FOILING CONCEPTS

Foil concepts may be classified as either surface piercing or fully submerged. A fundamental advantage of the surface piercing foils is that the ride height can be controlled passively; no control system is required. The height adjusts itself automatically, such that the submerged part of the foils develops just enough lift to carry the weight of the boat. The higher the speed, the smaller the part of the foil in the water. The most basic system of this kind is the V-foil, shown schematically in Fig 7.3(a).

In Fig 7.3(b) the simplest example of a submerged foil is presented: the T-foil. Since the lifting surface of the T-foil is independent of ride height, the control cannot rely on the same principle as the V-foil. There is, however, a weak control mechanism caused by the effect of the water surface. For reasons explained below, the lift of the foil is reduced when approaching the surface. In principle, this would prevent the foil from jumping out of the water, but since the effect is very weak it is hard to exploit it. Therefore, most T-foil configurations rely on an active control system, where the distance from the hull to the water surface is measured and used to control the lift from the foil. The lift is varied by changing the angle of a flap at the trailing edge of the foil. At the correct ride height, the lift produced is correct, and no change in flap angle required. If the boat flies too high, the flap angle (and therefore the lift) is reduced. For too low a ride height, the flap angle is increased. A control system of this kind will be explained below.

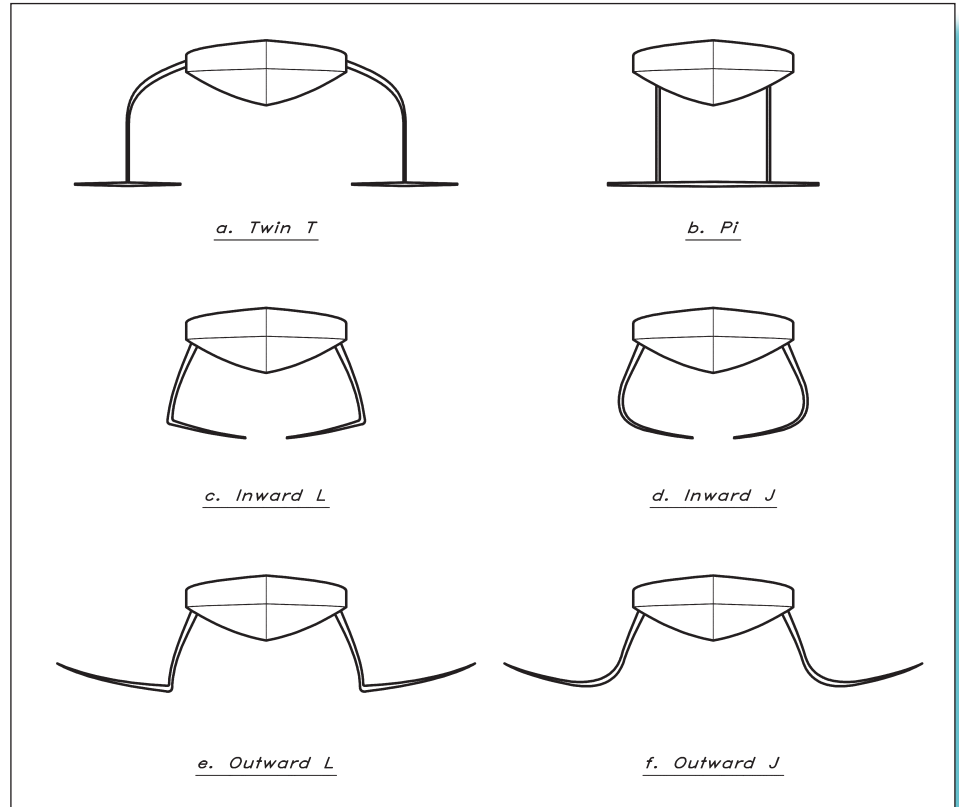
Note that for all concepts with the hull out of the water, pitch stability requires at least two foils separated longitudinally. By far the most common solution to this problem is to use the rudder for a second, smaller, horizontal foil, which will carry part of the lift. This is therefore a T-foil configuration.



**Fig 7.3** Basic shapes: V-foil and T-foil

Most foil configurations may be considered developments of the basic T- and V-shapes. Some examples will be given here.

**Fig 7.4** Variations of the T-foil



The most obvious development of the T-foil is the twin T-foil, shown in Fig 7.4(a). Stability can be achieved by lifting the windward foil out of the water. Alternatively, this foil can be arranged to create a downward force, thereby generating a righting moment. Then the stability gain will be larger, but the induced drag will increase and so will the friction, as compared to the case with a lifted foil. A typical example of a twin T-foil configuration is found on the AC75 America's Cup boats. Here the windward strut and foil are swung up into a horizontal position. Since they are ballasted, this contributes significantly to the righting moment. Note that in some designs the foils have a dihedral angle (see Chapter 6), so they may be classified as twin Y-foils.

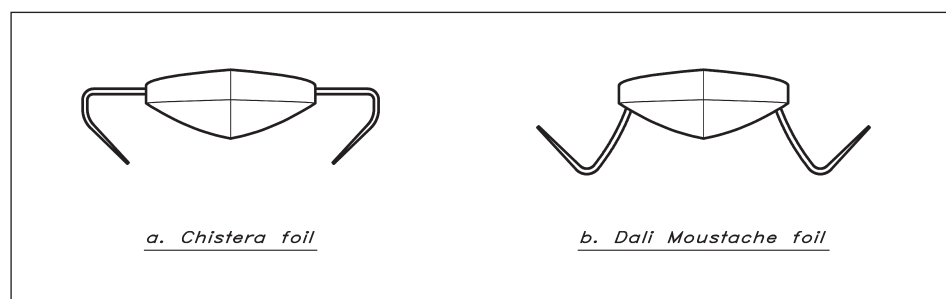
Another development of the T-foil concept is the pi-foil, seen in Fig 7.4(b). Here the centreboard has been replaced by two daggerboards. This system is slightly less efficient hydrodynamically, but more stable structurally.

If the maximum beam is limited, the outer half of the twin foils may be removed. This results in the inward L-foil, seen in Fig 7.4(c). Since there are negative effects of the corner between strut and foil, a more rounded variant is often used: the inward J-foil, shown in Fig 7.4(d). This concept was used for the AC72 and AC50 catamarans of the 2013 and 2017 America's Cups. The negative effects of an internal corner will be explained in the description of junction drag below.

These catamarans exploited an idea to give the foil a dihedral angle (i.e. a tilt upwards). With the windward foil hoisted, leeway and lift are linked on the leeward foil. This effect may be used for (at least partly) controlling ride height. When the hull moves up, above the equilibrium position, the submerged part of the daggerboard is reduced, hence leeway is increased. This increases the velocity component normal to the tilted foil, which reduces the effective angle of attack and hence the lift. So, the hull will move down. The opposite occurs when the hull is below its equilibrium position.

If there is no beam restriction it may be advantageous to remove the inner parts of the twin T-foils. This will increase the righting moment for a given foil span. An example of this outward L-foil configuration is shown in Fig 7.4(e). As for the inward L, a more rounded shape is preferable, hence the outward J (see Fig 7.4(f)).

With some exceptions (notably the AC75s) the foil configurations presented so far are used for monohull dinghies and catamarans and will lift the hull completely out of the water. There is, however, an increasing trend to use foils also on displacement yachts, such as IMOCA 60s. Even in this case it has been possible to lift the hull completely, but in most applications the hull will be only partly lifted by the foils. This will reduce hull resistance, but experiments indicate (Soupez *et al*, 2019) that the increased resistance due to the foil system may be larger than the gain in hull resistance. On the other hand, as mentioned above, there is also an increase in the righting moment, so the net result may be a faster yacht. The two most common configurations, called Chistera and Dali-Moustache, respectively, are shown in Fig 7.5.



**Fig 7.5** Foils for displacement yachts

Many foils are variations of the main types above. The Olympic Nacra 17, for instance, has a V-foil with a small vertical part at the tip. This is known as a Z-foil configuration. There are also other foil types like S-, U- and O-foils, but they are less common, so far.

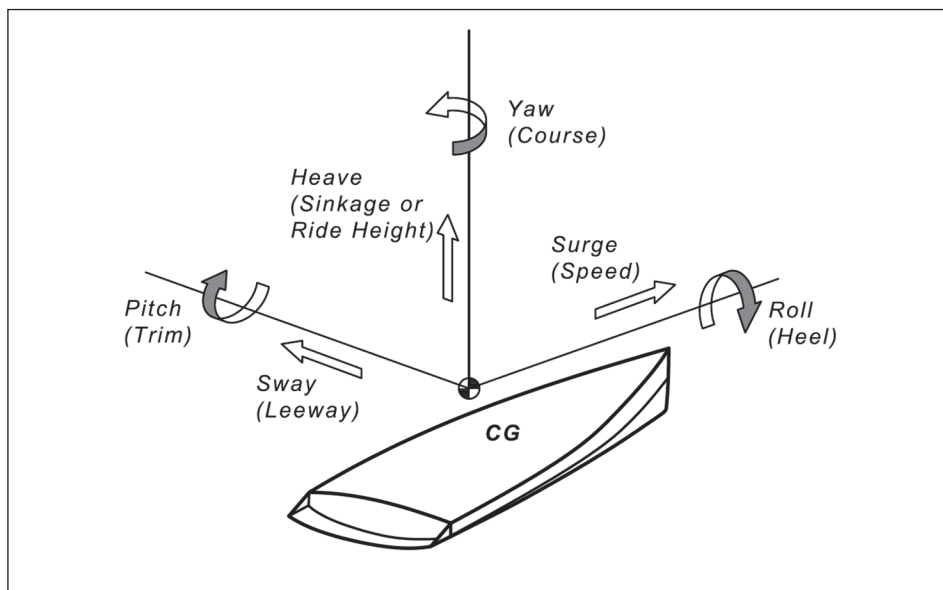
A detailed discussion of the performance of all concepts presented above would be very lengthy, so the discussion below will be limited to the basic shape for submerged foils: the T-foil.

## ■ FORCES AND MOMENTS

In Fig 7.6 we define the motions of the boat in all *six degrees of freedom* (DOFs). There are three translations:

1. Along the direction of motion (surge, speed)

**Fig 7.6** Definitions of the motions in six degrees of freedom



2. Along a horizontal direction at right angles to port of the direction of motion (sway, leeway)
3. Along the vertical direction upwards (heave, sinkage or ride height)

Further, there are three rotations:

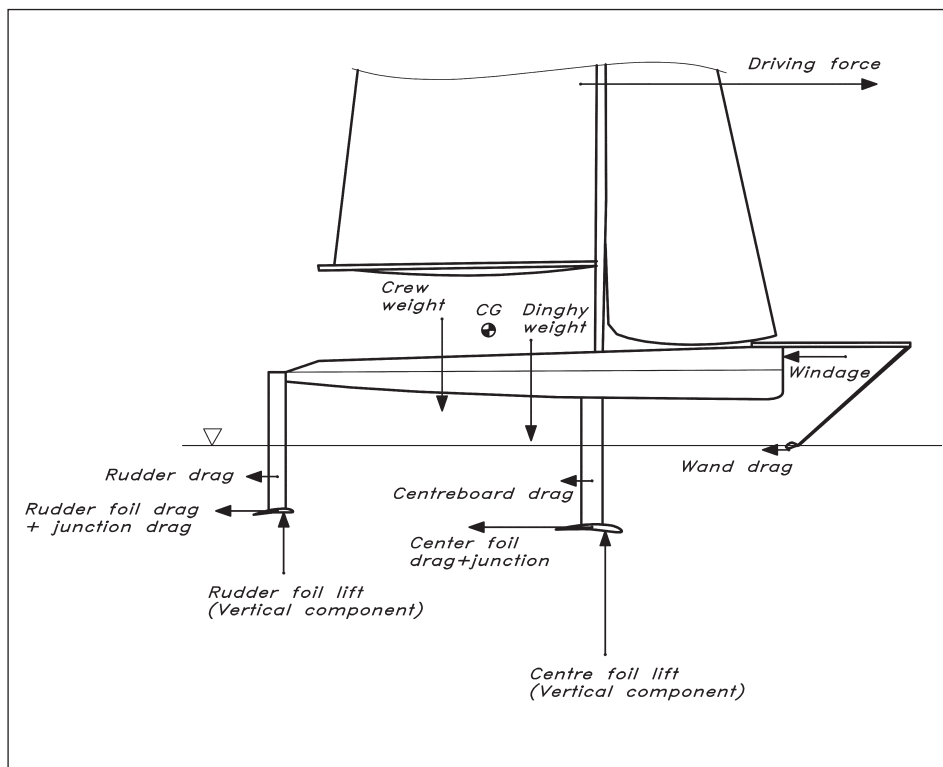
4. Around the direction of motion (roll, heel)
5. Around a horizontal direction at right angles to port of the direction of motion (pitch, trim)
6. Around the vertical direction upwards (yaw, course).

A body is said to be in *equilibrium* when the sum of all forces in each of the three directions, as well as the sum of all moments around each of the directions, is zero. This corresponds to the state shown in Fig 5.1 for a displacement hull and it is the basis for static Velocity Prediction Programs (VPPs). For a more extensive discussion of the equilibrium concept, see Chapter 17. In Fig 7.6 the relevant nomenclature is defined. The first word refers to the disturbance from equilibrium, while the one within brackets represents the equilibrium state.

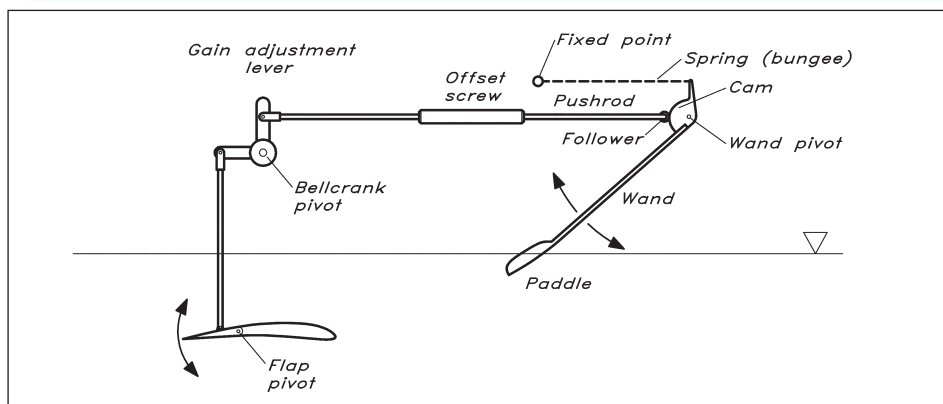
At equilibrium, the boat will continue at constant speed, leeway, ride-height (sinkage), heel, trim and course. In the present chapter we will concentrate on four DOFs: speed, ride height, trim and heel. The other two do not differ much from those discussed for a displacement hull in Chapters 6 and 9.

#### ◆ Vertical force balance (heave)

Fig 7.7 (overleaf) shows a side view of the forces acting on a foiling dinghy. For equilibrium, the sum of the vertical forces must be zero. That is, the total weight of the crew and dinghy must be balanced by the vertical component of the total lift from the centre foil and rudder foil. (At non-zero heel there is also a component of the centreboard



**Fig 7.7** Forces on a foiling dinghy, side view



**Fig 7.8** Flap angle control system

and rudder lifts, as described below). This is a problem since the weight is constant with speed, but the lift increases rapidly as speed goes up. According to the equations of Fig 6.5, the lift is proportional to the lift coefficient and the speed squared. To achieve vertical balance the lift coefficient must therefore be reduced with increasing speed. This can be achieved either by changing the angle of attack of the foils or by changing their shape. In most T-foil designs the shape of the centre foil is changed by rotating a flap at the trailing edge. A foil section with flap is presented in Fig 7.14. The flap angle is set by a control system sketched in Fig 7.8, based on the ride height.

The sensor of the system is the wand, normally attached to a bowsprit as in Fig 7.7. The wand has a small flat or spoon-shaped paddle at the lower end, facing the flow. The

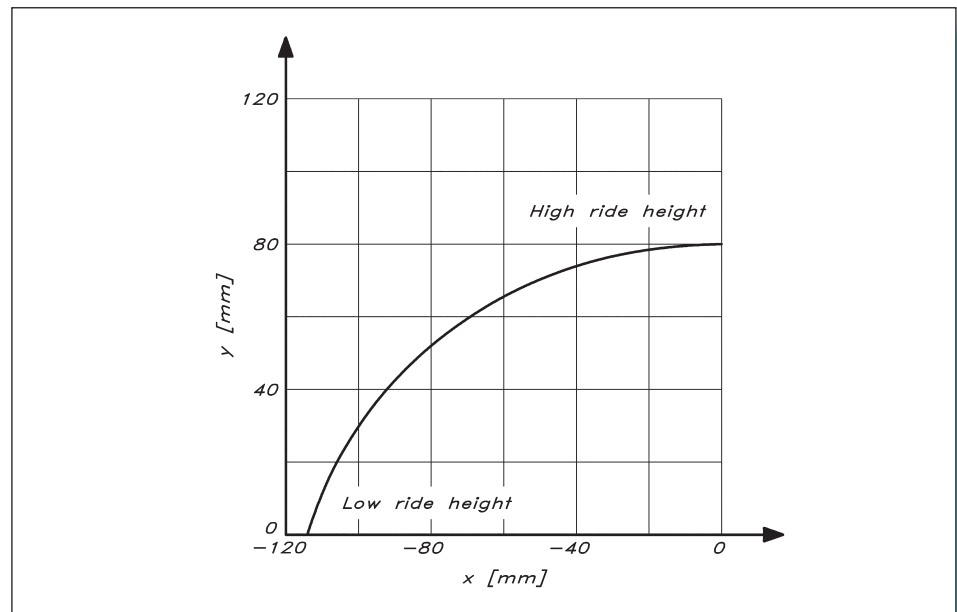


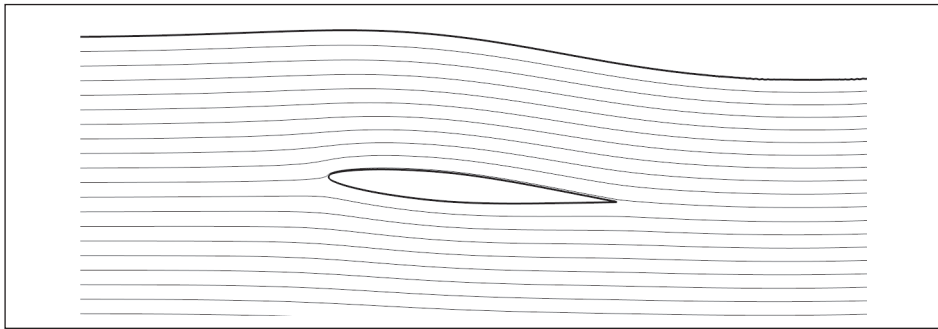
paddle skims along the water surface like a planing hull. For a given wand length, the vertical distance between the bowsprit and the water surface is thus determined by the wand angle. At the wand pivot point a cam is attached, which turns with the wand. Riding on the cam edge is a small wheel, the follower, attached to a pushrod, which is then moved axially when the cam is turned. The axial displacement is determined by the shape of the cam. The other end of the pushrod is linked to the upper arm of a bellcrank, which is thus turned by the axial movement of the rod. Turning the bellcrank, another pushrod attached to the other arm is moved vertically. This pushrod is linked to the flap, whose angle will thus be determined by the angle of the wand, and thereby the ride height.

There are two adjustments possible in the system. The connection point between the horizontal pushrod and the upper bellcrank arm determines the gain of the system (i.e. the flap angle/ride height ratio). Moving the connection upwards the gain is reduced, and vice versa. In sailing terms this is known as 'gearing'. The other adjustment is accomplished by the offset screw, which simply adjusts the length of the pushrod, and thus the flap angle for a given ride height. Note that the flap force can be negative; hence a spring is needed to push the paddle towards the surface.

The core of this system is the cam. By changing the shape of the cam profile, the system response to a ride height change may be varied within wide limits. For instance, it is possible to achieve a linear response function (i.e. a constant change of flap angle for a given ride height change, regardless of the height). The cam shape for a linear response function is shown in Fig 7.9. Now, a linear response is not necessarily the best. The BUGS CAM system, invented by Phil 'Bugs' Smith, has a constant flap angle before take-off; a high gain system right after take-off to control lift; a low gain system at stable ride height to maintain a smooth ride; and at maximum ride height a quick reduction of flap angle to zero lift to prevent the boat from jumping out of the water. The system is well described in Smith (2018).

**Fig 7.9** Cam shape for a linear response

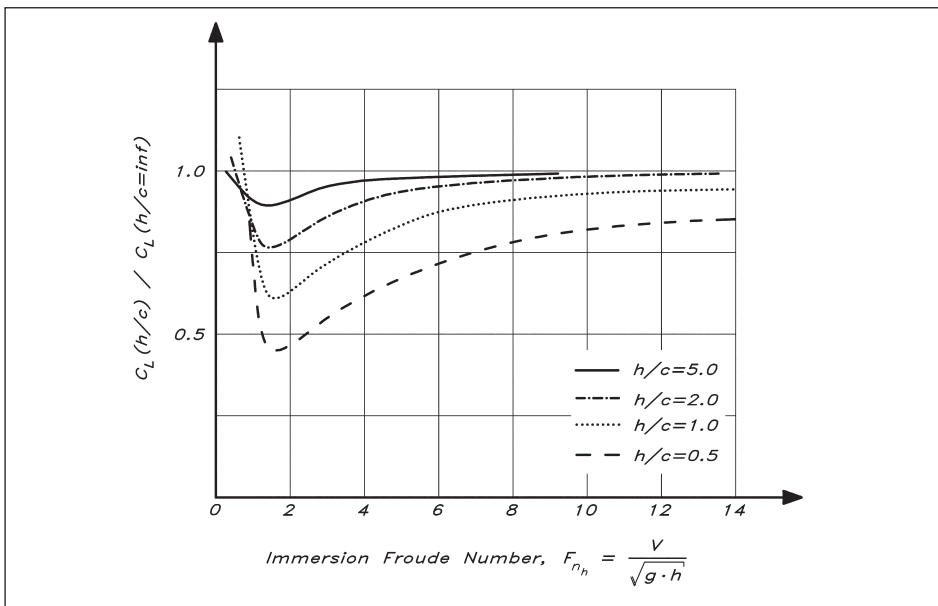




**Fig 7.10** Streamlines around a wing section (NACA 64A010) at a depth of 0.5 chord lengths, an angle of attack of 5° and a Froude number (based on chord length) of 1.2 (Andersson and Granli, 2019)

The rudder foil seldom has a flap. It is often fixed, but for instance the Moth has a variable rudder foil angle of attack, controlled by the helmsman via the tiller. If the rudder foil is fixed, the lift coefficient reduction with speed must come from the main foil, which means that load is gradually moved from the centre foil to the rudder foil as speed increases, provided the hull trim (pitch angle) is kept constant. If the pitch angle is changed such that the bow goes down, the angle of attack of the rudder foil is reduced, and so is the rudder foil lift. Note that some foil concepts are designed for negative lift. This is the case, for instance, for foiling boards, where the centre of gravity is in front of the main foil. But even Moths sometimes use negative rudder foil lifts.

For small foil submergences, there is a significant interaction between the water surface and the foil (see the CFD results by Andersson and Granli, 2019 in Fig 7.10). In front of the foil there is a high pressure, which makes the streamlines bend upwards, while above the foil the pressure is low, and the streamlines bend downwards. Therefore, there is a small wave crest at the nose and behind the foil there is a significant wave trough. Thus, there is a freedom of the free surface to adjust itself to the pressure generated by the foil. This reduces the suction on the upper side of the foil, and thus the lift.



**Fig 7.11** Lift coefficient reduction for varying immersion and Froude number (Faltinsen, 2005)

The lift reduction is presented in Fig 7.11, which shows the lift coefficient at a certain foil immersion, expressed as  $h/c$ , where  $h$  is the depth and  $c$  is the foil chord. This value is divided by the corresponding one at infinite depth (i.e. where there is no free surface effect). The horizontal scale is the Froude number based on the foil immersion. Curves are given for four immersions. It is seen that more than 50% of the lift is lost at the most critical point in the figure.

The lift reduction close to the surface has a stabilizing influence on the height control. Approaching the free surface, there is an automatic reduction in lift, which will cause the foil to sink. This effect may be exploited, but it is too weak for a stable flight, so a system like a wand for ride height control is required.

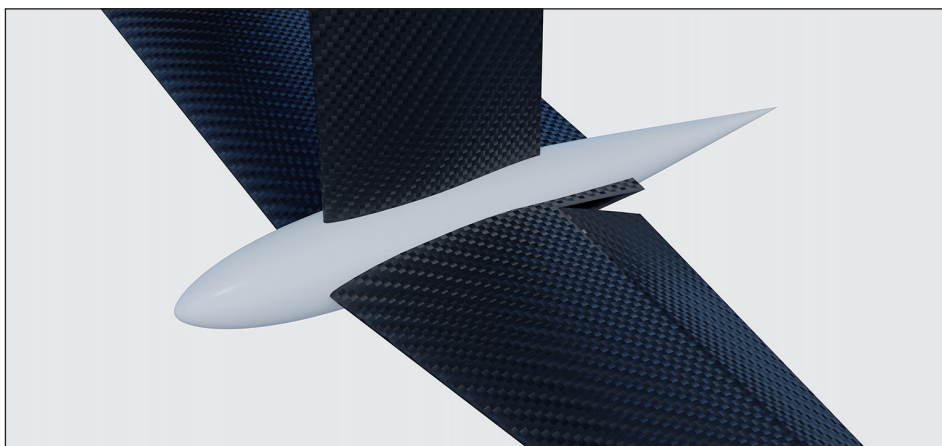
#### ◆ Longitudinal force balance (surge)

For horizontal equilibrium, the driving force from the sails must be equal to the sum of all drag components. For a fully foil-born condition there is no hydrodynamic resistance from the hull, but the aerodynamic drag may be considerable, particularly at high speeds. There are several drag components from the appendages:

- Centreboard/rudder
  - Profile drag
  - Induced drag
  - Wave and spray drag
- Centre foil foil/rudder foil
  - Profile drag
  - Induced drag
  - Wave drag
- Junction drag
- Wand drag.

The profile drag is the 2D drag of the section, as presented for instance in Figs 6.26–6.28. Induced drag is due to the slipping of the flow from the pressure side to the suction side around a free tip, as explained in Fig 6.3. Since both the centreboard and the rudder cut through the water surface, they will cause waves, just like a normal displacement hull. However, the Froude number, based on the chord length, is very high, so the waves are steep and break up into spray. As seen in Fig 7.10, a horizontal foil close to the surface generates waves, and thereby wave resistance.

The junction drag was briefly discussed in Chapter 6 in connection with the keel/hull or keel/bulb junction. To avoid a vortex in the corner, ‘fillets’ are recommended. However, if two wings are joined, like at the centreboard or rudder attachment to a foil, another phenomenon occurs. If the two parts are joined such that the minimum pressure on both sections coincide, the resulting pressure at that point will be very low. This means that the pressure recovery towards the trailing edges becomes very rapid, and the flow may separate, resulting in a considerably increased drag. Therefore, when two wings are joined, they should be staggered such that the maximum thicknesses are as far apart as possible. Another way to avoid this problem is to fit a torpedo in the



**Fig 7.12** Centreboard/foil junction torpedo (picture by Frowin Winkes)

corner, as seen in Fig 7.12. This is frequently used on Moths, for instance, and has the additional advantage of better structural integrity.

The final hydrodynamic drag component in the list is wand drag. This is the drag of the paddle at the lower end of the wand (see Fig 7.7). This paddle skims along the surface, like a planing hull. As appears from Figs 11.2 and 11.3 the force generated is at right angles to the planing surface, neglecting the small friction. For the small paddle, the buoyancy effect (hydrostatic pressure) can be neglected as well, as can its own weight, so the only force of importance is the hydrodynamic force caused by the deflection of the streamlines, as seen in Fig 11.2. This force is at right angles to the paddle surface, and it is this force that generates the required moment to turn the cam of Fig 7.8. The turning of the cam transmits a force through the linkage system to the flap. There is thus a direct coupling between the forces on the paddle and the flap. The link is the transfer function (flap angle versus ride height), which is determined by the cam shape and the gain adjustment lever described above. Knowing the flap and wand levers (i.e. the distances from the forces to the pivot points) the required paddle force for a given flap force may be computed. The wand drag is simply the horizontal component of the force on the paddle.

Even though the flap – for larger angles – will carry a considerable part of the total lift of the foil, the transfer function and the difference in levers reduce the wand force drastically, so the drag will be quite small, only a few Newtons. It will be neglected in the following.

#### ◆ Pitch moment balance

To achieve equilibrium in pitch, the net moment created by all forces in Fig 7.7 must be zero. With the pivot point at the centre of gravity (denoted CG in the figure) a bow-down moment is created by the aerodynamic driving force, all hydrodynamic resistance components, the rudder foil lift (if positive), and the dinghy weight. The bow-up moments come from the centre foil lift, the aerodynamic drag, and the crew weight. As mentioned, if there are no means to reduce the lift coefficient of the rudder foil, it will take over more and more of the total lift from the centre foil as speed increases. The lift from the centre foil is then reduced by a smaller flap angle. This means that the total lift force moves backwards, and to keep the boat on even keel the crew also needs to move backwards. This effect is in addition to the increased bow-down moment as the driving force and

hydrodynamic resistance increase (as for all sailing craft). Now, the even keel attitude may not be the best. Reasons for adopting other trims will be given below.

When computing the lift of the rudder foil the effective angle of attack should be used. This differs from the geometrical angle of attack (related to the horizontal direction) for two reasons:

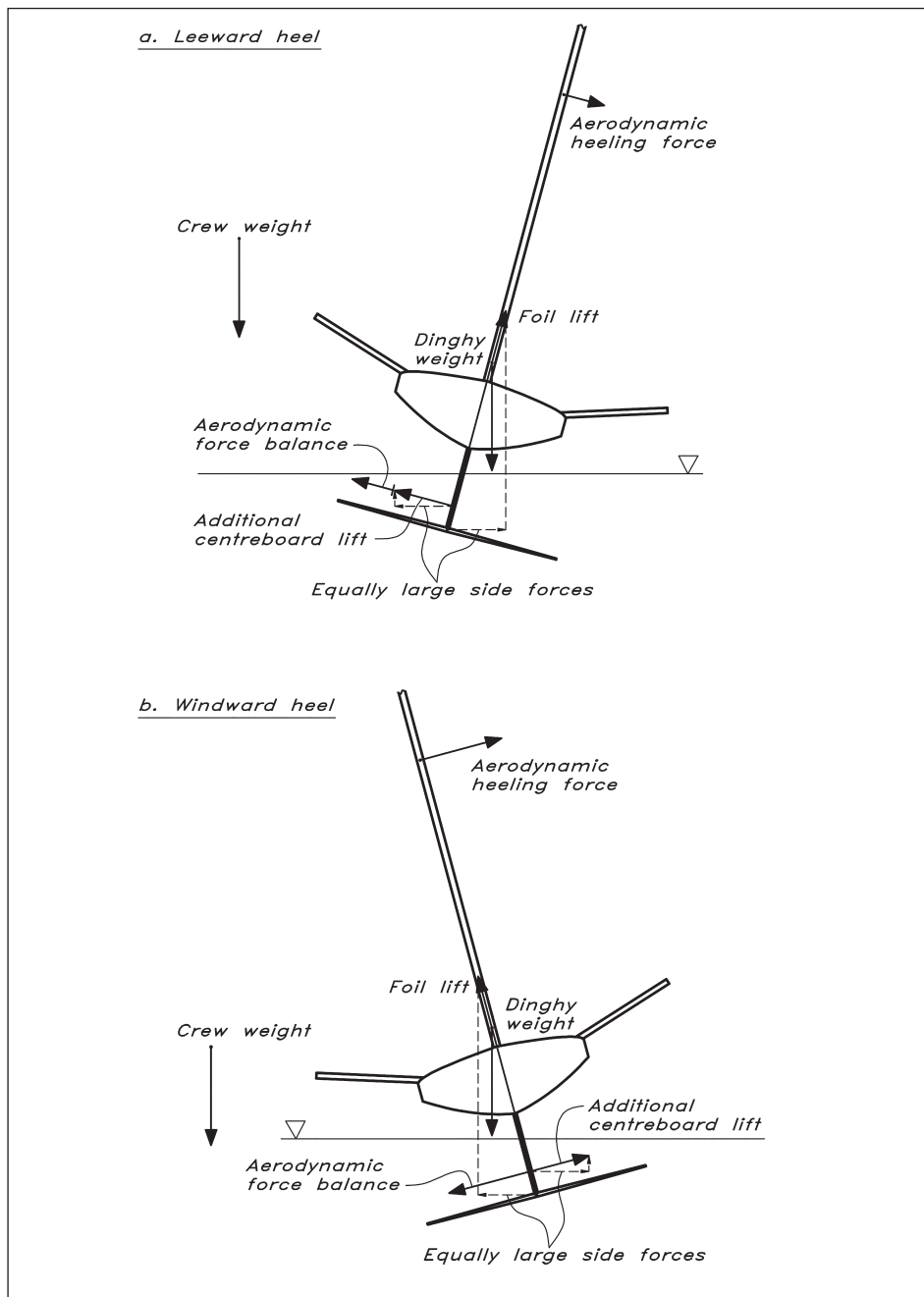
1. The rudder foil operates in the disturbed flow from the centre foil. The disturbance velocity is directed downwards and is called *downwash*. Using the lifting line theory, briefly introduced in [Fig 6.5](#), the downwash can be computed, but the mathematics is beyond that required for this book. Note that there is a similar disturbance from the keel on the rudder for all sailboats, as explained in [Chapter 6](#).
2. As seen in [Fig 7.10](#) waves are generated by the foils, and the rudder foil operates in the wave system of the centre foil. This will affect the flow direction, depending on both wave height and wavelength. While the wavelength is easily computed, as explained in [Fig 5.15](#), the height depends in a complex way on both foil lift and submergence. Without access to advanced methods, like computational fluid dynamics (CFD), this effect is hard to predict.

The pragmatic way to tackle the foil interference problem is to make the angle of attack of the rudder foil adjustable, and let practical experience determine the geometrical angle. Many boats, like the Laser (with a foil kit) have a pivoting rudder foil where the angle of attack can be adjusted easily. Others have a foil fixed to the rudder, but an adjustable rudder rake. In some classes the changes can be achieved when sailing, while in others it has to be done between the races. As explained above, the rudder foil takes over more and more of the lift with increasing speed, so the rake adjustment can be made based on the expected speeds of the race (i.e. based on the wind conditions).

#### ◆ Transverse moment balance (roll)

In [Fig 7.13](#) the forces acting on the dinghy in a transverse plane are displayed. At the top, the dinghy is heeled to leeward, and at the bottom to windward. Let us first look at the top panel. We note that the aerodynamic heeling force is balanced by an equally large, but opposite hydrodynamic force, just like for the displacement yacht in [Fig 5.1](#). There is, however, a difference in the vertical lifting force, which comes from the buoyancy in [Fig 5.1](#), but mainly from the foil lift in [Fig 7.13](#) (overleaf). The foil lift is directed at right angles to the foil span, and heels with the dinghy. This generates a side force to leeward. At equilibrium, this must be compensated by an equally large side force to windward. The latter is the horizontal component of an additional centreboard lift, generated by an increased leeway. Note that the vertical component of this force contributes to the vertical force balance.

Now let us look at the moments and take the boat centre of gravity as the moment point. By this choice neither the boat weight nor the foil lift will contribute. The main heeling moments comes from the aerodynamic side force and the corresponding hydrodynamic force. However, there is also a contribution from the additional centreboard lift. The only righting moment comes from the crew, so the stability depends entirely on the crew position.



**Fig 7.13** Forces on a dinghy heeled to leeward (TOP) and windward (BOTTOM) – seen opposite to the direction of motion

For the windward heel the tilted lift will be compensated by an additional centreboard lift, just as in the top panel. However, *it is now in the opposite direction*. This means that it counteracts the force balancing the aerodynamic side force. At a certain heel angle the forces cancel each other completely. Then there is no lift generated on the centreboard and there is no leeway! The foil generates enough side force to balance the sails. This has some interesting implications, as we will see below. However, the largest advantage is that the additional centreboard lift now co-operates with the crew in generating a heeling

moment (to windward) to balance the righting moment (to leeward) from the sails. Less depowering is then needed for the sails and the driving force can be increased. This is why most foiling dinghies are sailed with windward heel.

## ■ FLIGHT STABILITY

So far, we have looked at the forces and moments at equilibrium conditions. An important question is what happens if the boat is exposed to a disturbance in any of the degrees of freedom. Will the resulting motion die out and the boat return to equilibrium? If so, the boat is said to be *statically stable*. On the other hand, if the motion diverges away from equilibrium the boat is *statically unstable*. In both cases the development of the motion may be either monotonous or oscillatory. An oscillatory motion is *dynamically stable* if the oscillations die out in time. If they grow the motion is *dynamically unstable*.

An obvious necessary condition for static stability is the generation of a restoring force (moment) when the boat is disturbed from its equilibrium state. Without this restoring force (moment) there is no mechanism to bring the boat back to equilibrium and the disturbance will grow in time. For a foiling boat this will inevitably lead to a crash.

Let us look at the restoring forces and moments of the four degrees of freedom we considered above, namely surge, heave, roll and pitch.

A disturbance in surge, such as a speed increase, will automatically generate a restoring force for a displacement yacht. When the speed increases the resistance also increases, as seen in [Fig 5.3](#), and for a given driving force this means that there is a net force backwards. Now, the driving force is not exactly unchanged; the apparent wind speed increases (upwind) and the apparent wind angle decreases. The combined effect is a small reduction in driving force. This increases the force unbalance and hence the restoring force. For a speed reduction the opposite happens, and the restoring force will accelerate the boat towards equilibrium.

The resistance curve for a foiling boat is very different, as seen in [Fig 7.1](#). In the region between the hump and the hollow the resistance decreases. So, a small speed increase will result in a lower resistance, and hence in a net force forwards that will increase the speed even further. In this speed region the motion is unstable. This fact may be exploited by the crew when the speed is close to the hump. A small disturbance may then move the hull from displacement to foiling mode. Such disturbances may be a rapid pumping of the sails or a jump on the boat (that will generate a driving force on the foils). Note that there are two equilibrium states in the entire hollow region of [Fig 7.1](#): one to the left and one to the right of the minimum.

A foiling boat with an active height control system, as described above, always generates a restoring force in heave. When the boat flies too high the lift is reduced by the flap angle reduction, and the unbalance in vertical forces will move the boat downwards. For too low a ride height there will be a restoring force directed upwards.

As we have seen, the boat itself is not stable in roll. Instead, the balancing of the boat in roll relies entirely on the crew, requiring constant (and skilful) adjustment of sail power and crew position to keep the boat upright.



The final DOF discussed here is pitch. Suppose that the pitch angle is suddenly increased, for instance by a wave. Then both foils experience the same increase in angle of attack. For static stability this must result in a larger relative increase in the lift of the rudder foil than of the centre foil. If this is the case, the combined lift centre will move backwards, creating a bow-down (restoring) moment, trying to turn the boat back to the original trim. On the other hand, if the *relative* increase in lift is largest for the centre foil, the lift centre will move forwards and the pitch angle will increase. This is an unstable situation.

But the lift generated depends on several factors. It is proportional to the lift coefficient, which depends both on the slope of the 2D lift curve (see [Table 7.2, page 164](#)) and the aspect ratio (see [Fig 6.6](#)). This holds for both foils, but the centre foil lift also depends on the flap angle, as seen in [Table 7.2](#). As we will see in the example below, pitch stability puts a limit on the loading of the rudder foil (i.e. on the position of the crew). If too far aft, the relative change in lift of the rudder foil will be smaller than that of the main foil for a change in pitch angle, and that will cause the boat to crash.

Restoring forces and moments are *necessary* conditions for static stability, but they are *not sufficient*. Even if we have a restoring moment in pitch, for instance, the hull may start oscillating bow up/bow down. If the oscillation is damped, the boat is statically (and dynamically) stable, but if undamped, the static (and dynamic) instability will lead to a crash.

Unfortunately, there is no simple way to ascertain static stability. There are in principle two possibilities, but both include advanced mathematics. The most exact method is to solve the dynamic equations of motion in each of the six degrees of freedom as a function of time. This is done in the Dynamic Velocity Prediction Programs (DVPPs) presented in [Chapter 17](#). The other possibility is based on a simplification of the governing equations, whereby the equations are linearized by assuming linear relationships between forces (moments) and the state variables (position, velocity, and acceleration) in all six DOFs; but the mathematics behind this process is still far beyond the requirements for this book, and will not be further discussed. The interested reader is referred to the excellent paper by Masuyama (1987), where the theory is explained in detail and comparisons are made with the DVPP approach. Reference should also be made to a pioneering paper by Kaplan *et al* (1958) on pitch stability. Another basic paper on foiling stability is that of Heppel (2015). Applications to a Moth are described in Eggert *et al* (2020) and to a foiling catamaran by Bagué *et al* (2020).

## ■ PLANFORM AREA AND SHAPE

For the optimization of the foil system, a VPP should be available. See [Chapter 17](#) for an introduction to VPPs, including foiling. We will now discuss the optimization of the area, span and taper ratio for all four appendages: the centreboard, the centre foil, the rudder and the rudder foil.

### ◆ Centreboard

As mentioned above, foiling dinghies are often sailed with windward heel, which reduces the lift of the centreboard. For a certain heel angle, the lift will be zero, which means that the centreboard is not even required. But the centreboard is needed to support the foil, so there is

a minimum size from a structural point of view. Also, a certain area is needed for low speeds when the hull is still in the water. This area is, however, considerably smaller than the 3% of the sail area recommended for displacement yachts in [Chapter 6](#). This is because dinghies in general are fast even with small sail forces. The optimum area is thus a compromise between low-speed and high-speed performance considering structural aspects.

As pointed out above, the dinghy will be easier to balance for a small centreboard span, but there are disadvantages. For the centre foil to be efficient it should be submerged at least one chord length, even when sailing in waves. And the bottom of the hull must be sufficiently above the water surface to avoid the waves. There is thus a minimum span to satisfy these requirements. But there is also another very important aspect: the crew must be able to raise the boat to upright after a capsize! The mast, rig and sails generate a considerable heeling moment in a capsize, and the problem may be accentuated by water captured in the sail. When deciding about the centreboard span it should be ascertained that the righting moments from a crew standing as far out on the centreboard as possible (they will interfere with the foil!) is larger than the heeling moment from the mast, rig and sails.

Unlike a normal keel or centreboard, the elliptic shape is not optimum for a centreboard with a foil at the tip. In the non-foiling mode, there is a very efficient endplate at the root of the centreboard, namely the hull. This will act as a barrier for the overflow, as for all sailing craft. When foiling, the centreboard cuts through the water surface and the overflow prevention from the hull is lost. However, the water surface will deform, with a wave crest on the pressure side and a wave trough on the suction side. The vortex energy is thus transferred into wave energy. How to design the planform to minimize this effect is not well known. At the centreboard tip, the foil effectively prevents the overflow from the pressure to the suction side, so there is generally no reason to reduce the chord downwards. Therefore, most T-foil centreboards have a constant chord from root to tip.

However, when heeling to windward such that there is no side force generated by the centreboard, its submerged area should be minimized to reduce friction. This would speak in favour of a reduced chord towards the tip. In this condition, the chord should therefore be as small as possible, satisfying structural constraints. Heeling in this way also means that there will be no vortex generated at the surface and no corresponding wave drag, which is obviously an advantage.

#### ◆ Centre foil

The optimum centre foil area is a trade-off between early take-off and high-speed performance. A larger area will generate a larger lift, which is an advantage for early take-off. On the other hand, a larger area will also generate larger friction, so the speed will be reduced. It may well be that the optimum area for taking-off at minimum boat speed is not the best since it may require more wind to reach that speed. Therefore, the optimization of the area should be done based on the minimum wind speed. This is if early take-off is prioritized. If high speeds are prioritized the area should be reduced. The necessary lift can be accomplished by a much smaller area with less friction.

The importance of the aspect ratio was discussed in detail in [Chapter 6](#). For all wings with a free end, the lift is increased, and the induced resistance reduced when the aspect ratio is increased. Large spans are thus preferable, from a hydrodynamic point of view.

The span of the centre foil may be determined by a rule limitation in the class. If not, the optimum span is determined considering both hydrodynamic and structural aspects. A large span means a large bending moment, and thus a large cross-section (moment of inertia) is needed at the root. This may be achieved either as a thick section or one with a large chord (less efficient). Both are disadvantages from a hydrodynamic point of view. So, it is essentially a trade-off between induced drag and profile drag at the root. A way to increase the effective span without increasing stresses at the root is to add winglets at the tip, much like the bulb wings presented in [Chapter 6](#). An example of winglets is seen in [Fig 7.30](#) (page 177). Note that it is not only the risk of structural failure that needs to be considered; a large bending may cause problems with the flap hinge. Also, the dynamic forces developed for these fast craft are considerable. Based on measurements of accelerations onboard a Moth, a safety factor of at least 1.5 on the static loads is recommended for this class.

As shown in [Chapter 6](#), a certain taper is required to minimize drag for a given lift. According to [Fig 6.8](#), the best taper ratio for zero sweep is around 0.45. The foils do not normally have exactly zero sweep angle – this is impossible for the centre foil with a flap since the flap hinge must be on a straight line – but the deviation is small and may be neglected.

#### ◆ Rudder

The optimum rudder area is hard to determine even with a VPP since the task of the rudder is to generate sufficient side force to manoeuvre the dinghy at all speeds. This can in principle be studied by DVPPs, where the rudder could be optimized from a hydrodynamic point of view. But the problem is structural rather than hydrodynamic. In the ISO standard for sailing yachts, presented in [Chapter 15](#), the load case for the rudder is defined by the maximum lift coefficient, given for NACA sections in [Fig 6.31](#), and the maximum speed. This leads to completely unrealistic loads for a foiling dinghy with maximum speed of at least 15 m/s. The dinghy is so light that the smallest rudder angle will cause the boat to turn, thereby reducing the angle of attack of the rudder. A pragmatic solution is presented for the example dinghy below.

The draft of the rudder is often slightly smaller than that of the centreboard. There is no strong hydrodynamic reason for that. The downwash mentioned above will be slightly smaller if the rudder foil flies higher than the centre foil. But that is a very small effect and there is very little risk for the rudder to hit the viscous wake behind the centre foil since that is swept downwards by the downwash. On the other hand, the draft must be large enough to keep a sufficient area in the water even when the boat pitches in waves (and the rudder foil must certainly stay in the water at all times, otherwise the pitch stability will be lost and the boat will crash!).

Most rudders have a rectangular planform due to the endplate effect of the foil, but there might be an advantage in reducing the chord close to the tip. At higher speeds the rudder area can be reduced significantly, still providing the required side force. This would reduce the wetted area and thereby friction. To some extent this is accomplished through a bow-down trim at high speeds, but this is limited by the required submergence of the rudder foil. A smaller chord close to the tip could then contribute to the desired area reduction.

### ◆ Rudder foil

The rudder foil area should be determined based on the maximum lift to be carried by the rudder. This can be obtained from the pitch stability condition. For the example dinghy below, it is about 25% of the total weight. With lift given, there is a trade-off between area and lift coefficient, and an optimum can be found using [Tables 7.2 and 7.3](#). Note that structural aspects will call for a minimum moment of inertia of the root section at the largest load. Hence there is a minimum root chord.

A high aspect ratio is recommended for the rudder foil. This not only reduces the induced drag; it also alleviates the problem of satisfying the stability criterion. On the other hand, the bending moment at the root will increase with aspect ratio, calling for a larger root section. So, there is an optimum, considering both hydrodynamic and structural aspects. The taper ratio should be the same as for the centre foil: around 0.45.

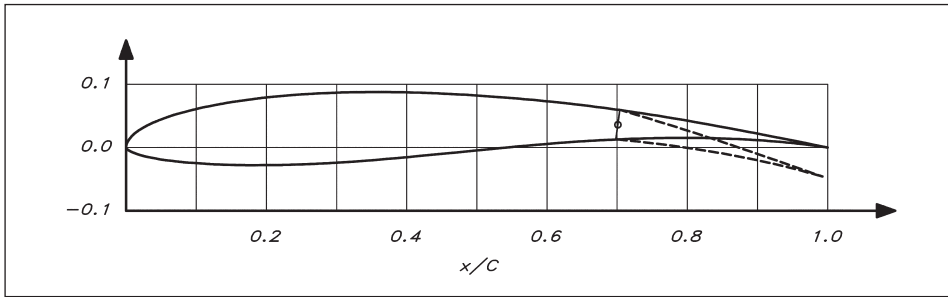
## ■ FOIL SECTIONS

The sections presented in [Chapter 6](#) are to be used for keels and rudders, so they must be symmetric. They are suitable for the centreboard and rudder in the present application, but not for the two foils, which will generate lift only in one direction. Here asymmetric sections may be more efficient. Such sections develop lift also at zero angle of attack, and they may be more efficient in terms of lift/drag ratio than the symmetric ones.

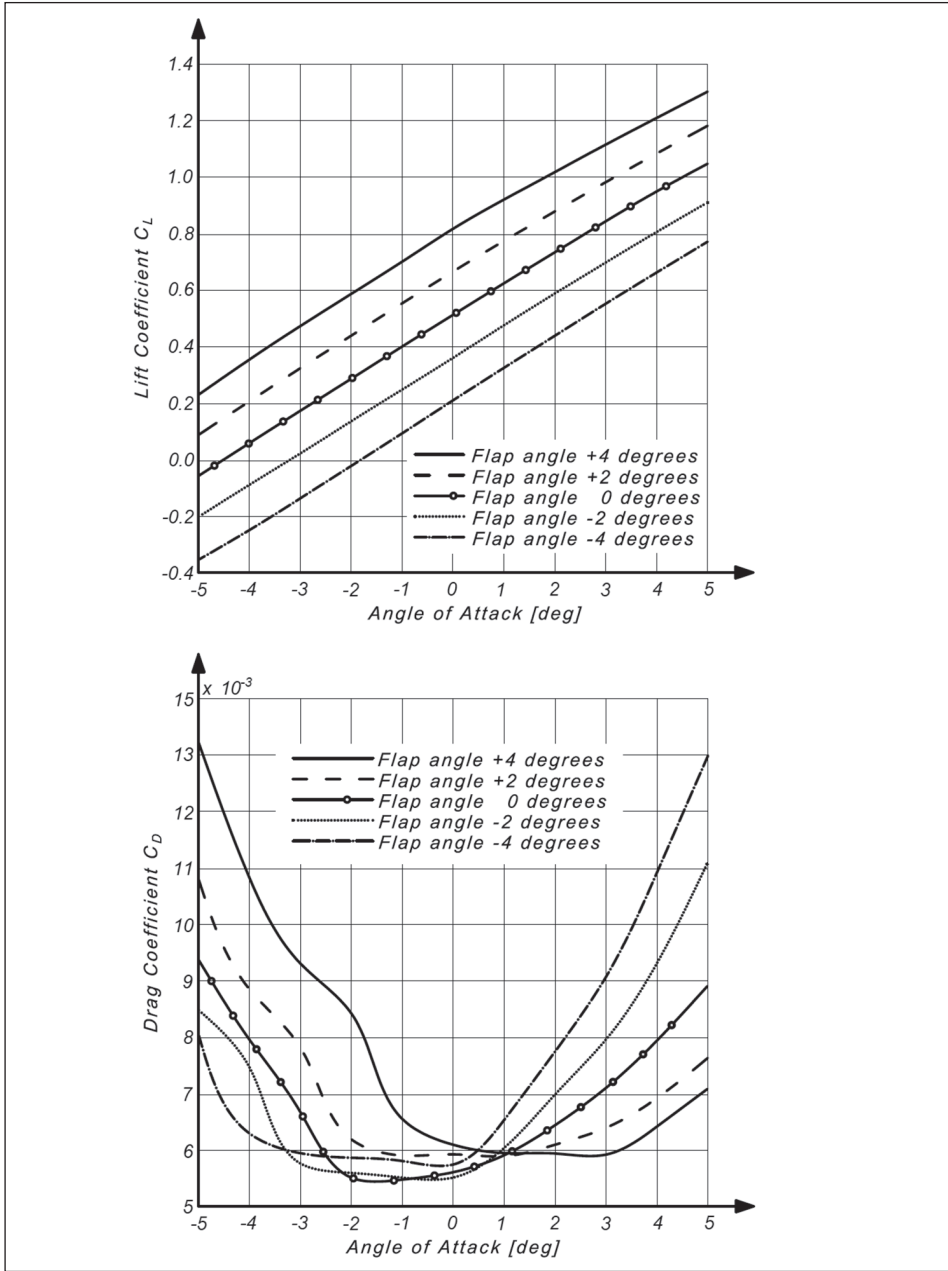
There are several asymmetric sections in the NACA series, and it would be natural to expand the information given in [Chapter 6](#) to such sections. However, as explained in that chapter, the NACA sections were developed for applications at relatively high Reynolds numbers. The data presented in [Chapter 6](#) are for a Reynolds number of 3 million. This corresponds to a keel chord of 1 m and a speed of 3 m/s (about 6 knots), typical for a medium-size sailing yacht keel upwind in a good breeze. However, it is too large for most sailing dinghies, at least in the non-planing speed range. For lower speeds, the Reynolds number for a centreboard or dinghy rudder is often well below one million. This turns out to have a considerable effect on the section characteristics.

In [Fig 5.8](#) we can see that friction is reduced with Reynolds number. This holds when the boundary layer on the section is fully turbulent (i.e. at higher Reynolds numbers). For lower Reynolds numbers transition from laminar to turbulent flow becomes important. As explained in connection with the description of the NACA section characteristics of [Chapter 6](#), the shape of the section can be designed to delay the transition, which reduces the drag. This works also for the higher Reynolds numbers of the NACA sections, but it is much easier to delay transition at a low Reynolds number. Therefore, sections developed for a lower Reynolds number range, are different from those of [Chapter 6](#).

A very useful section developed for the lower Reynolds numbers of gliders is the Wortmann FX 60-100. It is an asymmetric section with 10% thickness at 27.9% of the chord and max camber of 3.6% at 65.5% of the chord. It is shown in [Fig 7.14](#) (overleaf) with two flap angles, where the flap occupies 30% of the total chord. The camber is defined in [Fig 6.23](#). Coordinates of the section (with zero flap angle) are



**Fig 7.14** Wortmann FX 60-100 section with and without a deflected flap



**Fig 7.15** Wortmann FX 60-100: lift (TOP) and drag (BOTTOM) coefficients for varying angles of attack and flap angles at a Reynolds number of one million



**Table 7.1** Wortmann  
FX 60-100 coordinates

X	Y	X	Y	X	Y
0.000000	0.000000	0.777790	0.042000	0.278860	-0.022750
0.001070	0.005740	0.804380	0.037470	0.308660	-0.021000
0.004280	0.011440	0.829670	0.032980	0.339280	-0.018950
0.009610	0.017750	0.853550	0.028640	0.370590	-0.016370
0.017040	0.023680	0.875920	0.024470	0.402450	-0.013570
0.026530	0.029480	0.896680	0.020530	0.434740	-0.010450
0.038060	0.035230	0.915730	0.016810	0.467300	-0.007310
0.051560	0.040560	0.933010	0.013420	0.500000	-0.004050
0.066990	0.046090	0.948440	0.010350	0.532700	-0.000920
0.084270	0.050860	0.961940	0.007660	0.565260	0.002170
0.103320	0.055690	0.973470	0.005340	0.597550	0.004960
0.124080	0.059890	0.982960	0.003410	0.629410	0.007480
0.146450	0.064040	0.990390	0.001930	0.660720	0.009510
0.170330	0.067540	0.995720	0.000860	0.691340	0.011180
0.195620	0.070810	0.998930	0.000230	0.721140	0.012410
0.222210	0.073390	1.000000	0.000000	0.750000	0.013290
0.250000	0.075650	0.000000	0.000000	0.777790	0.013730
0.278860	0.077200	0.001070	-0.002000	0.804380	0.013810
0.308660	0.078380	0.004280	-0.004360	0.829670	0.013470
0.339280	0.078880	0.009610	-0.006910	0.853550	0.012800
0.370590	0.078980	0.017040	-0.009700	0.875920	0.011860
0.402450	0.078450	0.026530	-0.012470	0.896680	0.010720
0.434740	0.077500	0.038060	-0.014810	0.915730	0.009410
0.467300	0.075960	0.051560	-0.017300	0.933010	0.008020
0.500000	0.074090	0.066990	-0.019130	0.948440	0.006590
0.532700	0.071740	0.084270	-0.021100	0.961940	0.005150
0.565260	0.069110	0.103320	-0.022460	0.973470	0.003770
0.597550	0.066080	0.124080	-0.023770	0.982960	0.002510
0.629410	0.062750	0.146450	-0.024470	0.990390	0.001510
0.660720	0.059050	0.170330	-0.025030	0.995720	0.000700
0.691340	0.055110	0.195620	-0.025000	0.998930	0.000150
0.721140	0.050890	0.222210	-0.024750	1.000000	0.000000
0.750000	0.046520	0.250000	-0.023890		

given in [Table 7.1](#). Note that for very high speeds cavitation will be a problem. See below! This will call for very different foil sections.

The airfoil analysis tool XFOIL was introduced in [Chapter 6](#). To obtain input to Velocity Prediction Programs often many hundred computations are carried out using this software. Results of such systematic computations are presented in [Table 7.2](#), which gives the lift and drag coefficients for Wortmann FX 60-100 at varying angles of attack. The coefficients are given for five Reynolds numbers and five flap angles. Rather than running XFOIL, the reader may interpolate values in [Table 7.2](#) for this section. As an example, the coefficients are presented for a Reynolds number of one million in [Fig 7.15](#).

Data for the symmetric NACA 0012, computed with XFOIL are given in [Table 7.3](#) ([page 165](#)). This section is used for the centreboard and rudder in the example below. The shape can be obtained from [Table 6.3](#).

**Table 7.2** Wortmann  
FX 60-100: lift and  
drag coefficients from  
XFOIL at varying angles  
of attack, flap angles  
and Reynolds numbers  
(upper leftmost value  
for each Reynolds  
number extrapolated)

a. Lift coefficient												
Wortmann FX60100 - CL Data												
Re	Flap \ Alfa	-5	-4	-3	-2	-1	0	1	2	3	4	5
5,00E+05	-4	-0,4066	-0,2531	-0,1295	-0,0193	0,0937	0,2072	0,3209	0,4325	0,5403	0,6406	0,7548
	-2	-0,2345	-0,0940	0,0243	0,1362	0,2473	0,3594	0,4716	0,5829	0,6880	0,7922	0,9005
	0	-0,0522	0,0631	0,1777	0,2894	0,4009	0,5124	0,6231	0,7320	0,8371	0,9348	1,0376
	2	0,0946	0,2106	0,3264	0,4393	0,5515	0,6631	0,7727	0,8761	0,9772	1,0763	1,1660
	4	0,2404	0,3594	0,4739	0,5867	0,6997	0,8107	0,9192	1,0150	1,1084	1,1987	1,2825
Re	Flap \ Alfa	-5	-4	-3	-2	-1	0	1	2	3	4	5
7,50E+05	-4	-0,3645	-0,2421	-0,1356	-0,0217	0,0928	0,2077	0,3229	0,4370	0,5478	0,6567	0,7615
	-2	-0,2058	-0,0892	0,0213	0,1335	0,2461	0,3594	0,4735	0,5859	0,6954	0,7961	0,9050
	0	-0,0541	0,0585	0,1740	0,2876	0,4005	0,5127	0,6240	0,7331	0,8406	0,9442	1,0426
	2	0,0903	0,2064	0,3238	0,4379	0,5515	0,6642	0,7745	0,8760	0,9798	1,0813	1,1723
	4	0,2370	0,3572	0,4727	0,5870	0,7006	0,8128	0,9218	1,0143	1,1116	1,2041	1,2932
Re	Flap \ Alfa	-5	-4	-3	-2	-1	0	1	2	3	4	5
1,00E+06	-4	-0,3512	-0,2493	-0,1367	-0,0220	0,0933	0,2092	0,3241	0,4385	0,5506	0,6613	0,7702
	-2	-0,2016	-0,0913	0,0190	0,1323	0,2459	0,3603	0,4747	0,5872	0,6979	0,8059	0,9078
	0	-0,0570	0,0570	0,1723	0,2872	0,4004	0,5130	0,6245	0,7338	0,8424	0,9488	1,0458
	2	0,0890	0,2051	0,3230	0,4377	0,5518	0,6650	0,7713	0,8765	0,9818	1,0840	1,1820
	4	0,2363	0,3562	0,4724	0,5870	0,7012	0,8138	0,9141	1,0148	1,1140	1,2080	1,3002
Re	Flap \ Alfa	-5	-4	-3	-2	-1	0	1	2	3	4	5
2,00E+06	-4	-0,3646	-0,2514	-0,1359	-0,0198	0,0967	0,2119	0,3268	0,4412	0,5542	0,6666	0,7770
	-2	-0,2077	-0,0978	0,0165	0,1320	0,2483	0,3632	0,4771	0,5894	0,7012	0,8119	0,9194
	0	-0,0590	0,0559	0,1707	0,2869	0,4007	0,5137	0,6255	0,7359	0,8458	0,9531	1,0577
	2	0,0889	0,2050	0,3228	0,4386	0,5534	0,6626	0,7703	0,8790	0,9856	1,0890	1,1916
	4	0,2370	0,3553	0,4730	0,5884	0,7033	0,8080	0,9128	1,0175	1,1187	1,2170	1,3171
Re	Flap \ Alfa	-5	-4	-3	-2	-1	0	1	2	3	4	5
4,00E+06	-4	-0,3644	-0,2487	-0,1331	-0,0174	0,0983	0,2138	0,3285	0,4427	0,5560	0,6687	0,7800
	-2	-0,2121	-0,0972	0,0183	0,1342	0,2501	0,3648	0,4784	0,5910	0,7032	0,8140	0,9232
	0	-0,0590	0,0559	0,1709	0,2867	0,4013	0,5145	0,6263	0,7377	0,8479	0,9561	1,0635
	2	0,0907	0,2067	0,3237	0,4403	0,5507	0,6613	0,7711	0,8808	0,9884	1,0943	1,2009
	4	0,2396	0,3566	0,4753	0,5913	0,6990	0,8059	0,9138	1,0195	1,1232	1,2267	1,3304
b. Drag coefficient												
Wortmann FX60100 - CD Data												
Re	Flap \ Alfa	-5	-4	-3	-2	-1	0	1	2	3	4	5
5,00E+05	-4	0,02617	0,01398	0,01081	0,00943	0,00752	0,00762	0,00752	0,00700	0,00704	0,00713	0,00777
	-2	0,01594	0,01161	0,00931	0,00698	0,00699	0,00711	0,00729	0,00710	0,00717	0,00757	0,00860
	0	0,01259	0,01006	0,00737	0,00705	0,00695	0,00694	0,00705	0,00734	0,00787	0,00834	0,00979
	2	0,01104	0,00929	0,00760	0,00750	0,00740	0,00729	0,00723	0,00767	0,00881	0,00994	0,01150
	4	0,01039	0,00832	0,00829	0,00824	0,00811	0,00796	0,00772	0,00832	0,00998	0,01177	0,01422
Re	Flap \ Alfa	-5	-4	-3	-2	-1	0	1	2	3	4	5
7,50E+05	-4	0,01665	0,01172	0,01001	0,00885	0,00699	0,00678	0,00646	0,00631	0,00631	0,00674	0,00726
	-2	0,01240	0,00983	0,00833	0,00639	0,00629	0,00642	0,00640	0,00646	0,00667	0,00689	0,00796
	0	0,01050	0,00874	0,00676	0,00603	0,00599	0,00606	0,00628	0,00674	0,00740	0,00804	0,00922
	2	0,00943	0,00813	0,00637	0,00623	0,00616	0,00613	0,00619	0,00723	0,00826	0,00958	0,01094
	4	0,00882	0,00690	0,00671	0,00665	0,00657	0,00648	0,00640	0,00796	0,00938	0,01129	0,01358
Re	Flap \ Alfa	-5	-4	-3	-2	-1	0	1	2	3	4	5
1,00E+06	-4	0,01324	0,01083	0,00932	0,00843	0,00656	0,00611	0,00595	0,00595	0,00594	0,00643	0,00710
	-2	0,01079	0,00886	0,00783	0,00621	0,00592	0,00594	0,00590	0,00610	0,00640	0,00693	0,00764
	0	0,00938	0,00796	0,00667	0,00553	0,00550	0,00562	0,00591	0,00645	0,00712	0,00795	0,00892
	2	0,00850	0,00748	0,00578	0,00560	0,00554	0,00554	0,00604	0,00699	0,00796	0,00931	0,01109
	4	0,00803	0,00630	0,00596	0,00588	0,00582	0,00576	0,00655	0,00775	0,00909	0,01093	0,01298
Re	Flap \ Alfa	-5	-4	-3	-2	-1	0	1	2	3	4	5
2,00E+06	-4	0,00999	0,00881	0,00791	0,00715	0,00569	0,00517	0,00515	0,00530	0,00563	0,00588	0,00666
	-2	0,00822	0,00752	0,00696	0,00613	0,00510	0,00504	0,00520	0,00558	0,00607	0,00660	0,00754
	0	0,00740	0,00662	0,00610	0,00482	0,00478	0,00499	0,00540	0,00601	0,00668	0,00762	0,00881
	2	0,00688	0,00626	0,00498	0,00458	0,00454	0,00504	0,00582	0,00657	0,00752	0,00881	0,01018
	4	0,00658	0,00557	0,00479	0,00466	0,00461	0,00543	0,00641	0,00737	0,00865	0,01017	0,01147
Re	Flap \ Alfa	-5	-4	-3	-2	-1	0	1	2	3	4	5
4,00E+06	-4	0,00803	0,00723	0,00657	0,00615	0,00552	0,00471	0,00475	0,00500	0,00538	0,00584	0,00633
	-2	0,00712	0,00655	0,00609	0,00570	0,00469	0,00463	0,00489	0,00531	0,00581	0,00649	0,00733
	0	0,00618	0,00575	0,00548	0,00469	0,00446	0,00473	0,00522	0,00576	0,00644	0,00733	0,00826
	2	0,00581	0,00540	0,00468	0,00402	0,00449	0,00505	0,00568	0,00636	0,00726	0,00831	0,00921
	4	0,00557	0,00510	0,00412	0,00392	0,00497	0,00555	0,00626	0,00719	0,00829	0,00933	0,01027



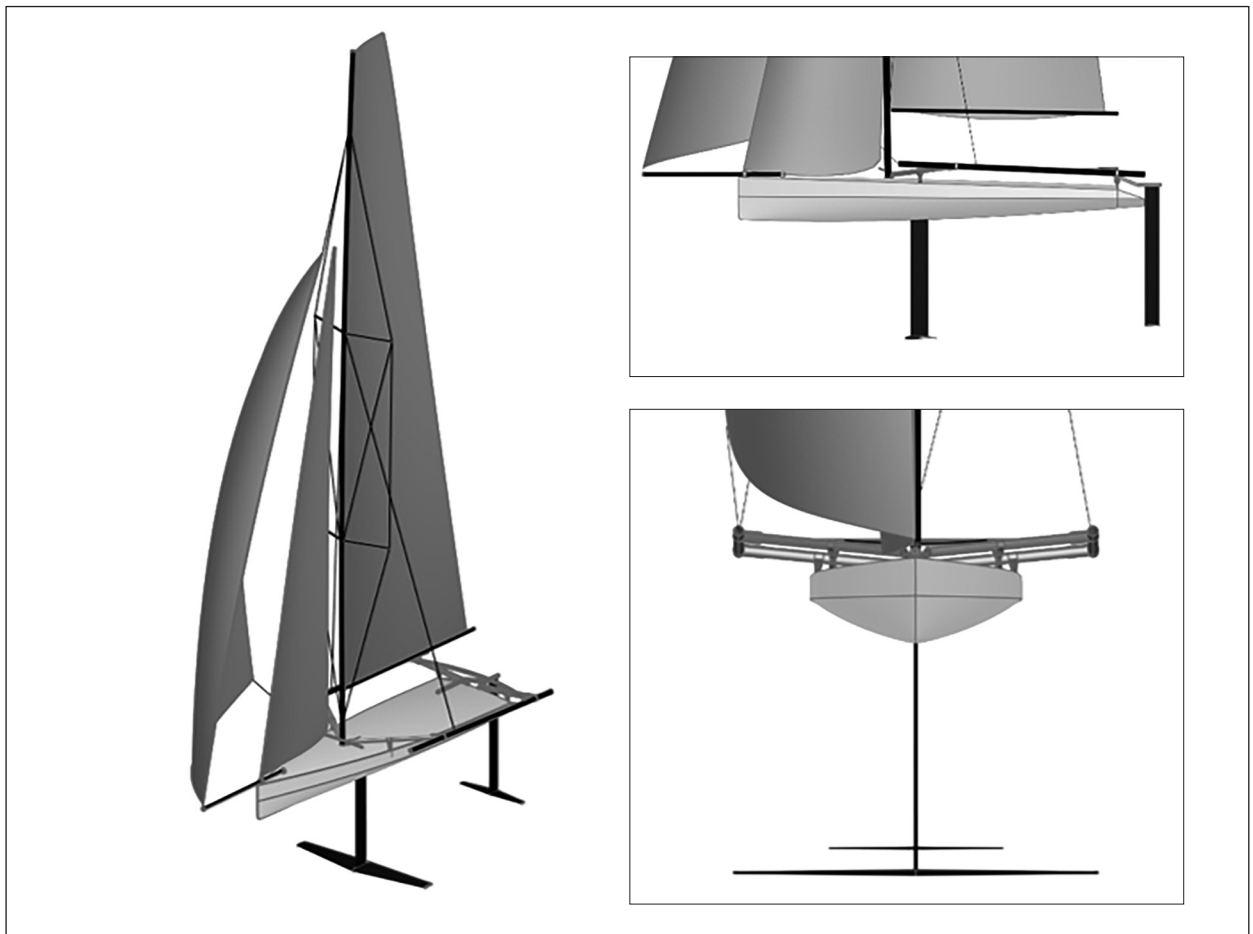
**Table 7.3** NACA 0012: lift and drag coefficients from XFOIL at varying angles of attack and Reynolds number

a. Lift coefficient									
alfa\Re	0	4,00E+05	8,00E+05	1,20E+06	1,60E+06	2,00E+06	2,40E+06	2,80E+06	3,20E+06
0	0,0000	0,0000	0,0000	0,0000	0,0000	0,0000	0,0000	0,0000	0,0000
1	0,0000	0,1028	0,1061	0,1085	0,1099	0,1108	0,1113	0,1117	0,1120
2	0,0000	0,2137	0,2116	0,2163	0,2191	0,2209	0,2220	0,2228	0,2234
3	0,0000	0,3545	0,3168	0,3227	0,3270	0,3296	0,3315	0,3328	0,3339
4	0,0000	0,5085	0,4341	0,4273	0,4325	0,4365	0,4394	0,4416	0,4432
5	0,0000	0,6322	0,5737	0,5439	0,5380	0,5410	0,5452	0,5486	0,5512
6	0,0000	0,7158	0,7146	0,6794	0,6614	0,6529	0,6512	0,6536	0,6569
7	0,0000	0,7962	0,8193	0,8156	0,7952	0,7827	0,7740	0,7683	0,7664
8	0,0000	0,8753	0,9021	0,9163	0,9263	0,9137	0,9041	0,8973	0,8919
9	0,0000	0,9534	0,9852	1,0005	1,0103	1,0179	1,0241	1,0249	1,0189
10	0,0000	1,0302	1,0695	1,0866	1,0970	1,1043	1,1101	1,1148	1,1188
b. Drag coefficient									
alfa\Re	0	4,00E+05	8,00E+05	1,20E+06	1,60E+06	2,00E+06	2,40E+06	2,80E+06	3,20E+06
0	0,00000	0,00668	0,00557	0,00532	0,00523	0,00517	0,00515	0,00513	0,00512
1	0,00000	0,00693	0,00569	0,00540	0,00529	0,00524	0,00521	0,00520	0,00519
2	0,00000	0,00762	0,00607	0,00568	0,00553	0,00546	0,00542	0,00540	0,00539
3	0,00000	0,00859	0,00675	0,00621	0,00598	0,00586	0,00580	0,00575	0,00572
4	0,00000	0,00971	0,00775	0,00702	0,00668	0,00649	0,00636	0,00627	0,00621
5	0,00000	0,01096	0,00905	0,00810	0,00759	0,00729	0,00707	0,00692	0,00679
6	0,00000	0,01240	0,01042	0,00931	0,00863	0,00818	0,00787	0,00764	0,00747
7	0,00000	0,01407	0,01163	0,01049	0,00972	0,00918	0,00878	0,00847	0,00823
8	0,00000	0,01598	0,01290	0,01160	0,01084	0,01024	0,00979	0,00943	0,00914
9	0,00000	0,01825	0,01443	0,01283	0,01192	0,01130	0,01085	0,01048	0,01016
10	0,00000	0,02098	0,01621	0,01428	0,01317	0,01245	0,01192	0,01151	0,01120

## ■ EXAMPLE – A FOILING SKIFF

Having presented the general guidelines for the design of foiling craft appendages, we will now be more specific. Formulae for computing forces and moments will be introduced and applied to an example, the 4.6 m foiling skiff *Linnea*. This skiff was designed by students at Chalmers University of Technology for participation in the 1001VELAcup (see [www.1001velacup.eu](http://www.1001velacup.eu)), a regatta for students from European universities. The boats are designed to a box rule called R3, with considerable freedom in most dimensions. Restrictions are applied to the length, beam, and sail area. Strict rules are applied to building materials, which, to a large extent, must be environmentally friendly. Thus, the hull is built in sandwich with skins of flax/bio epoxy. It is considerably heavier than a corresponding hull built in carbon fibre. For the appendages carbon fibre is allowed, however. *Linnea* was designed for the very light winds in Palermo in late September and has a very large sail area. The optimization was done for take-off at minimum wind speed, and all computations below are for the upright condition in light air.

CAD renderings of the foiling *Linnea* are shown in Fig 7.16. Both the main and rudder foils are T-foils. This is from the initial design stage and will be used to explain the basic principles. The more advanced final design with twin centreboards (pi-foil) will be presented at the end of the chapter. The main particulars of the dinghy are given in Table 7.4 and the dimensions of the appendages in Table 7.5 (page 166). Note the acronyms for the four appendages!



**Table 7.4** Main particulars – *Linnea*

Length [m]		Beam [m]		Draft [m]		Weight [kg]		Sail area [m <sup>2</sup> ]		
Total	Hull	Total	Hull	Design	Foiling	Boat	Crew	Main	Jib	Gen
5.7	4.6	2.1	1.22	1.5	0.75	175	140	16	6	11

**Table 7.5** Appendages – *Linnea*

	Centreboard, CB	Centre foil, CF	Rudder, RB	Rudder foil, RF
Span [m]	1.32 from hull	2.1	1.35 fr. D <sub>WL</sub>	1.0
Tip chord [m]	0.2	0.163	0.16	0.078
Root chord [m]	0.2	0.362	0.16	0.172
Mean chord [m]	0.2	0.263	0.16	0.125
Aspect ratio	6.6	8.0	8.4	8.0
Area [m <sup>2</sup> ]	0.264 from hull	0.551	0.216 fr. D <sub>WL</sub>	0.125
Section	NACA 0012	Wortmann	NACA 0012	Wortmann
Ang. of att. [deg]	–	0.0	–	0.0

**Fig 7.16** (LEFT) The foiling skiff *Linnea*

All computations for *Linnea* presented in this chapter were carried out by Nimal Sudhan Saravana Prabakar, whose contribution is gratefully acknowledged.

We will now give a motivation for the choices of area, span, and taper ratio for the four appendages, based on the general discussion above.

For the crew to manage a recovery from a capsize the draft of the centreboard (CB) must be at least 1.5 m. Since there is no reason to make it deeper this draft was selected. Note that this is the draft at zero speed. Once the hull starts moving, the foils will lift the hull gradually, as speed increases. At 4.1 m/s it will be completely lifted out of the water. The height then increases to about 0.4 m (between the hull and the water surface) at 6 m/s, thereafter remaining at this height.

The planform of the centreboard is rectangular. Since early take-off is prioritized, the possible gain at high speed with a tapered section was neglected. With the span given, the chord was optimized using the VPP of [Chapter 17](#). The earliest take-off in upwind sailing was achieved for a chord length of 0.17 m and a NACA 0010 section. However, preliminary strength estimations (sandwich with 3 mm carbon skins) indicated that the section modulus at the root would be too small with the crew at the tip in a capsize, so the section was changed to NACA 0012 and the chord was set to 0.2 m. For a definition of section modulus, and the computation of the maximum bending stress, see [Chapter 15](#).

The centre foil (CF) span was restricted to the maximum beam, 2.1 m (this restriction in the rule was later removed). With this span and a taper ratio of 0.45 the only remaining planform parameter is the mean chord. As explained above, the area of the foil is a trade-off between high-speed and low-speed performance. Using the VPP the mean chord length of the centre foil was obtained as 0.263 m for minimum take-off windspeed upwind. As the Wortmann FX 60-100 section has the largest lift/drag ratio of the two sections above it was selected for the centre foil.

Like the centreboard, the rudder (RB: rudder board) planform is rectangular. The draft is slightly smaller than that of the centreboard. As mentioned above, determining the area is not an easy task, since it is determined by strength requirements, and it is hard to estimate the loading. The pragmatic solution is to go by experience. In this case we have scaled the section modulus from a typical Moth rudder with the ratio of the mass moments of inertia around a vertical axis at the centre of gravity (see [Fig 5.24](#) for a definition of mass moment of inertia) between *Linnea* and the Moth. This ratio is around four and is achieved by a chord ratio of the third root of four, approximately 1.6. This gives a chord length of 0.16 m. The reason for scaling with the mass moment of inertia is that the moment required to accelerate the boat in yaw is proportional to this quantity.

The rudder foil (RF) area was determined considering the highest loading. To minimize induced drag, a large aspect ratio of 8 was selected, as well as the optimum taper of 0.45. Again, the Wortmann FX 60-100 section was selected. It should be stressed that this is not necessarily the best choice for rudder foils in general. Many designs have much smaller loading on the rudder foil, which means that a symmetric section could be preferable. The load may even be negative, which calls for an upside-down asymmetric section.

The performance of *Linnea* at varying true wind speeds and directions is presented as a polar plot in [Chapter 17](#) ([Fig 17.4](#)) in connection with the introduction to VPPs.

## ■ COMPUTED FORCES

Formulae for computing lift and all resistance components will be given in this section. As an example, the computations will be carried out for a speed of 5 m/s, close to the minimum in resistance after take-off. The conditions are specified in [Table 7.6](#). Note that the ride height is defined as the distance between deepest point on the hull bottom and the water surface.

Table 7.6 Data for the example calculations	
VTW [m/s]	3
BTW [m/s]	60
VAW [m/s]	7.0
BAW [m/s]	22
V [m/s]	5.0
Ride height* [m]	0.27
Submerged span (= foil draft) [m]	CB: 1.05, RB: 0.90
Submerged area [m <sup>2</sup> ]	CB: 0.210, RB: 0.144
Submerged geometric AR	CB: 5.25, RB: 5.63
Heel [degrees]	0.0
Trim [degrees]	−0.068
Leeway [degrees]	2.0
CF AOA [degrees]	−0.068
Flap angle [degrees]	−0.47
RF AOA [degrees]	−0.068
Density [kg/m <sup>3</sup> ]	1025
Viscosity [m <sup>2</sup> /s]	$1.0 \times 10^{-6}$

\*Distance between hull bottom and water surface

### ◆ Lift computation

The computation of the total lift, 3041 N (corresponding to a total weight of 310 kg) is presented in [Fig 7.17](#) as the sum of the centre foil and rudder foil lifts. Note that, in the computation of the latter, the effective angle of attack,  $a_{\text{eff}}$  is used. As explained above, this differs from the geometrical angle of attack  $a_{\text{geom}}$  (related to the horizontal direction) by the downwash angle,  $a_{\text{down}}$ , and the wave generated angle,  $a_{\text{wave}}$ , which is positive for a positive wave slope.

[Fig 7.17](#) shows that the main contribution to the lift, 2428 N, comes from the centre foil, while 613 N comes from the rudder foil. This is at 5 m/s. As mentioned above, this distribution will change with speed after take-off at 4.1 m/s (see [Fig 7.18](#)). Since the shape of the rudder foil is constant, the lift will increase as speed squared if the boat is kept on even keel (i.e. the angle of attack is unchanged). Then, to keep the total lift constant, the centre foil lift will have to be reduced by decreasing the flap angle, and this means that the rudder foil will carry an increasing portion of the lift with increasing speed. The redistribution of the load with speed is shown in [Fig 7.18](#). This figure also shows how the crew has to move

**Fig 7.17** Lift computation  
at 5 m/s of boat speed

$$L = 0.5 \cdot C_L \cdot \rho \cdot V^2 \cdot A$$

$$C_L = C_L^{2D} / (1 + 2/AR)$$

*L: Lift (Fig 6.5) [ $L_{CF}$ : 2428 N;  $L_{RF}$ : 613 N]*  
 *$C_L^{2D}$ : Table 7.2 [ $CF: \alpha = 0^\circ$ ;  $\alpha_F = -0.54^\circ$ ;  $Rn = 1.3 \cdot 10^6$ ;  $C_L^{2D} = 0.47$ ]*  
*[ $RF: \alpha_{eff} = \alpha_{geom} - \alpha_{down} + \alpha_{wave} = 0^\circ$ ;  $Rn = 6.25 \cdot 10^5$ ;  $C_L^{2D} = 0.51$ ]*  
*Free surface correction factor (Fig 7.11) [ $CF: 0.91$ ;  $RF: 0.94$ ]*  
 *$C_L^{2D}$ : Corrected for free surface effects*  
*[ $CF: C_L^{2D} = 0.43$ ;  $RF: C_L^{2D} = 0.48$ ]*  
 *$C_L$ : 3-D lift coefficient [ $CF: 0.34$ ;  $RF: 0.38$ ]*

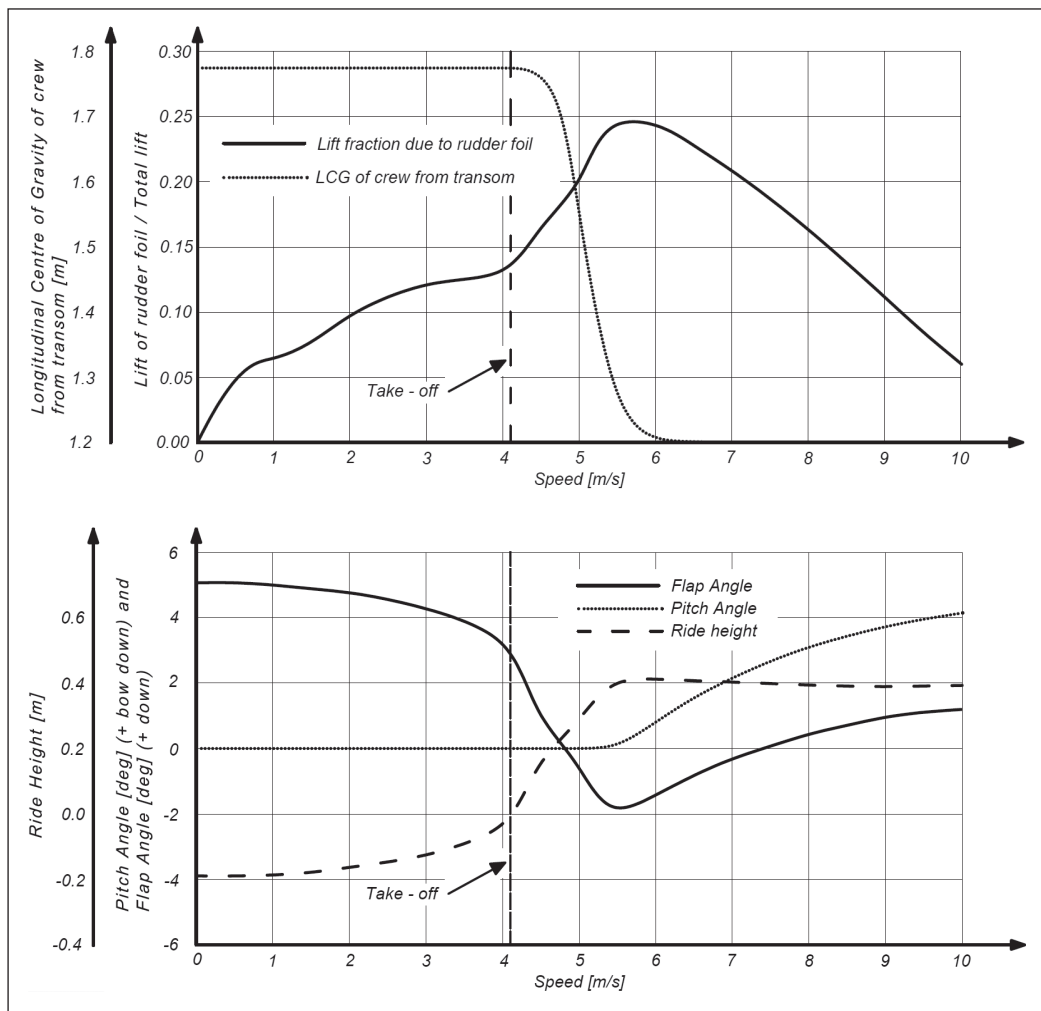
$$\text{Total lift: } L_{TOT} = L_{CF} + L_{RF} \quad [3041 \text{ N}]$$

*This corresponds to a total weight of 310 kg*

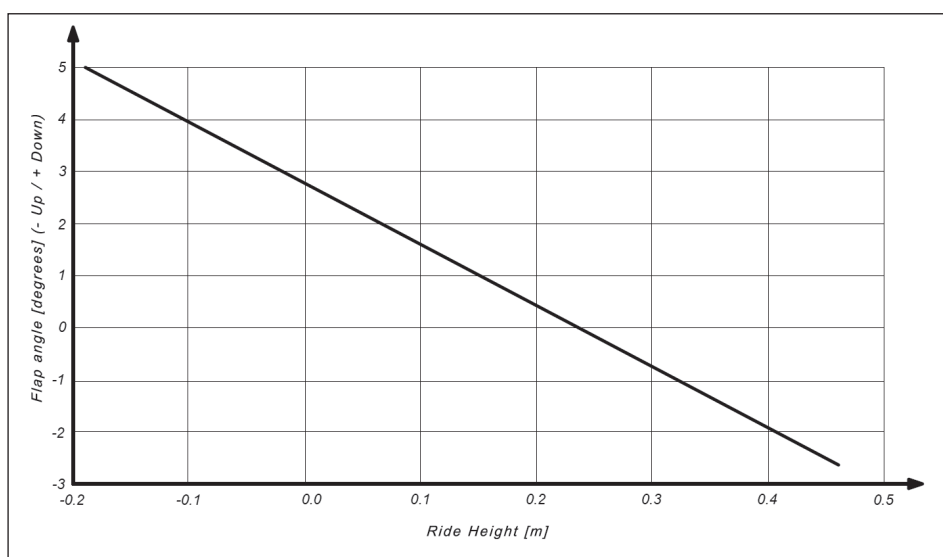
backwards to keep the boat on even keel. But they cannot move further than 1.2 m from the transom due to a constraint to be described below. This happens at 6 m/s of boat speed. So, at higher speeds the rudder lift cannot increase. In fact, its load drops off with speed due to the increased bow-down moment generated by the sail force. Thus, if the objective had been to keep the boat at even keel, the increased pitch moment by the sails could have been exploited to move the crew further back. However, there is no guarantee that the even keel attitude is the best. Before take-off a bow-up trim may be preferable to increase the lift, and at high speed a bow-down trim may be better since a high load on the rudder foil most likely increases the total induced drag. The optimum crew position at all speeds may be obtained from the VPP, but that was never done in this project.

Fig 7.18 (overleaf) also shows the ride height, which starts at  $-0.18$  m, the hull draft at zero speed. At 4.1 m/s the draft is zero (i.e. the hull is taking off). The final height, about 0.4 m, is achieved at 5.5 m/s. As expected, the flap angle is reduced progressively until the rudder lift attains its maximum value at 5.5 m/s. The pitch angle (trim) is zero as long as the crew can move backwards. After that the trim goes bow down, which reduces the lift on the rudder foil. The angle of attack decreases also on the centre foil, but the bow-down trim causes the wand to indicate a smaller ride height (since it is positioned on the bow sprit), and thereby the flap angle is increased. This, in turn, increases the centre foil lift.

The flap angle determined by the ride height according to the transfer function displayed in Fig 7.19 (overleaf). It is a linear relationship accomplished by a suitable shape of the flap cam. The line is determined by the flap angle at zero speed, where the hull is floating on the design waterline, and the slope of the line: the gain coefficient. A large flap angle at zero speed will increase the lift coefficient at non-foiling speeds, so the hull will take-off at a lower *boat* speed, but the resistance will increase for large flap angles, so when it comes to finding the lowest *wind* speed for take-off there is an optimum, which can be determined using a VPP. For *Linnea*, this optimum is  $2^\circ$  of flap angle, associated with a gain coefficient of  $-11.7$ . This is in combination with the optimum foil area presented above. It is the combination that needs to be optimized. Unfortunately, the optimum angle would result in a maximum ride height of only a few centimetres, so the angle was increased from  $2$  to  $5^\circ$ , which causes a small increase in take-off wind speed.



**Fig 7.18** Rudder foil load and crew position (TOP) and ride height, pitch angle and flap angle (BOTTOM) versus speed



**Fig 7.19** The flap angle/ride height relation

### ◆ Resistance computation

The profile drag is the sum of the friction and pressure drag of the 2D section and can be computed as described in Fig 7.20 for all four appendages. The input comes from Table 7.2 for the Wortmann sections of the foils, and from Table 7.3 for the NACA sections of the centreboard and rudder.

In Fig 7.21 the computation of the induced drag is presented. It is straightforward for the two foils, which are sufficiently submerged. Formulae from Fig 6.5 can be applied directly. However, it is very difficult to predict the induced drag of surface piercing foils, so the computation is very approximate for the centreboard and rudder. As mentioned above, the vortical energy normally found behind a wingtip is partly transferred into wave energy at the surface, but it is hard to say how much the free surface damps that energy transfer. At the tip, both have foils attached, so there is very little overflow at that end. A reasonable assumption (see e.g. Findlay and Turnock, 2009) is to assume a doubling of the geometric aspect ratio (of the submerged part) for the centreboard and rudder. This corresponds to the case with one end of a wing attached perpendicularly to an infinitely large flat plate, as explained in Chapter 6. The foil at the tip does not prevent the overflow that efficiently, but on the other hand, there may be some effect also of the free water surface. The doubling of the geometric aspect ratio is accounted for through the coefficient  $k_i$ , which is 2 for the centreboard and rudder, but 1 for the two foils.

**Fig 7.20** Profile drag at 5 m/s of boat speed

$$D_P = 0.5 \cdot C_D^{2D} \cdot \rho \cdot V^2 \cdot A$$

$D_P$  : Profile drag

[CB: 15.4 N; CF: 36.8 N; RB: 10.9 N; RF: 10.6 N]

$C_D^{2D}$  : Profile drag coefficient

[CB: Table 7.3;  $\alpha = 2^\circ$ ;  $Rn = 1 \cdot 10^6$ ;  $C_D^{2D} = 0.0058$ ]

[CF: Table 7.2;  $\alpha = 0^\circ$ ;  $\alpha_F = -0.54^\circ$ ;  $Rn = 1.3 \cdot 10^6$ ;  $C_D^{2D} = 0.0052$ ]

[RB: Table 7.3;  $\alpha = 2^\circ$ ;  $Rn = 8 \cdot 10^5$ ;  $C_D^{2D} = 0.0061$ ]

[RF: Table 7.2;  $\alpha = 0^\circ$ ;  $Rn = 6.25 \cdot 10^5$ ;  $C_D^{2D} = 0.0066$ ]

**Fig 7.21** Induced drag at 5 m/s of boat speed

$$D_i = 0.5 \cdot C_{Di} \cdot \rho \cdot V^2 \cdot A$$

$$C_{Di} = C_L^2 / (\pi \cdot K_i \cdot AR)$$

$D_i$  : Induced drag

[CB: 2.6 N; CF: 33.2 N; RB: 1.7 N; RF: 9.3 N]

$C_{Di}$  : Induced drag coefficient

[CB: 0.0010; CF: 0.0047; RB: 0.0009; RF: 0.0058]

$C_L$  : 3-D lift coefficient

[CB: 0.18; CF: 0.34; RB: 0.18; RF: 0.38]

CB and RB from table 7.3, with correction to 3D  
CF and RF from Fig 7.17

$K_i$  : Efficiency factor for Aspect ratio

[CB and RB: 2; CF and RF: 1]



$$D_{ws} = 0.5 \cdot C_{Dws} \cdot \rho \cdot V^2 \cdot t^2$$

$$C_{Dws} = C_{Dws, wave} + C_{Dws, spray}$$

$D_{ws}$  : Wave and spray drag [CB: 4.0 N; RB: 2.6 N]

$C_{Dws}$  : Wave drag coefficient = 0.54

$C_{Dws, wave}$  : Wave part of  $C_{Dws}$  = 0.30

$C_{Dws, spray}$  : Spray part of  $C_{Dws}$  = 0.24

$t$  : Foil thickness [CB: 0.024 m; RB: 0.019 m]

**Fig 7.22** Wave and spray drag of the centreboard and rudder at 5 m/s of boat speed

Since the centreboard and rudder cut through the free surface there will be waves and spray generated. The computation of the corresponding drag components is presented in Fig 7.22, based on empirical relations proposed by Hoerner (1965).

The waves generated by the two submerged foils contain energy, and the associated drag components are computed in Fig 7.23, based on measurements by Beaver and Zselezsky (2009).

$$D_w = 0.5 \cdot C_{Dw} \cdot \rho \cdot V^2 \cdot A$$

$$C_{Dw} = 0.025 \cdot C_L^2 \cdot c/h$$

$D_w$  : Wave drag [CF: 5.3 N; RF: 0.8 N]

$C_{Dw}$  : Wave drag coefficient [CF: 0.00075; RF: 0.00052]

$C_L$  : Lift coefficient [CF: 0.34; RF: 0.38]

$h$  : Foil submergence [CF: 1.03 m; RF: 0.88 m]

**Fig 7.23** Wave drag from the two foils at 5 m/s of boat speed

As mentioned above, the wand drag is very small. It is estimated to about 2 N for *Linnea* and is therefore neglected. So, the only hydrodynamic drag component left is the junction drag presented in Fig 7.24.

$$D_j = 0.5 \cdot C_{Dj} \cdot \rho \cdot V^2 \cdot t_m^2$$

$$C_{Dj} = 17(t_m/c)^2 - 0.05$$

$D_j$  : Junction drag  
[CF/CB: 0.78 N; RF/RB: 0.59 N]

$C_{Dj}$  : Junction drag coefficient  
[CF/CB: 0.068; RF/RB: 0.14]

$t_m$  : Mean thickness of joined sections  
[CF/CB: 0.03 m; RF/RB: 0.018 m]

**Fig 7.24** Junction drag at 5 m/s of boat speed

The aerodynamic drag, or windage, is significant also at 5 m/s but it becomes even more important at higher speeds. It is computed as explained in Fig 7.25, based on the aerodynamic model proposed by Hazen (1980) (see Chapter 8). Contributions are added from the hull and crew. The windage from the mast and rigging is included in the sail model. Note that this drag is in the direction of the apparent wind, not the direction of

**Fig 7.25** Aerodynamic drag at 5 m/s of boat speed

$$D_A = 0.5 \cdot C_{DA} \cdot \rho_A \cdot V_{AW}^2 \cdot A_F$$

$D_A$  : Aerodynamic drag parallel to apparent wind [58.4 N]  
 $C_{DA}$  : Aerodynamic drag coefficient [1.13]  
 $\rho_A$  : Density of air [1.23 kg/m<sup>3</sup>]  
 $V_{AW}$  : Apparent wind speed [7.0 m/s]  
 $A_F$  : Frontal area of hull, mast, rig and crew [1.72 m<sup>2</sup>]

$$D_{AM} = D_A \cdot \cos \beta_{AW}$$

$D_{AM}$  : Aerodynamic drag in direction of motion [54.3 N]  
 $\beta_{AW}$  : Apparent wind direction [22°]

motion. Therefore, the easiest way to include this drag is to add it to the sail model in the VPP. The component in the direction of motion is also computed in Fig 7.25.

All results so far have been computed for the speed of 5 m/s, when the hull is completely foil-borne. The forces are thus generated by the appendages alone. However, the hull contributes to the lift at all speeds before take-off. The resistance for this partly lifted hull may be computed as seen in Fig 7.26. As an example, a speed of 4 m/s is selected.

**Fig 7.26** Resistance of partly lifted hull (boat speed 4 m/s)

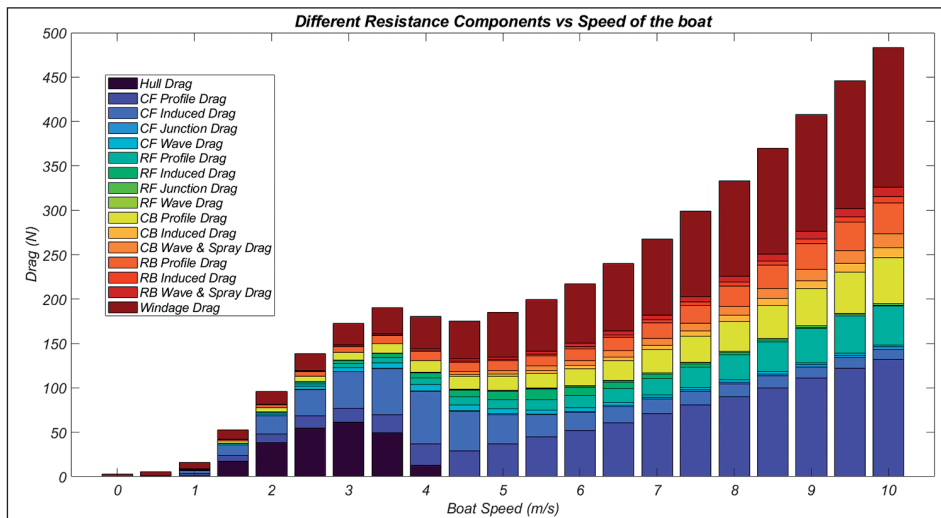
$$R_{pl} = S_{wpl} / S_w \cdot R_F + m_{pl} / m \cdot R_R$$

$$m_{pl} = B / g$$

$R_{pl}$  : Resistance of partly lifted hull [12.5 N]  
 $S_{wpl}$  : Wetted surface area of partly lifted hull [0.44 m<sup>2</sup>]  
 $S_w$  : Wetted surface below DWL [3.96 m<sup>2</sup>]  
 $R_F$  : Frictional resistance without foils [89.5 N]  
 $m_{pl}$  : Mass displacement of partly lifted hull [5.99 kg]  
 $m$  : Mass displacement below DWL [310 kg]  
 $R_R$  : Residuary resistance without foils [136 N]  
 $B$  : Buoyancy of partly lifted hull [58.8 N]  
 $g$  : 9.81 m/s<sup>2</sup>

Hull resistance was discussed in detail in Chapter 5. To obtain the resistance of a partly lifted hull, one way would be to derive the input parameters needed for the residuary resistance  $R_R$  of Fig 5.18 (LCB,  $C_p$ , etc.) and the frictional resistance  $R_F$  of Fig 5.8 for the partly lifted hull and add these two components. The problem with this approach is that the submerged hull shape will be rather distorted, particularly just before take-off, so the empirical relations for the residuary resistance might not be very accurate. Other possibilities are, of course, to make use of CFD or experiments, where the exact underwater shape of the partly lifted hull may be used. But without access to these more advanced tools, there is an approximate way, which may be more accurate than the direct application of the empirical relations to the partly lifted hull.

As appears from Fig 5.8, the frictional resistance is proportional to the wetted surface, while the residuary resistance, as seen in Fig 5.20, is essentially proportional to the displacement. Therefore, the resistance in the non-foiling state could be scaled to the partly lifted state by scaling the two components differently: the frictional resistance



**Fig 7.27** Drag components versus speed

in proportion to the wetted surface, and the residuary resistance in proportion to the displacement. This is the approach presented in Fig 7.26.

The distribution of drag components is shown in the bar chart of Fig 7.27 at different speeds. It is seen that the hull drag increases up until 3 m/s, but is then gradually reduced to zero at 4.5 m/s when the boat is foiling. The second-largest component around take-off is the induced drag of the centre foil, which is highly loaded (i.e. has a large lift coefficient). The load is however reduced with speed, and the induced drag becomes insignificant at the highest speeds. There, the dominating component is the profile drag of the centre foil, which steadily increases over the entire speed range. Similar tendencies are seen for the rudder foil, although with smaller contributions. The profile drag increases also significantly with speed for the centreboard and rudder, so the total profile drag dominates for speeds from 6 m/s upwards. The second-largest drag type is the windage, which contributes almost one-third of the total drag at 10 m/s. Note that these results are computed from a 'towing test' of the dinghy upright, at 2° of leeway. This is the only way to show a systematic trend like this. In real sailing, the same speed may be obtained in many different ways, depending on the course. So, the drag is not a unique function of the speed.

#### ◆ Pitch stability condition

Before finalizing the two foil designs a check of the pitch stability should be carried out. As mentioned above, a necessary condition for static stability is that there is restoring moment when the hull is exposed to a pitch disturbance. This is achieved if the relative change of the rudder foil lift is larger than that of the main foil. In Fig 7.28 this condition is checked for the 5 m/s case discussed above.

Assume that the hull is exposed to a force that will suddenly increase the pitch angle by 1° (bow up). The rotation is assumed to be around the centre of gravity. The increase in height measured by the wand may then be computed, and this may be transferred to a reduction in flap angle. From Table 7.2 the sensitivity of the lift on the flap angle for the Wortmann FX 60-100 section can be obtained, as can the sensitivity to angle of attack. The total change of the 2D lift coefficient for the centre foil may thus be computed and

transferred to a change in the 3D coefficient. Dividing by the original lift coefficient, the relative change is obtained for the centre foil. On the rudder foil, there is no flap, so it is only the angle of attack change that will influence the lift. The relative change in the 3D lift coefficient for the rudder may then be obtained, and this can be compared with that of the centre foil. In this example, it is larger, so the condition is satisfied.

The stability condition can be checked for all speeds, where the loading of the foils varies according to Fig 7.18. It turns out that above 6 m/s of boat speed the aft foil is so loaded that the relative change of its lift for a pitch disturbance is smaller than that of the main foil. The condition is then violated. That is why the crew cannot move further back than 1.2 m from the transom. Above that speed the hull then starts pitching bow down, but it can still sail. To avoid the bow-down trim the rudder rake can be set to reduce the rudder foil angle of attack, but then the boat will take-off at a higher wind speed. So, the rudder rake should be adjusted depending on the expected speed range in a race. Of course, it is an advantage to have a rake adjustable while sailing.

Unfortunately, as stressed above, a restoring moment is a necessary, but insufficient condition for static stability. To investigate whether the boat is statically stable two possible methods were mentioned. The first one relies on a DVPP, where the governing equations are solved as a function of time (for an introduction, see Chapter 17). A DVPP was developed by Prabakar *et al* (2021). Some results for *Linnea* are presented in Fig 7.29 (overleaf).

The graphs show the effect of a wind gust on several parameters. The true wind speed starts to increase from 3.5 m/s at 5 seconds. At 7 seconds it has reached 4.5 m/s and stays constant until 15 seconds, where it drops to the original speed in two seconds. The top

**Fig 7.28** Check of pitch stability (boat speed 5 m/s)

#### Pitch stability control

*Bow-up 1°, rotation around centre of gravity (CG)*

##### Centre foil

*Distance from CG to wand : 3m*

*Height increase of wand paddle :  $3 \cdot \sin 1^\circ = 0.052 \text{ m}$*

*Gain factor :  $-11.7^\circ/\text{m}$*

*Flap angle decrease :  $11.7 \cdot 0.052 = 0.61^\circ$*

*From Table 7.2 : Change in  $C_L$  per degree of flap change = 0.075*

*Change in  $C_L^{2D}$  due to flap =  $-0.61 \cdot 0.075 = -0.046$*

*From Table 7.2 :  $C_L^{2D}$  change per degree of  $\alpha = 0.112$*

*Total change in  $C_L^{2D} = 0.112 - 0.046 = 0.066$*

*Aspect ratio = 8*

*$C_L^{3D}$  change:  $0.066/1.25 = 0.053$*

*From Fig 7.17 Original  $C_L$  at 5 m/s = 0.34*

*% change in  $C_L$  :  $100 \cdot 0.053/0.34 = 15.6\%$*

##### Rudder foil

*From Table 7.2  $C_L^{2D}$  change per degree of  $\alpha = 0.112$*

*Aspect ratio = 8*

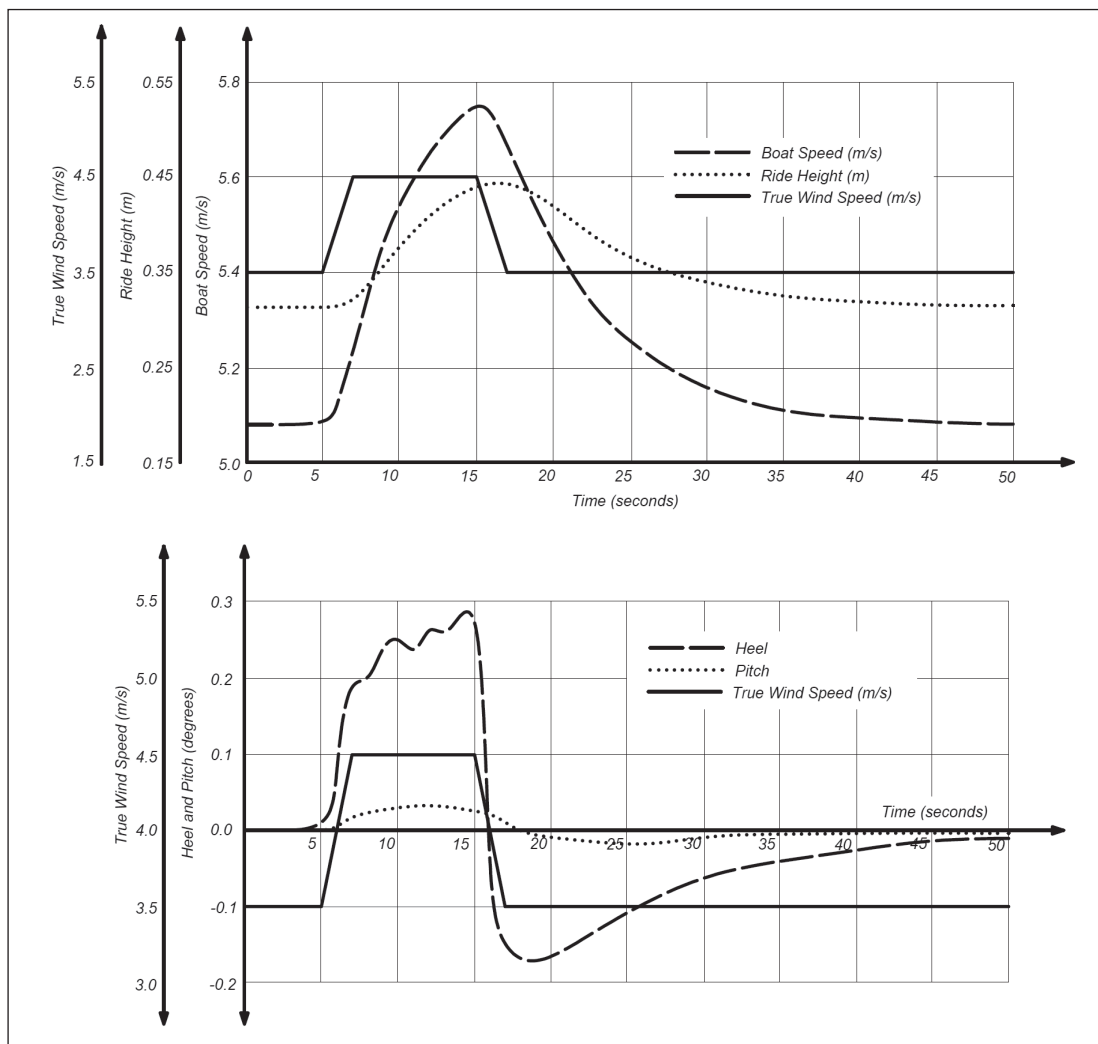
*$C_L^{3D}$  change :  $0.112/1.25 = 0.090$*

*From Fig 7.17 Original  $C_L$  at 5 m/s = 0.38*

*% change in  $C_L$  :  $100 \cdot 0.09/0.38 = 23.7\%$*

#### Conclusion

*Relative change of lift larger for rudder foil than centre foil  
=> pitch stability condition satisfied!*



**Fig 7.29** DVPP results for *Linnea* exposed to a gust

panel shows the effect on the heel and pitch angles. Both start to increase when the wind increases and reach their maximum when the wind speed starts to drop. Then they return smoothly to their original value, which is zero.

The bottom panel shows the effect of the gust on the ride height and the boat speed. As expected, the speed increases during the gust, but it returns smoothly to the original speed (5.1 m/s) after 50 seconds. The speed increase causes an increase in ride height, but this also returns to the original value (0.3 m) at the end of the simulation.

The most important feature of the two diagrams is the return to the original, equilibrium values for all variables. With the exception of the heel, all variations are smooth. For the heel some small oscillations occur during the gust, but they die out rapidly. Since the gust causes a significant disturbance in all degrees of freedom this test shows that the boat is statically (and dynamically) stable. But it should be kept in mind that this is with automatic control of three variables: the position of the crew transversely and longitudinally, and the sail depowering. The target for the controllers is zero heel and

trim. It may be that these controllers are more efficient than a human crew in adjusting these variables. So far, no attempts have been made to adjust the response times of the controllers to that of the crew.

A final check of the pitch stability was done using the simplified (linearized) method. It showed that *Linnea* is indeed statically and dynamically stable in pitch.

## ■ OTHER ASPECTS

In this section, more aspects of foiling will be presented. All may be significant, but require rather complex analysis, so they will only be discussed briefly. References to deeper analyses will be given. The following topics will be addressed:

- Stability increase by split flaps
- Cavitation and ventilation
- Fluid–structure interaction.

A double-handed foiling skiff with a rather extreme sail area will be very difficult to handle. In particular, heel stability will be an issue. To resolve this problem for *Linnea*, the centre foil flap was split into a port and a starboard half. When heeling, the leeward flap is deflected more than the windward one, thus generating a righting moment. To measure both ride height and heel angle two wands are needed, and they are coupled to the two flaps via a control system more complex than that described above. It turns out that with this system in place, and a reduction in centreboard span to 1 m, the foiling *Linnea* is as stable in heel as the non-foiling boat for all speeds. In fact, at high speeds, the heel stability is so high that there is a problem with the rig strength. The split-flap system is presented in Prabakar *et al* (2021).

Since the asymmetric loading of the centre foil will cause a large bending moment on the centreboard, the T-foil configuration was deemed too flexible, so the centreboard was replaced by two daggerboards in a pi-foil configuration. The problem with the small draft when righting the boat was resolved by adding winglets pointing downwards at the tip of the centre foil. These winglets were designed to be strong enough for the two crew members to step on. Standing on the winglets, leaning backwards the lever is sufficient. There is of course also a hydrodynamic advantage of the winglets, which were designed as proposed by Hoerner (1965). The final *Linnea* design is shown in Fig 7.30 (overleaf).

The pressure distribution around an airfoil was discussed in Chapter 6 in connection with Fig 6.2, where the pressure coefficient is defined, and in Fig 6.25, where some examples are given. Low pressures are found on the suction side near the nose, particularly at higher angles of attack, where the pressure minimum has moved forward of its optimum position. This low pressure may give rise to two different phenomena: cavitation and ventilation.

As explained in Chapter 10, Figs 10.16 and 10.17 (pages 220–1), water will start boiling if the pressure drops below the vaporization pressure. At 20° this pressure is 2–3 kPa. If the pressure at any point on a submerged foil reaches this low level, boiling will occur. This boiling is called cavitation. However, the ambient pressure around the foil



**Fig 7.30** *Linnea* – final design (picture by Frowin Winkes)

is the sum of the atmospheric pressure and the hydrostatic pressure at that depth (see Fig 10.16). The former is around 100 kPa, while the latter is an order of magnitude smaller for a submergence of the order of 1 metre. So, the local suction, represented by a negative pressure coefficient, must be quite large for the total pressure to drop to the vaporization level. The risk of cavitation can be computed knowing the minimum pressure coefficient for a foil section. This can be obtained for instance from XFOIL. Normally, the risk of cavitation is quite small, except at very high speeds, above 20 m/s. See Faltinsen (2005) or van Oossanen (2020) for good introductions to the subject.

Ventilation occurs when air is drawn into the fluid by a low pressure. There are three conditions for this to happen: the local pressure must be lower than the atmospheric pressure, the flow must be separated, and there must be a ‘channel’ from the atmosphere to the ventilated region, through which air can be continuously supplied. The most dangerous situation is when the surface piercing strut (centreboard or rudder) stalls and air is sucked down to the attached foil. For sufficiently low-pressure coefficients on the foil it may also ventilate. The result is a significant drop of side force on the strut and, more dangerously, a loss in lift of the foil. Since this may happen very rapidly, it may cause a crash of the foiling boat. Ventilation is a very complex phenomenon and beyond the scope of this book. The interested reader is referred to or Young *et al* (2017) or van Oossanen (2020).

When a foil is under load it will deflect, depending on its structural stiffness. This deflection causes the flow induced forces to change, which will change the deflection, etc. There is thus a two-way coupling between the fluid and the structure, called fluid–structure interaction (FSI). Since dinghy foils are slender, they may deflect significantly, which changes their performance. In advanced foil design this deformation is accounted for in the unloaded geometry, but it will not be further considered in this book. For a good introduction to the subject, see Marimon Giovannetti *et al* (2018).



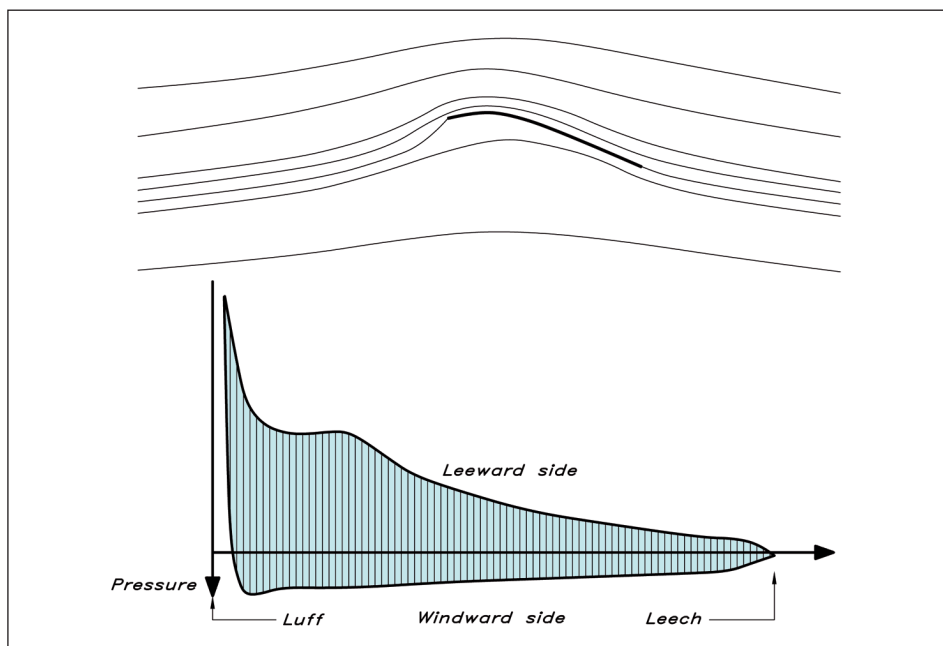
# 8 SAIL AND RIG DESIGN

A sail is a wing, which differs in some important respects from the wings of the previous chapters. Thus, the sail has virtually no thickness, but it has a camber which is quite large. It often works in the disturbed flow from a mast. Nevertheless, most of the principles described above still apply, and we will discuss them in connection with the design of sails and sailplan in this chapter.

## ■ FLOW AROUND SAILS

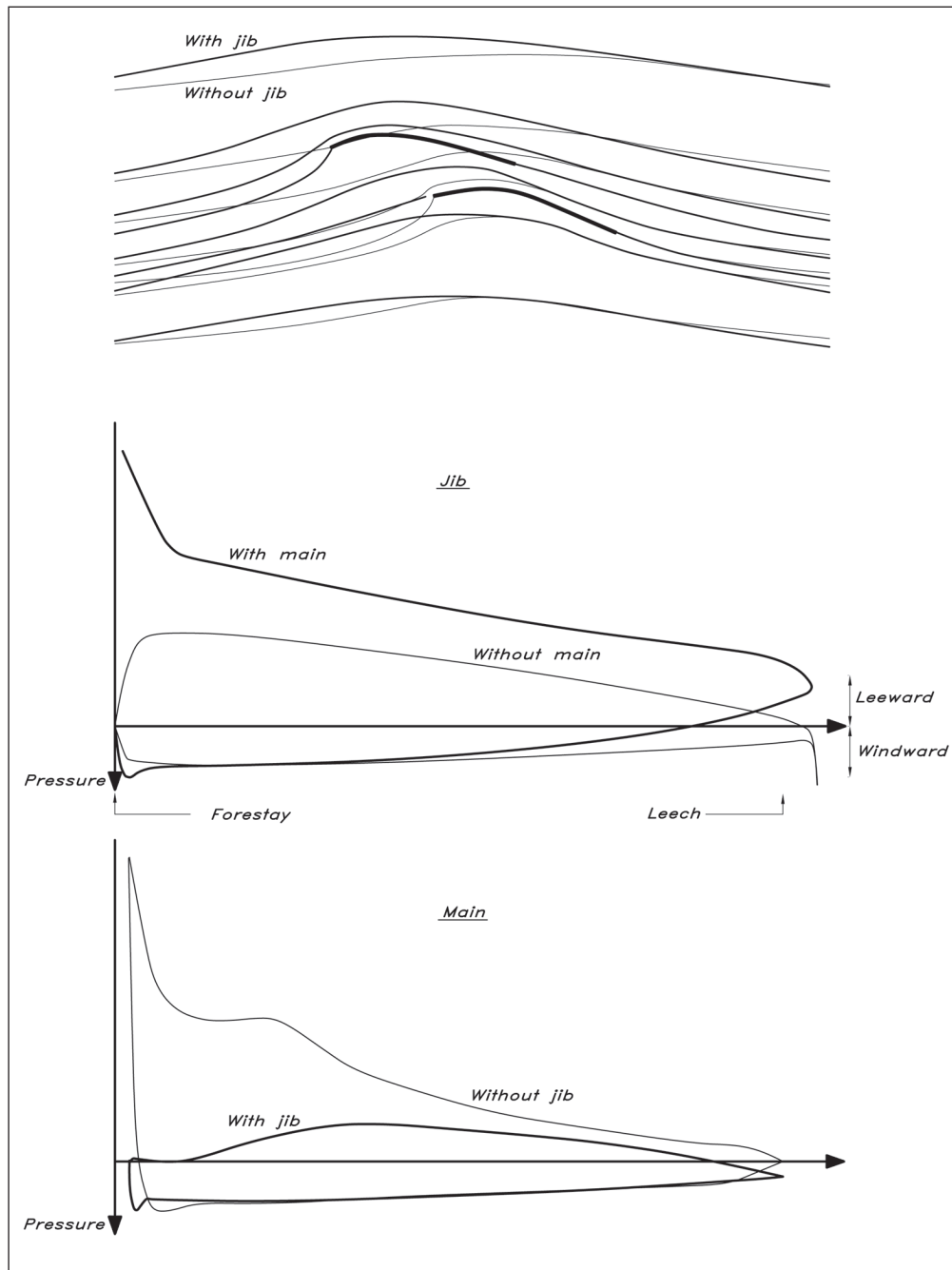
Fig 8.1 shows the flow around a single sail without a mast, together with the pressure distribution on the two sides. It can be seen that the negative pressures (upwards, cf Fig 6.2) on the suction side are much larger than the positive ones on the pressure side. Since it is the difference in pressure between the two sides (i.e. the vertical distance between the two curves) that gives the force, it is obvious that the major contribution to the sail force comes from the suction on the leeward side of the sail.

Fig 8.1 Flow around a sail



The flow around two sails close together is shown schematically in Fig 8.2. Streamlines for the two sails in combination are shown as thick lines, while streamlines for the single mainsail are shown as thin lines.

The latter are in principle the same as in the previous figure. Mast disturbances are neglected. There is a very interesting difference in the upstream flow between the two cases. Approaching the sails, the thick lines bend much further apart than the thin ones.



8.2 Flow around a mainsail/jib combination

This means that the air approaches the mainsail at a smaller angle than in the single sail case, while the opposite is true for the jib. Thus, as compared to the single sail case, the main gets unloaded, while the jib gets more load. This is reflected in the pressure plots in the lower part of the figure. Most of the suction over the forward half of the main has disappeared and the total force, represented by the area between the pressure curves on the two sides, has dropped considerably. On the other hand, the suction on the leeward side of the jib has increased from the leading to the trailing edge and the force is much larger.

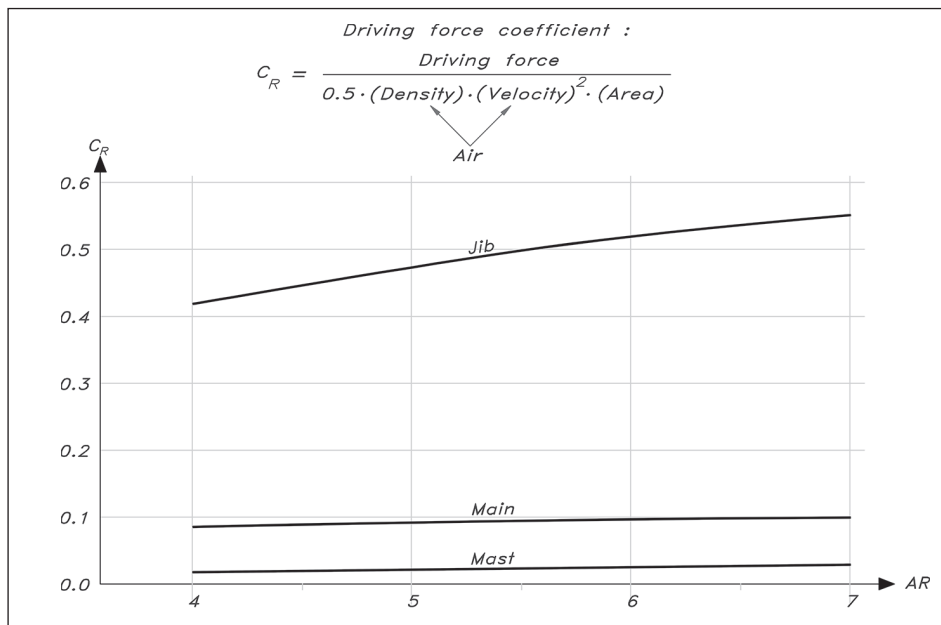
This interpretation of the slot effect was presented by the American aerodynamicist A E Gentry in the 1970s, and it represented a radical departure from the common belief that the suction behind the mainsail is increased by the presence of the jib. This opinion stems from an erroneous interpretation of the so-called Venturi effect. When the flow in a tube passes a restriction, i.e. a reduction in the cross-sectional area, the speed increases and the pressure drops. This is an indisputable fact, but the situation is different between the two sails. Unlike the flow in the tube the air approaching the sails has the freedom to avoid the restriction. Rather than going between the sails some of it may bend sideways and pass outside the jib/mainsail combination, i.e. to leeward of the jib and to windward of the main. As we have already noted, this is exactly what happens. Less air passes near the leeward side of the main if a jib is introduced in front of it.

Gentry's explanation is based on an idealized flow model, potential flow, where viscosity is neglected. (See [Chapter 17](#) for a discussion of different models.) This does not alter the main conclusion, but if viscosity is considered, some further conclusions may be drawn. Thus, the boundary layer on the suction side of the mainsail experiences a much smoother pressure distribution than for the single sail. The flow in the boundary layer does not have to make its way against a rapidly increasing pressure, so the risk of separation is very much reduced. This means that the sail can be sheeted at a larger angle to the main flow, at midship or even, in fact, somewhat to windward.

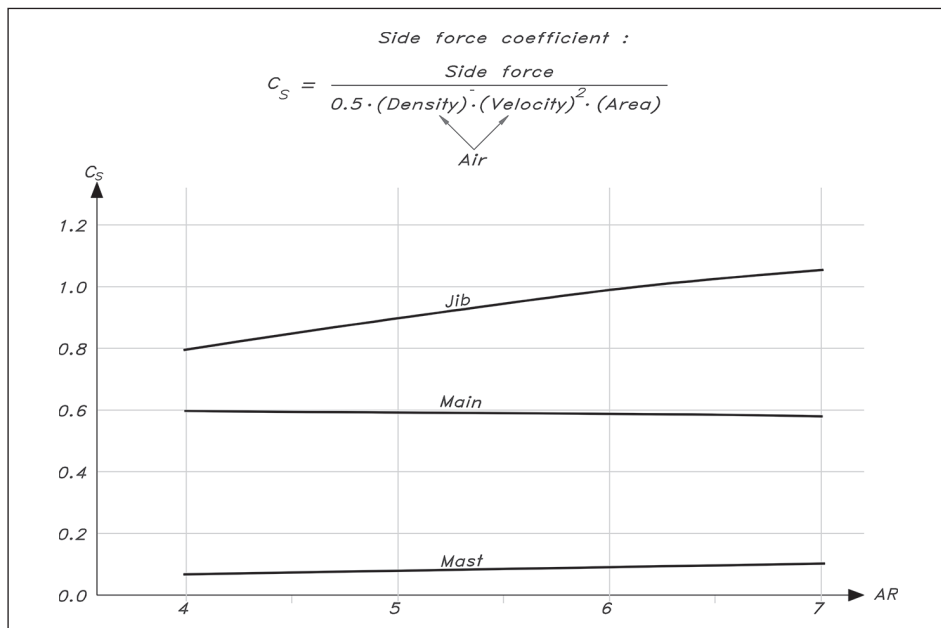
## ■ PLANFORM

At the top of the sail and at the boom the lift force goes to zero and vortices are shed, giving rise to an induced resistance. The larger the height of the sail, the smaller the effect of the vortices. As for the keel, the most important efficiency parameter for the sail is the aspect ratio. We define it here as the luff length divided by half the foot length, so, neglecting the roach, it corresponds to the definition of the previous chapters. It should be mentioned that in some sailing literature the foot length is not divided by two in the definition, so the aspect ratio is half as large.

Very interesting studies of sail physics were made by two Chalmers students, Jacobs and Sahlberg (2018), using computational fluid dynamics. Several systematic variations of a masthead rig in the upright condition were made. The aspect ratio of the whole rig was changed by stretching the sails in the vertical direction. Only upwind conditions were considered, and the computed force was resolved into its driving component  $R$  and side force  $S$ . These forces are given in coefficient form:  $C_R$  and  $C_S$  respectively, in [Figs 8.3 and 8.4](#) (overleaf).

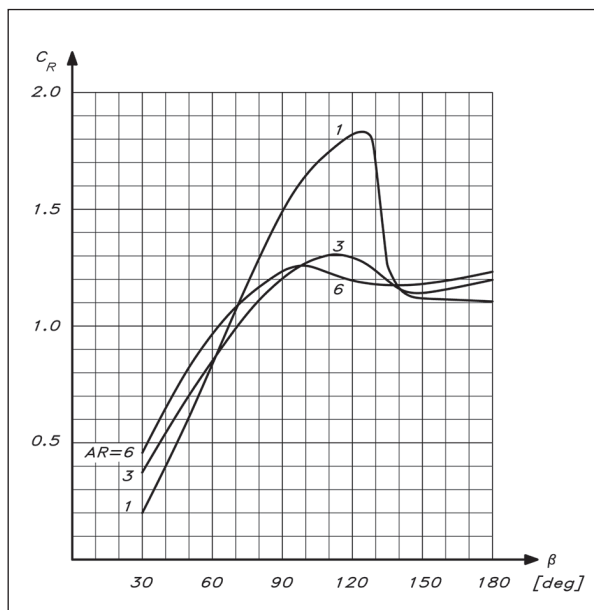


**Fig 8.3** Computed influence of aspect ratio on driving force. Each component dimensionless by total sail area

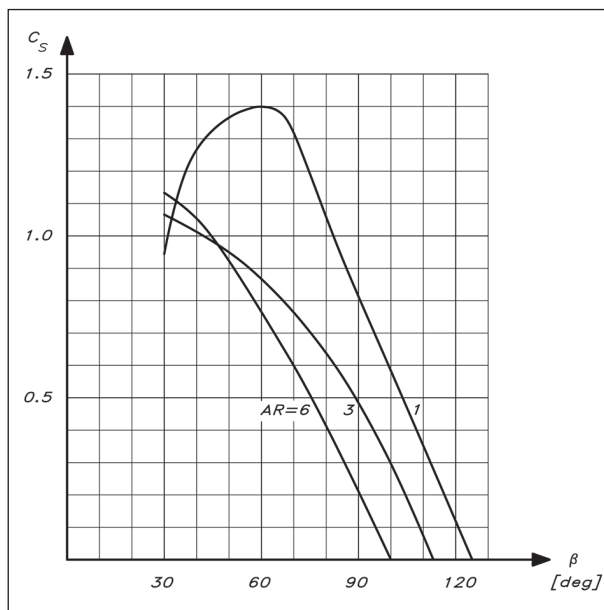


**Fig 8.4** Computed influence of aspect ratio on side force. Each component dimensionless by total sail area

Perhaps the most striking feature of Fig 8.3 is the contribution by the mast to the driving force. It contributes 4-5%, which may come as a surprise. But the mast is the most forward part of the wing created by the mast/sail combination, and, as we have seen in Fig 6.2, the largest suction is around the leading edge of a section. This does not mean that we will lose this force if we remove the mast. Then this effect would be transferred to the main. In fact, the mast destroys the flow in the most forward part of the sail, as we will see below, and this explains partly the second most interesting feature of Fig 8.3: the small



**Fig 8.5** (LEFT) Measured influence of aspect ratio on driving force



**Fig 8.6** (RIGHT) Measured influence of aspect ratio on side force

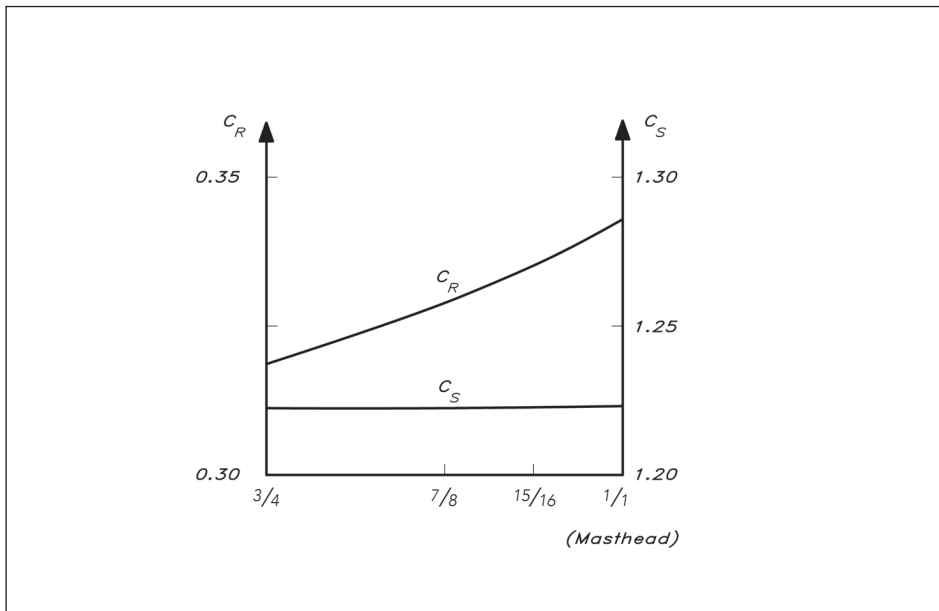
contribution by the main. For the smallest aspect ratio, the contribution is only 16% and it is even smaller for the largest AR: 12%. So, by far the most important contribution to the driving force comes from the jib, and this contribution increases significantly with aspect ratio. There is thus no optimum in driving force below 7 in aspect ratio.

As seen in Fig 8.4, the contribution to the side force by the main is considerably larger, even if the jib still contributes the most. The contribution from the mast is about the same (in per cent) as in Fig 8.3. The total driving force has increased by 31% from AR 4 to AR 7, and the side force by 19%. It should be stressed also that the heeling moment increases with aspect ratio due to the larger heeling arm. The net effect depends on the boat stability and can only be evaluated in a VPP.

The discussion so far has concerned only upwind conditions. In the CFD computations the apparent wind angle was 26 degrees. Aspect ratio effects at varying apparent wind angles were investigated in wind tunnel experiments by Marchaj (1979). Fig 8.5 shows the driving force and Fig 8.6 the side force for three aspect ratios: 6, 3 and 1. The latter is an almost square gaff sail. It can be seen that for small apparent wind angles, i.e. upwind, the force coefficients of the CFD investigation correspond well with the tunnel data. Around 30° the high aspect ratio sail develops more than twice the driving force of the square sail. However, at large wind angles the situation is different. Around 120° the square sail is superior and develops 50% more thrust than the narrow sail. At 70° the thrusts are almost equal. The side force of Fig 8.6 increases somewhat with aspect ratio at 30°, but the opposite is true above 45°. The general conclusion is that the positive effect of a high aspect ratio is reduced if all points of sailing are of interest.

Jacobs and Sahlberg (2018) also made a systematic variation of the height of the forestay attachment on the mast. Unfortunately, this was inconclusive, due to an inherent problem in systematic sail variation studies. When the forestay was lowered from the mast head, the flow on the leeward side of the main was completely separated in the part above

**Fig 8.7** Computed influence of foretriangle height on driving and side force



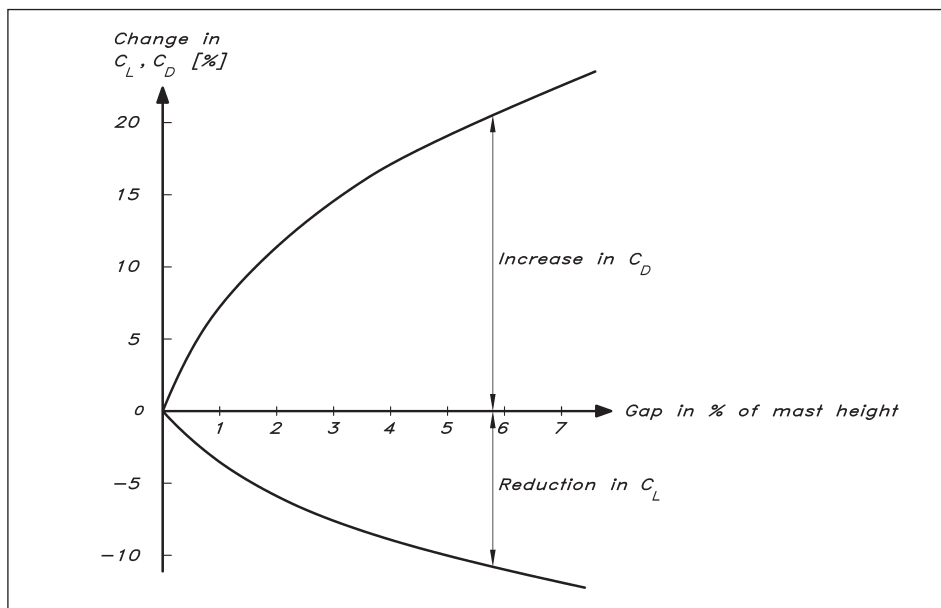
the attachment point. A perfect sail trim with the jib in front of the main did not work at all when that part of the jib was removed. For this study to be practically useful, the main would have to be retrimmed at the top. But then several parameters would have changed simultaneously, and the study would not have been systematic.

The separation problem can be avoided numerically if viscosity is neglected, i.e. in a potential flow (see [Chapter 17](#)). Such computations were carried out by Milgram (1971). Four rigs were computed, where the attachment point was at  $3/4$ ,  $7/8$ ,  $15/16$  and  $1/7$  of the full mast height, respectively. The results can be seen in [Fig 8.7](#). There is a significant gain in driving force when the foretriangle height is increased, while the side force is almost constant. Even though these computations are likely to overestimate the advantage, since they assume an attached flow on the main above the forestay attachment without a trim change, they indicate that the masthead rig is the most efficient one.

Modern yachts do not, however, feature masthead rigs, and the reason is the need for trimming the camber of the main. As will be seen below, there is a need for reducing the camber when the wind increases and that is most efficiently done by bending the mast. For a fractional rig, where the forestay is attached at a certain distance from the masthead, this can be easily achieved by tightening the backstay. For a masthead rig the bending has to be achieved in some other way, either through the lower shrouds or through a baby stay fitted between the fore deck and a point on the mast considerably below the head. Either way, the trimming possibilities are limited, not least because the mast is normally not tapered.

A high aspect ratio is not the only way to reduce the induced resistance of the sails. A very effective way is to try to seal the gap between the sail and the deck of the yacht. In [Fig 8.8](#) some results of wind-tunnel measurements by Bergstrom and Ranzén at the Royal Institute of Technology in Stockholm are presented. The change in lift and drag coefficients of the sails is given as a function of the gap size in per cent of the mast height. It may be seen that the lift is decreased, and the drag increased by an increasing gap. For

**Fig 8.8** Effect of gap between sail and deck



instance, a gap of 0.1 m and a mast height of 10 m give a drag increase of 7% and a lift decrease of 4% compared to the fully sealed case. Of course, it is impossible to seal the gap between the boom and the hull fully, so the figures should be relevant for the foresail only. Note that the drag and lift are the force components parallel to, and at right angles to, the apparent wind. They can easily be converted into the driving force parallel to, and the side force at right angles to, the direction of motion of the yacht (see Fig 8.21, page 196). For the YD-41 we have chosen a fractional rig with a relatively high attachment of the forestay (see Fig 12.15, page 248). The foretriangle area is large due to the large base. This is to increase the area of the non-overlapping jib, which is on a furler concealed below the deck. The foot of the sail is thus very close to the deck and the gap almost closed. To enhance performance on reaching and downwind legs a masthead asymmetric spinnaker and Code 0 sail are also included. For the mainsail the aspect ratio is 6.0, which is likely to be close to the upper limit, considering mast interference. The aspect ratio of the foretriangle is 6.4, a modest value due to the large foretriangle base.

## ■ SAIL CAMBER

Since the sail is a wing of practically zero thickness, the only characteristic feature of the section is the camber. We will now look at the effect of camber size and position. Figs 8.9 and 8.10 (overleaf) are obtained from measurements with plate sails without a mast reported by Marchaj (1979). Three different cambers were investigated:  $1/7$ ,  $1/10$  and  $1/20$  of the chord length. It is seen immediately that the larger the camber the larger the forces in both directions. There is a particularly large difference between the  $1/10$  and  $1/20$  sails. In fact, the latter sail is quite extreme. Sails that flat are rarely used in practice, but it is of interest to include it, since the trends then become clearer.

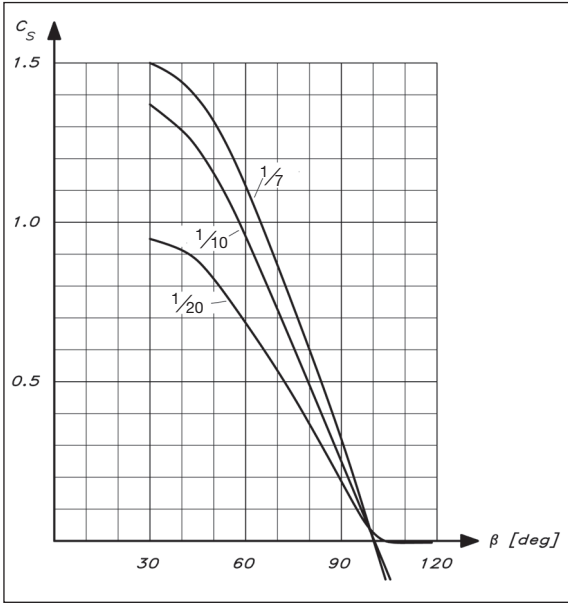
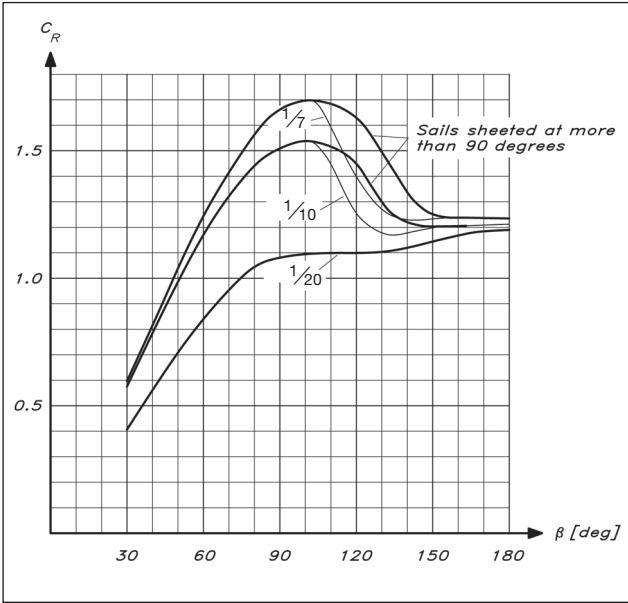


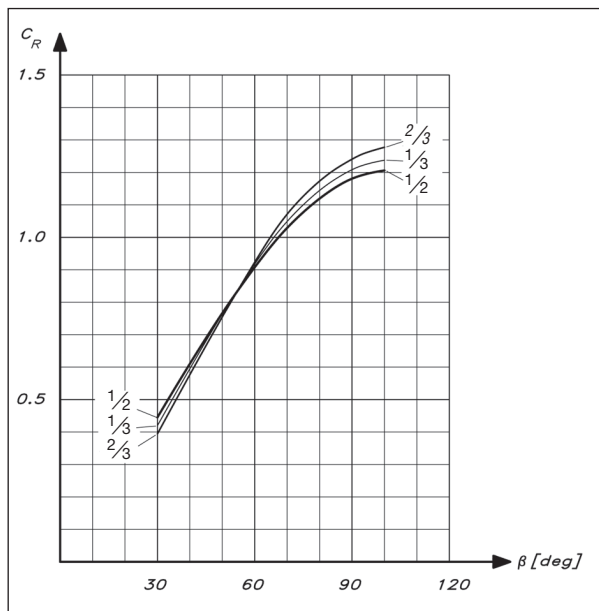
For the upwind case, at  $30^\circ$  and below, there is a very small difference in driving force between the two deepest sails, but the deepest one has a slight advantage. The difference in side force is somewhat larger: approximately 10%. Which sail is the best is hard to say, since it depends on the ability of the underwater body to balance the side force without producing too much induced resistance. The problem can be resolved in a complete equilibrium calculation for the yacht, such as in a VPP program (see [Chapter 17](#)), but the result is not obvious without such a calculation, unless heeling is a problem. In stronger winds the 10% smaller side force of the  $1/10$  sail has to be compensated by reefing of the  $1/7$  sail. Considering the fact that the centre of effort of the sails is then lowered, the area has to be reduced some 7%, which would reduce the driving force by an equal amount. This force would then be smaller than the  $1/10$  sail. It is thus better to flatten the sail than to reef it to reduce heeling, a fact well-known by most sailors.

From [Figs 8.9](#) and [8.10](#) it is obvious that for larger apparent wind angles the full sail is the best. At the maximum driving force around  $100^\circ$  there is a difference of about 10% between the  $1/7$  and  $1/10$  sails, while the side force is zero. An interesting feature of the measured results is that it is advantageous to develop a negative side force, i.e. to windward, for angles in the range  $100\text{--}150^\circ$ . The sails should thus be sheeted at more than  $90^\circ$  giving an angle of incidence of the sail small enough to avoid separation on the leeward side. The total force developed is then so large that, although it points somewhat to windward, the driving component is larger than if the sail is sheeted in the normal way. This possibility does not normally exist in practice, due to the shrouds, but it could be of interest for dinghies.

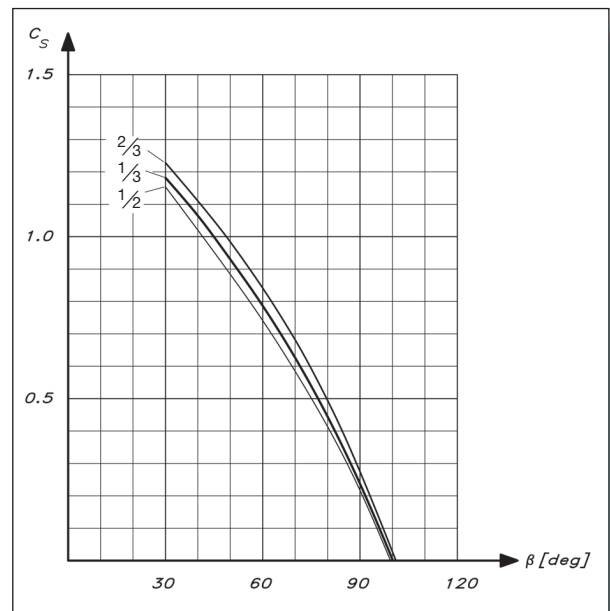
The effect of the position of the maximum camber is shown in [Figs 8.11](#) and [8.12](#). These figures are based on wind-tunnel measurements for a sail with a mast and are thus applicable to the mainsail. It can be seen that this effect is much smaller than that of the camber size. Interesting differences, however, are noted in the figures, which show results

.....  
**Fig 8.9** (LEFT) Influence of camber on driving force  
 .....  
**Fig 8.10** (RIGHT) Influence of camber on side force





**Fig 8.11** (LEFT) Influence of maximum camber position on driving force



**Fig 8.12** (RIGHT) Influence of maximum camber position on side force

for three sails with the maximum camber at  $1/3$ ,  $1/2$  and  $2/3$  of the chord. At small angles the  $1/2$  sail develops the largest driving force, followed by the  $1/3$  and  $2/3$  sails. Around  $55^\circ$  they are all equal, while at the maximum driving force around  $100^\circ$  the  $2/3$  sail is the best, followed by the  $1/3$  and  $1/2$  sails. The side force is smallest for the  $1/2$  sail and largest for the  $2/3$  sail in the range of angles up to maximum thrust. The results indicate that the sail with the maximum camber at mid-chord is the best upwind, while on broad reaches the maximum camber should be further aft. Note that these conclusions are for the single mainsail, not taking the interference with the foresail into account. Experiments by Marchaj (1979) indicate that with an overlapping genoa the maximum camber of the mainsail should be considerably more forward, for large overlaps even within the overlapping region. As to the foresail itself, a position of the camber forward of the middle is likely to be better. The aft position should definitely be avoided, since the flow approaching the mainsail might then be too disturbed.

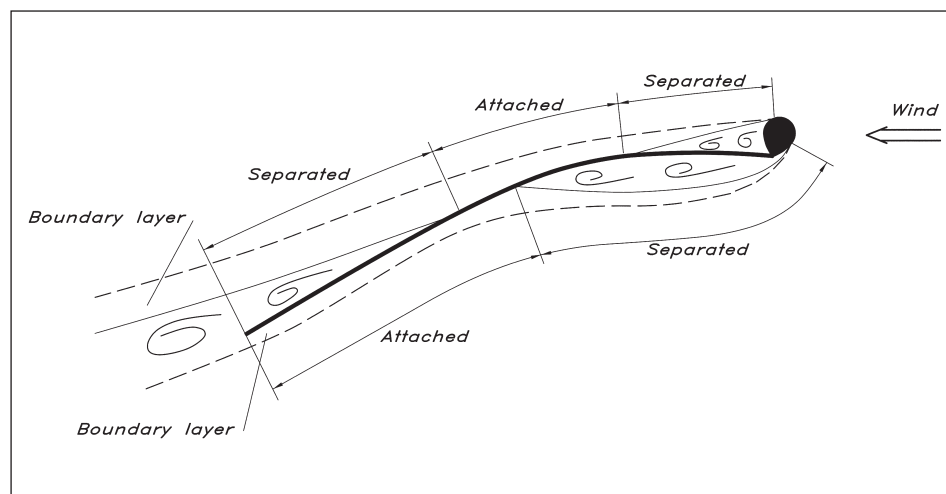
## MAST INTERFERENCE

Although the mast will contribute to the driving force sailing upwind, it has a negative effect on the total driving force. This is because of its negative effect on the main. The flow around a sail behind a mast in upwind sailing is shown schematically in Fig 8.13. As can be seen in the figure the flow is not attached to the sail all the way. Three zones of separation can often be distinguished. Two are immediately behind the mast, to windward and leeward, respectively, while the third zone is on the aft part of the leeward side. The separation behind the mast can be minimized by proper shaping of the mast section and by introducing turbulence stimulators. The aft separation zone depends, in fact, to some extent on the forward one, since a massive separation forward causes a thick boundary

layer to develop in the attached part of the flow. This layer separates more easily than a thin one. To a large extent the aft separation depends also on the loading of the sail. By proper sheeting and a good mast design this zone can be very small or even eliminated.

Experiments at Southampton University with a mast/sail combination indicated large effects of mast disturbance. Thus, when a circular mast with a diameter of 7.5% of the sail chord was put in front of the sail the driving force upwind was reduced by about 20%, as compared to the case without a mast. A thicker mast of 12.5% was also tested and the driving force was almost halved. It was, however, possible to regain almost half of the loss by turning the mast in such a way that the leeward side of the mast/sail junction became smooth.

The YD-41 has a light carbon mast. Being a performance cruiser, it should have a simple rig, manageable by a family on a cruise or a short-handed crew. Therefore, running backstays and inner forestays have been avoided, and a fractional rig with swept spreaders used instead. The dimensions (obtained from the rig calculation in [Chapter 12](#)) are  $229 \times 119$  mm. The average is 174 mm, which is about 5% of the average chord length of the sail, considering the roach. This is not much, so the major part of the sail should work properly, especially as we will employ the technique described in the next section to reduce the mast disturbance. There is no doubt, however, that the top part of the sail will be significantly disturbed.



**Fig 8.13** Flow around a mast/sail combination

## MEANS FOR REDUCING MAST DISTURBANCES

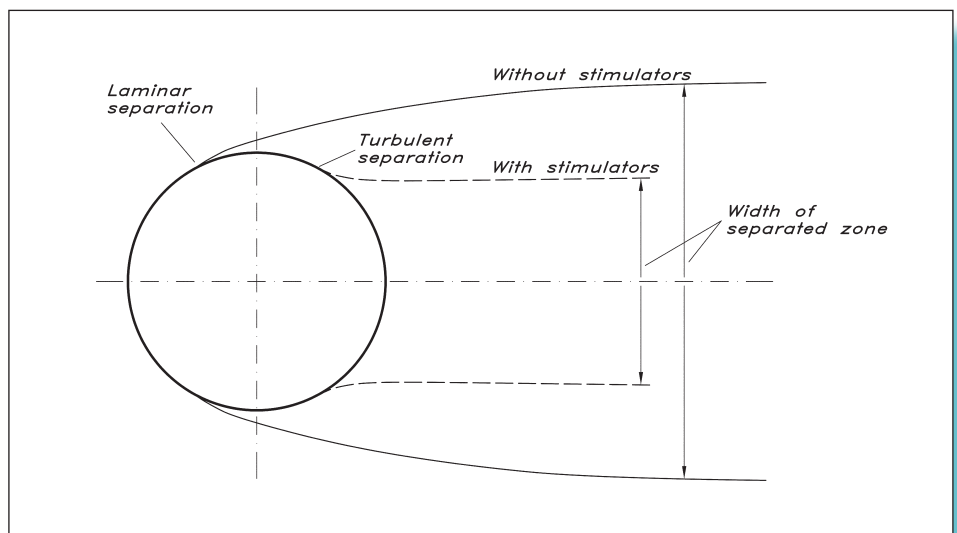
A well-known but seemingly paradoxical phenomenon in fluid dynamics is the reduction in drag of bluff bodies when their surface is changed from smooth to rough. As we have seen in [Chapter 5](#) a rough bottom of a yacht causes a considerable resistance increase. The reason for the different behaviour is that the viscous resistance of the hull, which is a slender body, is essentially due to direct friction (see [Fig 5.4](#)), while the resistance of a bluff body to a large extent is due to pressure losses in the wake (viscous pressure resistance).

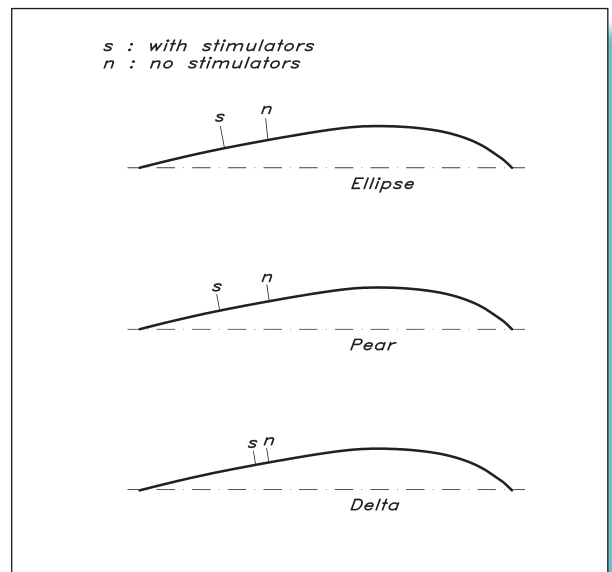
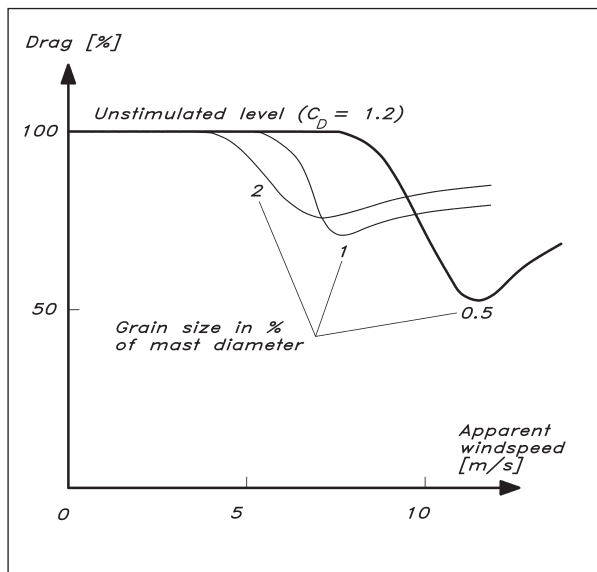
Let us return to Fig 5.5, showing the different regions in the flow around the hull. It can be seen that the boundary layer is laminar at the bow, but undergoes transition relatively quickly. Thereafter it is turbulent, and may, in rare cases, separate from the hull at a point near the stern. The same flow regions may exist around the cylinder, but not always. If the Reynolds number (i.e. the product of diameter and velocity, divided by viscosity, cf Fig 5.8) is small, the boundary layer never gets turbulent, but separates directly in the laminar part. This happens, in fact, before the maximum thickness (as shown in Fig 8.14). The wake then becomes quite wide and the drag is high. On the other hand, if the boundary layer gets turbulent before separation, the latter is delayed to a point well aft of the maximum thickness (see Fig 8.14). The wake is then narrower and the drag smaller. The reason why turbulence delays separation is that it has a stirring effect on the flow. High-speed fluid from outside the boundary layer is convected inwards and energizes the flow that is about to stop moving along the surface.

With this explanation in mind it is not difficult to understand why a rough cylinder may have a smaller resistance than a smooth one. If the Reynolds number is in the subcritical region, and laminar separation occurs, introducing roughness causes the boundary layer to turn turbulent earlier, maybe before separation. This is then delayed, as just explained, and the drag gets smaller. Now a mast is normally in the subcritical region and has a high drag, but it is close enough to the low drag region to make the roughness trick work. Fig 8.15 (overleaf) shows the drag coefficient of circular cylinders of around 0.1 m in diameter with different roughness heights. The height is given as a percentage of the diameter. It may be seen that at 11 m/s the drag is reduced by 50% if the roughness height is 0.5% of the diameter. The narrower wake also disturbs the sail much less, so there is a double gain. Unfortunately, the optimum roughness height varies with the wind velocity, but a height of 1% covers most of the interesting velocities quite well. Note that it is the apparent wind that is of interest.

Fig 8.16 shows results from measurements made by one of the authors and his students. A plate sail with different masts, with and without roughness, was tested in a wind tunnel,

**Fig 8.14** Effect of stimulators on the flow around a circular cylinder





and the position of the rear separation point was measured. The mast sections were the most common ones: ellipse, pear and delta. Practically no difference could be detected in the separation location for the three smooth masts, while the positive effect of the roughness was largest for the ellipse and pear masts.

It can be seen in the figure that a considerable increase in the effective length of the sail is obtained in all cases. The roughness in this test was 1% of the mast diameter and was created by sand grains of uniform size glued to the front half of the mast. Later tests have indicated that much less disturbance is required. In fact, a small riblet of the same height put at the leading edge of the mast produced the same effect. Note that when the sail is working, the stagnation point on the mast is always on the windward side, so the flow entering the leeward side of the sail has to pass the riblet, even if it is in the symmetry plane of the mast. There is no effect, however, on the flow on the windward side, so a better solution might be to put one riblet on each side of the mast, at  $45^\circ$ , say, on each side of the symmetry plane.

**Fig 8.15** (LEFT) Drag of circular cylinders with sand roughness

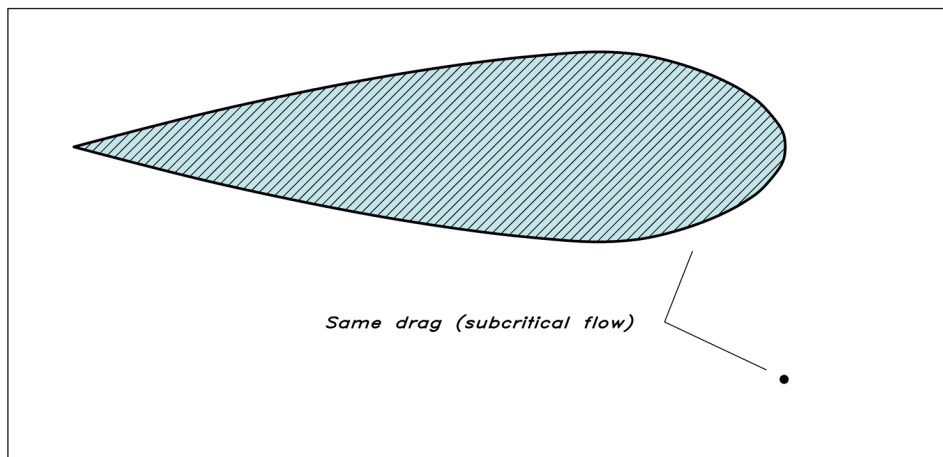
**Fig 8.16** (RIGHT) Position of trailing edge separation on a sail with three different masts

## ■ STREAMLINING

The windage of the mast and rig is considerable, as we will see in [Chapter 9](#), and all means of streamlining different components, such as spreaders and shrouds, are valuable. A striking figure is that of [Fig 8.17](#), which shows two 2-dimensional bodies with the same drag. The upper one is a streamlined foil, where most of the drag comes from friction, and the lower one is a round bar, for which pressure drag dominates. The drag coefficient for the bar is around 1.0, while it is only about 0.03 for the foil, based on the front area. The diameter of the bar thus has to be more than 30 times smaller than the foil thickness for the same drag.

In [Fig 8.18](#) results are presented from wind-tunnel tests at the Davidson Laboratory in New York. Drag measurements were made for three different types of shroud: a wire, a circular rod and an elliptic rod. It may be seen that the wire has the highest drag, somewhat

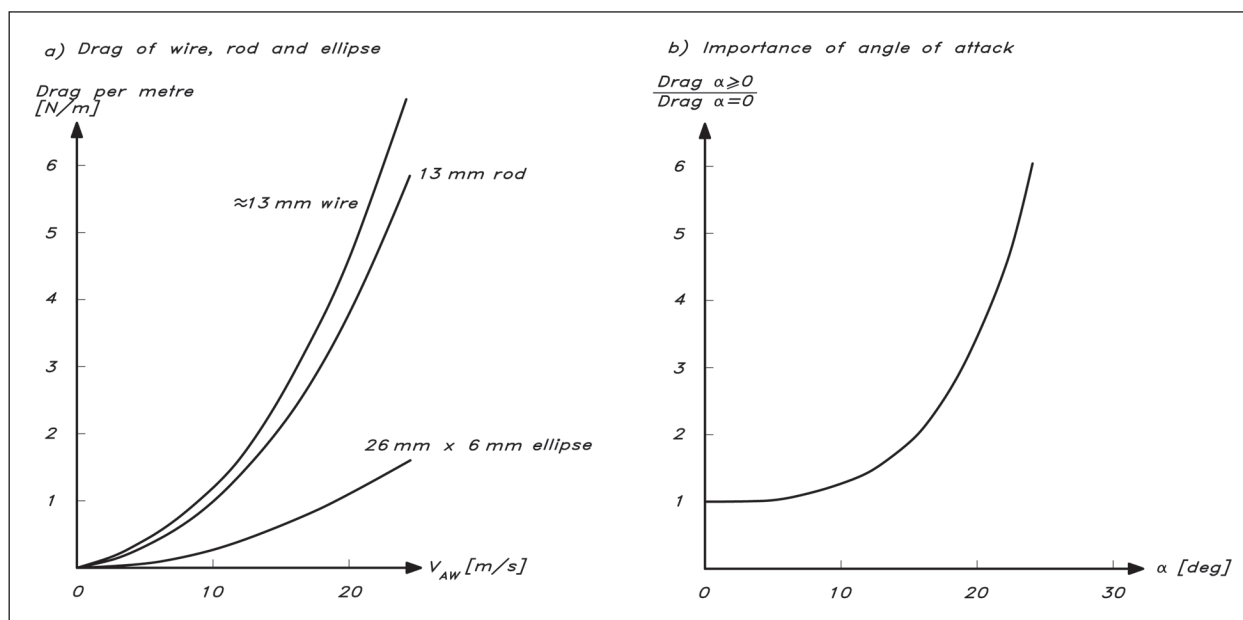
**Fig 8.17** Effect of streamlining



higher than that of the rod. At first sight this might seem contrary to the findings above (that a rough mast has a smaller drag than a smooth one), but the difference is that the wire has such a small Reynolds number (due to the small diameter) that the turbulent boundary layer never appears, even if the surface is rough.

The ellipse is outstanding with a drag that is only  $\frac{1}{4}$  of that of the wire. This is so in spite of the fact that the ellipse was tested at an angle of attack of  $19^\circ$ . Small as this may seem, it is probably realistic upwind, considering the fact that the sails guide the flow more in the longitudinal direction than the apparent wind. It is quite important that the angle of attack does not get too large for the ellipse, as can be seen in Fig 8.18(b). This diagram shows the relative increase in resistance when the angle increases from zero. Up to  $10^\circ$  the additional drag is small, but at  $20^\circ$  the drag is three times larger than the minimum. Thereafter, the increase is still faster.

**Fig 8.18** Drag of shrouds and stays



## ■ A PRACTICAL MODEL FOR SAIL AND RIG AERODYNAMICS

A model for the aerodynamics of sailing yachts was presented by Hazen (1980). This model is the basis for the aerodynamic modelling in most VPPs, as explained in [Chapter 17](#). For instance, the VPP of the currently most important international handicapping system, the Ocean Racing Congress (ORC) rule, uses a development of this basic model. We will describe the original model first and then introduce some improvements.

In Hazen's model the lift and viscous drag of each sail are prescribed as functions of the apparent wind angle. The corresponding coefficients are given in [Table 8.1](#). Only five angles are given in the original model: 27°, 50°, 80°, 100° and 180°. Interpolation between these angles is supposed to be done using spline functions. Manual fairing, for instance using physical splines, is also possible of course, but linear interpolation is too approximate.

Coefficients are given for five sails: main, jib, spinnaker, mizzen and mizzen staysail. To obtain the total lift or viscous drag (sometimes called the parasitic drag, which explains the index 'P') the area of each sail is to be multiplied by the corresponding coefficient and all sails added. The final coefficient is obtained by dividing by a nominal sail area, which is the sum of the foretriangle, main and mizzen areas. All areas are computed as triangular, i.e. the roach is neglected. In [Fig 8.19](#) the relevant equations are given. There is no explicit interaction between the sails, but the blanketing of the mainsail by the mizzen is taken into account in the mizzen coefficients. In view of the previous discussion on interaction the method is quite crude, but it has proved to be useful, nevertheless.

**Table 8.1(a)** Sail coefficients, lift

Angle	Main	Jib	Spinnaker	Mizzen	Mizz. stays.
27	1.5	1.5	0.0	1.3	0.0
50	1.5	0.5	1.5	1.4	0.75
80	0.95	0.3	1.0	1.0	1.0
100	0.85	0.0	0.85	0.8	0.8
180	0.0	0.0	0.0	0.0	0.0

**Table 8.1(b)** Sail coefficients, viscous drag

Angle	Main	Jib	Spinnaker	Mizzen	Mizz. stays.
27	0.02	0.02	0.0	0.02	0.0
50	0.15	0.25	0.25	0.15	0.1
80	0.8	0.15	0.9	0.75	0.75
100	1.0	0.0	1.2	1.0	1.0
180	0.9	0.0	0.66	0.8	0.0



	<u>Area</u>	<u>Centre of effort</u>
<i>Sail area and height of centre of effort above sheer</i>	Main: $A_M = 0.5 \cdot P \cdot E$	$CE_M = 0.39 \cdot P + BAD$
	Jib: $A_J = 0.5 \cdot \sqrt{I^2 + J^2} \cdot LPG$	$CE_J = 0.39 \cdot I$
	Spinnaker: $A_S = 1.15 \cdot SL \cdot J$	$CE_S = 0.59 \cdot I$
	Mizzen: $A_Y = 0.5 \cdot PY \cdot EY$	$CE_Y = 0.39 \cdot PY + BADY$
	Mizzen staysail: $A_{YS} = 0.5 \cdot YSD \cdot (YSMG + YSF)$	$CE_{YS} = 0.39 \cdot PY + BADY$
	Foretriangle: $A_F = 0.5 \cdot I \cdot J$	
Nominal area	$A_N = A_F + A_M + A_Y$	
Lift	$C_L = \frac{C_{LM} \cdot A_M + C_{LJ} \cdot A_J + C_{LS} \cdot A_S + C_{LY} \cdot A_Y + C_{LYS} \cdot A_{YS}}{A_N}$	
Viscous/parasitic drag	$C_{DP} = \frac{C_{DPM} \cdot A_M + C_{DPJ} \cdot A_J + C_{DPS} \cdot A_S + C_{DPY} \cdot A_Y + C_{DPYS} \cdot A_{YS}}{A_N}$	
Induced drag	$C_{DI} = C_L^2 \cdot \left( \frac{1}{\pi \cdot AR} + 0.005 \right) \left\{ \begin{array}{l} \text{close hauled: } AR = \frac{(1.1 \cdot (EHM + FA))^2}{A_N} \\ \text{other courses: } AR = \frac{(1.1 \cdot EHM)^2}{A_N} \end{array} \right.$	
Drag of mast and topsides	$C_{DO} = 1.13 \cdot \frac{(BMAX \cdot FA) + (EHM \cdot EMDC)}{A_N}$	
Total drag	$C_D = C_{DP} + C_{DI} + C_{DO}$	
Flattening: Multiply $C_L$ by flat factor $F$		
Reefing: Multiply $C_L$ and $C_{DP}$ by reef factor $R$ squared Multiply height of CE by $R$		
Standard IOR notation:	<div> <div> <math>P</math> : Mainsail hoist  <math>E</math> : Foot of mainsail  <math>I</math> : Height of foretriangle  <math>J</math> : Base of foretriangle  <math>LPG</math> : Perpendicular of longest jib  <math>SL</math> : Spinnaker leech length  <math>PY</math> : Mizzen hoist  <math>EY</math> : Foot of mizzen </div> <div> <math>YSD</math> : Mizzen staysail depth  <math>YSMG</math> : Mizzen staysail mid-girth  <math>YSF</math> : Mizzen staysail foot  <math>BMAX</math> : Max beam of yacht  <math>FA</math> : Average freeboard  <math>EHM</math> : Mast height above sheer  <math>EMDC</math> : Average mast diameter  <math>BAD</math> : Height of main boom above sheer  <math>BADY</math> : Height of mizzen boom above sheer </div> </div>	

**Fig 8.19** Hazen's model for rig and sail aerodynamics

The induced drag, which is more important than the viscous drag for upwind sailing, is computed from the simple wing theory presented in [Chapter 6, Fig 6.5](#) in particular. The induced drag coefficient is thus proportional to the square of the lift coefficient, and inversely proportional to the aspect ratio. In the present method the entire nominal sail plan is considered when computing the aspect ratio, and the induced drag is computed for all the sails together.

The aspect ratio of a wing was defined in [Chapter 6](#) as the span divided by the average chord. This may be expressed in another way. Since the projected area is equal to the span times the average chord, the aspect ratio may be defined also as the span squared divided by the area. In the present model this definition is used. However, due to some mirror effect of the water surface the effective span is taken to be 110% of the height of the masthead above the water, if the yacht is close-hauled. When the jib is eased and the gap to the deck opens up, only the mast height above deck level should be considered, and 110% of this height is used in the aspect ratio definition (see [Fig 8.19](#)).

Hazen argues that some of the viscous drag, originating from the separation on the leeward side of the sail, is proportional to the lift squared as well, so he introduces an addition to the induced drag to account for this effect. It appears as a constant, 0.005, in the expression for the induced drag.

In this model the drag of mast and topsides are included as well. The frontal area of the topsides is taken as the average freeboard multiplied by the maximum beam, while that of the mast is computed as the mean diameter multiplied by the mast height above deck. The drag coefficient is assumed to be 1.13. In [Chapter 10](#) we will discuss this drag component in more detail. The total drag is found as the sum of the viscous, induced and mast/topsides components.

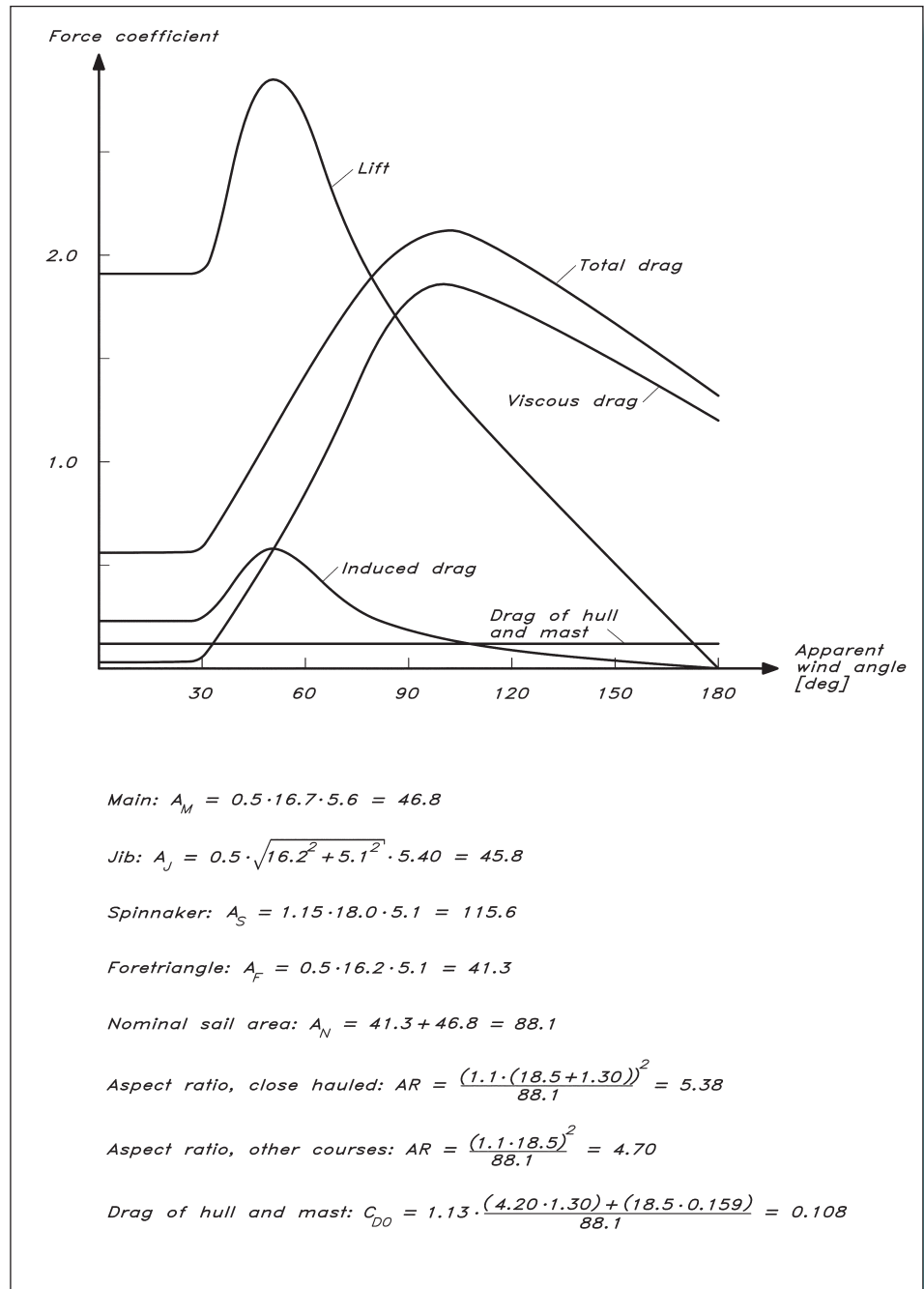
The height of the centre of effort of each individual sail is given in [Fig 8.19](#). For the main, mizzen and mizzen staysail it is taken to be at 39% of the luff length above the boom. For the jib and spinnaker it is at 39% and 59% of the foretriangle height, respectively, above the sheer line.

Sail coefficients computed for the YD-41 are presented in [Fig 8.20](#) for apparent wind angles from 0° to 180°. The curves were obtained from the tabulated values above, so only five points were computed on each curve. Splines were therefore used to find the intermediate points. As is common practice, the curves have been drawn horizontal below 27°. Angles smaller than about 20° will not be reached, since the driving force then becomes too small.

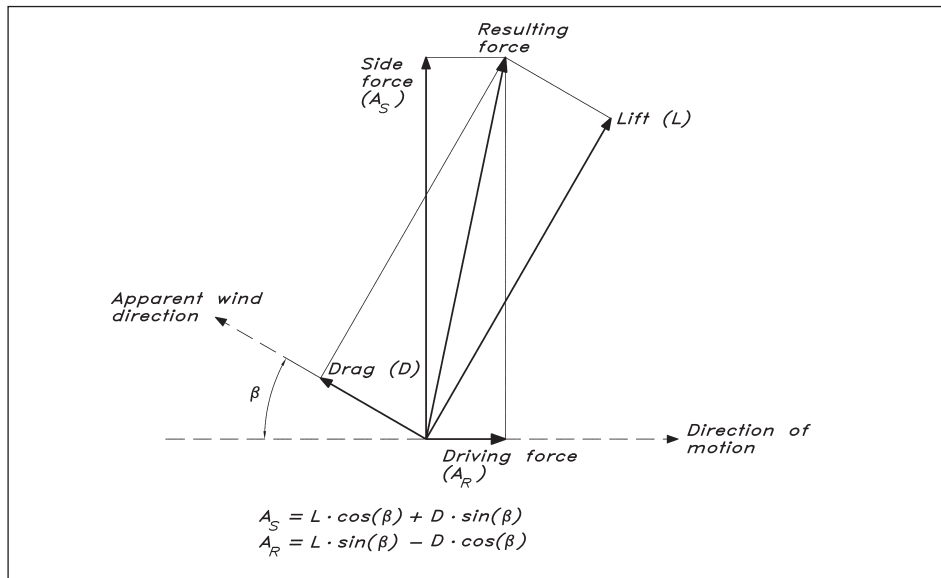
An interesting feature of the sail model is the possibility of considering reefing and flattening of the sails. The effect of these two actions is quite different. Reefing is specified by a factor  $R$  which defines the reduction in sail height.  $R$  is equal to 1 for the unreefed sail. The new height of the centre of effort is thus obtained as  $R$  times the original height, while the new area is found by multiplying by  $R^2$ . This means that both lift and drag (excluding mast/topsides) are reduced with  $R^2$ , while the major part of the heeling arm is reduced with  $R$ .

The flattening factor  $F$  specifies the reduction in lift due to the flattening of the sails. This factor, which is equal to 1 for the normal sail, cannot be directly related to the sail geometry, but the smaller the camber the smaller the factor. Note that  $F$  has no effect on the heeling arm, and that it has different effects on the lift and drag. Since the lift is proportional to  $F$ , the induced drag is proportional to  $F^2$ . This means that flattening reduces drag more than lift, i.e. the resulting force rotates forwards. It is therefore better to flatten the sails before reefing, as pointed out above. In most VPPs optimum values of  $R$  and  $F$  are found for all conditions, thereby providing information on the best sail setting.

**Fig 8.20** Sail coefficients:  
YD-41



The sail forces provided by the model are the lift and drag components. To be useful for predictions the components parallel to, and at right angles to, the direction of motion are required. Fig 8.21 (overleaf) explains how lift and drag can be converted to driving force and side force. Another geometrical transformation has to be made to obtain forces for the heeled condition. As has been seen above, no account has been taken of the effects of heel. This is done separately, in a somewhat unusual way.



**Fig 8.21** Relation between aerodynamic force components

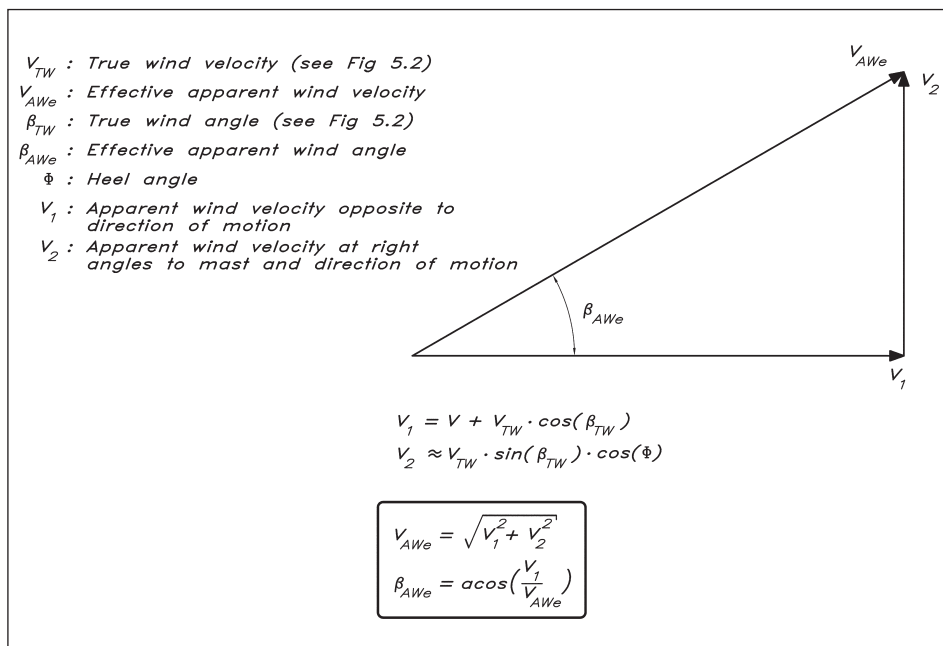
Rather than modifying all coefficients, the apparent wind speed and direction are computed in a plane that heels with the yacht. This can be done quite easily, as shown in Fig 8.22. The component of the apparent velocity along the hull is unchanged by heel, while the component at right angles thereto is proportional to the cosine of the heel angle. For simplicity, leeway is neglected in this computation, so the two directions to consider are along, and at right angles to, the direction of motion.

Since the original presentation of this aerodynamic model a number of improvements have been introduced. It would lead too far to explain all of them here, but the most important changes are listed below. For a detailed description, see the ORC VPP documentation.<sup>1</sup> A good overview is also found in Fossati *et al* (2008). The major improvements are:

- Mizzens and mizzen staysails are dropped in favour of asymmetric spinnakers and Code 0 sails.
- Coefficients are new and given at closer intervals down to smaller wind angles. Also, there are two sets given for main and foresail, depending on the trimming possibilities (fore-and-aft stays) of the yacht.
- There is a more exact computation of the areas, considering the roach and a possible fathead mainsail.
- Blanketing effects are introduced for the spinnaker (from the main).
- There is a more exact computation of the effective span in the induced resistance formulation.
- A twist function for depowering is introduced.
- Different drag coefficients are used for the hull, mast and rig, and even the crew is considered.

<sup>1</sup> The ORC VPP documentation may be found on the link: <https://www.orc.org/rules/ORC%20VPP%20documentation%202019.pdf>

**Fig 8.22** Effective apparent wind at non-zero heel angle



## SAIL STATISTICS

The sail area is obviously a measure of the driving force obtainable for a sailing yacht. To judge whether the area is large enough it must in some way be compared with the resistance-producing properties of the yacht. As we have seen in [Chapter 5](#) these are the wetted surface and the displacement. While the former determines the friction, which is dominant at low speed, the latter is the most important property for the wave resistance, the largest component at high speeds. Suitable non-dimensional parameters are therefore: sail area/wetted surface and sail area/(volume displacement)<sup>2/3</sup>.

Based on the statistics from the ORC fleet, the median value of the sail area to wetted surface ratio is 2.4. There is a slight increasing tendency with length, but it is so small that we can neglect it. The YD-41 has a value of 2.6. It should thus be fast in light airs when friction is dominant.

The median value of sail area/(volume displacement)<sup>2/3</sup> is 20.0. No dependence on length is seen. For the YD-41 the value is very high: 27.4, which is close to that of racing yachts like Class40. The high-speed qualities of the yacht should thus be very good.

Other interesting statistics from the ORC fleet are the aspect ratios of the main and foretriangle, as well as the distribution of area between them. The median value of the aspect ratio of the main is 5.8, and of the foretriangle 7.1. The YD-41 has a main with normal aspect ratio: 6.0, while the aspect ratio of the foretriangle is rather low, 6.4, due to the aim of having a large non-overlapping jib. The mainsail of the YD-41 has 53% of the total area, slightly smaller than the median, which is 54%. A picture of the YD-41 under sail is seen in [Fig 8.23](#).



.....  
**Fig 8.23** The YD-41 sailing  
upwind (Photo: Michal  
Korol)



# 9 BALANCE

One of the more difficult problems in the design of a sailing yacht is to find the best longitudinal position of the sail plan relative to the underwater body. If the sails are too far aft the yacht will require a considerable weather helm to go on a straight course, while lee helm will be required with the sails too far forward. The problem is complicated by the fact that neither the aerodynamic nor the hydrodynamic centres of effort are known, and that the yacht should behave reasonably well at all heel angles. An entirely theoretical solution to the problem has never been presented, but several semi-empirical methods have been proposed. Most of them, however, have the disadvantage of being less well tested, so in this chapter we will describe some simple rules of thumb used by designers to find the balance of the yacht. These methods work reasonably well for most hulls that are not too different from the common trend, but sometimes corrections have to be made after the first sailing tests.

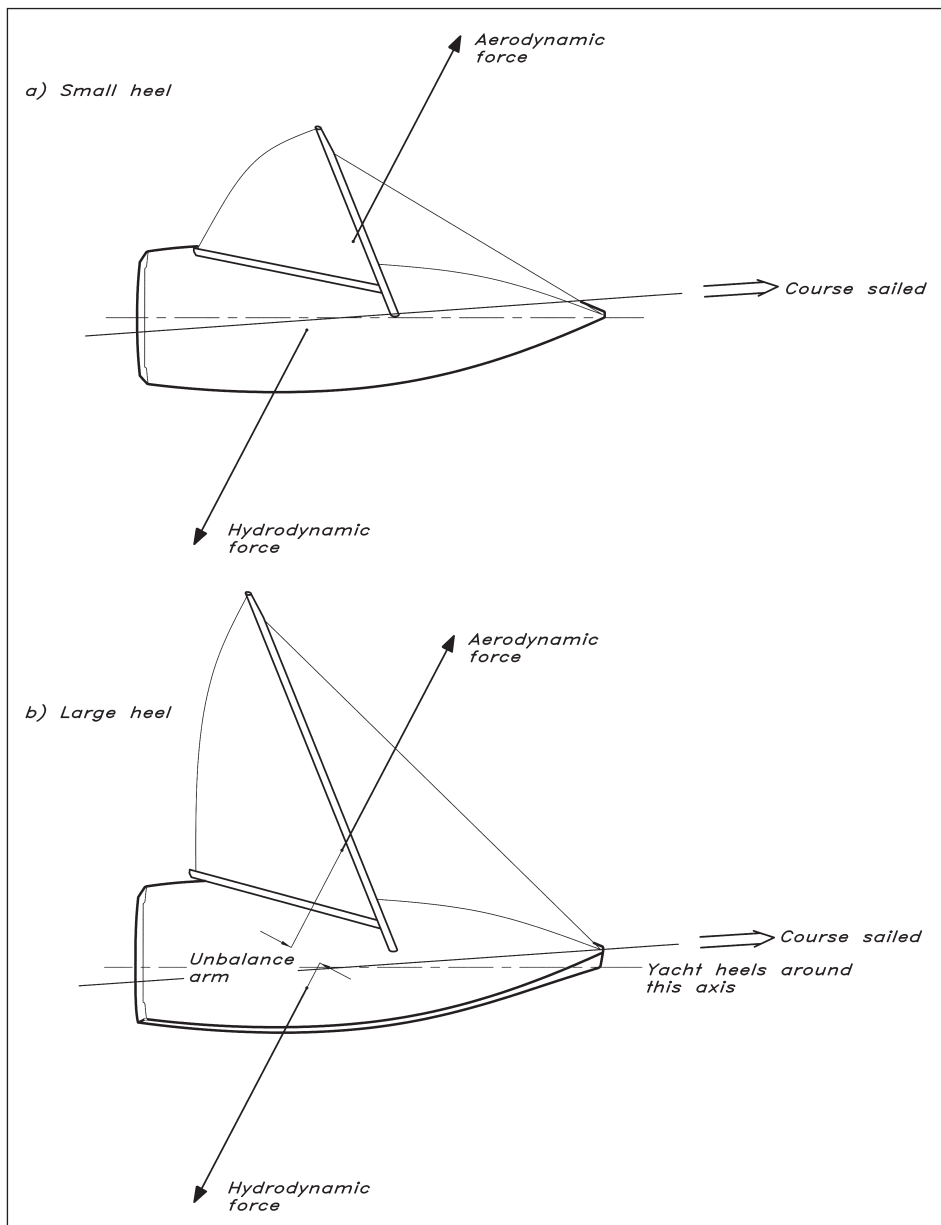
The chapter starts with an explanation of the effect of heel on balance and continues with a discussion on the location of the centre of effort, first of the underwater body and thereafter of the sails. The rule of thumb for selecting the 'lead' of the sails is then described, and, finally, some guidelines for balancing the rudder are given.

## ■ EFFECT OF HEEL

In [Chapter 5](#) the forces and moments acting on a sailing yacht were described. It was shown in [Fig 5.1](#) that under equilibrium conditions the hydro- and aerodynamic resulting forces must act along the same line, viewed from above. This situation is depicted in [Fig 9.1\(a\)](#), where the hull heels only a few degrees. If this yacht heels more, as in [Fig 9.1\(b\)](#), the centre of effort of the sails moves to leeward, while the opposite is true for the centre of effort of the underwater body. Since the hull rotates essentially around a fore-and-aft line, which is not at right angles to the hydro- and aerodynamic forces, the motion of the two centres will cause the forces to act along different lines. The aerodynamic force will act behind the hydrodynamic one, and the yacht will tend to luff up. To counteract this the helmsman has to give some weather helm, which will bring the hydrodynamic force astern until it hits the same line as the aerodynamic force.

Of course, if the heel is even smaller than in [Fig 9.1\(a\)](#), the opposite situation occurs, i.e. the yacht will tend to bear away. These effects are caused by the mere rotation of the hull, which will move the centres apart.





**Fig 9.1** Imbalance due to non-alignment of hydro- and aerodynamic forces

However, there is also a second effect of the heel on the hydrodynamics of the underwater body. Due to its asymmetric shape under heel, the hydrodynamic centre will move slightly forwards, thus increasing the imbalance. This effect depends very much on the shape of the hull and may be insignificant for slender yachts with fore-and-aft symmetry. For beamy yachts with flat stern sections it could be quite important, however.

This discussion points at the major difficulty in designing a balanced yacht. It is impossible to position the sail plan in such a way that the yacht is balanced at all angles of heel. Normally, the emphasis is placed on small angles, for which a good balance is sought. Larger weather helms are then tolerated under more heel.

## ■ GOOD BALANCE

So far, we have not defined what we mean by a well-balanced yacht. For several reasons this is not a yacht for which zero helm is required to steer it on a straight course. As we have seen in [Chapter 6](#), the rudder normally contributes to the side force, i.e. it unloads the keel to a certain extent. The larger the weather helm the larger the side force produced by the rudder. Experience shows, however, that there is a limit to the angle at which the total effect is positive. For a certain angle the total resistance of the yacht is minimum, and if this angle is exceeded the resistance grows larger.

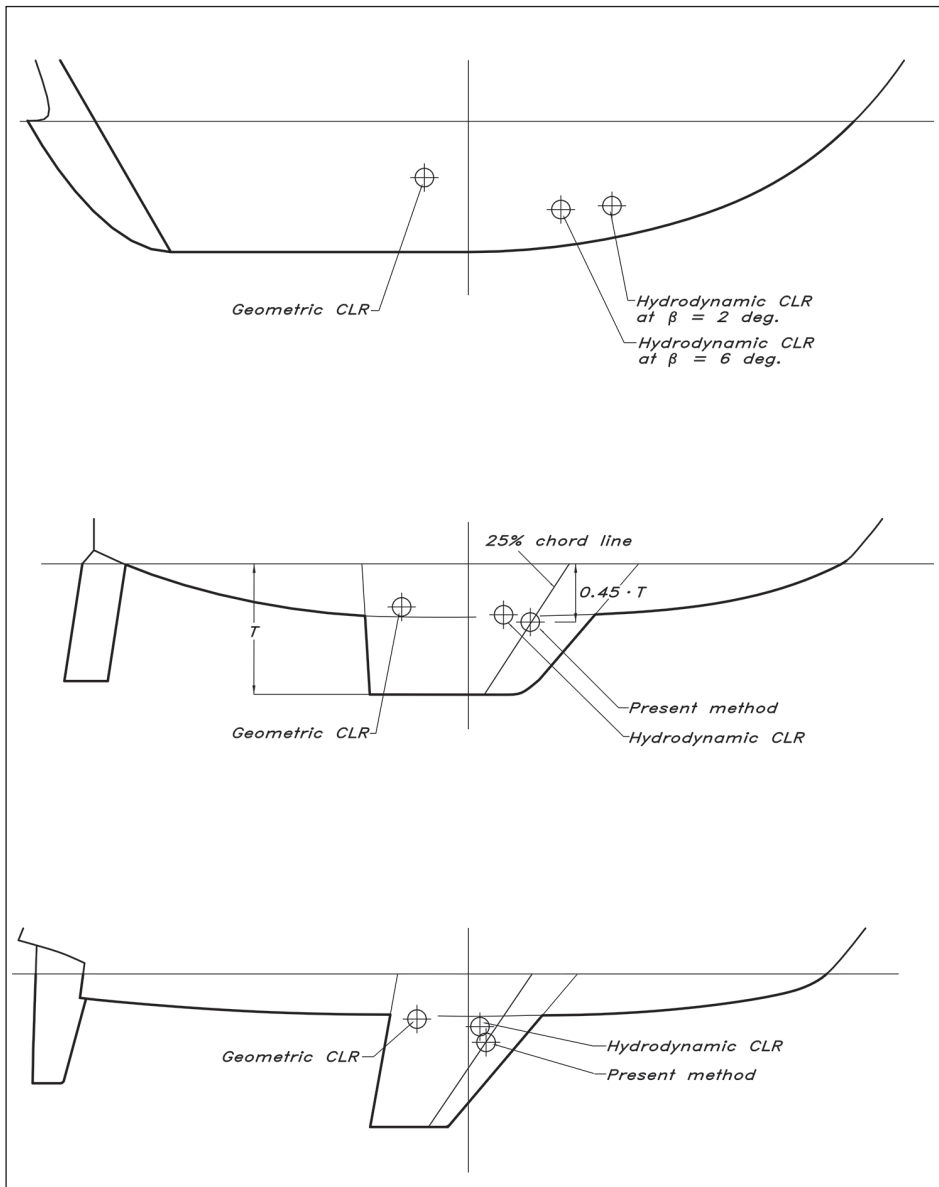
From the discussion of canard wings in [Chapter 6](#) we know that the keel/rudder combination may be analysed using biplane theory, and this shows that, since the wakes of the keel and rudder are separated due to the leeway, there is an advantage in distributing the load between the two lifting surfaces (see [Fig 6.14](#)). The rudder, however, is less effective due to the smaller draft (normally), and should therefore carry the smaller load. Theoretical optimization is possible but complicated. For extreme racing yachts the optimum rudder angle has traditionally been found from towing tank testing, but for most yachts the simple rule of thumb is to assume 5° of weather helm to be optimum.

Apart from the possible resistance reduction, there are other reasons for having a certain weather helm. From a safety point of view there is an advantage in having a yacht that automatically tends to luff up in a gust, thus unloading the sails and reducing the risk of excessive heel. Also, from a steering point of view it is an advantage to feel the effect of the gust as an increased force on the tiller or wheel. This helps the helmsman to react and makes the yacht feel livelier. Since the apparent wind angle instantaneously gets larger in the gust, due to the relatively smaller effect of the yacht speed on the apparent wind (see [Fig 5.2](#)), the yacht should luff up to take advantage of the gust, and this is more or less automatic for a well-balanced yacht.

## ■ CENTRE OF EFFORT OF THE UNDERWATER BODY

The centre of effort of the underwater body for three hulls, as tested by Nomoto and Tatano (1979) is shown in [Fig 9.2](#) (overleaf). In yachting literature this point is normally referred to as the Centre of Lateral Resistance (CLR). It is denoted 'hydrodynamic CLR' in the figure. The three hulls are quite different, the first being a traditional long keel rescue vessel, the second a heavy fin-keel cruising yacht and the third a typical IOR racer of the 1970s. It is seen that the hydrodynamic CLR is quite far away from the 'geometric CLR', which is simply the geometric centre of gravity of the underwater profile, including hull, keel and rudder. This is not surprising, in view of the fact that the centre of effort of a plane wing of large aspect ratio is at 25% of the chord from the nose, not at 50% where the centre of gravity lies. Certainly, the underwater body is a wing of a very peculiar shape and thickness distribution, and the aspect ratio is small, but wing theory at least shows that there is no reason to assume that the hydrodynamic CLR should coincide with the geometric one.

**Fig 9.2** Hydrodynamic centre of effort for three hulls (Nomoto)



Various ways to find an approximate position of the hydrodynamic CLR have been proposed. Professor J Gerritsma suggested a method for fin-keel yachts in which only the keel and rudder are considered. To some extent the effect of the hull is taken into account by extending the keel and rudder to the waterline, as can be seen in Fig 9.2 (only the keel needs to be extended in these cases). See also Fig 6.14 and the corresponding text. To find the side force and the CLR, the wing theory described in Chapter 6 is employed. This gives a good estimate of the side force, but the CLR is too far aft, if the keel and rudder are treated independently. A better estimate is obtained (as proposed by Gerritsma) if the force from the rudder is multiplied by a factor of 0.4. The physical justification for this is the change in inflow angle to the rudder caused by the keel, which reduces the lift

to about 40% for zero helm. Even with this modification Gerritsma's method tends to predict CLR too far aft, and the reason for this is that the forebody of the hull contributes somewhat to the position, even though the contribution to the force is very small. This is so, since the centre of pressure on the hull is very far forward.

Professor Nomoto and his co-workers suggested an improvement on Gerritsma's method, in which the force on the forebody is computed from a theory for slender bodies. Using Gerritsma's method, with a rudder reduction factor of 0.4, quite good results were obtained. Neither one of the two methods is very complicated, but they have the disadvantage that very little empirical data exists for linking the computed CLR to the centre of effort of the sails. We have therefore not presented the details of Nomoto's method. Instead, we propose a simplification for which empirical data is available.

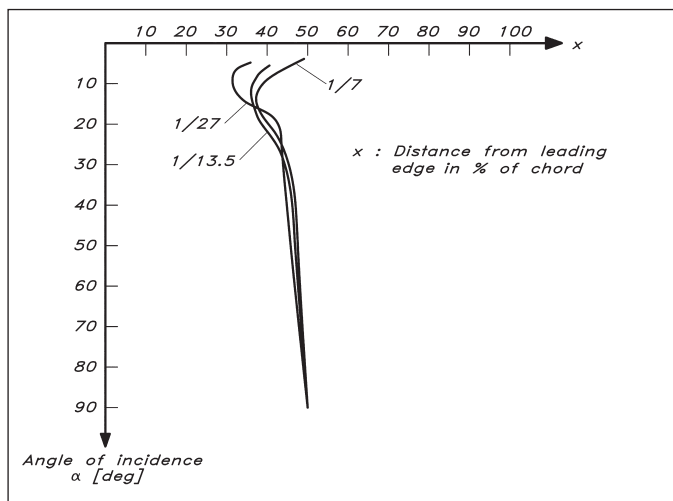
It turns out that for most fin-keel yachts the effect of the rudder and the forebody cancel each other reasonably well, so as a first approximation they may both be neglected in the CLR prediction. Thus, we use only the extended keel and compute the location of the centre of pressure on this, assuming that it lies on the 25% chord, at 45% draft. Inherently, we thus assume that the keel has a large aspect ratio and that the loading is nearly elliptical, but these approximations are not very important in the present context. In this method, CLR is easily found by connecting the points at 25% of the local chord at the waterline and at the tip of the keel by a straight line, and finding the point at 45% of the draft on this line. The procedure is shown in [Fig 9.2](#).

The obvious disadvantage of the proposed method is that it should be used only for fin-keel yachts. In principle, it could be tried also for long keels considering the whole lateral plane as a wing, but we lack experience of how to relate the CLR thus obtained to the centre of effort of the sails, and therefore do not want to propose this approach. For long keels the only feasible method is to use the geometric CLR and relate this empirically to the sail plan. This is the standard rule of thumb used for centuries and there is considerable experience available.

## ■ CENTRE OF EFFORT OF THE SAILS

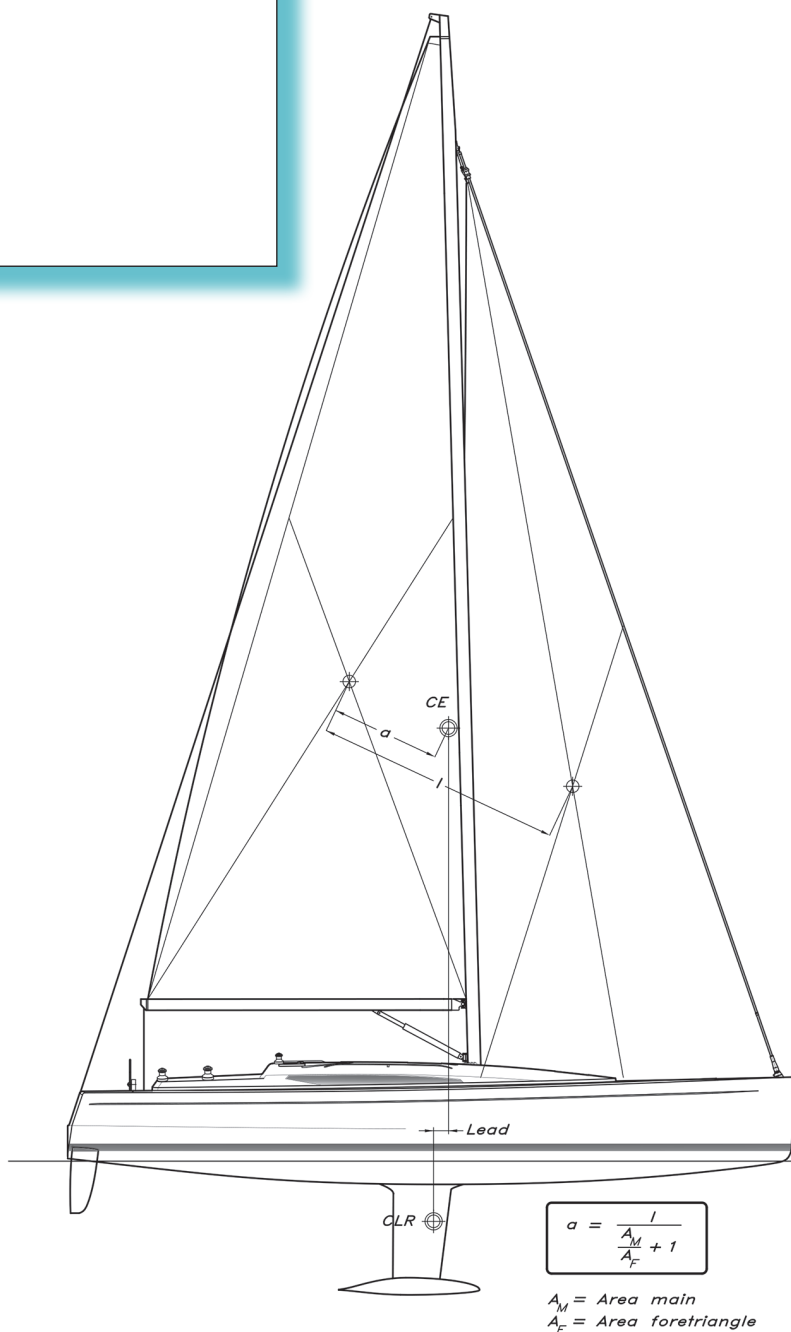
When the wind is at a  $90^\circ$  angle of attack to a sail the flow behind it is completely separated. The centre of effort (or CE, as it is normally denoted) is then at the geometric centre of gravity of the sail. This is what happens on a run. For other courses the angle of attack is usually considerably smaller and the CE further forward. As pointed out above, this centre is at the 25% chord for a plane wing of large aspect ratio. Now, the sail is not a plane surface, so even if it works like a wing at smaller angles of attack, the CE will not normally be located that far forward.

[Fig 9.3](#) shows how the CE moves with the angle of attack for different sail cambers. This is for a sail aspect ratio 5.0. It may be seen that the flattest sail with a camber ratio of 1:27 has its CE at about 30% of the chord at small angles, while this point has moved back to 37% for the full sail with the camber 1:7. A practical implication of this is the change in balance caused by changing from a flat to a full sail. More weather helm will be required for the latter.



**Fig 9.3** (ABOVE) Centre of effort for sails at varying angles of attack

**Fig 9.4** (RIGHT) Definition of lead



Another implication of Fig 9.3 is that there is normally a considerable distance between the geometric CE (corresponding to 50% of the chord) and the aerodynamic CE. In principle, it should be possible to determine a centre of the total sail plan based on, for example, 35% of the chord, but this approach is not normally used. Instead, only the geometric centre is employed. Fig 9.4 shows how this is found for a sloop rig. The centre for each sail is found first, as the intersection between straight lines from two corners to the mid-point of the opposite side. The fore and main triangles are used in this method. Having found the individual centres they are connected by a straight line, and the total CE is obtained as a point on the line, located as shown in the figure. If the yacht has a mizzen, only 50% of its area should be counted (*cf* Gerritsma's rudder efficiency factor 0.4). The common centre for the main and jib then has to be found as shown in the figure, and then the main plus jib area at this point is combined with the reduced mizzen area at the mizzen CE, in the same way.

## ■ LEAD

It is obvious from the above discussion that the positioning of the sail plan relative to the underwater body is very difficult. It can be done using modern CFD tools (see Chapter 17), but most designers still rely on empirical methods. Regardless of which method is used for finding CE and CLR their relative location has to be based on experience, if the yacht is to be as well balanced as possible under all conditions. In all the methods used, CE is in front of CLR, and the horizontal distance between them is called 'lead' (see Fig 9.4). The amount of lead depends, first, on which method is used for finding CLR and secondly on the type of yacht under consideration. In principle the following will increase the lead:

- A large beam. The beamy hull gets more asymmetric under heel, thereby creating a moment to windward.
- A large aspect ratio of the sails. The leeward displacement of the CE with heel angle is larger for a high sail.
- A low stability. Hulls with low stability obviously heel more and cause a larger displacement to leeward of the CE.

We recommend the geometric method for finding the CLR of long keel yachts. The lead, in percentage of  $L_{WL}$ , should then be as follows:

- Masthead sloops: 12–16%
- Sloops with a fractional rig: 10–14%
- Ketches: 11–15%.

For fin-keel yachts the extended keel method proposed here (Fig 9.2) should be used. The following leads are then recommended:

- Masthead sloops: 5–9%
- Sloops with a fractional rig: 2–6%.

The lead for the YD–41 is 2.2%.

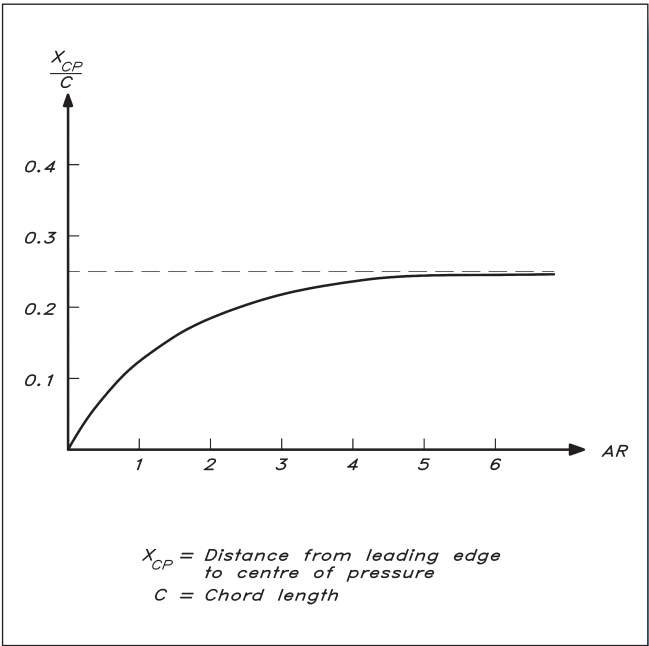
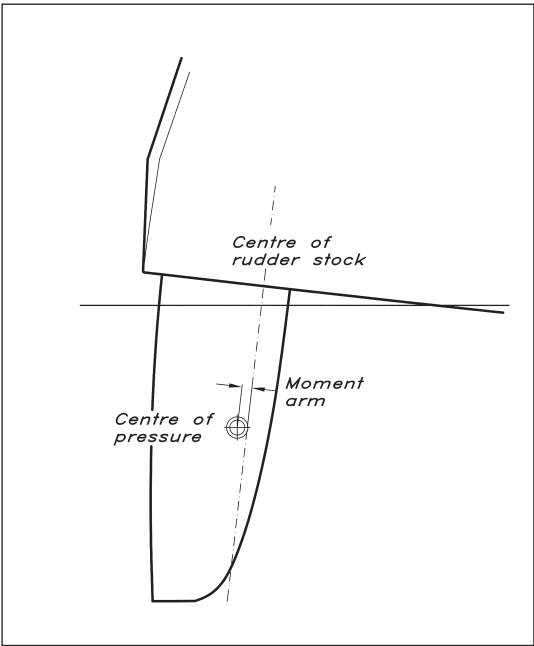
## ■ RUDDER BALANCE

Since the yacht should have a certain weather helm, it could be quite tiresome to steer it for long periods of time if the rudder is not properly balanced. The moment on the rudder stock is equal to the side force developed, multiplied by the distance between the centre of the stock and the centre of pressure (see Fig 9.5). The position of the centre of pressure may be obtained from Fig 9.6 for the actual aspect ratio. Note that for a rudder hung below the bottom of the hull the effective aspect ratio is twice the geometric one (as explained in Chapter 6). It is seen in the figure that the centre of pressure moves towards the leading edge when the aspect ratio goes to zero.

It is of the utmost importance that the rudder is not over-balanced (i.e. has its centre of pressure forward of the rudder stock centre), since it will then become unstable. A suitable location is 50 mm behind the centre of the stock. This will give a good feeling for the rudder force, without tiring the helmsman.

Fig 9.5 (LEFT) Rudder balance

Fig 9.6 (RIGHT) Position of centre of pressure for plane wings of varying aspect ratio





# 10 PROPELLER AND ENGINE

Since most sailing yachts today have auxiliary power, it is important to consider the design of the propeller and the power required under different circumstances. There may be three reasons for having an engine on a sailing yacht. First, yacht harbours are often crowded, and it is difficult to manoeuvre under sail in the limited space available. In some harbours it is not even permitted for safety reasons. Secondly, if sailing conditions are not perfect, many cruising skippers prefer to use the engine, particularly if they are short of time. Thirdly, the engine may be a life-saver under critical conditions in rough weather.

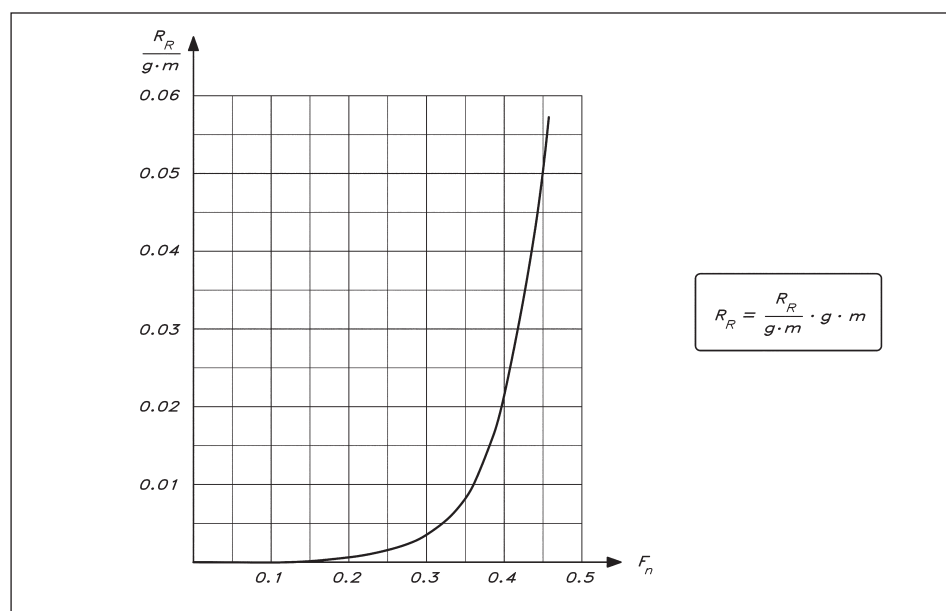
The first case does not put any major demands on the engine-propeller design, since only very limited power is required. It is important, however, that the propeller works reasonably well when going astern. In the second case, speed is an important factor, while in the third case enough thrust should be developed to escape from dangerous situations even against strong winds and heavy seas. These two latter cases put different demands on the propeller, and it is important to find a good compromise to achieve a reasonable performance in both situations. Perhaps the most important requirement is that the propeller allows the engine to work close to its optimum under severe weather conditions.

In the first part of this chapter we will consider the total resistance of the yacht. The contribution from the underwater part, i.e. the hydrodynamic forces, will be computed based on our discussion in [Chapter 5](#), while the aerodynamic drag will be obtained using formulae from [Chapter 8](#). Two cases will be considered: calm and rough weather. In the first case only the smooth water hydrodynamic resistance will be taken into account, while in the latter case the added resistance in a seaway will be added together with the windage from topsides, mast and rig. Having found the resistance under the two conditions we will show how the optimum propeller and the required power may be obtained under each condition. The final choice of the propeller has to be a compromise between the two requirements, and we must also consider what is available from manufacturers, both as to the propeller and the engine. After selecting a suitable combination we will investigate its performance. Finally, we will discuss the added resistance due to the propeller when sailing.

It should be pointed out that the calculations in the present chapter will be more approximate than those of [Chapters 5](#) and [6](#), in which the fine tuning of the yacht and appendages was discussed. To obtain a suitable propeller/engine combination this accuracy is not needed, and it is also very difficult to obtain, since many of the influencing factors are not known with great accuracy.

## ■ RESISTANCE IN CALM AND ROUGH WEATHER

Resistance was discussed extensively in [Chapter 5](#) (see [Fig 5.4](#) in particular). Since we are now interested in the upright case we can forget about heel and induced resistance, and if the hull is not too fouled we can also forget about the roughness drag. What is left in calm water is then the friction and the residuary resistance. How the friction is computed was explained in detail in [Fig 5.8](#), and the residuary resistance calculation was presented in [Figs 5.18](#) and [5.19](#). However, the formulae of the latter figures are quite complex and we could do with a more approximate estimate for the present case. As was pointed out in [Chapter 5](#), the residuary resistance, in percentage of the displacement, is more or less the same for all yachts at a given relative speed (Froude number), and we have plotted this approximate relation in [Fig 10.1](#). From [Figs 5.8](#) and [10.1](#) the reader can thus obtain an estimate of the resistance in calm weather.

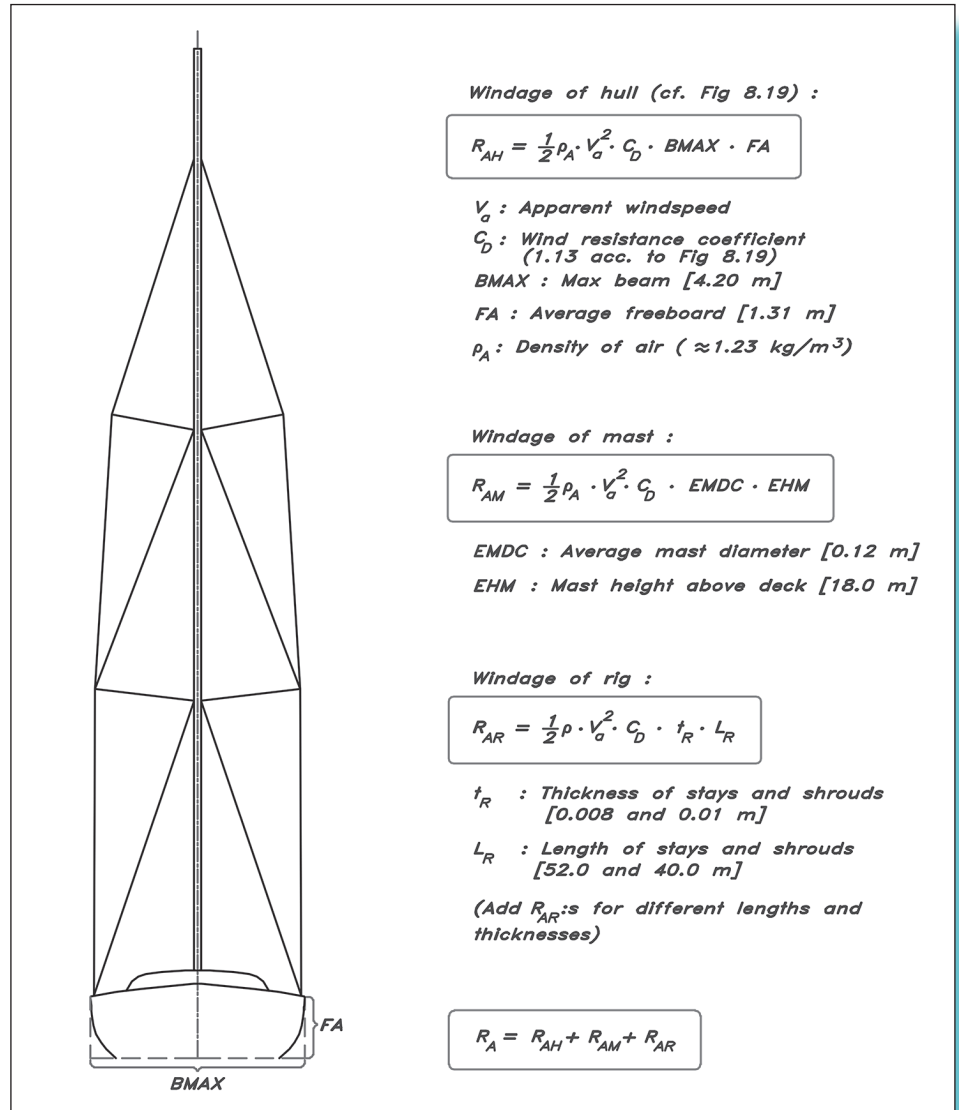


**Fig 10.1** Estimation of residuary resistance

In rough weather we also have the added resistance in waves (mentioned in [Chapter 5](#)), and the windage (discussed in [Chapter 8](#)). Let us start with the latter.

[Fig 10.2](#) gives the appropriate formulae for calculating the windage of the hull, mast and rig separately. In principle they have already been given in [Chapter 8](#), but they are repeated here for clarity. The frontal area of the hull and superstructure may be taken simply as the maximum beam times the average freeboard, and the drag coefficient is assumed to be 1.13 according to [Fig 8.19](#). For the mast the frontal area is taken as the mean diameter multiplied by the height above deck, and the drag coefficient is the same as for the hull, following the procedure of [Fig 8.19](#). This coefficient is also used for the stays and shrouds whose contributions from all parts of the rig have to be added. Most likely the total windage computed in this way is overestimated, but it is in accordance with the generally accepted procedure for sail force calculations in [Chapter 8](#). The main reason why

**Fig 10.2** Estimation of windage



the drag may be overestimated is the fact that the hull and a large part of the mast and shrouds for most yachts are exposed to a lower wind speed than the nominal one, which is measured at 10 m height. Note that it is only the straight upwind case that is of interest. Geometrical values for the YD-41 are given within square brackets, as usual, but no drag values are given, since the wind speed will vary in the example below.

In Fig 5.4 the added resistance in waves was computed for coastal waters with a wave height of 0.4 m and a mean wave period of 2.8 s. This corresponds to good weather sailing and the added resistance is quite small. Now, we are interested in rough weather and much worse conditions. We assume a significant wave height of 4 m and a wave period of 6 s. This corresponds to the conditions at 15 m/s in open, unsheltered areas, like the Skagerrak between Sweden and Denmark. In large oceans the wave period is larger, i.e. the waves are longer, and even if the waves are higher the added resistance is often smaller. Of course,

conditions worse than these may well be imagined, not least in shallow areas close to a windward shore, but it will be hard to optimize for these conditions without sacrificing the performance too much under more normal conditions. Since all necessary formulae are given in Chapter 5, the reader may well optimize for any conditions of interest.

The coefficients of Fig 5.27 are not available for straight upwind conditions (i.e. 180°), so the computations have been carried out for the wave angle 145°, corresponding to 35° from straight upwind. This may slightly underestimate the added resistance, but this approximation is small relative to the uncertainty of the appropriate wave climate.

Fig 10.3 shows the resistance computed for calm and rough weather cases. The three resistance components are added in the two tables, which give the total resistance at 8, 9 and 10 knots in calm weather and 6, 6.5 and 7 knots in rough weather. Note that the windage in calm weather is due to the motion through the still air. Results from the tables are presented in the graph.

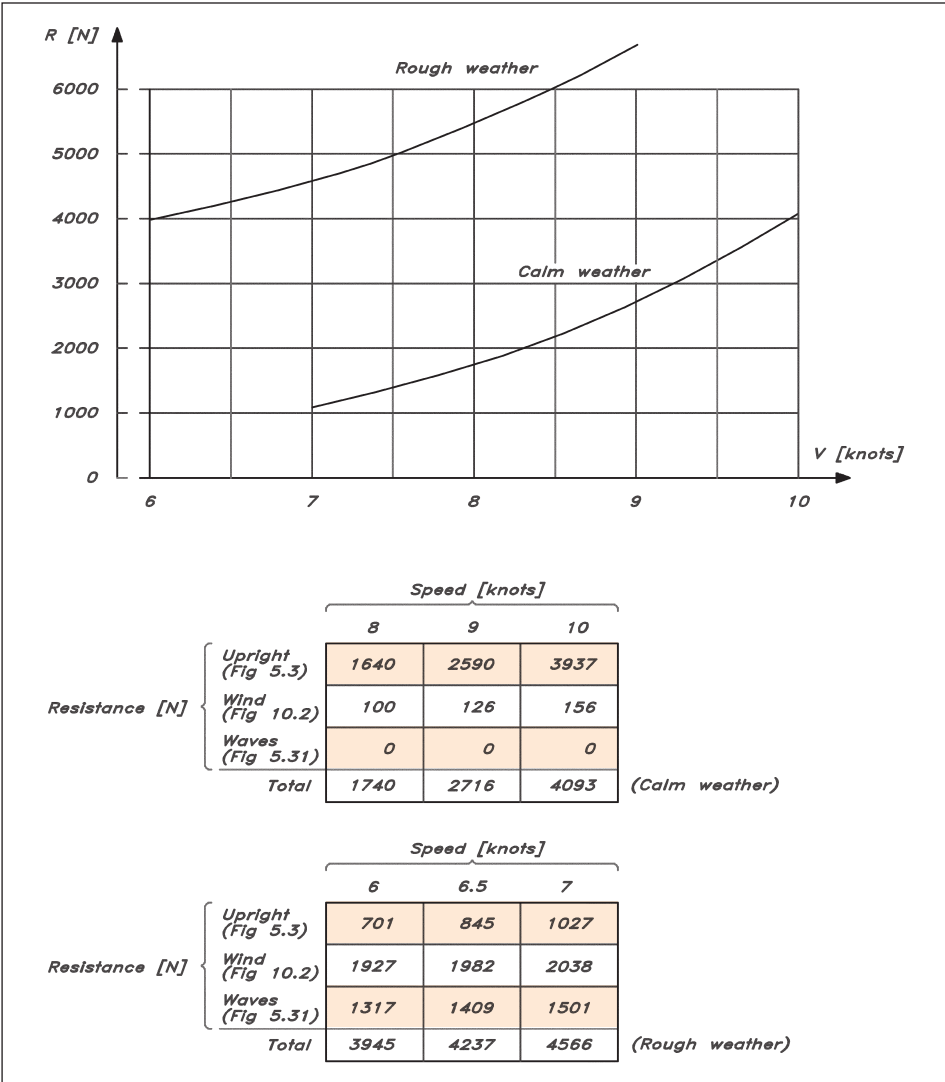


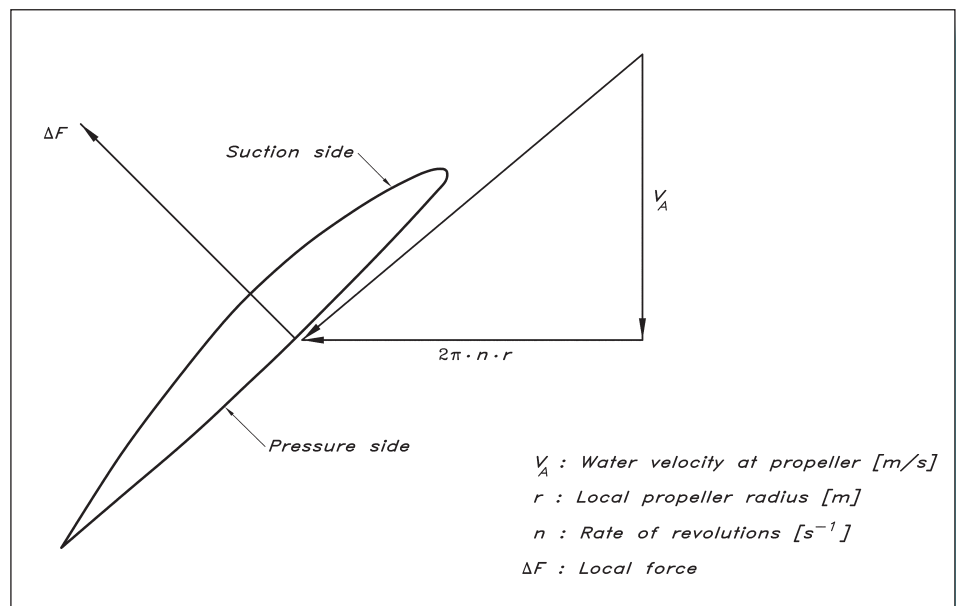
Fig 10.3 Resistance in calm and rough weather – YD-41

## ■ PROPELLER CHARACTERISTICS

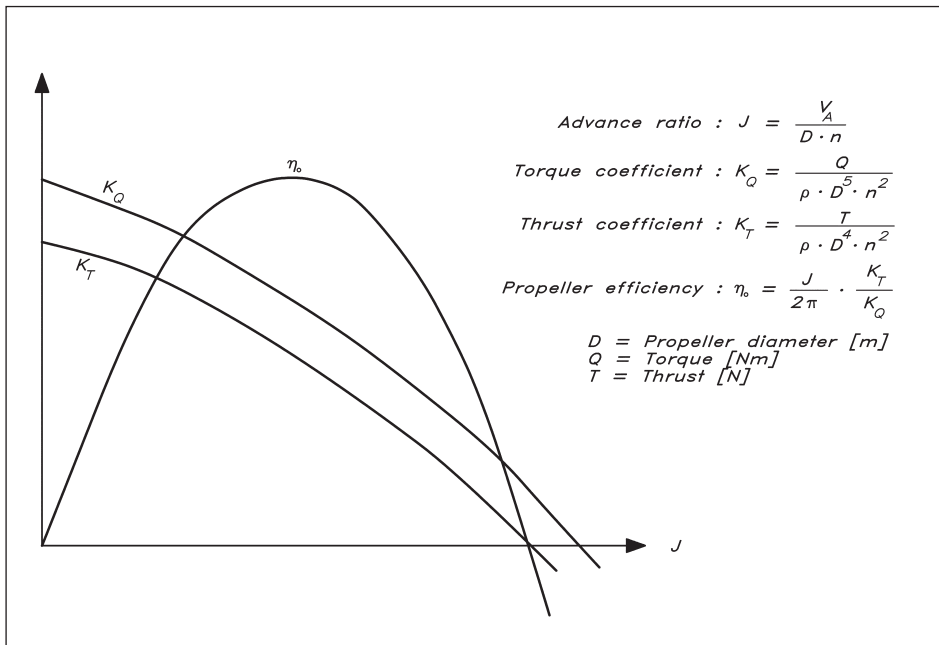
Propeller blades act as wings when the propeller rotates and advances through the water. A section of a blade at a certain radius is shown in Fig 10.4. It can be seen that the resulting velocity, to which the blade is exposed, is composed of the axial component (due to the forward motion) and the tangential component (due to the rotation). The former is normally not exactly equal to the yacht speed, but somewhat lower, since the propeller operates in the wake behind the hull. This effect can be quite significant for bluff ships, but for a sailing yacht with the propeller below the bottom of the hull it should be less than 10%, so we will neglect it in the following. The tangential component is proportional to the local radius and the rate of revolutions. It thus increases linearly with the radius, which means that the angle of the approaching flow gets smaller and smaller towards the tip. Therefore, the blades have to be twisted to become more and more at right angles to the propeller shaft further out. In fact, the propeller is normally designed so that the sections at all radii would advance the same distance for one turn of the propeller, had they been free from the others and cutting through a solid body. This distance is called the pitch, and is, together with the diameter, the most significant property of the propeller.

The pitch should be large enough to create a suitable angle of attack between the section and the approaching flow (as can be seen in Fig 10.4). A resulting force, more or less at right angles to the flow, is then developed. Had there been no resistance the angle would have been exactly  $90^\circ$ , but, since we have both induced and viscous resistance, the resulting force points more backwards (as explained in Chapter 6). The force has one component in the axial direction, the useful thrust, and one in the tangential direction, giving rise to an unwanted torque. These components may be made dimensionless in a similar way as described earlier for the various resistance components and the lift.

**Fig 10.4** Cut through a propeller blade



**Fig 10.5** Propeller characteristics



However, a typical velocity in the present case is the diameter multiplied by the rate of revolutions, and a typical area is the diameter squared. If these replace the normal velocity and area, a thrust coefficient may be defined as in Fig 9.5. To make the torque dimensionless the diameter should be raised to the 5th power in the denominator. The advance ratio, defined in the figure, is a measure of the angle of the approaching flow. By dividing the effective power (thrust times axial velocity) by the delivered power (torque times angular frequency), the efficiency of the propeller can be found. It may be expressed as seen in the figure.

The thrust and torque coefficients and the efficiency are called the propeller characteristics, and they are normally given as functions of the advance ratio (see Fig 10.5). To obtain this diagram the propeller is run in free water, often on a long shaft in front of a very slender hull containing the measuring equipment. Systematic variations in advance ratio are made either by varying the speed for a given rate of revolutions or vice versa. At zero speed a large thrust and torque are developed, but the efficiency is zero, since the propeller does not move forwards. At high speeds both the thrust and the torque go to zero, since the angle of attack of the blades goes to zero. At still higher speeds the propeller works as a turbine and negative thrusts and torques are developed. When the thrust is zero the efficiency is also zero. At some intermediate speed the efficiency reaches its maximum, and it is important to design the propeller for this condition.

A final remark should be made about Fig 10.4. Propeller specialists normally deal with the induced resistance in a way different to ours, as described in Chapter 6. In their approach, induced velocities from the trailing (helical) vortices are employed. If these were introduced, Fig 10.4 would be slightly more complicated. The methods are, however, equivalent and the following discussion is valid for both.

## ■ DESIGN OF AN OPTIMUM PROPELLER

To design the optimum propeller we need to know the advance velocity of the propeller, the thrust (or power) and the rate of revolutions. As we have already noted, the advance velocity is normally smaller than the speed of the yacht, due to the fact that the propeller operates in a wake. Considering the other approximations we will neglect this effect, which is small for a sailing yacht. Another approximation we will adopt is the assumption that the thrust of the propeller is equal to the total resistance of the yacht. This is not exactly true, since the propeller itself reduces the pressure around the stern, thereby increasing the resistance, but this effect should be very small for a yacht with the propeller below the hull and well in front of the stern.

There are several systematic series of propellers documented, but only a few of them include two-bladed propellers, which are of interest in connection with yachts. One series which does have two blades is the so-called Troost propeller series, developed and tested at the Netherlands Ship Model Basin (presently MARIN, Wageningen). The results are presented in the form of  $B_u$ - $\delta$  diagrams, where  $B_u$  is a thrust coefficient and  $\delta$  is an inverted advance ratio. Both are defined in Fig 10.6, which also explains the way to use the diagrams presented in Figs 10.7 (two blades) and 10.8 (three blades). (If the power is known, similar so called  $B_p$ - $\delta$  diagrams may be used.)

### Principles for using the $B_u$ - $\delta$ diagram

1. Compute  $B_u$  to obtain point 1 in Fig 10.6 (overleaf).
2. If optimum efficiency is requested, go to point 2 on the optimum curve.
3. Alternatively, if the propeller is already available, go to point 3, corresponding to the known pitch ratio  $P/D$ .
4. From point 2, go to the vertical axis and read the optimum pitch ratio.
5. Interpolate the efficiency between the  $\eta_0$ -curves at point 2 or 3.
6. Interpolate in a similar way between the  $\delta$ -curves.
7. Knowing  $\delta$  the advance ratio may be obtained from the definition of  $\delta$ , and from the advance ratio the diameter may be computed.
8. Finally, the delivered power may be found from the effective power (resistance  $\cdot$  speed) and efficiency. Note that this is the power available at the propeller. This is somewhat smaller than the nominal power of the engine, due to transmission losses. A 10% reduction is reasonable.

A suitable engine has to be selected from the product catalogue of an engine manufacturer. As a rough estimate, 4–5 kW per ton of displacement may be used for pure sailing yachts, while 5–7 kW per ton is appropriate for motor sailers. In the case of the YD-41, with a displacement of 6.5 tons the engine should have a power of around 26–33 kW. It is seldom possible to find an engine that exactly fits this requirement and we will assume in the following that the closest choice in our case delivers 30 kW at the shaft. The nominal



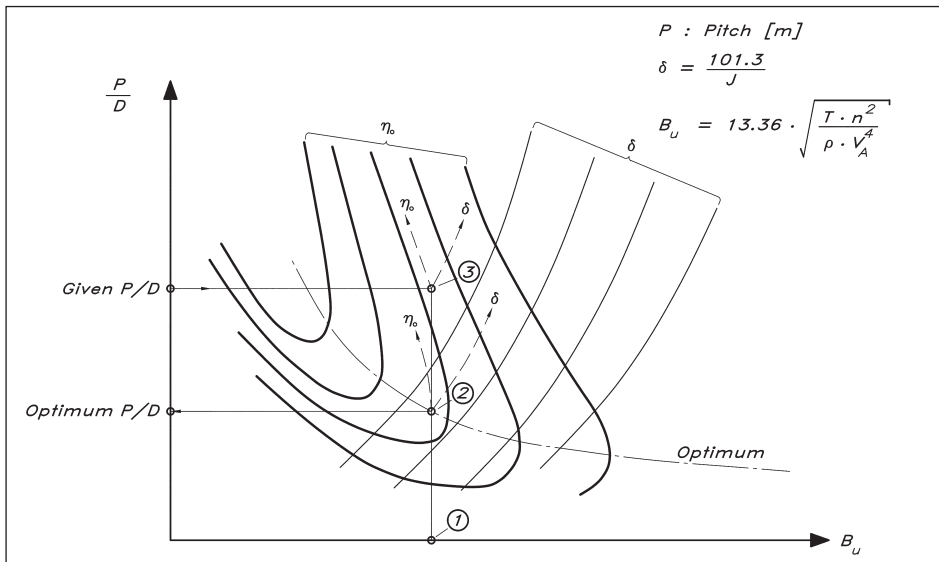


Fig 10.6 Principles for using the  $B_u$ - $\delta$  diagram

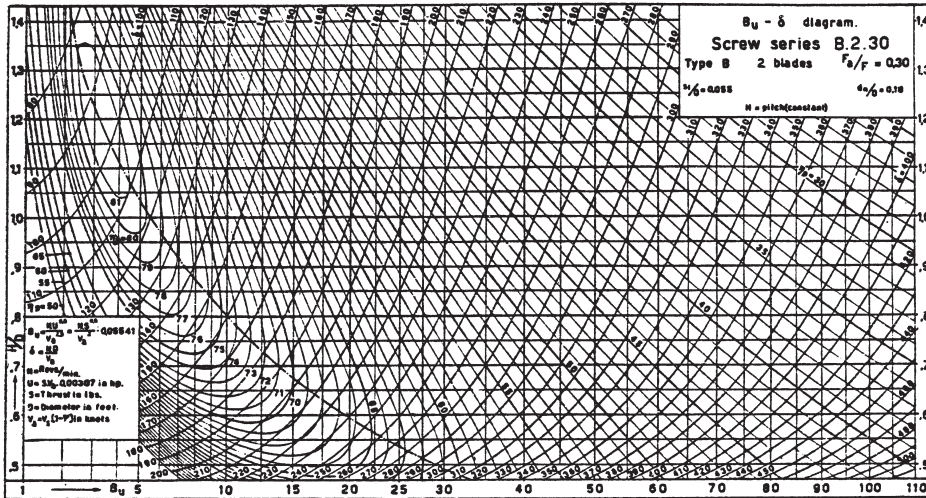


Fig 10.7  $B_u$ - $\delta$  diagram, two-bladed Troost propellers (courtesy of MARIN)

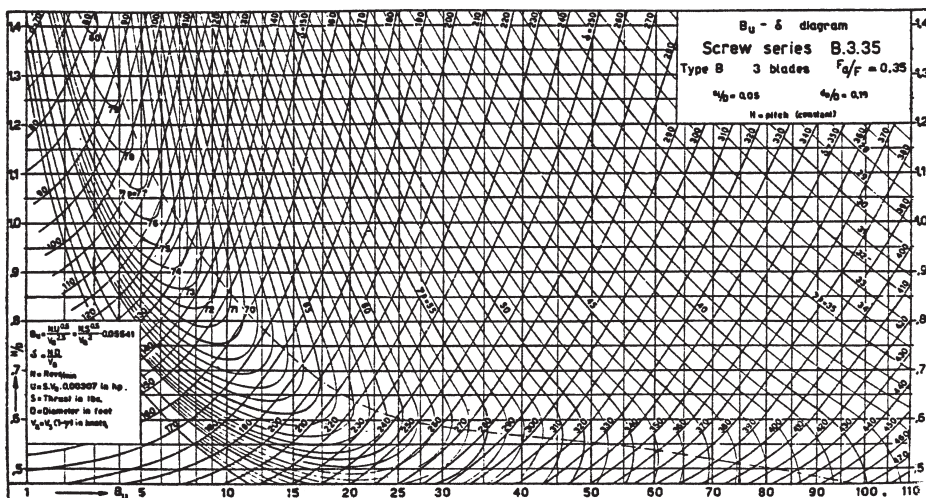


Fig 10.8  $B_u$ - $\delta$  diagram, three-bladed Troost propellers (courtesy of MARIN)

power of the engine is thus somewhat higher. We will also assume that this power is delivered at 3000 rpm and that the gear ratio is 2.5:1. This gives 20 revolutions per second of the propeller.

By computing the optimum propeller for different speeds it is possible to find the speed corresponding to the power available. Such a calculation is presented for the YD-41 in Fig 10.9. The speeds are the same as in Fig 10.3 for the calm and rough weather cases. In Fig 10.10 (overleaf) the computed results are displayed. The top figure (a) gives the power and the bottom one (b) the pitch and diameter. Since it turned out to be impossible to satisfy the cavitation requirements (see ‘Check of blade area’) with a two-bladed propeller the results are given for a three-bladed one, obtained using Fig 10.8. It is seen from the diagrams that the speed will be 9.77 and 6.76 knots, respectively, in the calm and rough weather cases. This yields an optimum diameter of 0.54 m for both conditions, while the optimum pitches are 0.34 m and 0.30 m. The differences between the two propellers are thus relatively small, and it should be possible to find a propeller that works well under both conditions.

**Fig 10.9** Design of optimum propeller – YD-41

	<i>Calm weather</i>			<i>Rough weather</i>		
$V_A = [\text{knots}]$	8	9	10	6	6.5	7
$V_A = [\text{m/s}]$	4.11	4.63	5.14	3.09	3.34	3.60
$T = [\text{N}]$	1740	2716	4093	3945	4237	4566
$B_u$	20.5	20.3	20.2	55.0	48.6	43.5
$\delta$ [diagram]	218	216	215	343	324	308
$D$ [m]	0.44	0.49	0.54	0.52	0.53	0.55
$P/D$ [diagram]	0.638	0.642	0.644	0.548	0.555	0.562
$P$ [m]	0.28	0.32	0.32	0.28	0.29	0.31
$\eta_b$ [diagram]	0.630	0.632	0.633	0.484	0.502	0.518
$P_D$ [kW]	11.4	19.9	33.2	25.1	28.2	31.7

Engine max :  $P_D = 30$  [kW] at  $n = 3000$  [rpm]

Gear ratio 2.5:1

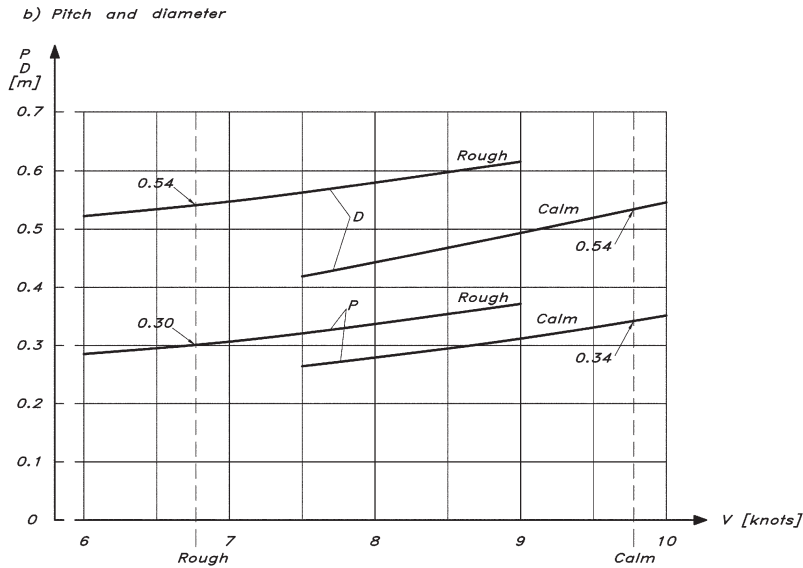
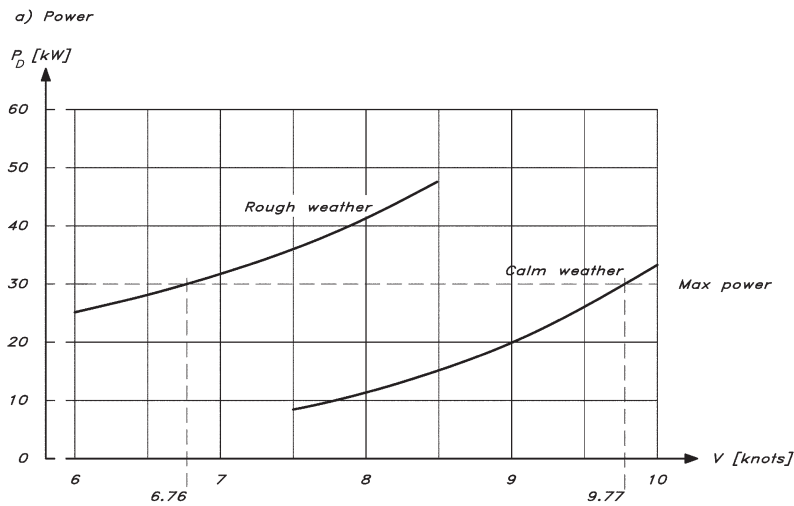
$$n = \frac{3000}{2.5 \cdot 60} = 20 \text{ [rps]}$$

$$B_u = 13.36 \cdot \sqrt{\frac{T \cdot n^2}{\rho \cdot V_A^4}}$$

$$D = \frac{\delta \cdot V_A}{101.3 \cdot n}$$

$$P_D = \frac{T \cdot V_A}{\eta_b}$$

Now we have to look again at what is available, in this case from the propeller manufacturers. There are three principally different types of propeller for sailing yachts: fixed, folding and vaning. As will be seen later, the folding propeller has superior drag properties when not in use, and it seems to be the most popular choice today. However, the only diagrams for propeller design that are available are for the fixed case, and we will have to use them even though we chose a folding propeller. The computed optimum diameter for the YD-41, around 0.5 m, is relatively large for this type and there is not much choice for this size from most manufacturers. As a general rule, the



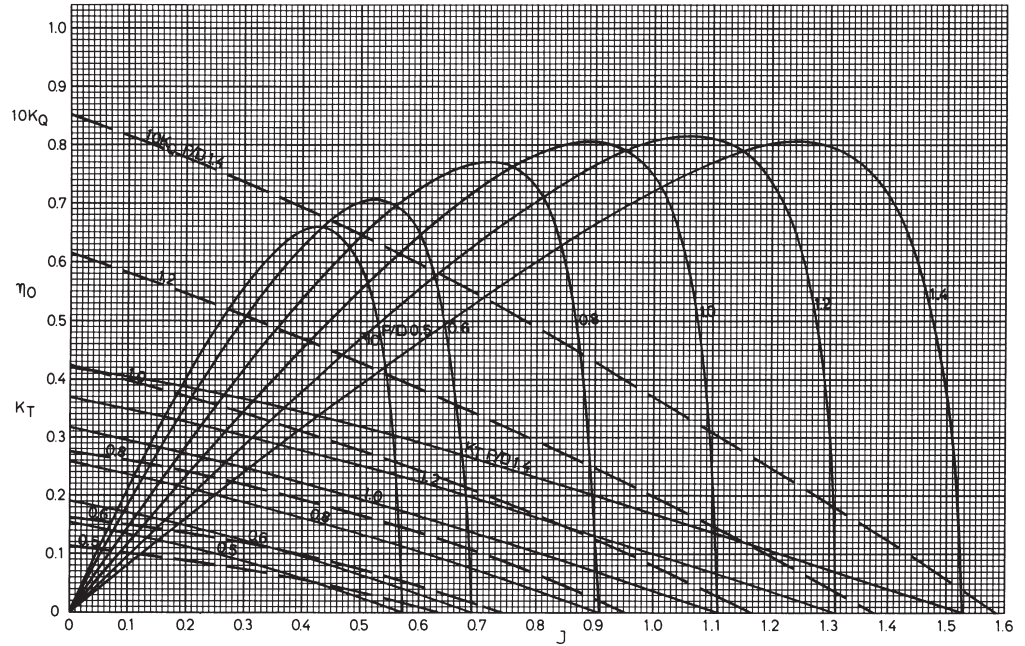
best compromise from an efficiency point of view is to select the propeller which comes closest to the requested one in terms of pitch multiplied by diameter, since that will load the engine approximately as much as computed for the optimum propeller. In our case we will assume that the best propeller we can find has a diameter of 0.56 m (22 in) and a pitch of 0.31 m (12 in). The pitch ratio is thus 0.55. We will now see how this non-optimum propeller performs.



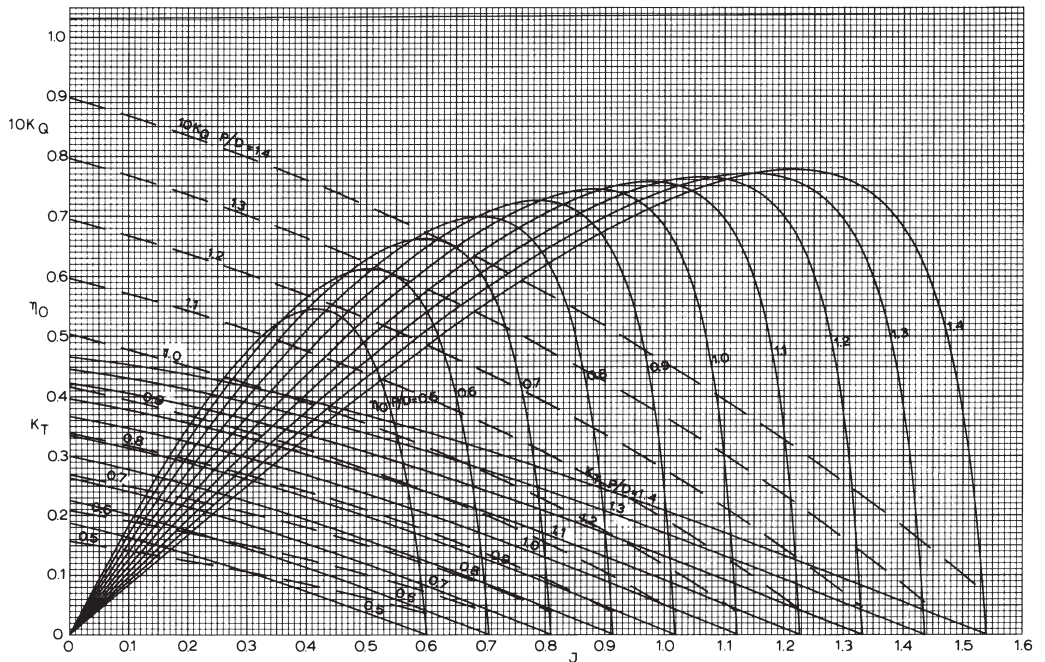
## ■ PERFORMANCE OF THE NON-OPTIMUM PROPELLER

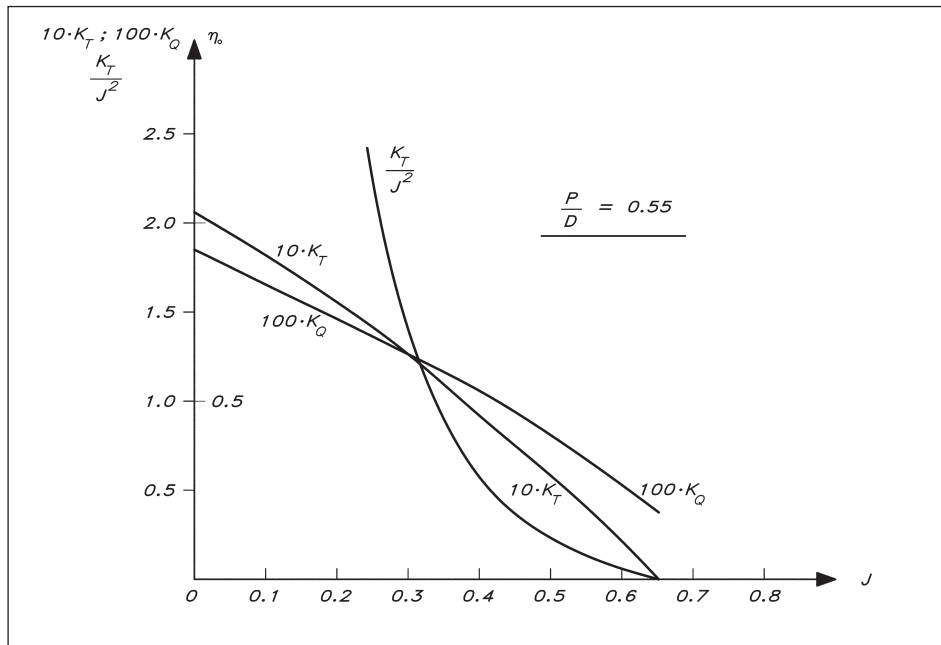
The propeller characteristics of three-bladed Troost propellers are given in Fig 10.12. This diagram is for a blade area ratio of 0.35, as was also the case for Fig 10.8. The blade area ratio is defined as the area of all blades together divided by the propeller disk area. We will return to the importance of this ratio later.

**Fig 10.11** Propeller characteristics, two-bladed Troost propellers (courtesy of MARIN)



**Fig 10.12** Propeller characteristics, three-bladed Troost propellers (courtesy of MARIN)





**Fig 10.13** Interpolated three-bladed propeller characteristics

To find the characteristics of the chosen propeller with a pitch ratio of 0.55, interpolation must be made between the curves of Fig 10.12. The characteristics thus obtained have been plotted in Fig 10.13. This diagram shall now be used to find the rate of revolutions and the power required for the propeller in question at different yacht speeds. These two quantities must match the output curve of the engine, as we will see.

If the thrust coefficient is divided by the advance ratio squared, a quantity independent of the rate of revolutions is obtained. This quantity,  $K_T$  divided by  $J^2$ , is often referred to as the propeller loading, and it can be computed from the characteristics. This has been done in Fig 10.13. The computation may now proceed as follows:

1. Assume that the velocity at the propeller is equal to the yacht speed, as before.
2. Compute the total resistance and assume that this is equal to the thrust, as before.
3. Compute the propeller loading,  $K_T$  divided by  $J^2$ .
4. Find the point on the loading curve in Fig 10.13 that corresponds to the computed value, and read the advance ratio and the torque coefficient on the same vertical line.
5. Compute the rate of revolutions from the definition of the advance ratio and the power from the torque and the angular frequency.

**Fig 10.14** Computation of power required for non-optimum propeller – YD-41

	Calm weather			Rough weather		
$V_A = V$ [knots]	8	9	10	6	6.5	7
$V_A = V$ [m/s]	4.11	4.63	5.14	3.08	3.34	3.60
$T = R$ [N]	1740	2716	4093	3945	4237	4566
$D$ (given) [m]	0.56	0.56	0.56	0.56	0.56	0.56
Coefficient	0.319	0.394	0.481	1.288	1.179	1.109
$J$ (diagram)	0.466	0.454	0.420	0.310	0.320	0.328
$K_Q$ (diagram)	0.0090	0.0093	0.0101	0.0124	0.0122	0.0121
$n$ [rps]	15.8	18.2	21.9	17.8	18.7	19.6
$P_D$ [kW]	12.5	19.9	37.6	24.8	28.3	32.3

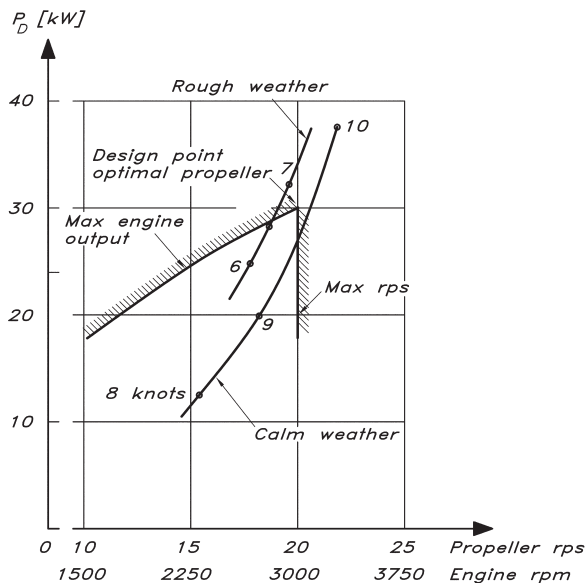
$$\text{Coefficient} = \frac{K_T}{J^2} = \frac{T}{\rho \cdot D^2 \cdot V_A^2}$$

$$n = \frac{V_A}{D \cdot J}$$

$$P_D = 2\pi \cdot K_Q \cdot \rho \cdot D^5 \cdot n^3$$

All formulae required are given in Fig 10.14, which also presents calculations for the YD-41 at the speeds used above. The results are plotted in the form of power versus rate of revolutions in Fig 10.15. Two curves are given, corresponding to the calm and rough weather cases. The limits for the engine are also indicated, representing the maximum engine output and the maximum rate of revolutions, respectively. The top corner of the ‘allowable region’ is the point for which the optimum propeller was designed, i.e. 30 kW and 20 rps.

**Fig 10.15** Engine and propeller power



The chosen propeller is a little too lightly loaded in calm weather, since the propeller diameter multiplied by the pitch is too small for this condition. This is seen in Fig 10.15 where the maximum rate of revolutions is reached at a power smaller than maximum. The opposite is true for the rough weather condition, where the propeller is somewhat too heavily loaded. It reaches the engine limit slightly below the maximum rate of revolutions, so only about 29 kW can be used. This is an unfortunate consequence of having to stick to available propellers, but the disadvantage is small in this case.

In principle, it is safer to have the rough weather curve to the right of the corner, meaning the power is limited by the maximum rate of revolutions. If, for some reason, the resistance goes up, the curve will move upwards, towards the corner and more power is available. In our case the available power drops somewhat if the resistance goes up.

## CHECK OF BLADE AREA

If the propeller is very highly loaded, the pressure on the suction side may get so low that the water evaporates, i.e. bubbles of vapour are created. If these are large the thrust is influenced and noise and erosion of the propeller blades occur. This is called cavitation. To avoid this problem the area of the blades carrying the thrust must be large enough. A simple check may be made using a method proposed by Burrill. We will describe this in the following discussion.

The relevant formulae are given in Fig 10.16. First, a cavitation number is defined. This is the 'margin' to cavitation at the propeller shaft in dimensionless form. The numerator thus contains the difference between the static pressure at the shaft and the vaporization pressure at the temperature in question, while the denominator is the dynamic pressure at

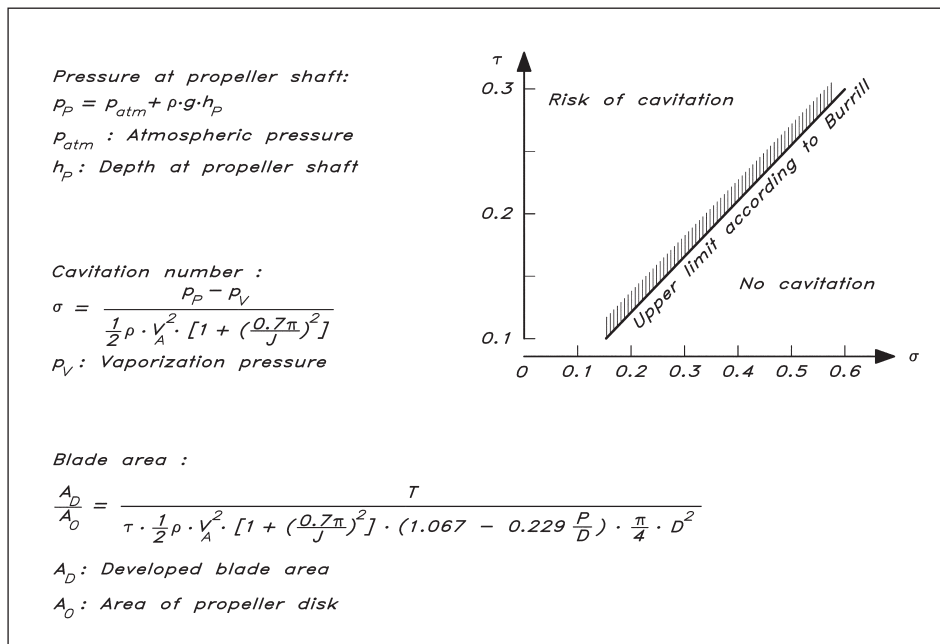


Fig 10.16 Burrill diagram



70% of the propeller radius. The static pressure at the shaft is the sum of the atmospheric and hydrostatic pressures at this depth, as shown in Fig 10.16.

Having computed the cavitation number, the diagram in Fig 10.16 may be used for finding the maximum value of the quantity  $\tau$  for non-cavitating conditions. This value is simply read from the line and used in the formula for the minimum blade area ratio. Note that this ratio is defined by the developed area, i.e. the sum of the areas of the blades considered 'flattened out and untwisted' and the area of the propeller disk.

In Fig 10.17 the blade area is checked for the YD-41. Computations are shown for 6.5 knots, which is the highest speed reached in Fig 10.15. Using the values of the table in Fig 10.14 and a propeller depth of 0.67 m, the minimum blade area ratio becomes 0.33. As we have already noted, the three-bladed Troost propeller had a ratio of 0.35, so this is large enough. Had the area been too small a larger diameter would have helped. A check was also done for 6 knots, but the requirement was smaller, only 0.31.

**Fig 10.17** Computation of blade area required – YD-41

*Calculation according to Fig 10.16*

$$h_p = 0.67 \text{ [m]}$$

$$P_{atm} = 101300 \text{ [Pa]}$$

$$P_p = 101300 + 1025 \cdot 9.81 \cdot 0.67 = 108037 \text{ [Pa]}$$

$$P_v = 2300 \text{ [Pa]}, \text{ at } 20^\circ \text{C}$$

$$\frac{P}{D} = 0.55$$

$$D = 0.56 \text{ [m]}$$

*Worst case – rough weather, 6.5 knots (see Fig 10.14):*

$$V_A = 3.34 \text{ [m/s]}$$

$$J = 0.32$$

$$T = 4237 \text{ [N]}$$

$$\sigma = \frac{108037 - 2300}{0.5 \cdot 1025 \cdot 3.34^2 \cdot [1 + (\frac{0.7\pi}{0.32})^2]} = 0.383$$

$$\tau = 0.20 \text{ (diagram Fig 10.16)}$$

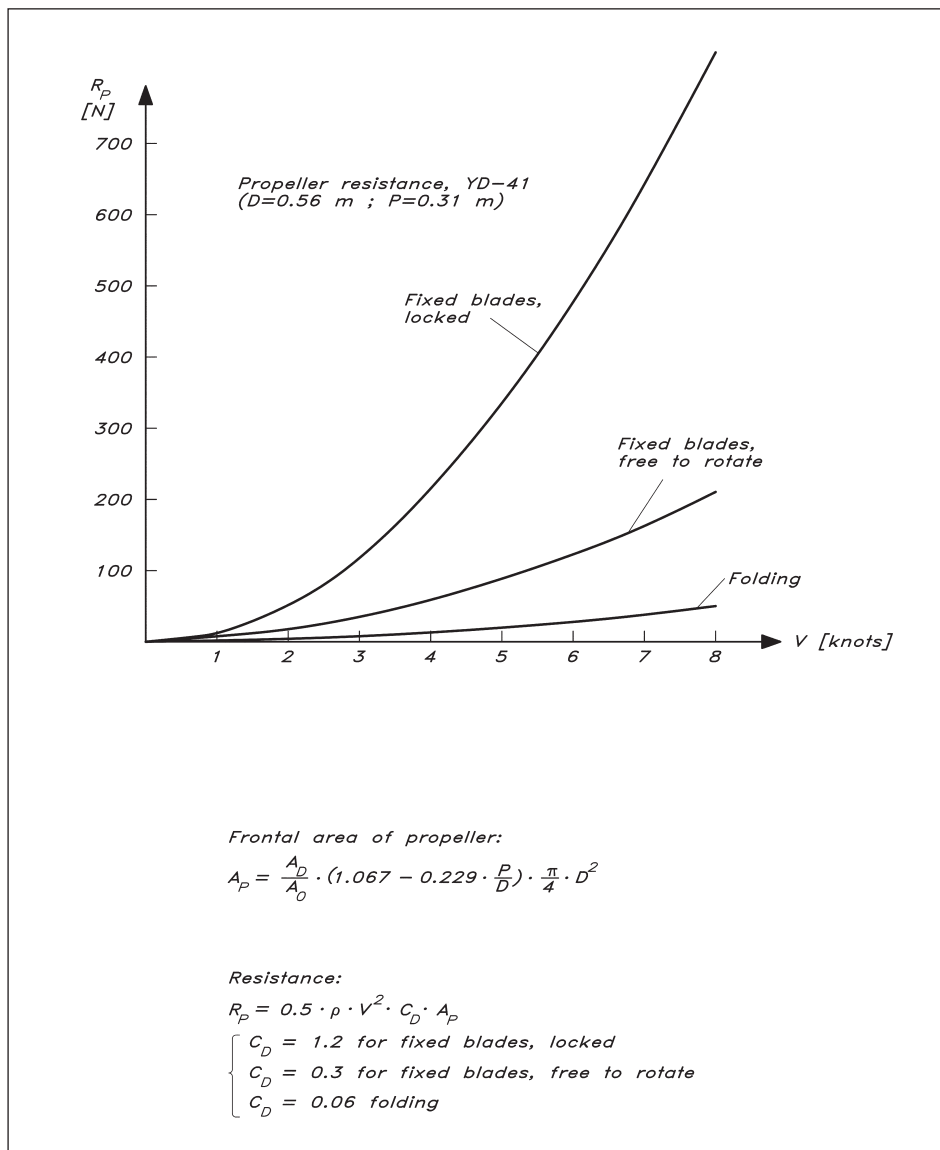
$$\frac{A_D}{A_0} = \frac{4237}{0.20 \cdot 0.5 \cdot 1025 \cdot 3.47^2 \cdot [1 + (\frac{0.7\pi}{0.326})^2] \cdot (1.067 - 0.229 \cdot 0.55) \cdot 0.25 \cdot \pi \cdot 0.56^2} = 0.33$$

## ■ PROPELLER RESISTANCE

The propeller resistance when sailing may be estimated using the frontal area of the propeller and some suitable drag coefficient. To obtain the area an approximate relation shown in Fig 10.18 may be used, and the drag coefficient for a fixed propeller, locked in position and outside the wake of the keel, may be set to 1.2. The resistance is then obtained easily as shown in the figure. If the propeller is completely free to rotate, its resistance is reduced to only about one fourth of that of a locked propeller. This is, however, an ideal situation. In practice the clutch and the friction will slow down the

rotation. Outstanding from a resistance point of view is the folding propeller with a resistance that is normally less than 5% of that of the fixed and locked one.

In Fig 10.18 the resistance of the YD-41 propeller has been plotted for varying speeds. If a propeller with fixed blades and locked in position were to be used, the resistance at the typical upwind sailing speed of 7.35 knots used in Fig 5.4 would be 700 N. This is almost half of the total resistance without propeller. If the propeller were completely free to rotate the resistance increase would be about 180 N. Most yachtsmen prefer to reduce the resistance even more and use a folding propeller, for which the resistance increase would be about 35 N, corresponding to an acceptable speed loss of about 0.07 knots.



**Fig 10.18** Propeller resistance when sailing

# 11

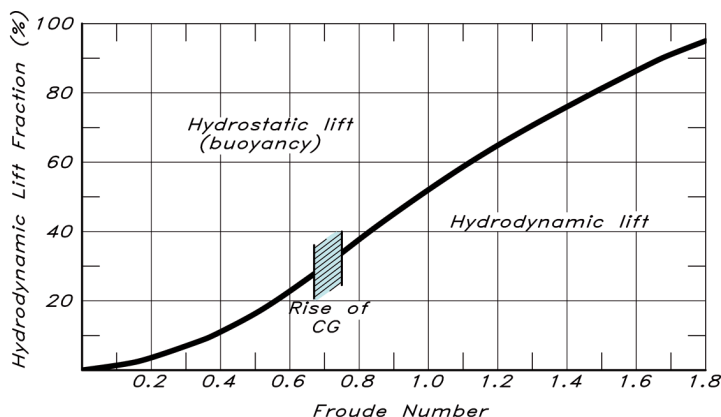
# HIGH-SPEED HYDRODYNAMICS

Although the emphasis of this book is on sailing yachts, much of the theory presented is the same for powerboats. There is no difference in the hull geometry definition or the principles for producing a drawing, manually or using a CAD system. The displacement of the yacht, as well as its static and dynamic stability properties, is computed in exactly the same way as for the sailing yacht. Neither is there any basic difference in the flow around the hull nor in the associated viscous and wave resistance components. The upright resistance may thus be obtained by the formulae presented in [Chapter 5](#) up to a Froude number of about 0.7 and the same is true for the added resistance in waves. Heel resistance is obviously irrelevant, but induced resistance as well as lift is of importance in the design of efficient powerboat rudders. Both planform and profile need to be considered. A reader only interested in powerboats can safely skip the two chapters on sails and balance, but should pay keen interest to the preceding chapter on propellers and engines.

An area not covered in the foregoing is the special hydrodynamics of high-speed craft, i.e. craft operating in the planing mode. Few sailing yachts reach this speed range, although some very special sailing craft like windsurfers or extremely light dinghies may be fast enough. Planing powerboats are, however, becoming more and more popular, and to satisfy the interested powerboat enthusiasts the present chapter on high-speed hydrodynamics has been included.

## ■ PLANING

According to Archimedes, the buoyancy of a body wholly or partly submerged in a fluid is equal to the weight of the displaced volume of fluid. The buoyancy, which is caused by the hydrostatic pressure in the fluid, was dealt with in [Chapter 4](#). At zero speed this force balances exactly the weight of a floating body. However, as soon as the body starts moving, the hull puts water particles into motion by exerting a force on each particle. The same force, but in the opposite direction, is exerted on the hull. This force per unit area may be called the hydrodynamic pressure. Although not distinguished in this way, we have seen this pressure in [Fig 5.4](#), and we have found in [Chapter 5](#), that it is responsible for both the viscous pressure resistance and the wave resistance. These two resistance components are caused by the longitudinal component of the pressure force over the hull surface. In the vertical direction the hydrodynamic pressure causes the hull to sink (or rise) and trim. At high speed this vertical pressure force may be considerably larger than the buoyancy,



**Fig 11.1** Distribution of hydrostatic and hydrodynamic lift components at varying Froude numbers (example)

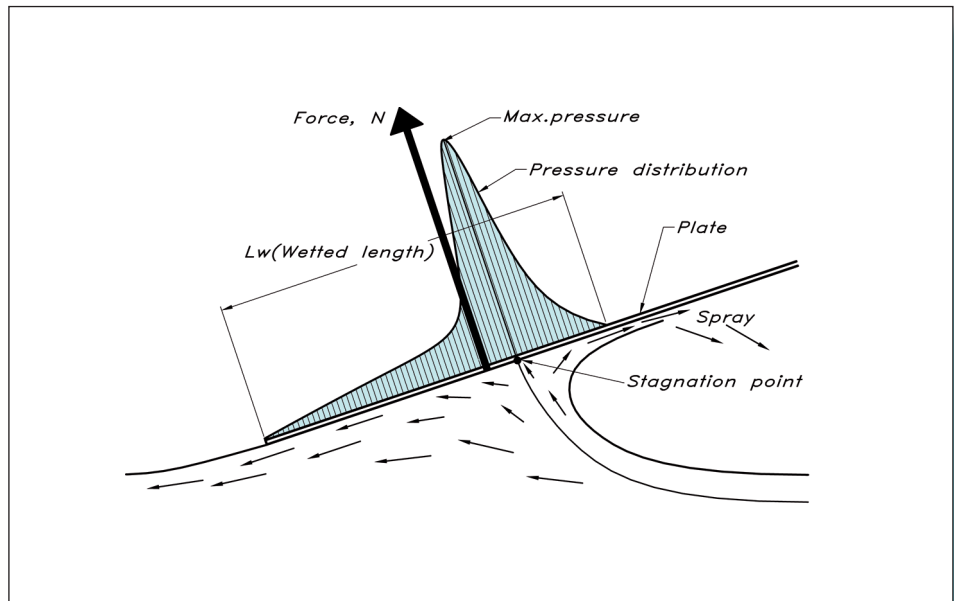
lifting the hull more or less completely out of the water. A hull predominantly supported by the hydrodynamic pressure is considered to be planing. Note that not all hulls may reach speeds high enough for this to occur. Fig 11.1 shows the hydrodynamic and the hydrostatic lift components for a typical high-speed hull at varying Froude numbers.

The basic principles of planing may be explained with reference to Fig 11.2, which shows the flow beneath a flat plate skimming along the water surface. Velocity vectors are displayed to show the direction of the flow relative to the plate. It is seen that at one point the flow hits the plate at right angles. This is the stagnation point, where the flow is divided into two parts, one going backwards and one forwards. At the stagnation point the pressure (hydrodynamic) is very high, since all the kinematic energy has been converted into pressure. There is no flow relative to the plate at this position. On both sides of the stagnation point the pressure is reduced and eventually it drops to zero. This happens at the trailing edge and at the forward location where the velocity has become parallel to the plate. Further forward the thin water sheet breaks down into spray, which drops down onto the water surface.

The high pressure creates a force at right angles to the plate, i.e. a force tilted backwards from the vertical at the same angle as the pitch angle of the plate. The vertical component is the lift, which has to balance the weight of the boat, while the horizontal component is the total pressure resistance, essentially the wave resistance.

The reality is somewhat more complicated than the idealized picture above. First, there is always some hydrostatic pressure present. Obviously this component is also at right angles to the plate and it adds to the pressure of Fig 11.2 (page 226). As appears from Fig 11.3, this means an increase in both lift and drag. There is thus a resistance component caused by the hydrostatic pressure. For a displacement hull the hydrostatic pressure forces acting backwards on the forebody are more or less balanced by those on the afterbody acting forwards. The latter forces are almost entirely missing on a planing hull where the transom is dry.

**Fig 11.2** Pressure and velocity distribution beneath a planing flat plate (principle)

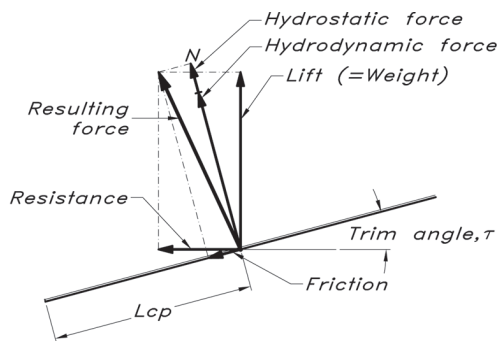


A second complicating factor is friction, which is parallel to the plate. Although there is some component in the forward direction in front of the stagnation point, the resulting frictional force essentially points backwards and increases resistance. There is also a small reduction in the lift force. It is interesting to note that if it were not for the friction the resistance of the plate would be uniquely defined by its weight (which is equal to the total lift) and the trim angle.

If the weight of the plate is changed the lift has to change correspondingly. A weight increase may thus be compensated by an increase in trim or wetted surface. In the latter case the plate is sunk a little deeper into the water and the friction is increased. To increase the trim angle the centre of gravity has to be moved backwards.

Savitsky at the Davidson Laboratory carried out a large series of systematic experiments for planing surfaces and proposed several general relations which are frequently used by designers of high-speed hulls. See Savitsky (1964). In Fig 11.3 a formula is found for computing the lift force, given the length to beam ratio of the wetted surface and the trim angle. Note that the beam is used as a reference length in the speed coefficient (corresponding to the Froude number) and the lift coefficient. The first term in the lift formula is the contribution from the hydrostatic contribution, while the second one is the hydrodynamic pressure.

At first glance it may appear as if both contributions to the lift would increase with an increasing length to beam ratio. However, this holds only for a lift coefficient which has been obtained by dividing by beam squared. Had this coefficient been defined in the usual way by the wetted surface the first term would have decreased with length to beam ratio. A wide and short planing surface is thus more efficient in generating dynamic lift than a long and narrow one. As we know from Chapter 6, this is also the case for wings. Wide hulls do, however, generate a much larger added resistance in waves, and in reality this puts a restriction on the beam.



**Fig 11.3** Forces on a flat planing surface

Lift according to Savitsky (neglecting friction):

$\lambda$  : Wetted length-beam ratio  $\frac{L_w}{b}$

$\tau$  : Trim angle [°]

$C_v$  : speed coefficient  $\frac{V}{\sqrt{g \cdot b}}$  (Beam Froude number)

$V$  : Speed [m/s]

$$C_{L_o} : \text{Lift coefficient} = \frac{m \cdot g}{0.5 \cdot \rho \cdot V^2 \cdot b^2}$$

$$C_{L_o} = \tau^{1.1} \cdot (0.012 \cdot \lambda^{0.5} + 0.0055 \cdot \frac{\lambda^{2.5}}{C_v^2})$$

Centre of pressure:

$L_{cp}$  : Distance from centre of pressure to trailing edge [m]

$$\frac{L_{cp}}{L_w} = 0.75 - \frac{1}{\frac{5.21 \cdot C_v^2}{\lambda^2} + 2.39}$$

Fig 11.3 also gives Savitsky's formula for the location of the centre of pressure of the planing surface. This location is important when determining the trim angle of a powerboat, as will be seen below.

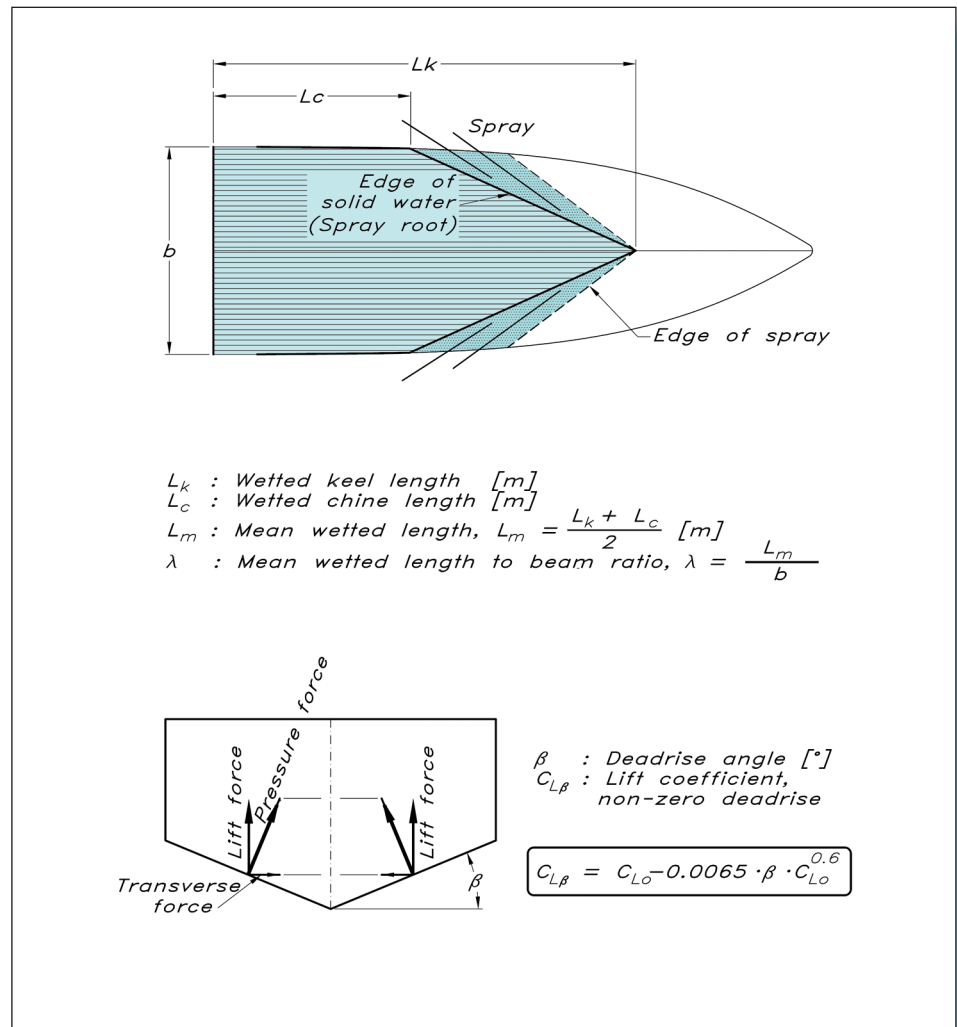
## DEADRISE

A flat plate skimming along a water surface may be useful for explaining the basic principles of planing, and it may be of interest for surfboards and water skis, but powerboat hulls almost inevitably have V-shaped sections, i.e. a so-called deadrise. The reason for this is the seakeeping qualities of the hull. A completely flat bottom would be impossible in a seaway, since the vertical accelerations would be too large. The ride would be extremely bumpy and put people on board in danger. V-shaped sections reduce the problem considerably; the deeper the V, the smaller the accelerations. However, the deadrise reduces the lift, so a larger wetted surface or trim angle is required, which both increase resistance.

The reason why deadrise reduces the lift force is that the water that hits the bottom of the boat may now be deflected sideways. In fact, for a normal deadrise angle most of the spray goes this way. As explained above, the hydrodynamic pressure that lifts the boat is caused by the reaction forces from the water particles which have been forced to change their direction when approaching the hull. For a flat plate the change in direction is almost  $180^\circ$  in the part of the flow in front of the stagnation point (see Fig 11.2). This results in high pressure. If the spray goes out sideways, however, the change in direction is much smaller and so is the reaction force. Further, this force is now tilted inwards, so a useless transverse component appears; see Fig 11.4, which also provides a formula for the change in lift due to the deadrise.

To understand the advantageous effects of the deadrise when it comes to seakeeping accelerations, compare the impact of a wedge hitting the free surface with that of a flat plate. In the latter case the entire surface of the plate hits the water simultaneously, while the wedge surface gets immersed gradually. The reaction force thus builds up much more slowly for the wedge.

**Fig 11.4** The influence of deadrise on spray and pressure forces





**Fig 11.5** Calculation of the frictional resistance of the hull

*Frictional resistance:*

$R_f$  : Friction [N]

$S_w$  : Surface wetted by water and spray [ $m^2$ ]

$C_F$  : Skin friction coefficient (see Fig. 5.8)

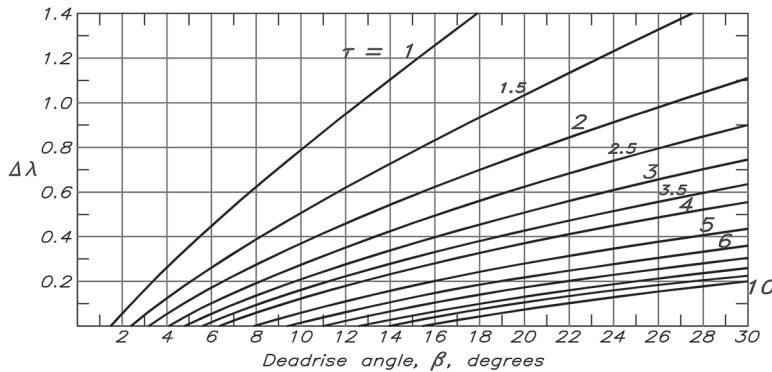
$\Delta\lambda$  : Increase in wetted length-beam ratio due to spray

$$R_f = C_F \cdot 0.5 \cdot \rho \cdot V^2 \cdot S_w$$

$$S_w = \frac{Lm}{b} \cdot b \cdot \frac{b}{\cos \beta} = (\lambda + \Delta\lambda) \cdot \frac{b^2}{\cos \beta}$$

$$R_f = C_F \cdot 0.5 \cdot \rho \cdot V^2 \cdot (\lambda + \Delta\lambda) \cdot \frac{b^2}{\cos \beta}$$

$\Delta\lambda$  is obtained from the following figure



Lever arm for  $R_f$  : ( $ff$  and  $VCG$ , see Fig. 11.6)

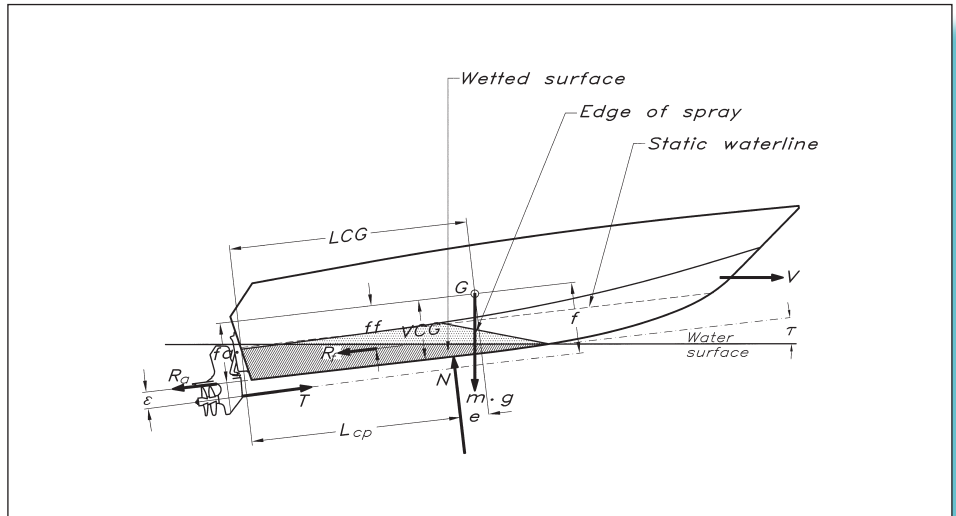
$$ff = VCG - \frac{b}{4} \cdot \tan \beta \text{ [m]}$$

The spray from a bottom with deadrise normally increases the frictional resistance, since most of the spray actually goes backwards. Savitsky measured this effect and devised a spray correction to the wetted length to beam ratio. This correction is shown graphically for different deadrise and trim angles in Fig 11.5, which also gives the appropriate formulae for computing the frictional resistance.

## FORCES ON A PLANING HULL

Fig 11.6 shows a planing hull with the most important forces acting on the hull displayed.  $N$  corresponds to the pressure force in Fig 11.3 (hydrostatic and hydrodynamic contributions) and  $R_f$  is the friction. There is also the propeller thrust  $T$  and the resistance of the propeller drive, denoted  $R_a$ , where the index 'a' stands for appendage. For a hull with a propeller on a shaft the resistance from all appendages like the shaft, shaft brackets and rudder must be considered. Useful formulae for streamlined shapes and inclined

**Fig 11.6** Forces on a planing hull



**Fig 11.7** Appendage resistance

*Resistance of rudders and brackets:*

$R_r$  : Rudder or bracket resistance [N]  
 $S_r$  : Wetted surface [ $m^2$ ]  
 $C_{Fr}$  : Skin friction coefficient (see Fig. 5.8)  
 $\frac{t}{c}$  : Thickness to chord length ratio

$$R_r = 0.5 \cdot \rho \cdot V^2 \cdot S_r \cdot C_{Fr} \cdot \left[ 1 + 2 \cdot \frac{t}{c} + 60 \cdot \left( \frac{t}{c} \right)^4 \right]$$

*Resistance of propeller shaft:*

$R_{sh}$  : Shaft resistance [N]  
 $l$  : Shaft length in water [m]  
 $d$  : Shaft diameter [m]  
 $\varepsilon$  : Shaft angle relative to flow [°]  
 $C_{Fsh}$  : Skin friction coefficient based on shaft length

$$R_{Fsh} = 0.5 \cdot \rho \cdot V^2 \cdot l \cdot d \cdot (1.1 \cdot \sin^3 \varepsilon + \pi \cdot C_{Fsh})$$

circular cylinders are given in Fig 11.7. The direction of the appendage forces varies somewhat, but without too much loss in generality they may be assumed parallel to the keel line. Some lift may be generated by the appendages, particularly the shaft, but this is neglected in the following.

The weight is shown as a force  $mg$  acting vertically through the centre of gravity  $G$ . To compute the moments this point may be taken as the origin. It is seen that  $N$ ,  $R_r$  and  $R_a$  create a moment to trim the boat by the bow and that their respective lever

arms are  $e$ ,  $f_f$  and  $f_a$ . The propeller thrust, on the other hand, creates a bow-up moment with the arm  $f$ . The hull automatically attains a trim angle where the moments cancel, i.e. the net moment is zero. Thus, for example, if there is a net moment to trim the boat by the bow the trim will become smaller and the force  $N$  moved forwards until balance is achieved.

If a bow-down moment is applied to a hull originally at an optimum trim angle, the new, smaller trim means that the hydrodynamic pressure is reduced. On the other hand, the wetted surface is increased, so it may be that the lift is still large enough. If it is not, the hull will sink down until the increased hydrostatic buoyancy will make up for the loss in hydrodynamic lift. In both cases there is an increase in friction that outweighs the advantage of having the force  $N$  pointing less backwards. This situation occurs if the centre of gravity is too far forward.

If the centre of gravity is too far aft, a net moment to trim the boat by the stern will increase the trim, thereby increasing the pressure and reducing the wetted surface. The hull rides higher, which is good, since friction is reduced, but the larger drag component of the force  $N$  makes the total resistance larger. When the centre of gravity is too

*Bow-down moment ( $M$ ):*

$$M_h = g \cdot m \cdot \left[ \frac{e \cdot \cos(\tau + \varepsilon)}{\cos \varepsilon} - f \cdot \frac{\sin \tau}{\cos \varepsilon} \right]$$

$$M_f = R_f \cdot \left[ f_f - e \cdot \tan \varepsilon - \frac{f}{\cos \varepsilon} \right]$$

$$M_a = R_a \cdot \left[ f_a - e \cdot \tan \varepsilon - \frac{f}{\cos \varepsilon} \right]$$

$$M = M_h + M_f + M_a \quad [\text{Nm}]$$

*Linear interpolation between two computed moments,  $M_1$  and  $M_2$ , at two trims,  $\tau_1$  and  $\tau_2$ , to find  $\tau_0$ , giving zero moment:*

$$\tau_0 = \tau_1 - \frac{M_1 \cdot (\tau_2 - \tau_1)}{M_2 - M_1}$$

*Linear interpolation between two computed frictional resistance values  $R_{f1}$  and  $R_{f2}$  to find  $R_{f0}$  corresponding to the trim angle  $\tau_0$*

$$R_{f0} = R_{f1} + \frac{R_{f2} - R_{f1}}{\tau_2 - \tau_1} \cdot (\tau_0 - \tau_1)$$

*Resistance:*

$$R = [g \cdot m \cdot \sin \tau_0 + R_f] \cdot \frac{\cos(\tau_0 + \varepsilon)}{\cos \varepsilon} \quad [\text{N}]$$

*Effective power*

$$P_E = V \cdot R \quad [\text{W}]$$

**Fig 11.8** Moments, trim and resistance

far aft, an instability often occurs. Increasing the trim, the force  $N$  moves too far aft, causing a bow-down moment. The bow falls down, and the process is repeated. We have a porpoising boat, a phenomenon not that uncommon. It is thus very important to design the boat to achieve equilibrium at the reasonable trim angle, and a procedure for calculating trim and resistance is described below. This scheme is a simplification of a procedure proposed by Hadler (1966), based on Savitsky's previous work. Hadler's original paper includes the effect of the propeller on the pressure forces on the hull and a procedure for correcting the propeller characteristics for the shaft inclination relative to the flow. Some lift forces on the appendages are also included. These effects are neglected here, as well as the air resistance. Although Hadler's work is old it still seems to be the most accepted procedure for planing hull predictions.

### Procedure for finding the equilibrium trim angle and the corresponding resistance and power

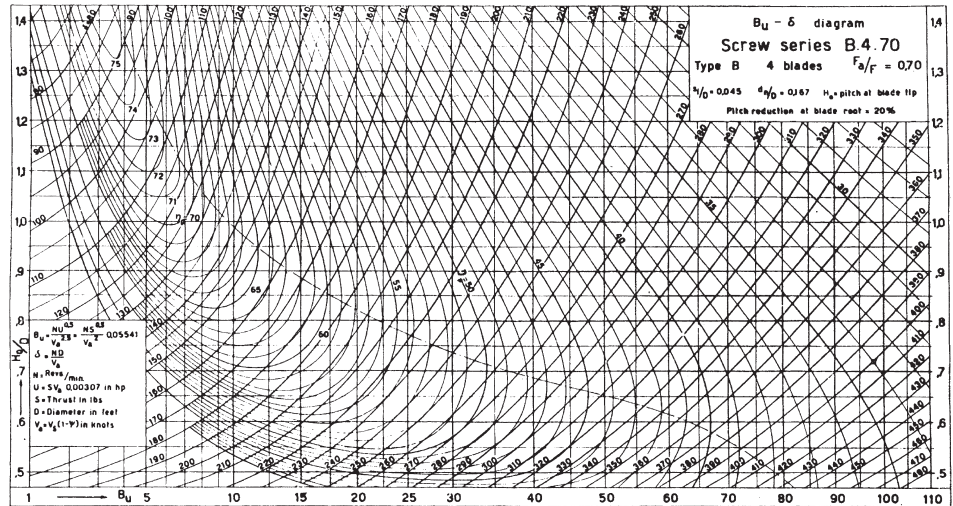
1. First determine the following quantities:  
 $m$ : Mass displacement  
 $LCG$ : Distance from transom to centre of gravity  
 $VCG$ : Distance from baseline (keel) to centre of gravity  
 $b$ : Maximum beam between chines (or between spray rails; see the next section)  
 $\epsilon$ : Propeller shaft inclination relative to baseline  
 $\beta$ : Deadrise angle (take the average of the angles at the transom and at the CG)  
 $f$ : Distance between shaftline and centre of gravity  
 $V$ : Speed
2. Compute the speed coefficient  $C_v$  (Fig 11.3).
3. Compute the lift coefficient from its definition in Fig 11.3 (i.e. use the formula including  $m$  and  $g$ ). In Fig 11.3, which is for flat plates, this gives  $C_{L0}$  but for a hull with a deadrise it will give  $C_{LB}$ .
4. Compute the corresponding  $C_{L0}$  from formula for  $C_{LB}$  (Fig 11.4) by trial and error, i.e. try to find the  $C_{L0}$  that gives the  $C_{LB}$  computed in step 3.
5. Assume a trim angle  $\tau$ , say  $4^\circ$ .
6. Compute the wetted length to beam ratio  $\lambda$  from the framed formula for  $C_{L0}$  in Fig 11.3 by trial and error, i.e. try to find the  $\lambda$  that gives the  $C_{L0}$  obtained in step 4.
7. Compute the mean wetted length  $L_m$  from  $\lambda$  (Fig 11.4) and calculate the Reynolds number.
8. Compute the skin friction coefficient  $C_f$  using the ITTC formula (Fig 5.8).
9. Find the increase in  $\lambda$  due to spray,  $\Delta\lambda$ , and compute  $R_f$  (Fig 11.5).

10. Compute the lever arm  $f_r$  for  $R_r$  relative to the centre of gravity (Fig 11.5).
11. Compute the resistance  $R_a$  for all appendages according to the formulae of Fig 11.7.
12. Compute the lever arm's  $f_a$  relative to the centre of gravity of the hull. Assume that the force acts on the centroid of the wetted surface for each appendage and is parallel to the baseline.
13. Compute the distance of the centre of pressure from the transom,  $L_{cp}$ , from the formula in Fig 11.3 ( $L_w$  is equal to  $L_m$  for a bottom with deadrise).
14. Compute the lever arm for the pressure force,  $e$ , as the difference between LCG and  $L_{cp}$ .
15. Compute the resulting bow-down moment  $M$  from the formula of Fig 11.8. This equation is derived in Hadler's paper considering the horizontal and vertical force balance.
16. Most likely, the computed moment will be different from zero, so the trim angle has to be changed to obtain balance. Go back to step 5 and repeat the calculations with another trim. (If the computed bow-down moment is positive, reduce the trim angle and vice versa.)
17. Compute the trim angle for zero moment by linear interpolation (extrapolation) between the two computed moments. Use the formula of Fig 11.8.
18. Compute the frictional resistance at this trim angle by linear interpolation between the two computed values (Fig 11.8).
19. Compute the resistance from the formula of Fig 11.8.
20. Compute the effective power from the formula of Fig 11.8.

The effective power  $P_E$  is the power made good when driving the boat. To obtain the real power required to turn the propeller (the delivered power  $P_D$ ),  $P_E$  must be divided by the propulsive efficiency. In Chapter 10 the total propulsive efficiency was assumed to be equal to the propeller efficiency, which can be read from diagrams of the type presented in Figs 10.8 and 10.9. The same approximation may be adopted here. However, a more appropriate diagram in this case is that of Fig 11.9, which is for four-bladed propellers with an area ratio of 0.70. The procedure for designing an optimum propeller described in Chapter 10 may now be used, assuming that the resistance obtained above is equal to the propeller thrust. Note that we have now neglected the resistance increase in rough weather. This is permissible, since the boat cannot normally drive at full speed in rough weather anyhow.

Although the procedure described in this section includes several simplifications it should be useful for optimizing the trim angle and the corresponding location of the centre of gravity, as well as for estimating the required power. Normally a good target for the trim angle is  $4^\circ$ . Readers interested in more details are referred to Hadler's original paper (Hadler 1996).

**Fig 11.9**  $B_u$ - $\delta$  diagram, four-bladed propellers with an area ratio of 0.70 (courtesy of MARIN)

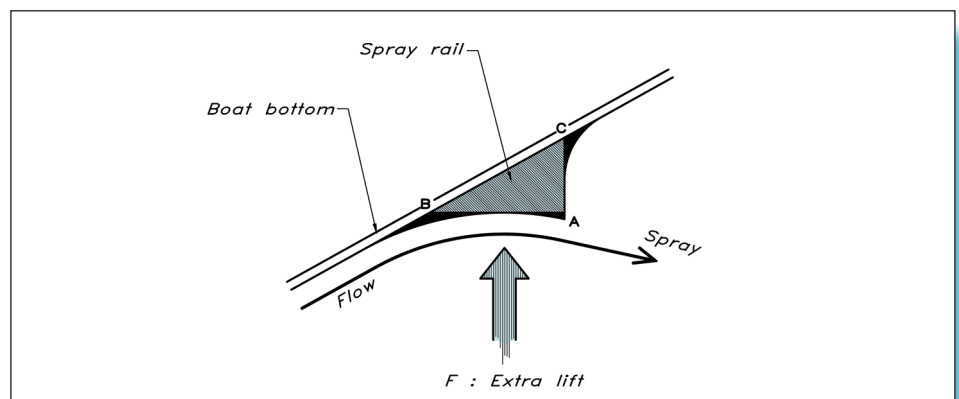


## ■ SPRAY RAILS, STEPPED BOTTOMS AND TRANSOM FLAPS

As we have seen above, a deep V-shape is good for seakeeping performance, but not very efficient in generating lift. One way to improve the lift production is to add spray rails along the hull. A typical cross-section of such a rail is shown in Fig 11.10. When the water flows sideways, as shown in Fig 11.4, it is forced to turn downwards by the rail. This creates a lift. The rail should be as sharp as possible at point A, where the water leaves the hull, but it should be smoothly blended into the main hull at point B to reduce resistance. In order not to create a larger resistance than necessary at speeds where the rail does not work, a smooth junction at C is also recommended. To increase the lift further, the surface between B and A may be inclined downwards.

Since the water runs sideways mainly on the forebody, the rails are most efficient in this region. Further back, where the flow is more or less parallel to the keel, they may be cut. Keeping them in this region may increase the resistance, but can be justified as providing anti-rolling results.

**Fig 11.10** Cross-section of a spray rail



Spray rails on a planing hull are shown [Fig 11.11](#). The wetted surface at two speeds is also indicated. If the speed will not exceed 25 knots it may be wise to cut the outer rail at D, since it will be useless further aft. However, if the hull may attain a speed of 40 knots the wetted surface must be reduced. Had the outer rail been cut, the water would have continued to clear the hull at the chine and the centre of pressure would have been moved too far aft. This would have caused the bow to fall, resulting in a larger resistance and also possibly steering problems. If the rail is kept all the way to the stern the wetted beam (between rails) becomes smaller, which means that the wetted length is not so much reduced when the speed increases. The centre of effort thus does not move that far backwards and the hull maintains its trim better. Note that the beam used in the calculations above is now the distance between the rails. There is no accurate procedure developed for the extra rail lift, but their effect may be roughly included by measuring the deadrise angle from the keel to the outer edge of the active rail. This angle is smaller than that measured along the surface and so yields a higher lift.

Spray rails should not be too effective on the forebody of the hull. If high lift is developed when the forebody hits a wave, large accelerations will occur, reducing the positive effect of the V-shape. Therefore, the rails should be made smaller in this region and the bottom side should be inclined upwards rather than downwards.

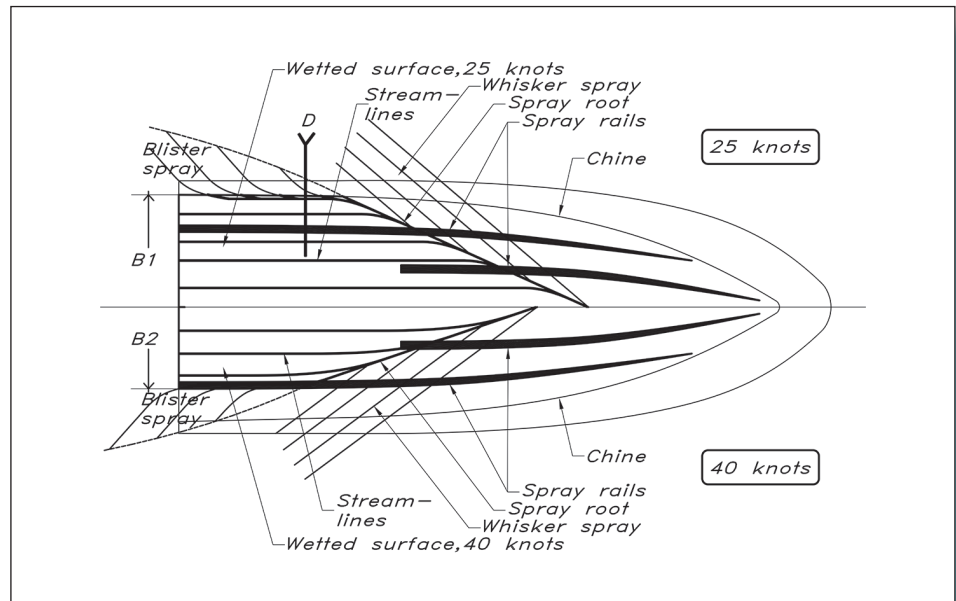
Stepped bottoms have been used for a very long time to improve performance. A very famous design was *Maple Leaf*, built in wood in 1912, and since then many successful racing hulls have had this type of bottom. The reason why stepped hulls are more effective is that the wetted area is divided into several smaller areas each with a large beam compared to the length; see [Fig 11.12](#). As we have seen above, the lift production is more efficient for a surface with a small length to beam ratio. (The planing bottom is different from a wing, where it usually does not help splitting the surface into several tandem wings.) The increased lift generation capability means that the total wetted surface may be reduced, as well as the friction.

[Fig 11.12](#) shows that the region behind each step has to be ventilated. Air thus has to be sucked into this region in sufficient quantities. Normally this is not a problem since the pressure is very low, but it is extremely important that the air supply is not cut. New air is continuously needed since the water entrains the air behind each step. This may be achieved most simply by extending the step sideways to the open air at the hull's side. However, this principle is somewhat dangerous, since these openings may be closed temporarily (and momentarily!) by waves. When the air supply is lost, a backflow occurs behind the step causing an excessive increase in resistance. The speed thus drops momentarily – a dangerous situation, which may even cause injuries to the crew. If the supply is cut only on one side, the hull will turn abruptly, and possibly even capsize. To avoid this problem, air is often sucked through openings well above the waterline, or it may be supplied through tubes from deck level. Another possibility is to discharge the exhaust gases through the step. In this way the gases will be sucked out, improving the efficiency of the engine.

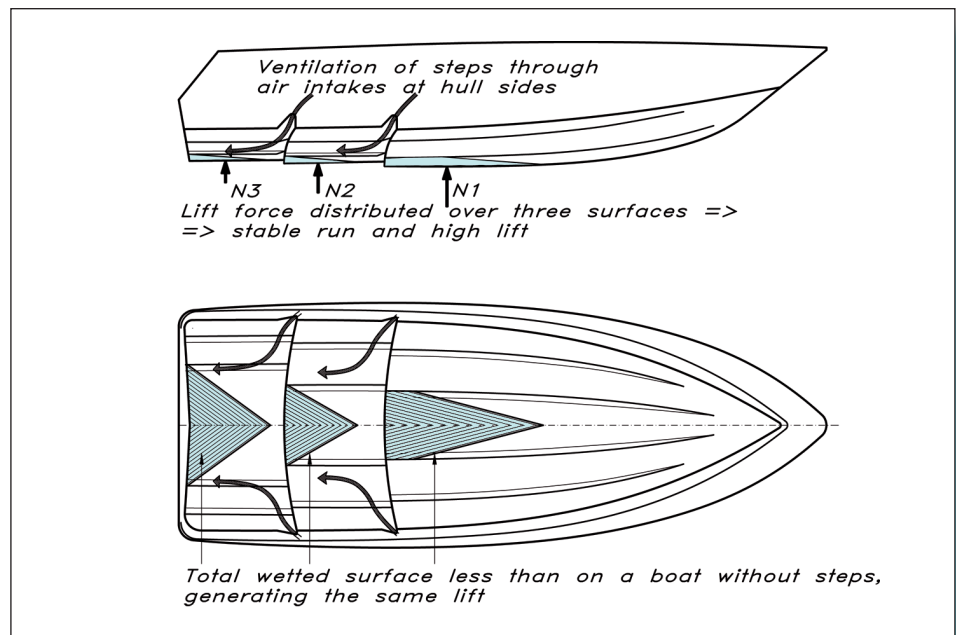
Since the lift is now spread to several surfaces along the hull (see [Fig 11.12](#)), the longitudinal stability becomes very large. It is difficult to change the trim. This is no problem in smooth water, but in a seaway the hull may tend to follow the contour of the waves. Larger hulls may acquire a tendency to bump into the next wave, making the ride



**Fig 11.11** Spray rails on a planing hull



**Fig 11.12** Hull with steps



very uncomfortable. Smaller boats, which tend to jump between the waves, are not so affected by this problem.

Another effect of spreading the lift to several efficient surfaces, one after the other, is that the transverse stability may be put in jeopardy. The hull rides high on a very narrow set of wetted surfaces. At very high speeds some designers have chosen to take advantage of the aerodynamics of the above-water part of the hull, using wing-like devices to keep the hull upright.

Transom flaps may be fitted to the hull to control the trim. Temporary adjustments for correcting changes in the centre of gravity may thus be made easily. The flaps may also be used to adjust the trim when the hull is running at off-design speeds, for instance in restricted waters or when the hull is under acceleration. This reduces the fuel consumption and, even more importantly, the generated waves, which may be excessive at these speeds. It is also possible to use the flaps for adjusting the trim in a seaway to reduce the bumpiness.

## ■ DYNAMIC STABILITY

There are two important dynamic stability phenomena for high-speed hulls. One is caused by the large centrifugal forces generated when a hull at high speed changes its direction. The other occurs due to the suction forces which may be generated near the chines due to convexity of the hull buttocks. We will deal with both in the following.

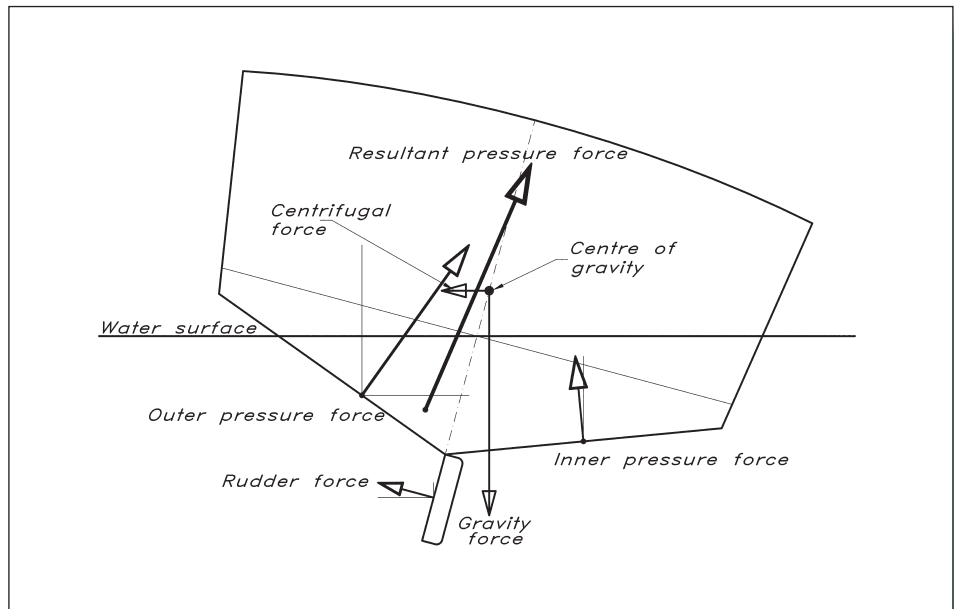
When the rudder is given an angle of attack a force is generated sideways. This causes the hull to start moving in this direction and, since the force is aft of the centre of gravity, the hull also starts to rotate. After a short while the hull has obtained an angle of attack to the flow and a side force opposing the rudder force develops, mostly on the forebody. Now the direction of motion has started to change; the path is curved. A centrifugal force directed 'outwards', i.e. in the same direction as the rudder force, is now gradually built up. (See [Fig 11.13.](#))

It is seen that the pressure force on the 'outer' side is larger than that on the 'inner' side. The difference in their horizontal components is the side force mentioned above. There is, however, also a vertical component, which is larger on the outer side and the resulting pressure force creates a moment (around the centre of gravity) that tends to heel the hull inwards. This moment is amplified by the rudder force. Taking the centre of gravity as the origin for the moment means that neither the gravity nor the centrifugal force contribute, so the total effect is a moment that will heel the hull inwards.

If the centre of gravity is moved upwards the resulting hull pressure force will soon pass through this point, thus creating no moment. At this stage, the rudder force still heels the hull inwards, but if the centre of gravity is moved still higher, the hull pressure forces will start heeling the hull outwards and at one position the moment from these forces will exactly balance the moment from the rudder. Now the hull does not heel at all. For any higher position of the centre of gravity the hull heels outwards.

Whether the hull is going to heel outwards or inwards thus depends on the height of the centre of gravity. Most planing hulls have their centre low enough to heel inwards, but some pleasure craft with a high flybridge may have it high enough to heel outwards, even dangerously so. For displacement hulls the pressure forces on the two sides are almost exclusively due to buoyancy, which is the same on the two sides (hull upright), thus creating no moment. The change in pressure force due to the turn is more or less horizontal and thus practically always directed below the centre of gravity. Even though the corresponding moment is to some degree compensated by the rudder, the result is a hull heeling outwards.

**Fig 11.13** Forces on a turning hull



The other type of dynamic instability, often called ‘chine walking’, occurs due to convexity of the buttocks. When a flow passes over a convex surface the pressure is reduced, and the larger the curvature, the lower the pressure. If the buttocks are too curved near the chine a suction force may develop. Of course, as long as the hull is exactly upright the effects from the two sides cancel, but if the hull gets a small heel angle, the side that is most submerged will generate the largest suction, and the more submerged it gets the larger the suction. The situation is thus unstable; the heel tends to increase all the time, until hopefully the static righting moment gets large enough to compensate the heeling moment. Now, any disturbance may reduce the suction, which means that the large righting moment will roll the boat back, and due to its inertia it will roll over to the other side, where the process is repeated. The hull thus rolls from side to side and may in fact eventually capsize. Further, it is very difficult to steer the boat when it is rolling in this way.

Normally, the buttocks on the wetted part of the hull are kept relatively straight, but it is very difficult to avoid convex buttocks on the forebody. The problem therefore normally occurs when the trim gets too small, i.e. when the forebody goes into the water at high speed. Situations when this may happen are:

- If the boat is overloaded
- If the load is put too far forward
- If the engine power has been increased without moving the centre of gravity backwards
- If the trim planes generate too large a bow-down moment.

The control of the trim is thus very important.

## ■ ALTERNATIVE PROPULSION DEVICES

Today, the most important alternative to the conventional propeller is the water jet. This device works like an aircraft jet engine, deriving its thrust from the reaction force when the fluid is accelerated. In the water jet the acceleration is achieved by an impeller. Water enters through an intake, normally in the bottom of the boat, and is ejected through a duct at the stern. Note that it is the acceleration of the water that creates the force, so it does not matter whether the water is ejected above or below the water surface.

The basic principle for obtaining the thrust is the same as for a propeller, and the requirements for efficiency are the same. To optimize propulsion, as much water as possible should be accelerated but the speed increase should be as small as possible. For a propeller this speaks in favour of a large diameter and a low rpm. Unfortunately, this is hard to achieve in a water jet, where the flow has to pass a channel inside the hull and the space is limited. The water jet has been less popular in the past, although the basic principles have been known for a long time. In fact, a patent on water jet propulsion was granted in England in 1661!

The reason why water jets have gained in popularity for high-speed propulsion is the fact that no outside appendages are required. The higher the speed of a planing hull the smaller the wetted surface to lift it. Appendages, such as brackets and open shafts, obviously have a constant wetted surface, and thus account for an increasing proportion of the resistance as the speed goes up. Although it is hard to claim that there are no corresponding losses in a water jet intake and channel, they are normally smaller, particularly as the need for rudders is relaxed. There is thus an advantage from a frictional point of view, and the advantage gets larger and larger as the speed increases. An example of a water jet driven hull will be given below. For more information on water jet efficiency, see Dyne and Widmark (1998).

The concept of cavitation was introduced in [Chapter 10](#). When the pressure at any point in the flow gets below the vapour pressure, the water evaporates. Bubbles of vapour and air dissolved in the water are created and these interfere with the flow and solid surfaces. Particular problems occur when the bubbles reach regions of high pressure where they may implode abruptly, causing large pressure pulses. Such pulses create vibrations and may erode the surface of, for example, a propeller. Further, the thrust of a cavitating propeller is often reduced.

When the speed goes up, the rate of revolutions of the propeller is increased, and both effects contribute to high velocities around the propeller blades. High velocities mean low pressures, so the risk of cavitation gets larger and larger with increasing speed. To avoid cavitation, large blade area ratios, as in [Fig 11.9](#), are required for high-speed boats. At speeds above 40 knots this may not help, however, and the problems with thrust reduction, vibrations and erosion may get large enough to prevent the use of conventional propellers. A possible alternative is then the so-called super-cavitating propellers. These are designed to have a steady cavitation bubble covering the entire suction side, thus effectively eliminating the problems due to cavitation.

The disadvantage of the super-cavitating propellers is the reduced thrust and efficiency. Once the blade speed is high enough to generate a bubble covering the whole back side of

the blade, the suction force cannot be increased any further. Higher speeds will only result in higher pressure side forces, so the increase in thrust is slower than normal. On the other hand, there is no friction on the suction side, which reduces the torque to some extent.

Since the back side of the blade is no longer in contact with the water it may be designed without the usual constraints on shape. It is, however, important to ensure that the water separates at the leading edge, so in contrast to conventional blade sections the super-cavitation one should have a sharp nose. This gives the section a wedge-like shape, designed to withstand the considerable forces generated at these speeds. Design methods for super-cavitating propellers are available. For references, see Kerwin and Hadler (2010).

Another typical high-speed propulsion device is the surface piercing propeller. This is usually placed behind the transom, with only part of the propeller disk in the water. Its main advantage is the same as for the water jet: no submerged appendages are needed. The shaft may stick out directly from the transom. In this case the restrictions on propeller diameter, normally imposed on a propeller behind the hull, are somewhat relaxed, thus increasing efficiency. Both super-cavitating and conventional blade sections are used, and since much air is entrained at the water impact of each blade the collapse of cavitation bubbles (now partly filled with air) is smoother.

The main disadvantage of surface-piercing propellers is the large variation in blade loading. At the top position, when the blade is in the air, the loading is zero, while it is at maximum when the blade points downwards. Apart from generating vibrations, this pulsating load causes fatigue which needs to be considered in the design. An exhaustive investigation of the problems may be found in Olofsson (1996).

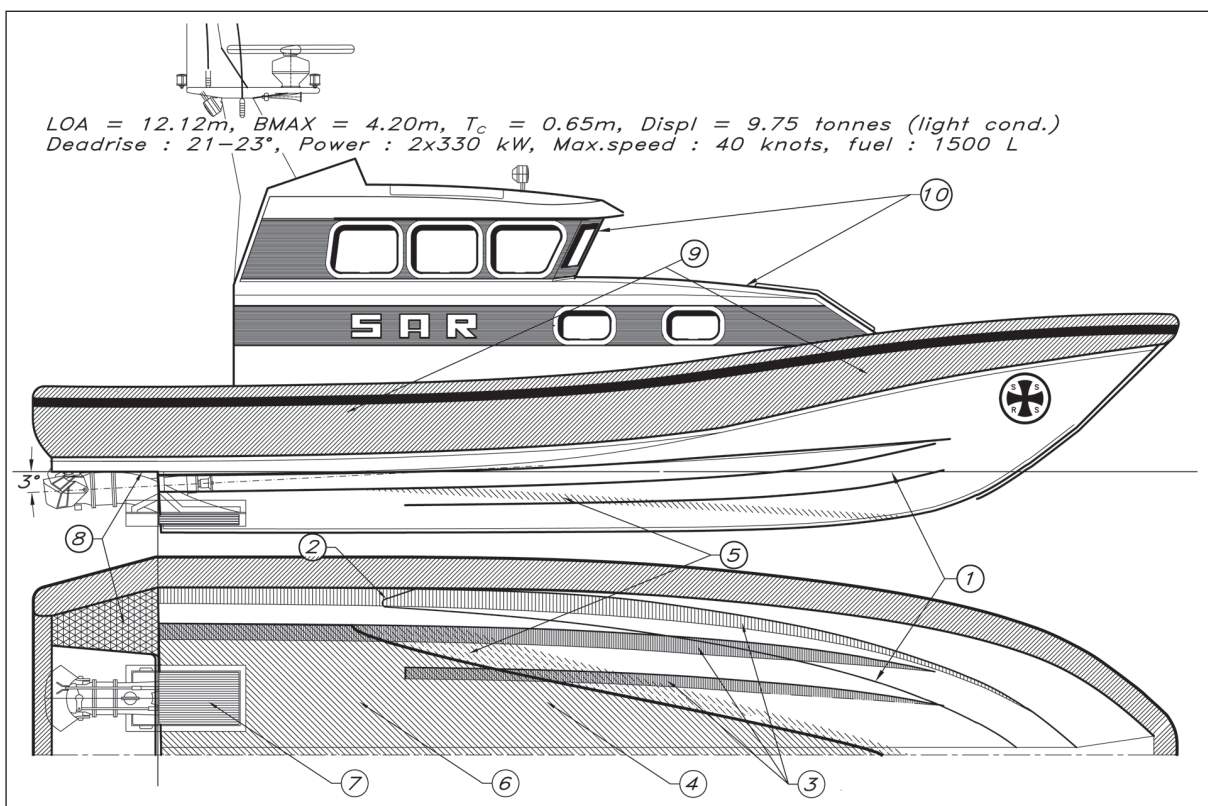
## ■ AN EXAMPLE

As an example of a contemporary high-speed boat, a rescue vessel for the Swedish Rescue Society, designed by one of the authors (Eliasson), will now be introduced. Fig 11.14 (overleaf) shows the 12 m craft landing after a jump in a 4 m wave. The hull is also shown in Fig 11.15 (overleaf), together with its main particulars. It is designed for an operating speed of 40 knots in smooth water and with good rough water capabilities.

To balance the hull at such a high speed the centre of gravity has to be relatively far aft. With a more forward location the trim would have been smaller with a risk of chine walking and broaching. In general, the craft would have been more difficult to steer in a seaway. For a pleasure craft it may be difficult to move the weight this far back, since the accommodation area and most of the equipment will be in the forward half of the hull.

The disadvantage of having the weight this far aft is that the ride may be bumpy in a head sea. Rather than hitting the next wave by the bow the hull will land on the afterbody after a jump. A remedy is to trim the hull slightly more by the bow using the trim flaps. Another disadvantage is the non-optimum low-speed performance. At lower speeds a larger wetted surface is required, which means that the pressure force is moved forwards and the hull trimmed by the stern. This creates large waves and resistance, but again the trim flaps may be used to reduce the problem.





## Key to Fig 11.15

**Fig 11.14** (TOP LEFT) Rescue boat in rough seas (Photo: Dan Ljungsvik)

**Fig 11.15** (LEFT) Main features of the rescue vessel

1. This is the still waterline. It has no relation to the waterline at full speed, as can be seen in the photo, but it gives an idea about the shape of the forebody. The bow is not particularly fine; a certain fullness is required to avoid problems with broaching in a following sea. On the other hand, it should not be too full, since this would hamper the performance in head seas and may lead to chine walking if the forward buttocks are too convex.
2. The waterline bends forwards at this position, showing that the bottom close to the chine has a negative deadrise. This is to generate a lift and to deflect the spray downwards. The hull runs dry, as can be seen in the picture.
3. The spray rails also have a negative deadrise as explained above. The inner one is cut off before the transom.
4. This is the boundary of the wetted surface (spray root) at 40 knots. There is no reason to extend the spray rails very far into this region. A certain overlap is desirable, however, since the spray root may move back and forth in a seaway.
5. In this area the spray should be deflected by the rails.
6. The wetted surface is not large at 40 knots! Compare with the waterline area at zero speed.
7. Modern water jets are used for propulsion. This is the intake, which is large enough to handle the enormous flow rate. As the flow into the intake should be as clean as possible, there should be no rails, keels or other devices ahead that can lead air into the jets.
8. The aftmost part of the bottom is raised over the full beam. This is to encompass the two water jets and to enable proper operation in reverse. Note that this part of the bottom is above the water at high speed. The trim flaps are hinged on the transom below the jets.
9. The collar is of a modified RIB type. It is not filled with air, but with an elastic polyurethane foam, covered with a skin of tough polyurethane and Kevlar. Tapering of the collar forwards is very important since otherwise too much buoyancy might be developed when the hull runs into a head wave, capsizing the boat backwards.
10. For stability reasons the deckhouse is relatively large.

The particular features of the design are described and keyed to Fig 11.15. The rescue vessel may be used as an example for the performance prediction above. Results are shown in Fig 11.16, where the numbering of the steps corresponds to that in the proposed procedure. The deadrise angle varies between  $21^\circ$  and  $23^\circ$ , but, as explained above, the angle used in the computations is measured to the edge of the spray rails and is the average of the angles at the transom and at the centre of gravity. Calculations were carried out for two trim angles,  $4^\circ$  and  $5^\circ$ . The smaller angle caused a bow-down moment



of 4.16 kNm and the larger one a moment in the same direction of 104.9 kNm. It is thus clear that the trim angle for zero moment must be slightly below  $4^\circ$  and a linear extrapolation yielded a trim angle of  $3.96^\circ$ . In turn this resulted in a resistance of 14.1 kN, corresponding to an effective power of 291 kW.

Now, the question is what engine power is required to achieve this. Since the vessel is equipped with water jets the propeller diagram cannot be used. An optimally designed propeller for this vessel would most likely have had an efficiency of at least 65% and so would an optimum water jet unit. This is a high efficiency, which is attainable due to the light loading of the propulsor at this high Froude number. At smaller Froude numbers the efficiency of the water jet deteriorates more than for a conventional propeller, but on the other hand the resistance is smaller due to the lack of external appendages, so it would be competitive also at somewhat lower speeds.

The water jet for the rescue vessel is also designed to produce a high thrust at very low speed (so called bollard pull), since the vessel must be capable of towing larger vessels. Therefore, the efficiency at full speed is reduced, and 50% may be a reasonable assumption for this case. Note that the deviation from the optimum may be important also for other cases. To obtain the optimum efficiency a specialist design of the water jet is required.

Assuming an efficiency of 50%, the delivered power must be 582 kW. This is the power at the impeller shaft. Due to mechanical losses in the gearbox and shaft bearings another 5% may be added, which would give approximately 610kW. The most suitable engines found for this vessel have a power of  $2 \times 330$  kW, so there should be some spare power if needed.

Step No	Variable	Computed value	Computed value	Computed value
1	$m$	9750 kg		
	LCG	3.550 m		
	VCG	1.145 m		
	$b$	2.740 m		
	$\varepsilon$	$3^\circ$		
	$\beta$	$17.9^\circ$		
	$f$	0.490 m		
	$V$	20.6 m/s		
2	$C_V$	3.970		
3	$C_{L\beta}$	0.059		
4	$C_{L\alpha}$	0.081		
5	$\tau$	$4.0^\circ$	$5.0^\circ$	
6	$\lambda$	1.79	1.20	
7	$L_m$	4.908 m	3.305 m	
	$R_n$	$101 \cdot 10^6$	$68 \cdot 10^6$	
8	$C_F$	$2.08 \cdot 10^{-3}$	$2.20 \cdot 10^{-3}$	
9	$\Delta\lambda$	0.32	0.24	
	$R_F$	7.53 kN	5.47 kN	
10	$ff$	0.920 m	0.920 m	
11	—	—	—	
12	—	—	—	
13	$L_{cp}$	3.510 m	2.420 m	
14	$e$	0.044 m	1.127 m	
15	$M$	4.16 kNm	104.9 kNm	
16	—	—	—	
17	$\tau_o$	—	—	$3.96^\circ$
18	$R_{Fo}$	—	—	7.6 kN
19	$R$	—	—	14.1 kN
20	$P_E$	—	—	291 kW
21	$P_D$	—	—	582 kW

**Fig 11.16** Summary of the rescue vessel calculation

# 12 RIG CONSTRUCTION

This chapter deals with the dimensioning and construction of the rig. Over the years different methods have evolved, ranging from old rules of thumb for solid wooden spars to sophisticated computer models for exotic composite materials. We will take a middle line, using accepted standard engineering practices as they are used in the Nordic Boat Standard (NBS). The reason for using this NBS standard instead of ABS or Lloyd's Register is the simple fact that NBS is one of the few yacht scantling standards that takes the rig into consideration. In [Chapter 15](#) we describe the ISO scantling standard's approach to the dimensioning of rigs. The ISO rig standard is rather comprehensive and also includes multihulls and form stable boats, while the YD-41 is a traditionally ballasted monohull which the NBS covers in a straightforward way. At the end of the chapter we will dimension the rig of the YD-41.

## ■ DEFINITIONS AND SCOPE OF THE STANDARD

The standard is valid for normal masthead and fractional rigs, with one or two pairs of spreaders. In [Fig 12.1](#) (overleaf) the required data for the calculations is defined. Other limits to this standard are, first, that the area of the foretriangle is not greater than 1.6 times the area of the mainsail ( $I \cdot J / (E \cdot P) < 1.6$ ) and, secondly, that the sail area is greater than the righting moment divided by 128 times the heeling arm. If this is not the case then the boat is classified as a motorboat with a steadying sail.

The starting point when dimensioning the rig is to calculate the righting moment. It is commonly agreed that a heel angle of  $30^\circ$  is a good design angle. This corresponds to a reasonably high wind strength with the sails still generating high loads and the boat making good speed through the water. Letting the boat heel over more (i.e. using a higher righting moment) in reality means a slower boat owing to increased resistance, with a correspondingly smaller dynamic force.

As can be seen from the box in [Fig 12.1](#) there are basically two ways of calculating the righting moment. We can start with calculating the moment for  $30^\circ$  of heel, or with the moment for  $1^\circ$  of heel. Calculating the  $RM_{30}$  means that we will have to make a calculation of the hull's heeled centre of buoyancy and the position of the centre of gravity in order to establish the righting arm. By using the  $RM_1$  instead, which we can get from the hull's upright hydrostatics (see [Chapter 4](#)), we need only estimate the centre of gravity of the vessel. Either way, the moment we get is to be that of the empty boat, which is then

$G$  Empty weight of boat [kg]  
 $\Delta$  Full load weight of boat [kg]  
 $g$  Ballast weight [kg]  
 $B$  Maximum beam [m]  
 $L_{OA}$  Length overall [m]  
 $A_S$  Sail area [m<sup>2</sup>]  
 $RM$  Dimensioning righting moment [Nm]  
 $RM_{30}$  Righting moment at 30 degrees heeling with empty weight of the boat [Nm]  
 $RM_1$  Righting moment at 1 degree heeling with empty weight of the boat [Nm]  
 $n$  Number of persons on board  
 $F_S$  Freeboard at mast [m]  
 $\delta_{RM}$  Additional moment from crew to windward [Nm]  
 $HA$  Heeling arm [m]

$$A_M = E \cdot P / 2$$

$$A_F = J \cdot I / 2$$

$$A_S = A_M + A_F$$

If  $A_S > RM / (128 \cdot HA)$   
 the boat is considered  
 to be a sailing boat,  
 and the rig is to be  
 dimensioned accordingly.

$$\delta_{RM} = 75 \cdot n \cdot (3.4B - 4.9F_S)$$

$$RM = RM_{30} \cdot \Delta / G + \delta_{RM}$$

or

$$RM = 27 \cdot RM_1 \cdot \Delta / G + \delta_{RM}$$

$$RM_{min} = 29 \cdot RM_1$$

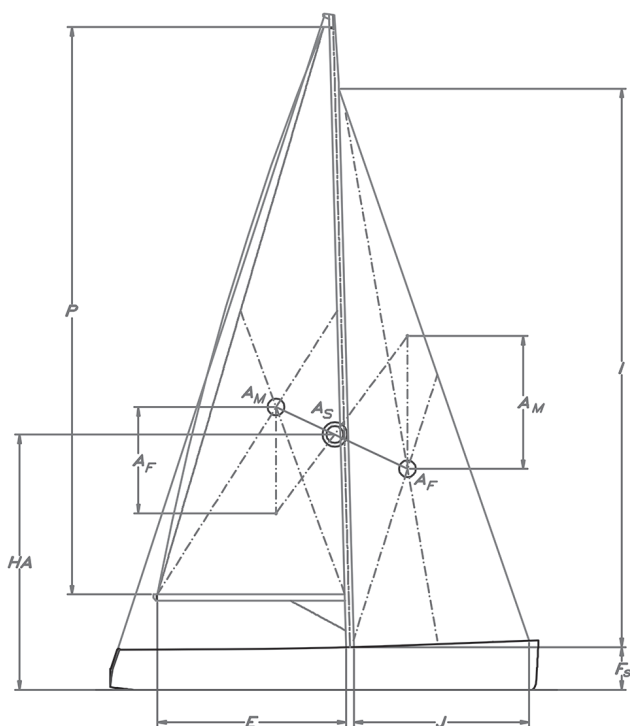


Fig 12.1 Definitions and  
 righting moments

modified to represent the fully laden boat including crew to windward, as shown in the box in the figure.

Fig 12.2 shows the different types of rig that this standard covers. The stability of the mast athwartship is dependent on the number of spreaders and the location of the mast foot, i.e. on deck or keel-stepped.

The longitudinal stability of the mast depends on the spread of lower shrouds, runners, inner forestay and location of the mast foot. It is common practice that the transverse and longitudinal stability are studied separately. Compared to a single-spreader, deck-stepped mast, we can increase overall mast stability by increasing the number of spreaders and/or bringing the mast down to the keel. At the same time we get the following pros and cons:

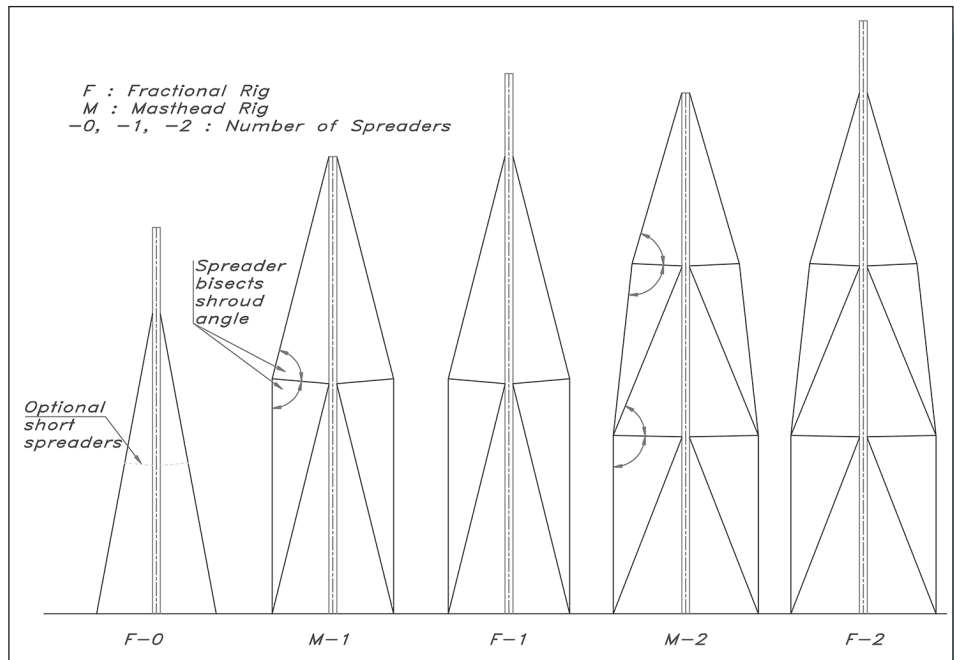
## Increased number of spreaders

- + Thinner mast, which gives better mainsail efficiency
- + Smaller outer dimensions/wall thickness give a lighter mast
- + Smaller foresail sheet angles are possible
- More difficult to trim
- Often, special measures must be made to take care of the longitudinal stability, i.e. runners, inner forestay and high longitudinal moment of inertia
- Higher cost.

## Mast through deck

- + Thinner mast, which gives better mainsail efficiency
- + Smaller outer dimensions/wall thickness give a lighter mast
- + Smaller foresail sheet angles are possible
- More difficult to trim, especially lengthwise
- High horizontal forces in deck level
- Risk of heat and water leakage.

Fig 12.2 Types of rigs



## FORCES ON THE SHROUDS

The forces come from the wind pressure on the sails and dynamic additions from wind and sea. Two load cases are considered in Fig 12.3: in Case 1 the rig is loaded by only a foresail, and in Case 2 the rig is loaded by a deep reefed mainsail. In Case 1 the transverse force  $T_1$  is simply the righting moment divided by the distance from the waterline to the uppermost shroud, as illustrated in Fig 12.3(A). It does not matter what kind of foresail is carried, since the dimensioning force comes from the righting moment.

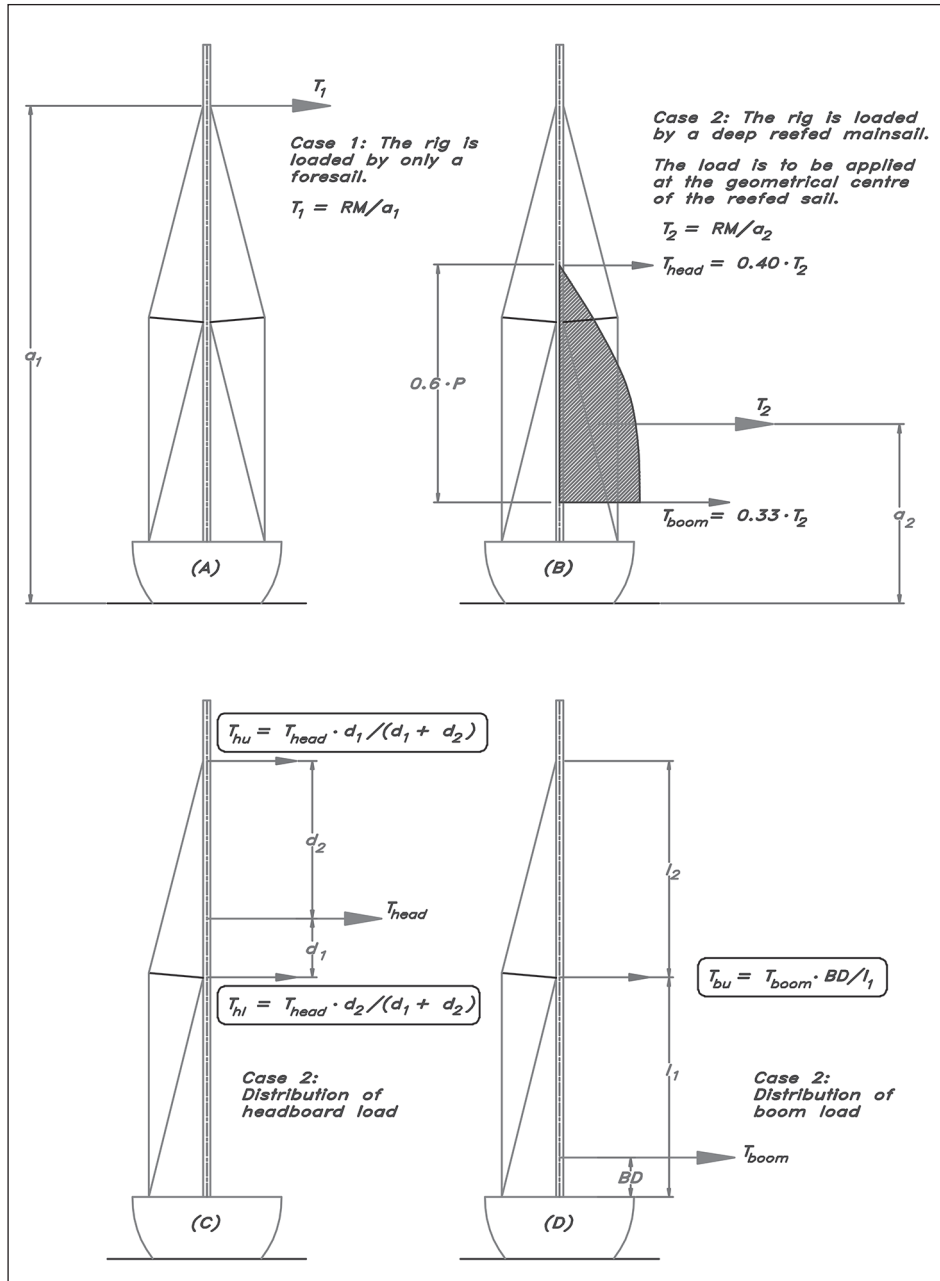


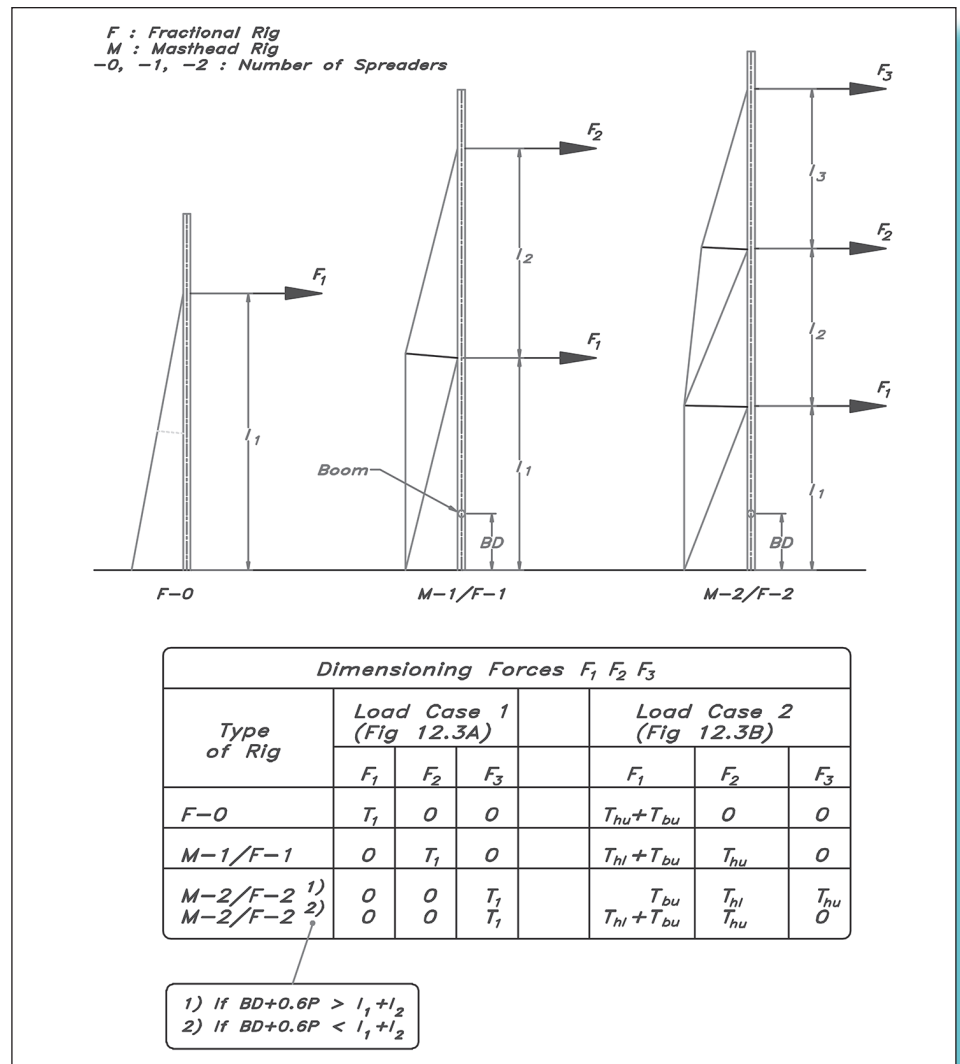
Fig 12.3 Transverse loads

In Case 2, with the reefed mainsail, the transverse force  $T_2$  is calculated by dividing the righting moment by the distance from the waterline to the geometric centre of the mainsail, approximately  $\frac{1}{3}$  of the luff up from the boom. This force is then distributed between the head of the sail,  $T_{\text{head}}$ , and the boom,  $T_{\text{boom}}$ , according to Fig 12.3(B).

When  $T_{\text{head}}$  lies between two shrouds, the force shall be distributed between the two shrouds proportionally to the distances from the shrouds' attachment points to the location of the force, Fig 12.3(C), and the resulting forces are  $T_{\text{hu}}$ , acting on the upper shrouds, and  $T_{\text{hl}}$ , on the lower shrouds. The boom force is working on the deck and on the lower shrouds, where we are interested to know the load on the shrouds. This load,  $T_{\text{bu}}$ , is a fraction of the boom force proportioned as the ratio of the boom height above deck to the distance of the shroud to the deck, Fig 12.3(D).

We now have all the components forming the transverse loads on the rig. Regardless of rig type, the dimensioning force is  $T_1$  in Load Case 1. In Case 2 the dimensioning force is different combinations of  $T_{\text{hu}}$ ,  $T_{\text{hl}}$  and  $T_{\text{bu}}$ , depending on rig type according to Fig 12.4.

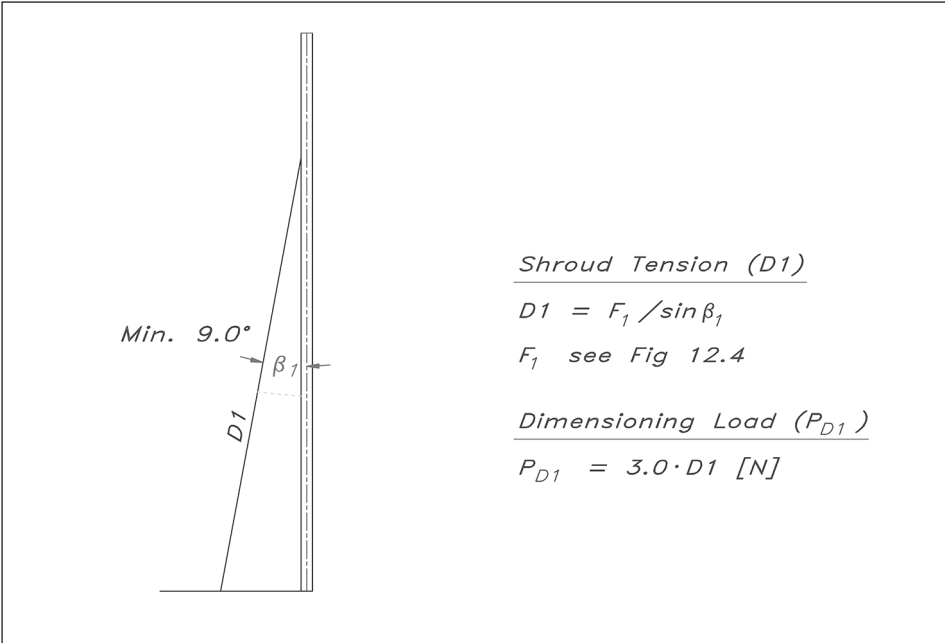
**Fig 12.4** Dimensioning forces for shrouds



Rig type F-0 only has  $F_1$  as a dimensioning force, type M-1 and F-1 have  $F_1$  and  $F_2$ , and type M-2 and F-2 include force  $F_3$  as well. For the dimensioning of the shrouds we use the maximum forces  $F_1$ ,  $F_2$  or  $F_3$  from Load Case 1 or Case 2. Note that there is no  $F_3$  force on a double-spreader rig in Case 2, if the reefed mainsail does not reach the upper spreaders (see notes 1 and 2 in Fig 12.4).

When calculating the shroud forces in the following figures, 12.5 to 12.8, it is essential to calculate the two above mentioned load cases separately, and then compare the results and choose the worse case, i.e. the highest load for each shroud.

Fig 12.5 gives the dimensioning load of the shrouds on an F-0 type rig. As can be seen it is the shroud tension multiplied by 3, and the smallest permissible shroud angle is  $9^\circ$ .



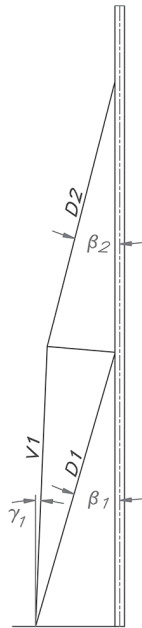
**Fig 12.5** Shroud load – rig F-0

Fig 12.6 shows the same thing for a single-spreader rig. Depending on whether we have single or double lower shrouds the dimensioning load is the shroud tension multiplied by 2.8 or 2.5. The upper shrouds are dimensioned from the shroud tension multiplied by 3 though, and the smallest permissible athwartship's angle is still  $9^\circ$ .

Fig 12.7 deals with the double-spreader rig. The method of calculation follows the same pattern as on the previous rigs. After calculating the shroud forces according to the formulae, we apply safety factors to the different parts and get the shroud loads. Basically, the safety factor distribution follows the one for the single-spreader rig, apart from the V1-position shroud, where the safety factor is 3.2. If we have separately coupled intermediate and upper shrouds to a common lower shroud, this shroud has to take the combined pull from the intermediate and upper shroud, which is the reason for the increased factor of safety. If, on the other hand, the intermediates and uppers run all the way down to the deck, their combined strength must at least equal V1.



**Fig 12.6** Shroud load – rig  
M-1, F-1



Shroud Tension (D#, V#)

$$D2 = F_2 / \sin \beta_2$$

$$V1 = F_2 / (\cos \gamma_1 \cdot \tan \beta_2)$$

$$C_1 = F_2 - V1 \cdot \sin \gamma_1$$

$$D1 = (F_1 + C_1) / \sin \beta_1$$

$$F_1, F_2 \text{ see Fig 12.4}$$

Dimensioning Load (P#)

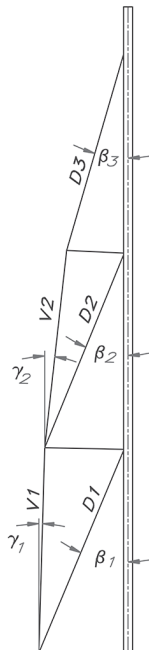
$$P_{D1} = 2.8 \cdot D1 \text{ [N] Single Lower Shrouds}$$

$$P_{D1} = 2.5 \cdot D1 \text{ [N] Double Lower Shrouds}$$

$$P_{D2} = 3.0 \cdot D2 \text{ [N]}$$

$$P_{V1} = 3.0 \cdot V1 \text{ [N]}$$

**Fig 12.7** Shroud load – rig  
M-2, F-2



Shroud Tension (D#, V#)

$$D3 = F_3 / \sin \beta_3$$

$$V2 = F_3 / (\cos \gamma_2 \cdot \tan \beta_3)$$

$$C_2 = F_2 - V2 \cdot \sin \gamma_2$$

$$D2 = (F_2 + C_2) / \sin \beta_2$$

$$V1 = (F_2 + C_2) / (\cos \gamma_1 \cdot \tan \beta_2) + V2 \cdot \cos \gamma_2 / \cos \gamma_1$$

$$C_1 = F_2 + C_2 + V2 \cdot \sin \gamma_2 - V1 \cdot \sin \gamma_1$$

$$D1 = (F_1 + C_1) / \sin \beta_1$$

$$F_1, F_2, F_3 \text{ see Fig 12.4}$$

Dimensioning Load (P#)

$$P_{D1} = 2.8 \cdot D1 \text{ [N] Single Lower Shrouds}$$

$$P_{D1} = 2.5 \cdot D1 \text{ [N] Double Lower Shrouds}$$

$$P_{D2} = 2.3 \cdot D2 \text{ [N]}$$

$$P_{D3} = 3.0 \cdot D3 \text{ [N]}$$

$$P_{V1} = 3.2 \cdot V1 \text{ [N]}$$

$$P_{V2} = 3.0 \cdot V2 \text{ [N]}$$

## FORCES ON THE STAYS

The longitudinal loads are primarily dependent on what tensioning devices there are on the boat: winches, tackles, hydraulics, etc. The NBS standard recognizes six different types of rig. Each basic type, masthead or fractional, is divided into three subgroups, according to Fig 12.8. For the masthead rig they are: (1) double lowers, (2) single lowers with inner forestay, and (3) runners with inner forestay. The fractional rig is divided into (4) runners with checkstay, (5) single lowers with swept spreaders, and (6) simple rig with no spreaders

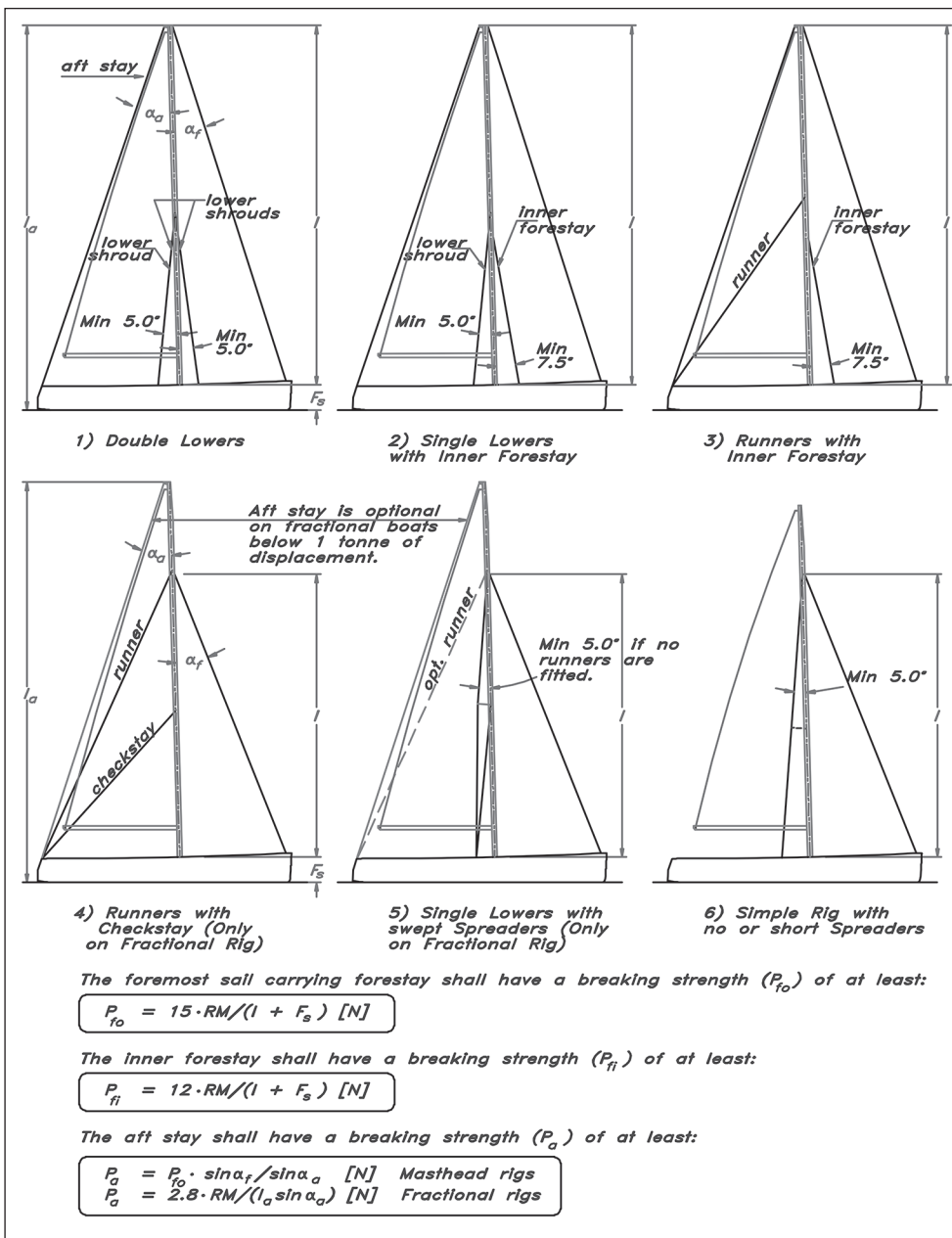


Fig 12.8 Loads on longitudinal stays

or short spreaders. The different staying types induce different loads on the mast itself, which have to be accounted for when dimensioning the mast. This will be discussed later.

As for the shrouds, the dimensioning force for the stays is derived from the righting moment at 30° of heel. The foremost sail carrying stay is required to have a breaking strength ( $P_{fo}$ ) of the righting moment multiplied by 15 divided by the distance of the stay above the deck plus the freeboard height at the mast. The inner forestay's load ( $P_{fi}$ ) is calculated accordingly, but using the righting moment multiplied by 12 instead.

The strength requirements for the aft stay ( $P_a$ ) differ between masthead and fractional rigs. For the masthead rig the aft stay is to have the same strength as the forestay, modified by a factor, depending on the angles that the aft stay and forestay make to the mast. The aft stay breaking strength for the fractional rig is calculated by taking the righting moment multiplied by 2.8 and dividing it by the mast height above the water multiplied by the sine of the aft stay angle to the mast. Runners on a fractional rig are dimensioned in the same way as the aft stay of a masthead rig.

The strength requirements calculated above include safety factors, and consequently the breaking strength of the wires can be used. When it comes to turnbuckles, though, it is wise to increase the dimensioning forces by 25% to ensure that if anything breaks it will be the standing rigging and not the attachment. For the same reason, it is prudent to allow for an equal increase in the loads for the chainplates.

## ■ COMPARISON BETWEEN WIRE AND ROD

In the following we will compare the two most common types of standing rigging, i.e. 19-strand stainless steel wire and solid rod of stainless steel. When choosing between wire or rod the following comparisons should be made:

- Breaking strength
- Fatigue
- Resistance to corrosion
- Elongation
- Weight
- Wind resistance
- Handling
- Price.

### ◆ Breaking strength

Breaking strength is the maximum load a wire/rod can carry without breaking. For every shroud and stay the breaking force is calculated and a proper wire/rod dimension is picked that can absorb the actual load. Depending on available sizes, the wire and rod form different stepped curves for breaking strength. Therefore, it is unlikely that there will

be the same relationship between wire and rod dimensions for every shroud/stay. For a certain stay, a wire dimension might fit well while the rod becomes over-strong. Normally, a rod is 20% stronger than a wire of the same diameter.

### ◆ Fatigue

Fatigue is normally regarded as the number of loads that can be applied before the wire/rod breaks. There are very few investigations regarding fatigue strength of 19-strand wire and rod.

Generally speaking, if the attachment points for the shrouds/stays are made in such a way that changes of angles can take place, wire is slightly more sensitive to fatigue because the individual strands rub against each other. Rod, on the other hand, is sensitive to surface damage, which can lead to fatigue-cracking. The wire has the advantage that the strands, when fatigued, break one at a time, and thereby give a warning that a change of wire is needed (provided, of course, that we regularly inspect the standing rigging). In a rod, a fatigue break comes without warning, and the beginning of cracking is almost impossible to detect by visual inspection.

### ◆ Resistance to corrosion

Resistance to corrosion is similar since the material is the same for both wire and the rod (AISI 316). This alloy might be discoloured, especially in the pockets between the strands of a wire, but this does not affect the strength.

### ◆ Elongation

Elongation ( $a$ ) of a loaded wire/rod increases proportionally to the load ( $P$ ) and length ( $L$ ), and inversely to the cross-sectional area ( $A$ ) and modulus of elasticity ( $E$ ):  $a = (PL) / (AE)$ .

As long as the load is within 70% of the ultimate breaking load (slightly more for rod) the wire/rod regains its original length when the load is released. A properly dimensioned rig should never get working loads greater than 50% of the breaking strength, i.e. there will be no plastic (permanent) deformations in the rig. The permanent deformations that can be measured come from first-time deformations of the attachment points and deformations of the hull girder. We will look more into this last item in the next chapter on hull construction.

In this comparison we assume the rod and the wire to be made of the same material. Due to the fact that the wire is constructed of strands that ‘compress’ and ‘straighten’ under load, the actual modulus of elasticity for the wire is approximately 20% less than for the solid rod. Comparing the cross-sectional area, the rod’s area is approximately 30% greater than the wire’s, due to air between the wire strands, rod and wire having the same diameter.

The following relations are valid with constant length and force:

- Same weight: rod elongation = 80% of the wire
- Same size: rod elongation = 60% of the wire.

The smallest elongation that it is possible to obtain by using rod gives two advantages when used in shrouds:

1. When loaded, the mast falls off to leeward; this, together with the heeling, puts the centre of effort of the sails outboard of the centre of lateral resistance, which tends to turn the boat into the wind (weather helm). With a stiffer rig the mast will not fall off as much to leeward, and the weather helm moment decreases, though not very much – normally 2–3%.
2. The lesser the mast top falls off to leeward, the straighter it is, and this makes it more resistant to bending and able to absorb greater loads.

The stiffer rod rig has one disadvantage though. A hull that becomes deformed is putting the ends of a shroud or stay closer to each other, and since the elongation of the rod is smaller than that of the wire at the same amount of pre-tensioning, the rod is losing more of its pre-tension compared to the more flexible wire.

To get a good pointing ability the forestay should be as straight as possible. This is achieved by tensioning the backstay or runners. When subjected to a wind load the forestay takes a curve; the smaller the curve, the stiffer a stay and/or boat. At temporary increases in the wind-load by 60% the depth of the curve of the wire forestay increases by 55% and for the rod forestay by 50%. The rod gives a slightly straighter forestay, but no account has been taken of the hull girder stiffness. The hull's flexibility makes the differences smaller, or, to put it another way, to really be able to utilize the rod rig, higher demands are put on the hull girder stiffness.

#### ◆ Weight

The boat's total displacement, stiffness and mass moment of inertia are influenced by the weight of different rigs. As we have shown earlier, the latter is of the utmost importance when sailing in a seaway.

Just as for the breaking strength, the weights of wire and rod form two different 'step-functions' which vary the result of the comparison for different rigs, although the same basis for the evaluation is used.

#### ◆ Wind resistance

Wind resistance of the shrouds and stays increases with increasing diameter.

Since a rod of equal strength to a wire is thinner, the resistance is less; and since the surface of the rod is smoother, the resistance, especially in low wind strengths, is still less than that for a wire. This latter effect (due to smoothness) diminishes with increasing wind strength.

#### ◆ Handling

Handling is better for wire compared to rod. It is possible to roll the wire into coils which have diameters of 0.5–0.8 m. Rod should not be coiled into smaller diameters than 200 times the rod diameter.

#### ◆ Price

The price of a rod rig is 50–100% higher than for an equally strong wire rig.

## TRANSVERSE MAST STIFFNESS

The tension in the shrouds and stays induces compression in the mast, and in order not to bend or break it has to have sufficient stiffness, i.e. enough transverse moment of inertia,  $I_x$ . The required stiffness depends on the load as well as on the length of the panel in question. In Fig 12.9 the formula for calculating the  $I_x$  required is given. The formula is common to all rig types, the differences in the results coming from the fact that the panel lengths vary. Another factor that differs between the rig types is the panel factor  $k_1$  and the 'foot factor'  $k_3$ . By letting the mast go through the deck we are able to decrease the moment of inertia by 35%. PT is the design load, and once again it is calculated using the righting moment, this

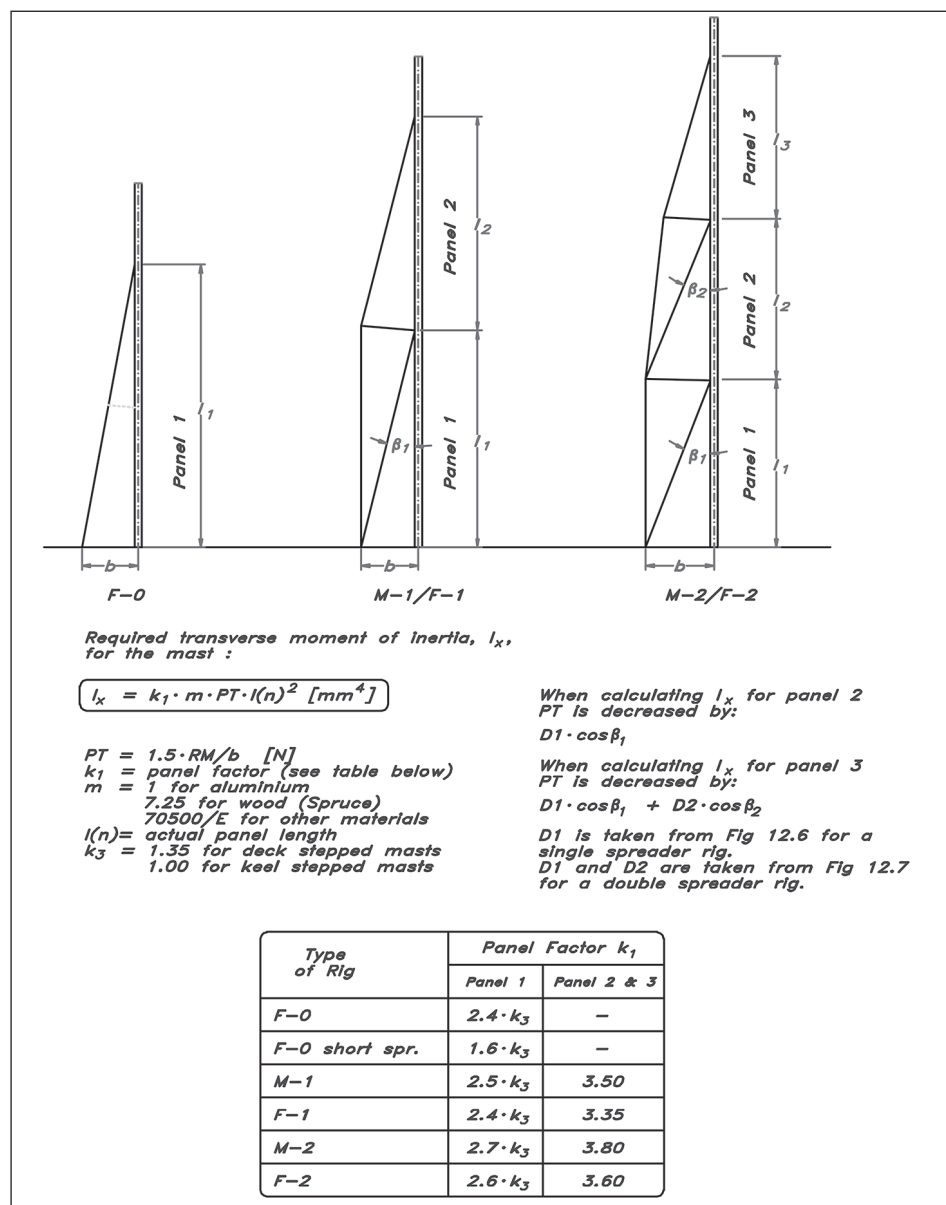


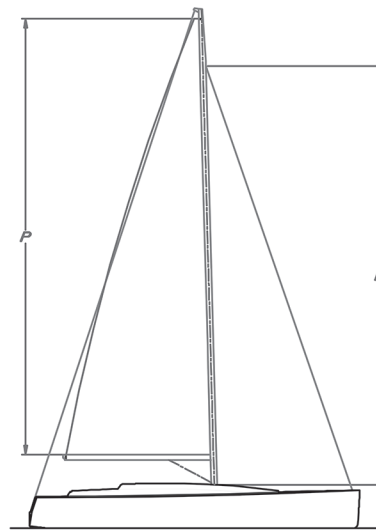
Fig 12.9 Transverse mast dimensioning

time divided by the horizontal distance between the mast centre and the chainplate for the shroud in question. The load thus arrived at is multiplied by 1.5 to handle the dynamic factors.

## LONGITUDINAL MAST STIFFNESS

The design load,  $PT$ , is obviously the same as for the transverse stiffness, and so is the 'foot factor',  $k_3$ . Fig 12.10 gives the rest of the data needed and the formula to calculate the required longitudinal moment of inertia,  $I_y$ . The different rig and staying types as defined in Fig 12.8 vary with the staying factor  $k_2$ , shown in the table of Fig 12.10.

**Fig 12.10** Longitudinal mast dimensioning



*Required Longitudinal Moment of Inertia for the Mast ( $I_y$ ):*

$$I_y = k_2 \cdot k_3 \cdot m \cdot PT \cdot h^2 \text{ [mm}^4\text{]}$$

$$PT = 1.5 \cdot RM/b \text{ [N]}$$

$k_2$  = staying factor (see table below)

$m$  = 1 for aluminium

7.25 for wood (spruce)

70500/E for other materials

$k_3$  = 1.35 for deck stepped masts

1.00 for keel stepped masts

$h$  = height above deck or superstructure to the highest sail carrying forestay

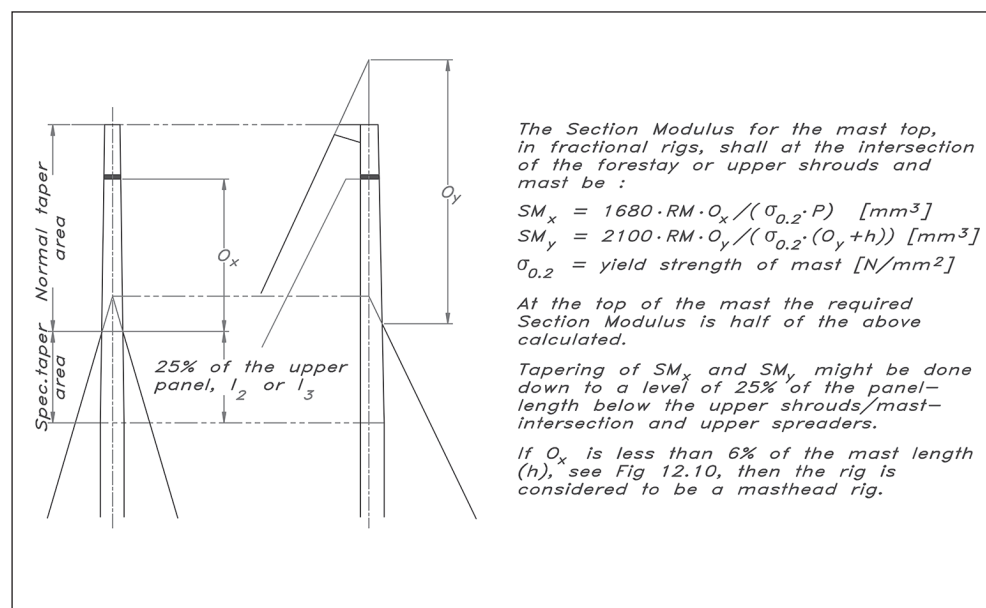
See Fig 12.8 for definitions of types of staying

Type of Staying	Staying Factor $k_2$				
	F-0	M-1	F-1	M-2	F-2
1) Double Lowers	-	0.85	0.80	0.90	0.85
2) Single Lowers, i.f.	-	0.80	0.75	0.85	0.80
3) Runners & i.f.	-	1.00	0.95	0.95	0.90
4) Runners & c.s.	-	-	1.00	-	0.95
5) Swept spreaders	-	-	0.85	-	0.80
6a) Short spreaders	1.05	-	-	-	-
6b) No spreaders	2.00	-	-	-	-



## FRACTIONAL MAST TOP

Special considerations for mast tops on fractional rigs are shown in Fig 12.11. Since there is no force from a foresail on the mast top, we are allowed to decrease the section modulus of the mast according to the formulae in the figure. We also see from the figure that if the distance from the top of the mainsail ( $O_x$ ) to the upper shrouds is less than 6% of the mast length ( $h$  in Fig 12.10), the rig is considered to be a masthead rig.



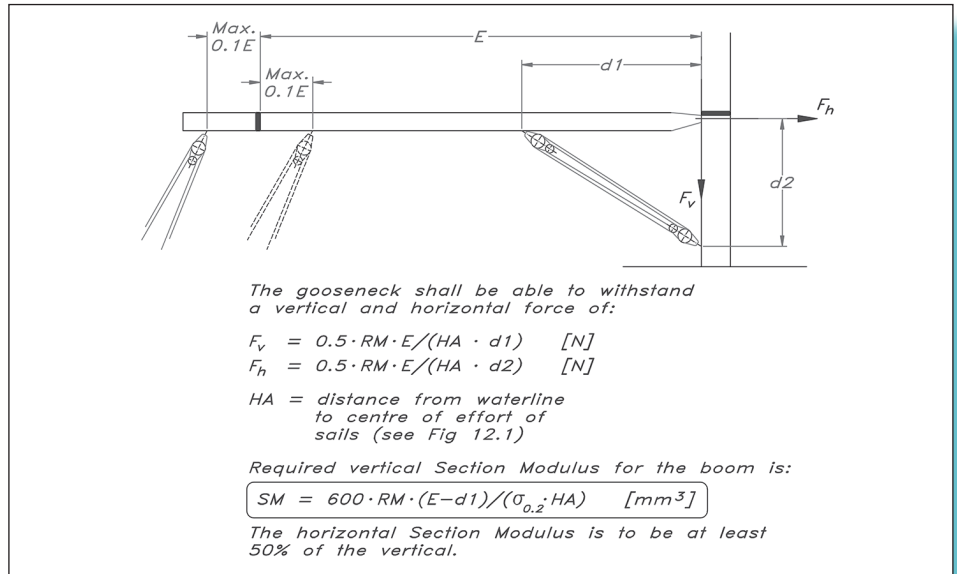
**Fig 12.11** Fractional mast top

## BOOM

The boom is subjected to bending forces coming from the wind pressure on the mainsail, which is counteracted by the sheet and kicking strap. This gives a vertical and horizontal force at the gooseneck, which has to withstand the forces  $F_v$  and  $F_h$  according to the formulae in the boom section of Fig 12.12. Once again the basis for the dimensioning force is the righting moment, in both cases the force is not to be less than 1000 N.

The bending forces that the boom has to withstand result in requirements for minimum section modulus,  $SM$ , as shown by the boxed formula in Fig 12.12. This section modulus is the vertical modulus, and the horizontal modulus is allowed to be half of the vertical. If we have a roller reefing boom, the section modulus must be that of the vertical modulus in all positions in which the boom can be locked. For the above formulae to be valid the sheet point on the boom is not allowed to be further from the end of the sail than 10% of the foot length. The attachment of the sheet must be able to withstand a force of at least the righting moment,  $RM$ , divided by the heeling arm,  $HA$ , with a minimum permissible value of 2000 N.

**Fig 12.12** Boom requirements

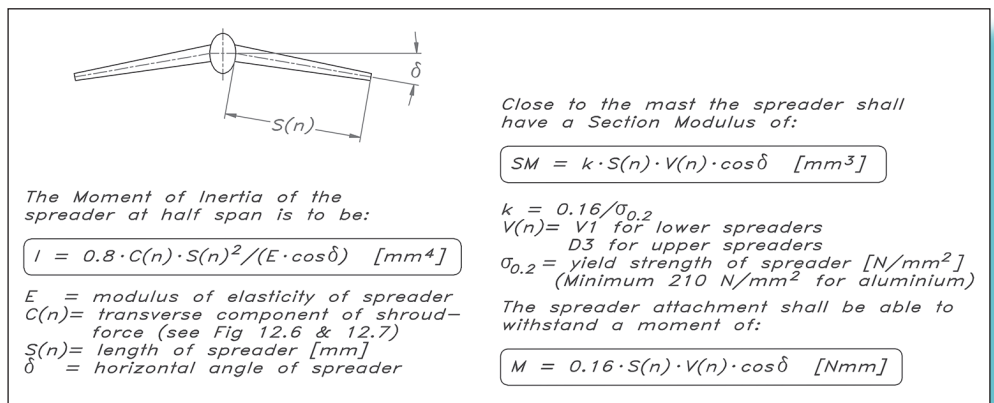


## SPREADERS

Spreaders are obviously put in to diminish the free length of the mast tube. As we have shown earlier (Fig 12.9), the required moment of inertia for the mast to carry a certain load is proportional to the free length squared. So if we halve the free length then we need a mast with a section of just ¼ of the moment of inertia. When installing the spreaders they should be set up in such a way that they cut the angle that the shroud is forming over the spreader tip into equal halves. This is easy to do on a one-spreader rig; on a two-spreader rig the intermediate and upper shroud come in at different angles. In this case, one has to make an intelligent adjustment and take the mean angle the shrouds are forming above the spreader. The reason for all this is to ensure that the spreaders are put into pure compression and do not tend to slide up or down.

Fig 12.13 gives the formulae for dimensioning the spreaders. The dimensioning force is the transverse component of the shroud force, C, which can be found in Figs 12.6

**Fig 12.13** Spreader requirements



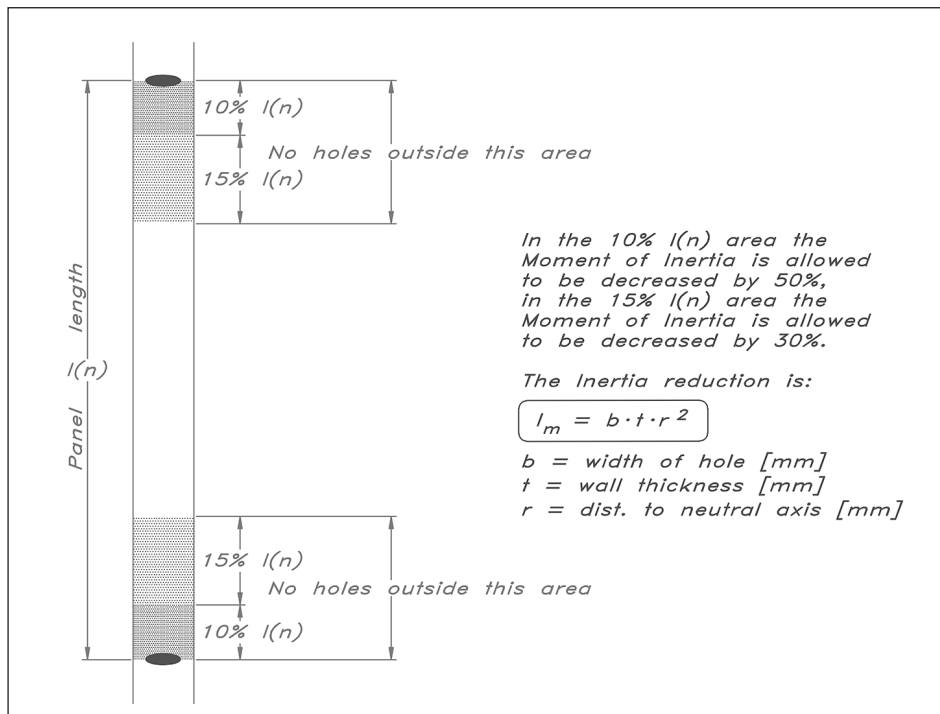
and 12.7. Multiplying this force by 0.8 and the length of the spreader,  $S_{(n)}$ , and then dividing the product with the modulus of elasticity and horizontal sweep angle of the spreader, the required moment of inertia at half span is found.

At the mast there is a requirement of a minimum section modulus,  $SM$ , as can be seen from the second boxed formula in Fig 12.13. Here the dimensioning force is the force of the V1 shroud for lower spreaders and of the D3 shroud for upper spreaders. The attachment of the spreader to the mast should furthermore be able to withstand a bending moment,  $M$ , according to the last formula in the figure. The reason for this is that by making the joint able to absorb a bending moment in the plane of the spreader, the longitudinal stability of the mast is enhanced.

## HOLES IN THE MAST

Holes in the mast are unavoidable. We need attachment points for stays, shrouds, winchpads, etc and exits for halyards. Every hole means a weakening of the mast, and the moment of inertia we have calculated takes no account of holes.

As Fig 12.14 shows, there are areas at the ends of each panel that are allowed to contain holes. Within 10% of the panel end we can reduce the moment of inertia by 50%, and for a further 15% of the panel length we are allowed to decrease the moment of inertia by 30%. The inertia reduction allowed is shown in the formula and is a function of the width of the hole, wall thickness of the mast and the distance to the neutral axis.

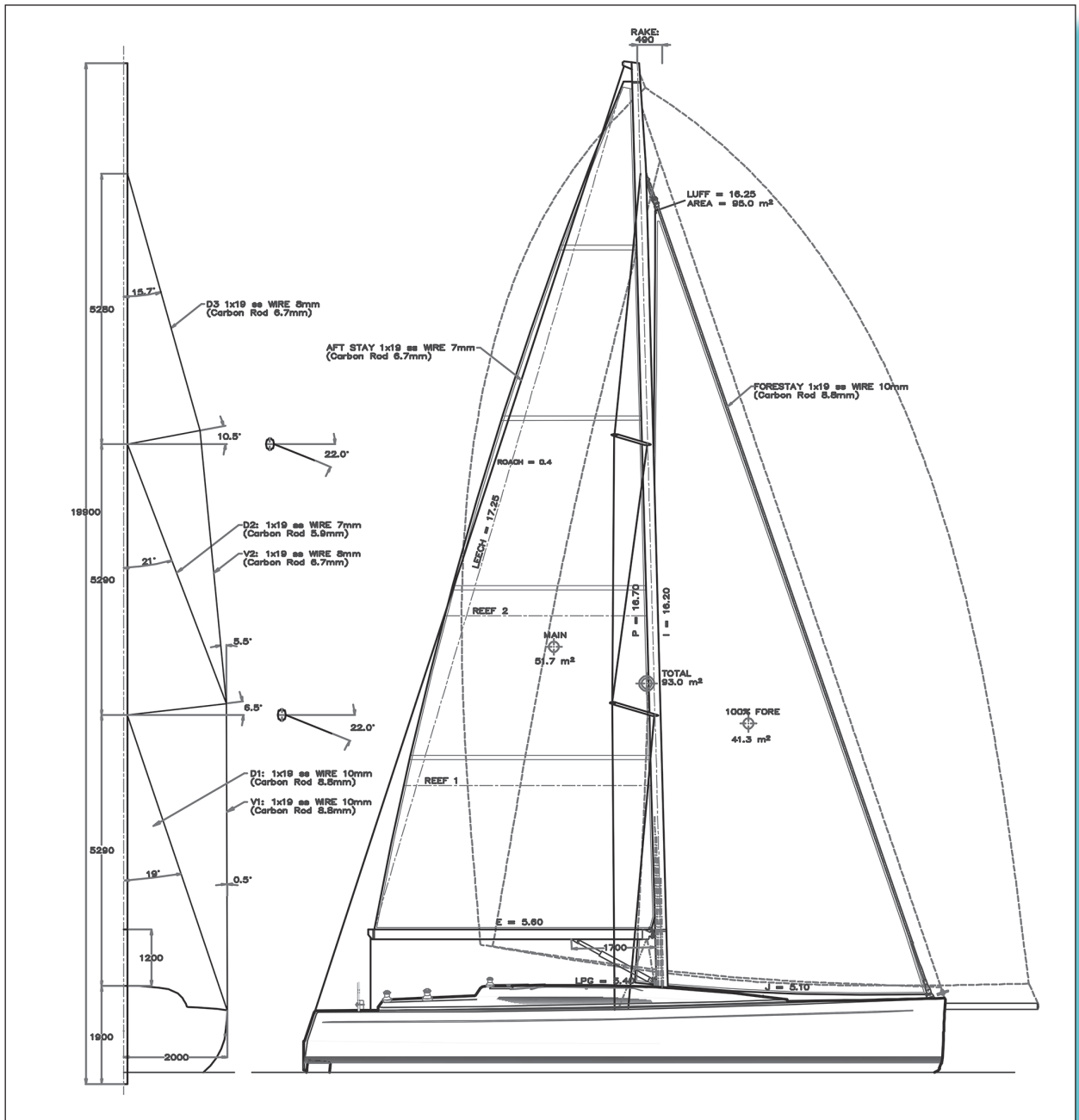


**Fig 12.14** Reduction of moment of inertia of mast

## THE YD-41 RIG

Fig 12.15 shows the type and dimensions of the YD-41 rig. We have chosen a fractional rig with a masthead asymmetric spinnaker and Code 0 sail, as it gives good performance, especially when no rating rule has to be taken into account. The foretriangle is larger than typical to increase the non-overlapping jib area. The jib is in on a furler concealed under the deck with the sail foot close to the deck for better performance.

Fig 12.15 YD-41 rig



As can be seen from the figure the mast is keel stepped, equipped with double spreaders and the shrouds have a wide base. In this way the mast weight is minimized and small sheeting angles are made possible due to the non-overlapping foresail, all of which enhance performance. Another factor that improves performance is the rake of the mast. Although not numerically proven, the rake of the mast together with the triangular planform gives a sweep back corresponding to an elliptical pressure distribution. And in terms of appearance, this is how a mast traditionally should look.

To calculate the rig we start with the righting moment, RM, calculated to be 69,000 Nm at 30° of heel in fully loaded condition. Since the crew is onboard this is the correct RM to use in the rig calculations. From the formulae in Fig 12.3 we get the transverse load values of  $T_1 = 3921 \text{ N}$ ,  $T_2 = 11060 \text{ N}$ ,  $T_{\text{head}} = 4424 \text{ N}$ ,  $T_{\text{boom}} = 3650 \text{ N}$ .

The input values for the dimensioning forces are the upper- and lower-mainsail head forces, and the upper mainsail boom force,  $T_{\text{hu}} = 201 \text{ N}$ ,  $T_{\text{hl}} = 4223 \text{ N}$ ,  $T_{\text{bu}} = 828 \text{ N}$ .

With these values we can enter Fig 12.4 and calculate the dimensioning forces  $F_1$ ,  $F_2$  and  $F_3$ . Since the rig is of the 2-spreader variety and  $BD+0.6P$  is greater than  $I_1+I_2$ , we




Typical properties for aluminium extrusions							
	Main Dim. (mm)	$I_y$ (cm <sup>4</sup> )	$I_x$ (cm <sup>4</sup> )	Wall Thkn. (mm)	Weight (kg/m)	$SM_y$ (cm <sup>3</sup> )	$SM_x$ (cm <sup>3</sup> )
Mast Sect. 	156/87	391	144	3.00	3.71	42.8	33.2
	175/93	558	191	3.24	4.18	53.6	41.0
	193/102	779	257	3.4	4.74	69.3	50.6
	211/110	1051	341	3.65	5.34	86.5	62.0
	227/119	1407	456	3.95	6.15	108	76.6
	245/127	1910	614	4.35	7.15	137	96.5
	264/136	2591	830	4.80	8.40	172	122
	285/147	3508	1127	5.20	9.72	214	153
	304/153	4686	1524	5.80	11.44	272	194
	176/93	526	187	2.89	4.20	58.2	40.0
Furl. Sect. 	194/101	709	254	3.04	4.79	70.8	49.8
	212/109	970	337	3.15	5.49	88.2	61.8
	228/118	1306	453	3.40	6.35	112	76.8
	246/126	1781	613	3.75	7.44	139	97.3
	265/135	2392	828	4.15	8.73	173	122
	286/146	3237	1122	4.50	10.10	220	154
	305/156	4389	1513	5.05	11.84	276	194
Boom Sect.	135/71	265	70	2.40	2.66	39.0	19.5
	152/82	433	126	2.70	3.59	54.2	30.4
	171/94	726	189	2.75	4.66	80.6	41.2
	200/117	1280	343	3.10	5.88	121	61.3
	250/140	2706	692	3.20	7.95	200	101
Spinn Pole Sect.	60/60	15.4	15.4	2.00	1.00		
	72/72	29.9	29.9	2.20	1.38		
	84/84	48.8	48.8	2.20	1.53		
	96/96	72.3	72.3	2.20	1.76		
	99/99	123	123	3.60	2.65		
Example properties for carbon sections							
	Main Dim. (mm)	$EI_y$ (GNmm <sup>2</sup> )	$EI_x$ (GNmm <sup>2</sup> )	Wall Thkn. (mm)	Weight (kg/m)	$SM_y$ (cm <sup>3</sup> )	$SM_x$ (cm <sup>3</sup> )
Mast Sect. 	158/88	399	117	3.60	2.80	49.0	37.0
	178/94	550	152	3.60	3.00	61.0	44.0
	196/103	815	235	4.20	3.70	85.0	61.0
	214/111	1036	293	4.20	4.00	100	71.0
	229/119	1259	365	4.20	4.20	115	82.0
	247/127	1641	448	4.20	4.60	134	95.0
	266/136	2264	638	4.80	5.40	176	124
	286/146	2804	800	4.80	5.80	205	145
	306/156	3762	1107	5.40	6.90	262	185
	158/87	292	92	3.00	2.10	50.0	30.0
Boom Sect.	179/93	492	120	3.00	2.50	71.0	37.0
	198/103	844	235	4.20	3.60	109	61.0
	249/127	1627	448	4.20	4.40	166	95.0

Fig 12.16(a) Typical spar dimensions and properties

use the penultimate row in the table of the figure, giving:  $F_1 = 0$ ,  $F_2 = 0$ ,  $F_3 = 3921$  N in Load Case 1, and  $F_1 = 828$  N,  $F_2 = 4223$  N and  $F_3 = 201$  N in Load Case 2.

Using the formulae in Fig 12.7, for a double-spreader rig we first calculate the tensions of the shrouds in Load Case 1, and by applying the relevant safety factors from the formulae we get the loads:  $P_{D1} = 41561$  N,  $P_{V1} = 66543$  N,  $P_{D2} = 16545$  N,  $P_{V2} = 42043$  and  $P_{D3} = 43471$  N.

Starting all over again with Fig 12.7 but using the forces of Load Case 2, we get:  $P_{D1} = 57195$  N,  $P_{V1} = 38616$  N,  $P_{D2} = 27950$  N,  $P_{V2} = 2156$  N and  $P_{D3} = 2229$  N.

Choosing the maximum values we get the dimensioning shroud forces:  $P_{D1} = 57195$  N,  $P_{V1} = 66543$  N,  $P_{D2} = 27950$  N,  $P_{V2} = 42043$  N and  $P_{D3} = 43471$  N.

From Fig 12.8 we can see that our boat is of type 5 concerning the longitudinal staying, and from the formulae we get the dimensioning forces,  $P_{fo} = 58817$  N for the forestay, and  $P_a = 29241$  N for the aft stay.

Fig 12.9 leads on to the requirements for mast transverse stiffness. The dimensioning force, PT, is calculated to be 51246 N according to the formula in the figure. Knowing

Fig 12.16(b) Typical rig dimensions and properties

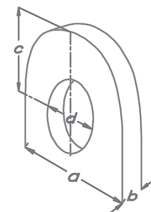
Approximate equivalents for 1x19 wire

1x19 Wire				Rod – Nitronic 50				Rod – Carbon		
Diam (mm)	Diam (in)	Br.str (N)	Weight (kg/m)	Size	Diam (mm)	Br.str (N)	Weight (kg/m)	Diam (mm)	Br.str (N)	Weight (kg/m)
–	7/32	24200	0.151	–4	4.37	20890	0.118	4.6	34000	0.026
6	–	28250	0.176	–6	5.03	28050	0.156	5.3	40800	0.034
7	9/32	34800	0.239	–8	5.72	36490	0.202	5.9	47600	0.044
8	5/16	45500	0.312	–10	6.35	45810	0.249	6.7	56600	0.054
–	3/8	64550	0.432	–12	7.14	55620	0.314	7.5	67900	0.068
10	–	71100	0.488	–15	7.52	63370	0.349	8.0	74700	0.076
11	7/16	86000	0.591	–17	8.35	77890	0.434	8.8	88300	0.094
–	1/2	114280	0.793	–22	9.53	100060	0.560	10.1	111000	0.122

Actual properties may vary slightly between different suppliers

Matching components made of stainless steel, type AISI-316

1x19 Wire			Rigging Screw		Chainplate lug (see fig.)			
Diam (mm)	Br.str (N)	Weight (kg/m)	Diam (in)	Br.str (N)	a (mm)	b (mm)	c (mm)	d (mm)
4	12550	0.078	5/16	22600	22.0	6.0	13.0	10.0
5	19620	0.122	3/8	33400	25.0	8.0	16.0	12.0
5.5	24200	0.151	7/16	46100	30.0	10.0	18.0	14.0
6	28250	0.176	7/16	46100	36.0	10.0	21.0	14.0
7	34800	0.239	1/2	66700	38.0	12.0	24.0	16.0
8	45500	0.312	5/8	93200	40.0	13.0	25.0	16.0
10	71100	0.488	3/4	123000	45.0	14.0	27.0	18.0
11	86000	0.591	3/4	123000	50.0	14.0	30.0	18.0
12	102000	0.703	7/8	167000	60.0	18.0	36.0	22.0
14	139100	0.957	1	218000	65.0	22.0	38.0	25.0



Chainplate lug

a = width  
b = thickness  
c = centre of hole to top of lug  
d = diameter of hole

the material of the mast and the way it is stepped, material and panel factors can be applied, and the requirement for each panel's transverse moment of inertia can be calculated. For the YD-41 the dimensioning panel is the lower one giving a  $I_x$  required of  $373 \cdot 10^4 \text{ mm}^4$ .

Doing the same calculations according to Fig 12.10 we can calculate the required longitudinal moment of inertia,  $I_y$ , which turns out to be  $1577 \cdot 10^4 \text{ mm}^4$ .

Entering values into Fig 12.12's formulae we get the requirement for the boom's section modulus. The vertical section modulus is not to be less than  $89.0 \cdot 10^3 \text{ mm}^3$  and the horizontal not less than  $44.5 \cdot 10^3 \text{ mm}^3$ .

Entering Fig 12.16(a) and Fig 12.16(b) with all these values we can pick the relevant shrouds, stays and rig components. In Fig 12.16(a) the upper table shows, in the shaded rows, the relevant aluminium mast and boom sections, and the lower table shows the carbon substitutes. In Fig 12.16(b) the upper table shows the required wire dimensions (with breaking strength), and their nitronic and carbon rod approximate equivalents. The lower table shows the corresponding sizes for rigging screws and chain plates.

The YD-41 ends up with an aluminium mast  $245 \cdot 127 \text{ mm}$  in diameter, weighing  $7.15 \text{ kg/m}$ , a boom measuring  $200 \cdot 117 \text{ mm}$ ,  $5.88 \text{ kg/m}$ , D1 and V1 shrouds and forestay of  $10 \text{ mm } 1 \cdot 19$  stainless wire, V2 and D3 of  $8 \text{ mm}$ , D2 and aft stay of  $7 \text{ mm}$ . With the wire dimensions go corresponding sizes of rigging screws and chain plate lugs,  $\frac{5}{8}$  in and  $\frac{1}{2}$  in rigging screws, 16 and 13 mm thick lugs, respectively.

However, for our yacht a carbon mast is used. For carbon spar sections shown in Fig 12.16(a), moments of inertia are combined with elastic modulus, and to calculate the required mast section the  $I_x$  and  $I_y$  in the formulae from Fig 12.9 and 12.10 need to be multiplied by the elastic modulus of aluminium. The mast section in this case is  $229 \cdot 119 \text{ mm}$ , weighing  $4.2 \text{ kg/m}$  and the boom is  $198 \cdot 103 \text{ mm}$ ,  $3.6 \text{ kg/m}$ . This, combined with carbon rod shrouds and stays, gives a substantial weight saving of approximately  $90 \text{ kg}$  for the rig of the YD-41.



# 13 HULL CONSTRUCTION

Is there really any need to calculate the strength of a boat? For centuries boats have been built from scantling rules that are based on experience, rules of thumb, guesswork and luck, with no actual strength or load calculations being made. The forces of the wind and sea are the same today as then, so reasons for the need to calculate boat strength must be sought elsewhere.

To begin with, modern boats of the 21st century have more highly loaded rigs compared with boats just 50 years ago. Aluminium and composite spars, stainless or fibre stays and shrouds and sails from synthetic fibres deliver more power and need not be reefed as early as before, which lead to high loads from the rigging which must be absorbed by the hull.

Another factor working in this direction is today's more aggressive way of doing things, comparing ourselves and competing with our neighbour and consequently driving our boats harder.

With series production of boats the cost of production has become more important. Since the cost relates directly to the weight of the boat, the importance of not building too heavy plays an increasingly important role. Performance, on the other hand (almost always sought), is inversely proportional to the displacement, but still this has pushed the development towards lighter and lighter boats. So, higher loads from the rig and a competitive owner must be taken care of by an increasingly lighter hull structure. All this means that the margin of error gets smaller and that the need for accurate calculations of strength becomes more important.

Other factors that put higher demands on the structure are the development of increasingly shorter fin keels that increase the stress on the keel/hull joint, and separate rudders that are supported only by their own rudder shafts, or by a skeg so small that it hardly contributes to the strength.

Before calculating strength requirements one must know the loads, and this is perhaps the most uncertain part of it all. The loadings can be divided into two parts: global and local. Global loads affect the vessel as a whole, i.e. loadings from the rig when under way try to bend the hull girder, and the stresses and deflections can be calculated by means of simple beam theory (to be discussed later). Local loads can be divided into hydrostatic/dynamic loads imposed on the vessel by the sea and waves, and loads brought into the hull from chainplates, keel, rudder, winches, sheet blocks and tracks, stanchions, etc.

In this chapter we will discuss the influence of different loads, global and local, and what deflections they induce. Then we will show how the keel and rudder affect the hull

structure, and finally survey different kinds of materials and their use, including exotic materials and sandwich construction. Details of the actual dimensioning of the YD-41 will be given in [Chapter 15](#).

## ■ CONCEPTS IN STRUCTURAL MECHANICS

Although this is not meant to be a chapter on general structural mechanics, we will describe some basic concepts in structural design that are used in this chapter.

When we talk of a material's stress, we mean the amount of force acting over the cross-sectional area of the item in question, expressed in Newtons per square millimetre ( $\text{N/mm}^2$ ). The ultimate breaking stress represents the actual breaking stress, and the yield stress for metals means the maximum useful static stress.

Strain is the extension of the material per unit length when loaded, and it is expressed as a percentage. So if we have a piece of wood, steel, glassfibre, etc., initially 100 mm long that when loaded to failure becomes 103 mm long, the strain is said to be 3%. Obviously the lower the strain value the more brittle the material is.

The stiffness of a material is the ratio of stress to strain. If we compare two equal wires, one of nylon and the other one of stainless steel, both carrying the same load and stress, the stainless one will stretch just a little while the nylon will stretch quite a bit more, reflecting the different levels of strain. Dividing the stress by the strain you get a measure of the stiffness known as the modulus of elasticity:  $E = \text{stress/strain}$  ( $\text{N/mm}^2$ ). This relationship is only true when the material is within its 'elastic region', which means that when the load is released the piece in question retains its original size. For metals this region is quite small. Typical permissible levels of strain are 0.2–0.3%. The level of stress at this point is called yield strength, as opposed to ultimate strength which is when the material actually breaks.

When bending a beam or a panel, one side will be subjected to compressional forces and the other side to tensional forces, both of them normal to the surfaces. Somewhere in between there will be a layer with no stress, called the neutral axis. In a homogeneous material this will pass through the geometrical centre of gravity for the cross-section. If the cross-section consists of parts of different moduli of elasticity, the cross-section is modified in the same proportion as the moduli of elasticity. If, for instance, one part has a 40% higher modulus of elasticity, this part is widened the same amount before calculating the centre of gravity for the cross-section.

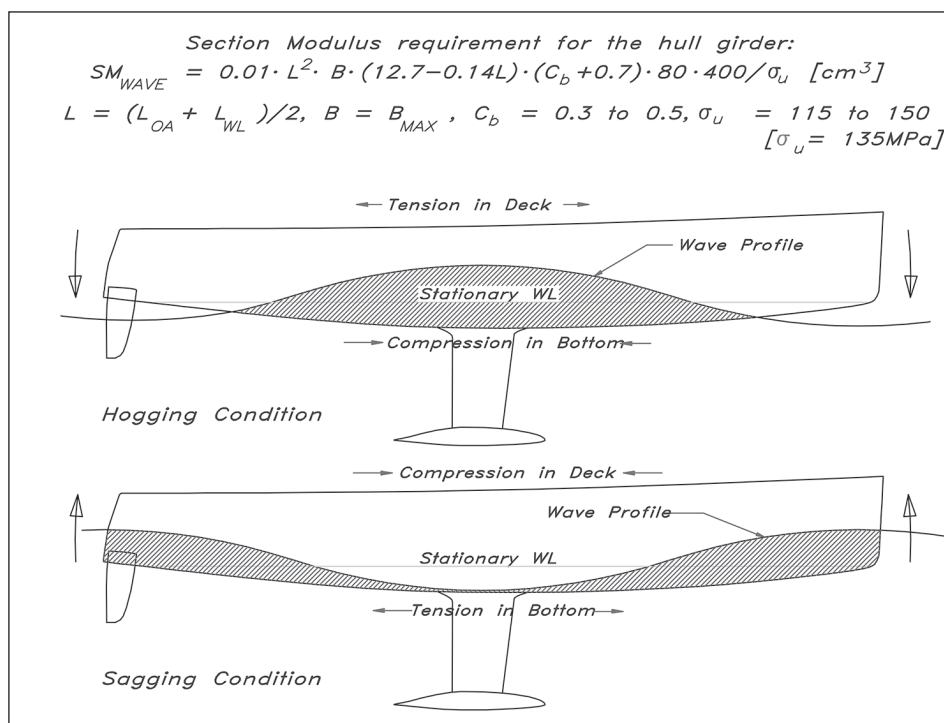
The combined moment of inertia ( $I$ ) for a composite section is the sum of each part's own moment of inertia plus each part's distance from the total neutral axis squared, multiplied by its area. When calculating the resistance to bending for a beam or a panel, we need to know the section modulus ( $SM$ ), which, put simply, is the moment of inertia divided by the longest distance from the neutral axis to one of the surfaces.

As stated earlier the bending force induces compressional and tensional forces on the surfaces, and also a transverse, or shear, force that is acting on the cross-section itself. This shear force also gives a shear stress along the beam or panel.

## GLOBAL LOADS

One case of global loadings, primarily concerning ships and bigger yachts, is the bending-moment conditions of hogging and sagging: hogging when the wave crest is amidships and sagging when the wave trough is amidships with the crests at bow and stern. Normally hogging/sagging calculations are not performed on pleasure yachts below approximately 100 ft (30 m) (Fig 13.1).

**Fig 13.1** Hull girder requirements (ABS)



The American Bureau of Shipping (ABS) guide for building and classing offshore racing yachts and the ISO 12215 Standard cover vessels up to 80 ft (24 m) and does not require the calculations of bending moments and hull girder strength, but the ABS rule for motor pleasure yachts stipulates a minimum hull girder section modulus  $SM$  at amidships varying with length, breadth and block coefficient. (See Fig 13.5 for how this is calculated for the YD-41.) This ABS formula is valid for yachts shorter than 45 m and made of fibre-reinforced plastic with speeds below 25 knots. The beam ( $B$ ) of the vessel is not to be greater than twice the depth of the canoe-body ( $D_c$ ).

The minimum ultimate strength of the hull material, tensile or compressive, is  $\sigma_u$ , whichever is less in  $\text{N/mm}^2$ .  $L$  and  $B$  are length and beam in metres, and  $C_b$  is the block coefficient of the vessel. Typical values for the block coefficient are 0.35 to 0.42.

The other big villain that inflicts deformations is loading from the rig in sailboats. The loads come from the shroud tension to windward, and the tension in the fore-and-aft stays. The former is directly coupled to the boat's righting moment and the latter to the need for a straight jib stay to get the best performance from the sails.

On a 'normal' ballasted sailing yacht the accumulated pressure on the mast foot, coming from stays, shrouds and halyard tension, can reach a value of double the boat's displacement. Loadings from the shrouds are of the same magnitude as the displacement, 7.4 tonnes for the YD-41, and halyard tensions are approximately 15% of displacement. The tension in the fore-and-aft stay, inducing a longitudinal bending moment in the hull girder, results in a bending force of approximately 85% of the displacement, i.e. 6.3 tonnes (a load that the hull girder must be able to absorb without undue deformations).

Transversely the hull section in the shroud area must be stiff enough not to lose its shape, so the mast falls off to leeward (Fig 13.2). To achieve this, the boat must have a 'strong cross' with the mast in its centre when seen from above. The hull for a

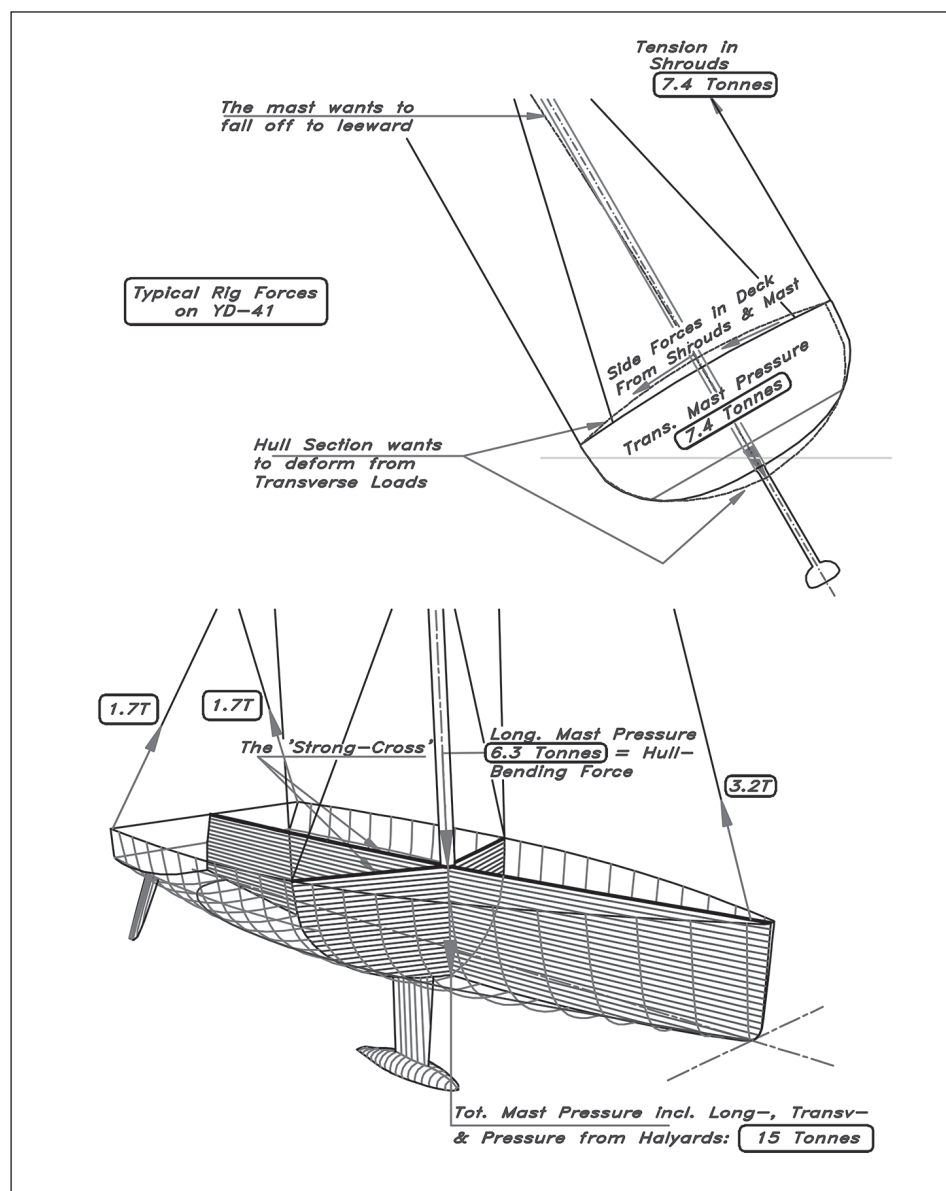
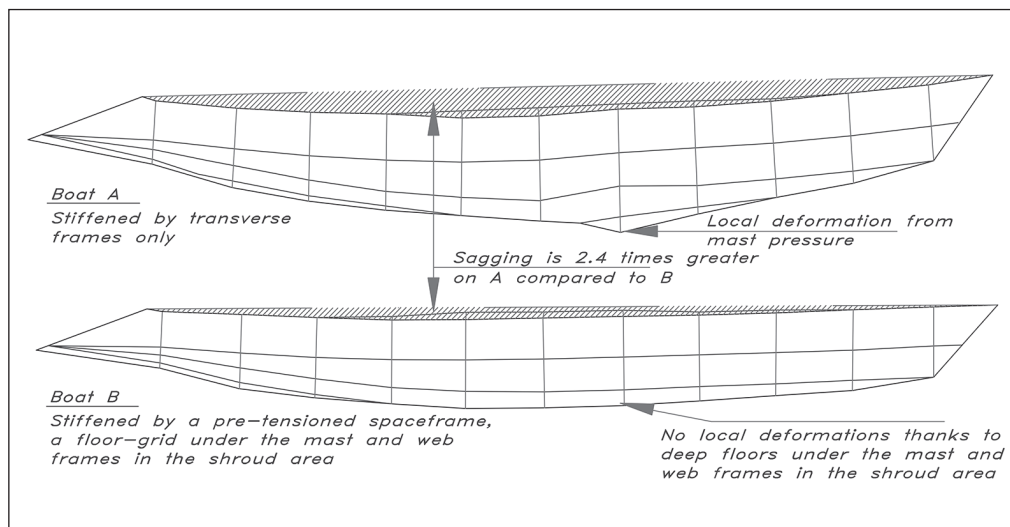


Fig 13.2 Forces from the rig

**Fig 13.3**

Longitudinal deformations from rigging loads (Hunyadi & Hedlund)

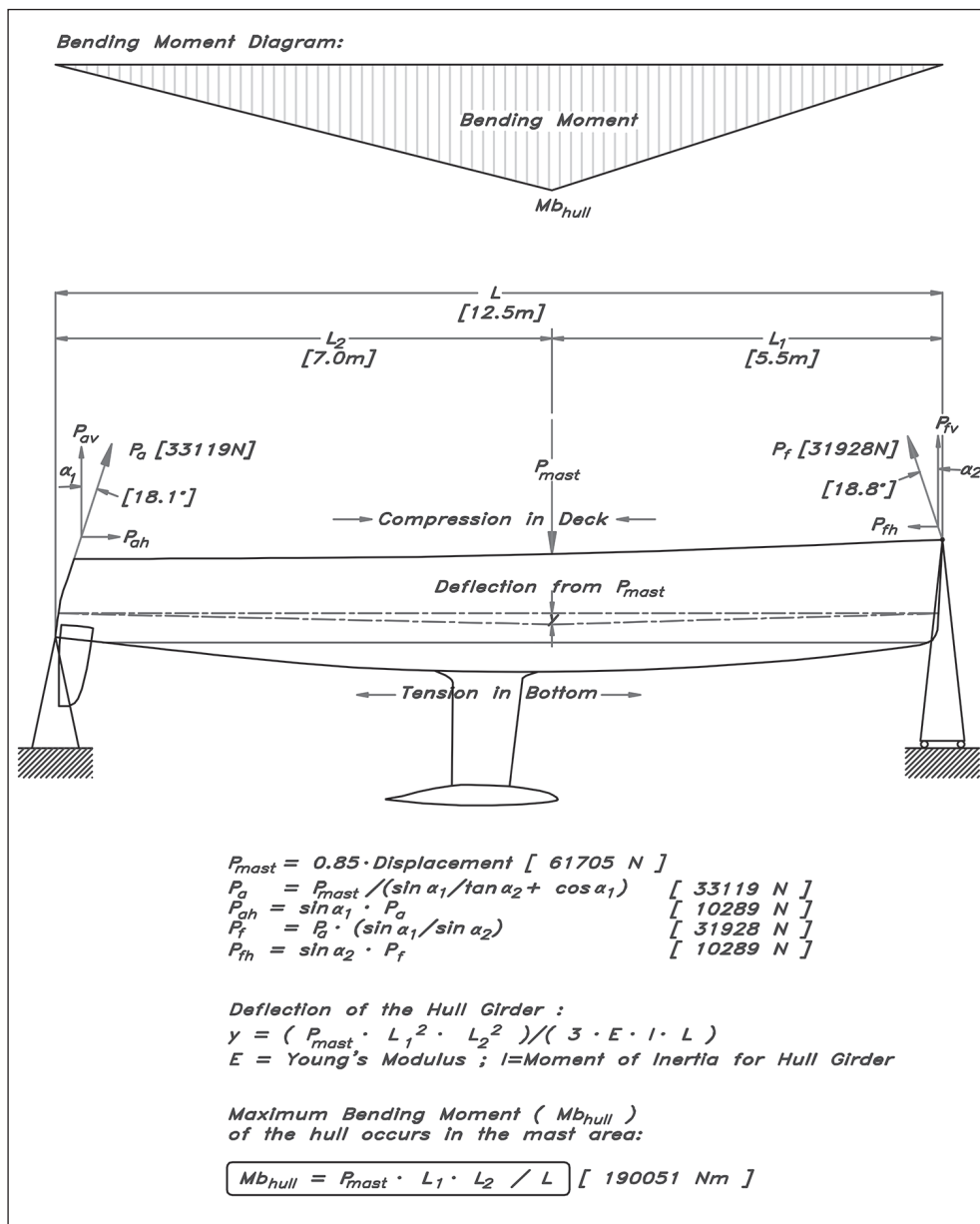


proposed Whitbread maxi was computed by the Royal Institute of Technology (KTH) in Stockholm (see Fig 13.3) with regard to longitudinal deformations due to rigging loads. Boat 'A' is stiffened by frames, spaced 2 metres, but no longitudinal members, and boat 'B' is stiffened by a pre-tensioned space frame. In both cases the hull is of sandwich construction, with a 40 mm PVC core and skins of S-glass in a vinyl-polyester matrix. As can be seen clearly it is not sufficient with just transverse frames to absorb the longitudinal rig-loadings, but a longitudinal stiffening system is needed. In the example shown it is in the form of a space frame, but a more usual approach today is to incorporate the stiffening system into the hull and deck structure, i.e. a monocoque type of structure. Most of the strength is put into the shell with this approach, with fewer internals and larger panels. The fibre orientation is crucial with the monocoque approach, and so is an analysis of the magnitude and direction of the forces involved. Boat size obviously plays an important role. Small vessels are almost self-supporting, i.e. monocoque, while the bigger ones need some sort of stiffeners, at least in specially loaded areas such as around the keel, mast, chainplates, etc.

The 'rig-sagging' condition is the most severe one for a sailing yacht as it puts the deck into compression and the keel into tension, whereas these parts are better suited to the reverse condition. Light decks are not fully effective in compression, as there is a risk of buckling which is worsened by the presence of deck hatches and other openings. A simple technique to counteract this weakening of the deck due to openings, is to use the reinforcement that should have been in the hole as an extra strengthening to the edge of the opening.

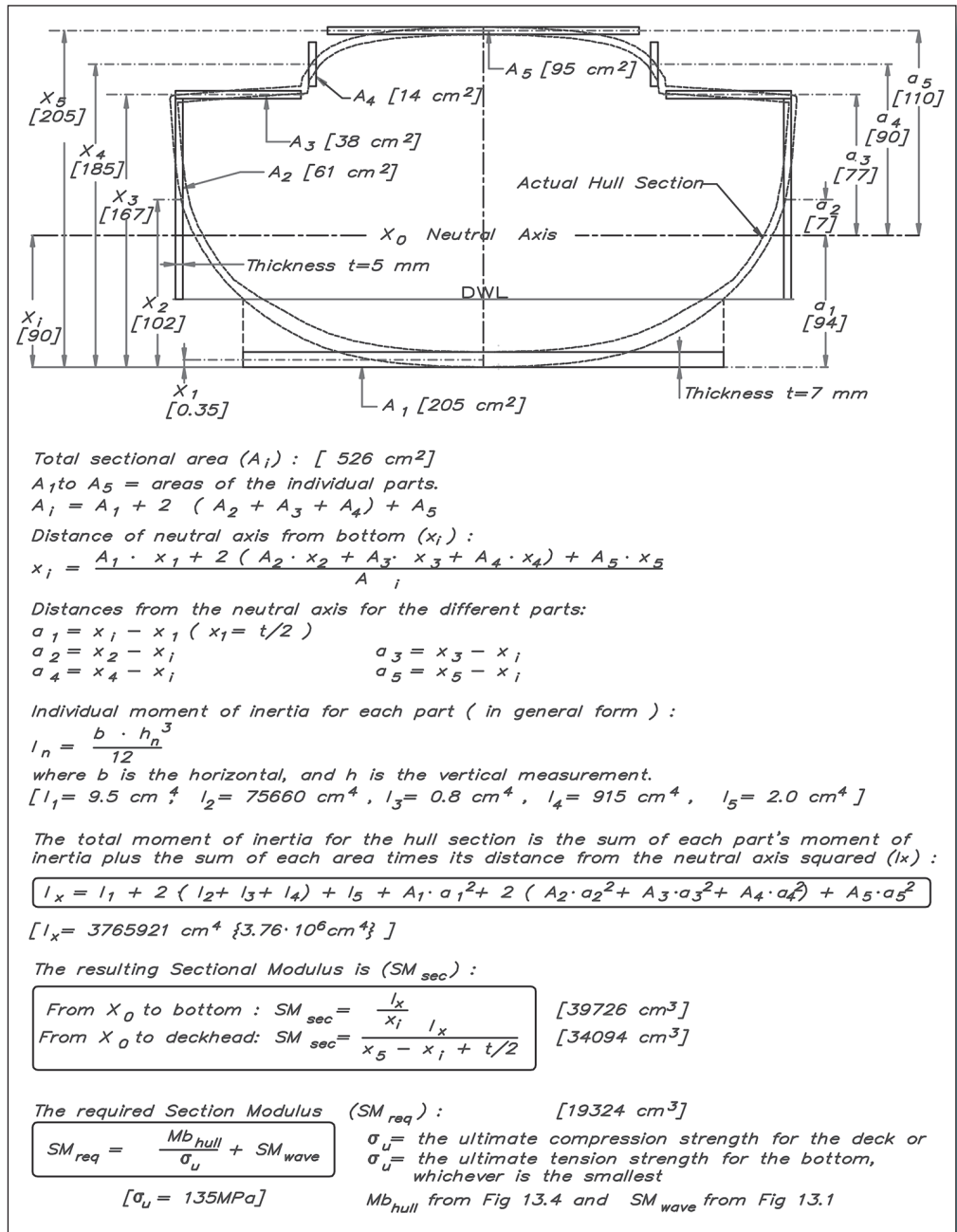
With regard to the YD-41, with 6.3 tonnes of pressure from the mast we can use a simplified model to estimate the required hull girder section modulus ( $SM_{\text{hull}}$ ). Considering the yacht to be a beam freely supported at its ends with the mast pressure trying to bend it, we will have a situation like that in Fig 13.4 (overleaf). The maximum bending moment occurs in the transverse section at the mast ( $M_{\text{b}_{\text{hull}}}$ ), so this is where we shall calculate the section modulus of the hull.

Fig 13.4 Longitudinal rig forces



In order to establish the required section modulus we must take our hull section at the mast and simplify it to make it practical to calculate. In Fig 13.5 the actual hull and deck is drawn with a dashed line, and the simplified section with a bold line. The aim with the simplification is to reduce the section to rectangular parts oriented orthogonally to the boat's Y and Z axis. Having reduced the section thus, it is comparatively easy to calculate the section's moment of inertia (I), area (A) and neutral axis ( $X_0$ ), and from these results the hull girder's section modulus (as shown in Fig 13.5). For the sake of simplicity the modulus of elasticity is assumed to be equal in all parts, otherwise corrections of areas have to be performed for the different parts, corresponding to the ratios of the different moduli.

**Fig 13.5** Hull girder section modulus at mast





In this example, the section is divided into five parts ( $A_1$ – $A_5$ ) with all parts of equal thickness ( $t$ ) except  $A_1$ , which is 60% thicker. In order to determine the section's neutral axis ( $X_0$ ) you calculate the geometrical centre of gravity for the parts, as shown in the figure.

The individual moments of inertia for the parts are then calculated and added to the areas of the parts, and their respective distances from the section's neutral axis squared. The resulting section modulus for the hull section is the moment of inertia, divided by the distance from the neutral axis to the deck and the bottom, respectively. Use the smallest value to compare with the required modulus to withstand the mast pressure, which is: maximum bending moment ( $M_{b_{hull}}$  from Fig 13.4) divided by the ultimate compressive strength for the deck and the ultimate tensile strength for the bottom.

For the YD-41 the moment from the mast pressure of 61705 N leads to a required hull girder section modulus of  $1408 \text{ cm}^3$  to take care of the longitudinal rig forces, and the actual boat has  $34094 \text{ cm}^3$ . The ABS requirement for hull girder strength on a 12.5 m motor yacht is  $17916 \text{ cm}^3$ , so the total required section modulus to handle all the forces becomes  $17916 + 1408 = 19324 \text{ cm}^3$  which leaves us with a factor of safety of 1.8 overall, and 24 looking only at rig forces. This is obviously enough, but if not, more or better material must be used if the section is to be geometrically unchanged.

A check of the maximum compression forces in the deck is now easily done:  $P_{deck} = M_{b_{hull}} / (a_5 + 0.5t) + P_{hd}$  ( $=179223 \text{ N}$ ). The expression  $(A_5 + 0.5t)$  is the distance from the top of the deck to the hull's neutral axis, see Fig 13.5.  $P_{hd}$  is the horizontal component of the fore and back stay tension, illustrated in Fig 13.4:  $P_{hd} = P_{fh} = P_{ah}$ . Dividing this value with the deck cross-sectional area, we will see if the deck is strong enough to absorb the compression forces. In our case the force in the deck leads to a compression stress of  $9.0 \text{ N/mm}^2$ , and with an ultimate allowable stress of  $135 \text{ N/mm}^2$  the safety margin is more than enough.

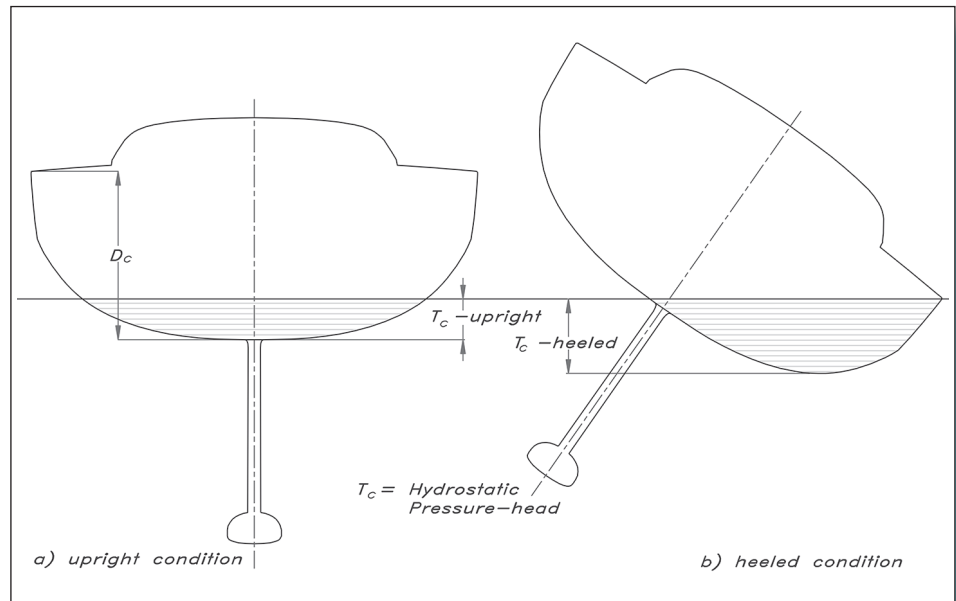
This might be considered the 'standard case'. A typical cruiser/racer dimensioned, by ISO 12215 or any other scantling rule, to withstand local pressure forces from the water, is strong enough to cope with the rigging forces. On extreme yachts though, with extraordinarily big rigs, low hull girder heights and built of 'exotic' materials with thin skins, it is wise to check the hull girder strength, and especially the compression and buckling stresses in the deck.

## ■ LOCAL HYDROSTATIC LOADS

To establish a proper design load let us begin with the hydrostatic part. The simplest case is when the boat is at rest and upright in calm water. Then the hydrostatic pressure head is simply the depth of the underwater body. This is the dimension  $T_c$ . For a vessel operating in a gale force breaking wave-train it is not excessive to assume that the crest reaches the sheer line, and so the static pressure would then become the  $D_c$  measurement (Fig 13.6(a)).

When under way and heeled in a rail-down condition, the immersed pressure head is approximately one-third to one-half of the full depth  $D_c$  depending on hull shape (Fig 13.6(b)).

**Fig 13.6** Hydrostatic pressures



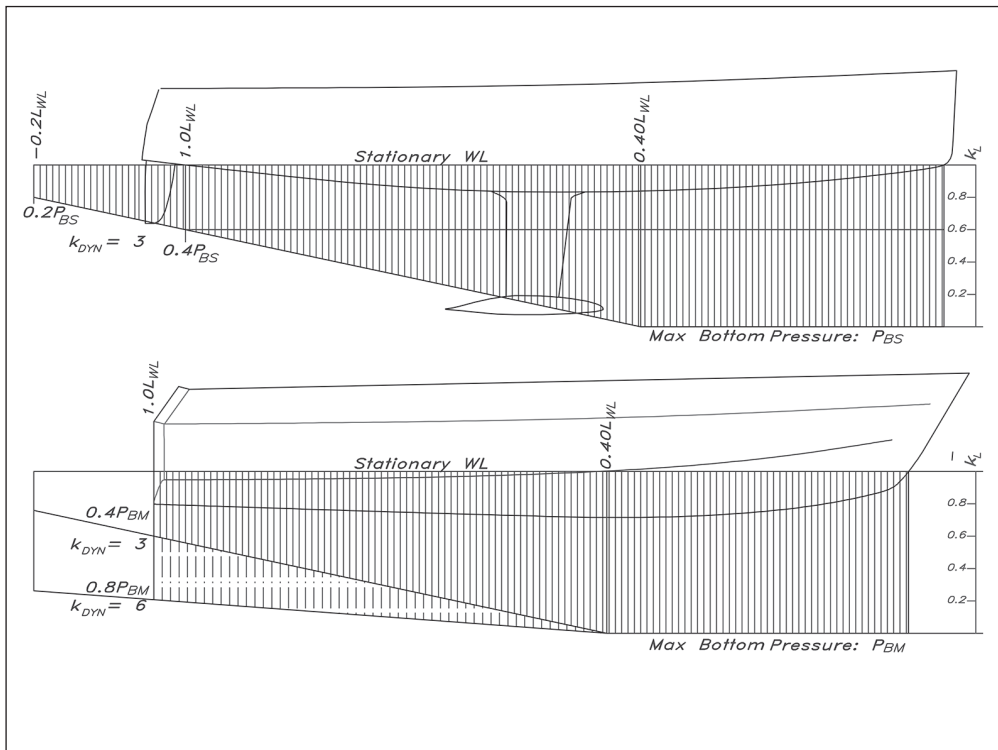
## LOCAL HYDRODYNAMIC LOADS

In the formula above no account is taken of speed, which naturally increases the pressure effects. It is commonly agreed that the pressure from speed varies with the speed squared, where speed is dealt with in terms of speed/length ratio. The ISO standard takes the speed as an absolute function of length for sailing craft, which means that ISO assumes a fixed speed/length ratio, plus an additional pressure-correcting factor for light boats. This additional loading is added to the hydrostatic pressure together with a constant pressure head to arrive at a bottom pressure ( $P_b$ ). We will deal with this in more detail when discussing the ISO rule.

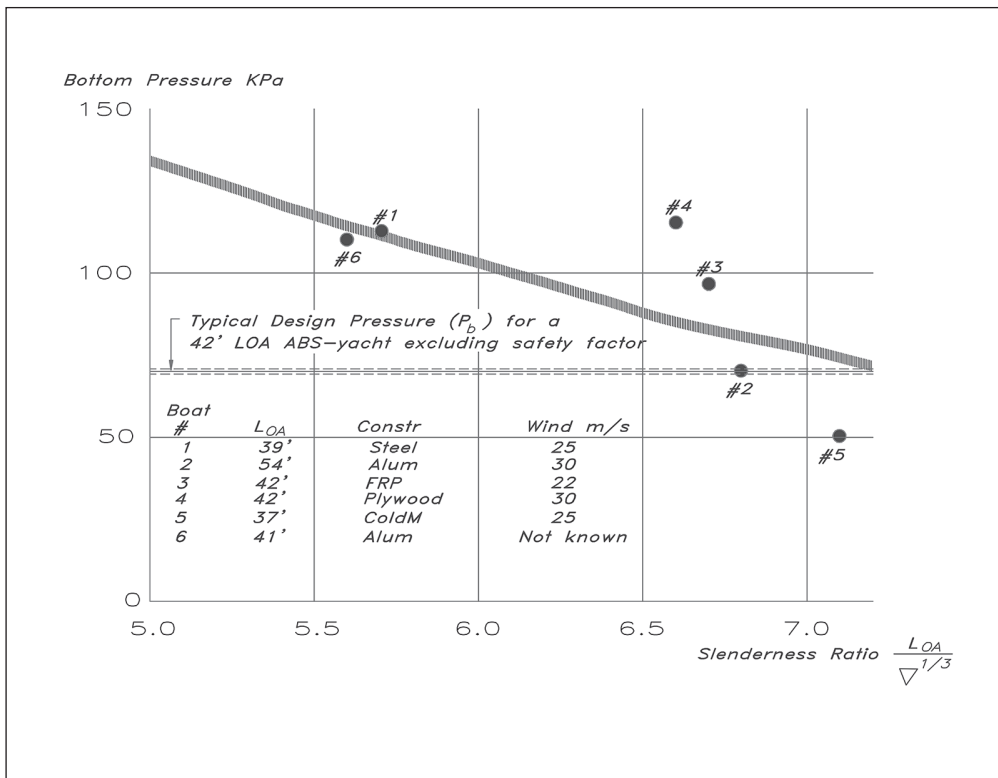
A vessel moving in a seaway is subjected to at least one more major load factor, that is, slamming. Several tests and measurements have been done to determine these loads, especially on planing powerboats, where the slamming effects are the most severe. One of the best recognized methods to deal with the slamming loads is made by Heller and Jasper, and this method, used by the ISO standard for power craft and fast sailing craft, gives a good fit for high-speed vessels. The formula takes speed, length, bottom deadrise, displacement and running trim into consideration when defining the bottom pressure ( $P_b$ ).

The work of Heller and Jasper has shown the primary slamming area to be in the forward sections of the boat, as can be seen from Fig 13.7 (overleaf). A word of caution though: on small fast boats with relatively high speeds ( $V(\text{knots})$  is greater than 6 times the square root of  $L(\text{m})$ ), the whole boat might be airborne in a big sea and land on the after part of the bottom, so it is wise to let the high pressure area be extended all the way to the transom on such a craft. Instead of dealing with speed length ratios ISO is using vertical accelerations ( $k_{\text{DYN}}$ ) to take speed into account.

**Fig 13.7**  
Longitudinal  
hydrodynamic loads  
(ISO)



**Fig 13.8** Calculated  
pressures from  
bottom failures  
(Joubert)



On the sailboat side Professor P N Joubert has calculated the bottom pressures for six sailing yachts that have been damaged by sea-forces but survived to be examined (Fig 13.8). The boats are:

1. *Odin*, a 39 ft steel yacht, buckled her bottom plating on a beat against a 25 m/s wind (50 knots). The deformed area was just ahead of the mast on one side between keel and  $L_{WL}$ .
2. *Pacha*, a 54 ft aluminium yacht, buckled a major part of the bottom in an area from the stem to the mast from keel to  $L_{WL}$ .
3. *Boomerang VII*, a 42 ft PVC-sandwich construction, delaminated in an area from stem to amidships from the keel up to some distance into the topsides.
4. *Destiny II*, a 42 ft plywood boat, got a transverse crack in her bottom where a structural bulkhead was attached.
5. *Magic Pudding*, a 37 ft cold moulded wooden boat, broke the same way as boat 4.
6. *Mary Blair*, a 41 ft aluminium boat, was injured in the same way as boat 2.

All these deformations, delaminations and cracks developed when the boats were on the wind. The reason for the failures were slamming loads, coming from the free falling of the boats from a crest down into the trough (a fall of 3 m (10 ft) or more).

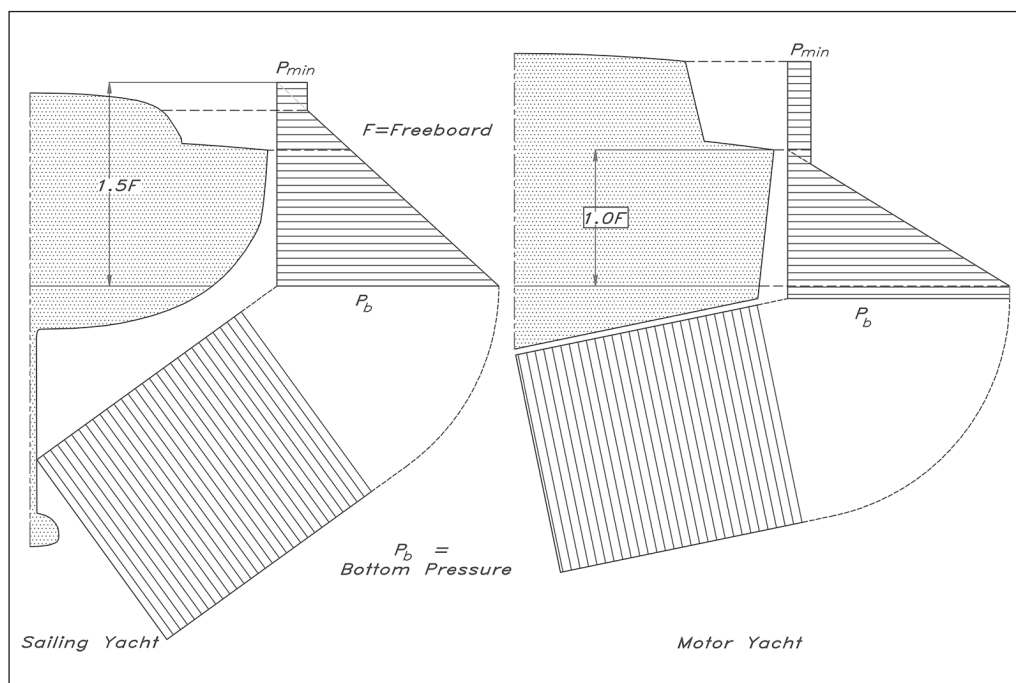
The pressure loads on the shells of the boats have been calculated 'backwards' by knowing the construction of each vessel. Depending on the calculation method, i.e. using simple beam theory or taking membrane stresses etc. into account, different pressures are reached. The more sophisticated calculation methods give a much higher pressure before the collapsing of the skin than does the beam theory. Fig 13.8 shows the result using the beam theory, with the boats ordered after slenderness ratio ( $L_{OA}/(\text{Displacement})^{1/3}$ ), and for comparison the ABS basic design head is represented by the dashed band. By including a design safety factor of 2 for the building materials, the allowable maximum pressures are taken care of by the ABS rule. Still the boats broke.

## ■ TRANSVERSE LOAD DISTRIBUTION

So much for the bottom pressure, but what about the sides? The longitudinal distribution follows that of the bottom, but transversely the pressure diminishes the higher up the topsides you move. And there is a difference between sail and power. Relatively speaking, a sailboat that in some instances has her topsides completely buried is more loaded in the side plating, compared to a planing powerboat, which is more subjected to slamming on its bottom.

On a sailboat the topside pressure falls off to zero at about 1.5 the freeboard height from full bottom pressure at the waterline. On a planning motorboat the side pressure

**Fig 13.9** Transverse load distribution (NBS)



according to ISO is 20% of the bottom pressure plus a minimum static pressure head corresponding to half hull depth ( $0.5 \cdot D_c$ ).

Deck and superstructure design pressures are functions of boat length and a constant. We will give more details of this when showing an example of a calculation using the ISO rule. Fig 13.9 shows typical transverse load distributions for sailing and motor yachts.

## LOCAL DEFORMATIONS

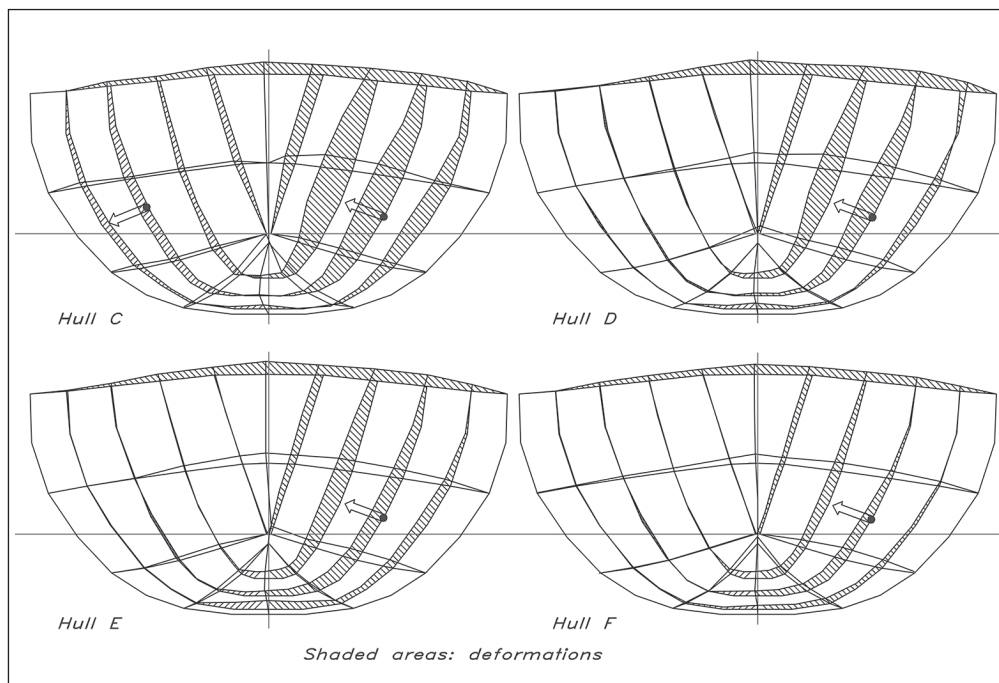
The Whitbread study of deformations made at KTH in Stockholm on different methods of stiffening a hull (Fig 13.10) shows that it is very important to have the forebody sufficiently stiffened. The hull is the same in all cases, with a different number of frames in the forward part. The hulls are basically stiffened by an inner space frame. The C boat has this space frame only, whereas the D boat has two additional stringers per side. In addition to this the E boat has one ring-frame before the mast, and the F boat has three ring-frames in the forebody.

The shaded areas in Fig 13.10 represent the deformed hull when subjected to slamming loads. As can be seen, the difference between the hull with only the space frame and the hull with stringers is not that great. The reason for this is that lacking transverse stiffeners the stringers get too long a span to effectively keep the deflections at a reasonable level.

By introducing a ring-frame into the forebody, i.e. frame spacing is 4.5 m, the deformations are diminished drastically, and by increasing the number to three the vessel starts to look like a boat even when under load (hull F in Fig 13.10). This ability to

**Fig 13.10**

Deformations due to slamming – shaded areas (Hunyadi & Hedlund)



withstand slamming pressures for the F hull shows roughly the same performance that a traditionally transversely frame-stiffened hull will give. As we have seen previously, the picture changes when dealing with longitudinal loadings. So, to summarize, the hull must be stiffened lengthwise as well as transversely to withstand the rigging and slamming forces. This can be done either by a separate stiffening system, by a monocoque structure or by a combination thereof.

## ■ FORCES FROM THE KEEL

Fig 13.11 shows an example of a calculation for stresses from the ballast keel on the YD-41. The ‘design-attitude’ for the boat is 90° heeled over and situated totally in air. Regarding the hull as in the air and applying a factor of safety of 4 to 6 takes care of the added loadings from dynamics, which are not incorporated in the formulae.

A simple calculation of moments around the keelbolts gives the transverse keel moment ( $M_{kt}$ ), and by dividing this moment with the distance between the windward keelbolts and leeward keel-edge ( $OF_{bolt}$ ) the keelbolt load ( $P_{kt}$ ) can be calculated (131686 N in our case).

The  $OF_{bolt}$  typically varies along the root chord of the keel, and to account for this it is reasonable to take a mean value of all  $OF_{bolt}$ s. Assuming the keel to have six pairs ( $n_{kb}$ ) of keelbolts, the loading on each bolt becomes ( $P_{kb} = P_{kt}/n_{kb}$ ) 16461 N. When calculating the required dimensions of the keelbolts it is the yield strength ( $\sigma_y$ ) of the material that shall be used, not the ultimate strength. The required diameter of the keelbolts ( $d_{kb}$ ), when using a safety factor of 5, becomes 23 mm, as can be seen from the formulae in Fig 13.11 (page 277).

The yield strength used in the example above is  $206 \text{ N/mm}^2$  which corresponds to stainless steel AISI-316. The diameter obtained is the minimum core diameter of the bolt, so the nominal bolt size will be a M27-bolt in the metric system or a 1  $\frac{1}{8}$  in bolt in the imperial system.

On the leeward side of the keel the tension in the keelbolts must be absorbed as a compression by the mating areas of the keel and hull. Since only the area nearest to the leeward edge is effective, it is reasonable to assume that 25% of the total area must be able to withstand a pressure corresponding to the total load on the bolts. The minimum required keel/hull area ( $A_{\min}$ ) is  $22510 \text{ mm}^2$ .

A typical ultimate strength in compression for a glassfibre laminate is  $117 \text{ N/mm}^2$  in compression. The actual keel has a 25% area of approximately  $100000 \text{ mm}^2$ , so the factor of safety is considerable in this case.

Each pair of keelbolts is connected to a floor, which has to absorb the moment induced by the tension in the windward keelbolt. The factor of safety for the floors is taken to be the same as for the keelbolts; in our example it is 5. So the bending moment working on each floor becomes the total transverse keel moment ( $M_{kt} \cdot 5$ ) divided by the number of floors, five in our example, which gives a bending moment ( $M_{fl}$ ) of  $36214 \text{ Nm}$ .

The required section modulus ( $SM_{fl}$ ) to withstand this moment is calculated by dividing the floor bending moment ( $M_{fl}$ ) by the floor laminate's ultimate strength in tension, typically  $125 \text{ N/mm}^2$  for a glassfibre laminate, and in this case it becomes  $290 \text{ cm}^3$ . The result comes out in  $\text{cm}^3$  when using  $\text{Nm}$  for the moment and  $\text{N/mm}^2$  for the strength value.

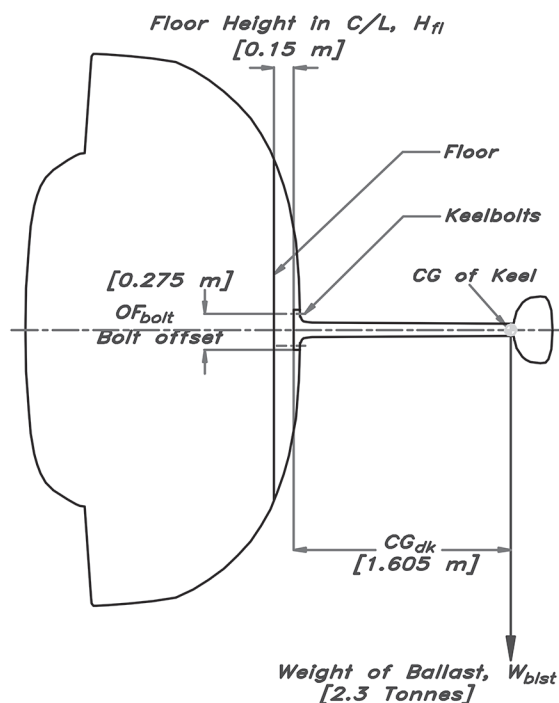
Entering the diagram of Fig 13.11 with an  $SM$ -value of  $290 \text{ cm}^3$  and choosing a floor height ( $H$ ) of  $15 \text{ cm}$  we need a flange area of  $16 \text{ cm}^2$  and a thickness of  $1.5 \text{ cm}$ . So the minimum floor breadth is  $10.7 \text{ cm}$ . If the keelbolts are passing through the floor, we must add their diameters to the breadth of the floor to achieve sufficient flange area, i.e. total breadth becomes  $13 \text{ cm}$ . These values are relevant for the floor section at the centreline; at the ends the required section modulus can be taken as half of that at the centreline,  $145 \text{ cm}^3$  for our boat. This leads to a section of  $8.0 \text{ cm}$  height, keeping the laminate thickness, breadth and flange area the same as at the centreline.

## ■ FORCES FROM GROUNDING

It is not practical to calculate the impact force  $F_i$  exactly. It depends on the weight and speed of the vessel, the relative weight of the ballast keel and its centre of gravity, as well as the shape of the seabed or rock (which governs the time of retardation) and the shape of the boat (which has great importance regarding the damping of the movement). For now it is sufficient to make some simplifications on the conservative side in order to guarantee the strength, since a slight increase of weight in this area seldom poses any substantial problems.

From Fig 13.12 (overleaf) it can be seen that the impact force  $F_i$  gives a moment in the keel/hull area ( $M_{kl}$ ) of  $203308 \text{ Nm}$ . In order to arrive at this figure and to solve the equations of Fig 13.12, some assumptions have to be made. We assume the boat's speed to be 8 knots,  $V_s = 4.11 \text{ m/s}$ , and that the time to a full stop ( $t_s$ ) is 0.25 seconds. This equals a 'stopping-distance' of approximately half a metre (which is rather a sudden stop) and gives





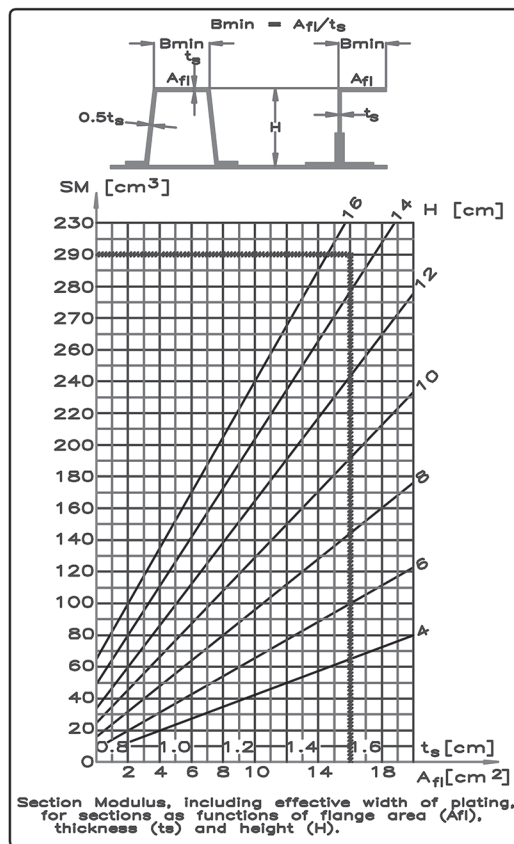
**Transverse Keel Moment ( $M_{kt}$ ) :**  
 $M_{kt} = CG_{dk} \cdot W_{blst} \cdot g$  [ 36214 Nm ]

**Total Keelbolt Load ( $P_{kt}$ ) :**  
 $P_{kt} = \frac{M_{kt}}{OF_{bolt}}$  [ 131686 N ]

**Required Keelbolt Diameter ( $d_{kb}$ ) :**  
 $d_{kb} = 2 \cdot \sqrt{\frac{P_{kb} \cdot \eta_{kb}}{\sigma_y \cdot \pi}}$  [ 23 mm ]

**Minimum Keel/Hull-Area ( $A_{min}$ ) :**  
 $A_{min} = \frac{P_{kb} \cdot \eta_{kb} \cdot \eta_{kb}}{0.25 \cdot \sigma_{uc}}$  [ 22510 mm<sup>2</sup> ]

**Required Section Modulus for Floors ( $SM_{fl}$ ) :**  
 $SM_{fl} = \frac{M_{fl}}{\sigma_{ut}}$  [ 290 cm<sup>3</sup> ]



**Keelbolt Tension ( $P_{kb}$ ) :**  
 $P_{kb} = \frac{P_{kt}}{\eta_{kb}}$  [ 16461 N ]

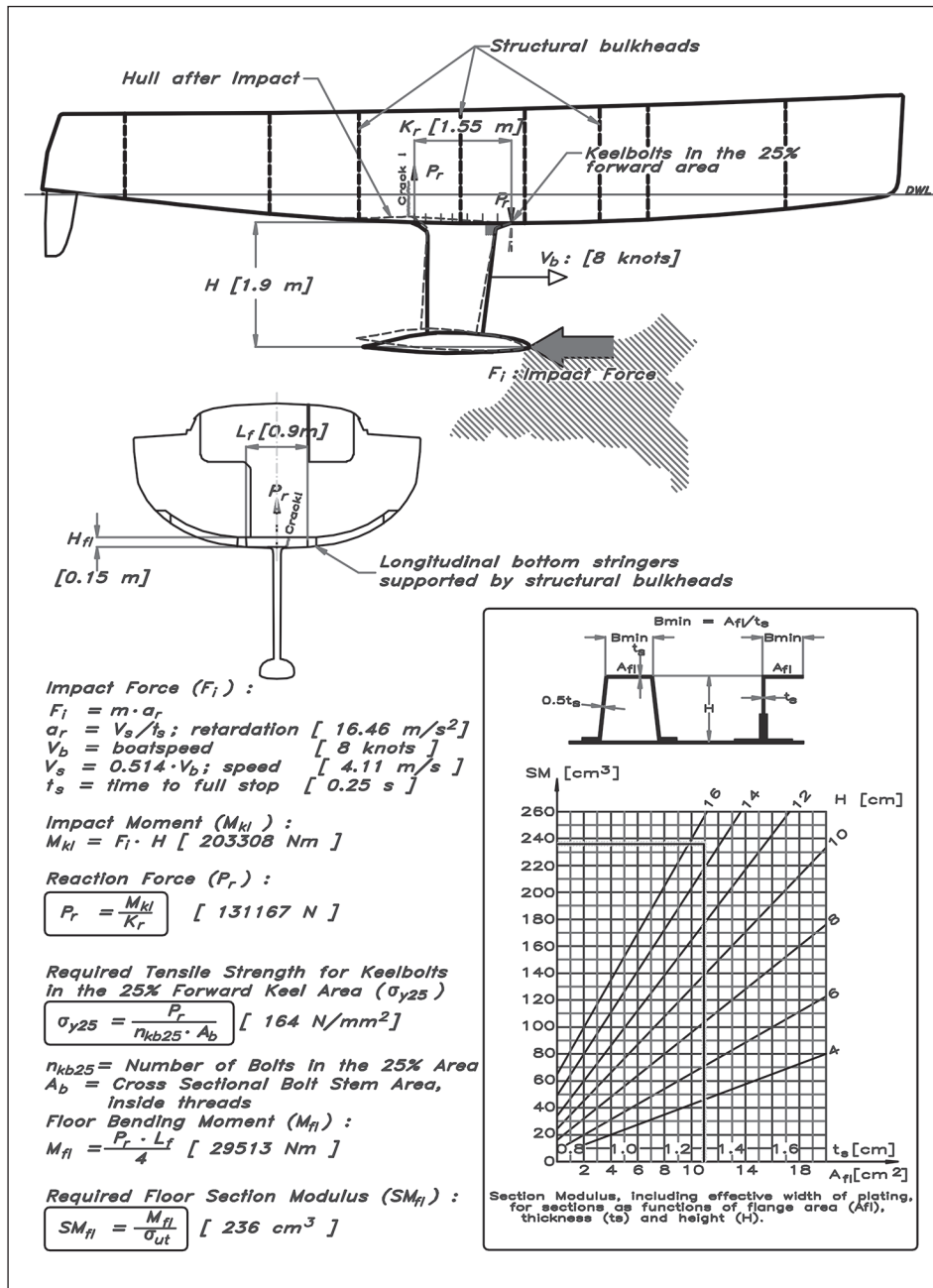
$\eta_{kb}$  = number of keelbolts [8]  
 $\eta_{kb}$  = factor of safety; 4–6 [5]  
 $\sigma_y$  = yield strength for keelbolts (206 N/mm<sup>2</sup> for AISI-316)

**Floor Bending Moment ( $M_{fl}$ ) :**  
 $M_{fl} = \frac{M_{kt} \cdot \eta_{kb}}{\eta_{fl}}$  [ 36214 Nm ]

$\eta_{fl}$  = number of floors over keel [5]  
 $\sigma_{uc}$  = typical ultimate strength in compression for GRP (117 N/mm<sup>2</sup>)  
 $\sigma_{ut}$  = typical ultimate strength in tension for GRP (125 N/mm<sup>2</sup>)

Fig 13.11 Loadings from the keel

Fig 13.12 Loadings from grounding



a retardation of  $a_r = V_s / t_s (= 16.46 \text{ m/s}^2)$ . Since the displacement of the vessel is 6500 kg this gives an impact force  $F_i = \text{Displ} \cdot a_r$ , 107000 N). Now it is easy to calculate the impact moment,  $M_{kl}$ , from the formula in the figure, and from this the resultant force  $P_r$ , 131167 N, can be calculated by dividing the impact moment by the length of the keel. This force acts as a pressure on the aft part of the keel, and as tension on the forward part. As can be clearly seen from these equations, a short and/or deep keel gives much higher loadings on the hull when running aground.

The centre of rotation for the keel is very uncertain and depends on the stiffness of different parts of the keel/hull joint as well as the slope and/or the geometry of the joint. Since the keelbolts and the material in the joint are more deformed the further you get from the rotational centre, it is probable that only the most forward bolts are fully tensioned, and that the joint area is subjected to maximum pressure only in its aft part.

A reasonable way to calculate the required tensile strength ( $\sigma_{y25}$ ) for the most forward bolts, is to assume that the number of bolts situated within the forward 25% of the keel ( $n_{kb25}$ ) takes care of the forces from the grounding ( $P_r$ ). In the YD-41 we have two bolts in the actual area, so the required tensile strength becomes  $164 \text{ N/mm}^2$ , as can be seen from the formula in Fig 13.12. Since the yield strength for AISI-316 stainless steel is  $206 \text{ N/mm}^2$  it is obvious that there is no risk of tearing the keelbolts apart by running aground with this boat. The most sensitive area is the aft part, where the keel meets the hull.

The maximum thrust from the grounding is  $P_r$  and occurs at the trailing edge of the keel. This force gives a bending moment in the floor supporting the aft part of the fin  $M_{kl}$  of  $29513 \text{ Nm}$ , and it is calculated by multiplying the thrust by one quarter of  $L_f$ , where  $L_f$  is the length of the floor supporting the keel as illustrated in Fig 13.12.

This bending moment requires a section modulus,  $SM_{fl}$ , of the floor of  $236 \text{ cm}^3$ . Entering the diagram in Fig 13.12 with this section modulus we read off a laminate thickness of  $1.3 \text{ cm}$  with the chosen floor height,  $H$ , of  $15 \text{ cm}$ . The minimum flange area is  $11 \text{ cm}^2$  which leads to a floor width of  $8.5 \text{ cm}$ . One potential problem in real life with a shallow hull is the lack of space between the sole and the bottom of the canoe body. It may not be possible to fit a floor of this height, and in that case we must use multiple floors in this area and divide the grounding force between them.

## ■ FORCES FROM THE RUDDER

The rudder forces are developed when the rudder is producing a side force, i.e. when you are (a) turning the boat or (b) trying to counteract a turning moment. In the first case it is not necessary that the maximum force is developed, since the boat gives way for the side force by actually turning. In the second case it is more likely that maximum forces will develop. A typical case is when trying to counteract a broach when spinnaker reaching.

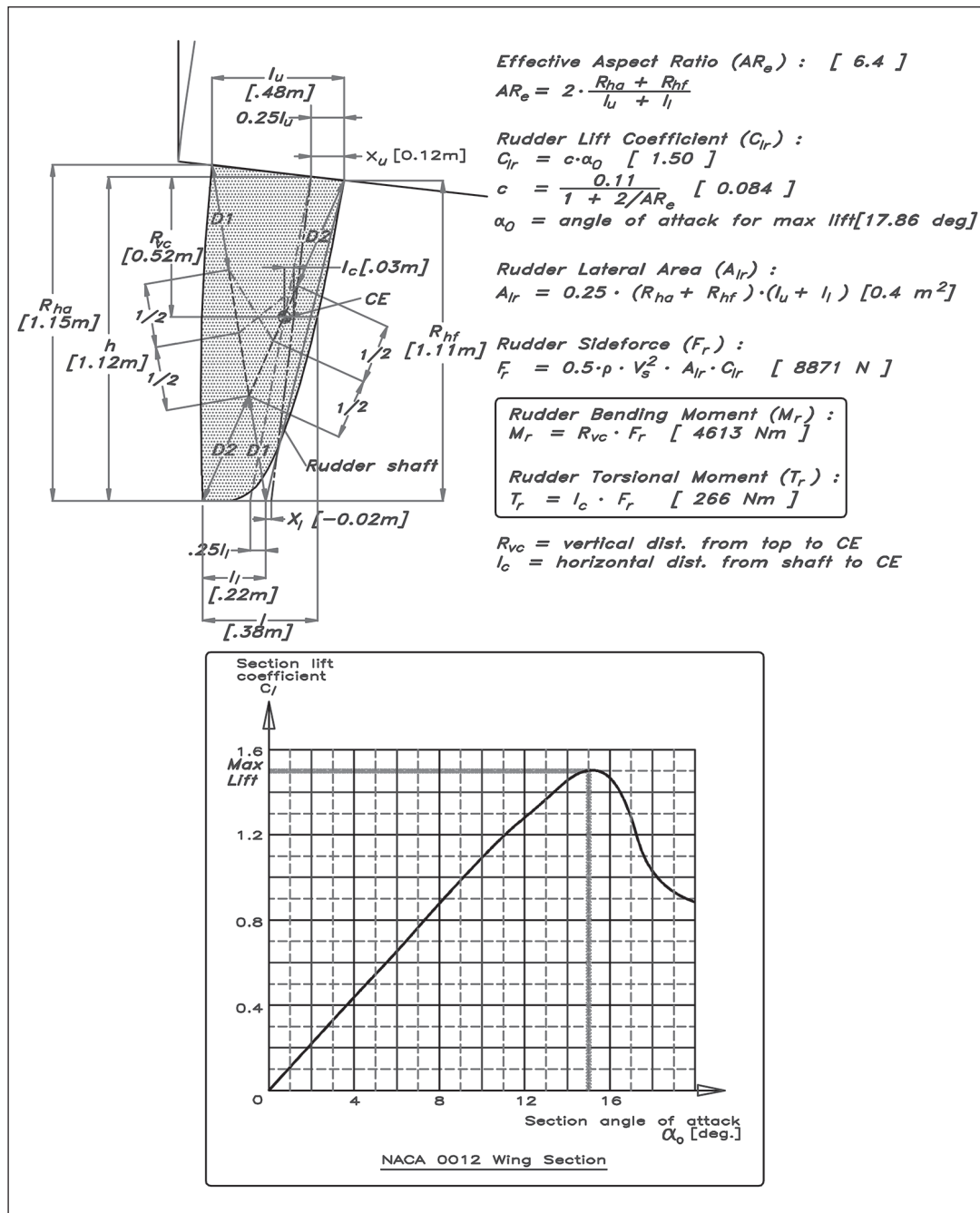
Fig 13.13 shows a typical spade rudder. In the following simplified calculations we have used double the geometric aspect ratio, the effective aspect ratio ( $AR_e$ ), which means that we do not take any ventilation into account and that the rudder is close to the boat bottom. This is hardly ever the case in reality, but it gives us an extra safety factor, because the forces are exaggerated this way.

The centre of effort for the rudder profile (NACA 0012) lies 25% aft of the leading edge ( $0.25l_u = 12 \text{ cm}$  &  $0.25l_l = 5.5 \text{ cm}$ ). Vertically, the position can be calculated as indicated in Fig 13.13. By deducting the short parts (D1 and D2) from the full-length diagonals and triangulating the remaining parts (showed as dashed lines) we can accurately position the geometric centre of effort, but here we only use the vertical distance,  $R_{vc}$ . Normally this figure will be in the region of 45% of the total height. Knowing the CE position and the 25% line, the distance from the leading edge to the CE can be calculated easily. Also,

knowing the position of the rudder shaft means that the corresponding distance (shaft centre line to CE)  $l = 5.3 \text{ cm}$  is easily determined.

The effective aspect ratio,  $AR_e$ , is double the ratio between the average height and the average length of the rudder (6.5). The lateral area  $A_{lr}$  of the rudder is the average height times the average length,  $0.4 \text{ m}^2$ . These values are used to compute the lift coefficient and side force, according to the formulae and diagram in Fig 13.13.

Fig 13.13 Loadings from the rudder



As can be seen from the diagram in Fig 13.13 the maximum section lift coefficient,  $C_{L_s}$ , is 1.5 and occurs at a section angle of attack,  $\alpha_0$ , of  $15^\circ$ . The resulting lift coefficient of the entire rudder,  $C_{L_r}$ , can be approximated also to 1.5, and, according to the rudder lift coefficient equation,  $C_{L_r}$ , of Fig 13.13, the angle of attack will be  $17.86^\circ$ . The reason for this difference between the section angle of attack and the actual angle of attack is that the section coefficient assumes an infinite aspect ratio and consequently no end leakage and induced resistance.

The side force ( $F_r$ ) this rudder delivers, at a speed ( $V$ ) of 10.5 knots ( $V_s = 5.4$  m/s) is 8871 N for our rudder. This side force is the load that determines the bending,  $M_r$ , and torsional,  $T_r$ , moments on the rudder shaft.  $M_r = 4613$  Nm and  $T_r = 266$  Nm in this example.

This bending moment in the rudder shaft occurs at the hull bearing, and the torsional moment in the shaft at the attachment of the tiller arm, quadrant or tiller. The loading in the upper part of the rudder is a combination of these two moments, but in the lower part only the torsional moment is involved.

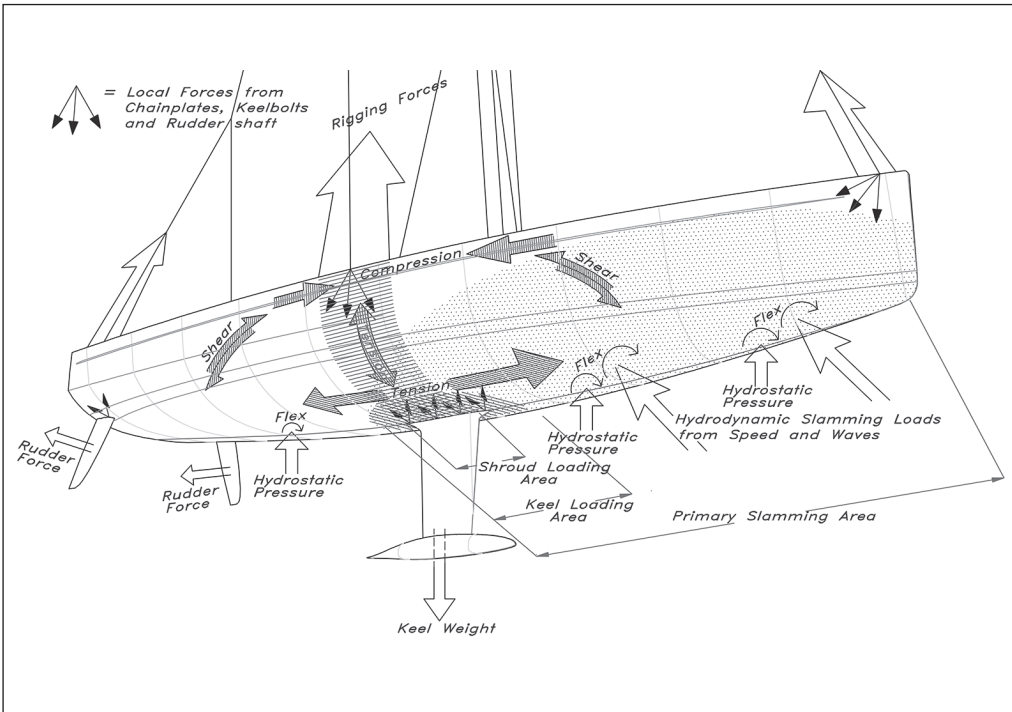
In the section on the ISO rule we will calculate the rudder shaft, but now let us see what demand the  $T_r$  puts on the steering mechanism. Assuming we are using a 10 in radius (0.25 m) rudder quadrant, the force in the steering cable will be  $266/0.3 = 887$  N. The mechanical losses (friction, etc.) are approximately 20%, so the required force from the steering gear is 3106 N. The drive gear has a radius of 6 cm, which means that the steering moment is  $976 \cdot 0.06 = 58.5$  Nm. With a wheel diameter of 0.9 m the force the helmsman must use becomes  $58.5/(0.9 \cdot 0.5) = 130$  N. The equivalent tiller length would be  $266/130 = 2.04$  m, quite a substantial tiller to match the wheel for power.

## ■ SUMMARY OF LOADINGS

Fig 13.14 shows the windward side of a sailing yacht beating into the wind. The shaded arrows indicate global loads imposed on the hull girder from the rigging forces. They are increased when the yacht is in hull sagging position, which is the case when travelling at hull speed in smooth water. As can be seen, the hull girder is subjected to bending which gives compression forces along the deck edge, tension along the bottom and shear forces in the topsides. On top of this there is transverse tension in the shroud area. Sailing in rough and steep seas might induce hull hogging too, not that the bending moment change sign, i.e. the deck comes under tension (the rigging forces are too great to let that happen), but there will be pulsating compression and tension in the hull with the inherent risk of fatigue in the long run.

Furthermore, we have the local loadings, the hydrostatic pressure, with additional loadings from slamming in the forward part of the boat, which tries to buckle the plating and bend the stiffeners. These are the most important forces when calculating the thickness of the skin and scantlings of the stiffeners. As previously shown, the global strength of the vessel is sufficient if it is dimensioned to withstand hydrostatic and hydrodynamic loads, at least if it is of a 'non-extreme' type. Other local loadings that must be taken into consideration are the ones that stem from attachments of shrouds and stays, keelbolts, rudder shaft, winches and other deck hardware.

**Fig 13.14** Forces on a sailing yacht



**Fig 13.15** Loaded areas

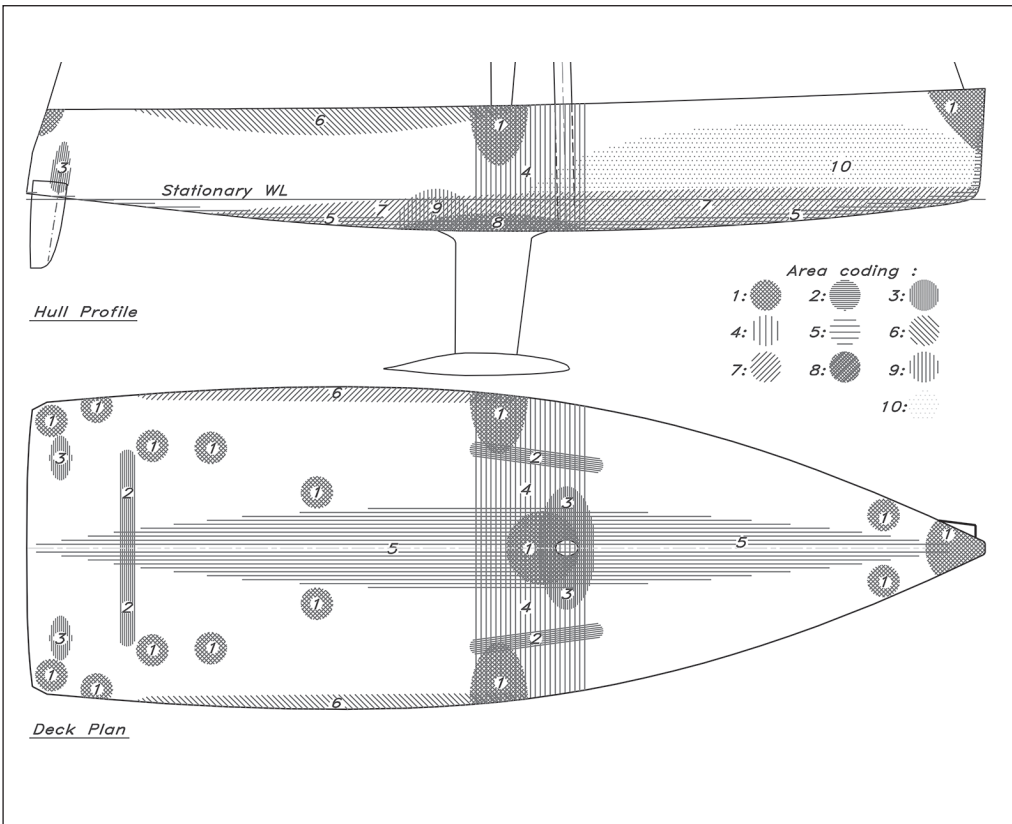




Fig 13.15 shows the boat divided into primary 'concern areas' regarding loadings. A qualitative look into the consequences for the different areas when it comes to dimensioning and building gives us the following points:

### Loaded areas

1. Local loadings from attachments, i.e. chainplates, stay fittings, cleats, winches, stanchions, etc. places demand on the laminate to be strengthened in order to cope with such big, local loads. To help the laminate, this means ensuring there are large washers under bolts and, in the case of a sandwich laminate, that the sandwich core is substituted for plywood, a very high density core or a single laminate. The last option, which might seem to be the most old-fashioned solution, actually has several advantages. First, regardless of core material (plywood or high density foam), the laminate in itself is better suited to withstand the compressional forces involved with through-bolting of deck fittings, and secondly, by going down into single laminate in these areas, the bolt heads or nuts will be countersunk into the core thickness, without disturbing the underdeck ceiling, etc. It is wise though to increase laminate thickness and not leave it as just the combined inner and outer laminates. An increase of approximately 40% would not be out of order.
2. Basically the same comments as in area 1 are valid, but since these (2) areas concern primarily sheet tracks, with a more spread out load distribution the demands on the area concerned also mean that the extremely local bolt loads are less, and the increase in laminate thickness of 25% would be enough.
3. These areas are loaded by transverse forces from the mast and the rudder. The laminate must be able to withstand the edge-pressure, i.e. use a hard core or rather change to a solid beefed-up laminate.
4. This is an area extraordinarily loaded by rigging forces from the shrouds and the mast. The whole section in this area must be exceptionally stiff and resistant to torsional forces, so as not to collapse transversely. To achieve this, framing has to be increased, a structural bulkhead has to be fitted or a load-bearing space frame has to be fitted to absorb and distribute the loadings.
5. Longitudinal forces from the rig and waves mean that the deck might need to be strengthened with stringers to withstand the pressure and the hull in the bottom area in order to withstand the tension. The demands on the bottom to cope with loadings from the keel and slamming make it strong enough to absorb the global bending forces in most cases, but there is still the risk of the deck not being able to withstand the resultant compression forces if the hull girder is shallow or the rig exceptionally large.
6. This is an extra stressed area due to pulsating loads coming from the vessel working in waves. Special consideration might be necessary regarding the compression/tension properties of the laminate, but more likely the weak link is the deck-to-hull joint, which must be strong enough not to move or buckle, in order to avoid leakage. When the joint is not glassed over, but fixed only with bolts and a bedding compound, it is wise to use an aluminium toe rail at the



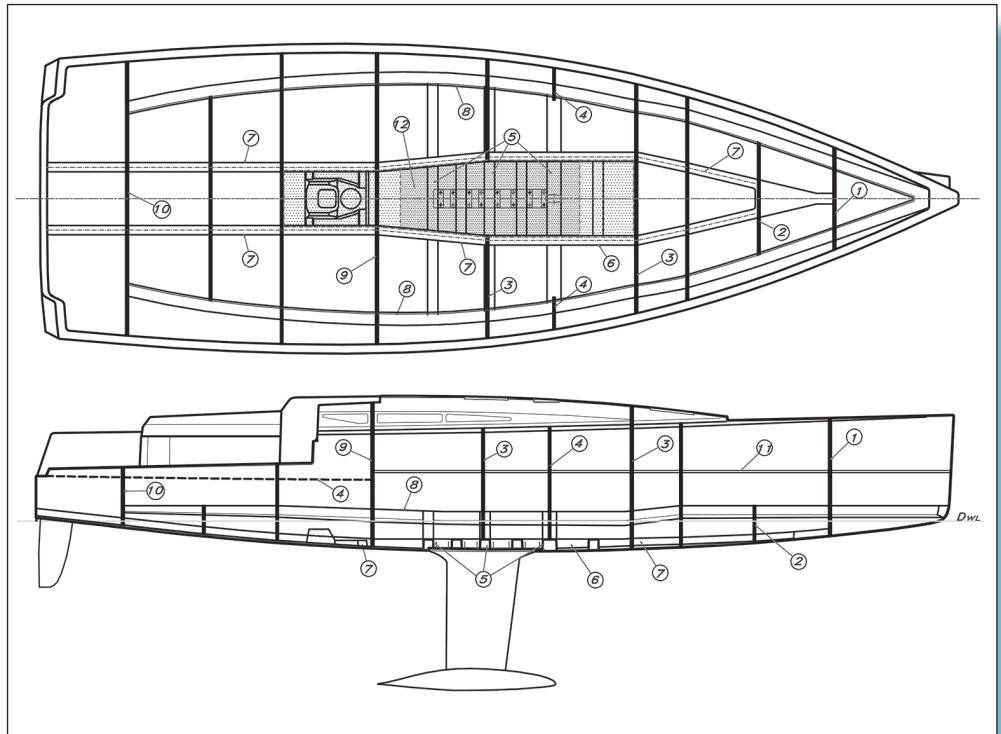
deck edge, which will stiffen the edge section so that it does not open under load. Another way to obtain the same effect is to design the edge of the deck as a box (top-hat) girder

7. The bottom panels in this area, i.e. forward of amidships and gradually tapering off towards the stern, are the most heavily loaded ones, with regard to hydrostatic and hydrodynamic loads. This puts a demand on the panels to be stronger and stiffer than on the rest of the bottom. When using a common lay-up over the entire bottom (which is the practice in series production), a 'strengthening effect' can be obtained by using a denser stiffening system in this area, thereby reducing the panel sizes
8. An area that is loaded by the keel. The demands on this area require that the laminate be thick enough to withstand high local pressures from the keelbolts
9. Transversely the area must be stiff enough not to let the keel act like a pendulum when beating in a seaway. The area in the aft part of the keel is most vulnerable when running aground. The grounding force must be spread over a larger area than the keel/hull joint itself
10. This is the primary slamming area, putting extra heavy demand on the strength and stiffness of the panels involved. The forces from waves are much greater than when sailing in flat water.

Fig 13.16 shows the YD-41, which is stiffened according to the points above. Basically, the boat is stiffened by a system of longitudinal stringers, transverse frames and load carrying bulkheads. Looking at the system, starting from the bow, we have the following:

1. A watertight, structural collision bulkhead of sandwich construction which effectively strengthens this slamming area
2. Extra floor in the forebody bottom to absorb slamming forces
3. Topside stringer running along the hull up to the point where a chine angle can be acute enough to be regarded as a stiffener
4. Structural sandwich bulkheads to strengthen the torsional rigidity of the hull/deck beam, to be stiff enough to resist the rig's transverse forces
5. Extra webs in the jib track and mast area
6. Structural sandwich bulkheads in the shroud area also supporting the longitudinal bottom stringers
7. A system of floors to distribute forces from the keel, the mast and from grounding
8. Integrated mast-step girders spanning between area four bulkheads, in order to distribute the mast load longitudinally over a number of bottom floors

**Fig 13.16** Stiffening system – YD–41  
– sandwich hull



9. Longitudinal bottom stringers from the collision bulkhead to the aftermost bulkhead. The bottom floors are connected to these stringers at their ends
10. Side stringers that run the entire length of the boat and whose support points are the structural bulkheads
11. A structural sandwich bulkhead also isolating the engine room from the accommodation, together with the engine casing
12. Hull chines used as a longitudinal stiffener
13. Additional structural sandwich bulkhead to strengthen the bottom and support cockpit sole
14. Extra web in the aft body strengthening the bottom
15. The aftermost structural, watertight sandwich bulkhead, stiffening the aft body not to bend or flex from rudder forces, and take forces from the main sheet track and the pedestals.

Detailed calculations of the actual dimensions of the panels and stiffeners for the YD–41 are to be found in [Chapter 15](#). We now turn to a discussion of materials.

# 14 MATERIALS

Fibre-reinforced plastic (FRP) has been used widely in boat hulls and decks. Recently, interest in this material has grown among the other fields of the marine industry as well. One of the advantages of FRP in primary structures is the possibility of tailoring the strength properties of the laminate according to the need, and thus obtaining lighter but stronger structures. However, optimum solutions demand sophisticated calculation methods and material evaluations.

In contrast to steel, aluminium and to some extent wood, you build your own material when using resin and reinforcement to produce FRP laminate. It can be made in different ways and with different ingredients, so to give just one typical FRP strength value is not meaningful. You must know the actual lay-up in order to calculate its strength. The most important parameter that affects the strength is the form of the reinforcement and what it is made of. The most widely used reinforcement in the boatbuilding industry is E-glass. There may be better materials strengthwise, but as yet the combined cost, strength and effectiveness of E-glass has not been equalled.

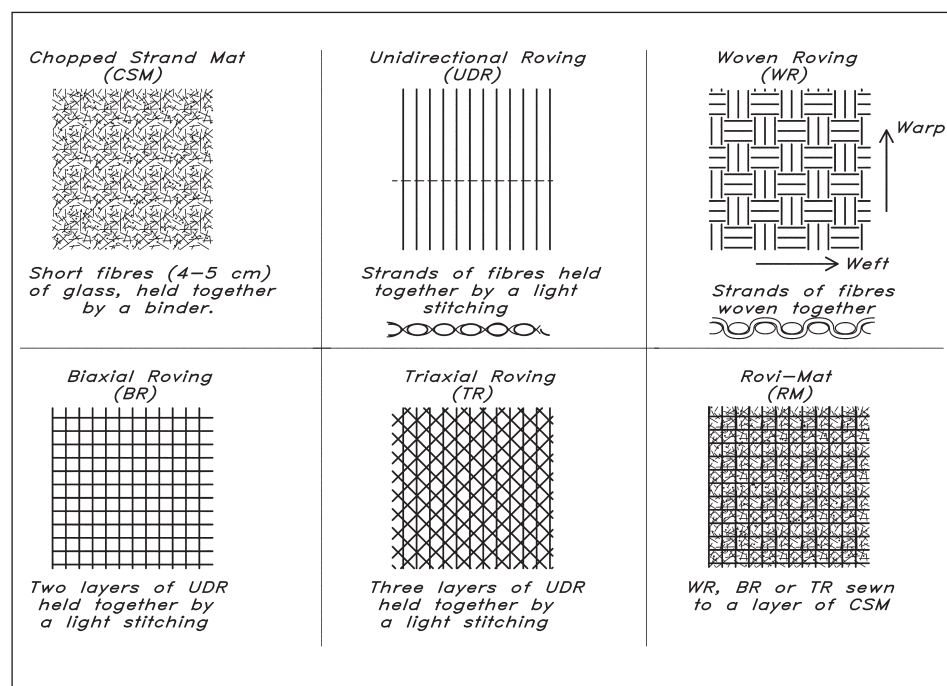


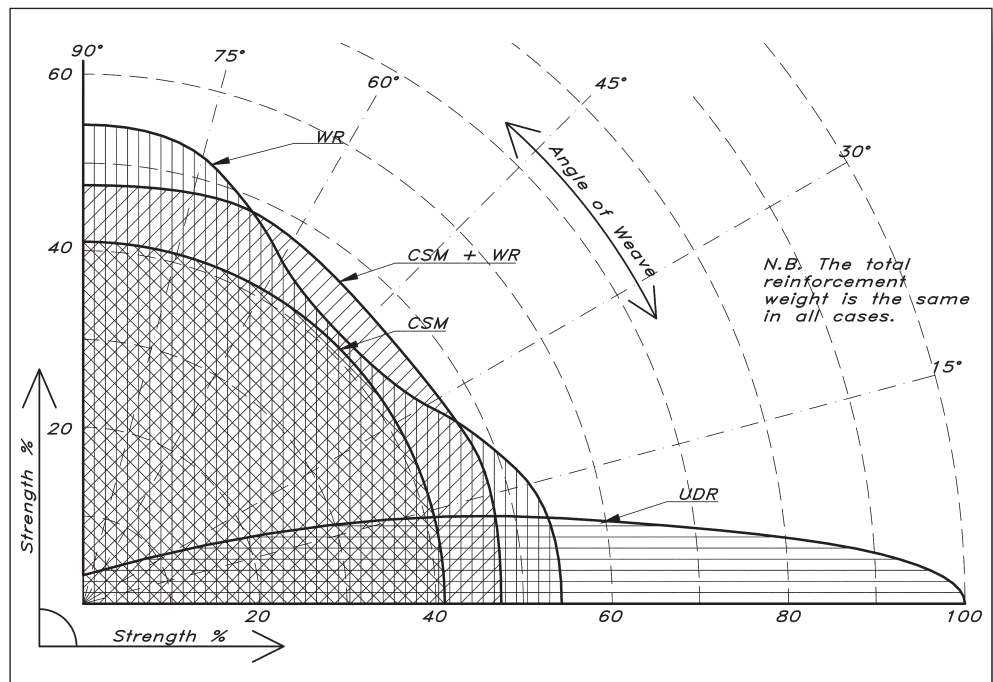
Fig 14.1 Reinforcement types

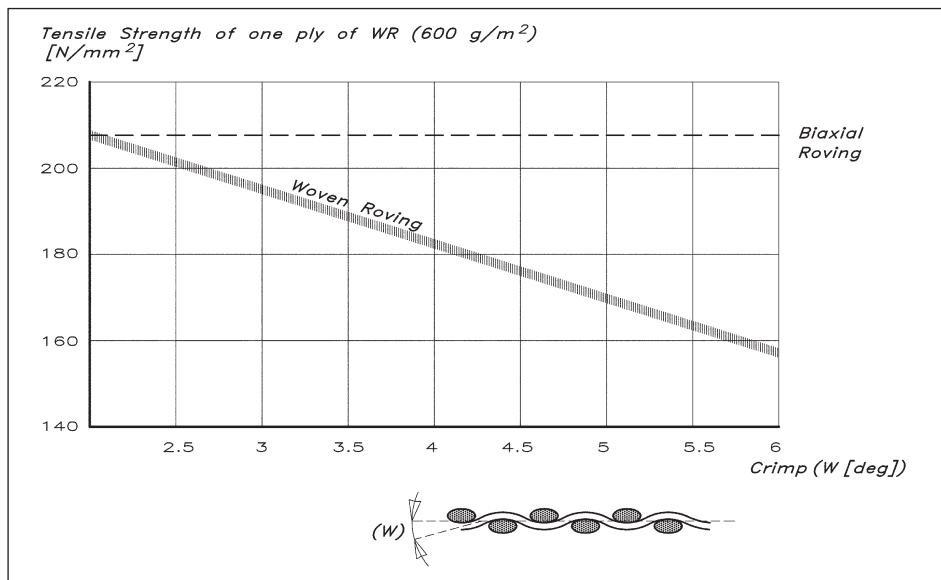
## GLASS REINFORCEMENT

Glass reinforcements come in a variety of shapes (as illustrated in Fig 14.1). The most commonly used type is chopped strand mat (CSM), which consists of short fibres, 4–5 cm long, evenly distributed and held together by a binder. The binder is of either an emulsion or powder type, which is dissolved by the styrene in the resin when wetting out the laminate. CSM is not suitable when using an epoxy resin as this does not contain any styrene, and consequently does not dissolve the binder. The emulsion type is slightly easier to work with because the powder type is more fragile and must be handled with care. One big drawback with the emulsion type, however, is that it is prone to osmosis, so in the outer part of a laminate at least the powder type should be used. While CSM is more or less isotropic (i.e. has the same strength in all directions), the other types are much more sensitive to the direction of load. This can become an advantage when building the lay-up, if one lines up the fibres with the primary load directions in order to take the best advantage of the available reinforcement materials. The use of rovings to take care of the primary loads is a good idea, but to ensure sufficient inter-laminar strength (strength between plies of reinforcement), the practice is to put in a layer of CSM between each roving layer. Manufacturers of glass reinforcement have noted this, and they have come up with a mat/roving combination: a roving sewn to a mat so that one can achieve the proper mix in one lay-up process. The most direction-sensitive type of reinforcement is the unidirectional type, which has virtually no strength in the 90° direction (see Fig 14.2).

The maximum slope of the fibres (crimp) in a woven roving (WR) has a strong influence on the tensile and compressive strength of the laminate (see Fig 14.3, overleaf). The tested laminate consists of two plies of 600 g/m<sup>2</sup> WR, and between them and also on

**Fig 14.2** Flexural strength vs angle of weave





**Fig 14.3** (Tensile strength vs crimp (Hildebrand & Holm)

the faces, one ply of 450 g/m<sup>2</sup> CSM. The fibre angle (W) is a measure of fibre curvature in degrees. The fibre curvatures in the warp and weft directions are not always the same in many woven roving products, so the tensile strength may vary up to 20% depending on direction. As can also be seen from Fig 14.3 a biaxial stitched roving has a higher tensile value, corresponding to a fibre slope of approximately 2°.

Another very important parameter regarding strength properties of the laminate is the fibre content, often expressed as a percentage by weight of the total laminate weight (see Figs 13.4 and 13.5). Generally speaking the higher the fibre content that can be reached, the stronger the laminate becomes, as long as the fibres are wetted out and not subjected to resin starvation. In practice, it is not realistic to count a fibre content higher than 37%, and lower than 27%, when using wet hand lay-up with a mat laminate. With a mix of mats and woven rovings in the laminate the fibre content usually varies from 35% to 45%, and with multidirectional material (rather than woven) up to 55%. The thickness of the cured laminate varies with fibre content as shown in Fig 14.6 (page 291).

To calculate the strength properties of a glass mat/roving composite we can use the values from the mat-only and roving-only values. The combined properties can be approximated by calculating the average weight of the respective reinforcements as:

$$P_c = P_m \cdot X_m + P_r \cdot (1 - X_m)$$

where:

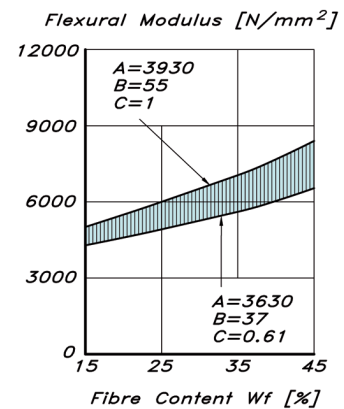
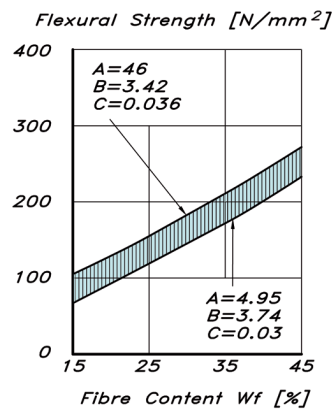
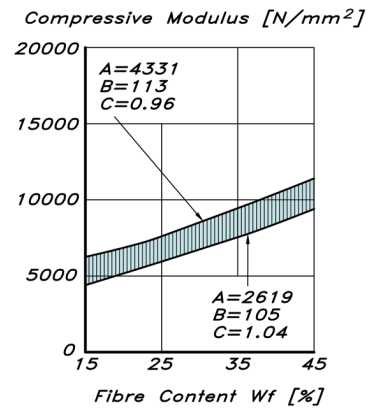
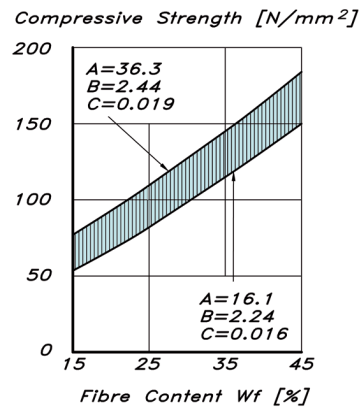
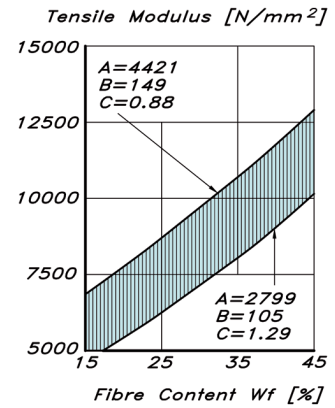
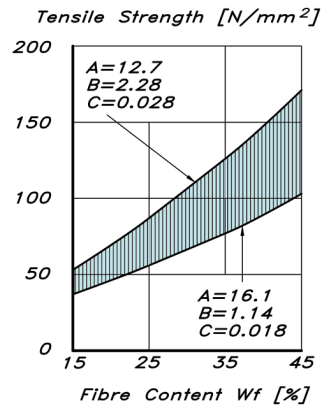
$P_c$  = Property of the mat/roving composite

$P_m$  = Property of the mat portion, having the same fibre content as the mixed composite, Fig 14.4

$P_r$  = Property of the roving portion, having the same fibre content as the mixed composite, Fig 14.5

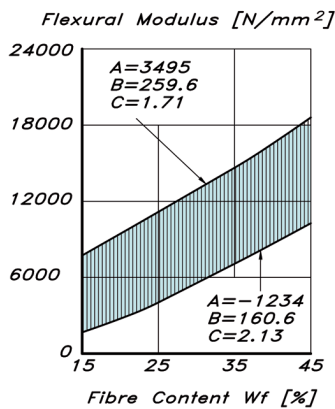
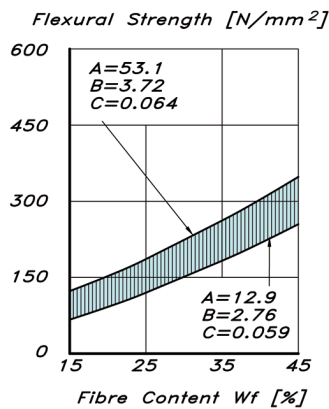
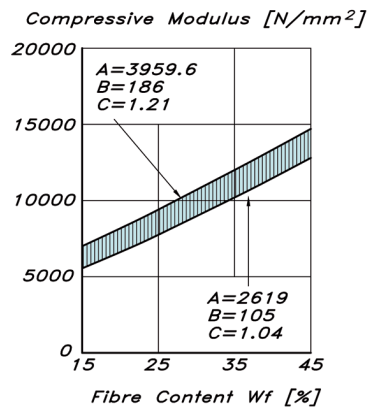
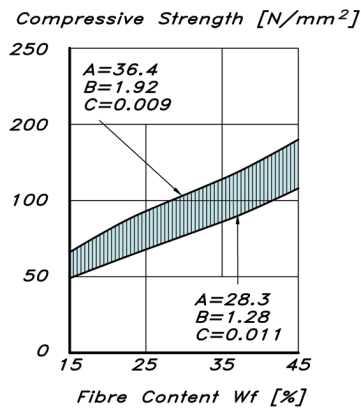
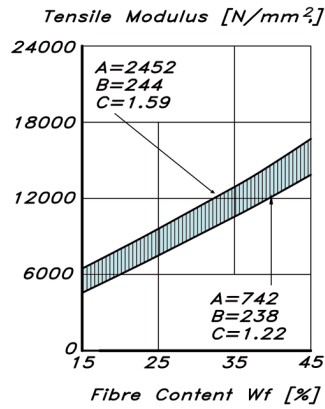
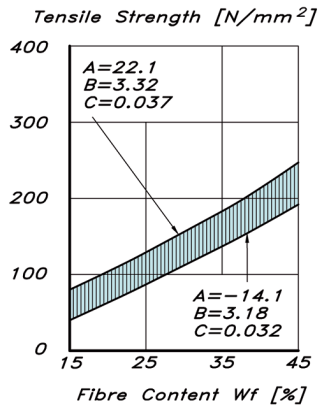
$X_m$  = Ratio of mat to the total mat/roving composite.

**Fig 14.4** CSM-polyester composite properties  
(Caprino & Teti)



The curves follow the general expression:  
 $\text{Strength/Modulus} = A + B(W_f) + C(W_f)^2$

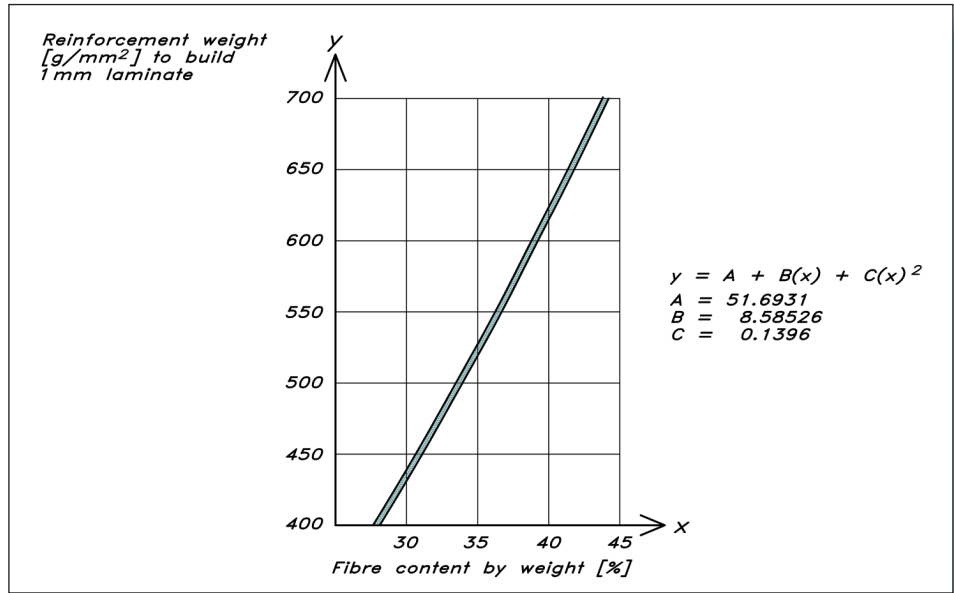
Fig 14.5 WR-polyester composite properties (Caprino & Teti)



The curves follow the general expression:  
 $\text{Strength/Modulus} = A + B(W_f) + C(W_f)^2$



**Fig 14.6** Thickness vs fibre content (NBS)



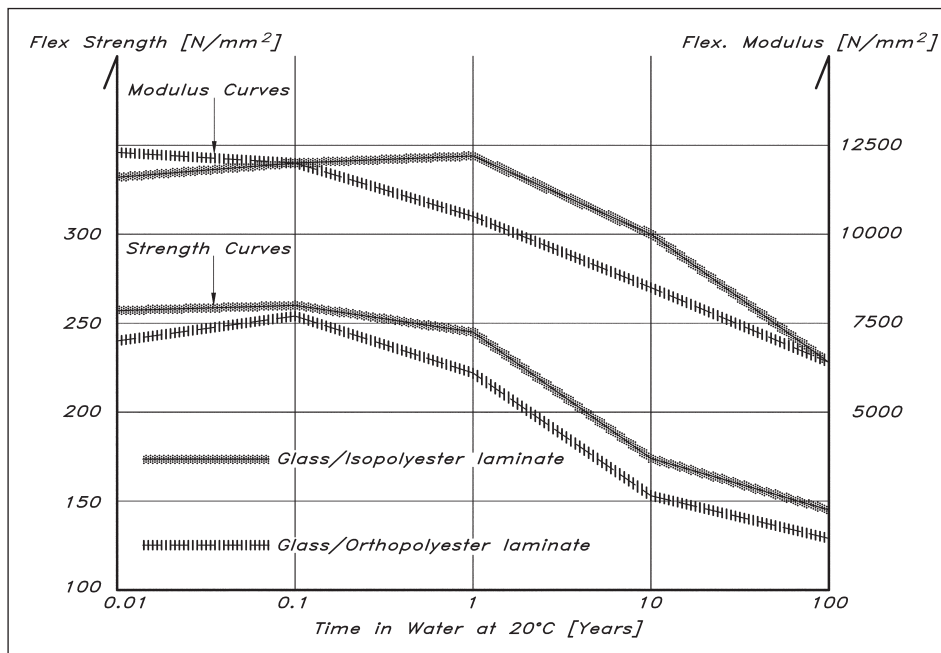
## WET LAMINATES

The values in Figs 14.4 and 14.5 are the ultimate strength and modulus values for dry laminates, but in practice this is not what can be expected from a boat laminate. The obvious reason is water, and the longer a laminate is submerged the weaker it becomes. Fig 14.7 (overleaf) shows the strength and elasticity properties for wet laminates as a function of time. The laminates are made of woven rovings with orthopolyester and isopolyester resin as a matrix. As can be seen the isopolyester laminate is not as prone to absorbing water as the orthopolyester type. One thing to remember though, is that if you store the boat on land during winter and let the laminates dry out, the process effectively starts from year 0 when you relaunch the boat again. To guard against osmosis the isopolyester gives a better protection, and gelcoats should be of isopolyester or of an NCA or better type of resin. Or, alternatively, use an all epoxy or vinyl ester resin.

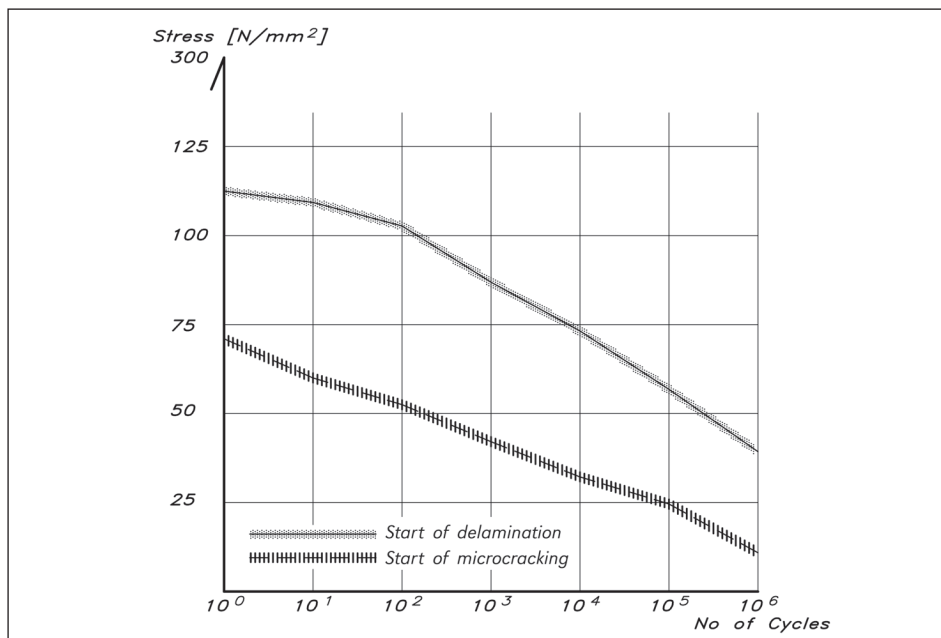
## FATIGUE

Another weakening factor for FRP laminates is fatigue. Yachts working in a seaway and with pulsating rig, keel and rudder loads are subjected to fatigue loadings. Fig 14.8 (overleaf) shows what happens to a CSM laminate.

The upper curve represents the failure of the laminate, and the lower curve corresponds to when microcracking first occurs. Microcracking is the first sign of laminate failure and it is obvious from the diagram that it takes place at a considerably lower level than the ultimate stress. What it means is that the resin, of orthopolyester type in this case, starts to develop cracks due to a low strain resistance: in other words it is too rigid. The strain level of this first failure is as low as 0.2% for an orthophthalic resin laminate compared



**Fig 14.7** Strength and modulus in wet laminates



**Fig 14.8** Fatigue properties of a CSM laminate

to 2% matrix elongation before break. Also obvious is the great fall in ultimate strength over stress cycles, from  $110 N/mm^2$  to  $40 N/mm^2$  after one million cycles, a reduction of 53%. This is something to bear in mind, especially when designing a yacht intended for long-range cruising over the oceans.

As said previously, the diagram is valid for an orthopolyester CSM laminate; switching to a better resin and a roving-based reinforcement, the fatigue properties are improved.

## ■ EXOTIC LAMINATES

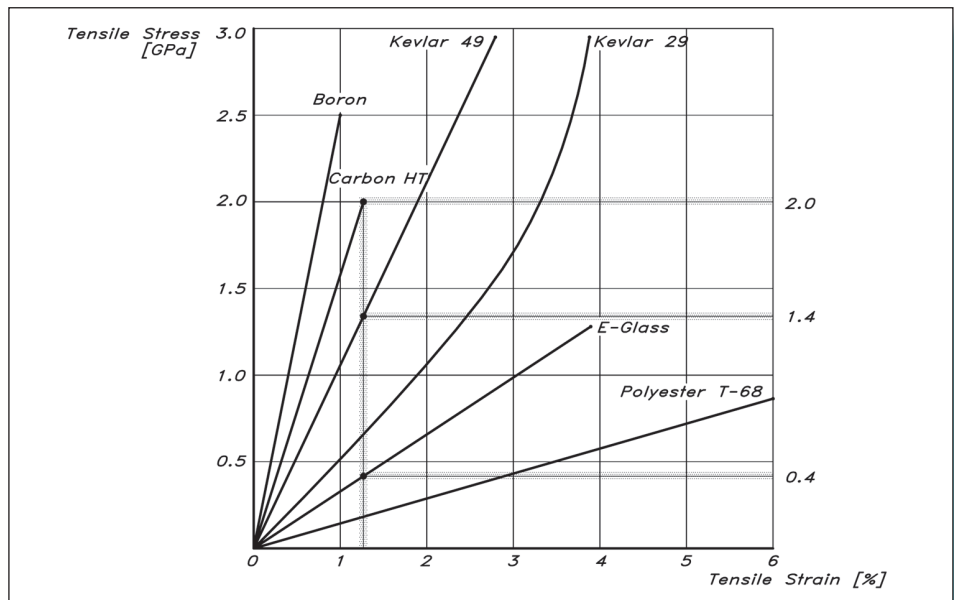
To improve a laminate, i.e. to make it stronger, stiffer and lighter, we can substitute the ordinary E-glass for better fibres, and switch from wet hand lay-up techniques with orthopolyester to better resins or better techniques, such as vacuum injection or 'prepreg' materials.

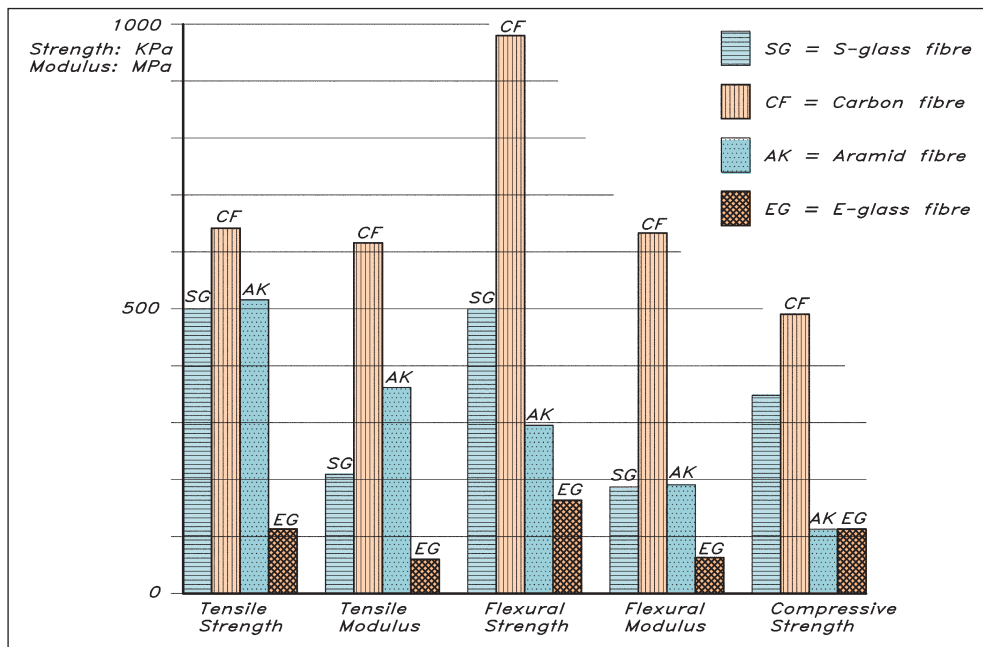
Fig 14.9 shows the strength and strain properties for different reinforcement fibres. As we can see, the Kevlar 49 is the strongest one, while Boron is the stiffest one closely followed by carbon fibre. These figures show the values for the fibres themselves; put into a laminate they will be considerably lower.

As previously stated, it is very important to use a resin with a higher strain level than the fibre, to discourage the start of microcracking. Thanks to the high strength of these exotic fibres much higher demands on the resin's adhesive characteristics must be made. Ortho or isopolyester are not particularly good glues, whereas vinylester or, better still, an epoxy resin formulated for laminating is an excellent glue with high strain values, making it possible to utilize the high-performance fibres to the full.

Usually the exotic fibres are used together with glass reinforcement and that leads to some consequences that must be taken into consideration. If, for instance, we have a laminate consisting of Kevlar 49, Carbon HT and ordinary E-glass, the carbon fibre is fully loaded when strained to 1.2% (the vertical line in Fig 14.9). Here the carbon develops its highest strength value of nearly 2 GPa, and if strained any further it will break. The other fibres in the laminate have their maximum strength at much higher strain values: Kevlar at 2.7% and E-glass at 3.8%. To make all the fibres in the composite co-operate, the total strain must not exceed 1.2%, which means that the Kevlar can only be used to 1.4 GPa and the E-glass to 0.4 GPa, roughly half their maximum values. If we are using all the materials at their maximum strength and disregarding the strain, the

**Fig 14.9** Fibre stress vs strain





**Fig 14.10** Typical composite properties

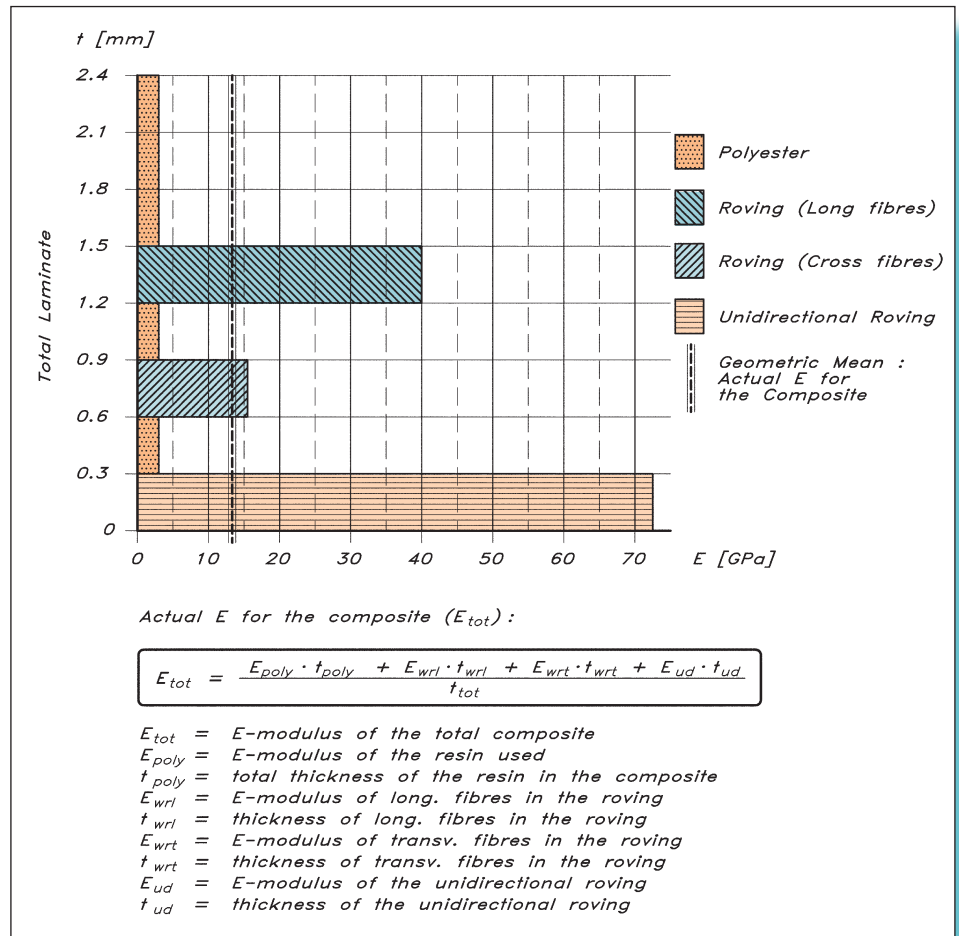
stiffest fibre will break before the structure is loaded to its maximum, since this fibre will then take on too big a load. Or to put it the other way: the other fibres are not allowed to develop their assumed maximum strength. So the stiffest fibre breaks first, which leads to overloading of the other fibres, and the structure collapsing.

Fig 14.10 shows some typical strength properties for composite laminates. The EG laminate is a common polyester/glass laminate hand laid wet, whereas the other laminates are epoxy preregs. A prepreg laminate is one where the manufacturer has already impregnated the fibre with a correct amount of resin, which makes it possible to obtain a high and even fibre ratio. In this example, the ratio is 60% compared to the EG laminate's 37%.

The drawback with preregs is that they are much more difficult to handle by the builder. He must store them at low temperatures so that they do not cure before they are used. When laminating, the tailored prepreg sheets are put into a mould, either male or female. This process is much more pleasant compared to wet lay-up because there are virtually no emissions, no sticky resin to handle and the available working timespan before it must be finished is much greater. When the preregs are in place the whole moulded area is covered with a vacuum bag, and air is removed to solidify the laminate. In order to cure the preregs heat is required, so the whole structure must be put into an oven or covered with electric heat blankets. The temperature control is quite crucial regarding both heat and the length of heating. The best prepreg systems need a curing temperature of 60°C. A similar result is achieved by infusing the resin with a vacuum bag over the dry fibre stack on the part to be infused. This is the technique used for YD-41.

To calculate the overall modulus of elasticity in a composite laminate we must know the individual modulus that the composite consists of. Fig 14.11 illustrates a way to determine the total modulus.

**Fig 14.11** E-modulus in a composite laminate



The laminate's total E-modulus,  $E_{tot}$ , is the weighted average of each component's modulus, with the weight equal to the thickness. By adding the product of each thickness and modulus and dividing the sum by the total thickness we get the total composite's modulus,  $E_{tot}$ . The fibre content in this example is 37.5%, i.e. directly proportional to the vertical axis (thickness). If it is possible to lessen the resin ratio, the total E-modulus will increase accordingly.

## SANDWICH

Basically there are three good reasons for building a yacht of sandwich construction:

- It gives a light building weight. However, practical considerations mean that the outer skin cannot be made too thin or else there will be insufficient strength to withstand docking, grounding and boatyard handling. The weight advantages for sandwich construction are therefore not so apparent in yachts below, say, 30 ft (9 m).

- Sandwich construction is able to utilize a stiffener free construction, making the whole hull totally self-supporting. In this case the scaling factors work in the reverse order. To build a boat of more than 25 ft (7.5 m) totally self-supported by its own hull panels, results in very high demands on the core material and skins.
- This method enables a boat to be built as a one-off where no moulds are available. This will be discussed in more detail later.

The greatest advantage with sandwich construction compared to solid laminates is that we can increase the strength and stiffness without a corresponding increase in the weight. Fig 14.12 shows clearly this advantage. By increasing the total thickness of the panel without increasing the total thickness of the laminates, the stiffness increases seven times for a doubling of the panel's thickness. By making the panel four times thicker the stiffness goes up 37 times compared to the solid laminate.

The strength increases 3.25 and 9.25 times, respectively, with the weight more or less equal. The core in this example is a honeycomb, with a foam or especially balsa core the weight would have increased slightly more. The reason for this drastic increase in strength and stiffness is illustrated in Fig 14.13.

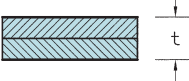

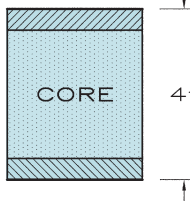
The critical load that a structure can withstand,  $P_{crit}$ , is proportional to the modulus of elasticity of the composite and the moment of inertia of the cross-section, and inversely proportional to the length squared of the test specimen.

Comparing two panels of the same length,  $L$ , we see that the only way to increase  $P_{crit}$  is to get a material with a higher  $E$ -modulus,  $E$ , or change the section to obtain a higher moment of inertia,  $I$ . To increase only the  $E$ -modulus by using better materials has its practical limits, not to mention the economical aspects. A better way is to increase the  $I$ -value of the panel. Since the moment of inertia is proportional to the thickness raised to the third power, it is not difficult to increase the stiffness of the panel by making it thicker. But we do not want to increase the weight, and here the 'sandwich-principle' comes into play. By dividing the laminate into an outer and an inner face and filling the space in the middle with something that is light, but still fulfils its structural tasks, we will have the increase in total thickness without an excessive increase of weight.

The faces carry the tensile and compressive stresses in the sandwich. The local flexural rigidity of the faces is so small that for all practical purposes it can be ignored, and therefore laminates specifically designed to carry tensile and/or compression loads can be used. Faces also carry local pressure at fastenings, etc., and where these pressures are high the face should be dimensioned for the shear force connected to it, so that we do not punch a hole in the face when applying the load.

The core has several important functions to perform. It has to be stiff enough to maintain a constant distance between the faces when the structure is loaded. It must also be so rigid in shear that the faces don't slide over each other. The shear rigidity of the core forces the faces to co-operate with each other. If the core is weak the faces do not co-operate, and the faces work as plates in bending, independent of each other. Since the local flexural rigidity is so small, the sandwich effect is lost and the structure collapses (see

**Fig 14.12** Strength and stiffness in sandwich vs solid

			
<i>Relative Stiffness</i>	100	700	3700
<i>Relative Strength</i>	100	350	925
<i>Relative Weight</i>	100	103	106

**Fig 14.13** Critical load in a sandwich structure

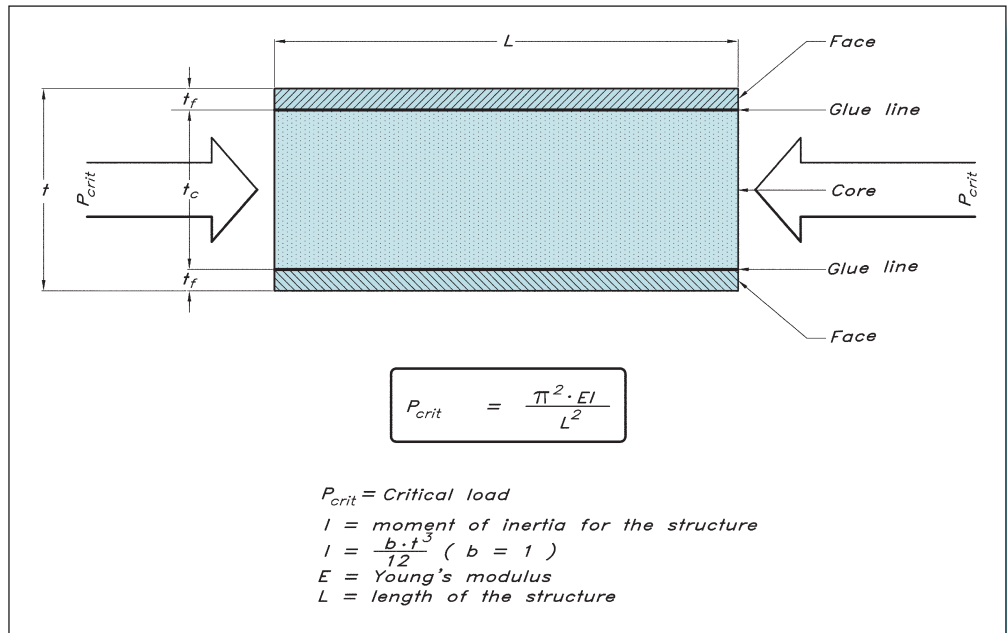
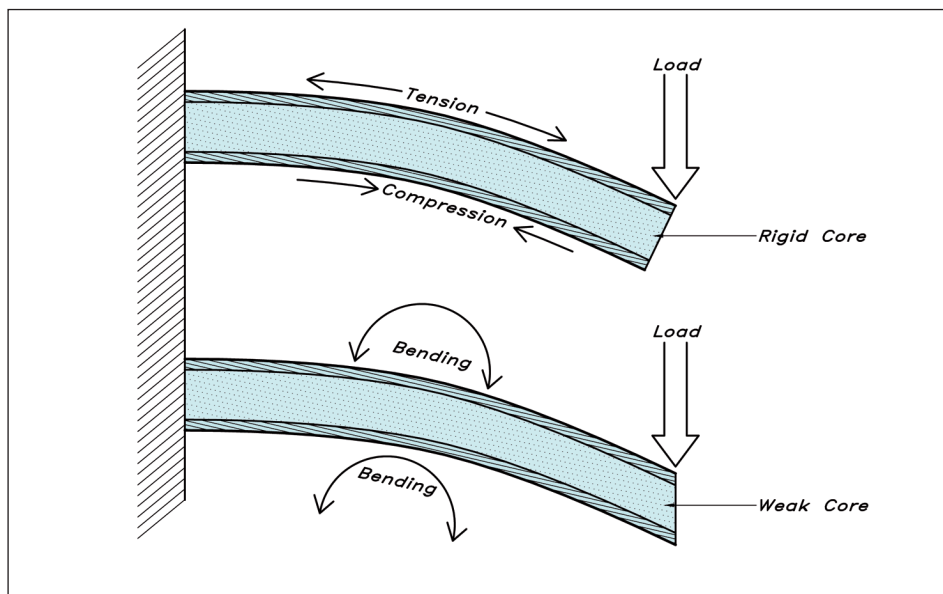


Fig 14.14, overleaf). To keep the faces and the core co-operating with each other, the face/core joints must be able to transfer the shear forces between the faces and the core, but it is hard to specify numerically the demands on the joints. A simple rule is that the joints should be able to absorb the same shear stresses as the core.

This basic description of the sandwich principle shows that it is the sandwich structure as a whole that generates the positive effects. However, we should mention that the core has to fulfil the most complex demands. Strength in different directions and low density are not the only properties that it must have; often there are special demands on buckling, insulation, absorption of moisture, fatigue, ageing resistance, etc.





**Fig 14.14** Comparison of cores that are rigid or weak

Each part of the sandwich has its specific property, and together they act as a unit. It is important not to break the co-operation between the parts. If for example reinforcing frames are made, they should be made of a material with the same or less strength than the face material. Otherwise most of the stresses will be taken by the frame reinforcement, which it is not designed for. Cracks at attachments often result from a combination of sandwich structure and frame structure which have not been properly balanced.

## ■ TYPICAL SANDWICH BUCKLING

A good understanding of a sandwich core's general qualities and the co-operation between faces and core can be obtained by carrying out a panel compression test. The panels are put into compression perpendicular to their plane, and the buckling characteristics are then studied. Possible results are depicted in [Fig 14.15](#) as follows:

### (a) General buckling

The core and the faces are co-operating well, but the panel is too slender, so the whole structure bends. If general buckling is feared, we can:

- Use facings with a higher elastic modulus
- Increase facing thickness
- Use a core with a higher shear modulus
- Increase core thickness.

### (b) Shear crimping

The faces and the face/core joint are strong enough but the core fails in shear. To increase the total critical crimping load we can:

- Increase core thickness
- Use a core with a higher shear modulus.

### (c) Wrinkling

The facings' buckling is prevented by the core which, when the facings are subjected to compression, supports them laterally. If the compression stress on the facings exceeds a certain limit, the core will not be able to prevent their buckling. In the first case the bonding of the face to the core is not strong enough, in the second case the core is failing in tension and the third case shows a core that does not have enough compression strength. If local wrinkling is feared, we can:

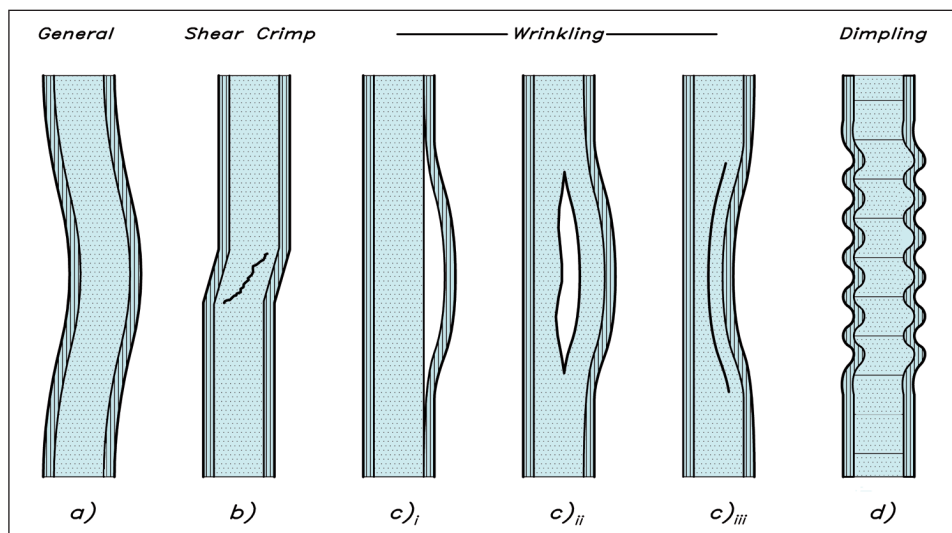
- Use a facing with a higher elastic modulus
- Use a core with higher elastic properties.

### (d) Dimpling

When the core is made of honeycomb, the bonding between faces and core only takes place at the honeycomb cells' edges. When the facings are subjected to a compressional force, they may therefore undergo buckling in the free spaces within the cells. When it is necessary to increase the critical dimpling stress, we can:

- Use a facing with a higher elastic modulus
- Use thicker facings
- Use a core with smaller size cells.

**Fig 14.15** Sandwich buckling characteristics



## SANDWICH BENDING

The normal load conditions for panels in boats are in the bending mode. Fig 14.16 shows the distribution and levels of stresses in a sandwich beam. The index 'f' refers to the faces and 'c' to the core in the formulae. As we can see from the figure the faces are considered to take all normal forces and the core all shear forces.

The faces' own moment of inertia ( $I_0$ ) are very small and can be ignored. The resulting moment of inertia ( $I_b$ ) gives the total section's moment of inertia:  $I_b = A_f \cdot d^2 / 2$ , i.e. the resulting moment of inertia is proportionally dependent on flange area, or face thickness, and the square of the sandwich thickness.

Thanks to this simplification the normal stress in the faces ( $\sigma_f$ ) can be approximated to:  $\sigma_f = P / A_f$ , i.e. the load carrying capability is directly proportional to the flange area, or face thickness.

If the core is too weak to contribute significantly to the flexural rigidity of the sandwich, which can be safely assumed in most cases, the shear stress may be regarded constant over the thickness of the core. If, in addition, the flexural rigidities about their own axes are ignored ( $I_0 = \text{small}$ ), the shear stress ( $\tau_c$ ) becomes:  $\tau_c = Q / (b \cdot d)$ , i.e. the shear stress is inversely proportional to the core thickness.

The approximations give a total error of 2–3% when the core is at least 5.77 times thicker than each facing and the modulus of elasticity of the faces is much greater than that of the core.

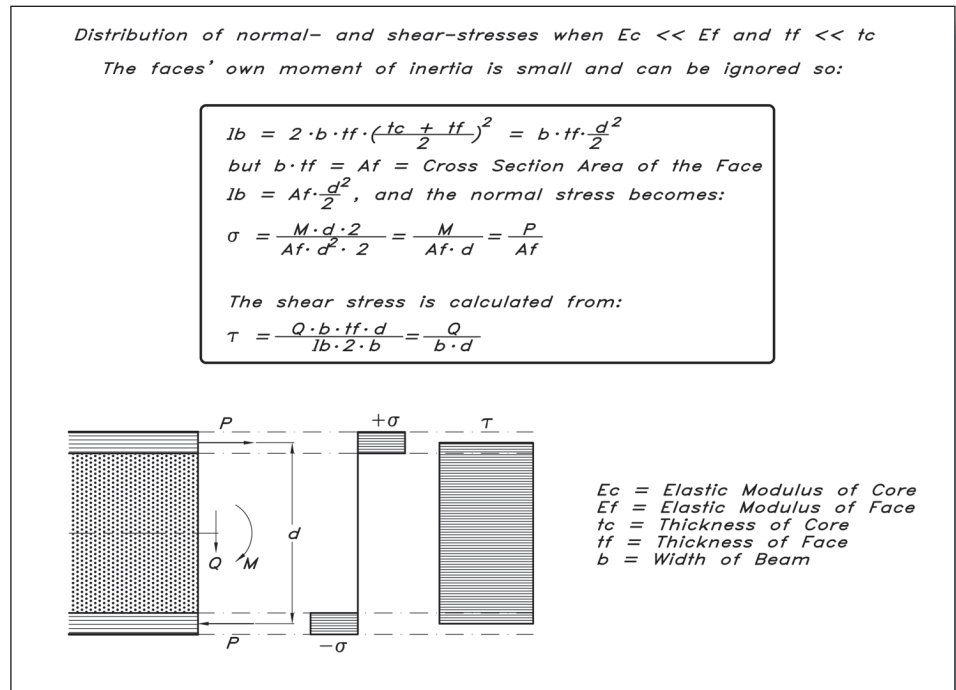
## SANDWICH IN PRACTICE

So far we have discussed the principles behind sandwich construction. Of a more practical nature is the choice of material. For the facings, since they are only subjected to tension or compression forces, and the thickness in itself is not of great importance compared to that of a solid panel, it pays to use directional fibres or perhaps exotic ones in the laminates.

The core is subjected to a lot of, sometimes conflicting, demands. Fig 14.17 shows a table listing different demands versus ratings for some core materials. The ratings are not weighted, so we have to decide the priorities when making a selection of the core material. The most commonly used core materials in boatbuilding are balsa and linear or cross-linked PVC foam. The best known linear type is Airex and the cross-linked types are Divinycell and Klegecell/Termanto. Recently there has been a development of the two types into a 'mixed linear/crosslinked' type which blends the linear's better impact properties with the cross-linked's better shear properties.

A problem that can arise when building a sandwich hull in a female mould is illustrated in Fig 14.18 (overleaf). In order to cover the curved mould the core material is divided into small cubes held together by a glass weave on one side. If the loose cubes are not glued together the shear properties of the core are drastically decreased: approximately 25% less than for the core material itself. It is not unusual for the builder to rely on the resin to fill the gaps between the 'core cubes' by itself and to glue them together. The drawbacks are many. First, you cannot be sure whether the voids really are filled; secondly,

**Fig 14.16** Stresses in a sandwich beam



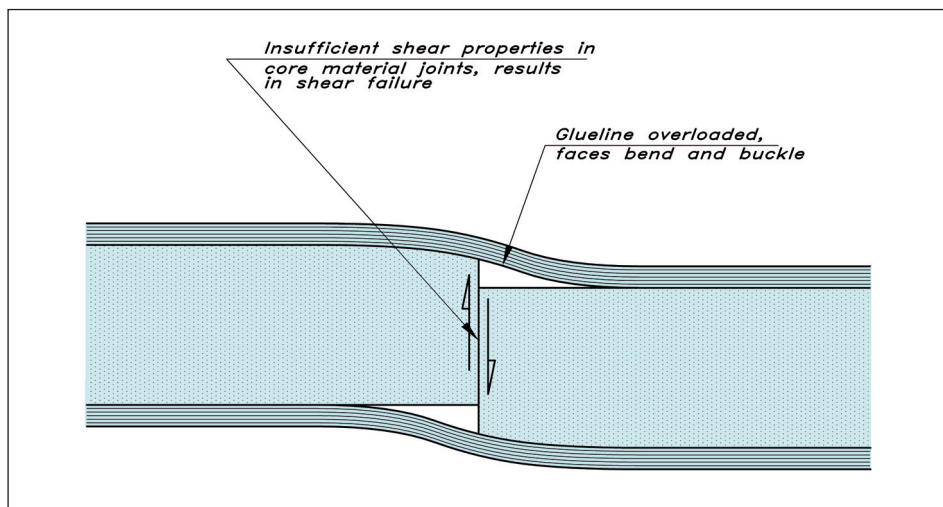
**Fig 14.17** Demands and ratings of core materials

Demands	Plywood	Balsa	Poly Urethane	Linear PVC	Cross-Linked PVC
Light Weight	-1	2	2	2	2
Water Absorb.	0	-1	0	2	2
Shear Strength	2	2	0	1	1
Fatigue	2	2	-1	2	2
Impact Strength	2	1	-1	1	0
Adhesion	2	2	1	0	2
Heat Resist.	2	2	1	1	1
Therm. Insul.	1	2	2	2	2
Fire Resist.	-1	-1	0	2	2
Ageing, rot	-1	-1	2	2	2
Water Resist.	0	0	0	1	2
Repair	0	0	0	0	0
Economy	0	2	1	0	0
<b>SUM</b>	<b>8</b>	<b>12</b>	<b>8</b>	<b>17</b>	<b>18</b>

-1 = Poor  
 0 = Adequate  
 1 = Good  
 2 = Excellent

you get hard spots between the faces which make the panel considerably less resistant to impact forces; and thirdly, the weight is increased due to an excess of resin.

One way to avoid this problem when laminating in a mould is to fill the voids with a microballoon filler that resembles the core material's strength and elasticity properties. To be sure that the voids are filled the core should be vacuumed down into the filler, which is spread over the already cured outer skin. By employing a vacuum/infusing technique on a dry stack of fibre skins, together with a core suitable for infusing, we can achieve a good

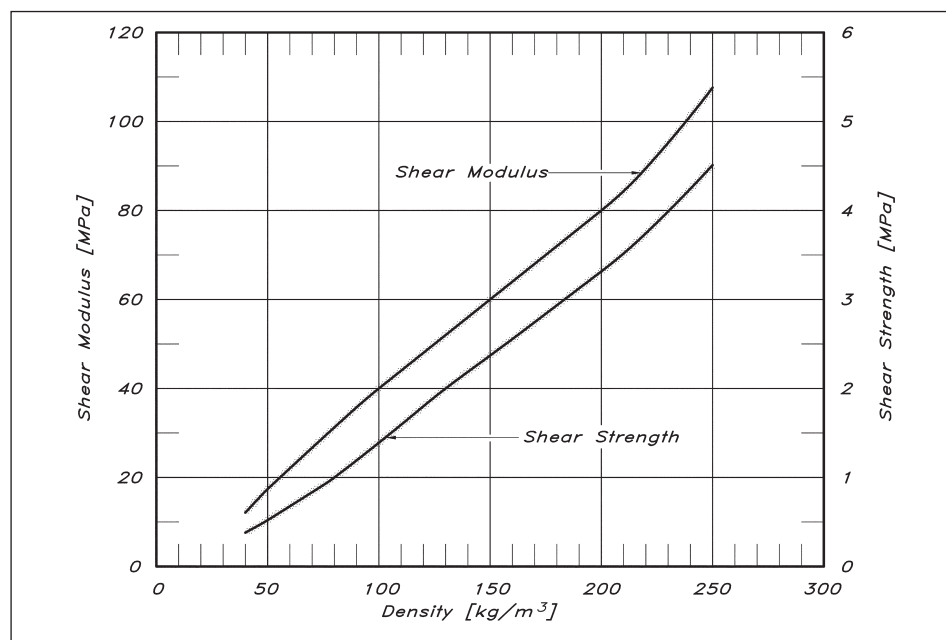


**Fig 14.18** Insufficient core joining

bonding quality between core and skins without using a filler. Another method is to inject a filler into the core after both skins have been laminated and cured.

To be certain of a good bond between the core and the skins, the core should be primed with a fast-setting resin that is left to cure partially before any laminating is made on top of it. This is to make sure that there will be no resin 'starvation spots' between laminate and core. This does not apply to vacuum infusion techniques.

The shear properties of PVC foam are almost proportional to density. In Fig 14.19 this dependence for shear strength and shear modulus is shown. We can use these diagrams to choose a correct core when dimensioning a sandwich panel, a task we will perform in the next chapter on scantling determination.



**Fig 14.19** Shear properties of cross-linked PVC foam

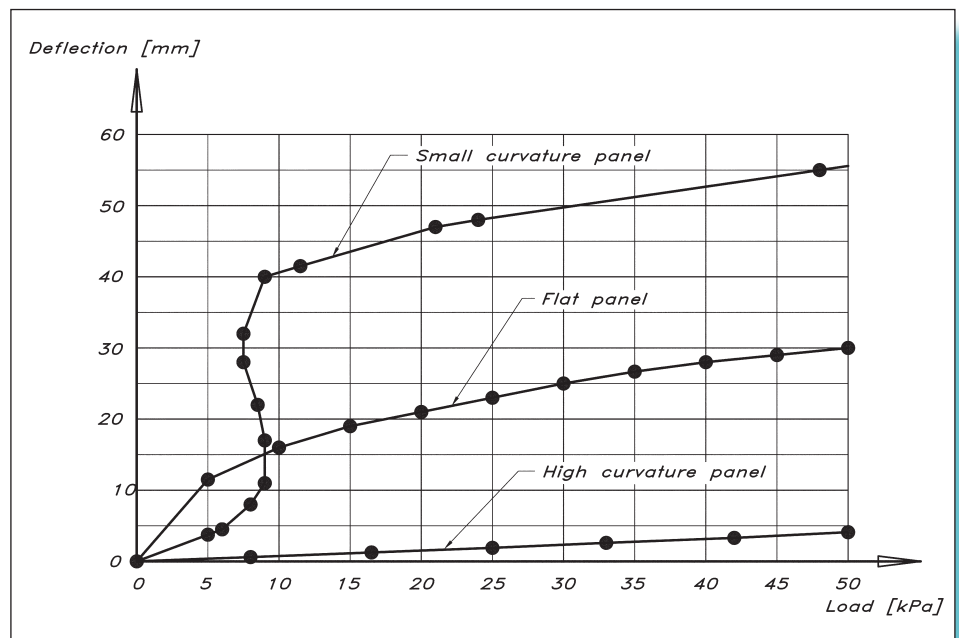
## ■ FINAL REMARKS

The simplified calculation methods outlined in this chapter, and in the ISO standard, can be used successfully if the sandwich faces are thin, the panels not too curved and the deflections small. Recent tests have shown that the bending behaviour of a sandwich panel varies greatly with curvature. The core shear stresses decrease significantly with increasing curvature (up to 80% compared to a flat panel), so the simplified calculation methods give us an increased factor of safety. If the deflection of single-skin panels exceeds half of the plate thickness (which is not uncommon for bottom panels), membrane effects must be expected and non-linear analysis applied, for which there are no simple rules of thumb. Fig 14.20 (overleaf) shows three different panels of the same lay-up but with different curvature, and their deflection behaviour under load. All panels are of sandwich construction and of a total thickness of 21.4 mm.

The non-linear behaviour of the flat panel is quite clear, as is the 'snapthrough', i.e. the deflection increases instantly without additional load, for the panel with a small curvature ( $A/s = 0.022$ ). The panel with higher curvature ( $A/s = 0.065$ ) shows an almost linear behaviour, with a stiffness substantially higher than the flat panel. This behaviour is not only true for sandwich panels – just look at eggs and their shells.

Another point to bear in mind is the non-exactness of the load assumptions that have to be made. As we shall see in the chapter on scantling determination, the size of the panels plays a significant role when deciding on what load to apply. Generally speaking we can reduce the load per unit area the larger the panel, since a big part of the design load relates to a slamming pressure that is limited in time and area, and consequently does not affect the entire panel with a constant pressure.

**Fig 14.20** Bending behaviour for sandwich panels (Hildebrand)



# 15 SCANTLINGS

## ■ DETERMINATION

In the previous chapter, we discussed different loads on the boat and their consequences on the construction. Due to the very complex interactions between loads and strength requirements, it is very difficult, by direct calculation, to determine the scantlings of the vessel. For this reason, different classification societies – Lloyd's, Bureau Veritas, American Bureau of Shipping (ABS) and others – have formulated scantling rules to follow to dimension a vessel that will hold together, if used as intended. For pleasure boats, an ISO standard has been developed that replaces the classification societies' standards for vessels below 24 m in length. The standard is now in its final format and harmonized into ISO 12215-5:2019. This ISO standard is mandatory if you want to market and sell boats up to 24 m in length into the European Union regardless of what the classification societies say in their rules. Having said that, it does not mean that the classing requirements are not valid, but to qualify to sell boats in Europe (EU) only the harmonized ISO standard has to be met, not any classification society's standard. In this chapter, we will look at the ISO standard 12215. Not all aspects of the standard will be dealt with by us since this will constitute a book of its own, but we will concentrate on some of the parts concerning glass-reinforced plastic that applies to the construction of the YD-41, updating the formulae used in the fourth edition of this book. Although this ISO standard is harmonized and approved by the Committee of European Norms (CEN), it is still under discussion by ISO working groups. Boatbuilders, be aware of this fact and be cautious when evaluating the result of the calculations. For the dimensioning of a production craft aimed at the general market, it is often good enough to use precalculated and simplified assessment methods, described in the standard, due to the cumbersome calculations otherwise demanded. This is the route we have taken with the YD-41.

## ■ STRUCTURE OF THE STANDARD

The ISO standard is a modern one in that it identifies the loads to consider, what material properties to use and what safety factors to apply. Naturally, older rules also consider these factors, but they are often hidden in constants or expressions so you do not know what you are doing. Comparing with old rules from classification societies and national standards, in which recommended practices for loads on the hull and the dimensioning of small



The dimensioning according to this standard is regarded as reflecting current practice, provided the craft is correctly handled in the sense of good seamanship and operated at a speed appropriate to the prevailing sea state.

**Fig 15.1** The ISO scantlings standard



scantlings – part 5: Design pressures, allowable stresses, scantling determination’. The first paragraph in part 5 covers the scope: this part of ISO 12215 applies to the determination of design pressures and stresses, and the determination of the scantlings, including internal structural members of monohull small craft, constructed of fibre-reinforced plastics, aluminium or steel alloys, glued wood or other suitable boatbuilding material, with a length of the hull ( $L_H$ ) according to ISO 8666 between 2.5 and 24 m. For the complete scantlings of the craft this part 5 of ISO 12215 shall be used in conjunction with part 6 for details, part 8 for rudders, part 9 for appendages (ballast keels) and part 10 for rig dimensioning and attachment. Where information is not available in the ISO standard, we will use industry practice when dealing with these issues. So, looking at Fig 15.1 and parts 5, 6, 8, 9 and 10 we have circled numbers in the boxes that refer to sections in the standards, circled letters that refer to annexes and hash signs (#) that indicate data from the actual design. Section 11 in part 5 of the standard describes the structural analysis and scantlings determination of six methods:

1. Simplified, enhanced ply-by-ply analysis
2. Developed use of classic laminate theory (CLT)
3. Direct test of actual laminate to reach the required value
4. Finite element method (FEM). The standard gives guidance for assessment by 3D numerical procedures, boundary assumptions, load application and model idealization
5. Drop-test. This only applies to a craft with a length of less than 6 m.

Only methods 1 and 2 will be described in detail in this chapter.

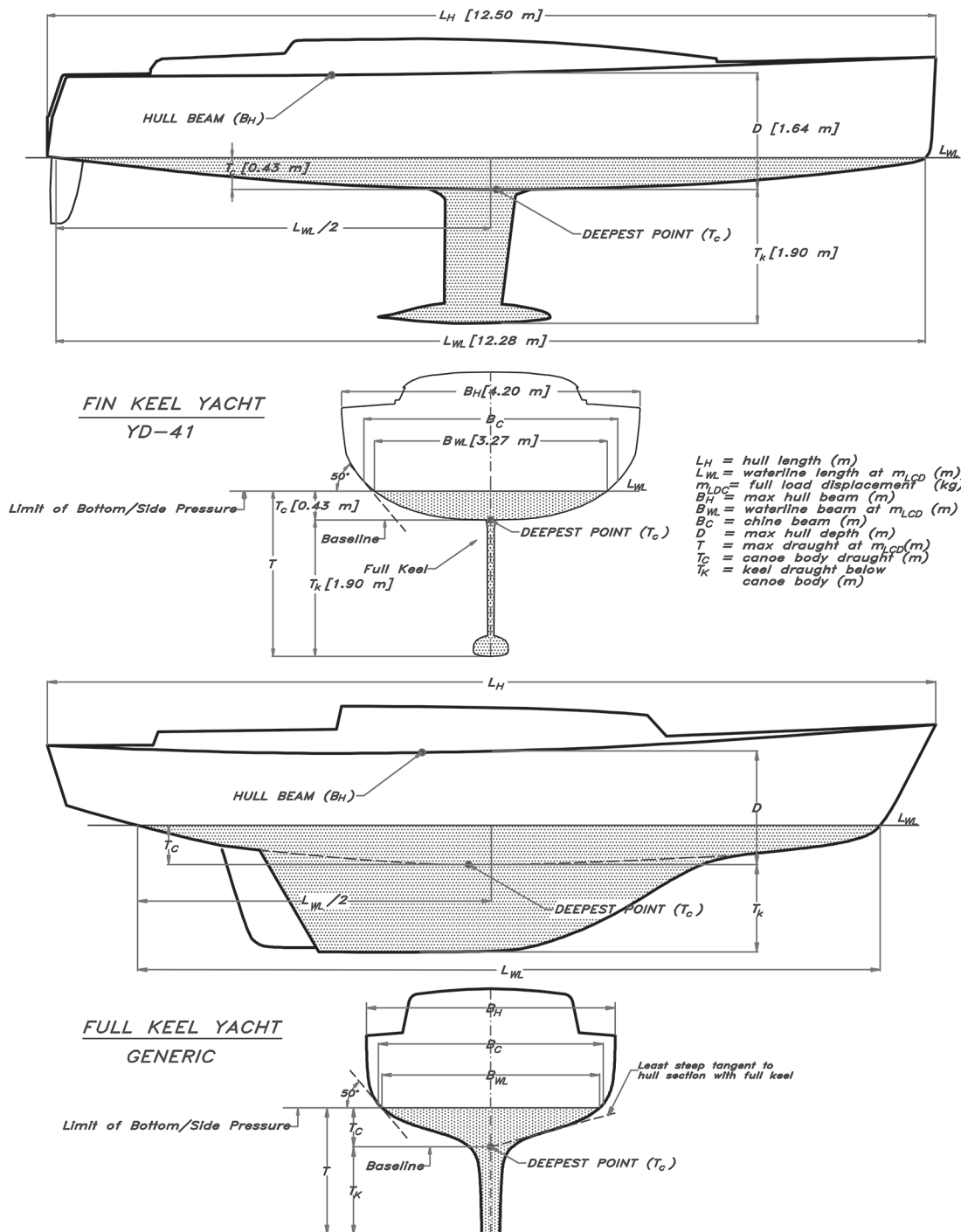
Although the standard does not explicitly state what documentation is needed in the form of drawings, in general, the plans listed below are essential, together with calculations, to show that the craft fulfils the scantling requirements. For a small boat the need for documentation is not that great due to the simplicity of the construction, but with increasing size, say from 10 m length upwards, the complexity increases and, along with this, the need for proper documentation. A typical set of plans is as follows:

- Framing sections
- Bottom construction, floors, girders, etc.
- Shell expansion
- Deck and cockpit
- Pillars
- Watertight and tank bulkheads
- Non-tight bulkheads, shelves and bunks which are glassed-in and used as structural supports
- Stern frame and rudder
- Keel bolt and chainplate connections
- Steering gear
- Cabin coach roof, sides and ends
- Closing appliances for hull, decks and superstructure.

**Fig 15.2** (RIGHT) ISO hull definitions

## HULL DEFINITIONS

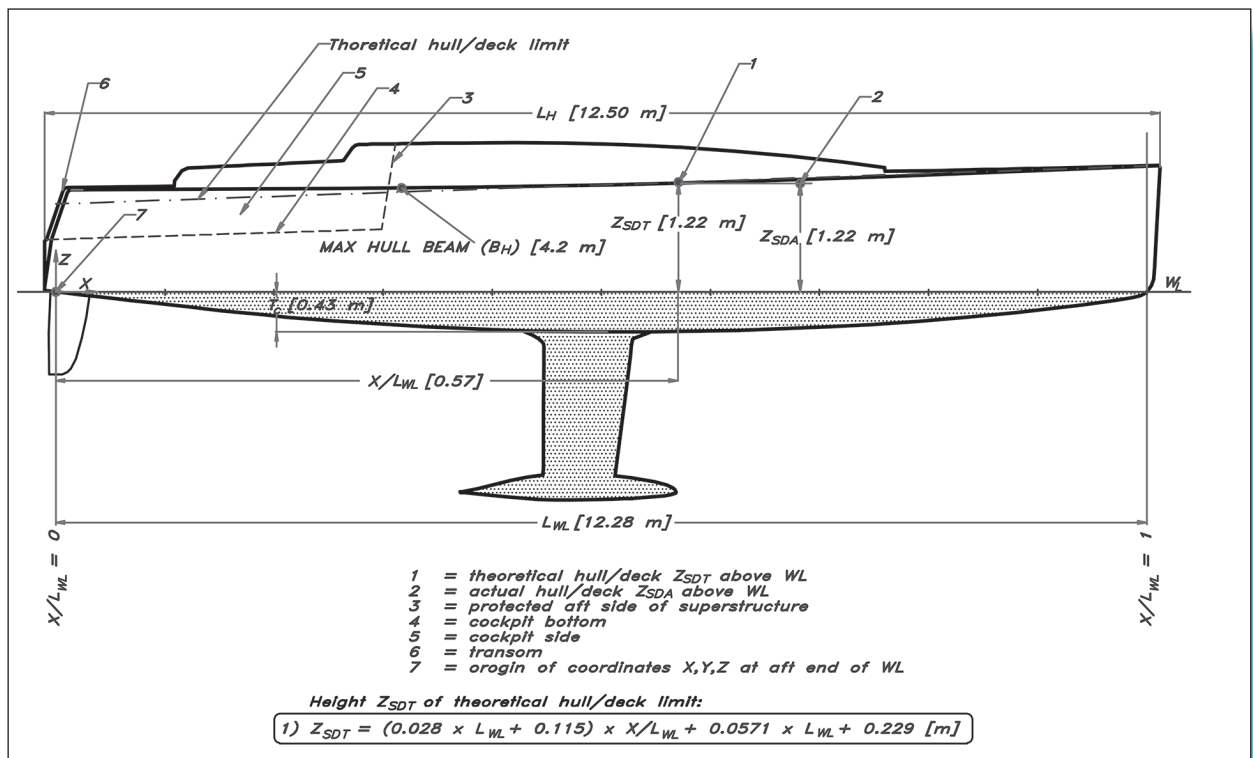
Fig 15.2 shows the measurements that must be taken to be able to determine the scantlings.



- $L_H$  = Length of the hull, excluding bolted-on extensions such as bowsprits, stern fittings, etc. [m]
- $L_{WL}$  = Length of waterline at full load displacement [m]
- $B_H$  = Hull beam, excluding bolted-on extensions [m]
- $B_{WL}$  = Waterline beam [m]
- $T_C$  = Immersed depth of canoe body measured vertically from the bottom of the hull at its deepest point at the centreline to the maximum estimated displacement waterline [m]
- $D$  = Maximum depth of the hull [m]
- $V$  = Maximum speed [knots] in calm water declared by the manufacturer with the craft in maximum load condition [ $m_{LDC}$ ]. This speed will never be taken less than  $2.36(L_{WL})^{0.5}$
- $T$  = Draft of a keel below  $L_{WL}$  [m]
- $m_{LDC}$  = Loaded displacement mass [kg]
- $\nabla$  = Loaded displacement volume [ $m^3$ ]
- $\beta$  = Deadrise angle at  $0.4L_{WL}$  forward of its aft end, measured according to Fig 15.2, not to be taken less than  $10^\circ$ , nor more than  $30^\circ$ .

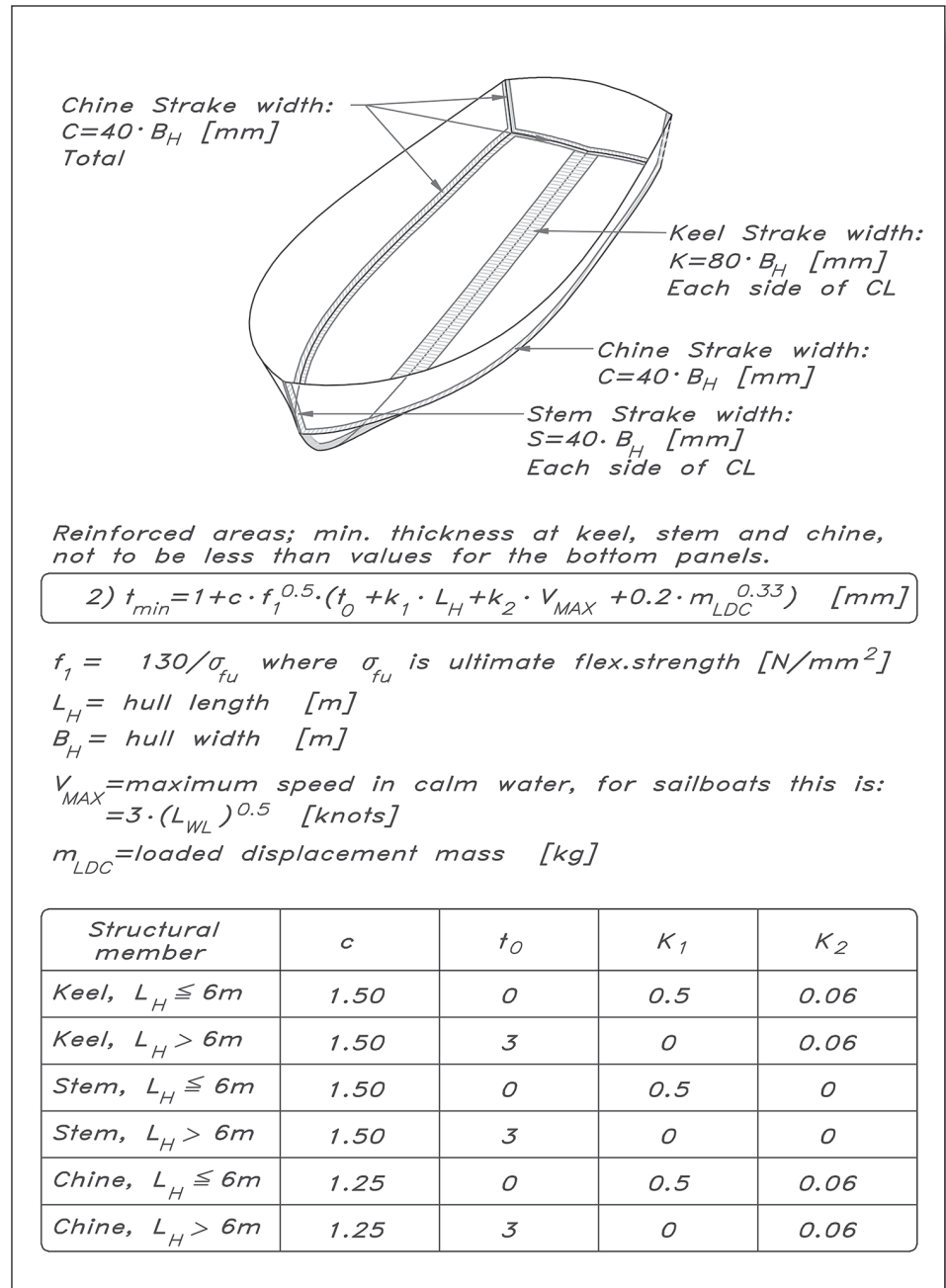
## AREAS

The hull, deck and superstructures are divided into specific areas as shown in Fig 15.3. Fig 15.3 Areas



All measurements are taken from the aft end of the flotation (X-direction) and vertically from the  $L_{WL}$  plane (Z-direction). The theoretical hull/deck limit  $Z_{SDT}$  (as defined in Fig 15.3, equation 1) sets the limit between side and deck pressures. The reason is to avoid penalizing a craft with a high freeboard. In contrast, where  $Z_{SDA} < Z_{SDT}$  (as in Fig 15.6(d)), the deck pressure is increased to mimic the side pressure at side/deck level. Fig 15.4 shows reinforced areas of the keel, stem and chine strakes as functions of  $B_H$ . Equation 2 gives the minimum thickness values, not to be less than the bottom panels.

Fig 15.4 Reinforced areas



## ■ DIMENSIONS OF PANELS AND STIFFENERS

A plating panel is subjected to local pressure. Any global loads are not considered in this standard as they are seldom significant on small craft, but one method is discussed in [Chapter 13](#) regarding global loads. Local pressure loads depend heavily on the design surface area ( $A_D$ ) of the panel, and hence from stiffener spacing and arrangement. The structure is often arranged so that the plating panels are supported at their edges by a set of ‘secondary’ stiffeners (stringers, intermediates, etc.), which in turn are supported by ‘primary’ stiffeners (frames, webs, bulkheads, etc.). Sometimes these stiffeners are not ‘dedicated’ stiffeners but ‘natural’ ones, which can include hard chines, round bilges, hull/deck connection, interior or coaming flanges, etc.

All structural arrangements must meet the three following conditions:

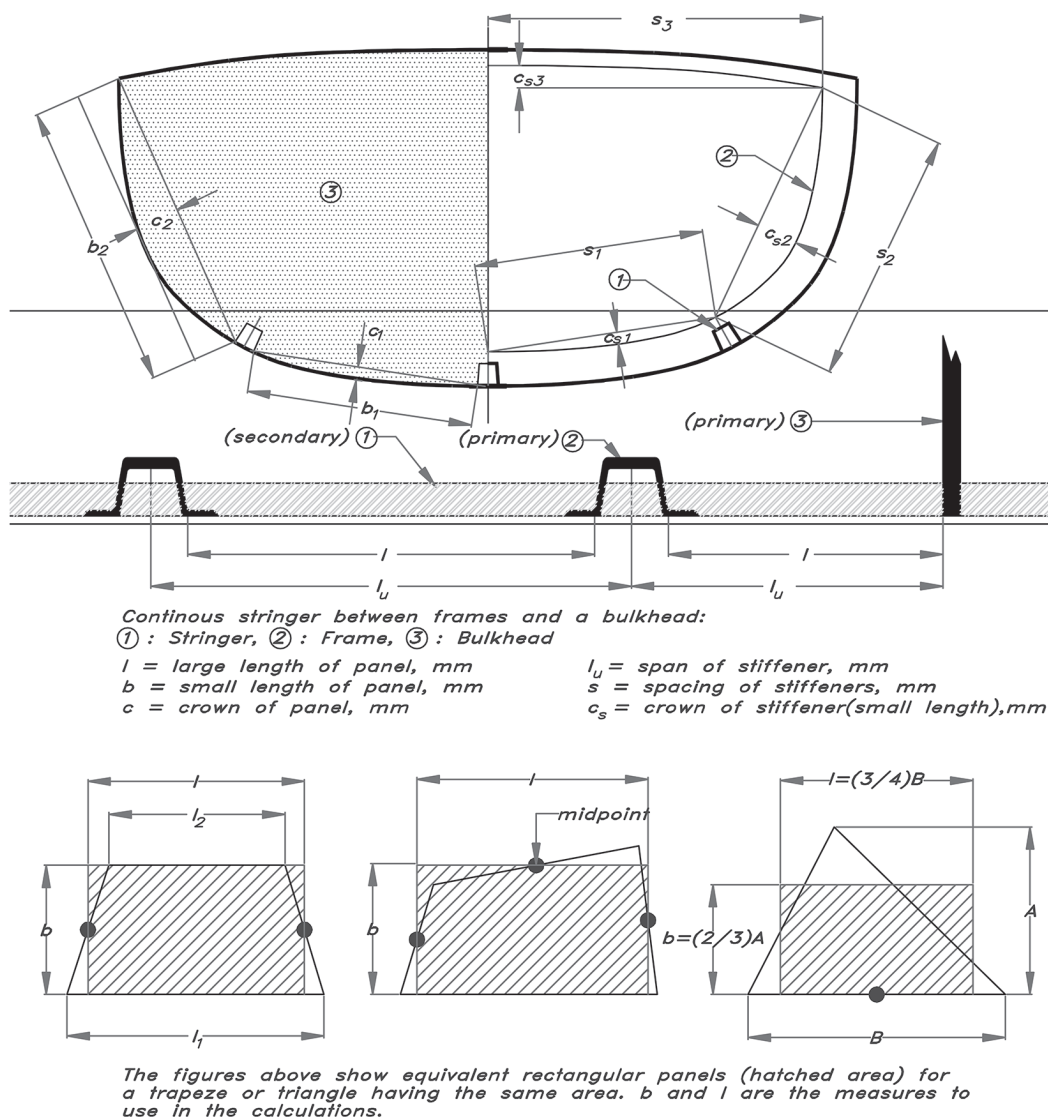
1. The primary stiffeners (where installed), are strong enough to keep their shape and transmit the shear force and bending moment from the secondary stiffeners to the rest of the structure.
2. The secondary stiffeners (where installed), are strong enough to keep their shape and transmit the shear force and bending moment from the plating to their supports, the primary stiffeners.
3. The plating is strong enough to keep its shape and transmit the shear force and bending moment resulting from the pressure load to its supports, the secondary stiffeners.

[Fig 15.5](#) shows an example of the dimensioning elements of stiffeners and rectangular panels in a system of primaries (frames and bulkheads) and secondaries (stringers). For non-rectangular panels (trapeze and triangular), the hatched area gives the equivalent rectangular panel.

## ■ PRESSURES ON PANELS AND STIFFENERS

[Fig 15.6](#) shows typical craft midsections and corresponding measurement definitions and pressure points. The pressure  $P$  ( $\text{kN/m}^2$ ) working on the different parts is applied to the centre of the panel or stiffener. The pressure on the bottom is the same for the whole area irrespective of depth below the waterline. Pressures on the topsides, decks and superstructures, on the other hand, depend on the distance from the waterline. For longitudinal positions different distribution factors,  $k_L$ , are applied as shown in [Fig 15.8](#) ([page 314](#)). Four different vessel cases are shown in [Fig. 15.6](#) ([page 312](#)):

a) Hard chine craft in displacement mode (i.e.  $V > L_{WL}^{0.5}$ ). The pressure  $P_1$  goes all way from the centreline up to the waterline. Along the keel, chine, stem and around the transom there shall be reinforced strakes according to [Fig 15.4](#). The side pressure is calculated at point  $P_2$  according to [Fig 15.11](#) or [Fig 15.12](#) ([pages 316](#) and [318](#), respectively). The deck pressure  $P_3$  runs from  $Z_{SDT}$  level up to the start of area 4. Since the side/deck connection forms a ‘natural’ stiffener the area is divided between deck and side that has the same



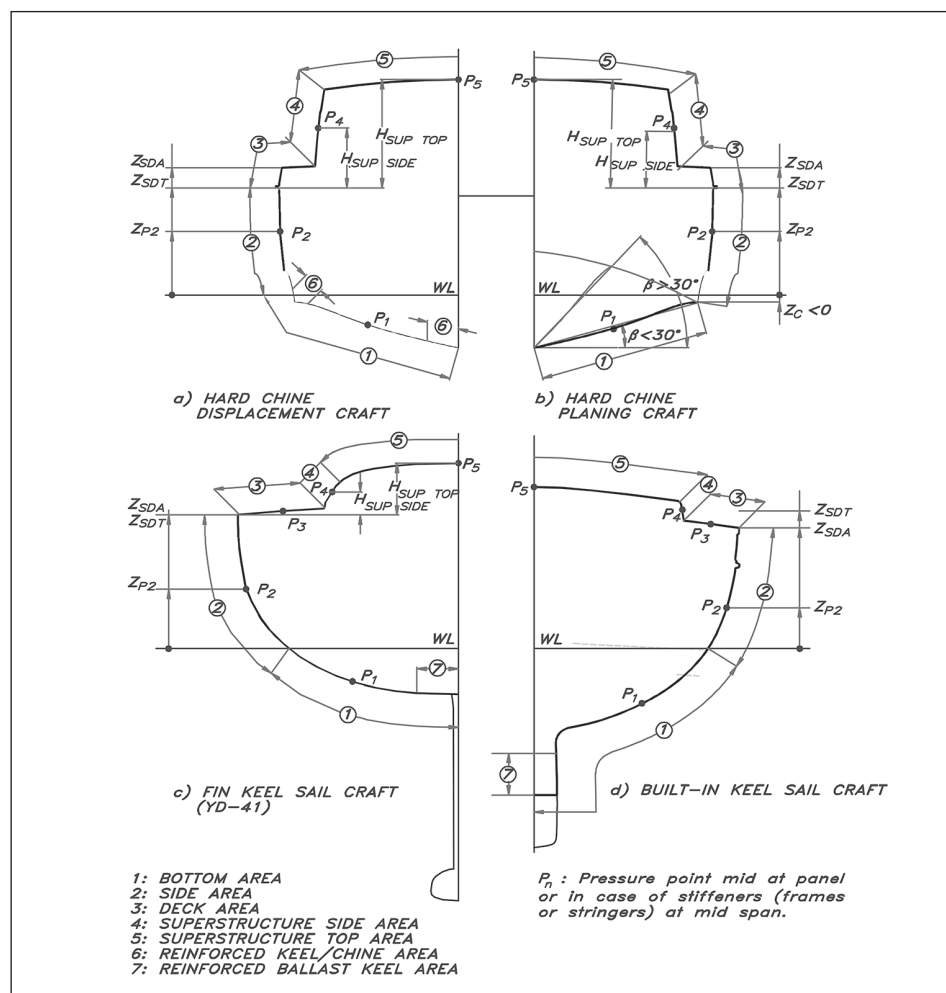
**Fig 15.5** Stiffener and panel dimensions

pressure (i.e. deck pressure). The coachroof side panel (4) has a transverse angle greater than  $55^\circ$  to the horizontal and is by definition a non-walking area. As  $Z_{SDA} > Z_{SDT}$  the value of  $H_{SUP}$  is measured from  $Z_{SDT}$  and the pressure on the upper part of the side is equal to the deck pressure.

b) Hard chine craft in planing mode (i.e.  $V \Rightarrow 5 \times WL^{0.5}$ ). The only difference is regarding the extent of the bottom panel that goes up to the chine, not the waterline. The standard stipulates that this condition is relevant as long as the deadrise angle ( $\beta$ ) is less than  $30^\circ$ . Moving forward in the hull the deadrise increases to more than  $30^\circ$  and the chine may move above the waterline. In this case, the extension of the bottom area that only goes up to the waterline with the remainder (up to the chine) is considered to be part of the side



**Fig 15.6** Pressure on panels and stiffeners



area. This might be good in theory, but not so in practice. To begin with, it complicates the lamination process by forcing a change in the lamination scheme in an area of maximum load, and there is a risk of damage occurring by grounding or hitting an object in the water. The advantage of minimizing weight in this comparably small area is probably very small, at least in a production situation.

c) Fin-keel sailing craft. This shows the midsection of the YD-41. The difference from the displacement craft (a) is the addition of a keel and that  $Z_{SDA} = Z_{SDT}$  (i.e. the actual freeboard is the same as the theoretical one). This means that the topsides (2) are fully in the side area and the actual deck pressure starts at the hull/deck intersection as described in Fig 15.11 or Fig 15.12. The pressures on the superstructure are measured from  $Z_{SDA}$  or  $Z_{SDT}$ . Due to the angle of the superstructure area (4), more than  $55^\circ$  from the horizontal, it is considered a non-walking area, but the top area (5) is a walking area. The top area spans the full width of the superstructure, so the pressure point will be at the centreline. The reinforced ballast keel area 7 has to withstand a pressure 1.8 times the bottom pressure. This area extends  $0.2 \times T$  around the ballast keel.

d) Built-in keel sailing craft. This shows a typical section of a full keel craft or one with a long fin keel. In this case, the ballast is external and bolted on to the keel stub, but it can also be encapsulated in the keel shell. The advantage with the latter is water tightness and no risk of leakage between the ballast and hull. The disadvantage is the difficulties to repair a heavy grounding that destroys the encapsulating skin with the risk of water ingress, and it also means a higher centre of gravity compared to the bolted-on variety. The difference from the fin keel craft (c) is that  $Z_{SDA} < Z_{SDT}$  (i.e. the actual freeboard is less than the theoretical one). This means that the topsides (2) are fully in the side area and the actual deck pressure is increased as described in Fig 15.11 or Fig 15.12. The pressures on the superstructure are measured from  $Z_{SDA}$ .

## ■ PRESSURE ADJUSTING FACTORS

The final local pressure is adjusted by a set of factors according to design, craft type, location, area, etc. These factors are used in defining the design pressures as shown in Fig 15.11 and Fig 15.12.

### ◆ Design category factor $k_{DC}$

The design category factors are dependent on which of the four categories, A–D, the craft belongs to. See Fig 4.22 (STIX stability index) regarding design categories. Values of  $k_{DC}$  are shown in Fig 15.7. The category factor considers the pressures and slamming loads due to sea conditions according to the design category.

### ◆ Dynamic load factor $k_{DYN}$

The dynamic load factor for power monohulls in planing mode,  $k_{DYN}$ , is the lesser of  $k_{DYN1}$  and  $k_{DYN2}$ . The dynamic load factor is used in the bottom pressure and  $k_L$  determination for planing motor craft. It shall be taken as the lesser of  $k_{DYN1}$  and  $k_{DYN2}$ , as defined in Fig 15.7.

**Fig 15.7** Design category and dynamic load factor

<i>Values of design category factor <math>k_{DC}</math> according to design category</i>				
<i>Design category</i>	A	B	C	D
<i>Value of <math>k_{DC}</math></i>	1	0.8	0.6	0.4

<i>Initial dynamic load factor for power monohulls in planing mode <math>k_{DYN1}</math></i>	
3) Dynamic Load Factor, $k_{DYN1} = 0.32 \cdot \left( \frac{L_{WL}}{10 \cdot B_c} + 0.084 \right) \cdot (50 - \beta) \cdot \frac{V^2 \cdot B_c^2}{m_{LDC}}$	
<i>This value represents the acceleration at <math>L_{CG}</math>, expressed in g's. <math>1g = 9.81 \text{ m/s}^2</math> and for calculations we check against 4) : (using the lesser value)</i>	
4) Dynamic Load Factor, $k_{DYN2} = \frac{0.5 \cdot V}{m_{LDC}^{0.17}}$ Not to be taken $>6$ nor $<3$	

$L_{WL}$ = Length of waterline
$B_c$ = Beam of chine
$V$ = speed in knots
$\beta$ = bottom deadrise in degrees, at $0.4 \cdot L_{WL}$
from transom, max. $30^\circ$ , min $10^\circ$
$m_{LDC}$ = loaded displacement mass (kg)

For sailing craft and motor craft in displacement, mode  $k_{DYN}$  is not used for pressure determination but is used for the determination of  $k_L$  using the value of  $k_{DYN} = 3$ . The dynamic load factor is considered to be close to the vertical acceleration measured at the craft centre of gravity expressed in units of  $g$ , where  $1g$  is the acceleration due to gravity.

#### ◆ Longitudinal pressure distribution factor $k_L$

The longitudinal pressure distribution factor described in Fig 15.8 shows the variation of pressure loads along with the lengthwise position on the craft. Fig 15.8 only shows values of 3, 4.5 and 6; for intermediate values,  $k_L$  shall be determined either by calculation or by interpolation in the graph.

#### ◆ Area reduction factor $k_{AR}$

The area pressure reduction factor described in Fig 15.9 shows the area distribution factor. It might seem strange that there is a reduction factor for stiffeners of long length and panels of large sizes. The reason for this is that the design pressure is considered to be static, but the peak pressures the vessel encounters are slamming loads of very short duration, acting over a very limited area. So, the longer the stiffener or larger the panel, the more the slamming pressure is spread out, so to speak. Fig 15.9, equation 6 shows the  $k_{AR}$  factor that applies to the stiffeners and the plating. The factor is not to be taken greater than 1 and not less than 0.

#### ◆ Pressure correction factor $k_{SL5}$

The pressure correction factor described in Fig 15.9 is aimed at a sailing craft that is very stable for its displacement equipped with canting keels, water ballast to windward,

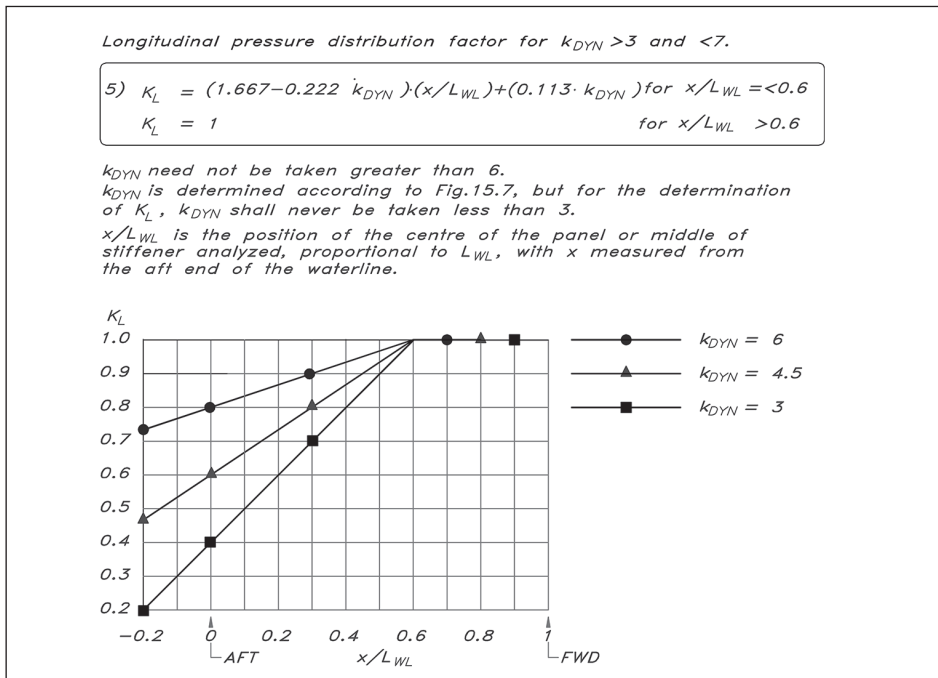


Fig 15.8 Longitudinal pressure factor  $K_L$

**Fig 15.9** Area reduction and pressure correcting factor

6)  $k_{AR} = k_R \cdot 0.1 \cdot m_{LDC}^{0.15} / A_D^{0.3}$

$k_{AR}$  = area reduction factor, not to be greater than 1 or less than 0

$k_R$  = structural component and boat type factor

- 1.0 for panels and stiffeners of motor craft in planing mode
- $1.5-3 \cdot 10^{-4} \cdot b$  for panels of sailing craft and motor craft in displacement mode
- $1.0-2 \cdot 10^{-4} \cdot l_u$  for stiffeners of sailing craft and motor craft in displacement mode

$m_{LDC}$  = loaded displacement mass, [kg]

$A_D$  = design area, [m<sup>2</sup>]

- $(1 \cdot b) \cdot 10^{-6}$  for plating not more than  $2.5 \cdot b^2 \cdot 10^{-6}$  [m<sup>2</sup>]
- $(l_u \cdot s) \cdot 10^{-6}$  for stiffeners, but not less than  $0.33 \cdot l_u^2 \cdot 10^{-6}$  [m<sup>2</sup>]

$b$  = shorter side of the panel [mm]

$l$  = longer side of the panel [mm]

$s$  = stiffener spacing [mm]

$l_u$  = unsupported span of stiffener [mm]

7)  $k_{SLS} = (10 \cdot GZ_{MAX<60} \cdot L_{WL}^{0.5} / m_{LDC}^{0.33})^{0.5}$

$k_{SLS}$  = pressure correcting factor, not to be greater than 1 if  $m_{LDC} > 5 \cdot L_{WL}^3$ , in design category A & B.

$k_{SLS}$  = pressure correcting factor, not to be less than 1 if  $m_{LDC} \leq 5 \cdot L_{WL}^3$ , in design category A & B.

$k_{SLS}$  = pressure correcting factor, = 1 in design category C & D.

$GZ_{MAX<60}$  = maximum righting lever in metres at a heel angle no more than 60 degrees, with all stability increasing devices such as canting keels or water ballast at their most effective position, in fully loaded condition. If the maximum righting lever occurs above 60 degrees, value of 60 degrees shall be used. The crew shall be in upwind hiking position

heavy and deep bulbs, etc. The limitation of the heel angle at 60° considers stability characteristics that can be achieved during high-performance sailing (i.e. at angles below 30° and ultimate stability below 60°).

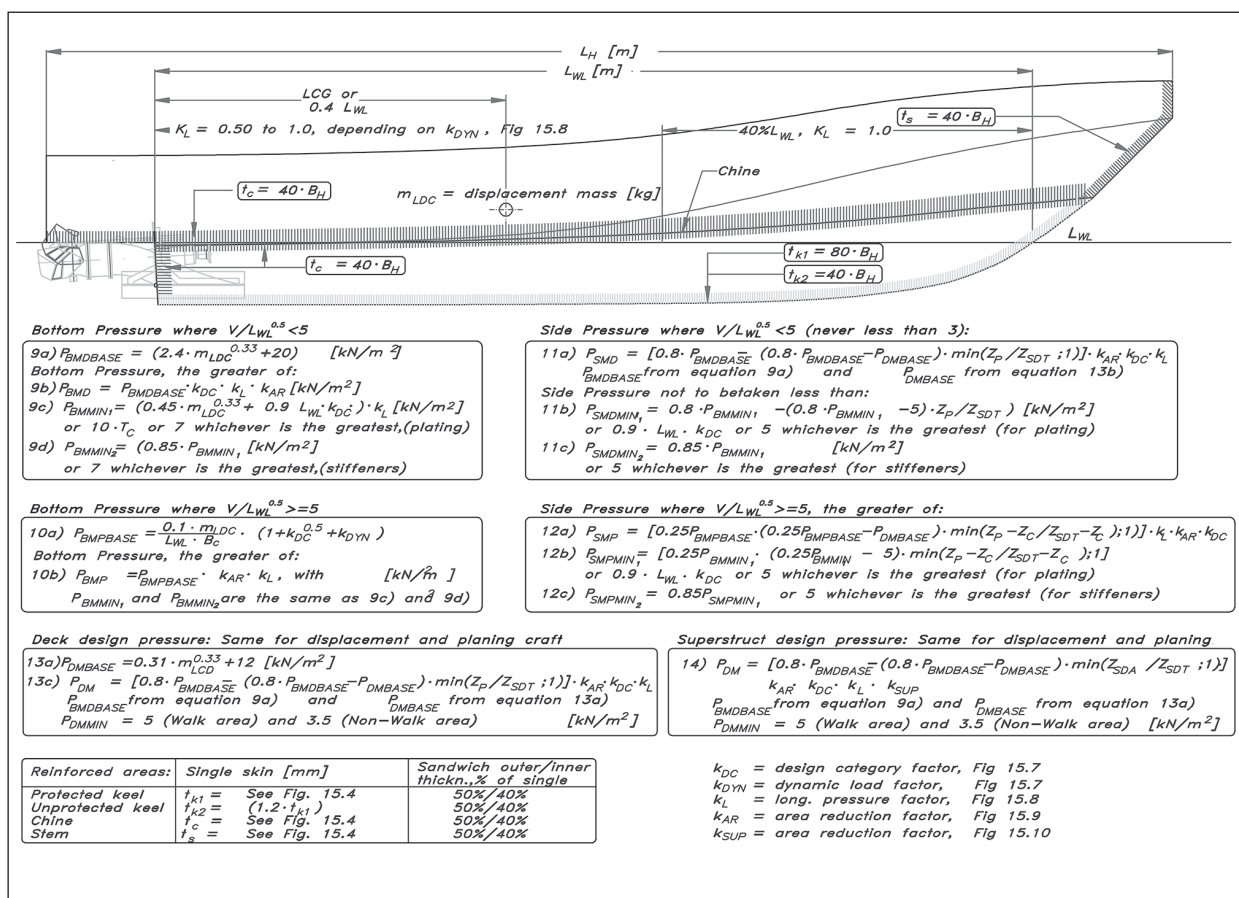
#### ◆ Superstructures correction factor $k_{SUP}$

The superstructure and cockpit side pressure reduction factor  $k_{SUP}$  is described in Fig 15.10. The height  $H_{SUP}$  is measured from the deck level to which the superstructure element is attached,  $Z_{SDA}$  or  $Z_{SDT}$ , whichever is the lower (see Fig 15.6). Superstructures, cockpits and decks can be walking or non/walking areas. Areas of an inclination of more than 25° degrees to the horizontal in the longitudinal direction or more than 55° to the horizontal in the transverse direction are non/walking areas. All other areas of deck, cockpit or superstructure are classified as walking areas.

Superstructure area	$k_{SUP}$
Superstructure front	8a) $1 - (0.3 \cdot H_{SUP}) / (\cos \alpha_L \cdot Z_{SDT})$ Walk. area min. 0.67 Non-walk. area min. 0.50
Superstructure side	8b) $1 - (0.4 \cdot H_{SUP}) / (\cos \alpha_T \cdot Z_{SDT})$ Walk. area min. 0.67 Non-walk. area min. 0.50
Superstructure top	8c) $1 - (0.5 \cdot H_{SUP}) / Z_{SDT}$ Walk. area min. 0.50 Non-walk. area min. 0.35
Superstructure aft aft side, non-protected	8d) $1 - (0.6 \cdot H_{SUP}) / Z_{SDT}$ Walk. area not relevant Non-walk. area min. 0.35
Superstructure aft aft side, protected	8e) $1 - (0.7 \cdot H_{SUP}) / Z_{SDT}$ Walk. area not relevant Non-walk. area min. 0.35
Cockpit side	Walk. area 0.67 Non-walk. area 0.50

Fig 15.10 Superstructure load factor

Fig 15.11 (BELOW) Motor craft design pressures



## ■ DESIGN LOADS

Fig 15.11 shows the magnitude and distribution of loads on the bottom, side, deck and superstructure for a powerboat that shall be used for the calculations. Fig 15.12 (overleaf) shows the same thing for a sailing boat. The loads are expressed as design pressures in kN/m<sup>2</sup> (kPa). To get a better feel for the loads it might be worth mentioning that 10 kPa gives a load of 1 metric tonne per square metre or a pressure head of 1 metre.

For the bottom of a powerboat, in displacement mode (i.e. operating at speed-length ratios less than 5), equations 9(a–d) in Fig 15.11 give the bottom pressure. Fast craft should be checked against this requirement also since, in rough seas, craft usually planing in flat water must progress at a slower speed in the same manner as a displacement craft. As can be seen in equations 9(c) and 9(d), there are different minimum requirements for plating and stiffeners.

For the bottom in planing mode (i.e. speed-length ratios of 5 or more), equation 10(a) in Fig 15.11 applies. The main formula 10a describes the bottom pressure  $P_{BMPBASE}$ . As can be seen, it consists of a term including displacement mass divided by length and width (i.e. a hydrostatic area pressure). To this is added a dynamic factor depending on speed, deadrise angle and bottom size. To calculate the bottom pressure, we start to calculate  $k_{DYN}$  (see Fig 15.7) at the worst condition (i.e. the highest speed at loaded displacement mass,  $m_{LCD}$ ), which might not be the maximum speed at a lower mass. The greatest of  $P_{BMP}$  and  $P_{BMPMIN}$ , in Fig 15.11, is used when calculating the scantlings for the bottom.

The extent of the bottom is defined to meet the chine at the LCG position if known, or at  $0.4 L_{WL}$  forward of the transom if the LCG is not known, as shown in Fig 15.11. In the case of a round bilged hull, the chine position is established by drawing a tangent of 50° from the horizontal to the hull contour, as can be seen in Fig 15.2.

For sailing craft, we calculate the bottom design pressure  $P_{BSBASE}$  according to equations 15(a–d) in Fig 15.12. This pressure depends on a function of the displacement mass (i.e. a hydrostatic pressure plus a pressure correcting factor for slamming,  $k_{SLS}$ ; see equation 7 in Fig 15.9). This factor should never be taken less than 1. The  $GZ_{MAX<60}$  used in the formula is the maximum righting lever at a heel angle less than 60°, with all stability increasing devices such as canting keels or water ballast at their most effective position, in the fully loaded condition. The crew shall be in the upwind hiking position ISO 12215-5 points out. This certainly maximizes the righting moment, but how realistic it is when calculating the stability characteristics of a cruising sailboat might be questioned. This since the standard specifically exempts racing yachts. But, since the practice today is that this is what's going on in racing (with cruising boats), it will increase the pressure for the bottom structure. To bear in mind is also that the  $k_{SLS} > 1$ -factor kicks in for boats with a light displacement,  $m_{LCD} < 5 \times L_{WL}^3$ , for yachts in design category A and B. Where  $m_{LCD} > 5 \times L_{WL}^3$ , and for design categories C and D the  $k_{SLS} = 1$ . To calculate the final design bottom pressure  $P_{BS}$  (equation 15b), the basic pressure is multiplied with  $k_{AR}$ ,  $k_L$ ,  $k_{DC}$  and when appropriate  $k_{SLS}$ . Be aware of equations 15(c) and 15(d), which set minimum values for  $P_{BS}$  that must be fulfilled.

The bottom is defined as reaching the level of the stationary waterline at fully loaded condition. In the YD-41 case the craft is divided into eight areas; A and B for the



<b>Bottom design pressure: (Fig 15.13 &amp; 15.14)</b> 15a) $P_{BSBASE} = (2.0 \cdot m_{LDC}^{0.33} + 18) \cdot k_{SLS}$ [kN/m <sup>2</sup> ] Bottom Pressure, the greater of: 15b) $P_{BS} = P_{BSBASE} \cdot k_{DC} \cdot k_L \cdot k_{AR}$ [kN/m <sup>2</sup> ] 15c) $P_{BSMIN1} = (0.30 \cdot m_{LDC}^{0.33} + 0.66 l_{WL} \cdot k_{DC}) \cdot k_L$ [kN/m <sup>2</sup> ] or $10 \cdot T_C$ or 7 whichever is the greatest (for plating) 15d) $P_{BSMIN2} = 0.85 \cdot P_{BSMIN1}$ [kN/m <sup>2</sup> ] or 7 whichever is the greatest (for stiffeners)		<b>Side design pressure: (Fig 15.13 &amp; 15.14)</b> 16a) $P_{SS} = [P_{BSBASE} - (P_{BSBASE} - P_{DSBASE}) \cdot \min(Z_P/Z_{SDT}; 1)] \cdot k_{AR} \cdot k_{DC} \cdot k_L$ $P_{BSBASE}$ from equation 15a) and $P_{DSBASE}$ from equation 17a) Side Pressure not to be taken less than: 16b) $P_{SSMIN1} = P_{BSMIN1} - Z_P/Z_{SDT} \cdot (P_{BSMIN1} - 5)$ [kN/m <sup>2</sup> ] or 5 whichever is the greatest (for plating) 16c) $P_{SSMIN2} = 0.85 \cdot P_{SSMIN1}$ [kN/m <sup>2</sup> ] or 5 whichever is the greatest (for stiffeners)	
<b>Deck design pressure: (Fig 15.6)</b> 17a) $P_{DSBASE} = 0.50 \cdot m_{LDC}^{0.33} + 12$ [kN/m <sup>2</sup> ] 17b) $P_{DS} = [P_{BSBASE} - (P_{BSBASE} - P_{DSBASE}) \cdot \min(Z_P/Z_{SDT}; 1)] \cdot k_{AR} \cdot k_{DC} \cdot k_L$ $P_{BSBASE}$ from equation 15a) and $P_{DSBASE}$ from equation 17a) $P_{DMIN} = 5$ (Walk area) and 3.5 (Non-Walk area) [kN/m <sup>2</sup> ]		<b>Superstructure design pressure</b> 18) $P_{SUPS} = [P_{BSBASE} - (P_{BSBASE} - P_{DSBASE}) \cdot \min(Z_{SDA}/Z_{SDT}; 1)] \cdot k_{AR} \cdot k_{DC} \cdot k_L \cdot k_{SUP}$ $P_{BSBASE}$ from equation 15a) and $P_{DSBASE}$ from equation 17a) $P_{DMIN} = 5$ (Walk area) and 3.5 (Non-Walk area) [kN/m <sup>2</sup> ]	
<b>Watertight bulkhead pressure: (Fig 15.15)</b> 19) $P_{WB} = 7 \cdot H_B$ [kN/m <sup>2</sup> ]		<b>Integral tank bulkhead pressure: (Fig 15.15)</b> 20) $P_{TB} = 10 \cdot H_B$ [kN/m <sup>2</sup> ]	

$k_{DC}$  = design category factor, Fig 15.7  
 $k_{DYN}$  = dynamic load factor, Fig 15.7  
 $k_L$  = long. pressure factor, Fig 15.8  
 $k_{AR}$  = area reduction factor, Fig 15.9  
 $k_{SLS}$  = dynamic load factor, Fig 15.9  
 $k_{SUP}$  = area reduction factor, Fig 15.10

$l$  = long edge of panel [mm], Fig 15.10  
 $b$  = short edge of panel [mm], Fig 15.10  
 $Z_P$  = local height from  $L_{WL}$  [m], Fig 15.6  
 $Z_{SDA}$  = Actual freeboard [m], Fig 15.6  
 $Z_{SDT}$  = Theoretical freeboard [m], Fig 15.6  
 $D_b$  = bulkhead depth, from bottom to deck [m], Fig 15.13 & Fig 15.15  
 $H_b$  = bulkhead pressure head [m], Fig 15.13 & Fig 15.15

bottom, C and D for the topsides, E for the transom, F and G for the deck and H for the superstructure. Areas A, C and F lie within the area from the forward perpendicular (FP) to 40% of  $L_{WL}$  aft of the FP (see Fig 15.13), and here the panel pressure is at maximum. From this position to the transom, the pressure drops down according to the  $k_L$ -factor.

Around the centreline, the stem and the chine, there are reinforced areas as shown in Fig 15.4. If the keel strake is unprotected (i.e. not fitted with a separate protective keel, which is the case for most planing powerboats) this strake extends  $80B_H$  mm on each side of the centreline. The stem strake extends  $40B_H$  mm on each side of the centreline and the chine strakes  $40B_H$  mm in total. When an external ballast keel is fitted the area around the keel, area K in Fig 15.13, shall withstand a bottom pressure 1.8 times bigger than the maximum bottom pressure.

## DESIGN LOADS FOR THE TOPSIDES

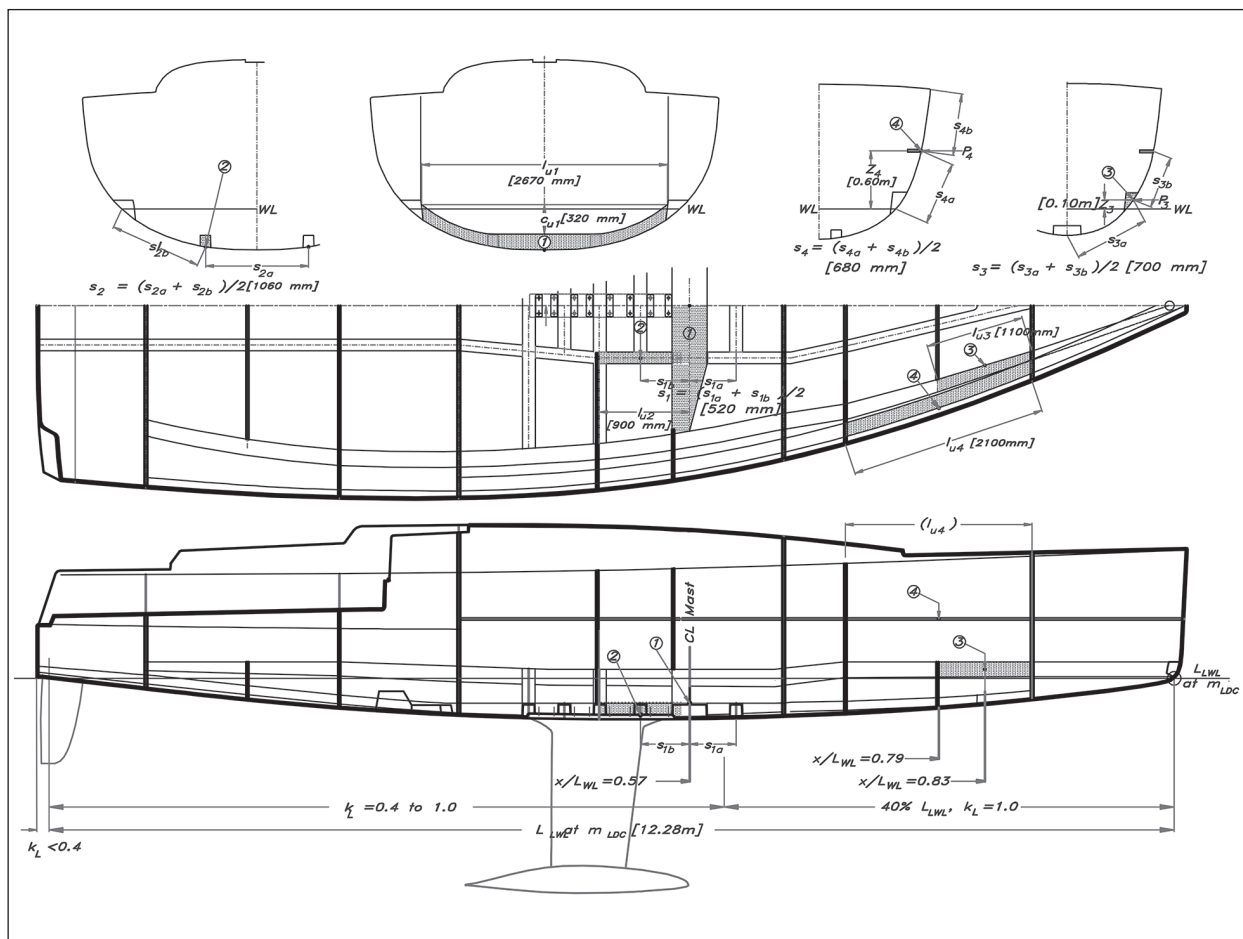
For the side panels, we must decide at which height above the bottom/side limit the pressure acts to establish the correct design pressure. This height ( $Z_P$ ) is measured from the waterline or chine, depending on whether the craft is non-planing or planing, to the pressure point P (Fig 15.6). If the chine is situated below the waterline the distance  $Z_C$  gets a negative value (Fig 15.6(c)). To be able to define the panels we must have a stiffening system layout so we can identify each hull panel. The pressure acts on the geometric centre of the panel in question, or at mid-length of the stiffener studied.

Fig 15.11 gives the equations to determine the side pressure for powerboats (11(a–c) and 12(a–c)), and Fig 15.12, equations 16(a–c) are for sailing boats, where it can be seen that sailing monohulls have a slightly higher value than other boats. The reason for this is the normal heeled position of this kind of boat when going upwind. The base pressure for the topside depends on a combination of bottom pressure and deck pressure, modified by the height of the pressure point above WL, for both power and sailing craft.

**Fig 15.12** Sailboat design pressures







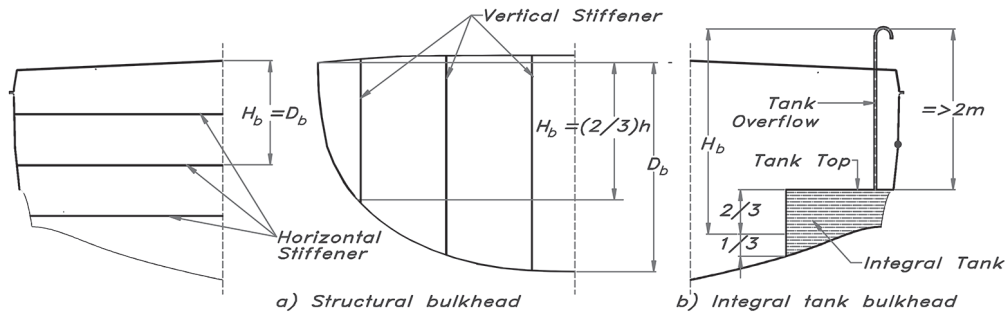
added to  $Z_p$ , according to equation 12(a) in Fig 15.11. Maximum and minimum values are calculated in a similar way as for displacement craft, in equations 12(b) and 12(c).

The sailing craft side pressure is described in Fig 15.12, equations 16(a–c), and is constructed similarly to the side pressure for displacement motor craft. From Fig 15.13 we can measure the different panel locations and dimensions. The panels marked A1, A2 and B1 are three bottom panels of the YD–41 used as examples of the pressure calculations. These are not used in the design pressure calculations but we will need them later when calculating the scantlings for the panels. In Fig 15.13 the panels marked C1 and D1 are two side panels of the YD–41 used as examples of the pressure calculations in Fig 15.16.

**Fig 15.14** Sailboat craft design pressure on stiffeners

## DESIGN LOADS FOR THE DECKS, SUPERSTRUCTURES AND BULKHEADS

For the pressures on decks and superstructures, motor craft and sailing craft are treated in a similar way. For motor craft decks the pressure  $P_{DM}$ , the same for displacement and



$D_b$  is the depth of the bulkhead, (m), measured as shown above:

$H_b$  is the water head, (m), measured as shown above:

1. for plating, the distance from a point  $2/3$  of the depth of the panel ( $D_b$  in m) below the top of the bulkhead, regardless of stiffening system
  2. for vertical stiffeners, the distance from a point  $2/3$  of the depth of the stiffener below the top of the bulkhead
  3. for horizontal stiffeners, the height measured from the stiffener to the top bulkhead
- Tank overflow to be considered at minimum 2 metres above tank top to determine  $H_b$

Structural plywood bulkheads:

$$21) \quad t_b = 7 \cdot D_b \quad [\text{mm}]$$

Tank plywood bulkheads:

$$22) \quad t_b = 10 \cdot D_b \quad [\text{mm}]$$

Structural and tank sandwich bulkheads:  
The skin thickness shall be such as

$$23) \quad t_s \cdot t_c \geq \frac{t_b^2}{6} \cdot \frac{25}{\sigma_d} \quad [\text{mm} \cdot \text{mm}]$$

The skin thickness shall be such as

$$24) \quad t_s \cdot t_c \geq \frac{t_b^3}{12} \cdot \frac{4000}{E} \quad [\text{mm} \cdot \text{mm}]$$

$t_b$  = plywood bulkhead thickness [mm]

$t_s$  = sandwich skin thickness [mm]

$t_c$  = sandwich core thickness [mm]

$\sigma_d$  = design strength [N/mm<sup>2</sup>]

$E$  = inplane modulus [N/mm<sup>2</sup>]

$\tau_d$  = design inplane shear strength [N/mm<sup>2</sup>]

$\sigma_d$  and  $E$  are values for the skins taken from Fig.15.21 and 15.24

Min. design core shear: [N/mm<sup>2</sup>]

$L_H$ [m]	<10	10 to 15	15 to 24
$\tau_d$	0.25	$0.25 + 0.03 (L_{WL} - 10)$	0.40

**Fig 15.15** Pressure bulkheads

planing craft, is based on  $P_{BMDBASE}$  as shown in Fig 15.11, equation 9(a), and  $P_{DMBASE}$ , equation 13(a).

For sailing craft, areas F and G in Fig 15.13, the procedure is similar which can be seen in Fig 15.12, equations 17(a) and 17(b). Comparing  $P_{DMBASE}$  with  $P_{DSBASE}$  gives the result that sailing craft deck pressure normally becomes greater than to a similarly sized motor vessel. The reason is that the sailing craft's deck is more heavily loaded because of the strains the rig puts on the entire hull-deck girder. Just as for the bottom the full deck pressure acts to 40% aft of the forward end of  $L_{WL}$ , as per Fig 15.8.

Superstructures are treated in a similar way as decks, see Fig 15.11, equation 14, and Fig 15.12, equation 18. The pressure  $P_{SUP}$  gets its basic value from the bottom- and side pressures which are corrected by the ratio of  $Z_{SDA}$  and  $Z_{SDT}$ , with a maximum value of 1, as per equations 14 and 18. The difference in load conditions between front, side and top area is taken care of by  $k_{SUP}$ , as shown in Fig 15.10.

When it comes to bulkheads that are structural, watertight or integral tanks, there are no differences between power or sailing vessels. Fig 15.13 shows a structural bulkhead, the area I, with required measurements to calculate the load for the YD-41. Fig 15.15 gives a more comprehensive picture of how to get the measurements, depending on the

bulkhead's stiffener layout or if the bulkhead is part of a tank. The actual design pressure calculations are given in equation 19 for watertight bulkheads and in equation 20 for integral tank bulkheads in Fig 15.12. For collision bulkheads, the same formula applies as for integral tank bulkheads. The thickness of an unstiffened structural bulkhead that is non-watertight may be obtained using equation 21 for a solid plywood bulkhead, and equation 22 for a plywood tank panel, in Fig 15.15. To transform this to sandwich FRP panels, equations 23 and 24 may be used.

To determine the tank design pressure, the top of the tank overflow shall be taken no less than 2 metres above the top of the tank, regardless of actual height, as per Fig 15.15(b). Integral tanks shall be subdivided as necessary by internal wash plates. Wash plates that replace hull framing shall have scantlings equivalent to the stiffeners they replace. In general, wash plates shall be fitted with perforation holes, not exceeding 20% of the total area of the bulkhead.

The scantlings of collision bulkheads shall be the same as for integral tank bulkheads. Regarding the design pressure of centreboard and lifting keel-well casings, it shall be at least  $10T_C$  (m).

## ■ SUMMARY OF DESIGN LOADS

Fig 15.16 shows some results of the pressure calculations of the YD-41. When we compare area A1 with A2, both with a  $K_L$  of 1, the only thing that differs from a pressure point of view, is the design area,  $A_D$ , which renders A1(smaller area) a pressure of 48 kPa with A2 (larger area) with a pressure of 44kPa. A prime example of  $K_{AR}$  in action. The actual load-carrying capability, when taken the panel area into consideration is for area A1 29.5 kN and for area A2 34.8 kN. Area B1, also a bottom panel, in the aft body is a large panel more than twice the size of panel A1. By being big and situated in the aft part of the bottom the pressure is down to 15.9 kPa, roughly one-third of the A1 pressure. This illustrates the working technique of spreading out the stiffening system the further back you go in the vessel, without increasing the panel scantlings. In fact, for pure strength reasons, you can often decrease the scantlings, but in practice in real-world boat-building, to keep the scantlings the same for the whole bottom is the most practical and economic, labour-wise.

Comparing the two stiffeners numbered 1 and 2 in Fig 15.14, we see that number 1 is a primary stiffener and number 2 a secondary. Both stiffeners are within the heavily loaded area by the ballast keel. Stiffener 2 of comparably short span and supporting a small panel gets the heaviest loading of 61.1 kPa compared with stiffener 1's 32.3 kPa thanks to its greater span and accompanied larger attached panel. The difference in total load carrying is comparatively smaller, though, 44.8 kN for stiffener 1 and 58.3 kN for stiffener 2.

The two side panels C1 and D1 in Fig 15.13 are very similar in shape and size, but with one in the forebody and the other in the aft body of the hull. This gives the significant difference of the  $K_L$  factors (1.0 versus 0.51), which reflects the big difference in the design pressure, 33.1 kPa for C1 and 15.7 kPa for D1. All deck areas F, G and H get the minimum allowable design pressure of 5 kPa, and I in Fig 15.13 gets a design pressure of 7.4 kPa.

Bottom Plating (Fig 15.13)				Bottom Plating (Fig 15.13)				Bottom Plating (Fig 15.13)			
Part # =	A1	KDC =	1	Part # =	A2	KDC =	1	Part # =	B1	KDC =	1
LWL(m) =	12.28	KDYN =	3	LWL(m) =	12.28	KDYN =	3	LWL(m) =	12.28	KDYN =	3
X(m) =	9.2	Tc(m) =	0.43	X(m) =	7.46	Tc =	0.43	X(m) =	3.8	Tc =	0.43
mLDC (kg)=	7400	kl =	1.00	mLDC (kg)=	7400	kl =	1.00	mLDC (kg)=	7400	kl =	0.65
GZMAX60(m) =	1.2	KAR =	0.58	GZMAX60(m) =	1.2	KAR =	0.53	GZMAX60(m) =	1.2	KAR =	0.29
Long Side,l(mm) =	990	KR =	1.314	Long Side,l(mm) =	1200	KR =	1.302	Long Side,l(mm) =	1200	KR =	1.17
Short Side, b(mm) =	620	KSLs =	1.491	Short Side, b(mm) =	660	KSLs =	1.496	Short Side, b(mm) =	1100	KSLs =	1.496
mLDC/5*LWL^3 =	4.00	Ad (m2)=	0.614	mLDC/5*LWL^3 =	4.00	Ad =	0.792	mLDC/5*LWL^3 =	4.00	Ad =	1.320
PBSMIN(kPa) =	13.8	PBSBASE =	83.2	PBSMIN(kPa) =	13.8	PBSBASE =	83.5	PBSMIN(kPa) =	13.8	PBSBASE =	83.5
PBS = 48.2		(kPa)		PBS = 44.4		(kPa)		PBS = 15.9		(kPa)	
		(29.5kN)				(34.8kN)				(21.0kN)	

Bottom Stiffeners (Fig 15.14)				Bottom Stiffeners (Fig 15.14)				Deck Plating Fore Deck (Fig 15.13)			
Part# =	1	KL =	0.90	Part# =	2	KL =	0.86	Part# =	F1	KL =	1.00
Spacing(mm), s =	520	KAR =	0.24	Spacing(mm), s =	1060	KAR =	0.47	Long Side(m), l =	2400	KAR =	0.21
Span(mm), lu =	2670	KR =	0.699	Span(mm), lu =	900	KR =	1.23	Short Side(m), b =	2000	KR =	0.9
X(m) =	6.86	AD =	1.388	X(m) =	6.42	AD =	0.954	X(m) =	9.65	AD =	4.800
PBSMIN(kPa) =	11.7	PBSBASE =	83.2	PBSMIN(kPa) =	11.7	PBSBASE =	83.5	Zp/ZSDT =	1	PDSBASE =	21.5
keel area PBS = 32.4		(kPa)		keel area PBS = 61.5		(kPa)		Pds = 5.0		(kPa) Min. pressure	
		(44.8kN)				(58.3kN)					

Side Plating (Fig 15.13)				Side Plating (Fig 15.13)				Deck Plating Cockpit Bottom (Fig 15.13)			
Part =	C1	KL =	1.00	Part =	D1	KL =	0.51	Part# =	G1	KL =	0.52
Long Side(mm), l =	2100	KAR =	0.51	Long Side(mm), l =	2100	KAR =	0.51	Long Side(m), l =	2100	KAR =	0.00
Short Side(mm), b =	480	KR =	1.356	Short Side(mm), b =	490	KR =	1.353	Short Side(m), b =	1086	KR =	1.1742
X(m) =	9.2	AD =	1.01	X(m) =	2.09	AD =	1.03	X(m) =	2.17	AD =	2.281
ZSDT(m) =	1.3	ZP(m) =	0.4	ZSDT(m) =	1.08	ZP(m) =	0.3	Zp/ZSDT =	0.5	PDSBASE =	21.5
ZP/ZSDT =	0.31	PSSMIN =	11.1	ZP/ZSDT =	0.28	PSSMIN =	11.3	Pds = 5.0 (kPa) Min. pressure			
Pss = 33.1		(kPa)		Pss = 15.7		(kPa)		Bulkhead (Part# [I] Fig 15.13)		Db = 1.58	
								PWB = 7.4		(kPa)	

Fig 15.16 YD-41 pressures

## MECHANICAL PROPERTIES AND DESIGN STRESSES

So far, we have established the design pressures for the various areas of the vessel, but still, there are some additional correction factors to apply before determining the scantlings. These correction factors do not concern design pressures and locations on the vessel, but rather building qualities, mechanical properties of the laminates and geometrical properties of the panel or stiffener in question. These are especially important for composite fibre-reinforced materials, where the boatbuilder fabricates the laminates and to a great extent determines the mechanical properties.

## BOATBUILDING QUALITY FACTOR $K_{BB}$

The standard assumes that the builder has properly followed the state of art regarding building and material supplier requirements, such as, where relevant:

- Building environment, temperature, hygrometry, etc. during storage and building
- Building process, preparation before building (e.g. dusting, degreasing, priming, etc.)
- Type of material, the proper combination of material, etc.

For fibre-reinforced plastic (FRP), which this book looks into, the factor  $k_{BB}$  reflects the quality of the as-built material obtained by the boat builder. In this respect, FRP differs from other boatbuilding materials, as the material is not bought ready to build from but



manufactured by the boatbuilder from ingredients bought from a supplier (resin, different fibres, sandwich cores, etc.). The only similar situation is when building a boat from ferro cement.

Fig 15.17 shows the different  $k_{BB}$  values connected to different builder characteristics and procedures. In one verified case two builders produced an identical 35 foot boat, to the same specifications regarding building materials, accommodations, engine, etc., with the result that one of the boats turned out 500 kg heavier than the other one. The only different amount of material used was the amount of resin used to build the laminate. Apart from being more expensive, the heavy boat also was not as strong as the lighter one but also of inferior performance. Also, when designing the boat by using optimum laminate properties without checking fibre content or better still, tested laminates there is the risk that the boat will not meet the strength requirements. As can be seen from Fig 15.17, the design material characteristics have to be reduced by 25% for the low non tested laminate. So, to summarize, the mechanical properties are significantly dependent on the craft manufacturing process.

## ■ ASSESSMENT METHOD FACTOR $K_{AM}$

This factor has the purpose of ‘balancing’ the results from the various assessment methods, mentioned earlier in this chapter, to ensure that simpler assessment methods give more conservative results than more scientifically developed ones. The assessment method factors are given in Fig 15.18.

Quality	Builder characteristics	$k_{BB}$	
		Hand laid	Infused, prepreg
TESTED	Mechanical properties of the laminates, as built, based on tests of the mechanical characteristics. Results and test procedures are drawn up into a quality procedure, such as ISO 9001.	1.00 of tested value	1.00 of tested value
HIGH	Fibre mass content obtained from sample thickness with theoretical approach, or from burning samples for a range of typical layups. Results and test procedures are drawn up into a quality procedure, such as ISO 9001.	0.95 of calculation or table value	1.00 of calculation or table value
LOW	No measurements or checking of fibre mass content. Volume content is taken from Fig 15.28, according to relevant building process.	0.75 of calculation or table value	0.80 of calculation or table value

Fig 15.17 Boatbuilding quality factor

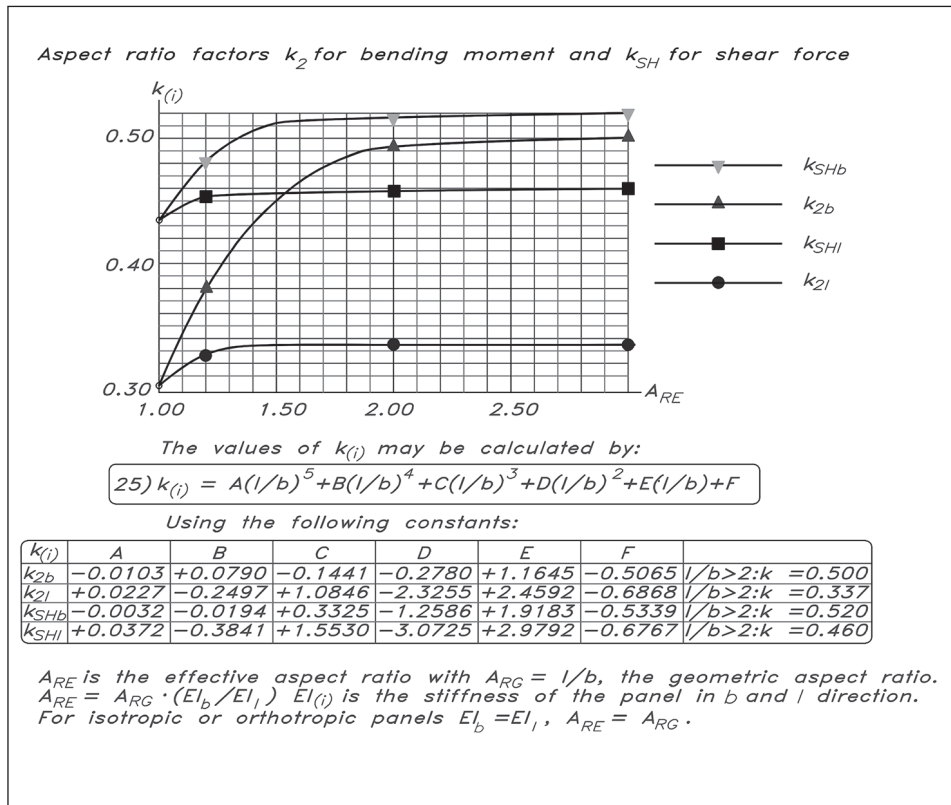
**Fig 15.18** Assesment  
method factor

Assessment method	$k_{AM}$	
	FRP & wood	Metal
Method 1 "Simplified" method	0.90	1.00
Method 2 "Enhanced" method	0.95	1.00
Method 3 "Developed" & "FEM"	1.00	1.00
Method 4 "Direct test"	1.00	1.00

## ASPECT RATIO FACTORS FOR PLATING $K_{2B}$ AND $K_{SH}$

These aspect ratio factors are for the calculation of bending moment ( $k_2$ ) and shear force ( $k_{SH}$ ) for rectangular panels, given in Fig 15.19. They are based on the effective aspect ratio ( $A_{RE}$ ) defined at the bottom of Fig 15.19.

**Fig 15.19** Aspect ratio  
factors

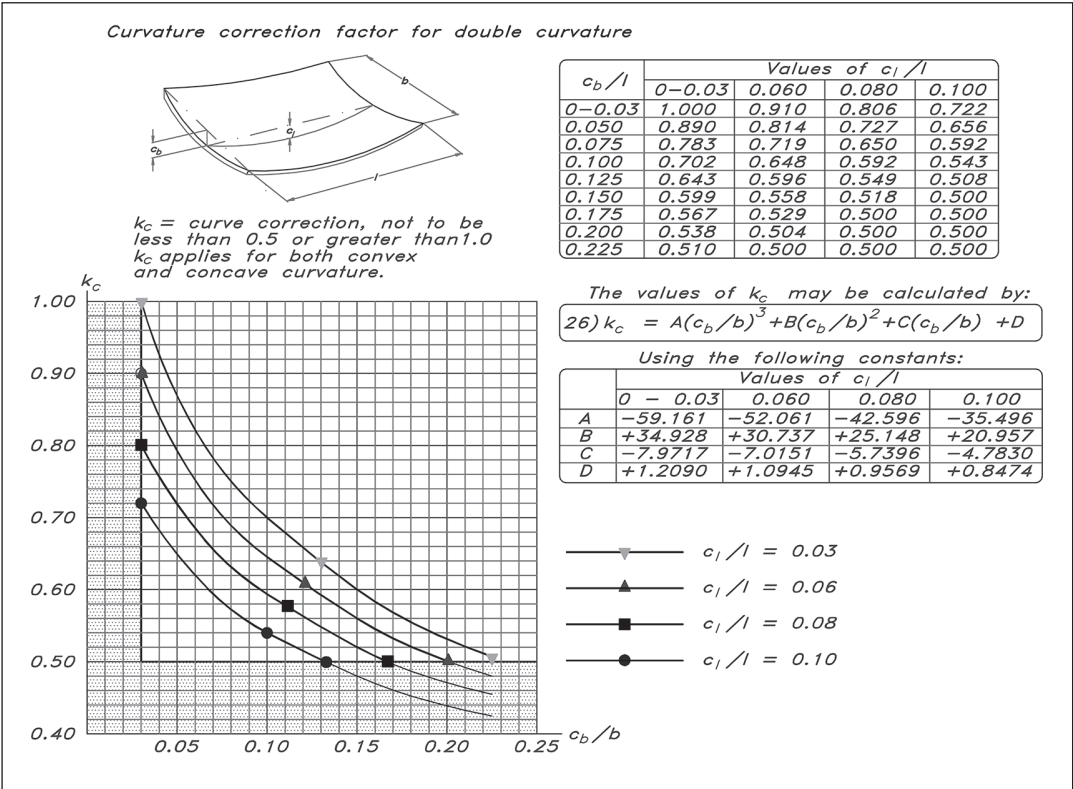




# CURVATURE CORRECTION FACTOR FOR PLATING $K_C$

The curvature correction factor  $k_c$  is given in Fig 15.20. It is a function of both the transverse curvature ratio  $c_b/b$  and the longitudinal correction factor  $c_l/l$ . It applies both for concave and convex surfaces and shall not be taken less than 0.5. Intermediate values may be calculated by linear interpolation of  $c_b/b$  and  $c_l/l$ .

Fig 15.20 Panel curvature correction factor



# DESIGN STRESSES

Fig 15.21 gives the design stresses that are allowed by the standard, compared to the ultimate direct and shear stresses (i.e. when the material actually breaks). The values given are for FRP materials, but the standard also tabulates values for other materials such as aluminium alloys, steel and different types of wood and plywood. Generally speaking, the design direct stresses are 50% of the ultimate stresses, which can be regarded as a safety factor of 2 for the materials, with additional considerations of  $k_{BB}$  and  $k_{AM}$ . An additional requirement regarding the inner skin of a sandwich panel is checking for skin wrinkling through the formula  $0.3(E_C \times E_{CO} \times G_{CO})^{0.33}$ .  $E_C$  is the compressive E modulus of the inner skin in direction b, in the plane of the panel.  $E_{CO}$  is the compressive modulus of the core perpendicular to the skins.  $G_{CO}$  is the core shear modulus in the direction parallel to the load.

Structural element	Direct Stress $\sigma_d$ N/mm <sup>2</sup>	Shear Stress $\tau_d$ N/mm <sup>2</sup>
Single skin plating	$\sigma_d = 0.5 \sigma_{uf} \cdot k_{BB} \cdot k_{AM}$	$\tau_d = 0.5 \tau_u \cdot k_{BB} \cdot k_{AM}$
Stiffeners	$\sigma_d = 0.5 \sigma_{ut} \cdot k_{BB} \cdot k_{AM}$	$\tau_d = 0.5 \tau_u \cdot k_{BB} \cdot k_{AM}$
Sandwich outer skin	$\sigma_{do} = 0.5 \sigma_{ut} \cdot k_{BB} \cdot k_{AM}$	$\tau_d = 0.5 \tau_u \cdot k_{BB} \cdot k_{AM}$
Sandwich inner skin	$\sigma_{di} = \min[0.5 \sigma_{uc}; 0.3(E_c \cdot E_{co} \cdot G_{co})^{0.33}] \cdot k_{BB} \cdot k_{AM}$	$\tau_d = 0.5 \tau_u \cdot k_{BB} \cdot k_{AM}$
Sandwich core	Compressive stress	Shear stress
Minimum of $\sigma_{uco}$ or $\tau_{uco}$ core value given by core provider in b and l directions, where relevant (see Fig 14.22)	Balsa	$\sigma_{dcco} = 0.50 \sigma_{ucco} \cdot k_{AM}$ $\tau_{dco} = 0.5 \tau_{uco} \cdot k_{AM}$
	Strain at break $\leq 35\%$	$\sigma_{dcco} = 0.55 \sigma_{ucco} \cdot k_{AM}$ $\tau_{dco} = 0.5 \tau_{uco} \cdot k_{AM}$
	Strain at break $> 35\%$	$\sigma_{dcco} = 0.65 \sigma_{ucco} \cdot k_{AM}$ $\tau_{dco} = 0.5 \tau_{uco} \cdot k_{AM}$
	Honeycomb	$\sigma_{dcco} = 0.50 \sigma_{ucco} \cdot k_{AM}$ $\tau_{dco} = 0.5 \tau_{uco} \cdot k_{AM}$

$\sigma_d$  = design stress     $\sigma_u$  = ultimate stress     $\tau_d$  = design shear stress  
 $\sigma_{do}$  = design stress outer skin     $\sigma_{uc}$  = ultimate compressive stress     $\tau_u$  = ultimate shear stress  
 $\sigma_{di}$  = design stress inner skin     $\sigma_{ut}$  = ultimate tensile stress     $\sigma_{dcco}$  = design core stress  
 $\sigma_{uf}$  = ultimate flexural stress     $\tau_{uco}$  = ultimate core shear stress  
 $\sigma_{ucco}$  = ultimate core comp. stress  
 $\tau_{dco}$  = core design shear stress

Fig 15.21 Design stresses

## DESIGN SHEAR FORCES AND DESIGN MOMENTS $F_D$ AND $M_D$

The design shear forces ( $F_d$ ) and bending moment ( $M_d$ ) are given in Fig 15.22. These requirements apply to both single skin and sandwich and only valid for rectangular panels with fully fixed ends.  $F_d$  and  $M_d$  are calculated incorporating the aspect ratio factors and the curvature ratio factors of Fig 15.19 and Fig 15.20. The value of the bending moment means bending moment on 1 mm wide stripe of the panel over the supports, where the maximum occurs, in compression on the inside when all sides are fixed.

Fig 15.22 Design shear forces and moments on panels

Force & moment	Unit	Formula
Design shear force in b direction	N/mm	$F_{db} = k_c \cdot k_{SHb} \cdot P \cdot b / 100000$
Design shear force in l direction	N/mm	$F_{dl} = k_c \cdot k_{SHl} \cdot P \cdot b \cdot (EI_l / EI_b)^{0.25} / 100000$
Design bend.moment in b direction	Nmm/mm	$M_{db} = -1/6 \cdot k_{2b} \cdot k_c \cdot P \cdot b^2 / 100000$
Design bend.moment in l direction	Nmm/mm	$M_{dl} = -1/6 \cdot k_{2l} \cdot k_c \cdot (EI_l / EI_b)^{0.5} \cdot P \cdot b^2 \cdot 10^{-5}$

For  $k_{SHb}, k_{SHl}, k_{k2b}, k_{k2l}$  see Fig 15.19 For  $k_c$  see Fig 15.20

## METHODS FOR SCANTLING DETERMINATION

As previously mentioned, the ISO standard recognizes six methods of analysis to determine the scantlings. We will look into one of them for GRP/FRP construction, the simplified method (method 1 in Fig 15.23). Method 2, called the enhanced laminate stack analysis method in the standard, calculates the first ply failure of the laminate. It will not be discussed here since it is done in Annex H of the ISO 12255-5 standard where it covers 14 pages to be properly dealt with. Methods 3–6, developed, direct test, FEM and drop test, need specialized software or test specimen. Methods 1 and 2 may be used in the design stage of the vessel without the need for specialized software.

<i>Analysis method</i>	<i>Material</i>	<i>Method</i>	<i>Element</i>	<i>Figures</i>	<i>Material properties</i>
#1 <i>Simplified</i>	GRP	<i>Formula for <math>t_p</math> into <math>w_f</math></i>	<i>Single skin &amp; sandwich</i>	<i>15.30 to 15.37</i>	<i>Fig 15.24 to Fig 15.28</i>
	GRP	<i><math>F_d, M_d, SM, t_{web}</math></i>	<i>Stiffener</i>	<i>15.37 to 15.42</i>	
#2 <i>Enhanced</i>	FRP	<i>Ply by ply analysis <math>F_d, M_d, SM, t_{web}</math></i>	<i>Plating &amp; Stiffener</i>	<i>Annexes A, C, H in ISO 12215-5</i>	

$t_p$  = laminate thickness mm       $SM$  = section modulus  $cm^3$   
 $w_f$  = dry fibre mass kg/m       $t_{web}$  = thickness of web mm  
 $F_d$  = design shear force N  
 $M_d$  = design bending moment Nm

**Fig 15.23** Methods for analysis and calculations

The ‘simplified’ method is valid for single skin or sandwich glass-reinforced plastics (GRP) with the same properties in b (short) and l (long) directions. This method (1) is explained in Fig 15.29 for single skin, 15.31–15.36 for sandwich plating and 15.37–15.42 for stiffeners.

## DETERMINATION OF MECHANICAL PROPERTIES

Mechanical properties to be used as input in determining the bending moment, stiffness and shear capabilities of FRP laminates and stiffeners may be derived either by testing or by calculations. Fig 15.24 shows properties of E-glass, aramid, carbon-HS fibres and polyester/epoxy resin. We must be aware that these values are valid for the fibres and matrices, and not for the total composites they form. One notable feature of Fig 15.24 is that polyester and epoxy matrices are given the same values. This might be true for the matrix itself, but put into a composite laminate the epoxy/glass laminate can have much better mechanical properties than the polyester/glass variety. The main reason for this is that epoxy adheres (‘glues’) much better to the fibres than the polyester does, and has

**Fig 15.24** Mechanical properties of fibres and matrices

Properties		E Glass	Aramid	Carbon HS	Polyester Epoxy
Specific gravity $\rho_f$ or $\rho_m$	$t/m^3$	2.56	1.44	1.78	1.20
E-modulus $E_{f1}, E_{f2}$ or $E_m$	$E_{f1} N/mm^2$ $E_{f2} N/mm^2$	73000	124000	235000	3300
G-modulus $G_f$ or $G_m$	$N/mm^2$	30000	2800	50000	1222
Poisson's rto $\nu_f$ or $\nu_m$	1	0.22	0.36	0.27	0.32

$\rho_f$  = spec.grav. of fibre       $G_f$  = Shear mod. of fibre  
 $\rho_m$  = spec.grav. of matrix       $G_m$  = Shear mod. of matrix  
 $E_{f1}$  = E-mod. along fibres       $\nu_f$  = Poisson's rto of fibre  
 $E_{f2}$  = E-mod. across fibres       $\nu_m$  = Poisson's rto of matrix  
 $E_m$  = E-mod. matrix

**Fig 15.25** Composite properties

Values of thickness for composite $\rho_c$ density depending on fibre content by volume or mass	
27a) $t = \frac{w}{\Phi \cdot \rho_f}$	27b) $t = \frac{w}{\rho_f \cdot \rho_m} \cdot \left[ \frac{\rho_f}{\psi} + \rho_m - \rho_f \right]$
Fibre content by volume or mass	
28a) $\Phi = \frac{\omega}{\psi + (1-\psi) \cdot (\rho_f / \rho_m)}$	28b) $\psi = \frac{\Phi \cdot \rho_f}{\Phi \cdot \rho_f + (1-\Phi) \cdot \rho_m}$
Composite density according to fibre content	
29a) $\rho_c = \rho_f \cdot \Phi + \rho_m \cdot (1-\Phi)$	29b) $\rho_c = \frac{\rho_f \cdot \rho_m}{\rho_f + \psi \cdot (\rho_f - \rho_m)}$
$t$ = Thickness of the laminate (mm) $w$ = Dry mass of fibre (kg/m <sup>2</sup> ) $\Phi$ = Fibre content by volume (fibre volume/laminate vol.) $\psi$ = Fibre content by mass (fibre mass/laminate mass) $\rho_f$ = Density of fibre (kg/m <sup>3</sup> ) $\rho_m$ = Density of matrix (kg/m <sup>3</sup> ) $\rho_c$ = Density of laminate (kg/m <sup>3</sup> )	

an elongation before break to inhibit microcracking (explained in Fig 14.8). The only polyester matrix that can come near to the epoxy's performance is vinyl-ester.

Fig 15.25 give the formulae to calculate the thickness, fibre content and specific density of the total composite laminate. To be able to calculate the scantlings we need a method to determine the mechanical properties for different laminates.

In Fig 15.26 theoretical equations are given for unidirectional and other fibre configurations. Except for E-glass chopped strand mat, the formulae apply to any FRP fibre (glass, carbon aramid, etc.) The values for UD laminates (equations 30–33) give the input for other laminate types (equations 34–41).

Fig 15.27 gives the breaking strains in % (ultimate strength/initial E modulus) for different fibres (E-glass and carbon HS) and configurations. Braking strains ( $\epsilon$ ) together with E modulus is the definition of a material's ultimate strength since  $s = \epsilon \times E$ . Other

*Theoretical formulae for UD in laminates of Fig14.27 & 14.28*

30a) $E_{UD1} = 0.975 \cdot [E_f \cdot \Phi + E_m(1 - \Phi)]$	30b) $E_{UD2} = E_m(1 + \eta_E \cdot \Phi) / (1 - \eta_E \cdot \Phi)$ $\eta_E = E_{f2} / (E_m - 1) / (E_{f2} / E_m + 1)$
31) $G_{UD12} = G_m(1 + \eta_G \cdot \Phi) / (1 - \eta_G \cdot \Phi)$	$\eta_G = (G_f / G_m - 1) / (G_f / G_m + 1)$
32) $T_{U/L} = 22.5 - (33 \cdot \Phi) / (\Phi + 0.89)$	
33a) $\nu_{UD12} = \nu \cdot \Phi + \nu_m(1 - \Phi)$	33b) $\nu_{UD21} = \nu_{UD12} \cdot (E_{UD1} / E_{UD2})$

*Theoretical formulae for CSM in laminates of Fig14.27 & 14.28*

34) $E_{CSM} = 3/8(E_{UD1} + 5/8 \cdot E_{UD2})$	35) $G_{CSM} = 1/8 \cdot E_{UD1} + 1/4 \cdot E_{UD2}$
36) $\nu_{CSM} = E_{CSM} / (2G_{CSM})$	

*Theoretical formulae for BD+ in laminates of Fig14.27 & 14.28*

37) $E_{BD+} = 0.5(E_{UD1} + E_{UD2})$	38) $G_{BD+} = G_{UD12}$
39) $\nu_{BD+} = \nu_{UD12} \cdot (E_{UD2} / E_{BD+})$	

*Theoretical formulae for DBx in laminates of Fig14.27 & 14.28*

40) $E_{DBx} = 4E_{BD+} / [(E_{BD+} / G_{BD+}) + 2(1 - \nu_{BD+})]$	41) $G_{DBx} = E_{BD+} / [2(1 + \nu_{BD+})]$
42) $\nu_{DBx} = E_{DBx} / (4E_{BD+}) \cdot [(E_{BD+} / G_{BD+}) - 2(1 - \nu_{BD+})]$	

*Theoretical formulae for Qx in laminates of Fig14.27 & 14.28*

43) $E_{Qx} = 0.5(A_{11} - A_{12}^2 / A_{11})$	44) $G_{Qx} = 0.5 / (G_{BD+} + G_{DBx})$	45) $\nu_{Qx} = A_{11} / A_{12}$
$A_{11} = E_{BD+} / (1 - \nu_{BD+}^2) + E_{DBx} / (1 - \nu_{DBx}^2)$		
$A_{12} = (E_{BD+} \cdot \nu_{BD+}) / (1 - \nu_{BD+}^2) + (E_{DBx} \cdot \nu_{DBx}) / (1 - \nu_{DBx}^2)$		

$E$  = Young's modulus  
 $G$  = Shear modulus  
 $\nu$  = Poisson's ratio  
UD = Unidirectional (basically only 0-direction)  
CSM = Chopped strand mat, E-glass  
BD+ = Biaxial (0/90), or woven Roving  
DBx = Double bias (+/-45)  
Qx = Quadriaxial (0/+45/-45/90)  
 $E$ ,  $G$  &  $\nu$  = see Fig 15.24

**Fig 15.26** Laminate mechanical properties

*Breaking strains (ultimate strength/E modulus) in %*

Type of fibre and resin	E-glass/polester	CarbonHS/epoxy
Unidirectional, UD	$\epsilon_{ut1}$ 1.90	1.00
	$\epsilon_{ut2}$ 0.50	0.50
	$\epsilon_{uc1}$ 1.40	0.70
	$\epsilon_{uc2}$ 1.40	1.90
	$\epsilon_{uf1}$ 2.02	1.21
	$\epsilon_{uf2}$ 0.92	1.16
	$\gamma_{u12}$ 1.70	1.50
Chopped mat, CSM	$\epsilon_{ut}$ 1.35	Not applicable
	$\epsilon_{uc}$ 1.70	
	$\epsilon_{uf}$ 1.88	
	$\gamma_u$ 2.00	
WR/0/90, BD+	$\epsilon_{ut}$ 1.55	1.00
	$\epsilon_{uc}$ 1.40	0.70
	$\epsilon_{uf}$ 1.84	1.21
	$\gamma_u$ 1.70	1.40
Double bias, DBx	$\epsilon_{ut}$ 1.06	0.77
	$\epsilon_{uc}$ 1.02	0.75
	$\epsilon_{uf}$ 1.30	1.12
	$\gamma_u$ 1.80	1.02
Quadriaxial, Qx	$\epsilon_{ut}$ 1.06	0.92
	$\epsilon_{uc}$ 1.02	0.74
	$\epsilon_{uf}$ 1.30	1.21
	$\gamma_u$ 1.80	1.02

**Fig 15.27** Breaking strain as percentage

types of glass or carbon, aramid, boron, etc., or other resins, may be used provided documented values are used.

Some guidance values for fibre content and composite density are given in Fig 15.28 (overleaf) (i.e. fibre content by volume, fibre content by mass, thickness/fibre mass and composite density). These values are given as a guide only, but it is the responsibility of the builder to check the values that his building methods are achieving. In other words: test. If better values are obtained then the better ones may be used. The starting point is the fibre content by volume which is the same irrespective of fibre material and measured as a ratio (fibre volume/matrix volume). The fibre content by mass, on the other hand, is heavily dependent on the specific density of the fibre material, which is obvious when comparing the values of E-glass versus carbon HS. For hand layup complex surfaces, the fibre content in volume is 80% of the ones for simple surfaces. Boat hulls are mostly of simple surfaces, where decks and cockpits are mostly of complex surfaces, which make them heavier per area unit. Utilizing infusion techniques raise the fibre content considerably compared to hand layup methods. In the complex surface case, the fibre content ratio can be doubled.

The final calculations of E, G and  $s_u$  or  $t_u$  follow the following relations:

1.  $s_u = E \text{ (Fig 15.26)} \times \varepsilon \text{ (Fig 15.27)}$ .
2.  $t_u = G \text{ (Fig 15.26)} \times g \text{ (Fig 15.27)}$ .

The design stress shall then be determined using Fig 15.21, with the relevant value of  $k_{AM}$  and  $k_{BB}$  from Fig 15.17 and Fig 15.18. The materials used in the building of the YD-41 are E-glass in CSM- and 0/90 Roving format, in ratios 20% and 80%, respectively, infused with vinyl-ester. To facilitate the computations the material properties are given in Fig 15.29, the underlined values. For other E-glass compositions, the equations from Figs 15.24–15.28 may be used. In the ISO standard, Annex C, these calculations have been performed for E-glass variations as well as for carbon fibre laminates.

## ■ SINGLE SKIN PANEL CALCULATION

Fig 15.29 (page 332) gives the formula that calculates the required thickness for a single skin panel. Equation 45 is the strength requirement and gives a thickness requirement in mm. This thickness shall be transformed to the mass of dry fibre reinforcement  $w_f$  (kg/m<sup>2</sup>) using the fibre content in volume or mass according to Fig 15.25 or 15.28. The calculated thickness shall not be less than stipulated by equation 46.

The design stress  $s_d$  is defined in Fig 15.21, aspect ratio factor  $k_{2b}$  from Fig 15.19 and curvature factor  $k_c$  from Fig 15.20. The resulting thickness  $t_p$  of the laminate shall be transformed into  $w_p$ , the mass of dry fibre, according to Fig 15.25 or Fig 15.28.

The minimum single skin thickness according to Fig 15.29 gives 5 mm as the result, but this does not apply to the YD-41 since the hull panels are of sandwich construction, except for the reinforced ballast keel area (Area K in Fig 15.13). Fig 15.30 shows the result for YD-41 regarding this reinforced keel area, a panel weight 22 kg/m<sup>2</sup>, corresponding to a thickness of 22 mm. This is the structural part of the laminate. In addition to this,



we have the gelcoat and surface layer of 300 g/m<sup>2</sup> CSM, so the total thickness will be roughly 23 mm. The total panel weight will be 40.3 kg/m<sup>2</sup> with an average fibre mass content of 55%. The pressure used is 1.8 times the calculated pressure for the bottom area, as stipulated in Fig 15.13 for keel reinforced area, K.

Fibre content in volume and mass, t/w and composite density

Build process	Material	Fibre content $\Phi$	E-glass/polester			CarbonHS/epoxy		
			$\psi$	t/w	$\rho_c$	$\psi$	t/w	$\rho_c$
Hand layup simple surface	CSM	0.167	0.300	2.340	1.430	—	—	—
	Woven Roving	0.300	0.478	1.302	1.610	0.389	1.870	1.370
	Rovimat	0.246	0.410	1.588	1.530	—	—	—
	Multidirection	0.319	0.500	1.255	1.630	0.410	1.760	1.390
	Unidirectional	0.364	0.550	1.073	1.700	0.459	1.540	1.410
Hand layup complex surface	CSM	0.134	0.248	2.924	1.380	—	—	—
	Woven Roving	0.240	0.403	1.628	1.530	0.319	2.340	1.340
	Rovimat	0.197	0.343	1.985	1.470	0.267	2.850	1.310
	Multidirection	0.255	0.422	1.531	1.550	0.337	2.200	1.350
	Unidirectional	0.291	0.467	1.341	1.600	0.378	1.930	1.370
Infusion	CSM	0.21—	0.36—	1.30—	1.49—	—	—	—
		0.30	0.48	1.860	1.61			
	Woven Roving	0.42—	0.61—	0.78—	1.77—	0.52—	1.12—	1.44—
		0.50	0.68	0.93	1.88	0.60	1.34	1.49
	Multidirection	0.45—	0.64—	0.87—	1.81—	0.54—	1.06—	1.46—
Prepreg	Unidirectional	0.53	0.71	0.96	1.92	0.63	1.25	1.61
	Multidir/Unid	0.53	0.706	0.737	1.92	0.626	1.06	1.51

Fig 15.28 Fibre content, t/w and density values

Thickness of hull, deck and bulkhead plating to be :

$$45) \quad t_p = b \cdot k_c \cdot \sqrt{\frac{P \cdot k_{2b}}{1000 \cdot \sigma_d}} \quad [\text{mm}]$$

$P$  = the reference pressure, given in Figs 15.11 and 15.12

$b$  = the short side of the panel, in mm, given in Fig 15.5

$k_{2b}$  = the aspect ratio factor, given in Fig 15.19

$\sigma_d$  = minimum allowable design stress, in N/mm<sup>2</sup>,  $0.5 \cdot \sigma_{uf} \cdot k_{BB} \cdot k_{AM}$

Minimum thickness for GRP single skin plating

$$46a) \quad t_{min} = k_5 \cdot k_6 \cdot (1.5 + k_7 \cdot V + k_8 \cdot m_{LDC}^{0.33}) \cdot k_9 \quad [\text{mm}]$$

$$46b) \quad w_{min} = 0.43 \cdot t_{min} \quad [\text{kg/m}^2]$$

$V$  = Speed in knots,

for sailing craft it shall be taken not less than  $2.36 \cdot (L_{WL}^{0.5})$

$k_5$	$\frac{\text{Glass CSM mass} + 0.9 \cdot \text{cont. glass fibre mass} + 0.7 \cdot \text{carbon/aramid mass}}{\text{Total fibre mass}}$	
$k_6$	Value of $k_6$ according to longitudinal position:	
	Front of $0.6 L_{WL}$	1.0
	aft of $0.6 L_{WL}$ adjusted for $k_{dyn}=4.5$ as per Fig 15.16, default Deck and cockpit	0.8
$k_9$	Value of $k_6$ according to vertical position:	
	Bottom	1.0
	Side and transom Deck and cockpit	0.75
$k_7 = 0.03$		$k_8 = 0.15$

Masses of fibres for glass, aramid, carbon etc. to be in kg/m<sup>2</sup>

Fig 15.29 Single skin panel calculation



**Fig 15.30** YD\_41 single skin keel plate

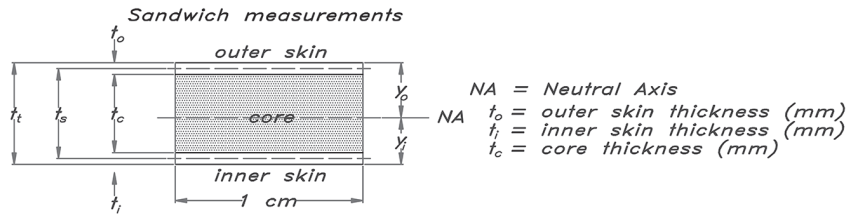
Bottom Plating (Increased keel area Fig 15.13)				Main formula for thickness:	
AREA # =	K1	k <sub>dc</sub> =	1	$t_p = b * k_c * (P * k_{2b} / (1000 * \sigma_d)^{0.5})$	Fig 15.29
LWL(m) =	12.28	k <sub>DYN</sub> =	3	Additional input:	
X(m) =	7.45	T <sub>C</sub> =	0.43	k <sub>2b</sub> =	0.44 Fig 15.19
m <sub>LDC</sub> (kg) =	7400	k <sub>L</sub> =	1.00	k <sub>c</sub> =	1.00 Fig 15.20
GZ <sub>MAX60</sub> (m) =	1.2	k <sub>AR</sub> =	0.34	$\sigma_d$ = (Pa)	255 Fig 15.21
Long Side, l(mm) =	900	k <sub>R</sub> =	1.35	M <sub>db</sub> = (Nmm/mm)	-0.93 Fig 15.22
Short Side, b(mm) =	500	k <sub>SLS</sub> =	1.491	E <sub>CSM</sub> +E <sub>DB</sub> =	30792 Fig 15.26
m <sub>LDC</sub> /5*LWL^3 =	4.00	AD =	0.450	$\epsilon_{uf}$ = (%)	1.84 Fig 15.27
P <sub>BSMIN</sub> (kPa) =	13.8	P <sub>BSBASE</sub> =	83.2	Thickness (mm) t <sub>p</sub> =	22.1 Fig 15.29
<b>P = 50.8</b> (kPa) keel area				<b>Fibre (kg/m2) W<sub>f</sub> =</b>	<b>22.2</b> Fig 15.28

## SANDWICH

In Fig 15.31 (overleaf) formulae needed to define sandwich panels to be calculated are shown. Fig 15.32 (page 335) gives the relevant equations given by the ISO standard to determine the dimensions for the skins and the core of a sandwich panel. This section applies to sandwich panels where outer and inner skins are similar in lay-up, strength and elastic properties. The laminates are considered similar when the ratio of their mechanical properties is within 25% of each other. The sandwich is also to be reasonably balanced (i.e. the inner skin shall not be less than 70% of the outer skin). Fig 15.33 (SM) and Fig 15.34 (I) give values for symmetrical sandwich panels (page 336).

Equations 47 and 48 are strength requirements and give the required section modulus for a 1 cm wide strip of the panel, to the outer skin and the inner skin, respectively calculated from the neutral axis, which is in the middle of the section if outer and inner skins are equal. If not, the neutral axis may be computed with the method described in Fig 13.5. When determining the outer skin, the tensile strength of the laminate is to be used, and for the inner skin, the compressive strength is to be used. This might seem a bit odd when looking at it at first, since a panel is flexing inwards when loaded by the sea, and consequently the inside is put under tension. The reason the ISO standard (and classification societies) takes an approach the other way around is that it considers the panels to be fixed at their edges, i.e. over the stiffeners or bulkheads defining them (the edges). Then we have a situation where the bending moments are greatest at the edges and with their signs inverted compared to the moments in the middle of the panel field. This is a simplification since in real life it can be debated whether the edges are fixed or not, the stiffeners and bulkheads bend or not, or if the whole yacht is flexing. Solving all this is not possible by simple panel/beam theory, but instead, we can do it by finite element analysis, which is far beyond the scope of this book. Anyway, the simplified approach has proven to give adequate results over the years, so obviously, the simplifications work.

The first thing to do when determining the sandwich scantlings is to define the panel dimensions and material properties. By using equations 47 and 48 (see Fig 15.32) we get the section modulus requirements. Equation 49 gives the minimum buckling strength requirement for the skin in compression, the inner one over the supports. If this value comes out less than the design compressive strength, the build of the panel has to be



**Fig 15.31** Sandwich formulae

**General formulae**

$t_t = t_o + t_o + t_i$	mm	total thickness of sandwich
$t_s = t_c + (t_o + t_i) / 2$	mm	distance between centroids of skins
$y_o = t_i \cdot t_s / (t_i + t_o) + t_o / 2$	mm	distance outside of NA
$y_i = t_o \cdot t_s / (t_i + t_o) + t_i / 2$	mm	distance inside from NA
$I = \frac{t_o \cdot t_i \cdot t_s^2}{t_o + t_i} + \frac{t_o^3 + t_i^3}{12} 10^{-3}$	cm <sup>4</sup> /cm	section modulus of outer skin
$SM_o = 10 \cdot I / y_o$	cm <sup>3</sup> /cm	section modulus of outer skin
$SM_i = 10 \cdot I / y_i$	cm <sup>3</sup> /cm	section modulus of inner skin
Only valid if skins of same material and $t_i \geq 0.7 \cdot t_o$		
$I = \frac{t_o \cdot t_i \cdot t_s^2}{t_o + t_i} \cdot 10^{-3}$	cm <sup>4</sup> /cm	second moment of inertia
$SM_o = t_c \cdot t_o / 100$	cm <sup>3</sup> /cm	section modulus of outer skin
$SM_i = t_c \cdot t_i / 100$	cm <sup>3</sup> /cm	section modulus of inner skin
Symmetric sandwich where $t = t_o = t_i$		
$I = t \cdot t_s^2 / 2000$	cm <sup>4</sup> /cm	second moment of inertia
$SM = t_c \cdot t / 100$	cm <sup>3</sup> /cm	section modulus

changed or the lesser value must be used. The final checks of the skins are that they are not lighter than the required minimum, shown in equations 50 and 51, and that the required bending stresses of the skins are less or equal to the achieved bending stresses, shown in equations 52 and 53.

Then we check that the core stands up to what is expected from it. From the equations 54 and 55, we calculate the required thickness and shear strength for the core. Ultimate mechanical properties for different core materials are given in Fig 15.35, and design values may be calculated from Fig 15.21.

Figs 15.33 and 15.34 show how the section modulus and moment of inertia vary with core and skin thicknesses for different sandwich laminates. They are valid only for panels with inner and outer skins being equal. With dissimilar material, Fig 15.32 gives equations, 52 and 53, to calculate minimum design stress in compression (inner skin) and tension (outer skin). The bending moment  $M_{db}$  is calculated from Fig 15.22. If the required stress levels are not obtained with the laminate used, SM has to be increased, i.e. more material must be used (thicker skins).

An example of a sandwich panel calculation is given in Fig 15.36, a side panel on YD-41, panel C1 in Fig 15.13. This is a panel receiving a lot of slamming when going

The section modulus of the skins about the neutral axis of a strip of sandwich panel 1 cm wide are to be not less than given by the following formulae :

$$47) SM_o \Rightarrow \frac{b^2 \cdot k_c^2 \cdot P \cdot k_{2b}}{6 \cdot 10^5 \cdot \sigma_{do}} \quad [\text{cm}^3/\text{cm}]$$

$$48) SM_i \Rightarrow \frac{b^2 \cdot k_c^2 \cdot P \cdot k_{2b}}{6 \cdot 10^5 \cdot \sigma_{di}} \quad [\text{cm}^3/\text{cm}]$$

$SM_o$  = required section modulus to outer skin from the neutral axis

$SM_i$  = required section modulus to inner skin from the neutral axis

$P$  = reference pressure for the location in question [ $\text{kN/m}^2$ ]

$b$  = short edge of panel, Fig 15.10

$k_c$  = correction factor for curvature, Fig 15.20

$\sigma_{do}$  = design stress of outer skin, Fig 15.21

$\sigma_{di}$  = design stress of inner skin, Fig 15.21

$k_{2b}$  = panel aspect ratio coefficient, Fig 15.19

Sandwich minimum skin fibre mass:

$$50) w_{os} = 0.6 \cdot w_{min} \text{ as in Fig 15.29}$$

$$51) w_{is} = 0.7 \cdot w_{os}$$

$w_{os}$  = fibre mass of outer skin, [ $\text{kg/m}^2$ ]

$w_{is}$  = fibre mass of inner skin, [ $\text{kg/m}^2$ ]

$w_{min}$  = fibre mass of single skin, [ $\text{kg/m}^2$ ] from eq. 46 in Fig 15.29

Bending stress requirements for sandwich skins

Location	Required Bending Stress ( $\text{N/mm}^2$ )
Outer skin	52) $\sigma_{to} = M_{db} / SM_o \leq \sigma_{do}$
Inner skin	53) $\sigma_{ci} = M_{db} / SM_i \leq \sigma_{di}$

$\sigma_{to}$  = required tension stress according to Fig 15.22

$\sigma_{do}$  = achieved tension stress according to Fig 15.21

$\sigma_{ci}$  = required compressive stress according to Fig 15.22

$\sigma_{di}$  = achieved compressive stress according to Fig 15.21

Inner skin buckling check,  $\sigma_{dci}$ :

$$49) \sigma_{dci} \leq 0.3 \sqrt{E_{ci} \cdot E_{cc} \cdot G_{cc} \cdot (k_{BB} \cdot k_{AM})} \quad [\text{N/mm}^2]$$

is not to be less than  $0.5 \cdot \sigma_u \cdot (k_{BB} \cdot k_{AM})$

$E_{ci}$  = compressive modulus of skin [ $\text{N/mm}^2$ ]

$E_{cc}$  = compressive modulus of core [ $\text{kPa}$ ]

$G_{cc}$  = shear modulus of core [ $\text{kPa}$ ]

$k_{BB}$  = build quality factor, Fig 15.17

$k_{AM}$  = assessment factor, Fig 15.18

The effective thickness,  $t_s$  of the core and skins are to be not less than given by formulae 54:

$$54) t_s = \frac{k_{SHb} \cdot k_c \cdot b \cdot P}{1000 \cdot \tau_d} \Rightarrow F_d / \tau_d \quad [\text{mm}]$$

$k_{SHb}$  = aspect ratio factor, Fig 15.19

$t_s$  = significant thickness, Fig 15.31

$k_c$  = curvature ratio factor, Fig 15.19

$k_{SHb}$  = aspect ratio factor, Fig 15.19

$\tau_d$  = design stress, in  $\text{N/mm}^2$ , according to Fig 15.21

Ultimate strength of the core material, given by manufacturer, or Fig 15.36

Min core shear stress,

$$55) \tau_{dco} = \min[\max(0.07 L_{WL} - 0.12); 0.3]; 0.58]$$

Min core compressive stress for bottom,  $\sigma_{dco}$

$$56) \sigma_{dco} \geq 0.008 \cdot P_{dco}$$

$\sigma_{dco}$  = design compressive strength, Fig 15.21 with  $\sigma_u$  and other core data from Fig 15.35. Applies for bottom plating, for side plating 70% is requested.

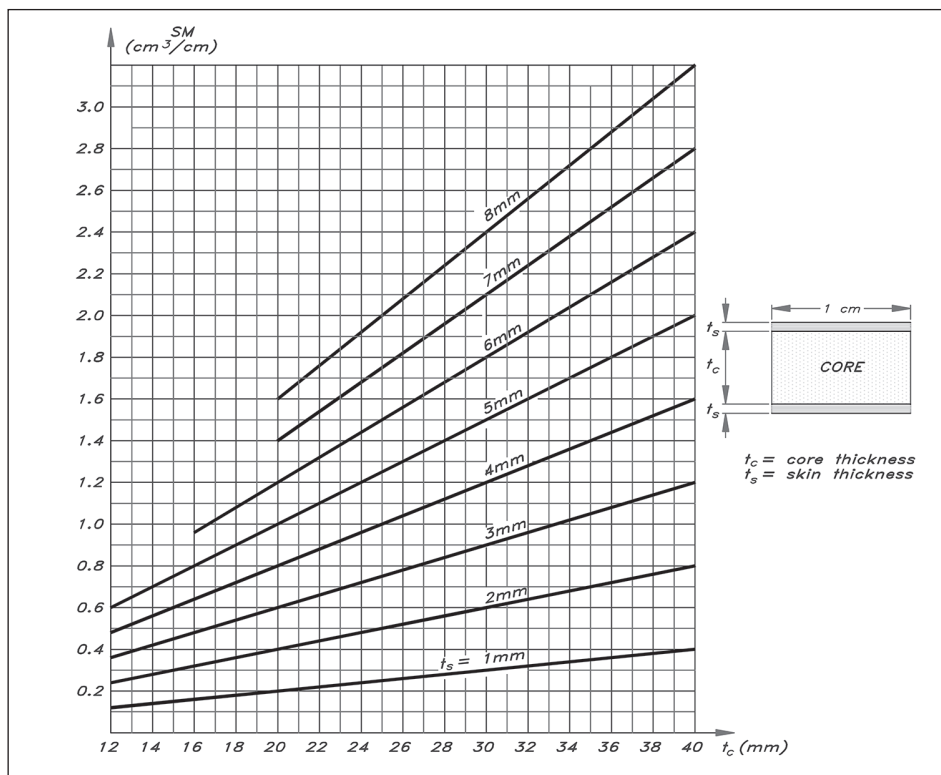
**Fig 15.32** Sandwich construction

upwind in a seaway. From spending some time there in the forecastle, it is quite obvious, especially in single laminate hulls, how the sides may deflect quite a lot when crashing into the waves. As can be seen from the results, it is the shear strength of the core that has the lowest compliance factor (1.15) and thus is the most likely failure reason if the panel gets overloaded.

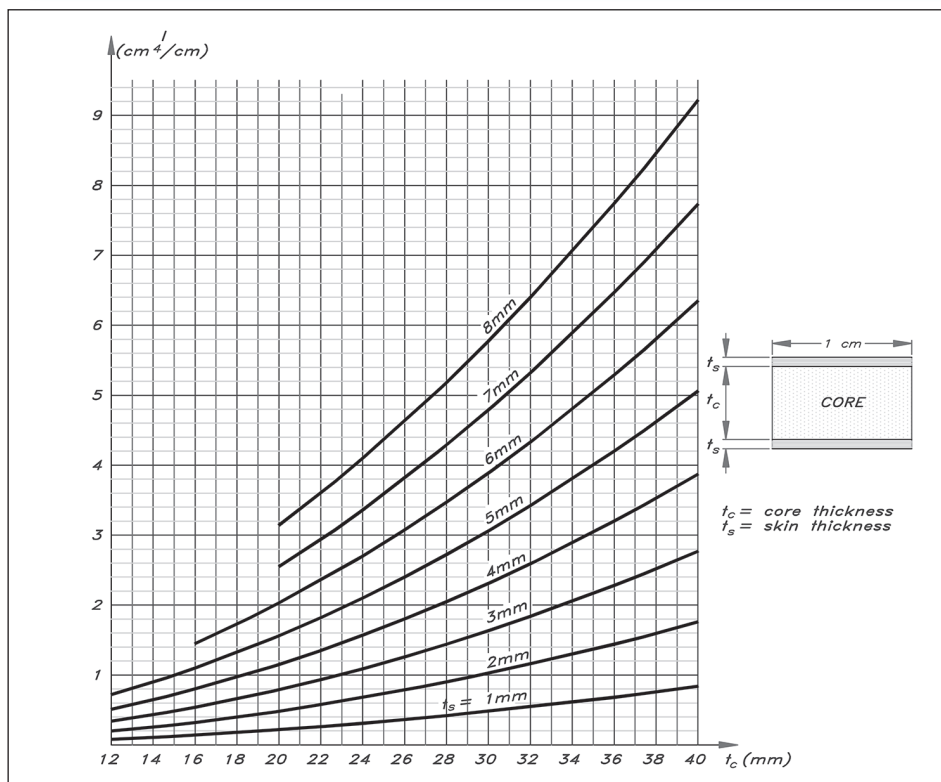
## STIFFENER DESIGN FORCES AND MOMENTS

Stiffeners are required to be such that loads are effectively transferred from secondary to primary, then to shell and bulkheads (see Fig 15.5). The shear forces and bending moments in stiffeners due to pressure loads are given in Fig 15.37, equations 57 and 58 (page 339). The shear and moment factors,  $k_{SF}$  and  $k_{BM}$ , given in Fig 15.37 are only valid for stiffeners with fully fixed ends, FF (see Fig 15.5 and Fig 15.14). For simply

**Fig 15.33** Section modulus for symmetric sandwich panels



**Fig 15.34** Moment of inertia for sandwich panels



supported ends, SS, and one end fully and the other simply supported, FS, the following relations may be used:

		Pt1	0.5	Pt2
SS:	$k_{BM}$	0.0625	0.125	0.0625
	$k_{SF}$	0.50	+0.25/-0.25	-0.50
FS:	$k_{BM}$	-0.125	0.07	0.0
	$k_{SF}$	0.625	0.312/-0.185	-0.5

## ■ STIFFENER CURVATURE FACTOR $K_{CS}$

Stiffeners are normally curved in one direction, the  $l_u$  direction. Fig 15.37 gives the formulae for the curvature factor,  $k_{CS}$ , in equation 59. It is derived from equation 26 in Fig 15.20 for  $C_t/b = 0.03$ . Values of  $C_t/l_u$  between the tabulated ones may be interpolated.

## ■ STRESSES IN STIFFENERS $\tau$ AND $\delta_{CRIT}$

The shear and tensile/compressive stresses in a stiffener given in Fig 15.39 are valid for materials as used in the simplified assessment method. In equations 60 and 61, covering requirements on shear stress,  $F_d$  is the shear force in equation 60 for stiffeners attached to plating, and equation 61 for stiffeners not attached to plating, in Fig 15.39 (page 340). The design values for shear and stresses can be found in Fig 15.21.

Equations 62 and 63 relate to bending stress and section modulus of the stiffener.  $\delta_{CRIT}$  relates to  $\delta_d$ , so parts subjected to compression (i.e. top flange of stiffener over a support) and parts subjected to tension (i.e. bottom flange (usually) the plating) governs the  $\delta_{CRIT}$ . When calculating  $I_{NA}$  consideration of the plating's effective attached breadth must be taken.

## ■ EFFECTIVE WIDTH OF ATTACHED PLATING $B_E$

Fig 15.39 shows the details of a top-hat stiffener, the most common type in FRP construction.

The ISO standard also covers metal construction where the sections mostly are of T-, L- or flat-bar type, but we will only describe the top-hat type that is used in the YD-41. Equation 64 gives the formula for the effective width,  $b_e$ , in mm. The values of  $s$  and  $l_u$  are taken from the actual stiffener we are calculating, and the E- and G-values are taken from Fig 15.26. A typical value for E/G for a GRP laminate is 3.3 which we will use in the example calculation of a YD-41 stiffener. The effective width may be applied to inner and outer skins and any padding or bonding angle that lies within this width. For stiffeners along with an opening, the effective width shall be 50% of the calculated width in Fig 15.41 (page 342). The effective width  $b_e$  is not to be taken more than  $s$ , the stiffener spacing.

# Conservative core properties

Core Type	Elong. break (%)	Density $\rho_c$ (kg/m <sup>3</sup> )	Shear Strength $\tau_u$ (N/mm <sup>2</sup> )	Shear Modulus $G_c$ (N/mm <sup>2</sup> )
Balsa, endgrain	n.a.	90–220	$0.0178 \cdot \rho_c - 0.34$	$0.868 \cdot \rho_c - 1.43$
Cross-linked PVC I	40	50–250	$0.0024 \cdot \rho_c^{1.334}$	$0.1633 \cdot \rho_c^{1.136}$
Cross-linked PVC II	12–30	45–80	$0.017 \cdot \rho_c - 0.29$	$0.33 \cdot \rho_c - 1$
Linear PVC	55	50–140	$0.014 \cdot \rho_c - 0.33$	$0.29 \cdot \rho_c - 5.3$
SAN A	40	60–210	$0.017 \rho_c - 210 \cdot \rho_c^2 - 0.613$	$0.46 \cdot \rho_c - 20$
Core Type	Elong. break (%)	Density $\rho_c$ (kg/m <sup>3</sup> )	Compressive Strength $\sigma_{uc}$ (N/mm <sup>2</sup> )	Compressive Modulus $E_{co}$ (N/mm <sup>2</sup> )
Balsa, endgrain	n.a.	90–220	$0.102 \cdot \rho_c - 5$	$30.7 \cdot \rho_c - 1350$
Cross-linked PVC I	40	50–250	$0.0014 \cdot \rho_c^{1.487}$	$0.1138 \cdot \rho_c^{1.449}$
Cross-linked PVC II	12–30	45–80	$0.025 \cdot \rho_c - 0.69$	$1.2 \cdot \rho_c - 18$
Linear PVC	55	50–140	$0.012 \cdot \rho_c - 0.24$	$0.84 \cdot \rho_c - 19$
SAN A	40	60–210	$6.7 \cdot 10^{-4} \cdot \rho_c^{1.59}$	$0.024 \cdot \rho_c^{1.75}$

PVC = Polyvinylchloride foam

SAN = Styrene Acrylic Nitrate foam

PVC I cores to be used in hull shell and load carrying areas,

PVC II in other areas.

## Typical cross-linked PVC core properties

Property		H45	H60	H80	H100	H130	H160	H200	H250
$\sigma_c$	Nominal	0.60	0.90	1.40	2.00	3.00	3.40	5.40	7.20
	Minimum	0.50	0.70	1.15	1.65	2.40	2.80	4.50	6.10
$E_c$	Nominal	50	70	90	135	170	200	310	400
	Minimum	45	60	80	115	145	175	265	450
$\sigma_t$	Nominal	1.40	1.80	2.50	3.50	4.80	5.40	7.10	9.20
	Minimum	1.10	1.50	2.20	2.50	3.50	4.00	6.30	8.00
$E_t$	Nominal	55	75	95	130	175	205	250	320
	Minimum	45	57	85	105	135	160	210	260
$\tau$	Nominal	0.56	0.76	1.15	1.60	2.20	2.60	3.50	4.50
	Minimum	0.46	0.63	0.95	1.40	1.90	2.20	3.20	3.90
$G$	Nominal	12	20	27	35	50	60	73	97
	Minimum	48	16	23	28	40	50	65	81
$\epsilon$	Nominal	12	20	30	40	40	40	45	45
	Minimum	48	60	80	100	130	160	200	250

$\sigma_c$  = Compressive Strength MPa

$E_c$  = Compressive Modulus MPa

$\sigma_t$  = Tensile Strength MPa

$E_t$  = Tensile Modulus MPa

$\tau$  = Shear Strength MPa

$G$  = Shear Modulus MPa

$\epsilon$  = Shear Strain %

$\rho$  = Density kg/m<sup>3</sup>

Fig 15.35 Typical core properties

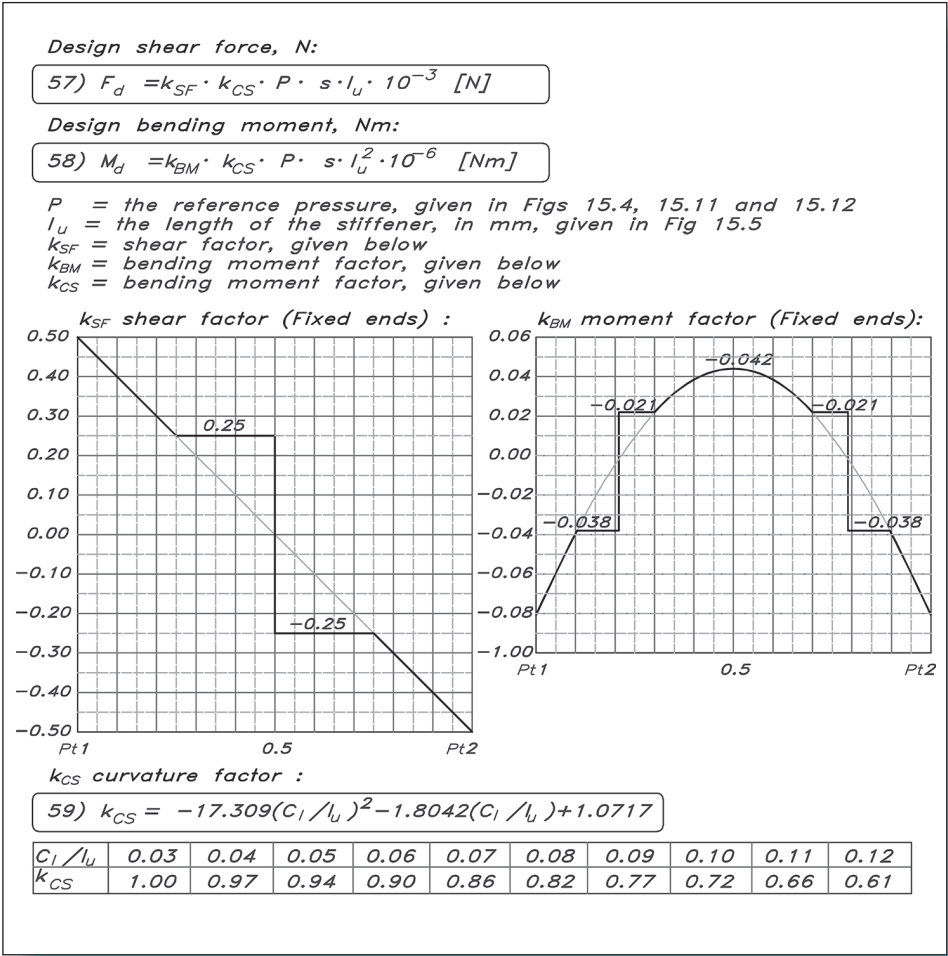
Fig 15.36 (BELOW) YD-41 side sandwich panel

VARIABLE	VALUE	VARIABLE	VALUE	VARIABLE	VALUE
P Kpa (15.16)=	33.1	k2b (15.19)=	0.50	Eci N/mm2 (15.29)=	12708 actual
b mm (15.13)=	480	kShb (15.19)=	0.52	Ecc N/mm2 (15.36)=	90 actual
l mm (15.13)=	2100	k2l (15.19)=	0.50	Gcc N/mm2 (15.36)=	27 actual
ARE (15.19)=	4.4	kShl (15.19)=	0.46	$\tau_u$ N/mm2 (15.36)=	61 actual
to mm (15.32)=	2.2	kc (15.20)=	1.000	$\tau_{ucco}$ N/mm2(15.36)=	1.00 required
ti mm (15.32)=	1.8	kBB (15.17)=	0.800	$\tau_{ucco}$ N/mm2(15.33)=	1.15 actual
tc mm (15.32)=	15	kAM (15.18)=	0.900	$\sigma_{ucco}$ N/mm2(15.36)=	1.20 required
ts mm (15.32)=	17	$\sigma_{ut}$ N/mm2(15.29)=	270	$\sigma_{ucco}$ N/mm2(15.33)=	1.40 actual
Fdb N/mm (15.22)=	8.3	$\sigma_{dt}$ N/mm2 (15.21)=	97	$\sigma_{dci}$ N/mm2 (15.36)=	67 required
Fdl N/mm (15.22)=	7.3	$\sigma_{uc}$ N/mm2(15.29)=	253	$\sigma_{dci}$ N/mm2 (15.33)=	91 actual
Mdb Nmm/mm(15.22)	636	$\sigma_{dc}$ N/mm2 (15.21)=	91	Wosmin kg/m2(15.36)=	0.82 required
Mdl Nmm/mm(15.22)	636			Wo kg/m2 (15.25)=	0.95 actual
SMo req. cm3/cm (15.33)	0.065	SMo act. cm3/cm(15.32)	0.33	Wismin kg/m2(15.33)=	0.57 required
SMi req cm3/cm (15.33)	0.070	SMi act. cm3/cm(15.32)	0.27	Wi kg/m2 (15.25)=	0.78 actual

Compliance factors: actual/required >1 fulfills requirements.



**Fig 15.37** Forces and moments on stiffeners



**Fig 15.38** (BELOW) Stiffener design stresses

Simplified formulae for shear stress, bending stress and section modulus		
Requirement on shear stress ( $\tau$ )	<div>60) <math>\tau = F_d / (H_s \cdot t) \leq \tau_d</math></div> <div>61) <math>\tau = 1.5 F_d / (H_s \cdot t) \leq \tau_d</math></div>	N/mm <sup>2</sup>
Requirement on bending stress ( $\sigma$ )	<div>62) <math>\sigma_{CRIT} = (M_d \cdot Z_{CRIT}) / I_{NA} \leq \sigma_d</math></div>	N/mm <sup>2</sup>
Section Modulus (SM)	<div>63) <math>SM = I_{NA} / Z_{CRIT}</math></div>	mm <sup>3</sup>
<div><div><math>\tau</math> = required shear stress (N/mm<sup>2</sup>) <math>\tau_d</math> = design shear stress (N/mm<sup>2</sup>) <math>F_d</math> = design shear force (N) <math>H_s</math> = height of stiffener (mm) <math>t</math> = web thickness (mm)</div><div><math>\sigma_{CRIT}</math> = required bending stress (N/mm<sup>2</sup>) <math>\sigma_d</math> = design bending stress (N/mm<sup>2</sup>) <math>M_d</math> = design bending moment (Nmm) <math>Z_{CRIT}</math> = distance to top or bottom (mm) from the Neutral Axis (NA) <math>I_{NA}</math> = cross section moment of inertia (mm<sup>4</sup>) (see Fig 13.5 for composite shapes)</div></div>		



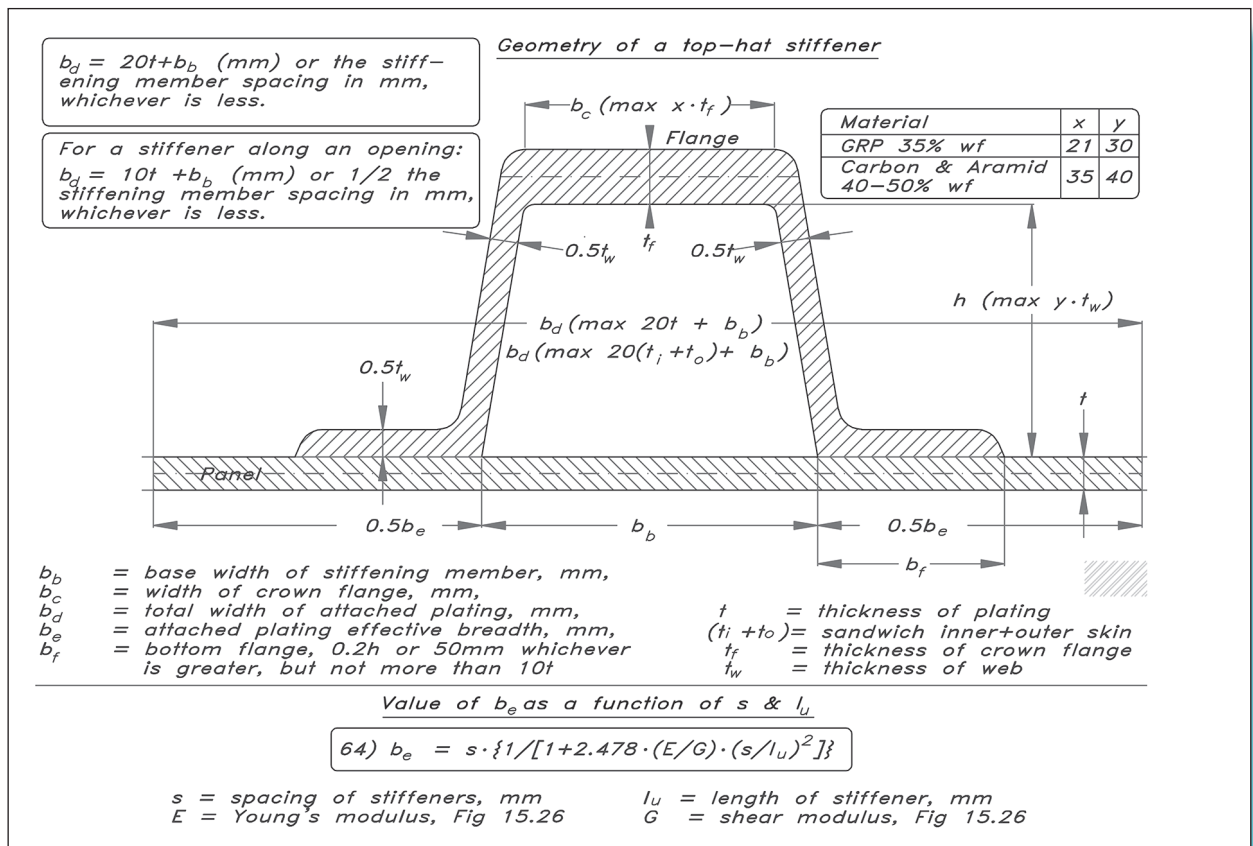


Fig 15.40 shows the geometry relations of stiffeners. The section modulus and moment of inertia diagrams are for simple cross-sections but are convenient to use for preliminary approximations. They can be turned around, combined or extended with an attached plating, keeping in mind to have the X-X axis in the correct direction and position as described in Fig 13.5. The neutral axis for the total of included parts has to be calculated.

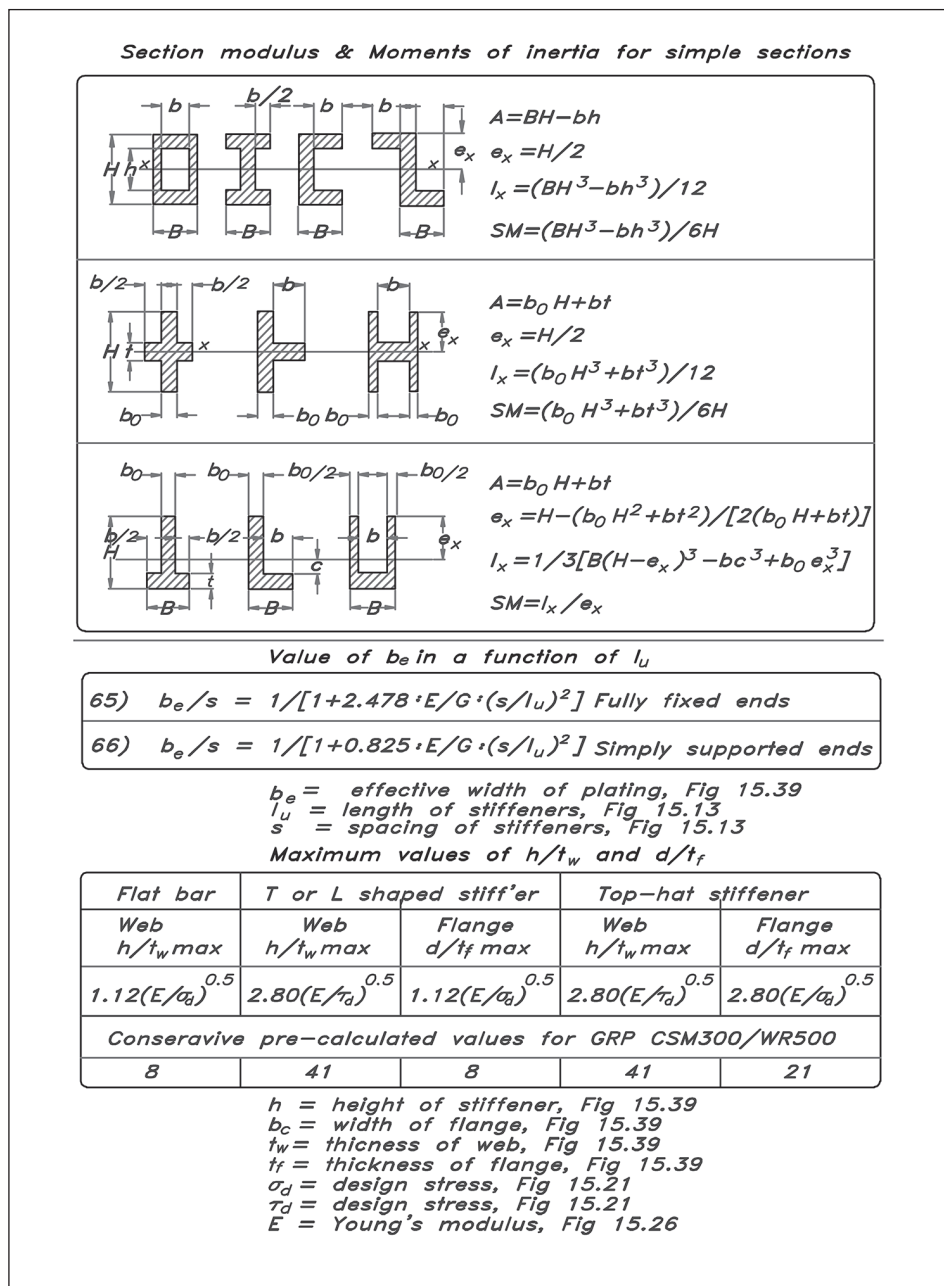
Equations 65 and 66 give the  $b_e/s$  ratio between the width of the attached plating and the actual stiffener spacing, not to be taken <0.1. For top-hat stiffeners, the final attached plating width is  $b_e + b_b$ , see Fig 15.39, but shall not be taken > $s$ . For GRP L-, T- or I-shaped stiffeners  $b_b$  is the thickness of the web.

## STIFFENER CONSTRUCTION

Fig 15.41 shows the requirements of a stiffener, in equations 67 and 68. If the obtained value of SM is less than the required, the most effective way to increase it is to increase the height of the stiffener, if there is space enough, as can be seen from Fig 15.41. The second-best option is to make the stiffening system denser (i.e. making  $l_u$  smaller). The third option is to use better materials to increase the stress resistance.

Fig 15.39 Stiffener details and effective width of plating

**Fig 15.40** Stiffener geometry



Equation 69 gives the requested web area to handle the shear forces. If the acquired area is not sufficient the most effective remedy is to increase the web thickness,  $t_w$ . To make the stiffening system denser, or by using better material, will also make things better.

For stiffeners in the reinforced ballast keel area (K in Fig 15.13) the calculated bottom pressure shall be multiplied with 1.8.

Fig 15.42 shows the result for a side stiffener (4) on YD-41. Equations from Figs 15.37–15.41 are used to calculate the result.

Required section modulus of a stiffener from the neutral axis

$$67) \quad SM_o \Rightarrow \frac{0.0833 \cdot k_{cs} \cdot P \cdot s \cdot l_u^2}{10^6 \cdot \sigma_{dt}} \text{ [cm}^3\text{]}$$

$$68) \quad SM_i \Rightarrow \frac{0.0833 \cdot k_{cs} \cdot P \cdot s \cdot l_u^2}{10^6 \cdot \sigma_{dc}} \text{ [cm}^3\text{]}$$

$SM_o$  = required section modulus for a flange in tension from the neutral axis

$SM_i$  = required section modulus for a flange in compression from the neutral axis

$P$  = reference pressure for the location in question [kN/m<sup>2</sup>]

$l_u$  = length of stiffeners, Fig 15.13

$s$  = spacing of stiffeners, Fig 15.13

$k_{cs}$  = correction factor for curvature, Fig 15.20

$\sigma_{dt}$  = design stress in tension, Fig 15.21, for the bottom flange/plating

$\sigma_{dc}$  = design stress in compression, Fig 15.21, for the top flange

Required web area,  $A_{wd}$

$$69) \quad A_{wd} = (P \cdot s \cdot l_u \cdot k_{SA} \cdot 10^{-6}) / \tau_d = < A_w \text{ [cm}^2\text{]}$$

$A_{wd}$  = required web area [cm<sup>2</sup>]

$A_w$  = aquired web area [cm<sup>2</sup>]

$k_{SA}$  = 5 for stiffeners attached to plating

$k_{SA}$  = 7.5 for floating stiffeners

Fig 15.37 to 15.41 for calc.

Required SM comp	96 cm <sup>3</sup>
Required SM tens	68 cm <sup>3</sup>
Required web area	9 cm <sup>2</sup>

Aquired calculated values:

SM in compression	110 cm <sup>3</sup>
SM in tension	183 cm <sup>3</sup>
Web area	11.5 cm <sup>2</sup>

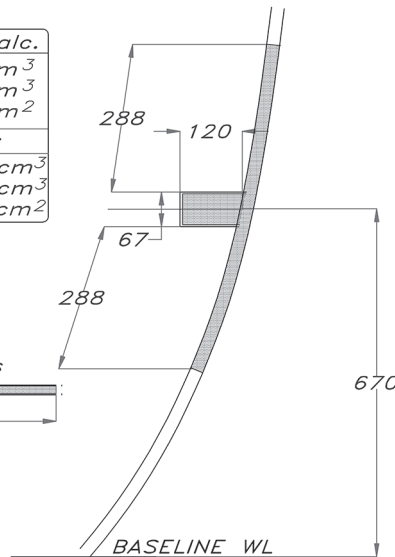
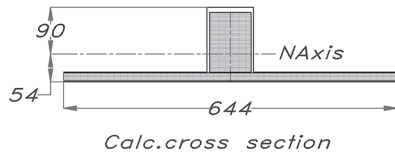


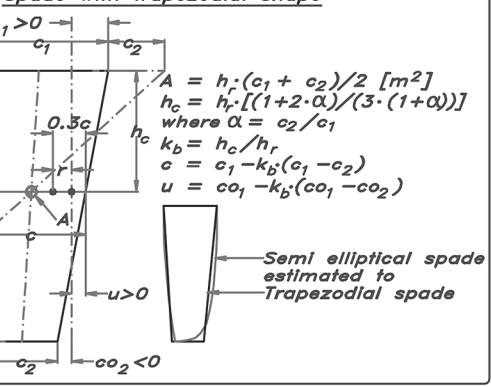
Fig 15.41 (ABOVE) Stiffener construction

Fig 15.42 YD-41 side stringer

## SPADE RUDDER STOCK

The first thing to do with the rudder stock calculation is to geometrically define the rudder. Fig 15.43 gives the definitions and equations. In the figure, we can see the measurements needed in equations 70 to 79. Basically, we need the height and average length of the rudder to determine the rudder lateral area, as well as the location of the centre of pressure, the length and the speed of the vessel.

By locating the rudder stock some way aft of the leading edge, we are diminishing the turning lever and hence the torque on the shaft. It is a good rule of thumb not to place the



To start the calculation, we first establish the side force the rudder is capable of delivering. This force  $F_1$  or  $F_2$ , given in equations 70 and 71, is dependent first of all on speed squared, which here is taken as  $L_{WL}$  and rudder lateral area,  $A$ . The lift is also modified by coefficients reflecting design category ( $k_{SEA}$ ,  $k_{USE}$ ,  $k_{SERV}$ ), length displacement ratio ( $k_{LD}$ ) and section type ( $k_{GAP}$ ,  $k_{FLAT}$ ).

The factor  $k_{LD}$  in the force formula is there to increase the dimension of rudder stocks in light sailboats. The reason for this is that they are simply faster than heavy boats, especially when reaching in strong winds, and this puts great strains on the rudder shaft. Now we can easily calculate the bending and torsion moments,  $M_H$  and  $T_r$ . Entering the equations with units according to ISO (i.e. N, knots, m, etc.) we get our results in N, Nm and mm. When calculating the rudder stock diameter, it is the yield stress of the stock material we shall use, or the ultimate tensile stress divided by 2 (whichever is less), in N/mm<sup>2</sup>. All these calculations lead to a solid rudder stock diameter of 44.5 mm when using stainless steel type 316 for the stock.

## ■ KEELBOLTS

Part 9 in the ISO scantling standard ('Sailing craft – Appendages') is a comprehensive standard containing guidance for designing different types of keels, centreboards and attachments. We will just show an example of a bulbed keel with a hull flange, as on the YD-41. Fig 15.44 shows what input and equations (80–87) we need. The different load cases correspond to:

- **Load case 1.** The yacht heeled over 90° in the air, giving a bending moment in the bottom and inner structure – equations 81 and 82. The required bolt diameter is calculated using equation 83. A notable thing to consider is that no additional safety factor is introduced: due to dynamic impacts in waves, only the static load is engaged. The calculated neck diameter of the bolts is 10.9 mm which gives a nominal diameter of 13.9 mm, but the nearest recommended bolt diameter according to the standard is 16 mm. If we do some reverse engineering in equation 83, to get a calculated bolt diameter of 16 mm, it turns out that there is an extra safety factor of approximately 1.5 worked in, in our case. On top of that, there is a material safety factor of 4 in equation 36, so bolts of 16 mm seem reasonable.
- **Load case 2.** Canted keel at 30° heel. This load case does not apply to the YD-41.
- **Load case 3.** Vertical pounding. Looking at equation 40 it is obvious that this is a very lean requirement. The force  $F_3$  only means that the yacht shall be able to stand on its own keel when hauled or vertically and gently grounding with no forward speed. No bending moment is given here as it depends on the floor and keel arrangement. The YD-41 bottom floors and girders fulfil this requirement.
- **Load case 4.** Longitudinal impact giving a bending moment of the bottom and inner structure – equations 85 and 86. The required bolt diameter is calculated

### ISO Keelbolt dimensioning

#### Design stresses for keel bolts:

Bolt metal	Class	Load case 1	Load case 4
		$\sigma_d$	$\sigma_d$
ISO SS bolts	50	105.5	157.5
	70	175.9	262.5
	80	201.0	300.0

Recommended bolt diameters:  $d_{bolt} = 1.18 \cdot d_{neck}$   
M12, M16, M20, M24, M30, M36, M42, M48

The general formula for design stress is:

$$(80) \sigma_d = \sigma_{LIM} \cdot 0.75 \cdot k_{LC} \cdot k_{DC}$$

$\sigma_{LIM}$  is either  $\sigma$  in tension or  $\tau$  in shear taken as  $\min(\sigma_y, 0.5 \cdot \sigma_u)$  where  $y$  means yield strength and  $u$  means ultimate strength for metal in unwelded state.

$k_{LC} = 0.67$  Load case 1

$k_{LC} = 1.00$  Load case F4

$k_{DC} = 1.00$  for Design Category A and B

$k_{DC} = 1.25$  for Design Category C and D

#### Load case 1:

$$(81) F1 = g \cdot m_{KEEL} \quad (N) \text{ vertical force at } 90^\circ \text{ knockdown} \quad [22563N]$$

$$(82) M1.1 = F1 \cdot a_K \quad (Nm) \text{ keel heeling design moment at keel junction} \quad [36214Nm]$$

$$(83) d_{neck} = \sqrt{\frac{1273 \cdot b_f \cdot M1.1}{\Sigma b_f^2 \cdot \sigma_d}} \quad [10.9 \text{ mm}] \quad d_{neck} = \text{diameter of each keelbolt at the bottom of the thread}$$

$d_{bolt} = 1.18 \cdot 10.9 = 12.9 \text{ mm}$  gives M16 recommended.

#### Load case 3:

$$(84) F3 = g \cdot (m_{LDC} - m_{KEEL}) \quad (N) \text{ vertical impact force} \quad [50031N]$$

#### Load case 4:

$$(85) F4 = 1.2 \cdot g \cdot (m_{LDC} - m_{KEEL}) \quad (N) \text{ longitudinal impact force} \quad [60037N]$$

$$(86) M4.1 = F4 \cdot h_{F4} \quad (Nm) \text{ longitudinal moment at keel connection level} \quad [114071Nm]$$

where  $h_{F4} = \min(T_K \text{ or } 0.2 \cdot L_{WL})$

$$(87) d_{neck} = \sqrt{\frac{1273 \cdot I_{Rimax} \cdot M4.1T}{\Sigma I_{Ri}^2 \cdot \sigma_d}} \quad [13.6 \text{ mm}]$$

where  $M4.1T = M4.1 \cdot L_{K2} / L_K$

and  $\Sigma I_{Ri} = I_{R1} + I_{R2} + I_{R3} + I_{R4}$

$I_{Rimax} = I_{R4}$

$d_{bolt} = 1.18 \cdot 13.6 = 16.0 \text{ mm}$  gives M16 recommended.

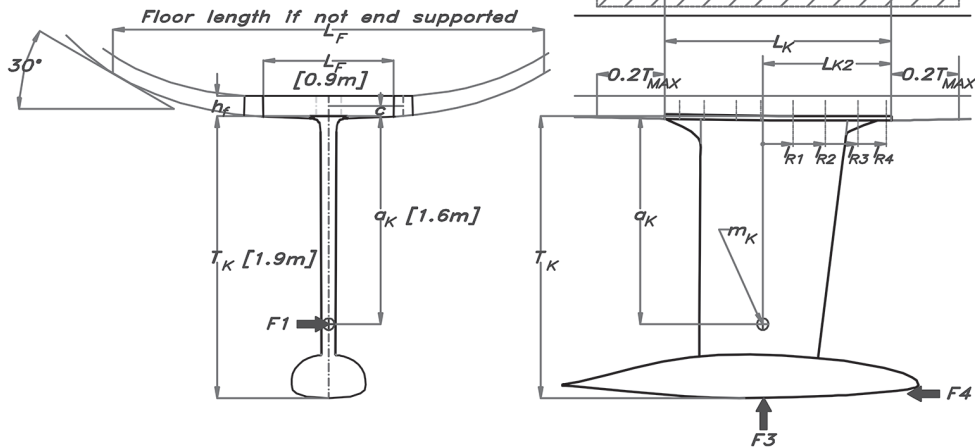


Fig 15.44 ISO keelbolts

using equation 87. The required bolt diameter refers to the forward bolts being put under tension when grounding. Also, in this case, the load is rather light, just 1.2 g times the yacht's mass minus the keel mass. It has been achieved by reverse engineering from actual boats. It is up to the designer to decide if this is good enough. Certainly, it is not a crash grounding scenario.



The resulting diameters of the keel bolts are to the bottom of the threads so the nominal size is bigger to account for this. These calculations only give the requirements in three load cases for the bolts themselves. Part 9 of the standard also gives the methods for calculating the supporting structure in the boat (i.e. girders, frames and structures, etc.) and different bolt materials.

## ■ RIG LOADS AND RIG ATTACHMENT

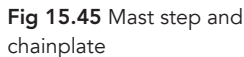
For the dimensioning of the mast, stays and shrouds, [Chapter 12](#) ('Rig construction') is valid. For a ballasted monohull, like the YD-41, part 10 of the ISO standard (which is quite comprehensive, covering 78 pages) really is a standard of itself; it uses the same load assumptions (i.e. using the righting moment at 30° of heel for a non-extreme monohull as the basis for the loads on the mast, rigging and attachments). The standard has procedures for ballasted monohulls, multihulls, form stable monohulls with max righting moment <30° and two-masted rigs, wing masts as well as masts stepped on the deck or the keel.

In this section, we will look into YD-41's keel-stepped mast and rig attachment, calculated using the standard's simplified method, based on 'established practice' or that the rig manufacturer provides the necessary in-data. In reality, the fact is that most boatbuilders let the mast manufacturer do all the calculations and select the proper mast section and rigging details. Nevertheless, the result must meet the standard's requirements. In [Fig 15.45](#) we have shown some examples that are covered by the standard. Hull sections (a) (deck stepped with a pillar) and (b) (deck stepped on bulkhead) are described and calculated in the standard, but we concentrate on case (c) (keel stepped), the YD-41 case. When it comes to chainplate attachment there are virtually countless variations but we will concentrate on case c), the YD-41 solution. Case (b) is covered in the standard with a calculation example, and case (a) may be calculated according to case (b) with the addition of dimensioning a tie rod lug in accordance with the deck lug.

The chainplates on the YD-41 sit on the edge of the hull, thereby minimizing the mast pressure and use as small and light mast section as possible. The chainplate material used is AISI 316, but other materials as well as fibre-reinforced lugs are covered in the standard. The shrouds are of a 10 mm carbon rod with a breaking strength of 75 kN. The chainplates shall be able to withstand 20% more load,  $2 \times 75 \times 1.2 = (2 \text{ shrouds}) 180 \text{ kN}$ . The hull where the chainplates are attached is of a solid laminate thick enough to absorb the bearing and shear load from the rigging.

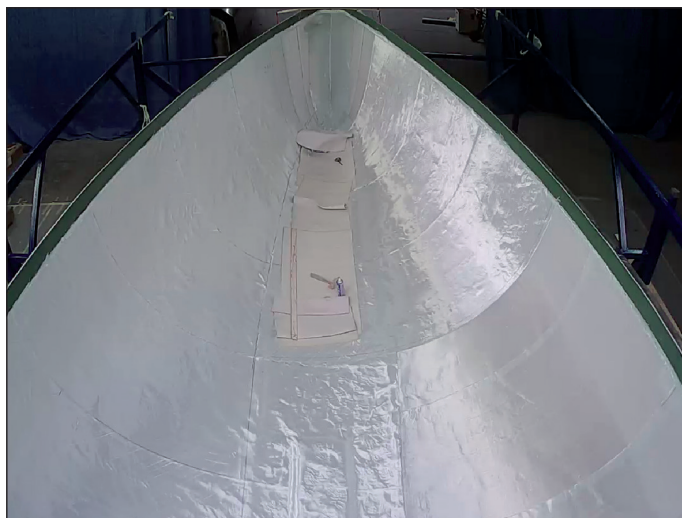
The mast step on the YD-41 consists of a pressure block of 250 kg/m<sup>3</sup> PVC foam encapsulated in an FRP vacuum-bagged bottom floor. The shear area,  $A_{SH}$ , is the actual cross-sectional area. Where the height of the floor is variable, the values of  $d_s$ , SM and  $A_{SP}$  shall be taken at 75% of the span  $L_{SP}$ . The formulae 88 to 93 may be used to calculate all requirements to make certain that the mast will remain in the boat. The factors  $k_{MSB}$  and  $k_{MSS}$  are approximate correction factors to make standard beam theory more applicable to short beams and high heights, as in the YD-41 case.





To meet the weight and strength properties that are required for our example yacht, the manufacturing process has to be well controlled. We decided, already at the preliminary design stage, that the boat had to be lighter than a typical production cruiser of this size but without the added cost of carbon fibre construction. The commonly used in the industry wet hand lay-up, solid laminates and full size, complex and heavy moulded liners are out of the question. The hull and the deck need to be light and the stiffening system needs to fit well with the interior arrangement, which should also contribute to the strength and rigidity of the boat. We choose a sandwich construction based on glassfibre reinforcement with a vinylester resin type matrix.

The vacuum infusion process is selected for building the GRP parts. The advantages of this method over the traditional hand lay-up are that a better fibre-to-resin ratio can be achieved with, at the same time, fewer air voids in the laminate. It is also much cleaner; less resin is wasted and – what is very important – the reinforcement can be set up without a time limit. The drawbacks are that it is a bit more complex and requires experience often gained through trial and error. In the worst-case scenario, the entire part can be ruined when something goes wrong.



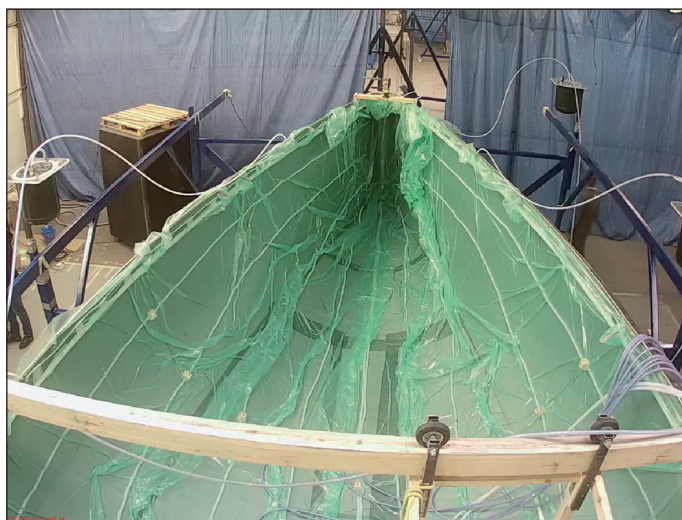
**Fig 15.46 (ABOVE)** Dry reinforcement and sandwich materials laid in the mould



**Fig 15.47 (LEFT)** Reinforcement materials covered with peel-ply and flow medium

**Fig 15.48 (BELOW)** Sealed off mould with visible flow lines

In our case, the building starts similarly to a traditional method. After the mould is prepared, the gelcoat is applied. However, on the bottom, which is painted later with an anti-fouling, a transparent gelcoat is used so that the finished laminate can be inspected visually. Then, to avoid the reinforcement texture being visible on the finished boat, so-called print-through, a thin skin coat is laminated using hand lay-up. When this protective layer is cured and sanded, the dry reinforcement and sandwich materials are laid down according to the laminate schedule (Fig 15.46). The entire area is then covered with a peel-ply and a special flow mesh to aid resin transfer (Fig 15.47).







A network of resin flow tubing with multiple resin inlet points is prepared. The material stack prepared this way is then covered with a vacuum bag and sealed properly so that low pressure can be maintained and there is no air ingress at any spot (Fig 15.48). It is important to test the air-tightness of the system before the resin infusion to avoid problems later.

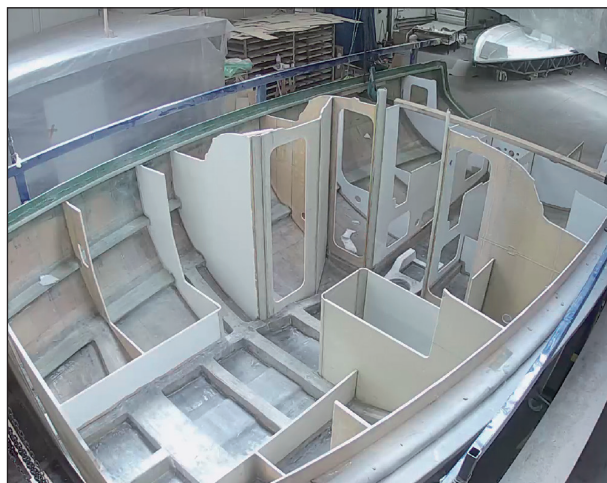
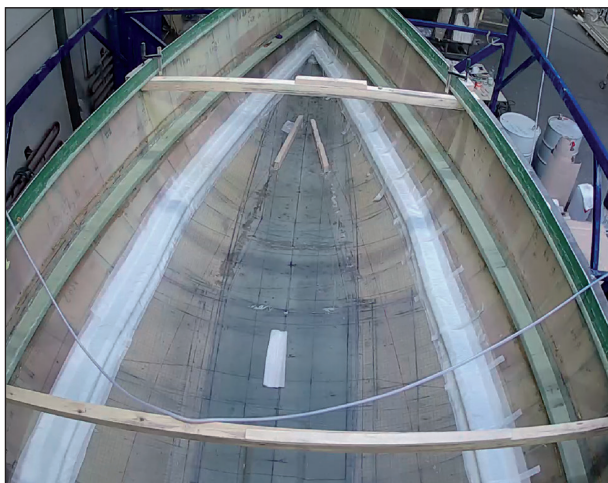
When the appropriate pressure is achieved and the resin prepared, the infusion process can start. The valves on feeding lines are opened in a prescribed order and the materials are gradually filled in with resin (Fig 15.49(a-c)).

**Fig 15.49(a-c)** (TOP TO BOTTOM) Infusion process – growing dark area shows the progress that resin makes through the material



The entire YD-41 hull, with an area of 75 square metres, is infused within one hour. The resin starts to gel after another hour but the vacuum is kept longer and the resin cures overnight at room temperature. Thereafter, the bag is removed and the flow mesh with the peel-ply separated from the laminate. The hull is post-cured at an elevated temperature to reach the desired mechanical properties.

The deck is built in a similar way but the shape complexity is greater so the network of resin feeding and distribution lines is more complicated to ensure that the resin reaches everywhere.



Hull stiffeners are built in place with a glass reinforcement on a sandwich foam, **Fig 15.50**. The vacuum is used to infuse the materials with resin. While the hull is still in the mould the composite sandwich bulkheads are bonded in to preserve the correct shape, **Fig 15.51**. In the end, the deck is bonded to the hull and the bulkheads to create a strong and light boat.

Some final remarks. If the YD-41 had been made of solid laminates hand laid up, the single skin for the hull to be strong enough would be 11 mm thick weighing 18 kg/m<sup>2</sup> compared to the infused sandwich laminate's 10 kg/m<sup>2</sup>. The total single skin structural weight including the deck, stiffeners and structural bulkheads would be 40% heavier compared to the sandwich structure. A better solution for a single skin design is to make the stiffening system denser, not to require too thick and heavy panel laminates. By reducing the panel sizes by about 20% the appropriate skin thickness would be 7.5 mm, which means 13.5 kg/m<sup>2</sup>, so the total hull laminate weight would be 35% higher compared to the sandwich construction.

The outer skin of the YD-41 is 2.2 mm thick and the inner skin is 1.8 mm. This might be regarded as a practical minimum for a boat of this size, not to be too sensitive to impact forces and crowded docking manoeuvres. Of course, we can use better fibres (S-glass, carbon, etc.), and then it is possible to get enough strength and stiffness with thinner skins and lower weights, which is acceptable and even desirable if the design is meant for high-level racing and maximum performance, but it is not necessarily ideal from a practical and robustness point of view for a cruiser or a cruiser/racer.

**Fig 15.50 (LEFT)**

Longitudinal stringers being built

**Fig 15.51 (RIGHT)**

The hull with the stiffeners and composite bulkheads in place

# 16 LAYOUT

The term ‘layout’ covers a wide area, and in this chapter we will discuss accommodation, cockpit, deck, instruments, hatches, ventilation and safety equipment. These different matters will be dealt with in general terms, but we will use the solutions used in YD-41 to show one way of meeting the demands.

## ■ GENERIC SPACE REQUIREMENTS

Before using the boat there are some general requirements that must be met, in order to make the vessel practical and comfortable to sail and live aboard. Fig 16.1 (overleaf) shows some important dimensions concerning the space required for a man standing, sitting and lying. The ‘module-man’ we are using is 1.8 m tall. Optimizing for a bigger or smaller person is done by *interpolating* the values according to size.

When standing up (Fig 16.1(A)), the reach forward measurement is meant to show the practical maximum to reach controls when movement forward is restricted. The eye height shown is just that; in order to see over an obstruction (the deckhouse for example), this height has to be decreased by at least 100 mm. The seat/wheel gap in the figure is the minimum comfortable; a greater distance makes it more comfortable to stand but on the other hand more difficult to reach the *wheel when sitting down*.

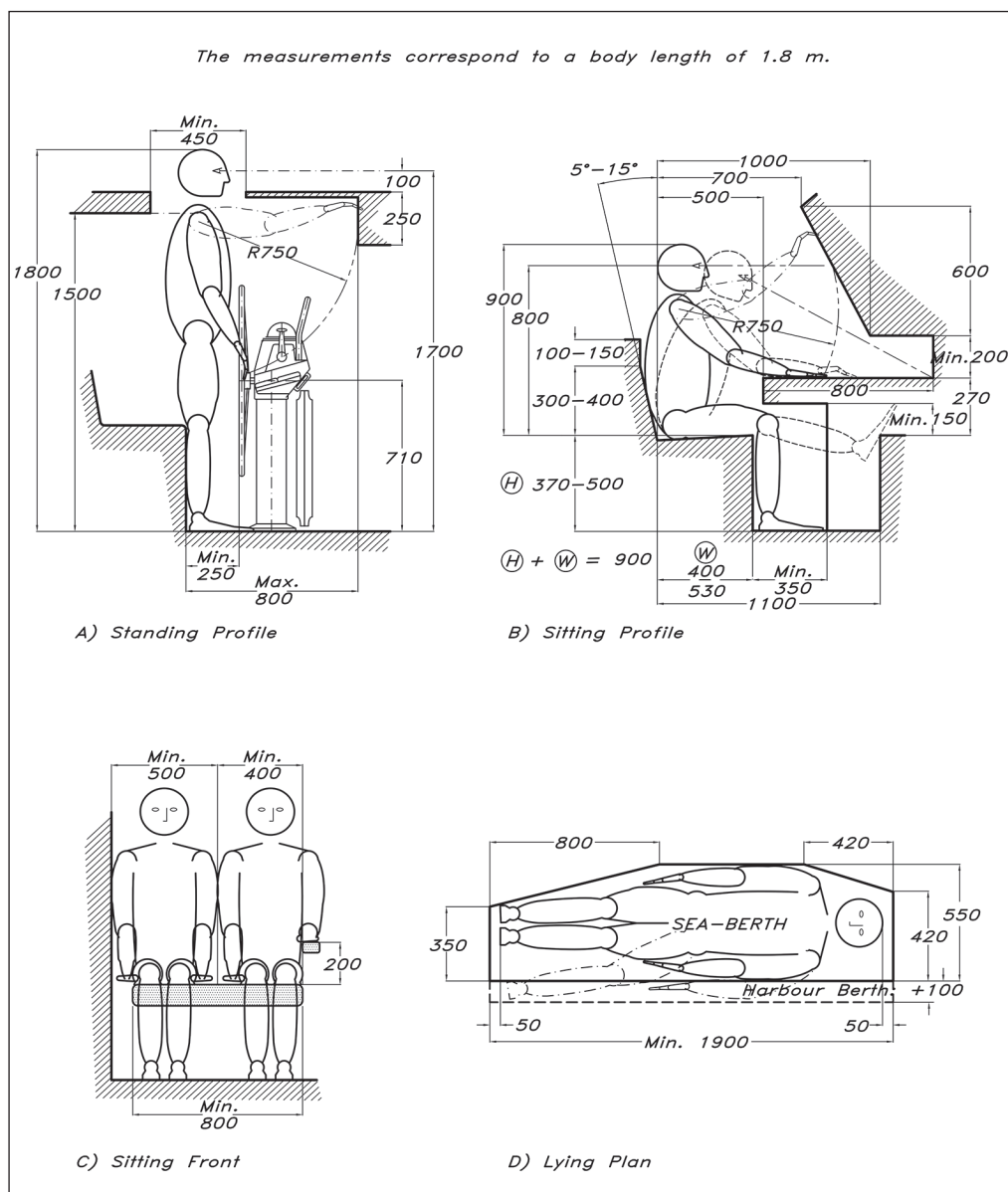
The seat height and depth shown in Fig 16.1(B) is for a rather upright seating position, for instance when eating or sitting by a navigation table. For a more relaxed sitting position the depth can be increased by 80 mm but at the same time the height is reduced by the same amount, to keep the sum of height and depth to 900 mm which produces a comfortable sitting *geometry*. The angle of the backrest can vary between 5° and 15° from vertical.

Fig 16.1(C) shows the width requirements when sitting down. It is worth noting that when the seat is beside a *bulkhead* the width required is greater than when it is free standing.

The picture in Fig 16.1(D) shows the minimum measurements for a comfortable seagoing berth. The narrowing of the ends is not necessary but this often happens due to the form of the hull. If the berth is a dedicated sea-berth these measurements are adequate, but if the berth is also to be used in harbour it might feel a bit cramped. Widening it by 100 mm will remedy this and doubling it will produce a usable double berth for harbour use, with a width of 1300 mm. If the double berth is free-standing with the sides not ‘walled in’ the width should be increased to 1400 mm minimum. A standard length of a berth is 2000 mm, but to tailor a berth for a specific body length, you need to add at least 50 mm to this body length at each end.



Fig 16.1 The human figure



## ACCOMMODATION

Looking at the YD-41's accommodation (Fig 16.2, page 354), there are some general features to consider. Basically the layout follows the principle that the activity areas are situated near the centre of motion of the boat, so that they can be used when under way. The lounging and sleeping areas, as well as stowage areas, are grouped forward and aft. As we have discussed previously, the aim with this design is to produce a comfortable offshore yacht for four persons, so we do not have to fill the boat to its extreme ends with bunks and accommodation. The numbers to follow (1-15) refer to the circled numbers in Fig 16.2.

## Accommodation

1. We start with the forepeak. One half of this part is dedicated to an anchor stowing system and the other is given to deck stowage for light items like fenders, lines, etc. By burying the headsail furler here we get a clear foredeck with the jib tack low down. Since this space has nothing to do with the rest of the accommodation the bulkhead to the forward cabin can easily be made watertight.

2. Another advantage of not pushing the accommodation too far forward is the position of the anchor windlass and chainlocker. These, along with the stowed-away anchor, are placed comparatively far back so as not to hamper the rough weather performance. Such heavy items placed far from the pitching centre play quite an important role in forming the gyradius of the boat.

3. This far back we are in the forward cabin. This is laid out as a cabin for harbour use, and that is why the double berth is placed here, a berth type that cannot easily be converted to a comfortable sea-berth. To achieve an acceptable width the berth is raised, and since this is too high to sit on, a separate seat is included. To make a cabin like this habitable, there is a hanging locker and a general stowage space for personal belongings in the aft-most part of the cabin, so they do not have to occupy the more public areas but still keep the weight closer to the centre of the boat.

4. Moving further aft to the saloon there are some other points to consider. There must at least be enough space around the table that all people who can sleep on the boat can also eat onboard. This is no problem for the YD-41, but on boats with an exceptionally large number of berths it might be. The saloon settees must be long enough (in our case) to sleep on, since the forward double berth is uncomfortable at sea. This dual function means that the backrests must fold up in order to have the berths wide enough to sleep on, while retaining a proper sitting depth while folded down. On a boat with a shallow hull like this one it might be a problem to locate water tanks big enough,

so here we use the space under the settees for tankage.

5. Thanks to the offset opening of the door to the forward cabin, the settee on the port side is deep enough to contain a big fixed table, while leaving a wide passageway to starboard. For large-scale dining there is a drop-leaf on the starboard side of the table, so it is possible to use the starboard settee as well.

6. Especially in boats under about 10 m (33 ft) it is often hard to fit in a full-size chart table and seat. Big charts may be 1300 × 800 mm when opened out, so the table top should ideally be this size. In the YD-41 this is possible without problems by fitting a generous navigation station between major structural bulkheads. If this is not possible we should at least strive for an area of 800 × 650 mm, i.e. a big chart folded once. For the navigator to be able to sit in the seat when the boat heels the seat must have a concave shape and possibly a sturdy armrest. Fig 16.3 shows clearly what it is like when sailing at a heel angle. Another thing to bear in mind when designing the interior is the narrowing of the boat the further down you get, and the effect of thickness of hull and other items. The circled area in Fig 16.3 shows just this. It is not sufficient just to deduct the sole width according to the relevant waterline on the lines plan without further deducting the hull and sole thickness. In this case they amount to a further deduction of 80 mm compared to the hull waterline.

Further demands on a good navigation station require it to contain plenty of stowage space as well as bulkhead areas for books and electronic instruments. A stowage bin under the working area is a good place to keep the charts flat, and by making it 50 mm deep it is possible to stow up to 200 charts unfolded, or, if the area is not enough, 100 charts folded once can be stowed per 50 mm depth. The best place for a bookshelf is on an athwartship's bulkhead, so the books in it can be handled on either tack without falling out when removing the retaining fiddle.



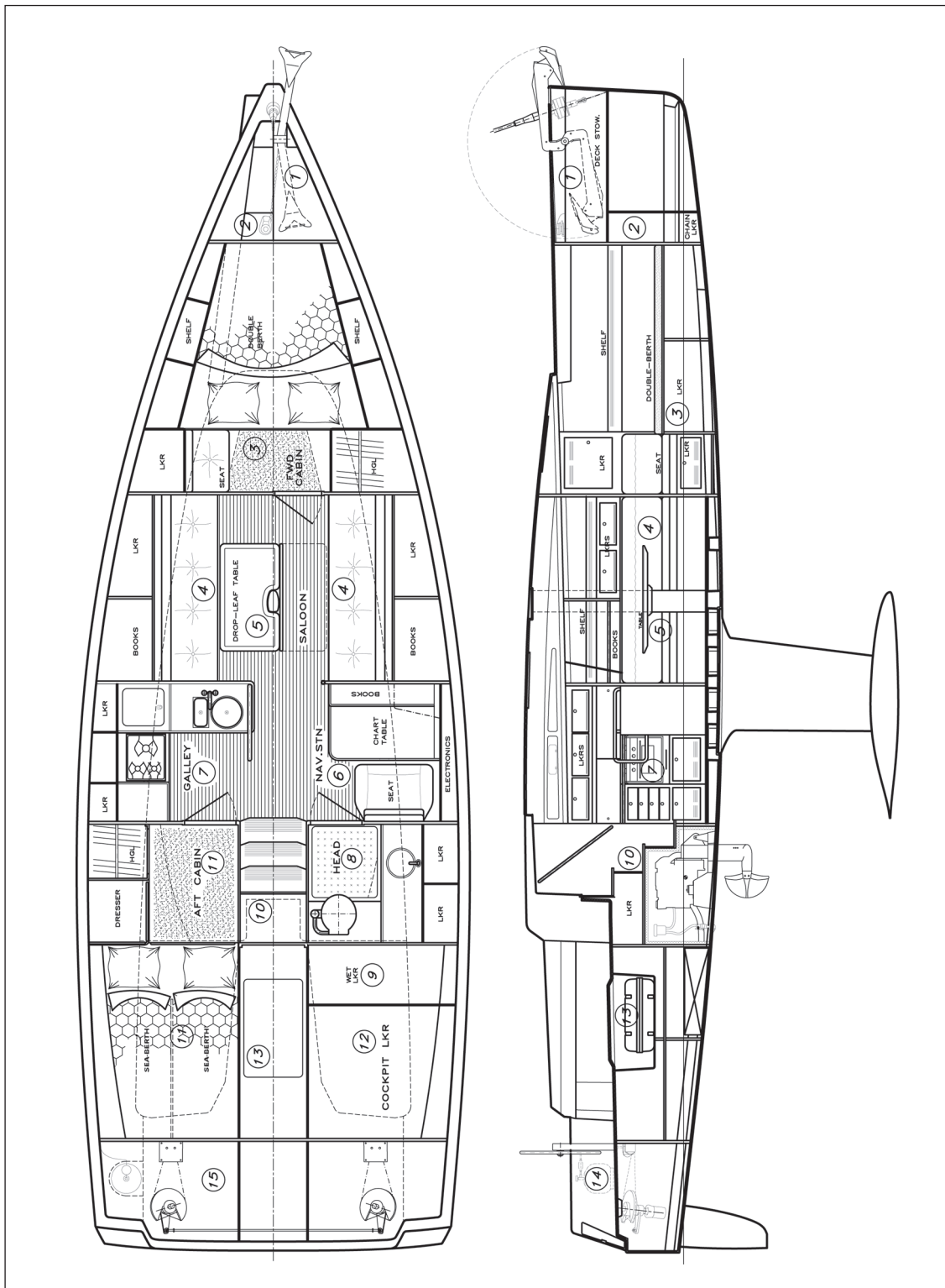


Fig 16.2 Accommodation layout – YD-41

Space requirements for electronic instruments will vary depending on owner preferences and the intended use of the boat. The single most important instrument that any boat should have is the compass. The primary one should not be electronic, but independent of the boat's electrical system, and it should be placed up in the cockpit to steer by. Instruments in the navigation area can be divided into three groups:

(a) *Navigation* instruments (compass, speed and distance meters, depth sounder, GPS, chart plotter, radar and AIS).

(b) *Weather and communications* instruments (barometer, wind speed and direction, air and water temperature, multiple band radio receiver, weather fax, VHF and other radio transmitters).

(c) *Boat performance* instruments (with the raw data gathered from instruments in (a) and (b), added to data such as heel angle, course and speed over ground from a GPS, the processing unit in the boat-performance instrument package can calculate VMG, leeway, direction and strength of current, time and distance to the next mark or waypoint, and calculate polar curves for the boat in actual conditions).

Most of these instruments are quite small and can generally be surface-mounted. Since many of them need input from the operator they must be placed within easy reach of the navigator. Radars and chart plotters take up more space, since the screens are often 20–30 cm (8–12 in) or more.

7. In the past galleys could be placed almost anywhere in the boat: forward, along one side of the saloon, or aft. Today, the common location for galleys is next to the aft companionway, and there are good reasons for this. This is the area where the violent pitching motions are smallest, the cook is not isolated from the rest of the crew, the ventilation through the companionway hatch is good and food may be passed to the cockpit easily.

In the YD-41 the galley is placed to port of the companionway, and thanks to the size of the boat it is sufficiently off-centre not to place the cook in the general traffic between the cockpit and saloon. The

planform is L-shaped, with an additional grab rail/bracing for the cook when the boat heels. As we can see from Fig 16.3 it is important that the distance from this bracing to the stove is great enough to allow the cook to take up the boat's heel angle. The heel angle shown is 30° which is certainly greater than the normal sailing angle, but temporarily, in squalls for example, it is not an exceptionally large angle. Another way of keeping the cook in place is by using a restraining belt. The disadvantage with this method is that the cook is strapped in and cannot escape if an accident, such as a boiling pot falling over, occurs.

As an added safety factor a crashbar should be set across the stove front to keep the cook from accidentally falling on to the burners.

Another vital feature to bear in mind when designing the galley is to make sure that there is enough space behind and in front of the stove to gimbal freely over approximately 60°. There are many stoves on the market, but generally the following features are desirable:

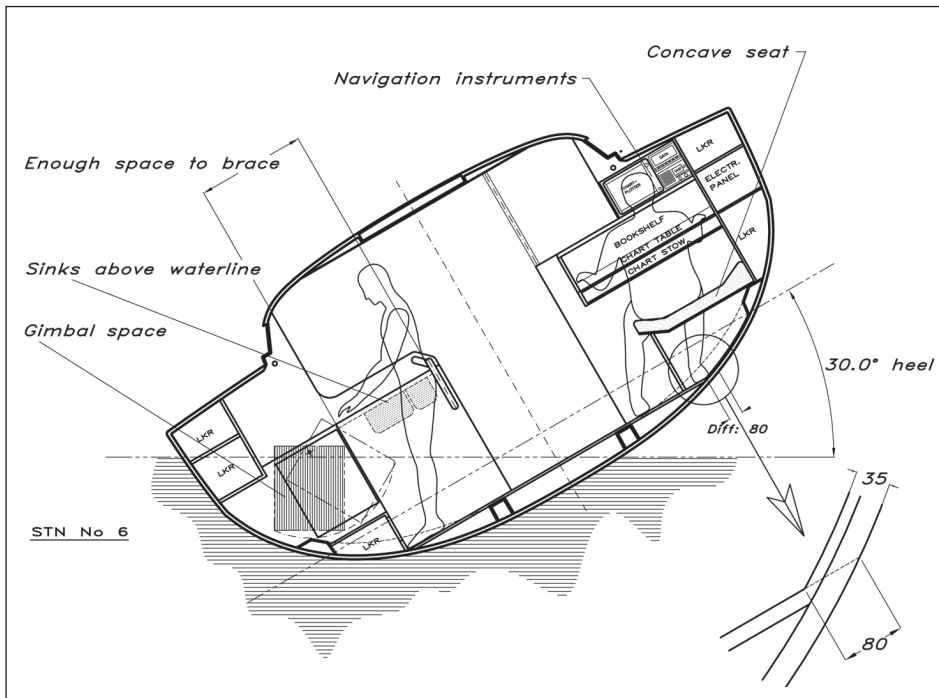
- Stainless steel construction
- Removable top gratings, for easy cleaning
- A high fiddle rail around the burners with pot-holders, to keep pots from falling over
- Sturdy gimbals positioned for good dynamic balance when the boat is rolling
- An oven
- A lock on the oven door, to keep things inside it in rough weather.

Several stove fuels are available:

(a) *Alcohol* has the coolest flame and therefore cooks the slowest. It is fairly safe, with no risk of explosion, and a fire can be put out with water. It has a tendency to smell sometimes to the point that crew members may be sick.

(b) *Kerosene* has the hottest flame. It was once the most common stove fuel, but it is becoming increasingly more difficult to obtain, and it is getting more expensive as well. It requires a vaporizing priming procedure to be lit, and tends to smell bad.

**Fig 16.3** Heeled section – YD-41



(c) *LPG* (liquefied petroleum gas) is the second hottest in flame heat. It is stored in liquid form and automatically vaporizes as it is released, so it can be lit just like household gas. The big drawback with *LPG* is that it is heavier than air, and mixed with air it forms an explosive mix. If it escaped inside the hull and settled in the bilge this could be highly dangerous. Therefore, it must be stored and handled with care:

- Stow *LPG* bottles in separate airtight compartments that drain overboard.
- Install a cut-off valve that is situated in the galley, and preferably an electric solenoid valve in the bottle stowage compartment, also operable from the galley.
- Install a leak-warning system in case of leakage into the bilges.
- Install a stove with a flame-out safety shutoff in the oven as well as on the top burners.

(d) *CNG* (compressed natural gas), unlike *LPG*, is lighter than air. Therefore, if it leaks, it will rise and can be ventilated away. It is not as

widely available as *LPG*, however, and it is more expensive.

The sink must be deep enough not to spill even with a half-load of dishwater, which means a depth of at least 160 mm. Having two sinks is a good idea, one for washing dishes and the other for rinsing and emptying cooking water, etc. By making the bigger sink round we make the most of the volume, i.e. we use a smaller amount of water to fill the sink up to a given level. As can be seen from [Fig 16.3](#), the sinks in the YD-41 are placed high enough and sufficiently inboard to allow them to drain when the boat is heeled over.

Some sort of refrigeration is essential, because ice is increasingly expensive and difficult to find (not to mention the awkward handling). Even small boats carry refrigeration in the form of insulated boxes cooled at home, and plugged into the boat's 12-volt system. On bigger boats like the YD-41, however, we need a permanent refrigeration system. To start with we need an efficient box or cabinet to hold the refrigerator.

By far the most important component is the insulation. There must be at least 100 mm of insulation all round the compartment. A very good insulating material is polyurethane or PVC foam. The door to the refrigerator can be either side or top-opening, with the latter considered to be more thermally efficient (since cold air does not pour out when opening the box). However, you often need items from the bottom of the box and to reach them you have to rearrange some food on the box top, where it will be warmed up during the search process. A way around this problem is to make the top opening as big as the box itself, and equip the box with 'modular inserts', stacked beside each other, containing food sorted by type, meal rations or any other system that is suitable, so that the entire contents of the box do not have to be disturbed when looking for a specific item.

Finally, there should be adequate counter space with high sturdy fiddles, with work areas on both sides of the stove. Having the stove directly against a bulkhead is not a good idea, since it is an uncomfortable place to stand in, and the process of preparing a meal benefits from having an area each side of the stove.

**8.** Like the galley, the head area traditionally has been placed almost anywhere in the vessel. Today just two areas are preferred: between the saloon and forward cabin, or (as in the case of the YD-41) close to the companionway. The advantage of the latter position is the same as for the galley: the motion of the boat is least felt here, so the head can be used under way in rough weather. As can be seen the WC is aligned fore-and-aft. This is the proper orientation for use at sea regardless of heel direction, provided the distance between the surrounding counter and bulkhead is not less than 650 mm and not greater than 750 mm. Anything smaller will render the WC useless, and if made greater the ability to offer good bracing is reduced.

One disadvantage of placing the WC this way is that the wash-basin is forced outboard, and will not self-drain on a port tack (YD-41) in fresh weather. Two solutions are given: either we install a holding tank, or pump out the waste water via a loop that goes up under the sidedeck.

The free area in front of the wash-basin and WC should be minimum 650 × 650 mm to be useful as a washing and showering area. It is not necessary, though, that the sole be completely flat: the hull might still show, especially if the head is placed aft in the boat since the hull lines are rather shallow in this area.

Having the head situated between the saloon and forepeak does prevent it from being used comfortably in a seaway, but since it is possible to use the full width of the boat here, it might be the only place to locate it in order to get enough elbow space, especially in smaller yachts. It also puts the saloon further back in the boat, where space is greater.

**9.** Foul weather gear is troublesome to stow. Not only is it bulky but also dampened by salt water. Therefore it is essential to have a separate wet gear locker. In the YD-41 it is situated directly aft of the head, so this compartment is used to take the wet gear without wetting the rest of the interior. There might also be a hatch on top of the locker leading directly to the cockpit so that people do not have to come down to get their foul weather suits. To make it possible to dry clothes stored here, there is a hot air outlet from the heating system into this locker.

**10.** The steps are formed by the engine compartment hatch. Enclosed by the longitudinal bulkheads to the head and aft cabin this gives a very secure companionway entrance. The locker above the engine is very useful for stowage of boots, tools, etc.

**11.** It is a good idea to place the sea-going berths in the aft part of the boat, as there is less motion here compared to the forward part. In smaller boats where it is impossible to fit a proper aft cabin there is usually room for a quarter-berth at least. In the YD-41 we have a proper cabin containing sufficient stowage and hanging locker space for two persons. There are some features in the berth area worth considering. To be suitable as a double sea-berth, there is a solid, fold-up dividing bunk board, stowed under the cushion when not in use. Lee cloths are good, but only when used on single berths.

To separate two sleepers effectively in a double-berth we need a substantial divider. It would have been possible to extend the berth into the centreline area and arrange the berths athwartship for better comfort during long ocean passages, but by not doing so the berth is not completely under the cockpit sole, where a claustrophobic feeling might have been experienced. At the same time we gain some cockpit stowage volume.

**12.** Extra sails, lines, fenders, fuel and water jerrycans, inflatable, outboard engine, cleaning compounds, lubricants, etc. are just a few things that most cruisers carry, in addition to the personal gear and food for the crew. This type of accessory does not belong in the accommodation, but should be placed in a cockpit stowage space. On the YD-41 it is situated under the starboard cockpit seat. This is quite large, but in real life it should be

subdivided with fiddles and dividers so as not to become a giant gear-mixer when the going gets rough.

**13.** At the centreline under the cockpit sole there is stowage for the liferaft and cockpit table. This location, while still easy to access, brings the heavy items lower and closer to the longitudinal centre of gravity.

**14.** A good place for LPG bottles is under the aftermost part of the side decks, but above the cockpit sole, in a moulded in self-draining compartment.

**15.** The aftermost part of the boat contains the steering mechanism, which is entirely isolated from the interior with a watertight bulkhead for safety in case of a rudder stock failure and possible leaks.

## ■ DECK LAYOUT

To design a deck layout that suits all types of boats and people is impossible. Like the accommodation, the intended use of the yacht has a profound influence on the layout. On a cruising boat the priorities are different compared to those of a racer. The racing deck is a working platform that has to perform efficiently for a well-defined crew with specific tasks. In contrast, the cruiser's deck must work with a smaller crew, offer space to sunbathe, protection from bad weather, and at the same time not be in conflict with the interior arrangement. On top of this we must not forget the performance side of it. The YD-41 is intended to be a performance-oriented cruiser, and looking at the deck more closely we can see what compromises are made in comparison to a pure racer. The numbers on the following pages (nos 16–37) refer to the circled numbers in [Fig 15.4](#).

## Deck layout

**16.** A stow-away telescopic emergency boarding ladder on the YD-41 is located to the side of the transom opening and at a level where it is possible to reach it from the water.

**17.** A nearly vertical stern creates more space in the cockpit for a given interior. On the YD-41 we have a wide foldaway transom platform. This gives the safety of a fully closed cockpit and, after opening it, creates a good deck to board the yacht from a dinghy or floating dock. It also makes it easier to recover a person who has fallen overboard, eases stern anchor handling and makes a nice showering and towelling area after a bath.

**18.** Generally speaking, a steering wheel takes up less space when under way than a tiller, but the opposite is true when at anchor. The feel of the boat is better with a tiller, and course adjustments can be made more quickly, which is especially important broad reaching in heavy weather, when broaching is most likely to happen. The disadvantage with a tiller is most obvious on a larger yacht. As we have shown in [Chapter 12](#), in the discussion of rudder forces, the tiller length has to be almost 2 m to equal the wheel-steering power on the YD-41. This makes it highly impractical on this cockpit design. To achieve a quick enough rudder action the number of turns from hard over port to hard over starboard should not exceed two on a performance-oriented boat, while on a heavy slow-reacting cruiser the number of turns may be allowed to reach three.

On a cockpit as wide as that of the YD-41, it is more practical to have two steering wheels offset to the sides leaving the centreline for communication. It also improves the visibility forward.

**19.** To give the helmsman a chance to remain behind the wheel, an efficient footbrace should be fitted. The cockpit sole behind each wheel has flip-up platforms that should be angled approximately 20°.

**20.** Mainsheet handling systems often collide with other cockpit requirements on cruisers. Therefore, it is becoming common to employ a mid-boom sheeting system for the main, with the sheet coming to a winch on the coachroof. In this way there will be virtually no lines in the cockpit. The disadvantage of the system is that the sheet loads will be much greater compared to an end-boom sheeting system, and the position of the mainsheet winch will be out of reach of the helmsman.

**21 and 22.** The system we have used consists of a mainsheet track just in front of the pedestals, and the traveller controls are lead to each side close to the helmsman position. The main sheet is led forward inside the boom and back on the sides to winches via turning blocks with clutches. The winches can be reached both by the helmsman and the crew sitting in front of the traveller. The sheet is double-ended so that it can be operated from either side of the boat. The coamings are wide, and angled to be comfortable to sit on when the boat heels.

**23.** The cockpit itself must be long enough to lie down in, even under way. This can be achieved even in quite small boats if considered in the early design stages. It might not be possible to have a long enough cockpit together with a heavily raked transom on a small yacht, and in this case the cockpit length should be given priority. On a racer it is not the lying-down requirement that dictates the length, but rather the number of crew that will be working in the cockpit, and the layout of the sail handling gear. On the YD-41 the benches are over 2 m long, and on the starboard side the bench contains hatches to the cockpit stowage space and the wet locker.

**24.** Since it is impossible to brace oneself against the opposite cockpit seat when the boat heels footbraces are necessary on the cockpit sole for the crew.

**25.** The primary winches are situated in the middle of the cockpit and are used also for the Code 0 and asymmetric spinnaker. The sizing of winches can be taken from most winch manufacturers' catalogues.

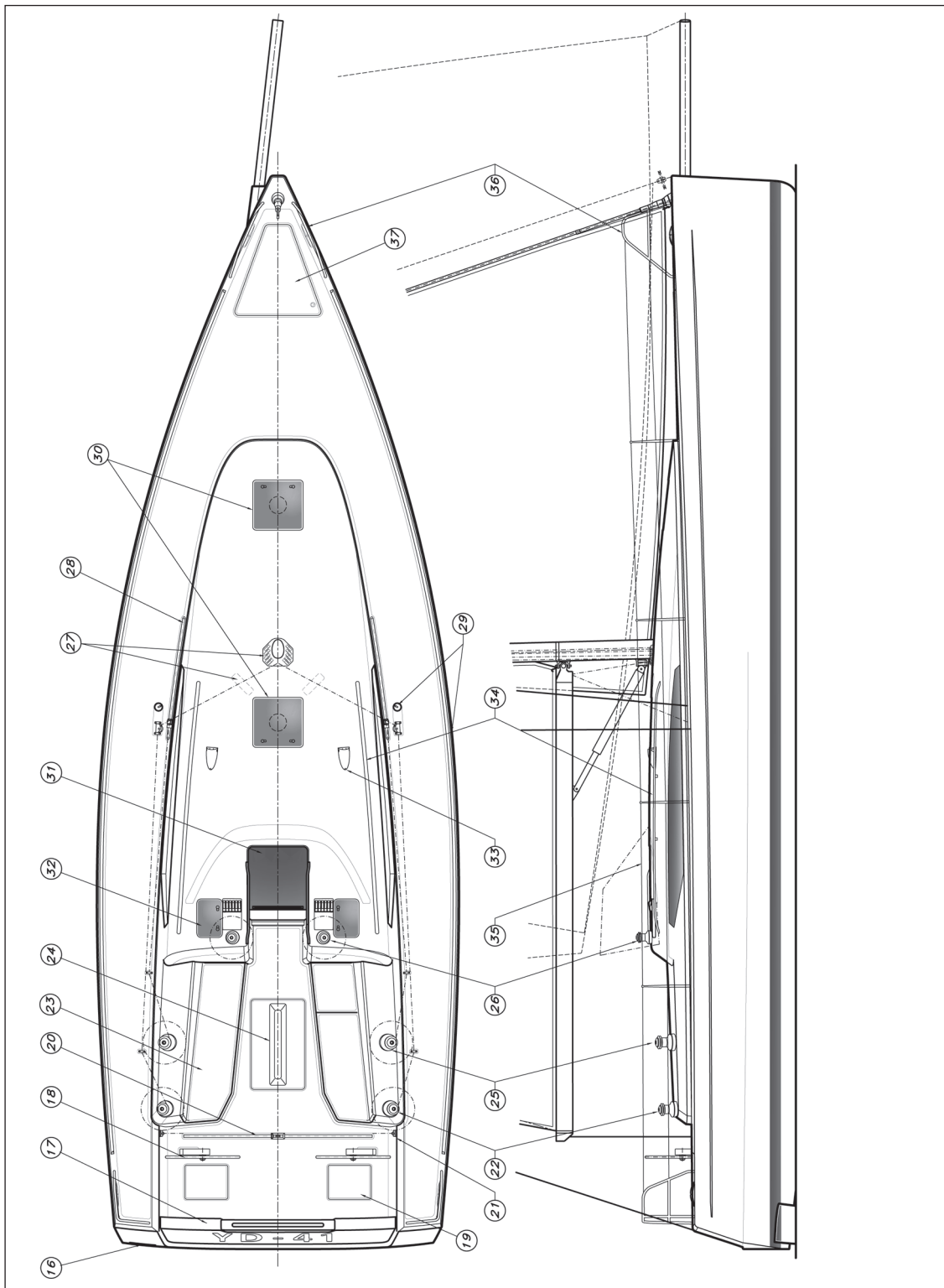


Fig 16.4 Deck layout – YD-41



**Fig 16.5** Calculation of winch size (Marshall)

*Foresail sheet load ( $F_F$ ):*

$$F_F = k_{bs} \cdot V^2 \cdot A_F \quad [ 1.45 \cdot 15^2 \cdot 43.3 = 14127 \text{ N} ]$$

*Main sheet load ( $F_M$ ):*

$$F_M = k_{bs} \cdot \frac{E \cdot P^2 \cdot V^2}{L_L \cdot T_R} \quad [ 1.45 \cdot \frac{5.60 \cdot 16.7^2 \cdot 15^2}{16.55 \cdot 3} = 10262 \text{ N} ]$$

$F_F$  = Foresail sheet load [N]  
 $F_M$  = Mainsail sheet load [N]  
 $V$  = Windspeed [m/s]  
 $A_F$  = Foresail area [m<sup>2</sup>]  
 $E$  = Mainsail foot [m]  
 $P$  = Mainsail luff [m]  
 $L_L$  = Mainsail leech [m]  
 $T_R$  = Mainsail tackle ratio  
 $k_{bs}$  = Boat size factor (2 for small boat, 1 for big boat)

*Winch power ratio ( $P_W$ ):*

$$P_W = \frac{F_F}{F_C} \text{ or } \frac{F_M}{F_C} \quad [ \frac{14127}{330} = 42.8 \quad \frac{10262}{330} = 31.1 ]$$

$F_C$  = Crew power on handle, 200 – 500 [N]

Fig 16.5 gives another way of determining the sheet loads from the main and foresails. The jib winches for the YD-41 should be at least of size 44, but preferably size 50. The mainsheet winch working through a tackle of 3:1 ratio should be at least of size 32.

**26.** On a cruising boat it is desirable to have the sail control lines (such as reefing lines, outhauls, halyards and kicking strap) lead to the cockpit. For this reason, the utility winches are placed either side of the companionway hatch, where they are easily reached from the cockpit. This layout of winches is not necessarily the best for single-handed sailing but prevent different crew members from getting in each other's way when operating the boat.

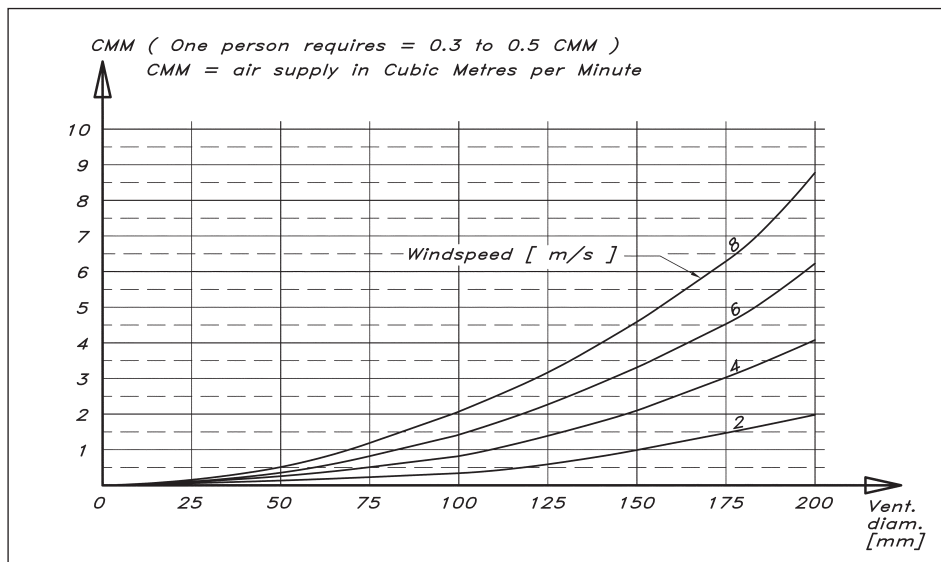
**27.** Leading sail control lines to the cockpit via turning blocks puts the roof under tension and exerts lifting pressure. Therefore, it is important to install tie rods between deck and hull in the mast area. Line organizers are used to direct the different lines to the cockpit. All the lines and turning blocks are concealed under the deck since stepping on exposed lines on the deck can be very dangerous.

**28.** On a racing yacht we usually have the opportunity to place the genoa tracks at an

optimum location. This means a foresail sheeting angle of between 7.5° and 10°. The sheeting angle obtained on the YD-41 is 12° with an optional in-haul to fine tune the angle when necessary.

**29.** The position of the chainplates is dictated by the rig calculation. The D1 is close to the coachroof for better passage on deck while the V1 uses the whole beam of the deck at its location. Having them both inwards while allowing for a larger foresail would mean higher rigging loads due to a narrower staying base. It is an iterative process to find the proper geometry that fits the available mast sections, wire/rod and intended deck layout. By using a three-spreader rig we might have succeeded in moving the chainplates inward to the deckhouse, but then they would have interfered with the saloon accommodation. It is difficult to please everybody.

**30.** Light and ventilation are needed below, and the deck is the obvious place to let both of them in. When a skylight hatch is open it ventilates and no other ventilation is needed. Ventilation is required, however, when the hatch is closed. The obvious place to put a ventilator is in the hatch itself. A standard 100 mm diameter clam shell ventilator is easy to fit, and is sufficient to ventilate a cabin for two people in temperate climates.



**Fig 16.6** Airflow through ventilators

**31.** Making the companionway hatch of smoke-tinted acrylic lets the light in but privacy is maintained. It should be possible to lock the hatch in an open position, so that it does not slide back and forth in a seaway. Installing a dodger over the companionway increases the ventilation; in fact it is the main factor in the boat's ventilation system. When the wind is forward it acts as a huge exhaust, and when the wind is aft it scoops in great amounts of air.

When sailing with the companionway hatch open it is extremely important that wash boards may be secured so that they do not fall out if the boat is knocked down. It is a good idea to carry two sets of wash boards: one good-weather set of lighter construction with built-in ventilation openings, and the other a heavy-weather set up, built solidly and tight.

**32.** As a general principle each compartment in the vessel should have its own ventilation. Quarter-berths or aft cabins in particular can become hot and uncomfortable if not properly ventilated. For obvious reasons the head also needs good ventilation. On the YD-41 these requirements are taken care of by two ventilation skylights each side of the companionway.

**33.** One very common, and good, ventilator is the dorade type. It consists of a scoop-type ventilator placed on top of a baffled water trap. By directing the scoop into or from the wind it can act either as an exhaust or an intake ventilator. However, on the YD-41 we can find slightly less efficient streamlined dorades, which suit better her sleek lines. By placing the ventilators high on the roof and as close to the centreline as possible, they can be left open during rather rough weather without letting in water. Another advantage of this design is that lines are less likely to be snagged and guards do not have to be installed around them.

To determine the total ventilation area needed we must start with the amount of fresh air that is needed below. For each person there should be a minimum air supply of 0.3 cubic metres per minute (CMM) and preferably 0.4 CMM. Fig 16.6 shows how much ventilation a certain size of vent provides, varying with wind speed. It is in rough weather sailing with the hatches closed that the ventilators must provide all intake and exhaust air. If we consider a six-person crew the required fresh air is  $6 \times 0.4 \text{ CMM} = 2.4 \text{ CMM}$ . Two 100 mm dorade vents provide 2.8 CMM at a wind speed of 6 m/s. The exhaust area must at least equal the intake area, and we have two 100 mm exhaust vents in the skylight hatches that take care of that.

**34.** The first and most important safety factor to consider on deck is the danger of falling overboard. A vital item is a long grab rail, so that you can move from the cockpit to the foredeck and have something to hold on to all the way. This rail also makes a good attachment for the safety harness. For boats with sail-handling systems (reefs, halyards, lifts, etc.) on the mast it is a good idea to incorporate a mast pulpit.

**35.** The last chance of rescue before hitting the water rests with the lifelines. Their height is often a compromise between looks and function. To be safe the height should be at least 750 mm but the desire for good looks combined with efficiency has established a height of 600 mm, with double lifelines. For small boats of lengths below 8.5 m the ISO 15085 standard accepts even 450 mm. The demands on the stanchions supporting the lifelines are quite high. They must be throughbolted, but even so they cannot be trusted to be strong points for the safety harness because a human body thrown against the lifelines during a violent roll can reach a force of 10000 N (one tonne).

**36.** The bow is an area where the combination of heaving and pitching movements is the greatest, so here it is essential to have something to hold on to, i.e. the pulpit. An open structure in the front of the pulpit makes the boarding from a dock or shore easier when moored stem to. A disadvantage of this solution is that the foot of the jib might get caught in the opening of the pulpit front of it requiring a crew to go to the bow. However, a detachable strap in the top part connecting the front corners efficiently solves the issue.

**37.** To have access to the forward deck stowage we must ensure that the deck hatch can be opened when the anchor is down. On the YD-41 the windlass and anchor chain is concealed under the hatch but in other arrangements the hatch must be offset or divided at the centreline. Thanks to the recessed foresail furler the deck is clear and unobstructed to aid anchor handling.

# 17 DESIGN EVALUATION

A basic aim of this book has been to provide the reader with the tools required for evaluating a design, not only qualitatively, but also quantitatively. Detailed formulae have been provided, enabling the designer to compute the performance characteristics of the yacht. In combination with the statistical information presented it is also possible to compare a proposed design with an existing fleet of yachts.

This chapter summarizes the use of non-dimensional parameters, composed of the main data, for quick estimates of the performance properties of the design. These parameters have all been defined in earlier chapters but they are collected here, and their usefulness in evaluating the total concept is discussed.

We then describe one of the most important tools available to the professional yacht designer today, namely the Velocity Prediction Program (VPP). This computer program predicts the speed, heel, leeway, apparent wind and many other quantities for a yacht under all possible wind conditions. By systematically changing the program input, while specifying the yacht, the designer may optimize his design with respect to different qualities.

The formulae given in this book are largely based on empirical information available from tests of different kinds. The hydrodynamic part, for instance, relies very much on the extensive series of yacht tests at the Delft University of Technology, while much of the aerodynamics comes from wind-tunnel tests and full-scale experiments. These kinds of results have been statistically evaluated to obtain the useful formulae in the book. Similar formulae are used in the VPPs.

If more exact information is required on a specific design the traditional way has been to model-test it. This, however, is quite expensive, and is done only in connection with large projects like the America's Cup or Volvo Ocean Races, or perhaps for very expensive luxury yachts. We will describe briefly how this testing is done.

A modern way to study a new design in detail is to carry out numerical flow calculations, i.e. using a technique known as computational fluid dynamics (CFD). This technique has become possible through the rapid development of computers, which enables very detailed studies of the flow and resistance properties of the design to be made. Its advantage is that it is faster and cheaper than model-testing, and the accuracy is continuously improving. For systematic variations and optimization, it has taken over much of the testing, while for very accurate predictions of absolute values testing is still often considered necessary. We will give a brief account of the status of CFD applied to yacht hydrodynamics at the end of this chapter.

## ■ NON-DIMENSIONAL PARAMETERS

The main data relevant to a yacht's speed potential are length, displacement, wetted area and sail area. To estimate stability the heeling arm and metacentric height are also required. For judging seaworthiness the beam, hull draft and some information on the righting moment at large heel angles are also required.

Since the sail area is a measure of the driving force, and friction is the predominant resistance component at low speeds, the sail area/wetted area,  $SA/S_w$ , is the most important speed parameter in light airs. This value should be above 2.0, otherwise the yacht will be very slow under these conditions. High performance will be obtained for ratios above about 2.5. Note that the sail area is defined here as the sum of the main and foretriangles. The value for the YD-41 is 2.6, so the yacht should be quite fast in light airs, when friction is the dominant resistance component.

In stronger winds the situation is much more complex. Not only the resistance but also the sail carrying capability come into play. As for the resistance, we have seen that the component due to the generation of a wave system becomes increasingly important when the speed increases. In fact, it is so important that very few yachts can leave the displacement speed regime at  $F_n = 0.45$  sailing upwind. The parameter of interest in this respect is the length/displacement ratio,  $L_{WL}/\nabla^{1/3}$  (see Fig 5.31). For a yacht to reach the semi-planing region downwind it has to have a ratio larger than around 5.7. Many modern high-performance yachts, even of the cruising type, reach this limit, and racers like the Open40s or IMOCA 60s are well above the limit. For the YD-41 the length/displacement ratio is 6.5 based on the light displacement (5900 kg) and 6.4 for the half-loaded case (6500 kg). As will be seen below, speeds up to 13 knots, corresponding to a Froude number of 0.6, are reached downwind.

For the upwind sailing, when practically all yachts operate in the displacement speed region, the wave resistance at a given Froude number is essentially proportional to the displacement. A parameter often used for the medium to strong wind performance is therefore the sail area/displacement ratio,  $SA/\nabla^{1/3}$ . This parameter is also a measure of the yacht's acceleration ability. It should be above 15 for reasonably good sailing performance. Very good performance may be expected for ratios above 25. The YD-41 has a value of 27.4, very close to that of Class40 yachts. It should be noted that the sail area/displacement ratio says nothing about the influence of length on speed. The ratio indicates the ability to reach a certain Froude number. If this is given the speed varies as the square root of the length.

A simple and reasonably accurate way of checking the stability is to compute the Dellenbaugh angle (as described in Chapter 4). Inserting the sail area, heeling arm, displacement and metacentric height into the formula of Fig 4.21 the heel angle in a breeze of approximately 8 m/s is estimated. The figure shows the variation between tender and stiff yachts.

The seakeeping qualities of the yacht are best checked by computing the stability index (STIX), as explained in Fig 4.22. This takes into account the proportions of the hull, the sail area and the righting moment curve. For ocean sailing, STIX must be at least 32, while 23 is enough for offshore cruising and racing. Inshore, STIX must be at least 14, while 5 is sufficient in sheltered waters. The YD-41 has a STIX of 42 and is thus well suited for ocean crossings.

## ■ THE VELOCITY PREDICTION PROGRAM (VPP)

Most VPPs are based on the equilibrium assumption, discussed in [Chapters 5](#) and [7](#). When the yacht is in equilibrium it moves on a straight course at constant speed, sinkage, heel and trim. The sum of all forces in each of the three main directions is then zero, as is the sum of all moments acting around the same directions. More specifically, the following relations apply (see also [Fig. 7.6](#)):

1. Along the direction of motion, the driving force from the sail is equal to the total resistance. (Surge equation)
2. At right angles to the direction of motion in the horizontal plane the side force from the sail is equal to the side force from the underwater body. (Sway equation)
3. Vertically, the buoyancy force is equal to the gravity force for a boat without foils. For a boat with foils the vertical component of the foil lift must be included in the force balance. There is also a possible vertical component of an additional centreboard lift at non-zero heel (see [Fig 7.13](#)). (Heave equation)
4. The heeling moment from the sails is equal to the righting moment from the hull and crew for a boat without foils. For a boat with foils the lift from the foils, and the possible additional lift of the centreboard, must be included in the moment balance (see [Fig 7.13](#)). (Roll equation)
5. The pitching moment from the sails is equal to the restoring moment from the hull and possible foils. (Pitch equation)
6. The total yawing moment is zero, since the hydro and aerodynamic forces act along the same line in the horizontal plane (see [Chapter 9](#)). (Yaw equation).

These are the equilibrium conditions in all six Degrees Of Freedom (6 DOFs). In some VPPs the vertical force balance (3) is assumed automatically satisfied, and so is the balance of the pitching moment (5). Few programs include the yawing balance (6) in their equations, but some have a model for non-zero rudder angles and may therefore consider this relation. The simplest VPPs thus take into account only the longitudinal and transverse forces, and the moment around the longitudinal axis, i.e. relations 1, 2 and 4. To explain the basic principles of a VPP, this simple version, for a non-foiling hull, will be presented first.

As for the first relation above, formulae for the resistance components are required, and those most commonly used are given in [Chapter 5](#). The aerodynamic driving force is normally computed as shown in [Chapter 8](#). Relevant formulae for the hydrodynamic side force are given in [Chapter 6](#), and the opposing aerodynamic force in [Chapter 8](#). The moment equation can be formulated using the stability relations of [Chapter 4](#), together with the heeling forces from [Chapter 8](#). Thus, the formulae required in a VPP have already been presented.

Using the formulae of [Chapters 4, 5, 6 and 8](#) relations 1, 2 and 4 may be formulated mathematically. The method for solving them is not obvious, however. It is necessary to use an iterative procedure. Thus, the value of some variables has to be guessed at the start. Based on these values a solution is obtained, which includes new values of the quantities guessed. These may now be used as a new start and the process is repeated. If the procedure is convergent, the computed values in each iteration get closer and closer to the initial ones, i.e. those obtained in the previous iteration, and when they are close enough the solution is considered converged. Some care is needed in the present case to obtain convergence, but the general sequence of operations is given in [Fig 17.1](#) (overleaf).

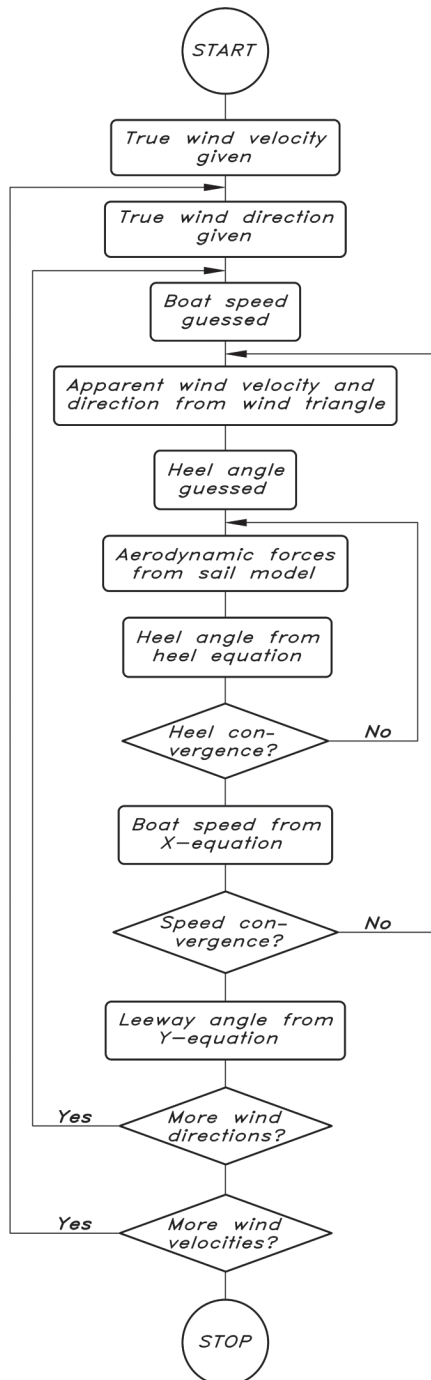
The program moves systematically through a set of given true wind speeds and for each speed a set of given wind directions is considered. These variations correspond to the two outer loops of [Fig 17.1](#). For a given combination of true wind speed and direction the procedure starts with a guess of the boat speed. The apparent wind speed and direction may then be obtained from the wind triangle (see [Fig 5.2](#)). Now the heel angle has to be guessed, and this angle, together with the apparent wind, yield the aerodynamic forces from [Figs 8.19, 8.21 and 8.22](#). The heeling moment may be computed, and the heel angle found from the heel equation (4). If the computed angle is not close enough to the guessed one, the latter is updated and the process repeated with new aerodynamic forces. This is the innermost loop of the diagram. When the heel angle has converged, a speed may be found that gives a resistance which is equal to the known aerodynamic driving force. Equation 1 is thus employed. The guessed speed may now be updated, a new apparent wind computed, etc. This is the outer loop to the right in the figure. Upon convergence of the speed the leeway may be solved from the side force equation (2).

Modern VPPs usually have more than three degrees of freedom and they utilize more efficient iterative techniques than that described above. With more equations to solve the number of iteration loops automatically increases, so efficient solution algorithms are required. A way to do this is to consider the solution an optimization problem. With speed, sinkage, leeway, heel angle, pitch angle and yaw angle as independent variables the optimizer tries to find the combination that satisfies the six equilibrium equations as well as possible, i.e. it tries to reduce the sum of all forces to zero in equations 1–3 and all moments to zero in equations 4–6. Optimizers are available in most programming languages and they utilize very efficient search algorithms.

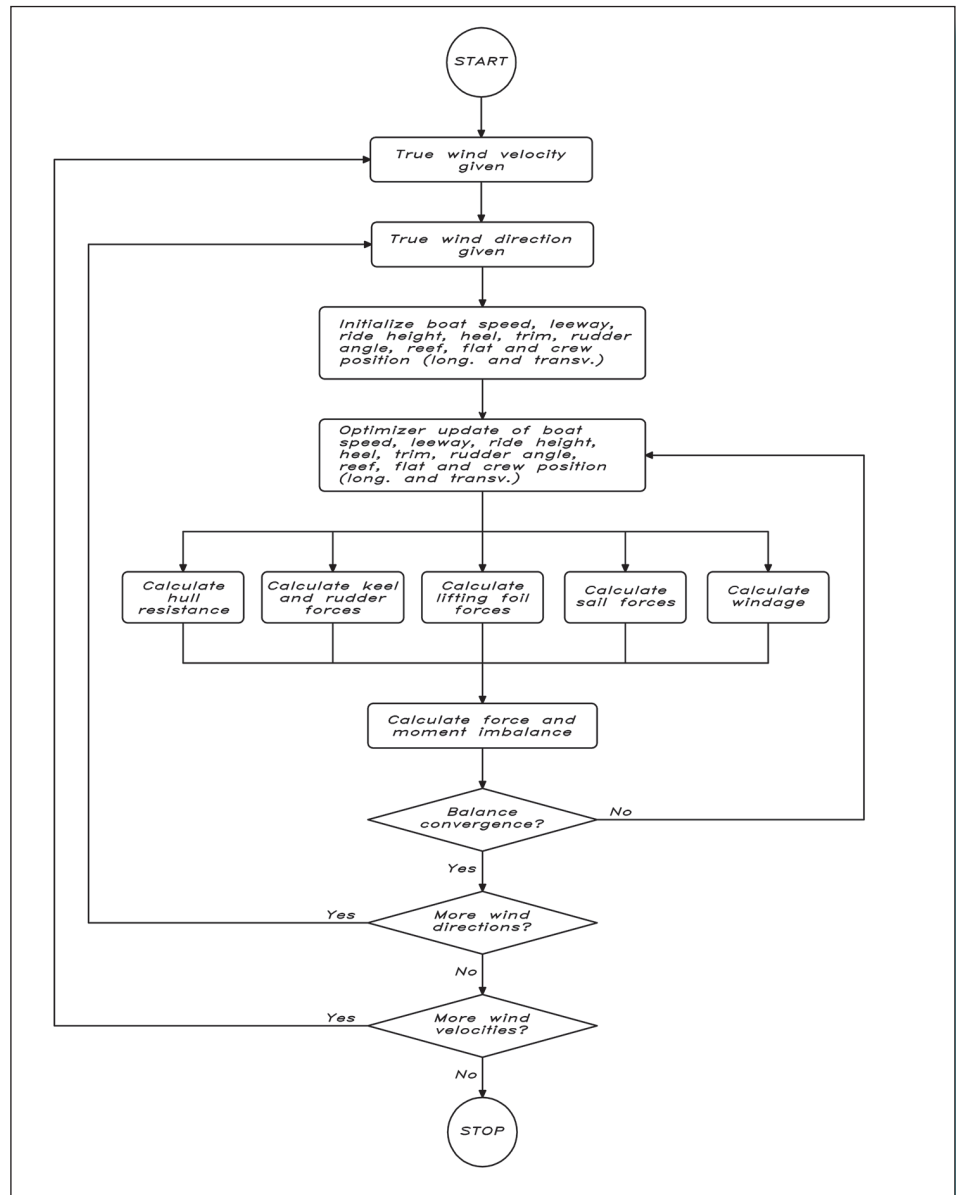
A flow chart for a modern VPP is shown schematically in [Fig 17.2](#) (page 369). This may be used with or without foils. If foils are included, they influence, in principle, all six equilibrium equations, which have to include the resulting forces and moments. As above, there are two loops for wind speed and direction. The optimization starts with a guess of all independent variables, which also include sail trim parameters and crew position. Separate modules then compute hull resistance (if the hull is still in the water), centrefoil and rudder foil forces (if any), keel and rudder forces, sail forces and windage. All forces and moments are inserted in the six equilibrium equations and the net force (equations 1–3) or net moment (equations 4–6) is larger than a specified limit for any equation, the program loops back and changes the independent variables. This continues until all equations have converged within a certain tolerance. Then the



**Fig 17.1** Flow diagram of a basic VPP



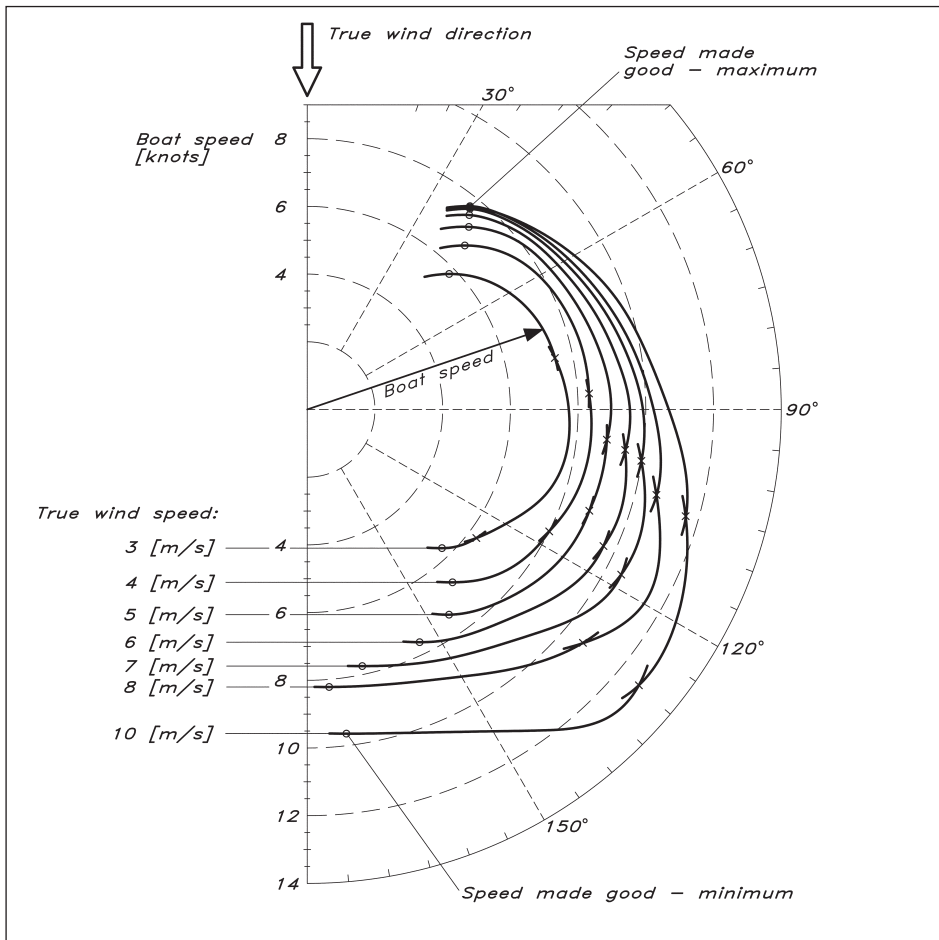
**Fig 17.2** Flow diagram of a modern VPP



program turns to the next wind direction. Note that for foiling boats, the solution is not unique in the hollow of the resistance curve (see Fig 7.1). Two different speeds are possible for a given driving force. This needs to be addressed in the choice of optimiser.

The result of the VPP calculation is often presented in the form of a polar plot. Fig 17.3 shows the VPP results for the YD-41. Each solid line represents the yacht speed at a certain wind velocity, and the speed may be found as the length of an arrow from the centre to the line. The angle between the arrow and the vertical is the true wind angle. Points of special interest are the upper- and lowermost ones of each curve (denoted by black dots), since these represent the best upwind and downwind performance of the yacht. The arrows to these points thus give the optimum pointing

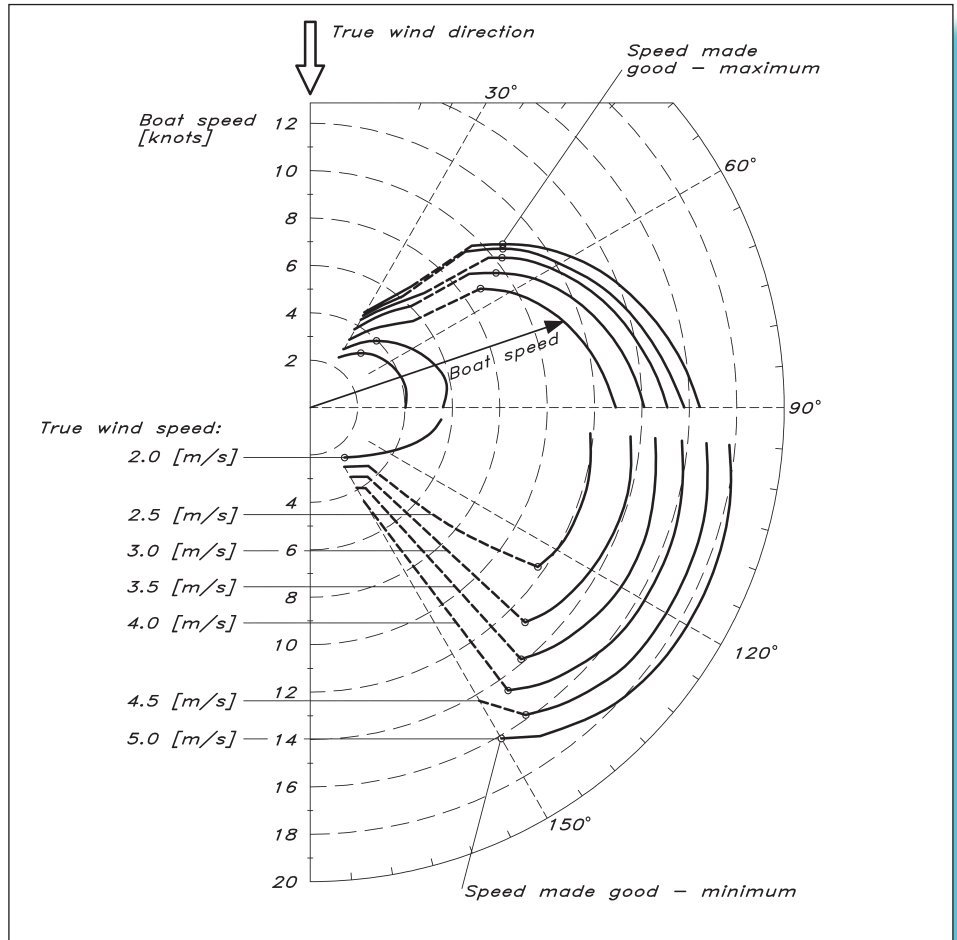
Fig 17.3 Polar plot YD-41



angles upwind and downwind. The latter information is particularly valuable, since it is normally very difficult for the helmsman to find the best course downwind. Note that each line has three segments, representing the different sail settings for upwind, reaching and downwind sailing. The dashed circles in the diagram represent boat speeds. It is seen that the YD-41 can reach speeds of almost 13 knots on a broad reach, 120–130 degrees from the wind. The maximum upwind speed at the optimum beating angle is about 7.5 knots, corresponding to a velocity component straight upwind (VMG) of 6 knots. A picture of the YD-41 on a broad reach is found in Fig 7.19 at the end of this chapter.

In Fig 17.4 the polar plot for the foiling *Linnea*, the example of Chapter 7, is presented. Take-off is indicated by dashed lines. Upwind, the lowest foiling wind speed is 3 m/s, where the boat takes off at 55 degrees of true wind angle. The speed is then about 9 knots and VMG is 5 knots. Downwind the lowest take-off wind speed is 2.5 m/s. The boat is then fully foilborne between 100 and 130 degrees of true wind. Since *Linnea* was designed for very light air the maximum wind speed in the plot is 5 m/s, where the boat speed in most downwind directions is about 18 knots. Note the break in the lines between 90 and 100 degrees, where the gennaker is hoisted.

Fig 17.4 Polar plot, Linnea



A polar plot is of interest not only to the designer, who can evaluate different alternatives rapidly, but also to the racing yachtsman. Apart from the information on the best course to sail, recommendations on the best setting of the sails may be obtained, and a target speed for all possible conditions may be computed. The size of the sail area and the optimum flattening and twist of the sails are normally computed in the program, based on the reefing, flattening and twist functions mentioned in Chapter 8.

Due to its ability to evaluate performance, VPPs are also useful in handicapping rules. The first handicapping system to make use of a VPP was the Measurement Handicapping System (MHS), which was popular in the United States in the 1980s. This system was replaced by the International Measurement System (IMS) in the 1990s and it has now been replaced by the Offshore Racing Congress (ORC) VPP.<sup>1</sup>

Although most VPPs are based on the equilibrium equations 1–6 above, there are programs that do not assume balance in the six degrees of freedom. These are the Dynamic Velocity Prediction Programs (DVPPs). The solution is now time dependent.

<sup>1</sup>The ORC VPP documentation may be found on the link: <https://www.orc.org/rules/ORC%20VPP%20documentation%202019.pdf>

It starts from a given initial state and computes the development of all motions in time. The optimiser is replaced by a routine that steps forward in time. At each time step the net force and moment, respectively, in equations 1–6 are computed. Dividing the force in equations 1–3 by the total mass of the yacht, the acceleration in each direction is obtained. Equations 4–6 give the angular acceleration dividing the net moment by the appropriate mass moment of inertia (see Fig 5.24 for a definition). Multiplying the accelerations by the time step, the change in velocity from the previous step is found and the solution may proceed to the next time step.

When the boat accelerates in any of the six degrees of freedom it causes the surrounding fluid (water and air) to accelerate as well. This gives rise to extra forces and moments compared to the equilibrium case. These forces and moments are considered by including an added mass from the fluid in the equations. The motions are also influenced by damping forces. Added mass and damping must therefore be considered in the DVPPs, but they are out of scope of the present book. The interested reader is referred to the references.

One of the authors was engaged in the development of a DVPP in the 1980s, and the program was the basis for a sailing yacht simulator; see Larsson (1990). A more detailed description of the method may be found in Ottosson *et al* (2002). For a modern 6 DOF DVPP for offshore racing yachts in waves, see Kerdraon *et al* (2019) and for foiling dinghies, see Eggert *et al* (2020). The presently most advanced DVPP, including foiling, is GOMBOC,<sup>2</sup> developed by Dan Bernasconi and used by the New Zealand America's Cup team since 2010.

As mentioned above, most standard VPPs use empirical relations like those presented in Chapters 4–8, to compute the required forces and moments. However, for more accurate predictions CFD (see below) is used. Then, systematic CFD calculations are carried out beforehand, where the independent variables: speed, leeway, heel, etc., are systematically varied and the corresponding forces computed. Results are stored in large matrices in which interpolation is carried out in the VPP. The most accurate VPP approach is, however, to use CFD for the entire VPP calculation. Then the forces, moments and all motions are computed within the CFD code. An early method of this kind was presented by Lindstand Levin and Larsson (2017) and this was further refined by Persson *et al* (2020). Recently, this method was extended to include incoming waves from any direction (Persson *et al*, not yet reported).

## ■ TOWING TANK TESTING

There are principally two different techniques for testing sailing yachts in towing tanks. The apparently most natural way is to tow the yacht at the correct centre of effort of the sails and, by means of an active rudder, let it attain its equilibrium heel and yaw angles. Each measured point in such a test represents a realistic sailing condition, so the number of test points may be kept to a minimum.

---

<sup>2</sup><http://sumtozero.com/products/gomboc-designer/>





**Fig 17.5** IACC hull under test at SSPA in Gothenburg (Photo: SSPA)

In the other technique the hull is kept fixed in all degrees of freedom, except heave (vertical motion) and pitch (rotation around a transverse axis), and the towing force, side force and their moments are registered for systematically varied speeds, heel angles and yaw angles. To evaluate such a test a special VPP is required. Rather than using the empirical formulae of the standard VPP, the measured forces and moments are introduced into the program. In this way, the evaluation will be specialized for the hull in question and the results may be expected to be more exact.

The first technique is called free-sailing and the second one semi-captive. Obviously, more test points are required in the latter, but the equipment required is less complicated and the results are independent of the stability of the model, since the heel is fixed. Different stabilities may be evaluated in the VPP. The free-sailing technique also calls for more expensive models, since a lead keel is required and the vertical centre of gravity has to be correct. At present, the semi-captive technique is by far the most common one in towing tanks all over the world.

A typical piece of semi-captive equipment is seen in [Fig 17.5](#), where an IACC yacht tested at SSPA in Gothenburg is shown. The forces and moments are measured through three posts, which fix the hull in the four degrees of freedom. Since these are vertical and attached to the hull below deck level, two corrections have to be made. The missing pitching moment caused by the distance between the sail centre of effort and the attachment point has to be compensated by moving weights onboard the model. Also, the downward component of the sail force, which is missing in the test, has to be simulated by additional weights onboard.

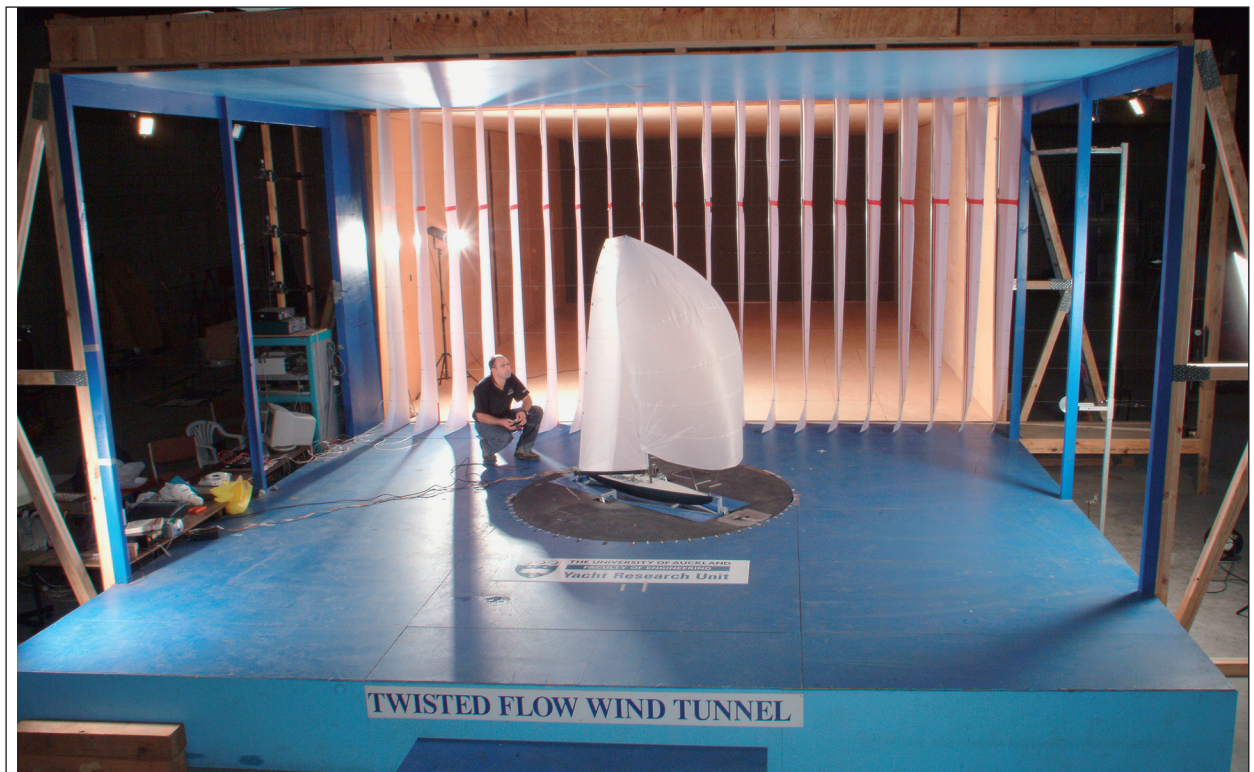
## ■ WIND TUNNEL TESTING

Wind tunnels may be used for different purposes in connection with yacht design. An obvious use is to measure aerodynamic forces on the sail and rig, but it may also be used for investigations of hydrodynamic quantities if the water surface effect can be neglected. Very often, keels are developed in wind tunnels, see for instance the America's Cup keel tests by Werner *et al* (2006), and the investigation of bulb keels, Ljungqvist *et al* (2018). Air can thus be used for hydrodynamic investigations; the only differences are the physical constants  $\nu$  (kinematic viscosity) and  $\rho$  (density), so results can easily be converted from one medium to the other.

The most advanced wind tunnel in the world for sail testing was the one at the Yacht Research Unit of the University of Auckland. A picture of the tunnel is seen in Fig 17.6. Unfortunately this tunnel is no longer in operation. It was the open type, where air blows from a nozzle into the surrounding still air. In closed tunnels the air moves in a closed loop, where the tests are carried out in a narrow part of the ducting system. Such a tunnel, also used for sail testing, is that at Politecnico di Milano.

Fig 17.5 shows a hull with sails in the Auckland tunnel. The most significant feature of the tunnel was the vertical white vanes spanning the height of the nozzle. As can be seen in the picture these were twisted in such a way that the flow close to the bottom was turned to the right when exiting the nozzle. This is to simulate the profile of the apparent wind experienced by a moving yacht. Referring to Fig 5.2, the apparent wind is composed of the true wind and the wind felt onboard the yacht when moving through still air. The

.....  
**Fig 17.6** Twisted Flow Wind Tunnel (TFWT) at the University of Auckland (Photo: Birgit Utech)





latter component is obviously the same at all heights above the water, while the true wind speed varies with height in the atmospheric boundary layer. This means that the resulting flow is directed more along the hull close to the water than further up. The vanes thus create the appropriate twisting of the flow, while obstacles further upstream create the vertical variation of the wind speed.

The model with its sails was mounted on a balance, which was connected to a computer with a real-time VPP. Based on the measured aerodynamic forces the heel angle was computed and adjusted automatically. Electrical winches were used to remotely sheet the sails and the optimum trim of the sails could be obtained by maximizing the speed computed by the VPP. The flying shape of the sails was recorded by a special photographic technique. More information about this tunnel can be found in Le Pelley and Richards (2011). It is a pity it is no longer in use.

## ■ COMPUTATIONAL FLUID DYNAMICS (CFD)

There are two main types of numerical methods for flow analysis in naval architecture. In the simplest approach, based on potential flow theory, the viscosity of the water is neglected. This enables calculations of the wave resistance, as well as the induced resistance and the side force, to be carried out rapidly without too much computer power. No quantities related to friction can be obtained, however.

In the second type, where viscosity is considered, some approximation of the fundamental equations of fluid mechanics, the Navier-Stokes equations, is used. As explained in [Chapter 5](#), the boundary layer is the thin region of water surrounding the hull, where the velocity relative to the hull changes from zero on the surface to approximately the yacht speed at the outer edge. By assuming that this layer is thin relative to the hull length the Navier-Stokes equations can be much simplified and the boundary layer equations obtained. However, this assumption breaks down under certain circumstances, such as in the hull/keel or keel/bulb junction. For most ships the boundary layer assumption breaks down also in the stern region, but yachts are normally sufficiently slender for the theory to hold all the way to the stern. Using boundary layer theory, the frictional resistance (including roughness effects) may be computed. The potential flow/boundary layer approximation is used also in aerodynamics, and the foil analysis tool XFOIL, referred to in [Chapters 6 and 7](#), is based on this technique.

More general viscous flow computations can be carried out using less approximate simplifications of the Navier-Stokes equations. The most widely used technique solves these equations for the mean flow, but not for the turbulence, which is considered through an empirical model. These methods are known as Reynolds-averaged Navier Stokes (RANS) methods. More computer demanding are the Large Eddy Simulation (LES) methods, where the largest eddies of the turbulence are computed and only the smaller eddies modelled empirically. There are also combinations of these two methods. Collectively, the RANS and LES methods are referred to as computational fluid dynamics (CFD). For a general introduction to numerical methods in hydrodynamics, see Larsson and Raven (2010).

CFD methods are rapidly becoming popular in general hydrodynamics and not least in yacht design. For general state-of-the-art reviews, see Larsson *et al* (2013) and Hino *et al* (2020). Using CFD the flow around the hull and all its resistance components may be computed. The disadvantage is the large computational effort required. By the time this edition of this book is published (2022) a simple boundary layer computation takes a few seconds on a desktop computer, while the potential flow methods take a few minutes. RANS methods are mostly run on multicore processors, but they still require several hours for a solution. If the detailed structures of the flow are of interest LES methods are superior, but the computer demands are excessive, in the region of 1000 times that of RANS methods, so they are seldom used in yacht design. In Table 17.1 the capabilities of the different types of methods are summarized, referring to the resistance components presented in Fig 5.4.

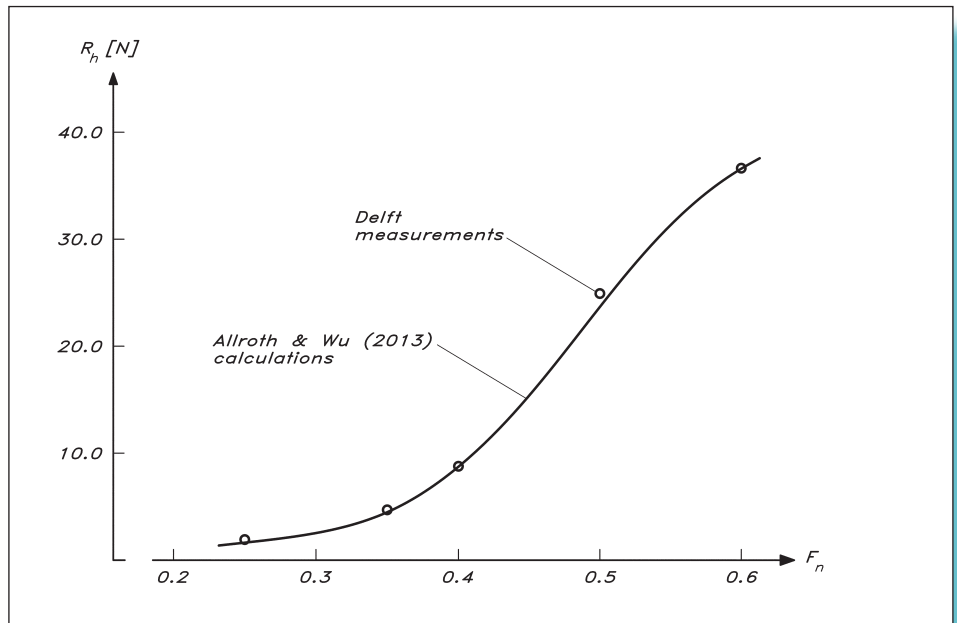
Table 17.1 Summary of CFD capabilities			
	Inviscid methods (Potential flow)	Viscous methods	
		Boundary layer	RANS (LES)
Friction	–	+	+
Roughness effects	–	+	+
Viscous pressure resistance	–	–	+
Wave resistance	+	–	+
Heel resistance	n/a*	n/a*	n/a*
Induced resistance	+	–	+
Added resistance in waves	+	–	+
Side force	+	–	+
Pressure distribution	+	–	+
Velocity distribution	Outside boundary layer	In boundary layer	+

\*Computations may be carried out in the heeled condition; hence no separate heel resistance component

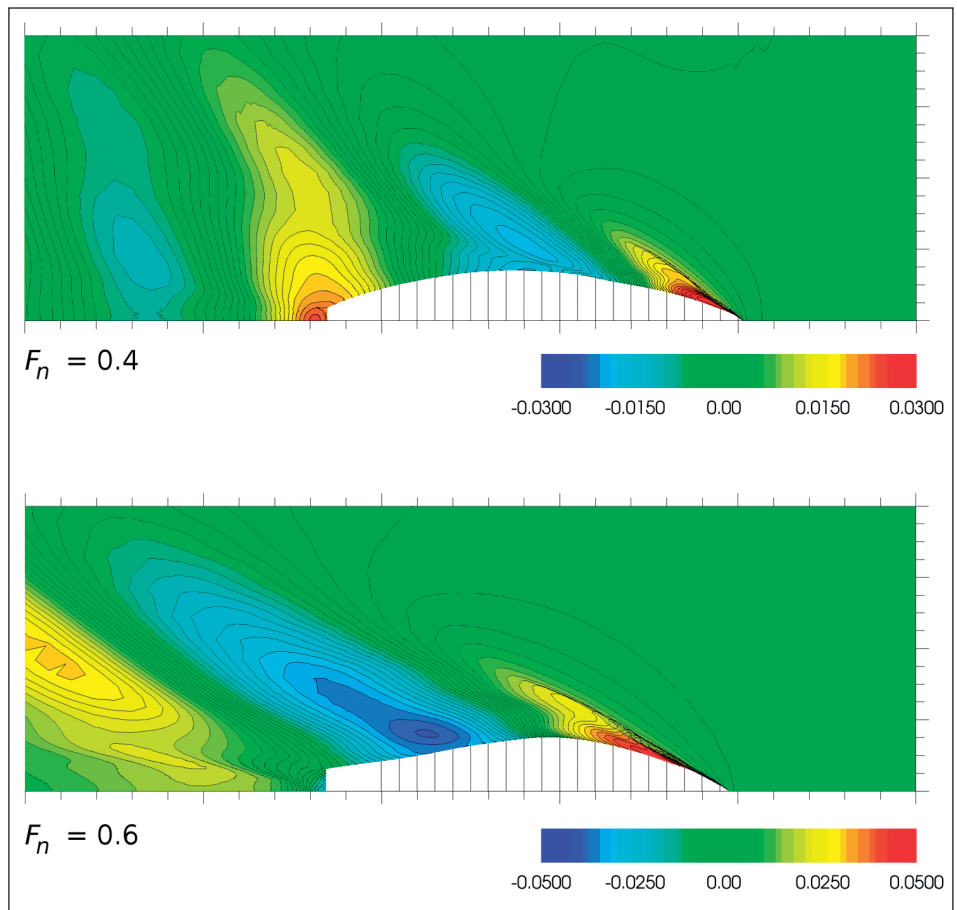
As seen in the table, almost all resistance components may be obtained from a combined potential flow/boundary layer computation. Then the potential flow is the first computed for the whole flow field, neglecting the boundary layer. Thereafter, the pressure distribution on the body is used for computing the boundary layer. Unfortunately, the viscous pressure resistance cannot be obtained in this way, unless there is a feedback from the boundary layer solution to the potential flow. However, this is complicated, and very seldom done. Also, the accuracy of the computed resistance components is generally lower for this approach than for the RANS computations. Therefore, the latter are gradually taking over from the simpler methods.

Even though a RANS computation takes considerable computer effort, it is considerably faster and cheaper than the towing tank. Another advantage is that very detailed information may be obtained on the flow everywhere around the hull. Wave

**Fig 17.7** Validation of resistance predictions for the Delft model #46



**Fig 17.8** Wave pattern of the Delft model #46 at two Froude numbers



patterns, pressure distributions, streamlines and velocity vectors are normally produced by the CFD programs, and especially interesting regions may be zoomed in on. This detailed information may guide the designer in the search for the best solution. To obtain all this information from the tank would be extremely expensive. CFD is also well suited for formal optimization, where the CFD code is linked to a CAD module and an 'optimiser' that automatically searches for an optimum solution under given constraints. For an example, see the bulbous keel optimization by Ljungqvist *et al* (2018).

SHIPFLOW is a CFD software developed especially for hydrodynamic problems by two of the authors and their co-workers. It includes all three methods in Table 16.1 (not LES). Although its major use is in ship design, the code has also been used for several yacht projects, not least in the development of the new YD-41. In the following discussion we will present some examples from SHIPFLOW computations.

First, a validation of the RANS code against measurements for one of the hulls in the Delft Series will be reported. This was part of an MSc thesis project carried out by Allroth and Wu (see Allroth *et al*, 2015) aiming at an optimization of the transom size and shape for sailing yachts at different Froude numbers. Upright results for hull #46 (canoe body) are seen in Fig 17.7. The resistance is given versus Froude number for the 1.71 m  $L_{WL}$  model. Good correspondence between computations and measurements is noted. There is a very elaborate process for formally validating a CFD computation against measured data (see for instance Zou and Larsson, 2013), but in the present context the apparently good correspondence will suffice. In Fig 17.8 the predicted wave pattern around the hull is seen for two Froude numbers, 0.4 and 0.6. The port half of the hull is shown in white with the bow to the right. Waves are represented by flooded contours, where red means a wave crest and blue means a wave trough. The numbers in the legend give the wave height divided by  $L_{WL}$ . At 0.4 the wavelength should be equal to the hull length (see Fig 5.15), and this is clearly borne out in Fig 17.8 (top). There is a large wave crest at both ends of the hull and a deep wave trough at midship. At 0.6 the wavelength is considerably larger than the hull, as can be seen in Fig 17.8 (bottom), where the second wave crest is now behind the hull and the wave trough on the afterbody. Note that the hull looks different in the two plots, since the sinkage, trim and wave profile along the hull are different. It is the hull up to the wave along the hull that is shown.

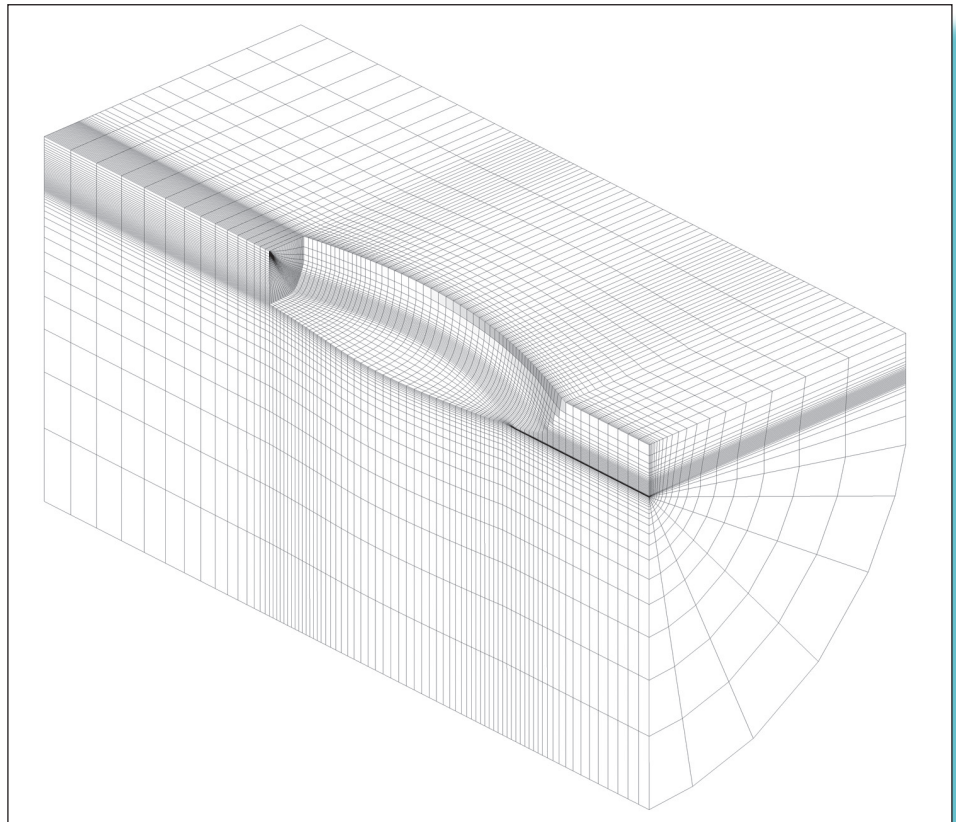
In all methods in Table 17.1 the relevant equations have to be discretized. For RANS this means that the computational domain is divided into cells. Rather than solving for a continuous variation of the variables (velocity components, pressure and some turbulence quantities) in the whole domain, there is now one value of each variable in each cell. If there are few cells the real (continuous) distribution is badly represented and the solution less accurate. However, as the number of cells increases, the accuracy improves. In principle, there is a minimum number of cells for a given accuracy, but the problem is complicated by the fact that the accuracy also depends on the 'quality' of the cells, as well as of the numerical method used. It would lead too far to go into more detail here, but the interested reader may find an introduction to RANS methods in Larsson and Raven (2010).

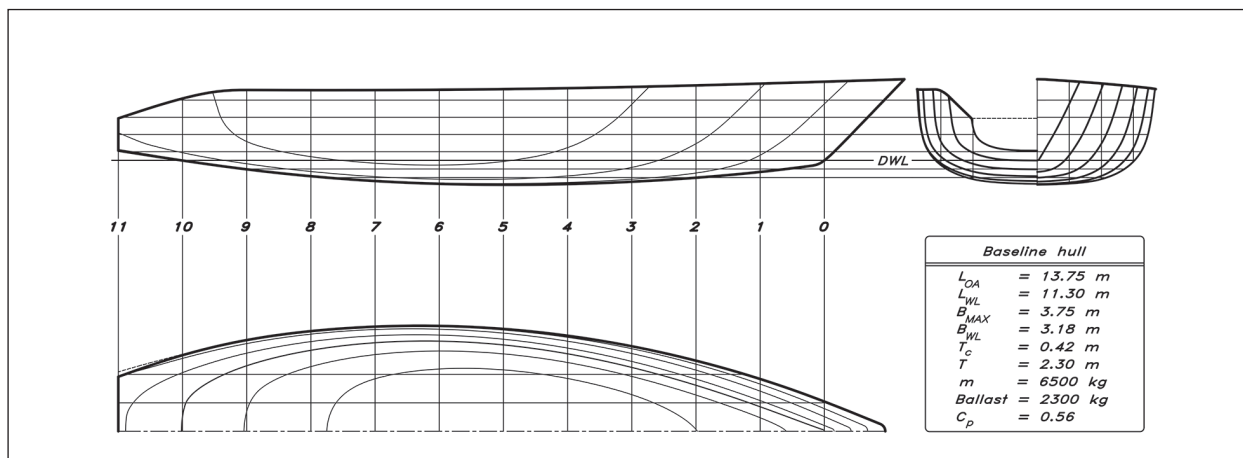
All the cells in the computational domain are collectively referred to as the *grid*, where the grid points represent corners in the cells. In the computations of Fig 17.7 and 17.8 a grid of 3.3 million cells was used. This is shown in Fig 17.9 where it has been coarsened

for clarity. The grid contains two blocks: one surrounding the hull, and one (denser) behind the transom to the left. Since the hull is symmetric, computations are carried out only for the port side. Note that the grid is extended upwards above the free surface level. The flow is computed both in the water and in the air just above the free surface. The density of the grid points increases towards the hull and around the horizontal level where the free surface is located. To obtain reasonable accuracy in RANS computations for hydrodynamic problems, the number of cells needs to be of the order of a few million (see Larsson *et al*, 2013 or Hino *et al*, 2020). Traditionally, the generation of a good grid has been an art that has required much experience, but modern computational methods can guide the user rather well in the grid generation process.

The second computation to be presented was initially carried out, when developing the YD-41, to look at possible gains with a new design compared to a more traditional one. For this purpose the YD-40 example used in previous editions of this book was scaled to similar dimensions as the YD-41, i.e. to the same displacement, beam of waterline and ‘dynamic’ length of waterline. By dynamic  $L_{WL}$  we mean the length from FP to the aft end of the transom. Since the overhang is quite different in the two designs, this was considered the fairest comparison. In Fig 17.10 (overleaf) the scaled YD-40 (‘Baseline hull’) is shown. It should be compared with the YD-41 in Fig 3.5. The upright canoe body resistance curves from RANS computations in SHIPFLOW are presented in Fig 17.11 (overleaf). It can be seen that there is a considerable reduction in total

**Fig 17.9** Grid used in the computations of Figs 17.7 and 17.8





resistance for the YD-41, starting at around 7 knots, reaching about 15% at the highest speeds. Apparently, this must be due to a wave resistance reduction, and this is confirmed in Figs 17.12 and 17.13. The former shows the predicted wave patterns for the Baseline hull (top half) and the YD-41 at a Froude number of 0.5. The wave crests are lower and the wave troughs shallower for the YD-41. A more quantitative comparison is shown in Fig 17.13, where the wave contour along the hull is presented for the two hulls. The hull is located between 0.0 and 1.0 on the horizontal scale. In front of, and behind the hull, the contour is shown at the centre plane.

An alternative computation of the upright resistance, using the potential flow and boundary layer methods in SHIPFLOW, is presented in Fig 17.14. A similar difference between the hulls is noted for this more approximate technique, although the absolute values are somewhat smaller. This is to be expected, since the viscous pressure resistance is

Fig 17.10 Baseline hull (scaled YD-40)

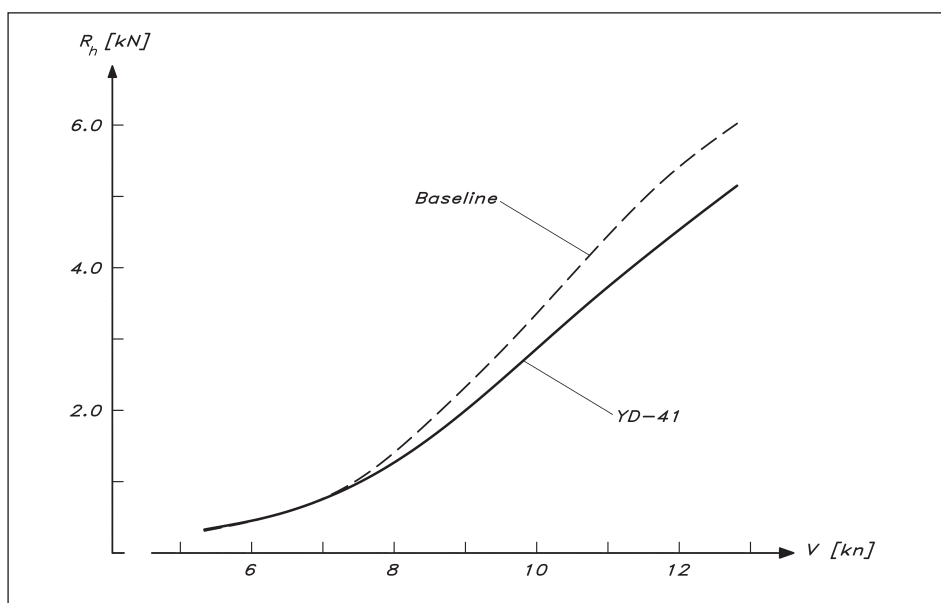
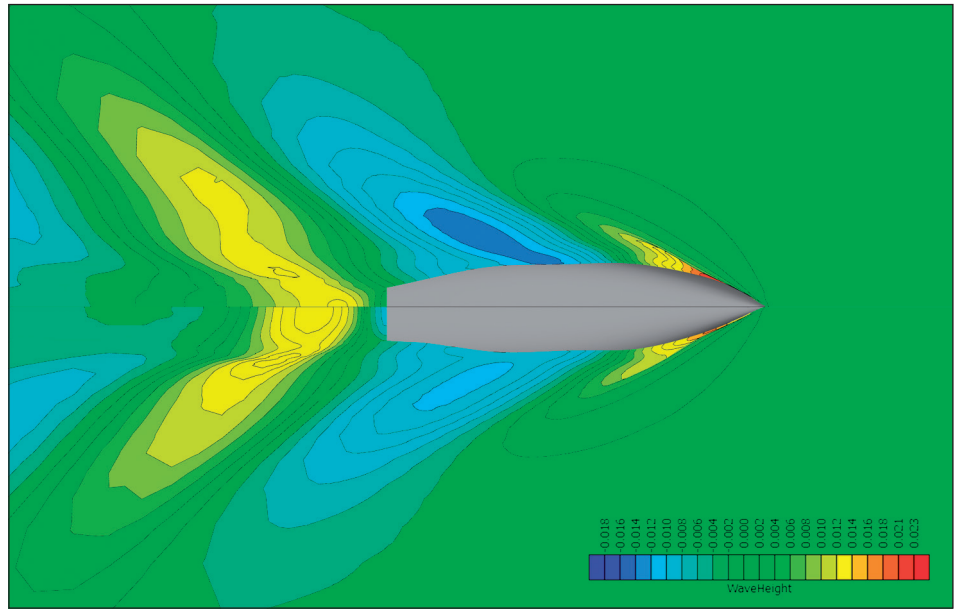
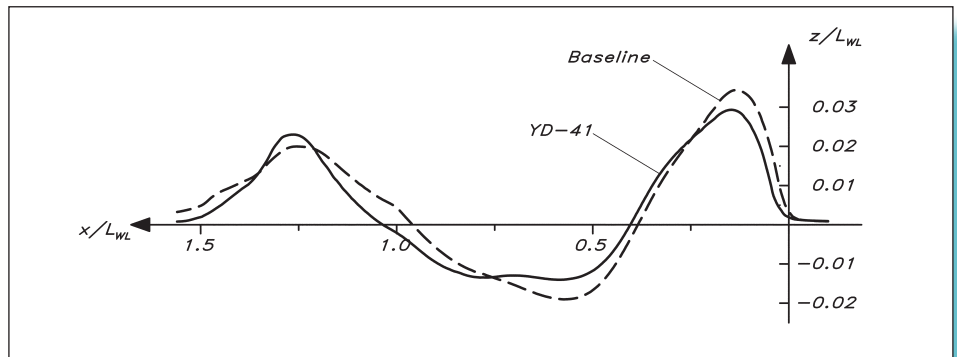


Fig 17.11 Resistance of the Baseline hull and the YD-41 predicted using a RANS method

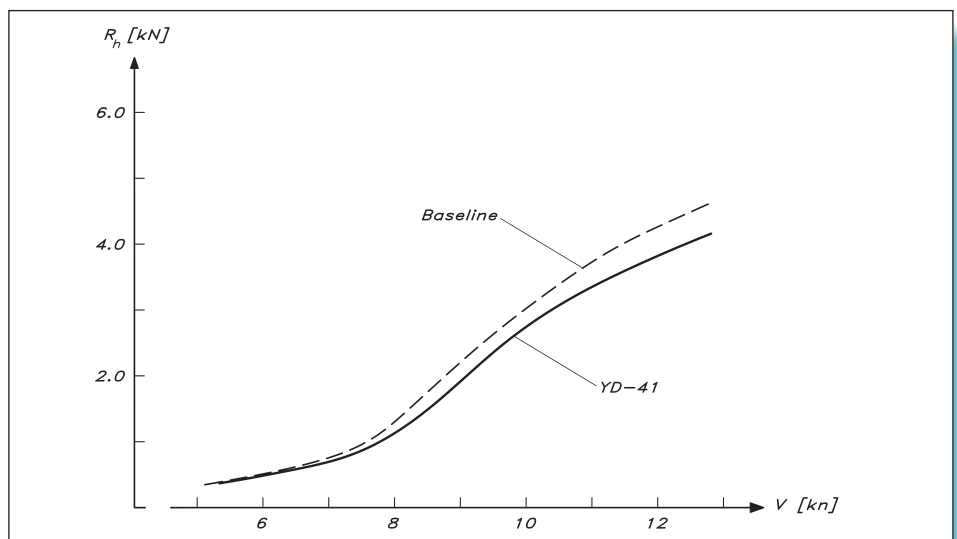
**Fig 17.12** Wave pattern of the Baseline hull (upper half) and the YD-41 (lower half). RANS method



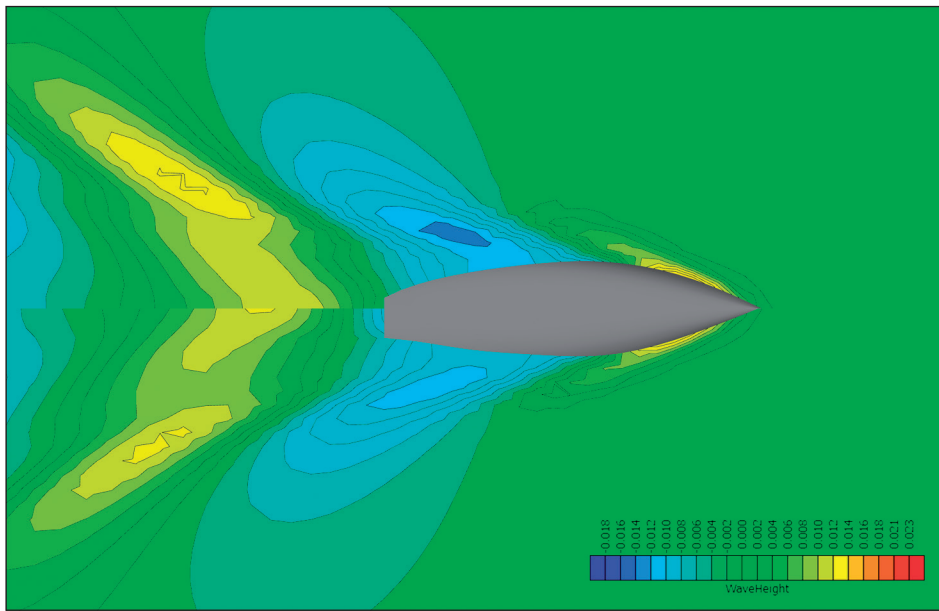
**Fig 17.13** Wave contour along the hull of the Baseline hull and the YD-41. RANS method



**Fig 17.14** Resistance of the Baseline hull and the YD-41 predicted using potential flow and boundary layer methods



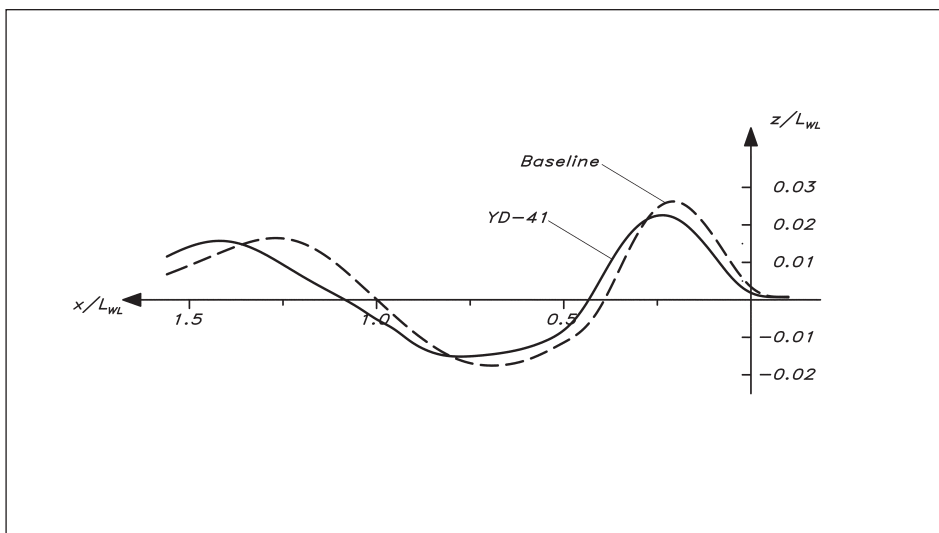




**Fig 17.15** Wave pattern of the Baseline hull (upper half) and the YD-41 (lower half). Potential flow method

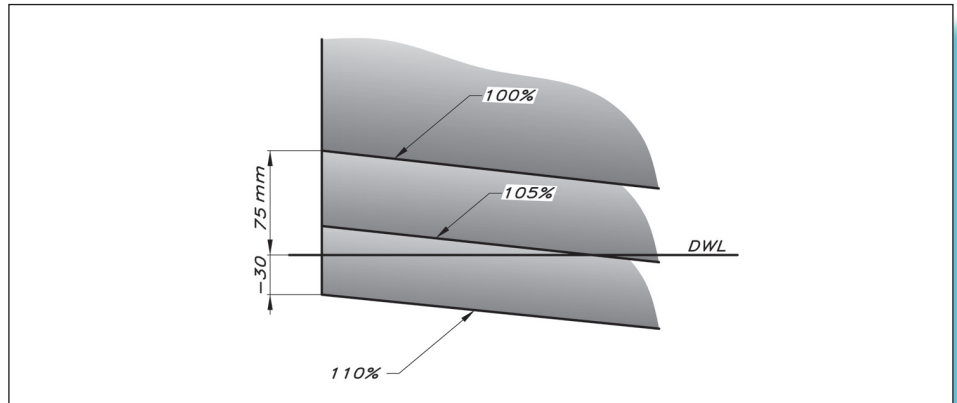
not taken into account this way, as explained above. Figs 17.15 and 17.16 correspond to Figs 17.12 and 17.13, but here the results were obtained using the potential flow method. The same conclusions may be drawn.

The third CFD computation to present is a preliminary investigation of the effect of the overhang height on the total canoe body resistance upright. An early version of the YD-41 was used, and to change the overhang the hull was stretched a certain percentage all the way from the bow but cut off at the same distance from the bow. Depending on the stretching the stern contour changed as shown in Fig 17.17. Note that the displacement of the hull was kept constant by adjusting the sinkage. The original hull had the transom 75 mm above the (zero speed) water level, while hull stretched to 110%

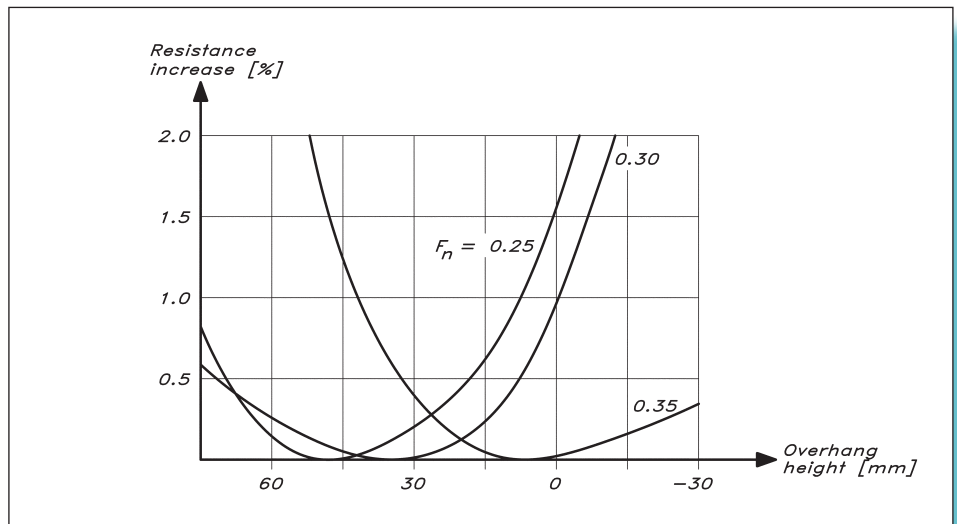


**Fig 17.16** Wave contour along the hull of the Baseline hull and the YD-41. Potential flow method

**Fig 17.17** Different sterns in the overhang height investigation



**Fig 17.18** Increase in upright hull resistance for different overhang heights



had the transom submerged 30 mm. In Fig 17.18 some quite interesting results are shown. The figure shows the increase in resistance relative to the minimum resistance for three Froude numbers, 0.25, 0.30 and 0.35, and different overhang heights (caused by the stretching). For the three Froude numbers, the minimum occurs for 50 mm, 35 mm and 5 mm, respectively. The higher the speed, the smaller the overhang height, which is in line with experience from power-boat design (Larsson and Raven, 2010). See also Orych and Larsson (2015) and Allroth *et al* (2015) for systematic CFD studies of the effect of transom size.

The three examples show the power of the CFD technique, which has developed rapidly over the past 30 years. It is not yet as common as the finite element analysis in structural mechanics, but the methods have matured considerably during the past few years (Larsson *et al*, 2013, Hino *et al*, 2020) and the user-friendliness has improved dramatically. There is no doubt that it will become a very useful tool for the common yacht designer within the not-too-distant future.



**Fig 17.19** The YD-41 on a broad reach (Photo: Michal Korol)

# APPENDIX 1

## Main particulars of the YD-41

Refer to List of Symbols on [page 6](#).

LCB and LCF are measured from midship, positive forwards, and are given in percent of the waterline length.

		Half-loaded displacement	Light displacement
$L_{OA}$	=	12.50 m	12.50 m
$L_{WL}$	=	11.90 m	11.62 m
$B_{MAX}$	=	4.20 m	4.20 m
$B_{WL}$	=	3.18 m	3.12 m
$T_C$	=	0.40 m	0.38 m
$T$	=	2.30 m	2.28 m
$\nabla_C$	=	6.05 m <sup>3</sup>	5.46 m <sup>3</sup>
$m_C$	=	6200 kg	5600 kg
$S_{WC}$	=	28.20 m <sup>2</sup>	26.92 m <sup>2</sup>
$S_W$	=	34.97 m <sup>2</sup>	33.64 m <sup>2</sup>
$A_W$	=	26.75 m <sup>2</sup>	25.64 m <sup>2</sup>
$m$	=	6500 kg	5900 kg
$Blst$	=	2300 kg	2300 kg
$l$	=	16.2 m	16.2 m
$J$	=	5.1 m	5.1 m
$P$	=	16.7 m	16.7 m
$E$	=	5.6 m	5.6 m
$ASL$	=	18.0 m	18.0 m
$SMW$	=	10.7 m	10.7 m
$SAF$	=	41.3 m <sup>2</sup>	41.3 m <sup>2</sup>
$SAM$	=	46.8 m <sup>2</sup>	46.8 m <sup>2</sup>
$SA$	=	88.1 m <sup>2</sup>	88.1 m <sup>2</sup>

		Half-loaded displacement	Light displacement
$C_{ku}$	=	1.00 m	1.00 m
$C_{kl}$	=	0.78 m	0.78 m
$T_k$	=	1.90 m	1.90 m
$C_{ru}$	=	0.48 m	0.48 m
$C_{rl}$	=	0.22 m	0.22 m
$T_r$	=	1.15 m	1.15 m
$\Lambda_k$	=	5.5°	5.5°
$\Lambda_r$	=	10.0°	10.0°
LCB	=	-4.2%	-4.5%
LCF	=	-7.3%	-7.3%
$C_P$	=	0.56	0.56
$C_{Mc}$	=	0.715	0.715
$SA/S_W$	=	2.52	2.62
$SA/\nabla^{2/3}$	=	25.7	27.4
$L_{OA}/B$	=	2.98	2.98
$L_{WL}/T$	=	5.17	5.10
$L_{WL}/T_C$	=	29.75	30.58
$L_{WL}/\nabla^{1/3}$	=	6.43	6.48
$L_{OA}/L_{WL}$	=	1.05	1.07
$F_f/L_{WL}$	=	0.121	0.123
$F_f/F_a$	=	1.23	1.23
$Blst\ Rto$	=	0.35	0.39

# APPENDIX 2

## Weight calculation

The mass of the different weights onboard the hull are given in kilograms and distances in metres.

LCG is measured from the forward end of the waterline and positive in the aft direction, denoted 'a' in the table, with negative values forward of the waterline, 'f'.

TCG is measured from the centreline with positive values to starboard, denoted 's' in the table and negative to port, 'p'.

VCG is measured from the waterline with positive values above and negative values below the waterline.

Group 1 <b>Structure</b>				
<i>Item name</i>	<i>Mass</i>	<i>LCG</i>	<i>TCG</i>	<i>VCG</i>
Hull gelcoat	52.6	6.40a	0.00	0.22
Hull GRP	488.1	6.30a	0.00	0.17
Hull sandwich core	115.0	6.40a	0.00	0.12
Hull sandwich adhesive	75.2	6.40a	0.00	0.25
Keel strake extra	32.9	2.60a	0.00	0.04
Keel area	91.8	5.90a	0.00	-0.40
Deck flange extra	36.7	6.60a	0.00	1.11
Deck gelcoat	43.2	7.50a	0.00	1.25
Deck GRP	303.3	7.50a	0.00	1.25
Deck sandwich core	30.5	7.50a	0.00	1.25
Deck sandwich adhesive	22.2	7.50a	0.00	1.25
Bilge stringer	95.2	5.40a	0.00	0.12
Bottom stringer	78.2	6.40a	0.00	-0.20
Mast step	24.0	3.80a	0.00	-0.40
Floors	57.6	6.20a	0.00	-0.26
Stiffeners adhesive	11.5	6.20a	0.00	-0.07
Engine bed	50.0	8.10a	0.00	-0.25
#1 bulkhead	15.4	1.50a	0.00	0.70
#2 bulkhead	33.5	4.20a	0.00	0.63
#3 bulkhead	24.6	6.30a	0.00	0.45
#4 bulkhead	31.6	7.73a	0.00	0.62
#5 bulkhead	28.7	9.00a	0.00	0.47
#6 bulkhead	21.6	11.10a	0.00	0.50
Bulkhead taping	48.6	6.70a	0.00	0.60
Floors extra taping	12.6	6.10a	0.00	-0.32
Misc	50.0	4.80a	0.00	0.40
<b>Group total</b>	<b>1874.6</b>	<b>6.48a</b>	<b>0.00</b>	<b>0.38</b>



Group 2 <b>Forepeak</b>				
<i>Item name</i>	<i>Mass</i>	<i>LCG</i>	<i>TCG</i>	<i>VCG</i>
Sole	5.2	0.90a	0.00	0.67
Shelf	6.0	0.90a	0.00	1.28
Anchor support	7.0	0.65a	0.00	1.00
Chainlocker	8.0	1.20a	0.00	0.65
Misc	3.0	0.80a	0.00	1.20
<b>Group total</b>	<b>29.2</b>	<b>0.91a</b>	<b>0.00</b>	<b>0.92</b>

Group 3 <b>Forward cabin</b>				
<i>Item name</i>	<i>Mass</i>	<i>LCG</i>	<i>TCG</i>	<i>VCG</i>
Berth top and framing	26.0	2.60a	0.00	0.20
Berth front	6.5	3.50a	0.00	0.00
Shelf front	3.4	2.50a	0.00	0.66
Hanging locker	10.6	3.70a	0.75s	0.65
Seat	3.4	3.80a	0.68p	-0.04
Locker	10.0	3.70a	1.10p	0.65
Sole	6.1	3.90a	0.00	-0.22
Berth cushion	12.9	2.60a	0.00	0.25
Seat cushion	1.2	3.80a	0.68p	0.06
Roof liner	5.0	2.90a	0.00	1.38
Side liner	5.0	2.85a	0.00	0.77
Saloon door	6.0	4.20a	0.28s	0.65
Misc	12.0	3.80a	0.00	0.50
<b>Group total</b>	<b>108.1</b>	<b>3.23a</b>	<b>0.04p</b>	<b>0.40</b>

Group 4 <b>Saloon</b>				
<i>Item name</i>	<i>Mass</i>	<i>LCG</i>	<i>TCG</i>	<i>VCG</i>
Port & stbd settee tops & fronts	25.0	5.20a	0.00	0.06
Port & stbd backrests	8.8	5.20a	0.00	0.40
Jib track reinforcement	14.0	5.25a	0.00	0.53
Bookshelves & lockers	20.0	5.20a	0.00	0.96
Table	14.0	5.30a	0.10p	0.40
Sole	25.9	5.20a	0.00	-0.25
Roof liner	8.5	5.20a	0.00	1.60
Side liner	8.0	5.20a	0.00	0.70
Port & stbd cushion	20.0	5.20a	0.00	0.15
Misc	15.0	5.30a	0.00	0.26
<b>Group total</b>	<b>159.2</b>	<b>5.22a</b>	<b>0.01p</b>	<b>0.36</b>

Group 5 Nav station				
<i>Item name</i>	<i>Mass</i>	<i>LCG</i>	<i>TCG</i>	<i>VCG</i>
Nav table top	9.5	6.80a	1.38s	0.66
Nav table fronts	10.0	6.85a	1.35s	0.47
Nav table seat	5.0	7.40a	1.10s	0.05
Nav table shelves	6.8	6.90a	1.70s	0.98
Nav table electr panel	4.0	7.50a	1.66s	1.10
Sole	20.3	6.93a	0.50s	−0.24
Roof liner	3.0	7.05a	1.10s	1.50
Side liner	2.0	7.05a	1.75s	1.00
Cushion	2.0	7.45a	1.25s	0.17
Misc	7.0	6.90a	1.50s	0.50
<b>Group total</b>	<b>69.6</b>	<b>6.98a</b>	<b>1.15s</b>	<b>0.40</b>

Group 6 Galley				
<i>Item name</i>	<i>Mass</i>	<i>LCG</i>	<i>TCG</i>	<i>VCG</i>
Counter tops	10.2	6.90a	1.40p	0.66
Counter fronts & shelves	12.0	7.00a	1.10p	0.20
Side locker	6.0	7.00a	1.75p	0.97
Drawers	7.0	7.50a	1.44p	0.25
Icebox liner & insulation	10.0	6.50a	1.40p	0.30
Sinks	3.0	6.50a	0.75p	0.55
Taps & plumbing	10.0	6.60a	0.80p	−0.05
Stove	22.0	7.03a	1.45p	0.46
Sole	16.9	7.10a	0.53p	−0.24
Roof lining	3.0	7.05a	1.10p	1.50
Side lining	2.0	7.05a	1.90p	1.00
Misc	10.0	7.30a	1.00p	0.45
<b>Group total</b>	<b>112.0</b>	<b>6.98a</b>	<b>1.16p</b>	<b>0.34</b>

Group 7 Head				
<i>Item name</i>	<i>Mass</i>	<i>LCG</i>	<i>TCG</i>	<i>VCG</i>
Wash basin countertop	6.2	8.40a	1.55s	0.66
Wash basin counterfront & shelf	6.0	8.40a	1.15s	0.25
Side locker	6.0	8.40a	1.61s	0.94
Door	6.0	7.72a	0.61s	0.72
Side bulkhead	12.3	8.30a	0.36s	0.64
WC base	5.0	8.70a	0.65s	−0.10
Wash basin & plumbing	5.0	8.30a	1.38s	0.30
WC & plumbing	15.0	8.80a	0.74s	0.10
Sole	8.0	8.10a	0.76s	−0.20
Roof liner	2.0	8.30a	1.15s	1.65
Side liner	1.0	8.40a	1.65s	0.95
Misc	10.0	8.20a	0.90s	0.45
<b>Group total</b>	<b>82.4</b>	<b>8.36a</b>	<b>0.90s</b>	<b>0.40</b>



Group 8 <b>Aft cabin</b>				
<i>Item name</i>	<i>Mass</i>	<i>LCG</i>	<i>TCG</i>	<i>VCG</i>
Hanging locker & dresser	12.0	8.20a	1.47p	0.50
Berth top	14.0	9.85a	0.99p	0.20
Berth stiffening	5.7	9.60a	1.30p	0.06
Door	6.0	7.72a	0.61p	0.72
Side bulkhead	15.0	9.05a	0.36p	0.48
Sole	9.0	8.10a	0.72p	-0.20
Roof liner	7.0	9.10a	1.15p	0.90
Side liner	5.0	9.30a	1.75p	0.65
Cushions	10.3	9.90a	0.99p	0.25
Misc	10.0	8.60a	0.80p	0.35
<b>Group total</b>	<b>94.0</b>	<b>8.98a</b>	<b>0.95p</b>	<b>0.37</b>

Group 9 <b>Cockpit stow</b>				
<i>Item name</i>	<i>Mass</i>	<i>LCG</i>	<i>TCG</i>	<i>VCG</i>
Locker sole	11.7	10.20a	0.94s	0.21
Transverse bulkheads	18.1	9.60a	0.86s	0.48
Longitudinal bulkhead	11.4	9.60a	0.36s	0.30
Shelves	10.2	9.95a	1.32s	0.57
Misc	10.0	10.30a	0.35s	0.24
<b>Group total</b>	<b>61.4</b>	<b>9.89a</b>	<b>0.78s</b>	<b>0.37</b>

Group 10 <b>Installations</b>				
<i>Item name</i>	<i>Mass</i>	<i>LCG</i>	<i>TCG</i>	<i>VCG</i>
Engine	150.0	8.10a	0.00	-0.02
Exhaust system	7.0	9.50a	0.00	0.05
Engine noise insulation	16.8	8.30a	0.00	0.10
Propeller	4.0	8.30a	0.00	-0.68
Fuel filter	2.0	8.70a	0.20p	0.20
Water filter	2.0	8.70a	0.00	0.30
Water intake & piping	2.0	8.70a	0.20p	-0.26
Fuel piping	2.0	8.60a	0.25p	0.15
Shore power	10.0	9.10a	0.40s	0.10
Batteries	60.0	3.20a	0.00	-0.14
Wiring	30.0	4.80a	0.00	0.40
Nav station instruments	15.0	6.40a	1.40s	0.90
Cool compressor & piping	10.0	6.50a	1.42p	0.30
Heater & ducting	10.0	9.20a	0.40s	0.40
Rudder blade	20.0	11.90a	0.00	-0.30
Rudder shaft	30.0	11.75a	0.00	0.00
Rudder sleeve	8.0	11.75a	0.00	0.35
Rudder quadrant	6.0	11.75a	0.00	0.50
Rudder linkage	8.0	11.60a	0.00	0.50
Steering wheel	5.0	11.20a	0.00	1.30

Group 10 Installations continued				
Steering pedestal	10.0	11.15a	0.00	1.05
Pedestal instruments	4.0	8.34a	0.00	1.62
Autopilot installation	15.0	11.60a	0.00	0.40
Bilge pumps & piping	7.0	7.50a	0.00	-0.20
Fuel tank	15.0	8.50a	0.00	-0.14
Water tank & piping	10.0	4.80a	0.00	-0.10
Holding tank & piping	11.0	8.10a	1.32s	0.20
Misc	57.0	4.80a	0.00	0.01
<b>Group total</b>	<b>526.8</b>	<b>7.63a</b>	<b>0.05s</b>	<b>0.10</b>

Group 11 Deck equipment				
<i>Item name</i>	<i>Mass</i>	<i>LCG</i>	<i>TCG</i>	<i>VCG</i>
Pulpit	7.5	0.50a	0.00	1.70
Stanchions	7.2	6.03a	0.00	1.54
Pushpit	9.0	11.67a	0.00	1.46
Lifelines	4.0	6.00a	0.00	1.65
Sheer rail	15.0	5.90a	0.00	1.25
Bollards	4.0	6.08a	0.00	1.24
Mast turn blocks	3.0	5.40a	0.00	1.65
Genoa tracks & cars	5.0	5.65a	0.00	1.26
Rope clutches	3.0	8.30a	0.00	1.69
#1 Winch	20.0	10.67a	0.00	1.45
#2 Winch	16.0	9.90a	0.00	1.49
#3 Winch	14.0	8.67a	0.00	1.75
Main track & blocks	4.0	10.90a	0.00	0.70
Chainplates	8.0	6.10a	0.00	1.02
Bow roller	11.0	0.60a	0.15s	1.08
Bow anchor (stowed)	20.0	1.16a	0.19s	1.08
Anchor windlass	20.0	1.30a	0.10p	1.25
Anchor chain	10.0	1.30a	0.00	0.00
Aft stay attachment	4.0	12.28a	0.00	0.90
Fwd deck hatch	4.0	0.97a	0.00	1.40
Fwd cabin deck hatch	5.0	3.64a	0.00	1.51
Saloon deck hatch	5.0	6.17a	0.00	1.68
Companionway hatch	10.0	8.10a	0.00	1.65
Aft cabin deck hatch	5.0	8.45a	0.00	1.66
Deckhouse windows	7.0	7.20a	0.00	1.40
Deck ventilation	3.0	6.17a	0.00	1.66
Misc	30.0	3.84a	0.00	1.06
<b>Group total</b>	<b>253.7</b>	<b>5.61a</b>	<b>0.01s</b>	<b>1.29</b>

Group 12 <b>Rig &amp; sails</b>				
<i>Item name</i>	<i>Mass</i>	<i>LCG</i>	<i>TCG</i>	<i>VCG</i>
Mast & spreaders	85.0	5.56a	0.00	10.65
Boom	21.0	8.20a	0.00	2.70
Forestay	2.0	2.85a	0.00	9.50
Shrouds D	2.0	5.80a	0.00	6.90
Shrouds V	3.0	6.27a	0.00	9.38
Running rigging	12.0	5.80a	0.00	7.50
Bowsprit (retracted)	13.0	0.90a	0.43p	1.29
Rigg screws & toggles	9.0	6.14a	0.00	1.30
Jib furler luff extrusion	11.8	2.80a	0.00	9.40
Jib furler drum	3.0	0.08a	0.00	1.40
Aft stay	3.0	9.00a	0.00	10.40
Genoa hoisted	12.0	3.60a	0.00	6.80
Main hoisted	18.0	7.40a	0.00	8.30
Rodkick & blocks & lines	6.0	6.10a	0.00	1.90
Mast top fittings	3.0	5.83a	0.00	19.70
Misc	25.0	5.50a	0.00	4.50
<b>Group total</b>	<b>228.8</b>	<b>5.44a</b>	<b>0.02p</b>	<b>7.44</b>

Group 13 <b>Ballast</b>				
<i>Item name</i>	<i>Mass</i>	<i>LCG</i>	<i>TCG</i>	<i>VCG</i>
Keel	2300.0	6.10a	0.00	-2.00
<b>Group total</b>	<b>2300.0</b>	<b>6.10a</b>	<b>0.00</b>	<b>-2.00</b>

<b>Light craft mass</b>	<b>5900</b>	<b>6.35a</b>	<b>0.00</b>	<b>-0.26</b>
-------------------------	-------------	--------------	-------------	--------------

Group 14A <b>Payload condition A – Minimum sailing condition</b>				
<i>Item name</i>	<i>Mass</i>	<i>LCG</i>	<i>TCG</i>	<i>VCG</i>
Helmsman	75.0	11.40a	0.00	1.55
One crew	75.0	9.30a	0.00	1.30
Forepeak gear	5.0	0.90a	0.00	0.85
Fwd cabin gear	0.0	3.80a	0.00	0.30
Saloon gear	10.0	5.10a	0.00	0.08
Nav station gear	10.0	6.60a	1.50s	0.40
Galley gear	10.0	6.70a	1.45p	0.25
Head gear	5.0	8.20a	1.40s	0.05
Aft cabin gear	15.0	8.30a	1.45p	0.10
Cockpit locker gear	10.0	10.10a	1.00s	0.40
Liferaft	40.0	9.70a	0.00	0.45
<sup>1</sup> / <sub>15</sub> Water	20.0	4.80a	0.00	-0.10
<sup>1</sup> / <sub>4</sub> Fuel	25.0	8.50a	0.00	-0.13
<sup>0</sup> / <sub>1</sub> Holding tank	0.0	8.10a	1.40s	-0.10
<b>Group total</b>	<b>300.0</b>	<b>9.01a</b>	<b>0.01p</b>	<b>0.81</b>
<b>Minimum operating condition</b>	<b>6200</b>	<b>6.48a</b>	<b>0.00p</b>	<b>-0.20</b>

Group 14B Payload condition B – Cruising crew of six				
<i>Item name</i>	<i>Mass</i>	<i>LCG</i>	<i>TCG</i>	<i>VCG</i>
Helmsman	75.0	11.40a	0.00	1.55
Five crew	375.0	7.80a	0.00	1.30
Forepeak gear	20.0	0.90a	0.00	0.85
Fwd cabin gear	80.0	3.80a	0.00	0.30
Saloon gear	80.0	5.10a	0.00	0.08
Nav stn gear	20.0	6.60a	1.60s	0.40
Galley gear	150.0	6.70a	1.30p	0.25
Head gear	20.0	8.20a	1.55s	0.05
Aft cabin gear	80.0	8.30a	1.40p	0.10
Cockpit locker gear	80.0	10.10a	1.25s	0.40
Liferaft	40.0	9.70a	0.00	0.45
<sup>4</sup> / <sub>4</sub> Water	300.0	4.80a	0.00	−0.05
<sup>2</sup> / <sub>2</sub> Fuel	100.0	8.50a	0.00	−0.07
<sup>2</sup> / <sub>2</sub> Holding tank	80.0	8.10a	1.40s	−0.05
<b>Group total</b>	<b>1500.0</b>	<b>7.07a</b>	<b>0.02p</b>	<b>0.49</b>

<b>Maximum load condition</b>	<b>7400</b>	<b>6.50a</b>	<b>0.00</b>	<b>−0.11</b>
-------------------------------	-------------	--------------	-------------	--------------

Group 14C Payload condition C – Racing crew of five				
<i>Item name</i>	<i>Mass</i>	<i>LCG</i>	<i>TCG</i>	<i>VCG</i>
Helmsman	75.0	11.40a	0.00	1.55
Four crew	300.0	6.80a	0.00	1.30
Forepeak gear	5.0	0.90a	0.00	0.85
Fwd cabin gear	30.0	3.80a	0.00	0.30
Saloon gear	30.0	5.10a	0.00	0.08
Nav station gear	10.0	6.60a	1.60s	0.40
Galley gear	25.0	6.70a	1.30p	0.25
Head gear	5.0	8.20a	1.55s	0.05
Aft cabin gear	15.0	8.30a	1.40p	0.10
Cockpit locker gear	20.0	10.10a	1.25s	0.40
Liferaft	40.0	9.70a	0.00	0.45
<sup>1</sup> / <sub>8</sub> Water	30.0	4.80a	0.00	−0.15
<sup>1</sup> / <sub>4</sub> Fuel	25.0	8.50a	0.00	−0.15
<sup>1</sup> / <sub>8</sub> Holding tank	10.0	8.10a	1.40s	−0.15
<b>Group total</b>	<b>620.0</b>	<b>7.41a</b>	<b>0.01s</b>	<b>0.89</b>

<b>Race-loaded condition</b>	<b>6520</b>	<b>6.45a</b>	<b>0.00</b>	<b>−0.15</b>
------------------------------	-------------	--------------	-------------	--------------

# APPENDIX 3

## STIX calculation

BOAT		YD-41		
Intended design category		A		PASS!
$L_H$	(m)	12.50		
$L_{WL}$	(m)	12.14		
$B_H$	(m)	4.20		
$B_{WL}$	(m)	3.12		
$T_C$	(m)	0.38		
T	(m)	2.28		
$V_C$	(m <sup>3</sup> )	2.30		
$F_M$	(m)	1.25		
<b>CREW LIMIT</b>	<b>(#pers)</b>	<b>6</b>	<b>(To be on Builder's Plate!)</b>	
GZ-90	(m)	0.91		
ASP	(m <sup>2</sup> )	92.00		
HCE	(m)	7.45		
HLP	(-m)	1.03		
Angle of vanishing stab. ( $A_{VS}$ )	(deg.)	132.00	Min $A_{VS}$	118
Area under GZ-curve to $A_{DH}$	(m deg.)	97.90		

LIGHT CRAFT CONDITION		Mass (kg)	X (m)	Z (m)
<b>LIGHT CRAFT MASS (<math>m_{LC}</math>)</b>	<b>(kg)</b>	<b>5900</b>	<b>6.35</b>	<b>-0.26</b>

MINIMUM OPERATING CONDITION				
Light ship	(kg)	5900	6.35	-0.26
Crew	(kg)	150	10.35	1.41
Liferaft	(kg)	40	9.70	0.45
Basic equipment	(kg)	110	6.80	0.50
<b>MIN. OPERATING MASS (<math>m_{MO}</math>)</b>	<b>(kg)</b>	<b>6200</b>	<b>6.48</b>	<b>-0.20</b>

LOADED ARRIVAL CONDITION		Mass (kg)	X (m)	Z (m)
Light ship	(kg)	5900	6.35	-0.26
Crew	(#pers)	300	7.80	1.25
Crew	(kg)	150	10.35	1.41
Liferaft	(kg)	40	9.70	0.45
Basic equipment	(kg)	110	6.80	0.50
Stores	(kg)	21	6.00	0.70
Water	(kg)	15	4.80	-0.15

LOADED ARRIVAL CONDITION <small>continued</small>		Mass (kg)	X (m)	Z (m)
Fuel	(kg)	10	8.50	−0.17
Hold	(kg)	80	8.10	−0.05
Personal gear	(kg)	210	5.75	0.20
<b>LOADED ARRIVAL MASS (<math>m_{LA}</math>)</b>	<b>(kg)</b>	<b>6851</b>	<b>6.53</b>	<b>−0.12</b>
Loaded volume	(m <sup>3</sup> )	6.75		
Maximum load (ML)	(kg)	951		
<b>MAX LOAD EX., FUEL, WATER</b>	<b>(kg)</b>	<b>911</b>	<b>(To be on Builder's Plate!)</b>	

STIX 12217-2 FDIS (March 2011)	
FDS	1.183
FIR	1.090
FKR	1.216
FDL	0.905
FBD	0.831
FWM	1.000
FDF	1.250
<b>STIX</b>	<b>42</b>

# REFERENCES

The literature on sailing theory and yacht design is extensive. For a comprehensive list of references, see the book by Fossati below. The following list contains essentially the references referred to in the present book.

- Abbott, I H, von Doenhoff, A E 1949. *Theory of Wing Sections*. New York: McGraw-Hill.
- ABS 1994. *Guide for Building and Classing Offshore Racing Yachts*. American Bureau of Shipping, New York.
- AIAA Symposium on the Aero/Hydraulics of Sailing. Held annually since 1969. Western Periodicals Company, North Hollywood.
- Allen, H G 1969. *Analysis and Design of Structural Sandwich Panels*. Oxford: Pergamon Press.
- Allroth, J, Wu, T-H 2013. *A CFD Investigation of Sailing Yacht Transom Sterns*. MSc thesis, Chalmers University of Technology, Dept. Shipping and Marine Technology, Gothenburg.
- Allroth, J, Wu, T-H, Orych, M, Larsson, L (2015). *Sailing Yacht Transom Sterns – a Systematic CFD Investigation*, Proceedings, 5th High Performance Yacht Design Conference, Auckland, 8-11 March 2015. s. 257–266. ISBN/ISSN: 978-1-909024-37-3.
- Andersson, R, Granli, S 2018. *Free Surface Effects on Horizontal Hydrofoils*. MSc thesis, 2018:87, Department of Mechanics and Maritime Sciences, Chalmers University of Technology, Gothenburg.
- Bague, A, Lataire, E, Demeester T, Degroote, J 2020. *Dynamic Stability Analysis of a Hydrofoiling Sailing Boat Using CFD*. INNOVAIL 2020, Gothenburg
- Beaver, B, Zselezcky, J 2009. *Full Scale Measurements on a Hydrofoil International Moth*, Chesapeake Sailing Yacht Symposium, Annapolis, USA.
- Bethwaite, F 1996. *High Performance Sailing*. McGraw Hill, New York.
- Bethwaite, F 2013. *Higher Performance Sailing*. Adlard Coles, London.
- Cannell, D, Leather, J 1976. *The Design of Sailing Yachts*. London: Adlard Coles Nautical.
- Caprino, G, Teti, R 1989. *Sandwich Structures Handbook*. Il Prato – Pelf SpA, Padua.
- Claughton, A R, Wellicome, J F, Shenoi, R A 1998. *Sailing Yacht Design – Theory*. Harlow: Addison Wesley Longman.
- Claughton, A R, Wellicome, J F, Shenoi, R A 1998. *Sailing Yacht Design – Practice*. Harlow: Addison Wesley Longman.
- DIAB 1991. *Divinycell Technical Manual H-Grade*. Divinycell International AB, Laholm.
- Dyne, G, Widmark, C 1998. *On the Efficiency of Water Jet Systems*. International Conference on Water Jet Propulsion – Latest Developments, Amsterdam 22–23 October.
- Eggert, F, Henrichs, J, Hansen, H, Hochkirch, K 2020. *Flight Dynamics and Stability Assessment of an International Moth*, INNOV'SAIL 2020, Gothenburg, Sweden.
- Faltinsen, O M 2005. *Hydrodynamics of High-speed Marine Vehicles*. Cambridge University Press, Cambridge, UK.
- Findlay, M W, and Turnock, S R 2008. *Development and use of a velocity prediction program to compare the effects of changes to foil arrangement on a hydro-foiling Moth dinghy. Proceedings – Innovation in High Performance Sailing Yachts*. Royal Institution of Naval Architects. pp. 43–55.
- Fossati, F 2009. *Aero-Hydrodynamics and the Performance of Sailing Yachts*, London: Adlard Coles Nautical, and Camden, Maine: International Marine/McGraw-Hill (US only).
- Gentry, A E 1971. *The Aerodynamics of Sail Interaction*. 2nd AIAA Symposium on the Aero/Hydraulics of Sailing.
- Gerritsma, J, Keuning, J A 1985. 'Model Experiments with Yacht Keels'. *Seahorse Magazine*, March/April 1985, pp. 23–26.
- Gerritsma, J, Keuning, J A, Onnink, R 1992. *Sailing Yacht Performance in Calm Water and in Waves*. 12th Symposium on Developments of Interest to Yacht Architecture, Amsterdam.
- Gerritsma, J, Onnink, R, Versluis, A 1981. 'Geometry, Resistance and Stability of the Delft Systematic Yacht Series'. *International Shipbuilding Progress* 28(328), pp. 276–97.
- Gutelle, P 1984. *The Design of Sailing Yachts*. London: Nautical Books.
- Hadler, J B, 1966. *The Prediction of Power Performance on Planing Craft*. Transactions Society of Naval Architects and Marine Engineer, Vol.74, New York.
- Hammitt, A G 1975. *Technical Yacht Design*. London: Adlard Coles Nautical.
- Hazen, G S 1980. *A Model of Sail Aerodynamics for Diverse Rig Types*. New England Sailing Yacht Symposium.
- Henry, R G, Miller R T 1963. *Sailing Yacht Design – An Appreciation of a Fine Art*. Transactions Society of Naval Architects and Marine Engineers, New York.
- Heppel, P 2015. *Flight Dynamics of Sailing Foilers*. 5th High Performance Yacht Design Conference, Auckland, New Zealand.
- Herreshoff, L E 1974. *The Common Sense of Yacht Design*. New York: Caravan-Maritime Books.
- Hildebrand, M, Holm, G 1991. *Strength Parameters of Boat Laminates* (in Finnish). Technical Research Centre of Finland, Research Notes No. 1289, Helsinki.
- Hildebrand, M 1991. *On the Bending and Transverse Shearing Behaviour of Curved Sandwich Panels*. Technical Research Centre of Finland, Research Notes No. 1249, Helsinki.
- Hino, T, Stern, F, Larsson L *et al* 2020. *Numerical Ship Hydrodynamics – An Assessment of the Tokyo 2015 Workshop*. Lecture Notes in Applied and Computational Mechanics 94. Springer Nature, Switzerland. ISBN 978-3-030-47571-0.
- Hoerner, S 1965. *Fluid Dynamic Drag*. Hoerner Fluid Dynamics, Albuquerque, USA.
- Honey, R A 1983. *Fibre Reinforcement Plastics in Boatbuilding*. University of Auckland, Department of Mechanical Engineering, Auckland.
- Hunyadi, B, Hedlund, P 1983. *Strength Comparison of Two Constructional Concepts for a 25 Metres Racing Yacht* (in Swedish). The Royal Institute of Technology (KTH), Department of Lightweight Structures, Publication No. 83–16, Stockholm.
- ISO/TC 188/WG 18. *Small Craft–Hull Construction/Scantlings EN ISO 12215-5: Design Pressures, Allowable Stresses, Scantling Determination. EN ISO 12215-6: 2008: Structural arrangements and details. EN ISO 12215-8: Rudders. EN ISO 12215-9: Sailing craft appendages*. International Standards Organization – SIS/SMS, Stockholm.
- ISO/TC 188/WG 22. *Small Craft–Stability and buoyancy assessment and categorization. EN ISO 12217-2: 2009: Sailing boats of hull length greater than or equal to 6 m*. International Standards Organization – SIS/SMS, Stockholm.
- Joint Committee on Safety from Capsizing. 1985. *Final Report of the Directors*. United States Yacht Racing Union, Newport and Society of Naval Architects and Marine Engineers, New York.
- Joubert, P N 1982. 'Strength of Bottom Plating of Yachts'. *Journal of Ship Research*, Vol. 26, No. 1, March 1982, pp. 45–49.
- Kaplan, P, Hu, P N and Tsakonas, S 1958. *Methods for estimating the longitudinal and lateral dynamic stability of hydrofoil craft*, Stevens Institute of Technology E.T.T. Report No. 691.



- Kay, H F 1971. *The Science of Yachts, Wind and Water*. London: G T Foulis.
- Kerdraron, P, Horel, B, Bot, P, Letourneur, A, Le Touzé, D 2019. 6DOF Behavior of an offshore racing trimaran in an unsteady environment. 23rd Chesapeake Sailing Yacht Symposium, Annapolis, USA.
- Kerwin, J E, Hadler, J B 2010. *Propulsion*, Principles of Naval Architecture Series, Society of Naval Architects and Marine Engineers, Jersey City, New Jersey.
- Keuning, J A, Sonnenberg, U B 1998. *Approximation of the Hydrodynamic Forces on a Sailing Yacht Based on the 'Delft Systematic Yacht Hull Series'*, 15th International HISWA Symposium on Yacht Design and Yacht Construction, Amsterdam.
- Keuning, J A, Katgert, M 2008. *A Bare Hull Resistance Prediction Method Derived From the Results of the Delft Systematic Yacht Hull Series Extended to Higher Speeds*. International Conference on Innovation in High Performance Sailing Yachts, Lorient.
- Keuning, J A, Verwerft, B 2009. *A new Method for the Prediction of the Side Force on Keel and Rudder of a Sailing Yacht based on the Results of the Delft Systematic Yacht Hull Series*. 19th Chesapeake Sailing Yacht Symposium, Annapolis.
- Kinney, F S 1973. *Skene's Elements of Yacht Design*. New York: Dodd, Mead & Co.
- Lackenby, H 1978. *ITTC Dictionary of Ship Hydrodynamics*. Marine Technology Monographs. Royal Institute of Naval Architects, London.
- Larsson, L 1990. 'Scientific Methods in Yacht Design'. *Annual Review of Fluid Mechanics*, Vol 22, pp. 349–385.
- Larsson, L, Raven, H C 2010. *Ship Resistance and Flow*, Principles of Naval Architecture Series, Society of Naval Architects and Marine Engineers, Jersey City, New Jersey.
- Larsson, L, Stern, F, Visonneau, M (eds) 2013 *Numerical Ship Hydrodynamics – An Assessment of the Gothenburg 2010 Workshop*, Springer Science+Business Media B.V., Dordrecht.
- Leer-Andersen, M, Larsson, L 2003. 'An Experimental/Numerical Approach for Evaluating Skin Friction on Full-Scale Ships with Surface Roughness', *J. Marine Science and Technology*, 8, pp. 26–36.
- Le Pelley, D, Richards, P 2011. *Effective Wind Tunnel Testing of Yacht Sails Using a Real-Time Velocity Prediction Program*. 20th Chesapeake Sailing Yacht Symposium, Annapolis.
- Lindstrand Levin, R, Larsson, L 2017. Sailing yacht performance prediction based on coupled CFD and rigid body dynamics in 6 degrees of freedom. *Ocean Engineering*, Vol. 144, pp. 362–373.
- Ljungqvist, K.; Orych, M.; Larsson, L.; Finnsgård, C. (2018) 'Comparison Of Modern Keel Types For Sailing Yachts', *International Journal of Small Craft Technology*, Vol. 159 (Part B2), pp. 81–88
- Lloyd's 1978–1993. *Rules and Regulations for the Classification of Yachts and Small Craft*. Lloyd's Register, Yacht and Small Craft Department, Southampton.
- Marchaj, C A 1979. *Aero-Hydrodynamics of Sailing*. London: Adlard Coles Nautical.
- Marchaj, C A 1982. *Sailing Theory and Practice*. London: Adlard Coles Nautical.
- Marchaj, C A 1986. *Seaworthiness. The Forgotten Factor*. London: Adlard Coles Nautical.
- Marchaj, C A 1996. *Sail Performance: Techniques to Maximise Sail Power*. Adlard Coles Nautical, London.
- Marimon Giovannetti L, Banks, J, Ledri, M, Turnock, S R, Boyd, S W (2018) 'Toward the development of a hydrofoil tailored to passively reduce its lift response to fluid load', *Ocean Engineering*, 167, 1–10.
- Marshall, R 1979. *Designed to Win*. London: Adlard Coles Nautical.
- Marshall, R 1980. *Race to Win*. New York and London: W W Norton & Company.
- Marshall, R 1990. *Designed to Cruise*. New York and London: W W Norton & Company.
- Masuyama, Y 1987. Stability Analysis and Prediction of Performance for a Hydrofoil Sailing Boat. Part 2: Dynamic Stability Analysis, *International Shipbuilding Progress* 34.398 (1987), pp. 178–188.
- Milgram, J H 1971. *Sail Force Coefficients for Systematic Rig Variations*. Technical Report No. 10, Society of Naval Architects and Marine Engineers, New York.
- Milgram, J H 1998. 'Fluid Mechanics for Sailing Vessel Design'. *Annual Review of Fluid Mechanics*, Vol. 30, pp. 613–653.
- Miller, R T, Kirkman, K L 1990. *Sailing Yacht Design – A New Appreciation of a Fine Art*. Annual Meeting, Society of Naval Architects and Marine Engineers, New York.
- NBS 1990. *Nordic Boat Standard*. Det Norske Veritas Classification A/S, Oslo.
- Nomoto, K, Tatano, H 1979. *Balance of Helm Sailing Yachts – a Ship Hydrodynamics Approach on the Problem*. 6th Symposium on Development of Interest to Yacht Architecture, Amsterdam, pp. 64–89.
- Nowacki, H, Bloor, M I G, Oleksiewicz, B (eds) 1995. *Computational Geometry for Ships*. World Scientific, Singapore.
- Obara, C J, van Dam, C P 1987. *Keel Design for Low Viscous Drag*. 8th Chesapeake Sailing Yacht Symposium.
- Olofsson, N 1996. *Force and Flow Characteristics of a Partially Submerged Propeller*. PhD Thesis, Chalmers University of Technology, Department of Naval Architecture and Ocean Engineering, Gothenburg.
- Orych, M 2005. *Calculations of the Flow and Resistance Components of Systematically Varied Keel/Bulb Winglets in Upright and Heeled Conditions*. Report No. X-05/168, Department of Shipping and Marine Technology, Chalmers University of Technology, Gothenburg.
- Orych, M, Larsson, L (2015). *Hydrodynamic Aspects of Transom Stern Optimisation*, Proceedings, 5th High Performance Yacht Design Conference, Auckland, 8–11 March 2015. pp. 247–256. ISBN/ISSN: 978-1-909024-37-3.
- Ottosson, P, Larsson, L, Brown, M 2002. *The Effect of Pitch Radius of Gyration on Sailing Yacht Performance*. 1st High Performance Yacht Design Conference, Auckland.
- Phillips-Birt, D 1966. *Sailing Yacht Design*. London: Adlard Coles Nautical.
- Persson, A, Larsson, L, Finnsgård, C 2020. *An Improved Procedure For Strongly Coupled Prediction Of Sailing Yacht Performance*. INNOV'SAIL 2020, Gothenburg.
- Poor, C L 1986. *The International Measurement System*. Offshore Racing Council, London.
- Prabakar, N S S, Larsson, L, Persson, A 2021. *Split Flaps for Increased Heel Stability of T-Foil Configurations*, 7th High Performance Yacht Design Conference, Auckland, New Zealand.
- Rousmaniere, J (ed) 1987. *Desirable and Undesirable Characteristics of Offshore Yachts*. New York and London: W W Norton & Company.
- Savitsky, D. 1964. 'Hydrodynamic Design of Planing Hulls'. *Marine Technology*, Vol. 1. No. 1.
- Sponberg, E W 1986. 'Carbon Fibre Sailboat Hulls: How to Optimize the Use of an Expensive Material'. *Marine Technology*, Vol. 23, No. 2, April 1986, pp. 165–174.
- Smith, P 2018. *Latest Update on the BUGS CAM*. Seahorse Magazine, May 2018.
- Street, D M 1973 and 1978. *The Ocean Sailing Yacht*, Vol 1 & 2. New York and London: W W Norton & Company.
- Soupeze, J-B R G, Dewavrin, J M M-A, Gohier, F, Borba Labi, G 2019. *Hydrofoil Configurations for Sailing Superyachts: Hydrodynamics, Stability and Performance*. Design & Construction of Super & Mega Yachts, Genoa, Italy.
- Tinoco, E N, Gentry, A E, Bogataj, P, Sevigny, E G, Chance, B 1993. *IACC Appendage Studies*, 11th Chesapeake Sailing Yacht Symposium.
- VTT 1997. *VTT-NBS Extended Rule*. Technical Research Centre of Finland, Technical Report VTT VALB172, Helsinki.
- Van Oossanen, P (2020) *The Science of Sailing*. Van Oossanen Academic Publishers, Wageningen, Netherlands.
- Werner, S, Larsson, L, Regnström, B 2006. *A CFD Validation Test Case – Wind Tunnel Tests of a Winglet Keel*. 2nd High Performance Yacht Design Conference, Auckland, February.
- Whicker, L F, Fehlner, L F 1958. *Free-stream characteristics of a family of low-aspect ratio, all movable control surfaces for application to ship design*. Technical report 933, David Taylor Model Basin, Bethesda.
- Young, Y L, Harwood, C M, Miguel Montero, F, Ward, J C, Ceccio, S L 2017. 'Ventilation of Lifting Bodies: Review of the Physics and Discussion of Scaling Effects'. *Applied Mechanics Reviews*, Vol 69.
- Zou, L, Larsson, L 2014. *CFD Verification and Validation in Practice – A Study Based on Resistance Submissions to the Gothenburg 2010 Workshop on Numerical Ship Hydrodynamics*. 30th Symposium on Naval Hydrodynamics, Hobart, Australia.

# INDEX

- Abbott, I H, *Theory of Wing Sections* 127, 136  
accommodation 21, 351–8  
aerodynamics: aerodynamic drag 172  
aerodynamic force 65, 66, 196, 199, 200  
practical model for sail and rig 192–6  
airflow 361–2  
Airfoil 140  
Allroth, J 378  
aluminium spars, typical properties for 260, 262  
American Bureau of Shipping (ABS) 16, 304  
rules 243, 265, 270  
America's Cup 71, 116, 118, 121, 364, 375  
foiling designs 144, 147–8  
angle of attack 102, 155, 191, 203  
apparent wind 65–7, 185, 186, 191, 196, 197, 201  
Archimedes Principle 40, 223  
area reduction factor 314, 315  
areas: calculation of 38–40  
ISO scantlings 308–9  
aspect ratio 158, 159–60  
aspect ratio factors for plating 325  
keel aspect ratio 105–8  
sail aspect ratio 181–5  
assessment method factor 324–5  
asymmetric spinnakers 185, 196, 259, 359  
*Australia II* 116, 119  
axial component, propellers 211  
balance 199–206  
ballast keels, calculation for stresses 275  
ballast ratio 100, 101  
Barkla, H M 18–19  
base length factor (LBS) 61  
beam 24  
beam displacement factor (FBD) 61  
beam/draft ratio 88  
beam of waterline 24  
length/beam ratio 88  
length overall/max beam 97, 98  
bending moment 325, 327  
Bergstrom, R 184  
berths 357–8  
Bethwaite, F 10  
bilge factor 40  
biplane theory 121, 201  
block coefficient 25, 26  
Blyth, A G 64  
boat type, choice of 17  
boatbuilding quality factor 323–4  
body plans 27, 28, 29, 30  
Boeing 120  
booms 256–7  
bottom: bottom pressure 271, 272–3  
design loads for 317–18  
bound vortex 106–7  
boundary layer 69–76, 129, 140, 161, 181, 189, 375, 376  
laminar 69, 70, 76  
turbulent 69, 70, 71  
breaking strain 329–31  
BUGS CAM 151  
bulb (keel tip shape) 119, 120  
bulkheads, design loads for 321–2  
buoyancy 223  
centre of buoyancy 26, 34, 42–5, 46, 87–8, 96  
Bureau Veritas 304  
Burrill diagram 220  
buttocks 27–8, 29, 30, 34, 86, 236, 237  
cam profiles 151  
canard wings 121–2  
canoe bodies, length of waterline/canoe body draft 98  
carbon spars, typical properties for 260, 262  
Carl, Bill 144  
cavitation 178, 220, 238–9  
centre of buoyancy 26, 34, 42–5, 46, 87–8, 96  
centre of effort (CE) 234  
of sails 203–5  
of the underwater body 201–3  
centre foils 153, 158, 159–60, 167, 174, 177  
centre of gravity (CoG) 26, 43, 46  
cardboard method to find 44, 46, 51–2  
methods of finding 43–4, 46  
planing hulls 230–1, 236  
centre of lateral resistance (CLR) 201–6  
centreboards 153, 158–9  
wave and spray drag 171–2  
centrifugal force 57, 58  
chainplates 346, 347, 361  
Chalmers University of Technology 113, 165  
chart table 353, 355, 388  
checklist of design considerations 22  
chine walking 237  
Chistera 148  
chopped strand mat (CSM) 287–9  
chord 105, 120  
Class 40 197, 365  
classification societies 16  
cockpits 315, 358, 359, 389  
Code 0 185, 196, 259, 359  
coefficients: block coefficient 25, 26  
drag coefficient 107–8, 129, 136, 193, 194  
lift coefficient 107–8, 109, 115, 129–33, 136, 150, 152–3, 154, 158  
prismatic coefficient 25, 34  
sail coefficient 192–6  
collision bulkheads 322  
Committee of European Norms (CEN) 304  
companionways 357, 362  
composites, properties of 329  
Computational Fluid Dynamics (CFD) 14, 116, 364, 375–83  
computed forces 168–77  
Computer Aided Design (CAD) 13, 15–16, 35–7, 38  
Contessa 32 53–4  
conversion factors 9  
Copenhagen ship curves 32  
corrosion, wire vs rod rigging 252  
cost: designing a boat 20–1  
wire vs rod rigging 253  
curvature: curvature correction factor 326  
curvature of lines 35–6  
daggerboards 123  
foiling 147  
Dali-Moustache 148  
damping 54, 55, 56, 57  
Davidson Laboratory, New York 116, 190–1, 225  
deadrise 226–8  
decks 315  
deck layout 358–63  
design loads for 321–2  
deep-V hulls 226  
deformations, local 274–5  
degrees of freedom (DOFs) 148–9, 157–8, 366  
Delft University of Technology 81, 364, 377  
keel concepts 123–6  
parent models 82, 87, 92  
Systematic Yacht Hull Series 81–3, 89  
Dellenbaugh angle 59–60, 365  
depth 24  
design: change in hull shapes 38  
checklist of considerations 22  
design category factor 313  
design loads for the bottom 317–18  
design loads for decks, superstructures and bulkheads 321–2  
design loads for topsides 318–20  
design stresses 323, 326–7  
evaluation of 364–83  
methodology 13–16  
parameters 18–20  
preliminary considerations 17–22  
shear forces and design moments 327  
spiral 13–14  
summary of design loads 322–3  
designed waterline length (DWL) 23, 27, 34  
water plane area 46  
diagonals 34  
dihedral angle 117, 118  
dimensions 18–20, 33  
definitions 23–7  
displacement 24, 33–4, 40, 42, 84–6  
displacement hulls 80–1  
displacement length factor (FDL) 61  
foils for displacement yachts 148  
length/displacement ratio 98–9  
Doenhoff, A E von, *Theory of Wing Sections* 127, 136  
downflooding factor (FDF) 63–4  
downwash 155  
draft 24  
beam/draft ratio 88  
length of waterline/canoe body draft 98  
length of waterline/draft 97–9  
drag 107–11, 112  
drag bucket 131, 133  
drag coefficient 129, 136, 193, 194  
foiling hulls 153–4  
induced drag 106, 107, 114–16, 171, 184, 194  
influence of roughness on 137–8

- influence of section shape on 131, 132, 133–4
- shrouds and stays 191, 208–9
- viscous drag 192, 194
- wave and spray drag 171–2
- Drela, Mark 140
- driving force 182, 183, 184
- ducks 31, 32
- dynamic load factor 313–14
- dynamic stability 236–7
- dynamic stability factor (FDS) 63
- Dynamic Stability System (DSS) 145
- Dynamic Velocity Prediction Programs (DVPPs) 158, 160, 175, 176, 371, 372
- E-glass 286, 293, 329
- elliptical force distribution 107
- elliptical keels 109, 125
- encounter frequency 54–6, 96
- engines 207–22
- equilibrium 149, 154, 157
- equilibrium trim angle 231–2
- exotic laminates 293–5
- extended keels 116
- fairing fillets 120, 153
- Fargot, Emmanuel Denis 144
- Fastnet Race (1979) 52–3, 59, 61
- fatigue: in FRP 291–2
- in metal rigging 252
- fibre reinforced plastic (FRP) 286, 324
- fatigue in 291–2
- fillets, fairing 120, 153
- fin keel yachts 312
- Finite Element Analysis (FEA) 383
- flare 26, 27
- flattening factor 194
- flight stability 157–8
- floors 276
- flotation, centre of 46
- flow: around the hull 69–70
- around the sails 179–81
- around a wing 102–5
- potential flow 376
- foiling 144–78
- computed forces 168–76
- concepts of 146–8
- flight stability 157–8
- foil sections 161–5
- foiling skiffs 165–7
- planform area and shape 158–61
- forces 65–6
- computed forces 168–77
- design shear forces and design moments 327
- foiling 148–57
- from grounding 276–9
- from the keel 275–6
- from the rudder 279–81
- longitudinal force balance (surge) 153–4
- rigging loads 265–8
- on a sailing yacht 281–2
- on shrouds 246–9
- stiffer design forces and moments 335–6, 339
- vertical force balance (heave) 149–53, 155
- forepeak 353
- Fossati, F 10
- fractional rigs 250–1
- fractional mast tops 256
- freeboard 26
- height of 100, 101
- frequency of encounter 54–6, 96
- frictional resistance 70–2
- calculation of 73
- Froude number 80–1, 83, 84, 85–6, 98, 144, 153, 223, 378
- full keel yachts 313
- galley 355–7, 388
- gearing 151
- Gentry, A E 181
- Gerritsma, Professor J 81, 125, 202–3, 205
- Gilruth, R. 144
- glass reinforcement 286–91
- gravity, centre of (CoG) 26, 43, 46
- cardboard method to find 44, 46, 51–2
- methods of finding 43–4, 46
- planing hulls 230–1, 236
- Grimalkin* 53–4, 56, 59
- grounding, forces from 276–9
- gyradius 91, 92, 93, 94, 96
- Hadler, J B 231, 232
- half breadth plans 27, 30, 32
- hard chine craft 310–12
- Hazen, G S 192, 194
- heads 357, 388
- heave 149–53
- heel 195
- angle of heel 66
- effect of heel 199–200
- heel resistance 88–90
- heeled waterline 50–1
- Heller, S R 271
- Heyman, G 134
- high speed hydrodynamics 223–42
- high speed rescue vessel 239–42
- hogging 57, 58
- hulls: buttocks 236, 237
- construction 263–85
- design 35–6, 65–101
- design loads for the bottom 317–18
- forces on a turning hull 236, 237
- form parameters 86
- frictional resistance calculation 73, 228
- geometry 15, 23–7
- girder requirements 265, 266, 269, 270
- hull girders 281
- ISO hull definitions 307–8
- local deformations 274–5
- pressure adjusting factors 313–16
- pressures on panels and stiffeners 310–13
- resistance of foiling hulls 144–5, 148, 153, 157
- sandwich construction 295–8, 300, 301–2, 303, 333–5, 336, 338
- scantlings 304–50
- single skin panel calculation 331–2
- statistics 96–101
- V-shape hulls 226, 233
- humps and hollows, wave 80–1
- hydrodynamics: Centre of Lateral Resistance (CLR) 201–6
- hydrodynamic force 114, 115, 199, 200
- design theories 65
- forces 65, 66
- high speed 223–42
- hydrodynamic loads 271–3
- lift components 224–6
- hydrofoils *see* foiling
- Hydroptère* 144
- hydrostatics and stability 16, 38–64
- hydrostatic loads 270–1
- IMOCA60 148
- inertia: hull 46–8
- longitudinal moment of 46, 47, 255
- mass moment of inertia 46, 90–1, 92, 96
- reduction of moment of inertia of a mast 258
- transverse moment of 46, 48, 254
- Initial Graphics Exchange Specification (IGES) 29
- integrator 51
- International America's Cup Class (IACC) 118, 120, 373
- International Measurement System (IMS) 59, 82, 371
- International Monohull Open Classes Association (IMOCA) 148, 365
- International Standards Organization (ISO) 60, 271
- hull definitions 307–8
- ISO Scantling Standard 12215 16
- scantlings standard 304–50
- International Towing Tank Conference (ITTC) 12
- inversion recovery factor (FIR) 63
- J-foils 147, 148
- Jasper, N H 271
- jets, water 238, 241, 242
- Joubert, Professor P N 272, 273
- keelbolts 275–6, 344–6
- keels: advanced planform design 116–22
- bulbous keels 113
- canting keels 123
- design 102–43
- elliptical keels 109, 125
- extended 202, 203, 206
- fin keels 108–9, 113–14
- foiling 146
- forces from the keel 275–6, 277
- keel planform 105–6
- long keels 108–9
- residuary resistance of 83, 84, 85, 89
- Scheel keel 124, 125
- statistics on area 140–2
- tandem keels 122
- tip shape 111–14, 117
- trailing edges 138–9
- trapezoidal 105, 123, 124
- winged 116–21
- Kelvin wave system 78
- Keuning J A 81
- Kinney, F S 10
- knockdown recovery factor (FKR) 63
- L-foils 147, 148
- laminar flow 69–71
- laminates: exotic laminates 293–5
- failure of 291–2
- fibre reinforced plastic (FRP) 286–91
- mechanical properties 330
- Large Eddy Stimulation (LES) methods 375, 376
- Laser 155
- layout 351–63
- accommodation 352–8
- deck layout 358–63
- lead 204, 205–6
- leeway 68
- leeway angle 66
- length: length/beam ratio 88
- length between perpendiculars 23
- length/displacement ratio 86, 98–9, 100, 365
- length/draft ratio 99
- length/hull draft ratio 99
- length overall 23
- length overall/length of waterline 99–100
- length overall/max beam 97, 98
- length of waterline 23
- length-weight ratio 18
- lift 107, 194, 195
- coefficient 107–8, 109, 115, 129–33, 136, 150, 152–3, 154, 158
- foiling hulls 150, 155, 158
- and induced resistance of the yacht 114–16
- influence of roughness on 137–8
- influence of section shape on 131, 133
- lift computation 168–70
- negative 152–3
- lifting line theory 106, 107, 110, 111, 121, 155
- light 361
- lines drawing 27–9
- tools 29–32
- work plans 33–4
- Linnea* 165–7, 169, 175, 176–7, 370, 371
- Lloyd's Register of Shipping (LR) 16, 243, 304

- loadings 265–74
  - design loads for the bottom 317–18
  - design loads for decks, superstructures and bulkheads 321–2
  - design loads for topsides 318–20
  - forces from grounding 276–9
  - forces from the keel 275–6, 277
  - forces from the rudder 279–81
  - global loads 265–70
  - keelbolts 344–6
  - hydrodynamic loads 271–3
  - hydrostatic loads 270–1
  - on panels and stiffeners 310–13
  - rig loads and attachment 346
  - rigging 265–8
  - summary of design loads 322–3
  - summary of loadings on a sailing yacht 281–5
  - transverse load distribution 273–4
- longitudinal centre of buoyancy (LCB) 44
- longitudinal force balance (surge) 153–4
- longitudinal pressure distribution factor 314
- longitudinal stability 46
  - at small angles 47–50
- Maas, Frans 82
- mainsheet system 359
- Maple Leaf 234
- Marchaj, C A 10, 137, 183, 185, 187
- MARIN 213, 214, 217
- Massachusetts Institute of Technology (MIT) 140
- mast steps 346, 347
- masthead rigs 181, 184, 250–1
- masts: airflow interference 187–90
  - dimensioning 251
  - fractional mast tops 256
  - holes in the mast 258
  - longitudinal mast stiffness 255
  - mast rake 260
  - tests 182, 183–4, 194
  - through deck masts 245
  - transverse loads 246–9
  - transverse mast stiffness 254–5
- materials 286–303
  - mechanical properties of fibres and matrices 328–30
  - stress in hull materials 263, 264
- maximum area section 25
- Measurement Handicap System (MHS) 371
- mechanical properties 323
  - determination of 328–31
- metacentre, transverse (M) 48
- midship sections 24, 33
- Milgram, Professor 184
- minimum operating condition 64
- moments: bending moments 325, 327
  - foiling 148–57
  - pitch moment balance 154–5
- stiffener design forces and moments 335–6, 339
- transverse moment balance (roll) 155–7
  - trim and resistance 230
- Moths 144, 152, 154, 167
- NACA sections 127–8, 129, 137, 140, 161, 163, 165, 167, 171
- Nacra 17 class 148
- Navier–Stokes equations 375
- navigation station 353, 355, 388
- Netherlands Ship Model Basin 213
- Newton's third law 102–3
- Nomoto, Professor K 201–3
- non-dimensional parameters 365
- Non-Uniform Rational B-Splines (NURBS) 15, 35
- Nordic Boat Standard (NBS) 243–5
- nose radius 128, 137
- offsets, table of 29
- Offshore Racing Congress (ORC) 81, 96, 192, 196, 197, 371
- Oossanen, P van 10
- Open-60 class 61
- orbital motion 58
- Orych, M 120
- osmosis 291
- panels: dimensions of 310
  - pressures on 310–13
  - single skin panel calculation 331–2
- parameters, non-dimensional 365
- particle motion 58
- perpendiculars: aft perpendicular (AP) 23
  - forward perpendicular (FP) 23
- pi-foils 147, 177
- pitch 158
  - pitch moment balance 154–5
  - pitch stability 146, 174–7
  - propeller 211
- pitching 96
- planform: advanced planform design 116–22
  - evaluation of planform keels 123–6
  - foiling planform area and shape 158–61
  - sail planform 181–5
- planimeters 32, 38
- planing 223–6
  - forces on planing hulls 228–32
- plank-on-edge cutters 61
- plans 306
- plating: aspect ratio factors for 325
  - curvature correction factor for 326
  - effective width of attached plating 337–40
- polar plot 370, 371–2
- potential flow 382
- pressure: around a wing section 103–4
  - bottom pressure 271, 272–3
  - on panels and stiffeners 310–13
  - pressure and velocity distribution beneath a planing flat plate 224, 225
  - pressure adjusting factors 313–16
  - pressure correction factor 314–15
  - pressure distribution 72–5, 129, 130
- prismatic coefficient 25, 34, 86
- profile plans 27, 28, 32, 33
- propellers 207–22
  - blade area 220–1
  - characteristics 211–12, 217–18
  - design of the optimum propeller 213–16
  - 4-bladed 233
  - performance of non-optimum 217–20
  - pitch 211
  - resistance 221–2
  - surface-piercing 238–9
  - tangential component 211
  - torque 211, 212
  - types of 215
- proportions, versus size calculation (Barkla) 18–19
- propulsion devices, alternative 238–9
- R3 rule 165
- rated length 24
- reefing 194
- refrigeration 356–7
- rescue vessel, high speed 239–42
- residuary resistance, waves and 81–8
- resistance 65
  - appendage resistance 229–30
  - in calm and rough weather 208–10
  - components 67–94
  - computed forces 170–4
  - foiling hulls 144–5, 148, 153, 157
  - frictional resistance 173, 228
  - lift and induced resistance of the yacht 114–16
  - predicting with CFD techniques 375–83
  - propellers 221–2
  - wind resistance of shrouds and stays 253
- resonance avoidance 56
- Reynolds–Averaged Navier–Stokes (RANS) method 375, 376, 378–80
- Reynolds number 71–2, 80, 136, 140, 161, 189
- Ridder, S O 116
- righting moment 47, 48, 50, 51, 243–4, 260, 317
  - influence of waves on 57–9
- rigs and rigging 391
  - construction 243–62
  - double spreader 250
  - forces on shrouds 246–9
  - forces on stays 250–1
  - loads 265–8
- number of spreaders 244–5
- rig design 179–98
- rig loads and attachment 346
- 'rig-sagging' condition 267
- streamlining 190–1
- types of 244–5
- weight 253
- wind resistance 253
- wire vs rod standing rigging 251–3
- YD-41 259–62
- rod rigging, vs wire rigging 251–3
- roll (transverse moment balance) 155–7
- rolling 54–7
  - amplitude 55, 56
  - roughness 75–7
  - influence of 137–8
- Royal Institute of Technology (KTH), Sweden 184, 267, 274
- rudders 136, 160–1, 359
  - aft rudder 121, 122
  - appendage resistance 229–30
  - balance 206
  - configuration 121–2
  - forward rudders 121–2
  - rudder design 102–43
  - foils 146, 152, 153, 154–5, 158, 161, 167, 170–1, 173–4
  - forces from the 279–81
  - forward rudder 122
  - rudder displacement 33–4
  - statistics on rudder area 140–2
  - wave and spray drag 172
- safety gear 363
- sagging 58
- sail control lines 361
- sails 391
  - air flow around 179–81
  - camber 185–7
  - sail area/displacement ratio 365
  - sail area/wetted area 365
  - sail and rig design 179–98
  - sail statistics 197
- saloons 353, 387
- sandwich construction 295–8, 333–5, 336
  - bending 300, 303
  - buckling 298–9
  - core materials 301–2
  - core properties 334, 338
- Savitsky, D 225, 226, 231
- scale factor 27
- scantlings 304–50
  - determination of 304, 328
  - structure of the standard 304–6
- Schaaf, D M W 92
- Scheel keel 124, 125
- seakeeping 94–6, 365
- seakindliness 94, 96
- seaworthiness, assessment of 60–4
- sections 56
  - advanced section design 140
  - definition of 126
  - foil sections 161–5
  - influence of deviations from theoretical section shape 137



- influence of shape on section characteristics 129–35
- midship sections 24, 33
- NACA sections 127–8, 129, 137, 140, 161, 163, 165, 167, 171
- practical conclusions regarding shape 136
- separation 70
- sheer line 15, 26
- SHIPFLOW 71, 378, 379, 380
- shrouds 254
  - drag 191, 208–9
  - forces on 246–9
  - rigging loads 265–8
  - wind resistance 253
- Simpson's rule 39–40, 42, 46
- single skin panel calculation 331–2
- sinks 356
- Skagerrak 209
- Skene, Norman 10
- skiffs, foiling 165–7
- skin friction 71, 72
- slamming 271, 317
- Smith, Phil 'Bugs' 151
- Sonnenberg, U B 81
- Southampton University 53, 188
- space requirements 351–2
- spade rudders 279–81
  - spade rudder stocks 342–4
- Sparkman and Stephens 82
- spars: aluminium 260, 262
  - carbon 260, 262
  - see also booms; masts
- speed: parameters 365
  - speed length ratio 81
- splines 31–2
- spray rails 233–6
- spreaders 244–5, 257–8
- SSPA 373
- stability 317
  - curve of static stability 52–4
  - dynamic stability 236–7
  - flight stability 157–8
  - foiling 146, 147
  - pitch stability 174–6
  - stability index (STIX) 60–4, 365, 393–4
  - stability programs 16
  - statistics 59–60
  - transverse and longitudinal 46, 47–52
- stagnation point 102, 103
- stainless steel rigging, wire vs rod 251–3
- stall, types of 134
- standing rigging, wire vs rod 251–3
- static stability, curve of 52–4
- stations 30
- stays 254
  - drag 191, 208–9
  - forces on 250–1
  - loads on longitudinal stays 250
  - rigging loads 265–8
- wind resistance 253
- wire vs rod rigging 251–3
- steering 359
- stem, 'ghost' 27
- stepped bottoms 233–6
- stiffeners 350
  - construction 340–2
  - design forces and moments 335–6, 339
  - dimensions of 310
  - pressures on 310–13
  - stiffener curvature factor 337
  - stiffening systems 284–5
  - stresses in 337, 339
- STIX (stability index) 60–4, 365, 393–4
- stoves 355–6
- stowage 363
- streamlining rigs 190–1
- stresses: design stresses 323, 326–7
  - in hull materials 263, 264
  - in stiffeners 337, 339
- stringers 350
- structural mechanics 264
- submerged foils 146
- Sunshine 91, 92, 93
- superstructures: design loads for 321–2
  - superstructures correction factor 315–16
- surface piercing foils 146
- surge 153–4, 157
- Swedish Rescue Society 239
- sweep angle 109, 110, 111
- Sydney-Hobart Race (1998) 61
- symbols 6–8
- T-foils 146–7, 148–78
- table of offsets 29
- tandem keels 122
- tangential component, propellers 211
- tank bulkheads 322
- tank testing 372–3
- taper ratios 109, 110–11
- Tatano, H 201–3
- Thébault, Alain 144
- tools 29–32
- top-hat stiffeners 337, 340
- topsides, design loads for 318–20
- torpedo, centreboard/foil junction 153–4
- torque, propeller 211, 212
- towing tank testing 372–3
- transom flaps 233–6
- transoms 34
  - 'ghost' 27
  - shape 96
- transverse metacentre (M) 48
- transverse moment balance (roll) 155–7
- transverse stability 46
  - at large angles of heel 50–2
  - at small angles 47–9
- trapezoidal keel 105, 123, 124
- trim tab 122, 133, 135
- Troost propeller series 213, 214, 217
- tumble home 26
- turning, forces on a turning hull 236, 237
- Twisted Flow Wind Tunnel (TFWT) 374–5
- University of Auckland 374–5
- USA 121
- V-foils 146–7, 148
- V-shape hulls 226, 233
- van de Stadt Design 82
- velocity distribution beneath a planing flat plate 224, 225
- Velocity Prediction Program (VPP) 14, 16, 81, 91, 113, 124, 149, 158, 163, 182, 364, 366–72, 373
- velocity triangle 65, 67
- ventilation (air) 361–2
- ventilation (foils) 178
- Venturi effect 181
- vertical force balance (heave) 149–53, 155
- vertical position of the centre of buoyancy (VCB) 45
- vertices 35
- vibration 139
- viscous flow 375
- viscous resistance 68, 69–70, 72–5, 77
- volume displacement, calculation of 43
- Volvo Ocean Race 364
- Volvo Open 70 123, 124
- vortex generation 56
- vortices 68, 90, 105, 106–7, 111, 117, 120, 121, 181
- vortex distribution 104
- wands 150–1, 172
  - drag 154
- water jets 238, 241, 242
- water plane area 46
- waterlines 86
  - beam of waterline 24
  - designed waterline length (DWL) 23, 27, 34
  - drawing 29, 30, 31
  - length overall/length of waterline 99–100
  - length of waterline/canoe body draft 98
  - length of waterline/draft 97–9
- waves: influence of on righting moment 57–9
- wave motion 90
- wave profile 57
- wave and residuary resistance 81–8
- wave resistance 77–81, 90–4
- wave systems 78–80
- weather helm 199, 200, 201, 203, 206
- weight, wire vs rod rigging 253
- weight schedule monitor 16
- Welbourn, Hugh 145
- wet gear locker 357
- wet laminates 291
- wetted surface 88
  - calculation of 40, 41
- wheel steering 359
- Whitbread maxi 267
- Whitbread Study of Deformations 274–5
- winches 359, 361
- wind moment factor (FWM) 63
- wind resistance, shrouds and stays 253
- wind tunnel testing 374–5
- windage, estimation of 208
- wings: flow around 102–5, 152
  - wing theory 106–11
- winged keels 116–21
- winglets 124, 125, 160, 177
- wire rigging, vs rod rigging 251–3
- work plans 33–4
- Wortmann FX 60–100 section 161–3, 164, 170, 175
- woven rovings (WR) 287–8, 290
- Wu, T-H 378
- XFOIL 140, 163, 165, 178, 375
- Y-foils 147
- YD-40 113, 379, 380
- YD-41 (Yacht Design 41-footer) 12
  - breakdown of total resistance 68
  - building 346–50
  - checklist of considerations 22
  - keel design 142–3
  - lines drawing 28
  - main particulars 385
  - mast 260, 262
  - maximum speed 77
  - optimum propeller 215–16
  - perspective views 36, 37
  - preliminary layout 21
  - propeller resistance 222
  - resistance curve 67
  - rig 259–62, 267, 270
  - rig loads and attachment 346
  - righting moment 260
  - rudder design 143
  - stiffening system 284–5
  - weight calculation 386–92
- Z-foils 148